Cheminformatics bioprospection and experimental validation of corn silk for interventive type 2 diabetes therapeutics

Ayesha Akoonjee

August, 2024

Cheminformatics bioprospection and experimental validation of corn silk for interventive type 2 diabetes therapeutics

Submitted in fulfilment of the requirements for the degree of
Master of Applied Science (MAppSc.) in Biotechnology
in the Department of Biotechnology and Food Science,
Faculty of Applied Sciences,
Durban University of Technology,
South Africa.

Ayesha Akoonjee
Student number: 22290008

Supervisor: Professor Saheed Sabiu

August 2024

Declaration

It is hereby declared that the work in this dissertation submitted by me for the qualification of Master of Applied Science Degree in Biotechnology at the Durban University of Technology is my independent work and has not previously been submitted by me for qualification at another Institution of higher education. The copyright of this thesis is hereby ceded in favour of the Durban University of Technology.

_____ _____

Ayesha Akoonjee **Date**

Student

As the candidate's supervisor, I agree to the submission of this thesis.

_____ _____

Professor Saheed Sabiu **Date**

Acknowledgements

1. My supervisor, Professor Saheed Sabiu, for his guidance, wisdom, patience, time, compassion, kindness and mentorship throughout this project. I have so much to be grateful for that I cannot put it into words. I am forever thankful for every single thing I have learnt from you in the past two years.
2. Professor Nokwanda Makunga for introduction and exposure to metabolomics. I am grateful for the knowledge gained in your laboratory and highly grateful for your kindness during my research expedition to Stellenbosch University.
3. Professor Mazibuko-Mbeje and the Biochemistry Research Group at the North-West University (Mahikeng campus) for introducing me to cell culture and teaching me the skills needed to complete this project.
4. Professor Anil Chuturgoon and Dr. Terisha Ghazi for the help and guidance provided to complete my tissue culture work and gifting me HepG2 cells. Thank you for welcoming me into your lab at the Department of Medical Biochemistry, University of KwaZulu-Natal, Durban, South Africa.
5. The members of the Computational and Systems Biology Research Group, Durban University of Technology (DUT) whose assistance and advice molded the project into what it is now. I am so happy to have made friendships that I will treasure forever.
    a. Mr. Jamiu, thank you for the computational skills gained from you.
    b. Dr. Balogun, many thanks for your time and assistance on the editorial aspects of my writing and advice, for which I am forever grateful.
    c. Mr. Dayo, I am forever grateful for your help throughout this project with my writing.
    d. Miss Athika, for your advice, support and help throughout this project.
6. My family, to whom I am forever grateful
    a. My parents Dawood and Suraiya, without whom I would not exist. Mum and Dad, I'm sorry for every time I have inconvenienced you throughout this project and am forever grateful for everything you have done for me. Without you two, I would not be the person I am today.
    b. My husband, Suhail Dada, without you, I would not have been able to do this. You have helped me more times than I can ever count. Thank you for always helping me and I apologize for when I have inconvenienced you.
    c. My sister, Zahra and her son Umar, for being in my life and bringing me happiness when I needed it most.
7. The Durban University of Technology for the opportunity to do this program.
8. The DUT Scholarship Scheme under the auspices of the Directorate of Research and Postgraduate Support, for funding me throughout this project.
9. I acknowledge and appreciate the financial assistance of the National Research Foundation (NRF) Competitive Programme for Rated Researchers Support (SRUG2204193723) to S. Sabiu
10. Each and everyone whose invaluable input facilitated the success and completion of this project.

Publications and presentations

Primary publications and manuscripts emanating from this study

1. **Akoonjee, A**., Lanrewaju, A.A., Balogun, F.O., Makunga, N.P. and Sabiu, S., 2023. Waste to medicine: Evidence from computational studies on the modulatory role of cornsilk on the therapeutic targets implicated in type 2 diabetes mellitus. *Biology*, 12(12), 1509.
2. **Akoonjee, A**., Saheed Sabiu., 2024. Unveiling the mechanism of action of corn silk intype 2 diabetes mellitus intervention through down regulation of *ADORA1* and *GABBR1* in HepG2 cells (Submitted and under review for publication in *Journal of Functional Foods*).
3. **Akoonjee, A**., Saheed Sabiu., 2024. Metabolomics and computational bioprospection of corn silk against key enzymes implicated in type 2 diabetes mellitus and itscomplications. (Submitted and under review for publication in the *South African Journal of Botany*).

Secondary publications

1. **Lukman, H.Y.**, Aribisala, J.O., Akoonjee, A., Sulyman, A.O., Wudil, A.M. and Sabiu,S., 2024. Modulation of dipeptidyl peptidase IV by rooibos tea metabolites towards type 2 diabetes care: Evidence from molecular dynamics simulation and densityfunctional theory. *Scientific African*, 24, 2173-2187.
2. **Balogun, F.O.**, Singh, K., Rampadarath, A., Akoonjee, A., Naidoo, K. and Sabiu, S., 2023. Cheminformatics identification of modulators of key carbohydrate-metabolizing enzymes from *C. cujete* for type-2 diabetes mellitus intervention. *Journal of Diabetes and Metabolic Disorders*, 22, 1299-1317.
3. **Akoonjee, A.**, Rampadarath, A., Aruwa, C.E., Ajiboye, T.A., Ajao, A.A.N. and Sabiu,S., 2022. Network pharmacology-and molecular dynamics simulation-based bioprospection of *Aspalathus linearis* for type-2 diabetes care. *Metabolites*, 12, 1013- 1034.

Conference proceedings

1. **Akoonjee, A**. and Sabiu S., 2024. Unveiling the mechanism of action of corn silk as an interventive therapy in type 2 diabetes mellitus through integrated network pharmacology and downregulation of *ADORA1* and *GABBR1*. An oral presentation at the Computational and Systems Biology Research Conference held at Coastlands Hotel, Musgrave, Durban, held on the 26th of June 2024.
2. **Akoonjee, A.** and Sabiu, S., 2023. Cheminformatics bioprospection of corn silk as an interventive therapy in type 2 diabetes mellitus. An oral presentation delivered at the Durban University of Technology's Faculty of Applied Sciences 2023 Research Day, held at Coastlands Hotel, Musgrave, Durban, South Africa, on the 17th of November 2023.
3. **Akoonjee, A.** and Sabiu, S., 2023. Turning waste into medicine- Corn silk as an intervention in type 2 diabetes treatment. An oral presentation delivered at the Three Minutes Flash Fact Competition of the Department of Biotechnology and Food Science, Faculty of Applied Sciences, Durban University of Technology, Durban, South Africa, held on the 12th of October 2023. The presentation was awarded ***First Place for Oral Presentation (Masters)*** *and* ***First Place for People's Choice Award***.

4. **Akoonjee, A.** and Sabiu, S., 2022. An integrated network pharmacology approach in unveiling the mechanism of action of corn silk in type 2 diabetes care. A poster presentation delivered at the Durban University of Technology's Faculty of Applied Sciences 2022 Research Day, held at Coastlands Hotel, Musgrave, Durban, South Africa, on the 17th of November 2022.
5. **Akoonjee, A.** and Sabiu, S., 2022. Network pharmacology study of corn silk phenolics against targets related to type 2 diabetes mellitus. A virtual oral presentation at the 2022 South African Society of Basic and Clinical Pharmacology (SASBCP) Conference held on the 12th of October 2022.
6. **Akoonjee, A.** and Sabiu, S., 2022. Network pharmacology study of corn silk phenolics against targets related to type 2 diabetes mellitus. A virtual oral presentation at the South Africa Sweden University Forum (SASUF) held on the 19th of September 2022.

General abstract

Diabetes mellitus (DM) is one of the oldest known human diseases, with type 2 diabetes mellitus (T2DM) being the most prevalent form. Type 2 diabetes mellitus (T2DM) is characterized by elevated blood glucose levels due to defective insulin production and/or resistance to insulin. If left untreated, it can lead to severe complications affecting various body systems. While synthetic medications are commonly used to treat T2DM, their associated drawbacks, such as high cost, inaccessibility and side effects, mitigate their application in managing T2DM. Consequently, there has been a growing interest in natural products with antidiabetic potential. Natural products, including medicinal plants and plant-derived products, have been used for centuries, and their active compounds continue to be explored for therapeutic applications. For example, corn silk (CS), a waste material of corn cultivation, possesses several therapeutic properties, including antidiabetic potential. Although, studies reporting the promising hypoglycaemic potentials of CS exist, its exact mechanism of action remains incompletely elucidated, a research gap that was fulfilled in this study through metabolomics, cheminformatics bioprospection and *in vitro* experimental validation.

To identify the constituents in CS, ultra-performance liquid chromatography-mass spectrometry analysis and principal component analysis was performed on its three extracts (aqueous, hydro-ethanolic and ethanolic) at two developmental growth stages (premature and mature). A library consisting of 128 metabolites was generated from all the samples of CS with qualitative and quantitative variations observed between the two growth stages of CS and the type of solvent used for extraction. Specifically, the mature CS had a higher abundance of most metabolites, with the hydro-ethanolic extract of CS being the most metabolites-rich compared to the aqueous and ethanolic extracts of CS. These metabolites were thereafter subjected to bioprospection against the therapeutic targets, such as enzymes and genes implicated in the pathogenesis of T2DM using computational techniques.

The modulatory role of CS metabolites on six enzymes implicated in the pathogenesis of T2DM and its secondary complication, particularly alpha-amylase (AA), alpha-glucosidase (AG), aldose reductase (AR), dipeptidyl peptidase-4 (DPP-4), protein tyrosine phosphatase 1B (PTP1B) and sorbitol dehydrogenase (SDH), was analysed using molecular docking complemented with molecular dynamics (MD) simulation. Molecular docking analysis identified aesculin (-8.1 kcal/mol), austricin (-7.8 kcal/mol), (6E)-1-(4-hydroxyphenyl)-7-phenylhepta-4,6-dien-3-one (-9.9 kcal/mol), (-)-11-hydroxy-9,10-dihydrojasmonic acid 11-beta-D-glucoside (-8.6 kcal/mol), phaseic acid (-6.0 kcal/mol), and erythronolide B (-9.2 kcal/mol) as compounds with the most negative scores against AA, AG, AR, DPP-4, PTP1B and SDH, respectively. However, a further insight into the binding free energy (ΔG_{bind}) calculations of the putative leads against each enzyme over a 150-ns simulation period revealed that R-7-butyl-6,8-dihydroxy-3-[(3e)-pent-3-en-1-yl]-3,4-dihydroisochromen-1-one (BHP), 1-O-vanilloyl-beta-D-glucose (VBJ), (-)-11-hydroxy-9,10-dihydrojasmonic acid 11-beta-D-glucoside (HDJ), p-coumaroyl malic acid (CMA), 2-hydroxydecanedioic acid (HDA), and (-)-11-hydroxy-9,10-dihydrojasmonic acid 11-beta-

D-glucoside (HDJ) hold remarkable therapeutic promise as modulators of AA, AG, AR, DPP-4, PTP1B, and SDH, respectively. The post-MD dynamic simulation analysis and interaction plots in each case revealed the formation of thermodynamically stable complexes suggestive of the putative leads as potential modulators of the respective investigated enzymes and their possible applications in the management of T2DM and its secondary complications. Density functional theory (DFT) analysis was used to determine the molecular characteristics of the top ranked CS metabolites identified to modulate the investigated enzyme targets. Although the lower energy gaps, higher softness and lower chemical hardness of the metabolites did not correlate with their high negative binding free energy (potentially due to the observed relative residue fluctuations and increased surface area of the targets upon ligand binding), their electrophilicity indices which were above 1.5 electron volt (eV) alluded to their strong electrophilic potential. This highlights their ability to interact with amino acids with nucleophilic side chains of the target enzymes that is indicative of enhanced specificity and binding to the enzymes.

Subsequently, a network pharmacology study was conducted to elucidate the relationship between CS constituents and signaling pathways implicated in T2DM. The analysis identified the cAMP pathway as the central signaling pathway, with adenosine receptor A1 (*ADORA1*), hydroxycarboxylic acid receptor 2 (*HCAR2*) and gamma-aminobutyric acid type B subunit 1 (*GABBR1*) as key therapeutic targets. Gallicynoic acid (-48.74 kcal/mol), dodecanedioc acid (-34.53 kcal/mol), and tetradecanedioc acid (-36.80 kcal/mol) interacted effectively with *ADORA1*, *HCAR2*, and *GABBR1*, respectively, relative to the reference standards (metformin and resveratrol) and formed thermodynamically stable complexes, as indicated by post-MD analysis results. These findings suggest the compounds as potential drug candidates for T2DM through modulation of cAMP pathway genes. The cAMP pathway is implicated in the pathogenesis of T2DM through various levels including glucagon and epinephrine-stimulated cAMP production, increased glucose release from the liver, modulation of insulin signaling, insulin resistance and the regulation of gut hormone secretion, including glucagon-like peptide-1.

To complement and validate the results obtained through network pharmacology as a further way of elucidating the mechanism of antidiabetic action of CS, experimental validation employing the use of HepG2 cells was performed. The effect of different CS formulations on HepG2 cells was firstly assessed using the 3-(4,5-dimethylthiazol-2-yl)-2,5-diphenyltetrazolium bromide (MTT) viability and glucose consumption assays, followed by real-time polymerase chain reaction (RT-qPCR) to understand the effect of CS on the expression of *ADORA1* and *GABBR1*, the top two target genes modulated by the CS metabolites as identified by the network pharmacology study. For the MTT assay, CS extracts at concentrations 75 – 100 µg/mL promoted viability of HepG2 cells, with the ethanolic extract of the mature CS being the most viable relative to the controls (insulin- and metformin-treated) and the untreated cells. Generally, higher HepG2 cell viability and glucose uptake were observed following treatment with mature CS extracts compared to premature CS. Specifically, the most significant and enhanced glucose uptake level was observed with both normal and insulin-resistant HepG2 cells following treatment with the aqueous extracts of mature CS extract compared to the controls. Furthermore, compared to

the untreated cells, as well as insulin- and metformin-administered cells, treatment with CS extracts remarkably inhibited the expression of *ADORA1* and *GABBR1* in insulin-resistant HepG2 cells with the most prominent effect observed with the aqueous extract of premature CS. These observation with the CS aqueous extracts may be attributed to their relatively higher abundance of the profiled metabolites such as gallicynoic acid B and tetradecanedioc acid, which were more than 40% each by composition in both the mature and premature extracts. These findings regarding the high concentrations of gallicynoic acid B and tetradecanedioc acid in CS aqueous extracts are not only significant in modulating the expression of *ADORA1* and *GABBR1*, resulting in increased glucose uptake in the treated cells but consistent with the results of MD simulation that profiled the two compounds as putative leads against the two most significant therapeutic targets in the cAMP signalling pathway associated with T2DM. Overall, the findings from this study have contributed to the elucidation of the mechanisms of antidiabetic action of CS metabolites which would be vital in the development of CS as a therapeutic agent for the management of T2DM and its associated secondary complications.

Keywords: Computer-aided drug design; Corn silk; Network pharmacology; Molecular dynamics simulation; Type 2 diabetes mellitus

Table of contents

Chapter one
General Introduction

Chapter one

1. Introduction

Diabetes mellitus (DM), a chronic metabolic disease characterized by elevated blood glucose levels, is a significant contributor to morbidity, mortality, and health costs worldwide (Mazibuko-Mbeje *et al*., 2022). In 2024, approximately 540 million adults between the ages of 20 – 79 years were diabetic globally, and this figure is expected to rise to 783 million by 2045, if no practical solution is provided (IDF, 2024). Just like the global trends, the rapidly increasingly prevalence of DM in South Africa is also alarming, especially since DM is the leading underlying cause of death in women and the second highest cause of death for the entire South African population (Sifunda *et al*., 2023). Approximately 55.5% of South Africans are living in poverty (Statistics South Africa, 2024) and when coupled with the already overburdened healthcare system , the economic toll of DM on the country is tremendous (Sifunda *et al*., 2023). Among several factors that contribute to the rising prevalence of DM in South Africa, sedentary lifestyles, unhealthy diets, obesogenic environments, urbanization and an aging population are the most pertinent (Pheiffer *et al*., 2018). Accounting for approximately 90% of cases, type 2 diabetes mellitus (T2DM) remains the most prevalent form of DM (Lankatillake *et al*., 2019) and its untreated cases have culminated in severe complications such as kidney disease, ocular damage, cardiovascular disease, heart attack, stroke, bone fracture risks, nerve damage, skin conditions, foot related complications (ulcers, loss of feeling, amputation etc.), increased risk of Alzheimer's disease and hearing impairment (Xiao *et al*., 2019; Yagasaki *et al.*, 2022).

To improve the health and quality of life of patients suffering from T2DM, mitigate the onset of T2DM-related secondary complications, minimize the number of hospitalizations, alleviate the strain on healthcare systems, and reduce the risk of premature death, effective T2DM management is imperative (Michaelidou *et al*., 2023). Lifestyle modifications (a healthy diet, regular physical exercise, weight management therapy), constant blood sugar monitoring and regular healthcare visits to monitor overall health and prevention of secondary complications can be used in the management of T2DM (Dludla *et al*., 2020). However, the long-term application and sustainability of these approaches are usually not feasible for several patients (Lankatillake *et al*., 2019). Consequently, there is a significant reliance on the use of conventional oral antidiabetic medications to achieve and maintain glycaemic control (Sabiu *et al*., 2019). However, the long-term regimens, cost, accessibility, lower therapeutic efficacy,

differing individual variability, low drug solubility and permeability, lack of target specificity and low potency are major drawbacks associated with the use of conventional synthetic drugs in T2DM management therapy (Padhi *et al*., 2020). In addition, prolonged usage of T2DM synthetic medications results in drug resistance and unwanted side effects such as weight fluctuations, nausea, diarrhoea, hypoglycaemia, liver and kidney failure, cardiovascular complications and lactic acidosis (Michaelidou *et al*., 2023; Yao *et al*., 2024). Consequently, several anti-hyperglycaemic agents with promising antidiabetic potentials have been identified as alternatives or complementary adjuncts to synthetic medications (Padhi *et al*., 2020).

Natural products, such as plants, herbs and organic materials with promising antidiabetic properties have served as abundant sources of non-synthetic anti-hyperglycaemic compounds that can be used to maintain blood glucose concentration, reduce the impact of side effects and prevent secondary complications associated with T2DM (Xiao *et al*., 2018; Sukhikh *et al*., 2023). Among the various crops produced in South Africa, corn stands out as a predominant field crop as it is an economical staple food consumed by most of the population (ADAMA, 2023). While the edible corn kernels are the main product produced by corn cultivation, a by-product of corn proliferation is corn silk (CS) which is often treated as waste and discarded (Hasanudin *et al*., 2012). However, CS is an abundant, low-cost natural plant material with promising therapeutic properties (Sabiu *et al*., 2019; Wang *et al*., 2019), and has been used as a traditional medicine to treat several diseases including T2DM (Zhang *et al.,* 2015; Dardouk *et al*., 2019; Alimin L, 2020). Corn silk (CS) consists of several metabolites, including flavanoids, saponins, alkaloids, tannins, phytosterols, terpenoids, steroids, polysaccharides, cerebrosides, allantoin and vitamins (Thoudam *et al*., 2011), many of which are responsible for its reported bioactivities including antidiabetic (Singh *et al*., 2022; Fougere *et al*., 2023). Despite several studies reporting CS as a promising antidiabetic material (Chen *et al*., 2013; Zhang *et al*., 2015; Jia *et al*., 2020; Chaudhary *et al*., 2022; Dong *et al*., 2022; Liang *et al.*, 2024), its mechanism of anti-hyperglycaemic action has not been fully elucidated to date, a gap in research that needs to be further explored.

A major challenge in T2DM therapy involves the optimization of current T2DM therapies (conventional and non-conventional), which is crucial for the development of promising antidiabetic agents for the effective maintenance of blood glucose levels (Padhi *et al*., 2020). With technological advancements, researchers can identify plant secondary metabolites, which can be used to further investigate the pharmacological potential such as antidiabetic

properties of a plant (Yao *et al*., 2024). This is crucial for the isolation and/or synthesis of lead compounds that can serve as a foundation for future drugs (Rahman *et al*., 2022). Metabolomic profiling is a powerful technique used to comprehensively analyse metabolites present in a plant allowing investigations on its developmental stages, responses to external stresses, and genetics (Desai *et al*., 2013) as well as its pharmacological properties and mechanisms of action (Lu *et al*., 2013). For instance, metabolomic studies can offer insights on the potential role of plant-derived metabolites in modulating insulin resistance and glucose homeostasis (Hu *et al*., 2014; Wang *et al*., 2020).

Among the high throughput tools used in metabolomic studies, mass spectrometry (MS) and proton nuclear resonance spectroscopy remain the most used techniques (Nicholson *et al*., 1999). Hailed as the most frequently used technique in metabolomics, MS provides information on mass-to-charge ratio which enables the structure of a compound to be determined, allowing for its detection and quantification in a biological sample (Hasanpour *et al*., 2020; Lu *et al*., 2013). It is usually coupled with other suitable analytical techniques such as gas chromatography (GC) and liquid chromatography (LC) to enhance the detection of distinct metabolite classes (Lu *et al*., 2013). da Hora *et al*. (2021) employed high performance liquid chromatography-mass spectrometry (HPLC-MS) analysis and GC-MS to identify 34 metabolites in different organic solvent extractions of CS (da Hora *et al*., 2021). Ultra-high performance liquid chromatography-mass spectrometry (UHPLC-MS) of a 50% ethanolic extract of Martinique CS revealed the detection of 104 therapeutic compounds consisting of 55 flavonoids, 13 organic acids, 29 lipids and 7 nitrogenous compounds (Fougere *et al*., 2023). Although there has been increasing efforts in terms of exploring the phytochemical composition of CS, a comprehensive phytochemical profile of CS could be further improved, particularly in terms of investigating various types and varieties of corn, and establishing correlations between CS metabolites and reported biological activities, which could be improved using computational approaches.

Integrating metabolomic data with computational approaches allows for identification of novel therapeutics through drug targets prediction and biomarkers' identification, which will enable drug repurposing, understanding of drug mechanisms, drug response predictions, investigating drug-drug interactions and optimizing drug combinations as well as enabling personalized medicine (Pang *et al*., 2023). Through the constant evolution of technology, computational techniques have revolutionized the field of drug discovery, accelerating the process and expanding the possibilities for identifying, designing and developing new drug

agents (Koparde *et al*., 2023). Network pharmacology, an interdisciplinary field encompassing pharmacology, network science, systems biology and computational biology, allows for the study of drug leads, targets and biological systems at a network level (Leung *et al*., 2013). The integration of distinct largescale datasets from heterogenous sources in network pharmacology allows for the construction of disease-specific networks (Agamah *et al*., 2020), and to foster a genome-centric strategy which can be used to elucidate crucial nodes that can serve as potential targets, owing to their influence within the network (Katsila *et al*., 2016).

Together with network pharmacology, computer-aided drug design (CADD) approaches such as structure-based drug design, structure-based pharmacophore modelling, virtual screening, quantum mechanical modelling (density functional theory), molecular docking, ligand-based drug design, quantitative structure–activity relationship models, ligand-based pharmacophore modelling and molecular dynamics (MD) simulation can be used to further explore the relationship between targets and lead drugs (Asadi *et al*., 2013; Xin *et al*., 2021; Hasan *et al*., 2022; Wang *et al*., 2022). Through CADD, the discovery and development of lead compounds by employing theoretical calculations, simulations and prediction of relationships between drug leads and target receptors is made possible, accelerating the process of drug discovery (Gu *et al*., 2023; Sharma *et al*., 2023).

While computational approaches have offered valuable insights into the discovery and development of therapeutic agents for T2DM, experimental validation to ensure the reliability, accuracy, efficacy, and safety of potential drugs and/ or treatments is imperative (Shalaby *et al*., 2014; Ponnulakshmi *et al*., 2019; Kifle *et al*., 2020). Of the experimental validation strategies, the use of mammalian cell lines has been identified as one of the most reliable ways to screen potential drug candidates in providing insights into their safety profiles and possible mechanisms of action (Jaroch *et al*., 2018, Venkateswaran *et al*., 2020; Feraco *et al*., 2021). While numerous studies have reported the anti-hyperglycaemic properties of CS using animal models (Zhao *et al*., 2012; Zhang *et al*., 2015; Pan *et al*., 2017; Han *et al*., 2019; Sheng *et al*., 2021), there is limited reports on the use of mammalian cell lines investigating the effect of CS on T2DM and its related secondary complications. The only available cell line studies on the mechanism of antidiabetic action of CS are through the restoration of beta-cell function, reduction of pathological oxidative stress, inhibition of protein glycation, reduction of advanced glycation end-product formation, inhibition of extracellular matrix, induction of glucose uptake and enhancing the translocation of glucose transporter type 4 (Chang *et al*., 2016; Guo *et al*., 2019; Wang *et al*., 2019; Hamzah *et al*., 2021). Out of the mammalian cells

exploring the anti-hyperglycaemic activities of CS, there is no reports validating the antidiabetic potentials of CS using HepG2 cells. HepG2 is a human hepatoma cell derived from human foetal liver tumour cells and is one of the commonly used cells in studies related to DM (Liu *et al*., 2017). While the use of HepG2 cell line studies have been employed to investigate the relationship between many plants and their chemical components on the pathogenesis of T2DM and the prevention of secondary complications associated with T2DM (Huang *et al*., 2015; Mokashi *et al*., 2017; Chen *et al*., 2019; Aladejana *et al*., 2020; Bourebaba *et al*., 2021; Yarahmadi *et al*., 2021), there is no information available validating the antidiabetic potentials of CS using a HepG2 cells, one of the knowledge gaps this project aims to fulfil.

This study focuses on exploring the antidiabetic mechanism of action (MoA) of CS, an abundant natural waste product that remains underutilized in South Africa, through metabolomics, computational and experimental validation approaches. Ultra-performance liquid chromatography-mass spectrometry was utilized to identify the metabolites present in different formulations of CS at two developmental growth stages. Thereafter, computational approaches such as network pharmacology, molecular docking and MD simulation were employed to unearth the antidiabetic MoA of CS by exploring the relationship between its metabolites and therapeutic targets implicated in the pathogenesis of T2DM. Subsequently, a HepG2 cell line study aimed at investigating the effect of CS on glucose uptake and expression of target genes implicated in the pathogenesis of T2DM, was performed to validate the anti-hyperglycaemic potential of CS *in vitro*.

2. Research problem

Type 2 diabetes mellitus (T2DM) is a complex metabolic disorder that affects millions globally (Lankatillake *et al*., 2019). If left untreated, it can lead to serious complications, such as cardiovascular disease, stroke, kidney damage, blindness, and even limb amputation (Michaelidou *et al*., 2023). The high cost, long-term regimen and adverse side effects associated with the currently available oral antidiabetic drugs make the disease difficult to manage (Padhi *et al*., 2020). Plants serve as sources of various phytochemicals which have been reported with promising antidiabetic properties (Rahman *et al*., 2014; Zhang *et al*., 2015). Although, studies have reported the antidiabetic properties of CS, the exact MoA are not fully elucidated. Seeking to understand the underlying mechanism of antidiabetic action of CS prompted this study.

3. Aim and objectives of the study

The aim of this study was to determine the metabolite profiles and molecular mechanism of action of corn silk as an interventive therapy in the management of T2DM using computational and experimental approaches.

This aim was achieved through these specific objectives:

i. Metabolomic profiling of the metabolites presented in different extracts of CS of a commonly consumed corn in South Africa at two different developmental stages (premature and mature) using ultra performance liquid chromatography-mass spectrometry and principal component analysis;
ii. Establishment of the structural mechanism of interaction between CS metabolites and the key enzymes (alpha-amylase, alpha-glucosidase, dipeptidyl peptidase-4, aldose reductase, sorbitol dehydrogenase and protein tyrosine phosphatase 1B) implicated in the pathogenesis of T2DM using molecular dynamic (MD) simulation approach;
iii. Investigation of the relationship between CS metabolites with the signalling pathways and genes implicated in T2DM using network pharmacology-based strategy complemented with MD simulation; and,
iv. Validation of the molecular mechanism of antidiabetic potential of CS in vitro using HepG2 cells.

4. Organization of dissertation

The dissertation includes a contribution of a published article as well as submitted articles for publication. Chapter one provides the general background to the study with details on the core research problem and aim of the study, while Chapter two focused on the literature review assessing information available on the medicinal properties, particularly the antidiabetic potential of CS. Chapter three explores the intermolecular mechanism of interaction between CS metabolites identified through metabolomics against the key enzymes implicated in the pathogenesis of T2DM using molecular docking and MD simulation approaches. Chapter four on the other hand focused on elucidating the relationship between CS metabolites and therapeutic genes as well as signaling pathways implicated in the pathogenesis of T2DM through integrated network pharmacology and advanced computation approaches. The findings on the experimental validation of the anti-hyperglycemic potentials of CS using HepG2 cells are presented in Chapter five. In Chapter six, the general discussion and conclusions to consolidate the overall results obtained from the study are presented.

References

ADAMA. 2023. Maize farming in South Africa, retrieved from https://www.adama.com/south-africa/en/maize-farming/maize-farming-south-africa, accessed on 11/03/2024.

Agamah, F.E., Mazandu, G.K., Hassan, R., Bope, C.D., Thomford, N.E., Ghansah, A. and Chimusa, E.R. 2020. Computational *in silico* methods in drug target and lead prediction. *Briefings in Bioinformatics*, 21, 1663-1675.

Aladejana, A.E., Bradley, G. and Afolayan, A.J. 2020. *In vitro* evaluation of the anti-diabetic potential of *Helichrysum petiolare* Hilliard and BL Burtt using HepG2 (C3A) and L6 cell lines. *F1000Research*, 9. 1240.

Alimin, L. 2020. Effects of corn silk (*Stigma Maydis*) against blood glucose levels of type 2 diabetes mellitus patients. *Buletin Farmatera*. 5. 202-207.

Assadi, M.H. and Hanaor, D.A. 2013. Theoretical study on copper's energetics and magnetismin TiO2 polymorphs. *Journal of Applied Physics*, 113, 233913.

Bourebaba, N., Kornicka-Garbowska, K., Marycz, K., Bourebaba, L. and Kowalczuk, A. 2021. *Laurus nobilis* ethanolic extract attenuates hyperglycemia and hyperinsulinemia-induced insulin resistance in HepG2 cell line through the reduction of oxidative stress and improvement of mitochondrial biogenesis–Possible implication in pharmacotherapy. *Mitochondrion*, 59, 190-213.

Chang, C.C., Yuan, W., Roan, H.Y., Chang, J.L., Huang, H.C., Lee, Y.C., Tsay, H.J. and Liu, H.K. 2016. The ethyl acetate fraction of corn silk exhibits dual antioxidant and anti-glycation activities and protects insulin-secreting cells from glucotoxicity. *BMC Complementary and Alternative Medicine*, 16, 1-11.

Chaudhary, R.K., Karoli, S.S., Dwivedi, P.S. and Bhandari, R. 2022. Anti-diabetic potential of cornsilk (*Stigma maydis*): an *in-silico* approach. *Journal of Diabetes and Metabolic Disorders*, 21,445-454.

Chen, F.C., Shen, K.P., Ke, L.Y., Lin, H.L., Wu, C.C. and Shaw, S.Y. 2019. Flavonoids from *Camellia sinensis* (L.) O. Kuntze seed ameliorates TNF-α induced insulin resistance in HepG2 cells. *Saudi Pharmaceutical Journal*, 27, 507-516.

Chen, S., Chen, H., Tian, J., Wang, Y., Xing, L. and Wang, J. 2013. Chemical modification, antioxidant and α-amylase inhibitory activities of corn silk polysaccharides. *Carbohydrate Polymers*, 98, 428-437.

da Hora, N.R., Santana, L.F., da Silva, V.D.A., Costa, S.L., Zambotti-Villela, L., Colepicolo, P., Ferraz, C.G. and Ribeiro, P.R. 2021. Identification of bioactive metabolites from corn silk extracts by a combination of metabolite profiling, univariate statistical analysis and chemometrics. *Food Chemistry*, 365, 130479.

Dardouk, F., Arandi, H. and Makharzeh, M. 2019. Extraction of corn silk and its applications in healing and cosmetics, retrieved from: https://repository.najah.edu/items/360298b5-d108- 4221-b0a1-9e9575122cd6, accessed on 29/01/2024.

Desai, N. and Alexander, D. 2013. Metabolite profiling for plant research. *From Plant Genomics to Plant Biotechnology*, Woodhead Publishing. 2013, 49-65.

Dludla, P.V., Muller, C.J., Louw, J., Mazibuko-Mbeje, S.E., Tiano, L., Silvestri, S., Orlando, P., Marcheggiani, F., Cirilli, I., Chellan, N. and Ghoor, S. 2020. The combination effect of aspalathin and phenylpyruvic acid-2-o-β-d-glucoside from rooibos against hyperglycemia-induced cardiac damage: an *in vitro* study. *Nutrients*, 12, 1151.

Dong, W., Zhao, Y., Hao, Y., Sun, G., Huo, J. and Wang, W. 2022. Integrated molecular biology and metabonomics approach to understand the mechanism underlying reduction of insulin resistance by corn silk decoction. *Journal of Ethnopharmacology*, 284, 114756.

Feraco, A., Gorini, S., Armani, A., Camajani, E., Rizzo, M. and Caprio, M. (2021). Exploring the role of skeletal muscle in insulin resistance: lessons from cultured cells to animal models. International *Journal of Molecular Sciences*, 22, 9327.

Fougère, L., Zubrzycki, S., Elfakir, C. and Destandau, E. (2023). Characterization of corn silk extract using HPLC/HRMS/MS analyses and bioinformatic data processing. *Plants*, 12, 721.

Guo, Q., Chen, Z., Santhanam, R.K., Xu, L., Gao, X., Ma, Q., Xue, Z. and Chen, H. 2019. Hypoglycemic effects of polysaccharides from corn silk (*Maydis stigma*) and their beneficial roles via regulating the PI3K/Akt signaling pathway in L6 skeletal muscle myotubes. *International Journal of Biological Macromolecules*, 121, 981-988.

Hamzah, N., Safuan, S. and Wan Ishak, W.R. 2021. Potential effect of polyphenolic-rich fractions of corn silk on protecting endothelial cells against high glucose damage using *in vitro* and *in vivo* approaches. *Molecules*, 26, 3665.

Han, Y.C., Wu, J.Y. and Wang, C.K. 2019. Modulatory effects of miracle fruit ethanolic extracts on glucose uptake through the insulin signaling pathway in C2C12 mouse myotubes cells. *Food Science and Nutrition*, 7, 1035-1042.

Hasan, M.R., Alsaiari, A.A., Fakhurji, B.Z., Molla, M.H.R., Asseri, A.H., Sumon, M.A.A., Park, M.N., Ahammad, F. and Kim, B. 2022. Application of mathematical modeling and computational tools in the modern drug design and development process. *Molecules*, 27, 4169.

Hasanudin, K., Hashim, P. and Mustafa, S. 2012. Corn silk (*Stigma maydis*) in healthcare: a phytochemical and pharmacological review. *Molecules*, 17, 9697.

Hasanpour, M., Iranshahy, M. and Iranshahi, M. 2020. The application of metabolomics in investigating anti-diabetic activity of medicinal plants. *Biomedicine and Pharmacotherapy*, 128, 110263.

Hu, X., Wang, S., Xu, J., Wang, D.B., Chen, Y. and Yang, G.Z. 2014. Triterpenoid saponins from *Stauntonia chinensis* ameliorate insulin resistance via the AMP-activated protein kinase and IR/IRS-1/PI3K/Akt pathways in insulin-resistant HepG2 cells. *International Journal of Molecular Sciences*, 15, 10446-10458.

Huang, Q., Chen, L., Teng, H., Song, H., Wu, X. and Xu, M. 2015. Phenolic compounds ameliorate the glucose uptake in HepG2 cells' insulin resistance via activating AMPK: anti-diabetic effect of phenolic compounds in HepG2 cells. *Journal of Functional Foods*, 19, 487-494.

International Diabetes Federation. 2024. Diabetes facts & figures. Retrieved from: https://idf.org/about-diabetes/diabetes-facts-figures/, accessed on 16/11/2024.

Jia, Y., Xue, Z., Wang, Y., Lu, Y., Li, R., Li, N., Wang, Q., Zhang, M. and Chen, H. 2021. Chemical structure and inhibition on α-glucosidase of polysaccharides from corn silk by fractional precipitation. *Carbohydrate Polymers*, 252, 117185.

Jaroch, K., Jaroch, A. and Bojko, B. 2018. Cell cultures in drug discovery and development: The need of reliable *in vitro-in vivo* extrapolation for pharmacodynamics and pharmacokinetics assessment. *Journal of Pharmaceutical and Biomedical Analysis*, 147, 297-312.

Katsila, T., Spyroulias, G.A., Patrinos, G.P. and Matsoukas, M.T. 2016. Computational approaches in target identification and drug discovery. *Computational and Structural BiotechnologyJournal*, 14, 177-184.

Kifle, Z.D., Yesuf, J.S. and Atnafie, S.A. 2020. Evaluation of *in vitro* and *in vivo* anti-diabetic, anti-hyperlipidemic and anti-oxidant activity of flower crude extract and solvent fractions of *Hagenia abyssinica* (rosaceae). *Journal of Experimental Pharmacology*, 151-167.

Koparde, A.A., Doijad, R.C. and Magdum, C.S. 2019. Natural products in drug discovery. *Pharmacognosy-medicinal plants*. IntechOpen. Retrieved from: https://books.google.co.za/books?hl=en&lr=&id=JJn8DwAAQBAJ&oi=fnd&pg=PA269&dq=Natural+products+in+drug+discovery.+In+Pharmacognosy-medicinal+plants&ots=8KhC4SIxRm&sig=2q_71McvA4G6una8gFVN9rrx-kg&redir_esc=y#v=onepage&q=Natural%20products%20in%20drug%20discovery.%20In%20Pharmacognosy-medicinal%20plants&f=false, retrieved on: 29/01/2024.

Lankatillake, C., Huynh, T. and Dias, D.A. 2019. Understanding glycaemic control and current approaches for screening antidiabetic natural products from evidence-based medicinal plants. *Plant Methods*, 15, 105.

Leung, E.L., Cao, Z.W., Jiang, Z.H., Zhou, H. and Liu, L. 2013. Network-based drug discovery byintegrating systems biology and computational technologies. *Briefings in Bioinformatics*, 14, 491-505.

Liang, H., Zhang, R., Zhou, L., Wu, X., Chen, J., Li, X., Chen, J., Shan, L. and Wang, H. 2024. Corn stigma ameliorates hyperglycemia in zebrafish and GK rats of type 2 diabetes. *Journal of Ethnopharmacology*, 325, 117746.

Liu, L., Zhang, X., Chen, F., Hu, J. and Zeng, B. (2017). The establishment of insulin resistance model. *BIO Web of Conferences*. EDP Sciences. 8, 03005.

Lu, J., Xie, G., Jia, W. and Jia, W. 2013. Metabolomics in human type 2 diabetes research. *Frontiers of Medicine*, 7, 4-13.

Mazibuko-Mbeje, S.E., Dludla, P.V., Johnson, R., Joubert, E., Louw, J., Ziqubu, K., Tiano, L., Silvestri, S., Orlando, P., Opoku, A.R. and Muller, C.J. 2019. Aspalathin, a natural product with the potential to reverse hepatic insulin resistance by improving energy metabolism and mitochondrial respiration. *PloS One*, 14, 0216172.

Michaelidou, M., Pappachan, J.M. and Jeeyavudeen, M.S. 2023. Management of diabesity: current concepts. *World Journal of Diabetes*, 14, 396-411.

Mokashi, P., Khanna, A. Pandita, N. 2017. Flavonoids from *Enicostema littorale* blume enhances glucose uptake of cells in insulin resistant human liver cancer (HepG2) cell line via IRS-1/PI3K/Akt pathway. *Biomedicine and Pharmacotherapy*, 90, 268-277.

Nicholson, J.K., Lindon, J.C. and Holmes, E. 1999. 'Metabonomics': understanding the metabolic responses of living systems to pathophysiological stimuli via multivariate statistical analysis of biological NMR spectroscopic data. *Xenobiotica*, 29, 1181-1189.

Padhi, S., Nayak, A.K. and Behera, A. 2020. Type II diabetes mellitus: a review on recent drug-based therapeutics. *Biomedicine and Pharmacotherapy*, 131, 110708.

Pan, Y., Wang, C., Chen, Z., Li, W., Yuan, G. and Chen, H. 2017. Physicochemical properties and antidiabetic effects of a polysaccharide from corn silk in high-fat diet and streptozotocin-induced diabetic mice. *Carbohydrate polymers*, 164, 370-378.

Pang, H. and Hu, Z. 2023. Metabolomics in drug research and development: The recent advances in technologies and applications. *Acta Pharmaceutica Sinica B*, 13, 3238-3251.

Pheiffer, C., Pillay-van Wyk, V., Joubert, J.D., Levitt, N., Nglazi, M.D. and Bradshaw, D. 2018. The prevalence of type 2 diabetes in South Africa: a systematic review protocol. *BMJ Open*, 8, 021029.

Ponnulakshmi, R., Shyamaladevi, B., Selvaraj, J., Valli, G., Purushothaman, V., Alsawalha, M. and Mohan, S.K. 2019. Effect of chebulagic acid on apoptotic regulators in prostate cancer cell line-PC-3. *Drug Invention Today*, 12. 281-285.

Rahman, M.M., Dhar, P.S., Anika, F., Ahmed, L., Islam, M.R., Sultana, N.A., Cavalu, S., Pop, O. and Rauf, A. 2022. Exploring the plant-derived bioactive substances as antidiabetic agent: an extensive review. *Biomedicine and Pharmacotherapy*, 152, 113217.

Sabiu, S., Madende, M., Ajao, A.A.N., Ogundeji, O.A., Lekena, N. and Alayande, K.A. 2019. The scope of phytotherapy in southern African antidiabetic healthcare. *Transactions of the Royal Society of South Africa*, 74, 1-18.

Shalaby, N.M., Abd-Alla, H.I., Aly, H.F., Albalawy, M.A., Shaker, K.H., Bouajila, J. 2014. Preliminary *in vitro* and *in vivo* evaluation of antidiabetic activity of *Ducrosia anethifolia* Boiss. and its linear furanocoumarins. *BioMed Research International*, 2014, 480545.

Sharma, P., Sharma, K. and Nandave, M. 2023. Computational approaches in drug discovery and design. *Computational Approaches in Drug Discovery, Development and Systems Pharmacology*, 2023, 53-93.

Sifunda, S., Mbewu, A.D., Mabaso, M., Manyaapelo, T., Sewpaul, R., Morgan, J.W., Harriman, N.W., Williams, D.R. and Reddy, S.P. (2023). Prevalence and psychosocial correlates of diabetes mellitus in South Africa: results from the South African National Health and Nutrition Examination Survey (SANHANES-1). *International Journal of Environmental Research and Public Health*, 20, 5798.

Singh, J., Rasane, P., Nanda, V. and Kaur, S. 2022. Bioactive compounds of corn silk and their role in management of glycaemic response. *Journal of Food Science and Technology*, 60, 1695-1710.

Sheng, L., Chen, Q., Di, L. and Li, N. 2021. Evaluation of anti-diabetic potential of corn silk in high-fat diet/streptozotocin-induced type 2 diabetes mice model. *Endocrine, Metabolic and Immune Disorders-Drug Targets (Formerly Current Drug Targets-Immune, Endocrine and Metabolic Disorders)*, 21, 131-138.

Sukhikh, S., Babich, O., Prosekov, A., Kalashnikova, O., Noskova, S., Bakhtiyarova, A., Krol, O., Tsvetkova, E. and Ivanova, S. 2023. Antidiabetic properties of plant secondary metabolites. metabolites, *Metabolites*, 13, 513.

Statistics South Africa. 2024. Poverty trends in South Africa: An examination of absolute poverty between 2006 and 2024. Statistics South Africa, Pretoria. Retrieved from: https://www.statssa.gov.za/publications/P03101/P031012024.pdf, accessed 16/11/2024.

Thoudam, B., Kirithika, T., Ramya, J. and Usha, K. 2011. Phytochemical constituents and antioxidant activity of various extracts of corn silk (*Zea mays* L). *Research Journal of Pharmaceutical, Biological and Chemical Sciences*, 2, 986-993.

Wang, K.J. and Zhao, J.L. 2019. Corn silk (*Zea mays* L.), a source of natural antioxidants withα-amylase, α-glucosidase, advanced glycation and diabetic nephropathy inhibitory activities. *Biomedicine and Pharmacotherap*y, 110, 510-517.

Wang, J., Wu, T., Fang, L., Liu, C., Liu, X., Li, H., Shi, J., Li, M. and Min, W. 2020. Anti-diabetic effect by walnut (*Juglans mandshurica* Maxim.)-derived peptide LPLLR through inhibiting α-glucosidase and α-amylase, and alleviating insulin resistance of hepatic HepG2 cells. *Journal of Functional Foods*, *69*, 103944.

Wang, Z. and Gao, H. 2022. Computer-aided drug design combined network pharmacology to explore anti-SARS-CoV-2 or anti-inflammatory targets and mechanisms of Qingfei Paidu Decoction for COVID-19. *Frontiers in Immunology*, 13, 1015271.

Venkateswaran, M., Jayabal, S., Hemaiswarya, S., Murugesan, S., Enkateswara, S., Doble, M.. Periyasamy, S. 2021. Polyphenol-rich Indian ginger cultivars ameliorate GLUT4 activity in C2C12 cells, inhibit diabetes-related enzymes and LPS-induced inflammation: an *in vitro* study. *Journal of Food Biochemistry*, 45, 13600.

Xiao, E., Luo, L. 2018. Alternative therapies for diabetes: a comparison of western and traditional Chinese medicine (TCM) approaches. *Current Diabetes Reviews*, 14, 487-496.

Xin, W.A.N.G., Zi-Yi, W.A.N.G., Zheng, J.H. and Shao, L.I. 2021. TCM network pharmacology: a new trend towards combining computational, experimental and clinical approaches. *Chinese Journal of Natural Medicines*, 19, 1-11.

Yagasaki, K. and Muller, C.J. 2022. The effect of phytochemicals and food bioactive compounds on diabetes. *International Journal of Molecular Sciences*, 23, 7765.

Yao, Y., Chen, Y., Chen, H., Pan, X., Li, X., Liu, W., Bahetjan, Y., Lu, B., Pang, K., Yang, X. and Pang, Z. 2024. Black mulberry extract inhibits hepatic adipogenesis through AMPK/mTOR signaling pathway in T2DM mice. *Journal of Ethnopharmacology*, 319, 117216.

Yarahmadi, A., Sarabi, M.M., Sayahi, A. and Zal, F. 2021. Protective effects of quercetin against hyperglycemia-induced oxidative stress in hepatic HepG2 cell line. *Avicenna Journal of Phytomedicine*, 11, 269-280.

Zhang, Y., Wu, L., Ma, Z., Cheng, J. and Liu, J. 2015. Anti-diabetic, anti-oxidant and anti-hyperlipidemic activities of flavonoids from corn silk on STZ-induced diabetic mice. *Molecules*, 21, 7.

Zhao, W., Yin, Y., Yu, Z., Liu, J. and Chen, F. 2012. Comparison of anti-diabetic effects of polysaccharides from corn silk on normal and hyperglycemia rats. *International Journal of Biological Macromolecules*, 50, 1133-1137.

Chapter two
Literature review

Chapter two

Literature review

1. Introduction

Diabetes mellitus (DM), a chronic metabolic disease resulting from abnormal glucose metabolism, is responsible for significant morbidities, mortalities and economic expenditures worldwide (Pheiffer *et al*., 2018). In 2021, approximately 537 million adults (between 20-79 years old) were living with DM globally, and this number is expected to rise to 783 million by 2045 if no practical solution is provided (Yagasaki *et al*., 2022). The prevalence of DM in South Africa has surged significantly, nearly tripling from 4.5% in 2010 to 12.7% in 2019 (Grundlingh *et al*., 2022). An estimated 52.4% of the 4.58 million individuals aged 20 to 79 years old with DM in South Africa in 2019 were undiagnosed (Grundlingh *et al*., 2022). The alarming rise in the prevalence of DM in South Africa is a cause for concern (Khan *et al*., 2020), particularly considering that DM is the primary natural cause of death in women and the second-highest cause of death in the entire South African population (Sifunda *et al*., 2023). Comprising of approximately 90% of DM cases, type 2 diabetes mellitus (T2DM) is the most widespread form of DM (Lankatillake *et al*., 2019) and sadly if not properly treated, can result into a number of significant complications such as renal disease, damage to the eyes, cardiovascular disease, heart attacks, strokes, heightened risks of bone fractures, nerve damage, skin conditions, complications related to the feet (ulcers, loss of sensation, amputation), increased risk of Alzheimer's disease, and hearing impairment (Xiao *et al*., 2019; Yagasaki *et al.*, 2022).

Lifestyle modifications, such as a healthy diet, regular physical exercise, weight management therapy, constant blood sugar monitoring and regular healthcare visits to monitor overall health and prevent the occurrence of complications can be used for the effective management of T2DM (Dludla *et al*., 2020). However, the long-term application and sustainability of these approaches are usually not feasible for several patients (Lankatillake *et al*., 2019), who therefore become reliant on the use of synthetic medications to uphold glycemic control (Sabiu *et al*., 2019). However, the drawbacks associated with conventional synthetic drugs in the management of T2DM are significant. These include the need for long-term regimens, high costs, limited accessibility, lower therapeutic efficacy, individual variability, poor drug solubility and permeability, lack of target specificity, and low potency (Padhi *et al.,* 2020). In addition, prolonged use of these medications can lead to drug resistance and a range of unwanted side effects, such as weight

fluctuations, nausea, diarrhea, hypoglycemia, liver and kidney failure, cardiovascular complications, and lactic acidosis (Michaelidou *et al*., 2023; Yao *et al*., 2024). As a result, there is growing interest in exploring alternative or complementary approaches to synthetic medications, focusing on anti-hyperglycemic agents from natural sources with promising antidiabetic potential (Padhi *et al*., 2020).

When searching for these alternative agents, it's important to recognize the role plants play in treating several diseases and illnesses including T2DM (Lankatillake *et al*., 2019). Natural products, including plants, herbs, and organic materials (Rahman *et al*., 2022), offer ample reservoirs of non-synthetic anti-hyperglycemic compounds that exhibit promising antidiabetic properties. These natural compounds can help regulate blood glucose levels, mitigate the effects of side effects, and deter secondary complications associated with T2DM (Xiao *et al*., 2018; Sukhikh *et al*., 2023). The ethnopharmacological knowledge available on natural products in traditional African medicine systems serves as a means to uncover and develop novel antidiabetic drug candidates is gaining traction in Africa (Mohammed *et al*., 2022), which is fueled by the recognized high nutritional and therapeutic worth of native African plants (Hostettman *et al*., 2000). Although there has been increasing interest in the therapeutic properties of South African flora, many plants or plant materials with pharmacological potential have been overlooked or underutilized when searching for novel therapeutic agents (Sabiu *et al*., 2016). An example of an underutilized plant material in South Africa is corn silk (CS), an abundant waste product discarded following corn cultivation, which has been traditionally used for the treatment of many diseases and illness (Sabiu *et al*., 2019). Several studies report the therapeutic properties of CS including antioxidant, anti-inflammatory, anti-hypertensive, anti-cancer, anti-microbial and antidiabetic (Hasanudin *et al*., 2012; Chen *et al*., 2013; Žilić *et al.,* 2016; Chaiittianana *et al*., 2017; Wang *et al*., 2019; Shalihah *et al*., 2020; Chaudhary *et al*., 2022). In this review, an overview of DM is covered, with a particular focus on T2DM, its associated complications, and both conventional and non-conventional T2DM therapies, including the utilization of the waste material CS as an antidiabetic agent. The nutritional, phytochemical, and biological properties of CS are thoroughly examined, underscoring the significance of this waste material as a pharmacological asset, particularly in combating T2DM. This comprehensive review is essential for evaluating CS as a potential therapeutic candidate against T2DM and for advocating the exploration of novel therapies as viable treatment options for T2DM, complementing existing conventional treatment modalities. It is

believed that this will contribute significantly to the advancement of novel antidiabetic agents, which is vital in the fight against the ever-increasing prevalence of T2DM and will contribute towards the improvement of T2DM management systems.

2. Methodology for the review

Information was gathered from published journals, books, reports from national, regional and international institutions, conference proceedings and other intellectual resources. Keywords such as “diabetes mellitus”, “classifications of diabetes mellitus”, “prevalence of diabetes mellitus”, “type 2 diabetes mellitus”, “type 2 diabetes mellitus in South Africa”, “complications of type 2 diabetes mellitus”, “type 2 diabetes mellitus therapy”, “conventional treatment for type 2 diabetes mellitus”, “antidiabetic plants”, “corn silk”, “corn silk in healthcare”, “pharmacological properties of corn silk”, “ antidiabetic compounds in corn silk” were used to retrieved information from online databases such as Google, Google Scholar, PubChem, Elsevier, Consensus and Science Direct.

3. Review of diabetes mellitus

3.1.Brief history of diabetes mellitus

The earliest observations of clinical features resembling those of DM such as weight loss and polyuria, date back over 3000 years to ancient Egyptian records wherein concoctions of bowes, wheat, and earth were recommended by the Egyptians to alleviate the symptoms (Ahmad, 2002). The association between polyuria and sweet tasting urine was documented in Indian literature between the 5th and 6th centuries AD by Sushruta (Peumery, 1987). Araetus of Cappadocia, Greece (81 AD – 133 AD), was the first to identify excessive thirst and abnormal urine production as symptoms of a condition he termed polyuria, which aligns with modern-day symptoms of DM (Kaul *et al*., 2012). Ancient Chinese medical texts, around the years 160–219, described polyuria, polydipsia, and weight loss as indicative of a specific (but unclassified) disease. Additionally, in the 7th century AD, a disorder called ‘Hsiao kho ping’ was characterized by symptoms resembling those of DM, including sweet-tasting urine and intense thirst (Karamanou *et al*., 2016). From the 8th century onwards, physicians noted the propensity of diabetic patients to develop skin infections, ulcers, furuncles, and visual impairments (Karamanou *et al*., 2016). The modern terminology of diabetes mellitus emerged in 1675 when Thomas Willis of Britain introduced the term "mellitus" (Latin for honey) to describe the condition due to the presence of excess sugar in the urine and blood of afflicted patients (Ahmad, 2002). This

term continues to serve as a hallmark of typical diabetic symptoms to this day (Kaul *et al*., 2012). Two significant milestones in understanding the pathogenesis of DM occurred in medical history: firstly, the application of chemistry for diagnostic purposes in the 18th century, and secondly, the pioneering work of Claude Bernard (1813-1878) and Charles-Édouard Brown-Séquard (1817-1895), which laid the foundation for the emergence of endocrinology as a medical discipline (McGrew, 1985). In the 19th century, Oskar Minkowski and Joseph von Mering played pivotal roles in the discovery of the relationship between the pancreas and diabetes, particularly in understanding the role of the pancreas in glucose metabolism. A major collaborative action that took place in the early 20th century between Frederick Banting, Charles Best, James Bertram Collip and John Macleod led to the discovery of insulin, a hormone crucial for regulating blood sugar levels in the body (Karamanou *et al*., 2016). A summarized timeline highlighting major contributions to the history of DM is depicted in Figure 1.

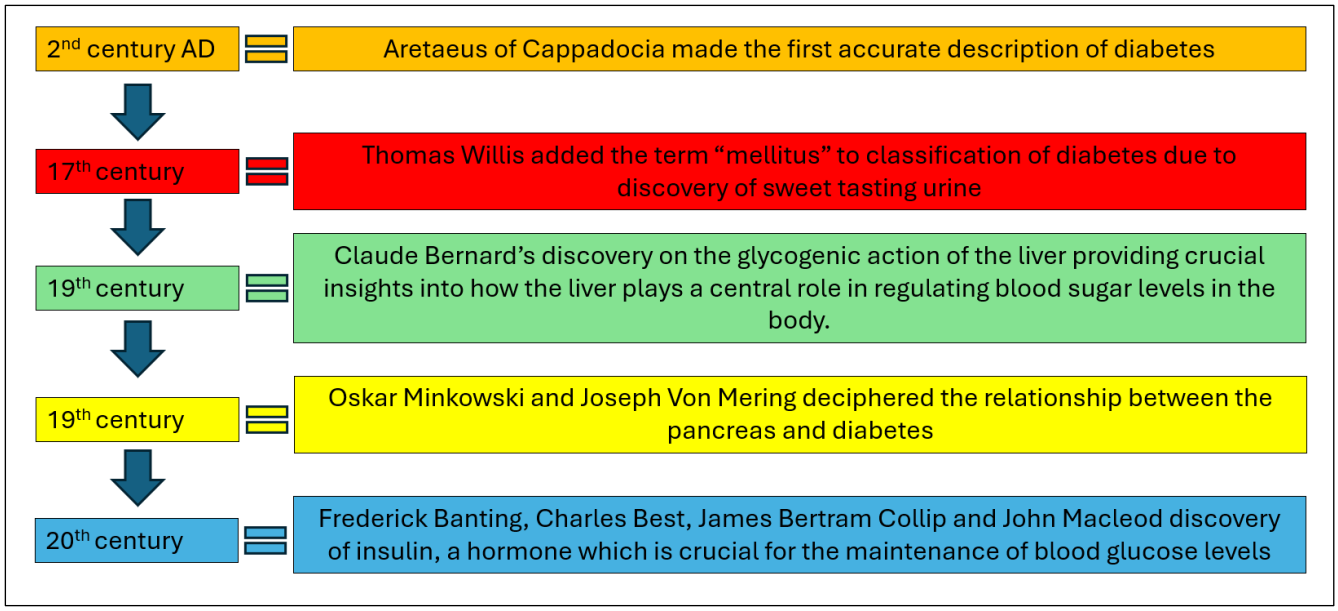

Figure 1: Major contributions made in the history of diabetes mellitus

3.2.Overview and prevalence of diabetes mellitus

Several systems and pathways in the human body function synergistically to bring about and maintain a healthy physiological state, however, an aberration to the stable state can result in dire consequences to the body, including injury (Kaul *et al.*, 2012). Diabetes mellitus (DM), regarded as the epidemic of the century (Kharroubi *et al.*, 2015), is a group of chronic and complex metabolic diseases characterized by impaired blood glucose control

due to defective insulin production and/or action resulting in dysfunctional glucose metabolism (Patel *et al*., 2012; Yagasaki *et al.*, 2022). The emergence of DM as a global epidemic is closely correlated to the onset of industrialization worldwide as well as the staggering rise in the prevalence of obesity (Kaul *et al.*, 2012)**.** According to the International Diabetes Federation (IDF), approximately 537 million people have DM in the world, with around 24 million adults (aged 20-79 years) affected in Africa alone (IDF, 2023). Interestingly, out of the 24 million African adults with DM, 13 million are undiagnosed (Mthembu *et al*., 2022). Projections suggest a staggering 134% increase in DM prevalence across the African continent by 2045, making it the region with the highest percentage increase globally (IDF, 2021). In 2021, the IDF reported that 416,163 deaths of individuals aged 20-79 years old in Africa were attributed to DM (IDF Diabetes Atlas, 2021). In South Africa, a country where roughly 55.5% of the population lives in poverty (Sulla., 2020), an estimated 4,234,000 adults are reported to have DM, leading to significant social, health, and economic burdens (IDF, 2023). The surge in the prevalence of DM in South Africa is driven by various factors including an aging population, economic transition, urbanization, genetic predisposition, lifestyle choices (such as poor diet, sedentary behavior, and obesity), insulin resistance, advancing age, specific ethnicities, pregnancy, and other health-related condition (hormonal disorders) (Pheiffer *et al*., 2017; Yagasaki *et al*., 2022). For the early detection and treatment of DM, identifying the occurrence of symptoms associated with the disease is crucial (McAulay *et al*., 2001). The most commonly observed symptoms associated with DM include polyuria, polydipsia (increased thirst), polyphagia (increased hunger), unexplained weight loss, fatigue, blurry vision, slow wound healing, frequent urinary and/or genital infections, frequent skin infections (cellulitis, styes, folliculitis, candidiasis and skin ulcers), neuropathy, increased incidence of foot ulcers and darkened skin patches (Ramachandran, 2014; Cloete, 2021). The symptoms experienced by individuals with DM vary based on the stage of the disease, the type of DM, and the overall health status of the patient (McAulay *et al*., 2001). Recognizing the specific type of DM is essential for effectively managing the condition, preventing complications, and enhancing long-term health outcomes (Kharroubi *et al*., 2015).

The classification of DM is important; allowing for proper treatment, it is however a difficult task because many patients do not easily fit into a single class especially younger adults (Kharroubi *et al*., 2015). In 1997, the American Diabetes Association proposed three major types of DM: type 1 diabetes mellitus (T1DM), type 2 diabetes mellitus (T2DM) and gestational diabetes mellitus (GDM) (American Diabetes Association, 2014), each distinguished by unique characteristics and underlying causes as discussed further (Surya *et al*., 2023).

3.3.Types of diabetes mellitus

3.3.1. Gestational diabetes mellitus

Gestational diabetes mellitus (GDM) is a type of DM that develops during pregnancy, typically during the second or third trimester, and usually resolves after childbirth (McIntyre *et al*., 2019). Gestational diabetes mellitus (GDM) is characterized by elevated blood glucose levels, a condition known as hyperglycemia, which occurs due to hormonal fluctuations and heightened insulin demands associated with pregnancy (Glovaci*e et al*., 2019). Woman suffering from GDM have reduced insulin response to nutrients resulting in hyperglycemia in comparison to woman who do not have GDM (Petry *et al*., 2023). Additionally, woman who previously suffered with GDM reported a significant defect in pancreatic β-cell function in comparison to woman with normal pregnancies (Kautzky-Willer *et al*., 1997). Several risk factors contribute to the development of GDM, including being overweight or obese, environmental factors (overeating and a sedentary lifestyle), family history, age, and previous history of GDM in prior pregnancies, along with specific ethnic backgrounds (Turgut *et al*., 2022). Certain ethnic groups, particularly women from South Asia and Southeast Asia, have historically exhibited a higher prevalence of GDM compared to Caucasian, African-American, and Hispanic communities (Schiavonem *et al*., 2016). In 2021, the IDF reported that approximately 1 in every 8 live births are affected by GDM (IDF, 2021). If left uncontrolled, GDM not only increases the risk of maternal and fetal complications during pregnancy but also raises the risk of long-term complications for both mother and child (Schneiderman, 2010). Gestational diabetes mellitus (GDM) has been linked to an increased risk of pre-eclampsia, cardiovascular disease, and T2DM in affected mothers (Chiefari *et al*., 2017), while the fetus may face obstetrical and neonatal complications such as pre-term delivery, polyhydramnios, macrosomia, shoulder dystocia,

neonatal respiratory distress syndrome, fetal hypoglycemia, and hyperbilirubinemia (Lende *et al*., 2020). A long-term follow-up study by Kim *et al*. (2002) revealed that most, but not all, woman with GDM progress to DM following pregnancy (Kim *et al*., 2002). Long-term complications, such as high blood pressure, obesity, insulin resistance, impaired glucose tolerance and dyslipidemia have been reported in offsprings of GDM patients (Chiefari *et al*., 2017). Antepartum care for GDM involves the use of standard antidiabetic treatments such as nutritional changes, regular healthcare visits, regular exercise, constant blood glucose monitoring, exogenous insulin therapy and administration of selected oral antidiabetic agents, all of which aim to normalized pre- and postprandial glucose levels (Buchanan *et al*., 2005; CDC, 2020). Post-pregnancy care in patients with GDM includes minimizing the risk of DM and detecting and treating DM if it were to occur (Buchanan *et al*., 2005).

3.3.2. Type 1 diabetes mellitus

Type 1 diabetes mellitus (T1DM) is a chronic heterogenous disorder characterized by auto-immune destruction of insulin-producing pancreatic β-cells, culminating in an absolute deficiency of insulin, leading in elevated blood glucose levels (Padhi *et al*., 2020; Parviainen *et al*., 2022). While T1DM is less prevalent compared to T2DM, it accounts for approximately 5-10% of DM diagnoses (Glovaci*e et al*., 2019) and still impacts a considerable number of individuals globally who require lifelong management (Patterson *et al*., 2019). According to IDF, the number of youth (0-20 years old) diagnosed with type 1 DM worldwide in 2022 was 8.75 million people (IDF, 2022). Several factors, including genetic and environmental, contribute to the prevalence of T1DM, including genetic predisposition, viral factors such as congenital rubella and infection with enterovirus, rotavirus, herpes virus, cytomegalovirus and endogenous retrovirus, low vitamin D levels, prenatal exposure to pollutants, early infant nutrition and obesity (Stene *et al*., 2010; Kharroubi *et al*., 2015). Type 1 diabetes mellitus (T1DM) tends to develop suddenly and symptoms such as frequent urination, excessive thirst, inability to control urination, unexplained weight loss, increased hunger, fatigue, slow-healing wounds, blurred vision, recurrent infections as well as severe dehydration and diabetic ketoacidosis are experienced by children and adolescents (Parviainen *et al*., 2022). In comparison to adults, children and adolescents develop more severe symptoms and are often more likely to develop other autoimmune disorders such as Graves' disease, Hashimoto's thyroiditis, Addison's disease, vitiligo, celiac sprue, autoimmune hepatitis, myasthenia gravis, and pernicious anemia

(Kharroubi *et al*., 2015). Additionally, the incidence of T1DM cases continues to increase worldwide which results in higher prevalence of serious short-term and long-term complications, such as diabetic retinopathy, macular oedema, diabetic nephropathy, microalbuminuria, diabetic neuropathy (carpal tunnel syndrome, peroneal nerve and third cranial nerve palsies, proximal nerve conditions), foot complications (foot ulcers and foot infections), hypertension, lactic acidosis, metabolic acidosis, hyperketonemia, anxiety, depression, and cardiovascular disease (Daneman *et al*., 2006). The overall goals for the management of T1DM includes setting of realistic goals which consider factors such as patient's age, developmental status, family involvement, social and economic situation and medical history, near normalization of blood glucose levels and hemoglobin A1C measurements, prevention of diabetic ketoacidosis, avoidance of severe hypoglycemia, maintenance of normal growth, development and maturation of children, provision of nutritional and psychological support, prevention of microvascular and macrovascular complications (Haller *et al*., 2005). Along with continuous glucose monitoring, patients with T1DM require lifelong insulin therapy in the form of rapid, short, intermediate and long-acting insulin preparations, making the disease easier to manage and preventing the risk of complications (Khardori *et al*., 2023).

3.3.3. Type 2 diabetes mellitus

Type 2 diabetes mellitus (T2DM) is a metabolic disorder characterized by the body's resistance to insulin and/or insufficient insulin production, causing an accumulation of glucose in the body and giving rise to significant healthcare complications (Lankatillake *et al*., 2019). Alongside insulin resistance and defective insulin synthesis in the pancreas, a decreased metabolic response to insulin in several tissues, including adipose tissue, the liver and skeletal muscle, is observed in T2DM (Daryabor *et al*., 2020). Among the types of DM, T2DM distinguishes itself as the most widespread form, accounting for approximately 90-95% of all DM cases (Galicia-Garcia *et al*., 2020). Globally, most individuals with T2DM fall within the age bracket of 40-59 years old (Grundlingh *et al*., 2022), and there is a higher prevalence of T2DM reported in males compared to females (Kharroubi *et al*., 2015). Approximately 80% of global T2DM diagnoses are in low and middle-income countries (Kharroubi *et al*., 2015), particularly in African countries such as South Africa (Sabiu *et al*., 2019), where the epidemic is occurring at an alarming rate (Khan *et al*., 2020). Interestingly, South Africa holds the top position among all African countries in terms of T2DM prevalence (Kharroubi *et al*., 2015), with an observed 22% prevalence of T2DM in

2022 (Grundlingh *et al*., 2022). A staggering 67% of South Africans were found to be pre-diabetic without previously being tested, thus a large proportion of South African population remain undiagnosed (Grundlingh *et al*., 2022). The increased incidence in the number of T2DM cases is influenced by many factors, including a genetic predisposition, rapid urbanization, a sedentary lifestyle, an unhealthy diet, obesity and body fat composition, insulin resistance, age, and other medical conditions like hypertension, dyslipidaemia, and hormonal disorders (Chandler-Laney *et al*., 2011; Yagasaki *et al*., 2022). The pathogenesis of T2DM is due to insulin resistance (inability to use insulin produced by the pancreas) and/or defective insulin production in the body resulting in abnormally high and persistent plasma glucose levels, a condition known as hyperglycaemia (Galicia-Garcia *et al*., 2020) (Figure 2). While symptoms of T2DM is not limited to increased thirst, frequent urination, increased hunger, unintended weight loss, fatigue, blurred vision, slow-healing sores, frequent infections, numbness or tingling in the hands or feet and areas of darkened skin (armpits or neck), if poorly managed or left untreated T2DM cases can lead to a range of serious complications that negatively impact diverse areas of the body and in severe cases, mortality (Lankatillake *et al*., 2019).

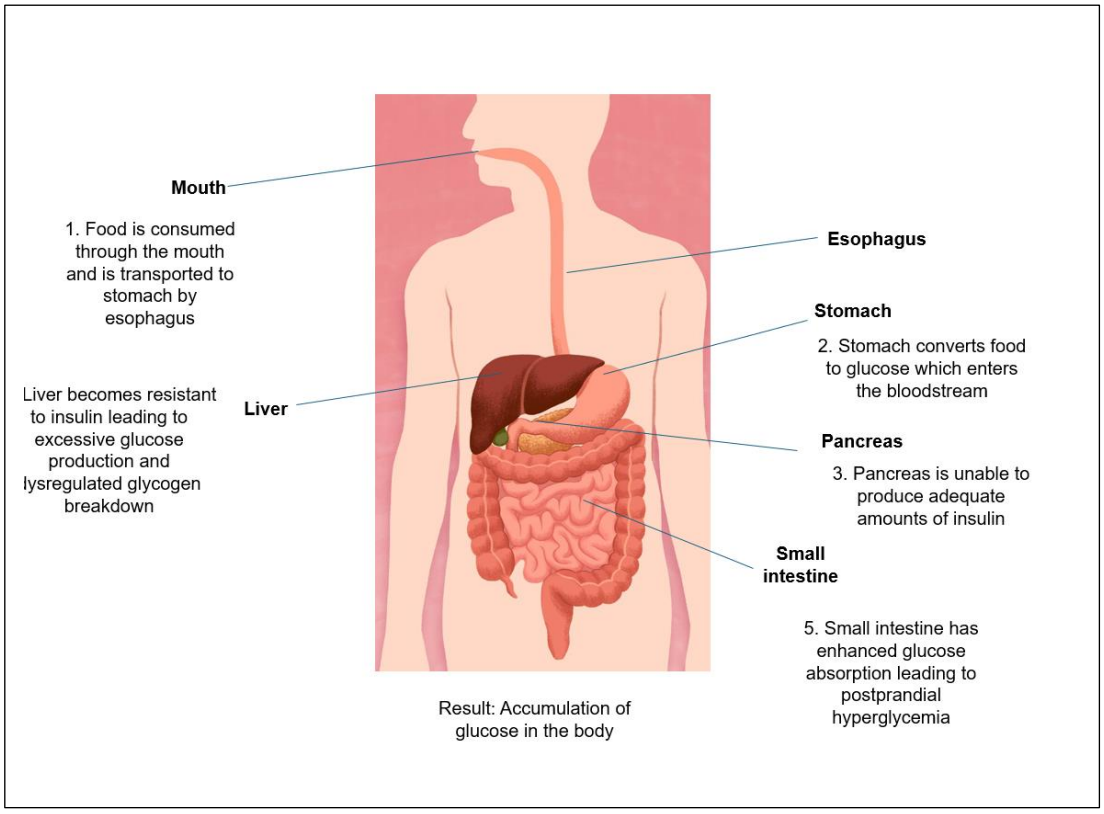

Figure 2: The pathogenesis of type 2 diabetes mellitus which affects diverse areas of the human body. Under T2DM conditions, the pancreas is unable to produce enough insulin and the liver

becomes resistant to insulin produced. Therefore, large amounts of glucose enter the bloodstream, resulting in severe secondary complications which affect diverse areas of the human body

3.3.3.1. Secondary complications associated with type 2 diabetes mellitus

The inflammatory state resulting from chronic hyperglycemia can affect every organ system in the human body including the circulatory system, pancreas, liver, gastrointestinal tract and skeletal muscle, although the degree of organ damage primarily hinges on the severity and duration of the disease (Guimaraes *et al*., 2014; Daryabor *et al*., 2020). Delayed and ineffective management of T2DM results in the occurrence of severe secondary complications (Lankatillake *et al*., 2019). These secondary complications include cardiovascular complications (including coronary heart disease, myocardial infarction, hypertension, atherosclerosis and stroke), diabetic neuropathy (numbness, tingling and loss of sensation in extremities), nephropathy (chronic kidney disease and kidney failure), diabetic retinopathy (blurred vision and blindness), liver cirrhosis, heightened susceptibility to infections (urinary tract infections, skin infections and frequent yeast infections), slow wound healing, sexual dysfunction and mental health-associated problems (depression and heightened anxiety) (Lankatillake *et al*., 2019; Galicia-Garcia *et al*., 2020). Therefore, to minimize the risk of secondary complications as well as prevent premature mortality, effective management of this disease is crucial (Lankatillake *et al*., 2019).

3.4.Conventional treatments for type 2 diabetes mellitus

The main objective of the various treatment options for T2DM is to address the chronic hyperglycaemia, mitigate the risk of associated complications, and above all enhance the overall health and well-being of patients (Paddy *et al*., 2014). Non-pharmacological T2DM treatment is achieved through various components including lifestyle modifications like adopting a healthy diet, engaging in regular physical activity, weight management therapy, receiving education and support (therapy visits) and attending regular healthcare visits to monitor overall health and prevent the occurrence of secondary complications (Lankatillake *et al*., 2019; Dludla *et al*., 2020). However, the long-term application and sustainability of these approaches are usually not feasible for several patients (Lankatillake *et al*., 2019). Consequently, the use of synthetic medications become necessary for the alleviation of hypoglycaemia (Paddy *et al*., 2014; Sabiu *et al*., 2019). Biguanides (metformin), sulfonylureas, thiazolidinediones, meglitinides, dipeptidyl peptidase-4 (DPP-

4) inhibitors, sodium-glucose co-transporter 2 (SGLT-2) inhibitors, glucagon-like peptide-1 (GLP-1) receptor agonists and injectable insulin are among the varying classes of orthodox treatment options employed in the management of T2DM (Paddy *et al*., 2014; Michaelidou *et al*., 2023). Each of these medications exerts its effects through distinct mechanism of action as illustrated in Figure 3 (Kokil *et al*., 2015; Tyagi *et al*., 2021; Michaelidou *et al*., 2023).

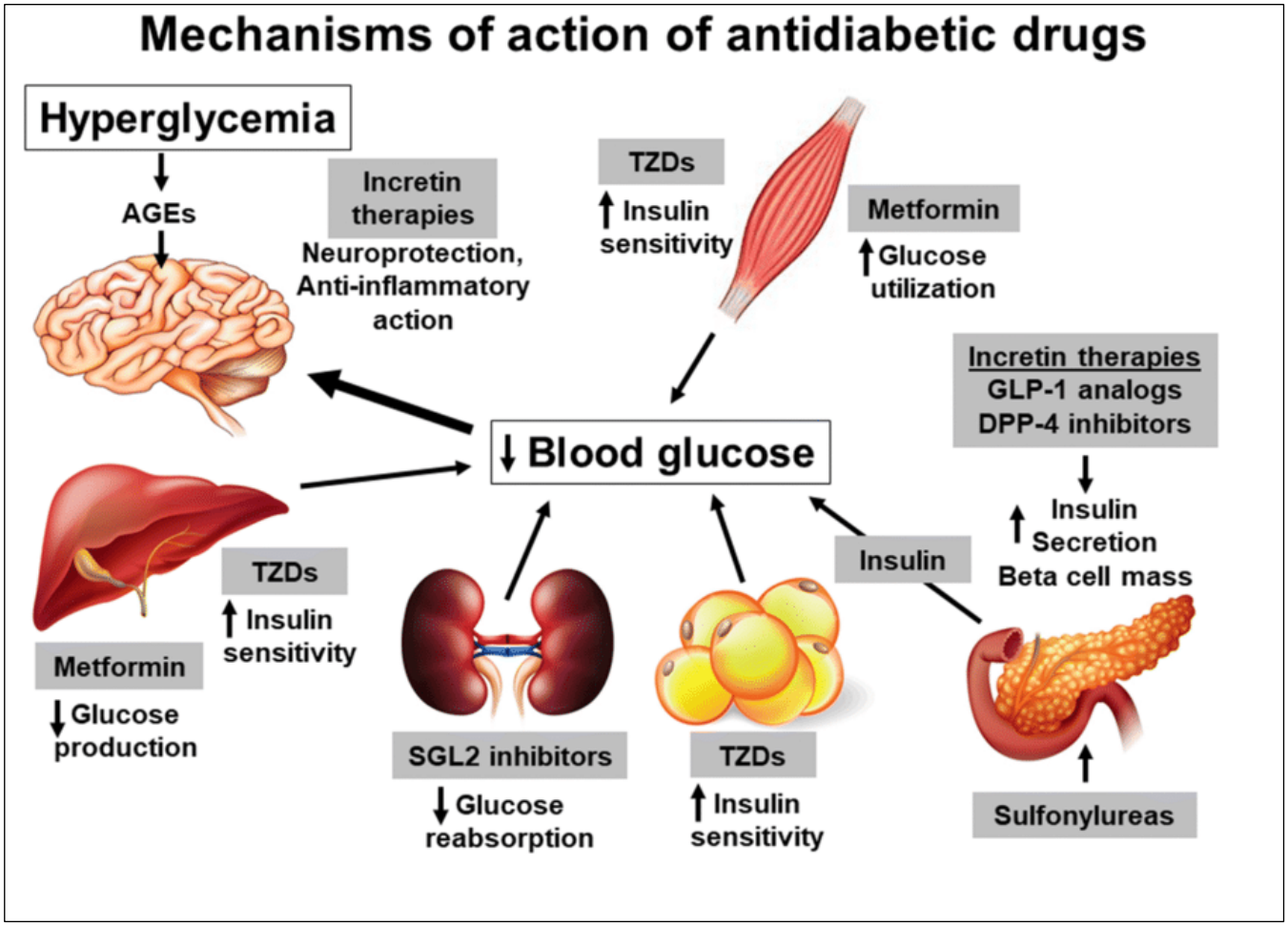

Figure 3: The mechanism of action of oral hypoglycaemic agents. Incretin therapies, such as glucagon-like peptide-1 (GLP-1) receptor agonists and dipeptidyl peptidase-4 (DPP-4) inhibitors affect the gastrointestinal system and target the incretin system, including hormones releases from the gut in response to food intake, resulting in an increase in insulin secretion and β-cell mass. Additionally, incretin therapies have neuroprotective and anti-inflammatory action. TZDs (thiazolidinediones) improve insulin sensitivity in adipose tissue, muscle, liver, pancreas and the cardiovascular system. Metformin reduces the production of glucose in the liver and increase the utilization of glucose in the body's muscle muscle. SGL2 (sodium-glucose co-transporter 2 inhibitors) decrease the absorption of glucose in the kidneys. Insulin and sulfonylureas exert their action primarily in the pancreas and result in the stimulation of insulin secretion and increase in β-cell mass (Tyagi *et al*., 2021)

3.4.1. Biguanides

Three potent biguanides, namely phenformin, buformin and metformin, were discovered in the 1950s and have been used for the treatment of T2DM as well as to prevent secondary complications associated with the disease (Meneses *et al*., 2015). However, due to the high risk of lactic acidosis associated with their use, phenformin and buformin are discontinued in many countries, leaving metformin as the primary example of biguanide medication used worldwide (Michaelidou *et al*., 2023). Metformin is commonly prescribed as the initial medication for managing T2DM, particularly in newly diagnosed patients, in conjunction with dietary adjustments and exercise (Sabiu *et al*., 2019). It functions by reducing glucose production in the liver and improving insulin sensitivity in muscle tissues (Paddy *et al*., 2014). Additionally, metformin aids in glucose uptake by cells and may affect gut hormones involved in blood sugar regulation (Paddy *et al*., 2014; Sabiu *et al*., 2019). Combining metformin with lifestyle modifications is acknowledged as a preventive strategy for T2DM in individuals at high risk (Sabiu *et al*., 2019; Michaelidou *et al*., 2023). The adverse reactions associated with the use of metformin include diarrhoea, vomiting, dyspepsia, flatulence, metallic taste, weight loss, lactic acidosis and megaloblastic anaemia (Mane *et al*., 2012). Contraindications implicated in the use of metformin are renal disease, heart failure, hypoxia, acute or chronic metabolic acidosis and active liver disease (Bosenberg *et al*., 2008; Mane *et al*., 2012).

3.4.2. Sulfonylureas

Since their discovery in 1942, sulfonylureas have stood out as the most commonly employed medications in the treatment of patients with T2DM (Sabiu *et al*., 2019). Sulfonylureas lower blood glucose levels by stimulating insulin secretion endogenously, enhancing peripheral insulin receptor sensitivity and reducing glycogenolysis (Moher *et al*., 2018). Initially, sulfonylureas such as tolbutamide, chlorpropamide, acetohexamide, and tolazamide were commonly used for T2DM therapy, but were largely replaced by the newer second-generation sulfonylureas such as gliclazide, glipizide, glibenclamide (glyburide) and the latest addition to the class glimepiride (Meneses *et al*., 2015). While sulfonylureas are generally well tolerated, the incidence of side effects has been reported with its use (Rendell, 2004). The side effects include hypoglycaemia, weight gain, gastrointestinal disturbances (nausea, upset stomach and diarrhoea), skin reactions (rashes, itching, erythema multiforme, exfoliative dermatitis and photosensitivity), allergic

reactions (hives, swelling, breathing difficulties, anaphylaxis), liver dysfunction and cardiovascular complications (Rao *et al*., 2008; Sola *et al*., 2015).

3.4.3. Thiazolidinediones

Glitazones, more commonly known as thiazolidinediones are a class of anti-hyperglycaemic medications that work by activating a nuclear receptor known as peroxisome proliferator-activated receptor-gamma (PPAR-gamma), which plays a role in regulating glucose and lipid metabolism (Sabiu *et al*., 2019). Through PPAR-gamma activation, these medications improve insulin sensitivity in peripheral tissues, including adipose tissue and skeletal muscle (Paddy *et al*., 2014; Sabiu *et al*., 2019). The two main types of thiazolidinediones used in T2DM therapy are pioglitazone and rosiglitazone, which works by increasing insulin sensitivity in muscle and adipose tissues (Lebovitz, 2019). Although periodically used as a monotherapy, thiazolidinediones are more frequently used in combination with other oral antidiabetic agents and/or insulin in patients who are unable to maintain glycaemic control with just one form of medication (Lebovitz, 2019). The adverse reactions associated with thiazolidinedione use include weight gain, oedema, hypoglycaemia, hepatic failure, heart failure, anaemia, increased fluid retention, increased peripheral fractures and bone loss (Bosenberg *et al*., 2008; Lebovitz, 2019).

3.4.4. Meglitinides

In the late 1970s, meglitinides were developed through the addition of a carboxyl (COOH) group to the non-sulfonylurea end of a glibenclamide molecule (Banwari *et al*., 2023). Repaglinide and nateglinide, which are the two commonly known meglitinides, are short-acting hypoglycaemic insulinotropic agents used for treating adults with T2DM (Sabiu *et al*., 2019). This class of drug acts similarly to sulfonylureas by binding to ATP-sensitive potassium channels in pancreatic β-cells which causes calcium ion influx and increased insulin secretion (Timmons *et al*., 2022). One of the significant advantages of using meglitinides as a therapy in T2DM treatment is the fact that the drug is excreted mainly by hepatic clearance making it safe for patients suffering with chronic kidney disease (Ritz *et al*., 2013). Another advantage of meglitinide use is the lack of sulphur in its composition, making it safe for patients with a sulphur allergy (Ray *et al*., 2023). Although effective in managing hyperglycaemia, the most frequent adverse effects associated with its use include hypoglycaemia, weight gain, gastrointestinal disturbances (nausea, upset stomach, diarrhoea), upper respiratory infections, headache, joint or muscle pain, allergic reactions

(hives, itching, swelling and difficulty breathing) and liver dysfunction (Blahova *et al*., 2021).

3.4.5. Dipeptidyl peptidase-4 (DPP-4) inhibitors

Sitagliptin, saxagliptin, linagliptin, alogliptin and vildagliptin form part of a class of prescription anti-hyperglycaemic drugs known as DPP-4 inhibitors that have been approved for use in the treatment of T2DM in adults since 2006 by the Food and Drug Administration and the European Medicine Agency (Kasina *et al*., 2023). Although often available as a single-ingredient product taken once a day following a meal, DPP-4 inhibitors can sometimes be used in combination with metformin (Kasina *et al*., 2023). Dipeptidyl peptidase-4 inhibitors inhibit DPP-4, an ubiquitous enzyme that degrades incretin hormones such as glucagon-like peptide-1 (GLP-1), thus increasing the levels of GLP-1 and glucose-dependent insulinotropic peptide, resulting in the elevation of incretin which facilitates insulin release, decreases glucagon secretion, decelerates gastric emptying, and fosters a sense of satiety (Sabiu *et al*., 2019). Adverse reactions associated with the use of DPP-4 inhibitors include nasopharyngitis, nausea, diarrhoea, vomiting, hypoglycaemia, decreased appetite, weight loss, acute pancreatitis, abdominal pain/discomfort, severe joint pain, muscle weakness, muscle spasms, upper respiratory tract infections, peripheral oedema, headache and dizziness (Gilbert *et al*., 2020).

3.4.6. Sodium-glucose co-transporter 2 inhibitors

Ipragliflozin, dapagliflozin, canagliflozin, empagliflozin, luseogliflozin, and tofogliflozin form part of a class of prescription oral anti-hyperglycaemic agents known as sodium-glucose co-transporter 2 (SGLT-2) inhibitors which are employed in T2DM therapy for adults The drug work by inhibiting the SGLT-2, a transporter responsible for the absorption of glucose in renal tubules (Sabiu *et al*., 2019; Sohail *et al*., 2021). The blocking of SGLT-2 prevents the reabsorption of glucose, leading to increased urinary excretion of glucose and thus lowering blood glucose levels (Paddy *et al*., 2014). The use of SGLT-2 inhibitors, along with diet and exercise, for T2DM patients with chronic kidney disease and/or heart failure is approved by the Food and Drug Association and has been found to reduce the risk of kidney failure and death in people with chronic kidney disease and T2DM (National Kidney Foundation, 2023). Although as an effective anti-hyperglycaemic agent, it does not rule out the development of adverse effects including hypoglycaemia, nausea, abdominal pain, ketonuria, ketonemia, urinary tract infections, mycotic genital infections, diabetic

ketoacidosis, lower limb amputation, low blood pressure and dehydration (Nagahisa *et al*., 2019).

3.4.7. Glucagon-like peptide 1 receptor agonists

Exenatide, liraglutide, dulaglutide and semaglutide form a class of oral and injectable medicines known as glucagon-like peptide 1 (GLP-1) receptor agonists which are used to treat T2DM by mimicking the actions of GLP-1, an incretin hormone naturally released by the intestines in response to food intake (Ahrén, 2011). Glucagon-like peptide-1 (GLP-1) help the body to produce more insulin, thus reduce the amount of glucose produced in the liver, and the rate of digestion of food reducing the amount of glucose absorbed in the blood as well as reduction in appetite (Müller *et al*., 2019). In addition, GLP-1 receptors agonists bind to the GLP-1 receptor stimulating the release of insulin from the pancreatic β-cells, reduce glucagon secretion, slow down gastric emptying, and promote a feeling of fullness (Sabiu *et al*., 2019; Michaelidou *et al*., 2023). There are currently four GLP-1 agonists that are used in T2DM therapy, namely exenatide, liraglutide, dulaglutide and semaglutide (Helmstädter *et al*., 2021). Although, GLP-1 agonists are generally well-tolerated and have a favourable safety profile, however, the incidence of adverse reactions has been reported with its use. These include nausea, vomiting, diarrhoea, constipation, injection-site reactions, antibody formation, increased heart rate, acute pancreatitis, weight loss, gallstone formation (Meier, 2012; Wharton *et al*., 2022).

3.4.8. Insulin therapy

Insulin therapy is one component of a treatment plan commonly used in the management of T2DM when other treatment modalities are insufficient or unlikely to achieve adequate blood sugar control (Paddy *et al*., 2014). Insulin treatment involves administering exogenous insulin (a hormone that ensures that sugar from foods are correctly utilized and stored in the body) via subcutaneous injections or insulin pumps to supplement and/or replace the body's natural insulin production, with the goal of regulating blood glucose levels and preventing and/or minimizing complications (Wallia *et al*., 2014; Sabiu *et al*., 2019). The type of insulin used is dependent on the type of diabetes one suffers from, the blood glucose levels, differences in blood sugar levels during the day and the lifestyle of T2DM patients (American Diabetes Association, 2023). The adverse reactions associated with insulin therapy for the management of T2DM include hypoglycaemia, weight gain, fluid retention, oedema, injection site reactions, lipodystrophy, allergic reactions (skin

rashes, itching and difficulty breathing) and insulin resistance (Mane *et al*., 2012; Sorli *et al*., 2014).

3.5.Challenges of synthetic medications used in type 2 diabetes mellitus therapy

Despite the array of synthetic medications employed in T2DM therapy, it is noteworthy that they do not offer a definitive cure for the disease (Kokil *et al*., 2015). Alternatively, their effects can be regarded as potentially postponing or delaying the onset of secondary complications associated with different degrees of the disease (Lankatillake *et al*., 2019; Sabiu *et al*., 2019). These synthetic medications are not able to consistently achieve satisfactory blood glucose levels in all patients (Paddy *et al*., 2014; Sukhikh *et al*., 2023), and individuals who are able to maintain satisfactory blood glucose levels using synthetic medication may develop secondary symptoms related to T2DM (He *et al*., 2019; Sukhikh *et al*., 2023). The use of these synthetic medications is linked with several drawbacks, including long-term regimens, cost, inaccessibility, lower therapeutic efficacy, differing individual variability among individuals, low drug solubility and permeability, lack of target specificity and low potency (Padhi *et al*., 2020). The prolonged usage of these medications is linked to the occurrence of undesirable side effects in many individuals (Lankatillake *et al*., 2019), as depicted in Figure 4, many of which are concerning as it can affect the overall well-being and quality of life of individuals with T2DM (Lankatillake *et al*., 2019; Yao *et al*., 2024). The limitations of the synthetic medication pose challenges for patients in terms of tolerability and adherence to treatment (He *et al*., 2019; Singh *et al*., 2022b). Consequently, an advent of novel anti-hyperglycaemic agents with promising antidiabetic potentials have been identified as alternatives or complimentary additions to synthetic medications (Padhi *et al*., 2020), many of which have been discovered in products of natural origin like medicinal plants (Salehi *et al*., 2019).

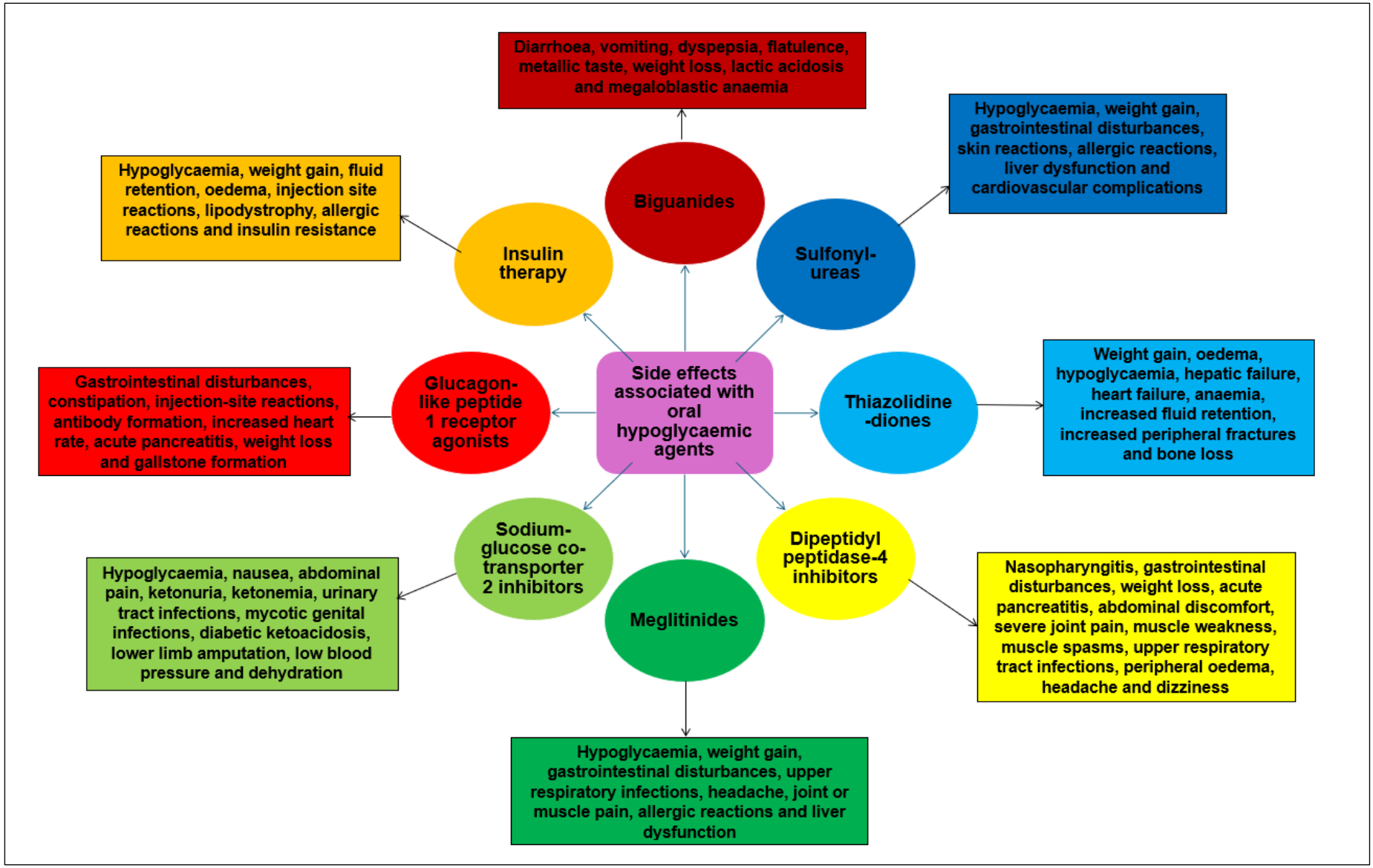

Figure 4: Synthetic oral hypoglycaemic agents and their associated side effects

3.6.Medicinal plants as alternative medicines

Natural products, especially those of plant origin, are abundant sources for drug lead candidates and play a fundamental role in drug discovery and development programs worldwide (Salehi *et al*., 2019). A medicinal plant harbors substances that possess therapeutic and/or medicinal properties (Sofowora *et al*., 2013). Several cultures, including Chinese, Indian, European, African, Korean, Middle Eastern, American (North, South and Central) and Australian, have employed medicinal plants for the treatment and/or alleviation of a variety of health conditions (Van Wyk *et al*., 2018). Employing medicinal plants to treat DM has been highly accepted as a form of medical intervention, mainly due to their efficacy, probable fewer side effects and affordability (Hasani-Ranjbar *et al*., 2008). In developing countries, medicinal plants are an acceptable alternative to the high cost of western medicine (Salehi *et al*., 2019). Through centuries of using medicinal plants to treat diseases and illnesses in traditional medicine system, an extensive repository of information on therapeutic properties of many medicinal plants has been culminated (Rahman *et al*., 2014; Zhang *et al*., 2015). Several attributes place immense value on medicinal plants as cogent sources for the development of effective and culturally relevant antidiabetic agents (Mushtaq *et al*., 2018). Firstly, indigenous communities and traditional healers possessed deep-rooted ethnobotanical knowledge, which provides a deep foundation for identifying plants with potential antidiabetic properties (Rahman *et al*., 2014; Sabiu *et al*., 2019). Secondly, the chemical diversity found in these plants or natural products, encompassing alkaloids, flavonoids, terpenoids, phenolic compounds, etc., containing a wide array of bioactive constituents with likelihood to exhibit promising pharmacological activities (in this case antidiabetic effect) (Rahman *et al*., 2014). Thirdly, plant-based remedies often have a history of safe usage and are perceived as natural and potentially safer alternatives to synthetic drugs (Singh *et al*., 2022a). Fourthly, plants are renewable resources that can be sustainably sourced, making them accessible for research and developmental purposes (Chen *et al*., 2016). Lastly, the cultural acceptance of plant-based remedies in managing diseases particularly T2DM arises from the beliefs and practices of many of these different cultures; fostering increased acceptance and adherence among patients (Sabiu *et al*., 2016; Sabiu *et al*., 2019). The field of ethnopharmacology, which consists of investigating the biological activities of herbal medicines has contributed to the development of several therapeutic agents (Suntar, 2020). Naturally derived therapeutic agents allicin (anti-inflammatory), artemisinin (anti-malarial), berberine (hepatoprotective and antimicrobial), morphine (pain relieving), taxol (anti-tumour), codeine (pain relieving and cough

suppressing), cocaine (pain relieving, mood stimulating, anesthetic inducing), digitoxin (used in heart conditions), quinine (anti-malarial and anti-parasitic), vinblastine (anti-cancer) and vincristine (anti-cancer) (Balunas *et al*., 2005; Shakya, 2016), as well as antidiabetic agent metformin were developed using ethnopharmacological knowledge available on medicinal plants (Mohammed *et al*., 2022). Using the ethnopharmacological knowledge available on natural products in traditional systems of medicine as a tool for the discovery and development of novel antidiabetic drug candidates is becoming increasingly popular in Africa (Mohammed *et al*., 2022), which is attributed to the high nutritional and therapeutic value of native African plants (Hostettman *et al*., 2000).

3.6.1. African medicinal plants

Africa's exceptional plant biodiversity, combined with its rich and dynamic tradition of cultural medicine, provides a promising foundation for discovering and developing novel therapeutic agents. These resources offer immense potential for creating new treatments, drawing from both traditional knowledge and modern scientific research (Mohammed *et al*., 2022; 2023). Several native African flora have a fundamental role in African traditional systems of medicine used for the treatment of DM and its associated complications (Odeyemi *et al*., 2018). In North and West Africa, several plant species including *Gongronema latifolium*, *Momordica charantia*, *Allium cepa*, *Vernonia amygdalina*, *Moringa oleifera, Hyphaene thebaica*, *Balanites aegyptiaca* and *Cymbopogon citratus* in Nigeria (Ugochukwu *et al*, 2002; Abo *et al*., 2008; Gbolade, 2009; Popoola *et al*., 2013; Shinkafi *et al*. 2015; Oguntibeju. 2019), *Zygophyllum coccineum*, *Acacia albida* and *Lupinus albus* in Morocco (Soumyanath; 2005; Chaachouay *et al*., 2019; Mechchate *et al*., 2020), *Allium sativum*, *Aloe sinkatana* and *Guiera senegalensis* in Sudan (Mohammed *et al*., 2022), *Dichrostachys glomerata* and *Allium sativum* in Guinea (Diallo *et al*. 2012), have been used as a traditional medicine for the management of DM, including T2DM (Mohammed *et al*., 2022). Among the plant species in South Africa, *Aloe vera*, *Artemisia afra*, *Brachylaena discolor*, *Brachylaena elliptica, Bulbine frutescens, Carpobrotus edulis*, *Catharanthus roseus*, *Catha edulis*, *Chilianthus olearaceus*, *Chironia baccifera*, *Chironia baccifera*, *Cissampelos capensis*, *Cnemaspis Africana*, *Dicoma anomala*, *Eriocephalus punctulatus, Gnidia deserticola*, Hypoxis *hemerocallidea*, *Laseria frutescens*, *Leonotis Leonurus*, *Momordica foetida*, *Momordica cymbalaria*, *Ornithogalum longibracteatum*, *Ruta graveolens*, *Sclerocarya birrea*, *Tarchonanthus camphoratus*, *Tulbaghia violacea* and *Xysmalobium undulatum* are some of the many plants that are used as traditional

antidiabetic medicine (van de Venter *et al*., 2008; Afolayan *et al*., 2010; van Huyssteen *et al*., 2011; Balogun *et al*., 2016; Davids *et al*., 2016; Oguntibeju, 2019; Sagbo *et al*., 2022). Although, South Africa has a wide array of medicinal plants that are used for the treatment of DM, a scientific understanding behind these plants' reported bioactivities is still largely unexplored (van de Venter *et al*., 2008). For example, a study performed in the Eastern Cape of South Africa identified 48 plant species as widely used antidiabetic therapeutic agents, but knowledge on the mechanism of action of those plant species was lacking (Sagbo *et al*., 2022). Despite the huge potential the African continent possesses in the drug discovery field, only a limited number of drugs have been commercialized globally (Atawodi, 2005). Although, there has been an increasing number of publications in the scientific literature focusing on assessing the effectiveness of medicinal plants from South Africa, which are thought to play a significant role in maintaining health and introducing new treatments, many plants or plant materials with pharmacological potential have been overlooked or underutilized (Sabiu *et al.,* 2016). An example of an underutilized plant material in South Africa is corn silk (CS), an abundant waste product with promising therapeutic properties (Hasanudin *et al*., 2012). *Zea mays*, commonly known as corn plays a crucial role in food security in many African countries, including South Africa where it is one of the top five cereal crops produced each year, in addition to sorghum, rice, wheat, and millet (Kamer, 2022; Shahbandeh, 2023). Following the proliferation of the edible corn kernels, an excessive amount of waste biomass is generated in the corn cultivation industry in South Africa, forfeiting huge potentials for the generation of valuable products (Mohlala *et al*., 2016).

3.7.Corn silk: a waste product with therapeutic potential

3.7.1. Descriptive and physiological characteristics of corn silk

The Food and Agriculture Organization (FAO) of the United Nations estimates that approximately 2.819 million tonnes of cereal crops were produced globally from January to July 2023 (FAO, 2023). Among the different cereal crops cultivated in Africa, corn is notably one of the most extensivelt grown (Shahbandeh, 2023). While the edible corn kernels are the primary product of corn cultivation, other parts of the plant, such as the husk and silk are typically considered by-products and often discarded as agricultural waste (Zhang *et al*., 2015). Corn silk (CS) are tuffs if hair-like strands that form part of the elongated stigmas from the female flower of the maize plant as shown in Figure 5 (Sabiu *et al*., 2015). Corn silk (CS) serves as fine hair-like strands which trap pollen for pollination,

allowing for the production of corn kernels (Hasanudin *et al*., 2012; Singh *et al.,* 2022a). The coloration of CS varies according to the developmental stage of the plant, initially displaying lighter green hues and transitioning to shades of yellow, red and light brown as it matures (Sabiu *et al*., 2015). The growth of corn can be categorized into two main phases: the vegetative stage and the reproductive stage. During the vegetative stage, which includes germination, leaf emergence, node development, root growth, stem elongation, and tasseling, the plant focuses on establishing its structure and foliage (Figure 6a). Conversely, the reproductive stage involves silking, blistering, milking, doughing, and denting phases, where the plant transitions to producing and maturing kernels (Figure 6b). Ultimately, the growth process culminates in physiological maturity (Singh *et al*., 2022a).

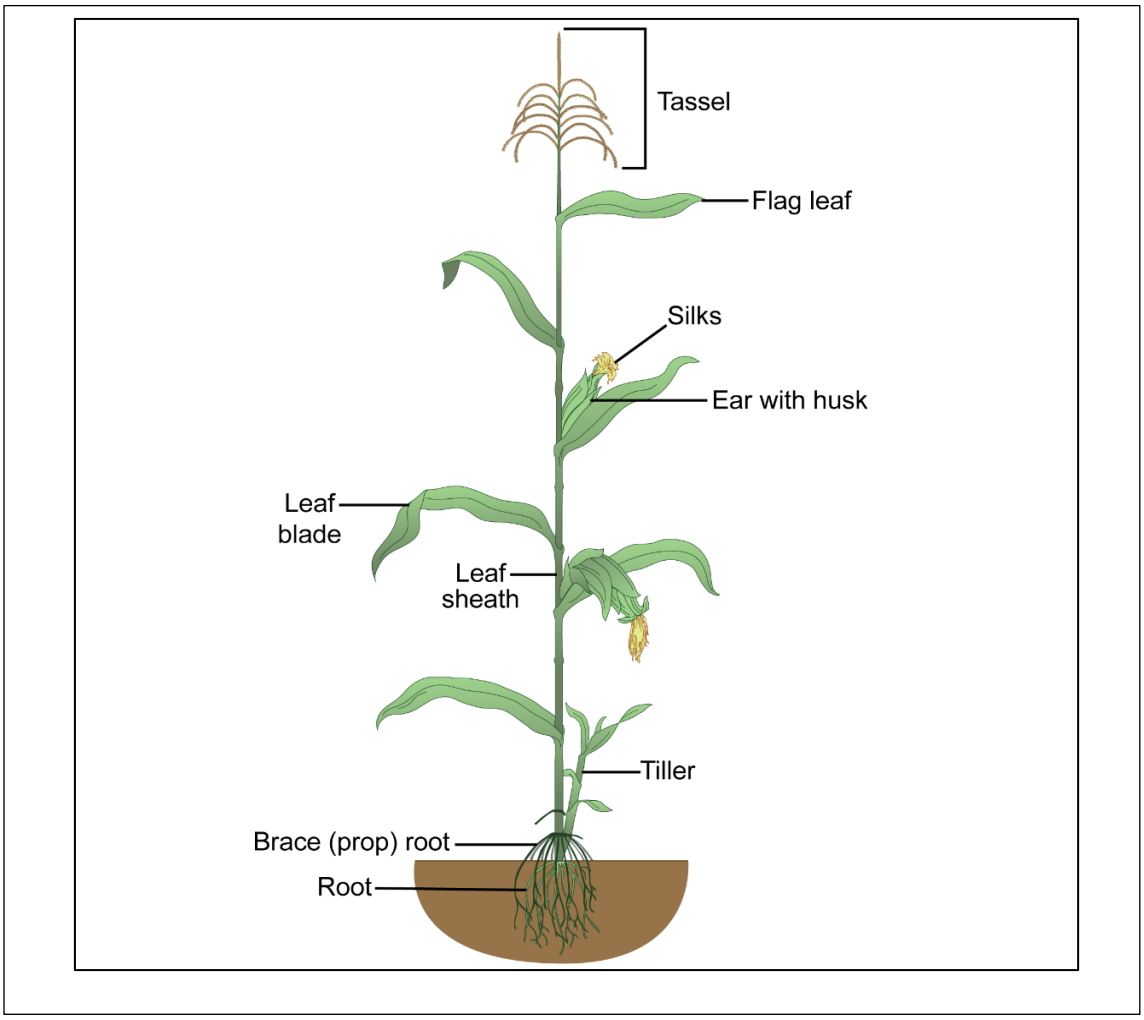

Figure 5: Mature corn plant showing corn silks circled in red (Paleontological Research Institution, 2021)

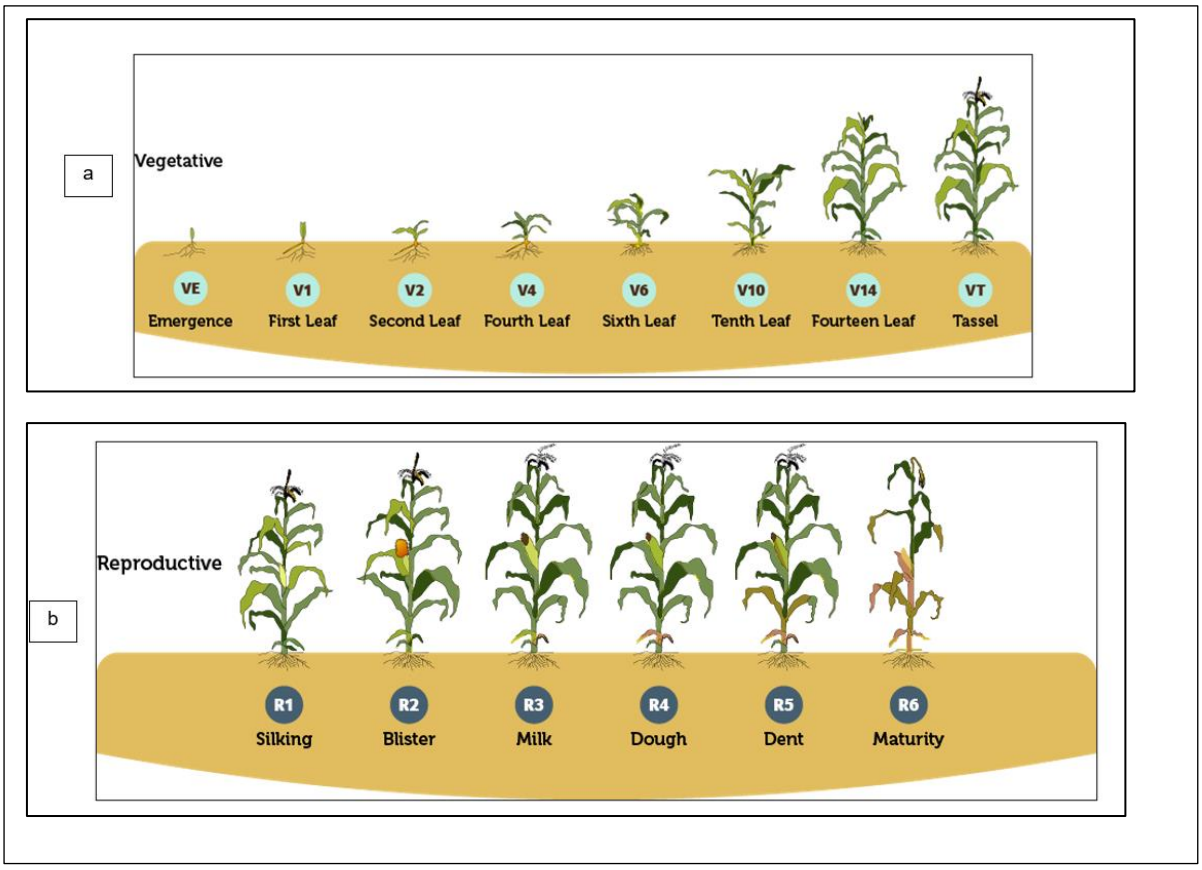

Figure 6: Stages of growth of corn: a) vegetative stage and b) reproductive stage (eKonomics news team, 2023). The vegetative stage of corn begins with the emergence of the radicle (first root), followed by the emergence of the coleoptile (protective sheath), which pushes through the soil surface during the VE (vegetative emergence) stage. This allows the first true leaf to emerge. The plant's growth during the vegetative stages is tracked by the number of fully developed leaves (V1-Vn). The final stage of vegetative growth, known as the VT (vegetative tasselling) stage, is characterized by the full emergence of the tassel, the male reproductive structure, at the top of the plant. The reproductive stage of corn begins with the R1 (silking) stage, where silks emerge for pollination. This is followed by the R2 (blister) stage, with small, fluid-filled kernels, and the R3 (milk) stage, where kernels fill with a milky fluid as they develop. In the R4 (dough) stage, kernels thicken with accumulating starch. The R5 (dent) stage then occurs, where kernels harden and form a dent, indicating maturity is near. The final R6 (physiological maturity) stage marks full kernel development, with maximum dry weight and a black layer signalling readiness for harvest

3.7.2. Nutritional composition of corn silk

Corn silk consists of various nutritional components including water, protein, lipid, crude fibre, carbohydrates, essential vitamins (including A, D, E and K) and minerals (calcium, magnesium, potassium, sodium, copper, iron, manganese, zinc) (Kaur *et al*., 2023). The moisture content and water activity of CS are closely linked to its shelf stability and microbiological safety, both of which are low and fall within acceptable ranges for shelf stability (Singh *et al*., 2022a). Aside from environmental factors (atmosphere, soil type, irrigation and fertigation type etc.), differences in the type of CS—including cultivar, stage

of maturity, processing methods, and storage conditions—contribute to the nutrient and mineral composition of CS (Rahman *et al*., 2014; Singh *et al*., 2022a). When powdered and dried, CS consists of a significant amount of soluble dietary fibres, such as pectin, glucan, and glucomannan, and insoluble dietary fibres such as cellulose, hemicellulose, and lignin as well as crude protein and carbohydrates (Nawaz *et al*., 2018). Investigating the variations in nutrient composition between three different varieties of CS: Sweet L. var. corn (*Zea mays* L. var. *saccharata*), Sweet corn (*Zea mays saccharata*), Waxy corn (*Zea mays ceratina*), revealed that sweet corn exhibited the highest moisture, protein, and fat content. Conversely, waxy corn demonstrated the highest ash and fibre content, while Sweet L. var. corn displayed the highest carbohydrate content (Hongsuwan *et al*., 2019). A study on the nutrient composition of dried and powdered Indian CS of the variety G5417 obtained during the silking stage was revealed the content of moisture, carbohydrate, fibre, protein, ash and fat was 7.89 %, 56.16 %, 14.82 %, 15.29 %, 5.29% and 0.55% respectively (Singh *et al*., 2022a). Differences in the nutrient composition between premature and mature Malaysian sweet-processed CS showed higher levels of moisture, lipids, and proteins, with slightly lower levels of ash, dietary fibre, and carbohydrates in CS obtained during the premature stage compared to the mature stage (Rahman *et al*., 2014). Additionally, there were discrepancies in the mineral composition between premature and mature CS, with elevated levels of certain minerals including calcium, magnesium, copper, and zinc, and reduced levels of potassium, sodium, manganese, and iron observed in premature CS compared to mature CS (Rahman *et al*., 2014). Corn silk (CS) can serve as a supplementary ingredient in various food products (such as pasta, bread, different types of flours, meat products) to enhance their protein, ash, and dietary fibre content, thereby boosting their nutritional value (Hasan *et al*., 2021; Rozan *et al*., 2022).

3.7.3. Phytochemical composition of CS

Phytochemicals are naturally existing non-nutritional compounds predominantly found in fruits, vegetables, medicinal plants and/ or natural products (Guo *et al.,* 2018). These plant constituents play a crucial role in numerous processes including growth and development of a plant, protection against viruses, bacteria, fungi and parasites while contributing to various plant characteristics, such as colour, fragrance, flavour, and texture of a plant (Martinez *et al*., 2017; Kaur *et al.,* 2023). Corn silk consists of diverse phytochemicals, such as polyphenols, phenolic acids, flavonoids, anthocyanins, carotenoids, sterols, tannins, volatile compounds, sugars, vitamins. minerals, polysaccharides, proteins, amino acids,

glycosides, terpenoids and peptides (Nawaz *et al*., 2019; Wang *et al*., 2019; Shalihah *et al.,* 2020) which are responsible for the biological effects of the plant material (Hasanudin *et al*., 2012; Wang *et al*., 2019). The wide array of bioactive metabolites found in CS significantly enhance its medicinal value, underscoring its importance as a pharmaceutical agent (Nawaz *et al*., 2019). Corn silk contains a significant amount of flavonoids, a diverse group of polyphenolic compounds, which confer various biological activities including antidiabetic antioxidant, antibacterial, antiviral and anti-inflammatory nature (Hasanudin *et al*., 2012). The isolation and identification of reduced derivatives of maysin and 3'-methoxymaysin were found to be abundant in CS obtained from several corn inbreeds (Snook *et al*., 1995). The isolation and identification of two novel flavone glycosides, a subclass of flavonoids namely 2''-O-α-L-rhamnosyl-6-C-3''-deoxyglucosyl-3-methoxyluteolin and 6,4'-dihydroxy-3'-methoxyflavone -7-O-glucoside was performed using high performance liquid chromatography-mass spectrometry analysis on 16 samples of air-dried Chinese CS (HPLC-MS) (Ren *et al*., 2009). Singh *et al*. (2022a) determined the total phenolic content (94.01 mg of gallic acid equivalent (GAE)/g,), total flavonoid content (163.93 mg quercetin equivalent (QE)/g), ascorbate content (270 mg/100g) of CS of the G5417 variety of *Zea mays*, due to their role in the quality, nutritional value and biological activity of CS (Singh *et al*., 2022a). Several studies investigated the different classes of metabolites in CS, identifying key phytochemical components and the estimated amounts present as indicated in Table 1. Among the different phytochemical classes, CS contains a significant portion of terpenoids (99% of which are volatile compounds) (El-Ghorab *et al*., 2007). Although terpenoids are typically used in perfumery and flavour applications (soaps, household products and cosmetics) (Hasanudin *et al*. 2012), their diverse chemical structure and biological properties make them promising candidates for various healthcare applications (Yang *et al*., 2020), including anti-inflammatory, antioxidant, antimicrobial, anti-viral and antidiabetic (El-Ghorab *et al*., 2007; Masyita *et al*., 2022). The generation of maize specialised metabolome networks revealed the presence of organ-preferred metabolites, in which 21 amino acids, 22 benzenoids, 22 indoles and 77 mixed glycosides were found to be more abundant in the silks of corn in comparison to the leaves, ears, stem and corn cobs (Desmet *et al*., 2021).

Table 1: The type and amount of phytochemical constituents and biological activities of different phytochemical classes of CS

Class of phytochemicals	Phytochemical components	Amount of phytochemicals estimated	Biological activities of phytochemical class	Reference
Polyphenols	Tannins, flavonoids, saponins, alkaloids, cardiac glycosides, steroids, anthocyanins, allantoins, hesperidin and resins, antioxidant	Total phenolics: 8101.6 ± 73.5 to 10,160.8 ± 250 mg CGAE/100 g Flavonoid: 5565 ± 40.9 to 6478.3 ± 409.9 mg CE/100 g Anthocyanins: 192.9 ± 0.3 mg CGE/100 g Proanthocyanidins: 69.4 ± 6.6	Antioxidant, antidiabetic, antimicrobial anti-inflammatory, prebiotic property and act as vasodilator	Žilić *et al*. (2016)
Phenolic acids	Para-aminobenzoic acid (PABA), vanillic acid, p-coumaric acid, chlorogenic acid, protocatechuic acid, caffeic acid, ferulic acid, maizenic acid, hydroxycinnamic acid ester, 3-O-caffeoylquinic acid, quinic acid, p-	3-O-caffeoylquinic acid: 22.6 ± 0.9 to 49.9 ± 1.4 mg/100 g	Antimicrobial activity, anti-inflammatory, anti-allergic properties, antidiabetic, inhibit oxidative damage diseases including coronary heart diseases, cancer, stroke	Žilić *et al*. (2016)

	coumaric acid, gallic acid			
Flavonoids	Catechin, protocatechin, quercitin, rutin, 3, 4, 5, 7-hydroxy flavones and isoflavones, cardiac glycosides, Maysin derivatives, methoxymaysin derviative	Rutin: 0.1398 mg/L Quercitin: 0.11 mg/L Maysin derivatives: 1.1 ± 3.6 Methozymaysin derivative: 1.2 ± 0.1 to 4.9 ± 0.3	Anti-cancer, prevents coronary heart diseases, osteoporosis, neurodegenerative diseases and postmenopausal bone loss, antidiabetic, antimicrobial	Ismael *et al*. (2017)
Carotenoids	B-carotene and zeaxanthin	Total carotenoid count: 11.3 mg CGAE/100 g dry weight (ethanolic extract)	Treat cardiovascular diseases, cancer, eye related disorders, protects skin and show high antioxidant power and reduces oxidative stress	Laeliocattleya *et al*. (2014)
Sterols	Phytosterols such as stigmasterol and β-sitosterol	Stigmasterol: 10.5886 mg/g Beta-sitosterol: 963.86 ± 198.39 mg/g to 1783.37 ± 57.70 mg/g	Regulation of membrane permeability and fluidity, control metabolic process, substrate for synthesis of secondary metabolites and precursor in	Haslina *et al*. (2017)

			cellular and developmental process	
Tannins	Gallotannins and phlobatannins	–	Improves cardiovascular health, inhibit atherogenesis, treat ischemia, reduce platelet aggregation, modulate immune responses and lipid peroxidation	Hu *et al*. (2010)
Vitamins	Vitamin C, Vitamin K and Vitamin E	–	Reduces oxidative stress, helps in collagen synthesis, prevents cancer, sepsis and neurodegenerative diseases, prevents blood clotting and oxidation of low density lipoprotein	Rahman *et al*. (2014)
Minerals	Sodium, Potassium, Calcium, Magnesium, Copper, Iron, Manganese, Zinc	Sodium- 12.5 ± 0.5 to 28.9 ± 0.3 mg/100 g Potassium- 1359.9 ± 46.6 to 1832.6 ± 37.5 mg/100 g	-	Žilić *et al*. (2016)

		Calcium- 0.1465 mg/g Magnesium- 0.1602 mg/g Copper- 0.0072 mg/g Iron- 0.0198 mg/g Manganese- 0.0187 mg/g Zinc- 0.0136 mg/g		
Sugars	Fructose, glucose, sucrose	Fructose: 14.20 ± 0.12 Glucose: 22.20 ± 1.10 Sucrose: 4.40 ± 0.20	Effective treatment for hypoglycaemia (abnormally low blood glucose levels)	Rosli *et al*. (2015)
Miscellaneous compounds	Polysaccharides (galactan), terpenoids, apigenin, anthraquinones, xanthoproteins	–	-	Singh *et al*. (2022b)

Key: CGAE: catechin or gallic acid equivalents, CE: catechin equivalent, mg/L: milligram per litre, mg/g: milligram per gram.

Several factors, such as developmental stage, extraction time, solvent used for extraction, cultivar type and environmental conditions play a role in the type and amount of metabolites detected when analysing CS (Sarepoua *et al*., 2013; Nurraihana *et al*., 2018; Singh *et al*., 2022b; Fougere *et al*., 2023). Fougere *et al*. (2023) investigated the phytochemical characterization of 50 % ethanolic extract of CS obtained from sweet corn cultivated in Martinique using ultra-performance liquid chromatography-mass spectrometry (UPLC-MS) analysis in which allowed the detection of 104 compounds, including 7 nitrogenous, 28 lipidic and 67 phenolic compounds (Fougere *et al*., 2023). Yucharoaen *et al*. (2023) investigated the variations in total phenolic content in extracts of CS made using two

different solvents, ethanol and ethyl acetate, which showed a phenolic content of 28.27 and 12.81 mg GAE/g respectively. Moreover, the total flavonoid content of ethanolic and ethyl acetate extracts of CS were 4.71 and 2.23 ± 0.57 mg QE/g extract, respectively (Yucharoaen *et al*., 2023). Nurraihana *et al*. (2018) revealed that ethanolic and ethyl acetate fractional extracts of CS was found to be rich in flavonoid compounds such as flavones, flavonols, flavanols, flavone C-glycosides, flavonols, flavonol O-glycosides, and isoflavonoids, many of which can be useful for application in both nutraceutical and pharmaceutical sectors (Nurraihana *et al*., 2018). In addition to the 22 flavanoid compounds (mirificin, isoorientin 7-o-rhamnoside, violanthin, chrysoeriol 7-neohesperidoside, 8-c-beta-d-glucofuranosylapigenin 2″-o-acetate, 3′-o-methylmaysin, pectolinarin, acacetin 7-(2″-acetylglucoside), gossypetin 7,4′-dimethyl ether 8-acetate, irisolone, theaflavanin, torosaflavone D, 6a,7-dihydroxymedicarpin, 5,7,4′-trihydroxy-3′-c-methylflavone 4′-rhamnoside, gallocatechin 3-o-gallate, epicatechin monogallate, epiafzelechin 3-o-gallate, epigallocatechin 3-o-(3-o-methylgallate), wedelolactone, epicatechin 3-O-(4-O-methylgallate) and (−)-acanthocarpanm) identified in the CS, 1 bis-coumarin derivative (daphnoretin), 1 fatty acid (9S,10S,11R-trihydroxy-12Z-octadecenoic acid), 1 chalcone (okanin 4-methyl ether 3′-glucoside) and 2 alkaloids (theobromine and 1,3,7-trimethyluric acid) were identified (Nurraihana *et al*., 2018). da Hora *et al*. (2021) identified thirty four metabolites (15-oxo-18Z-tetracosenoic acid, 1-cinnamoylpiperidine, 1-diphenyl-2- (4-methoxyphenyl) propene (4), 1-propenyl 1-(1-propenylthio)propyl disulfide, 2-keto-l-gluconic acid, 2-O-α-l-rhamnosyl-6-C-3- deoxyglucosyl-3′-methoxyluteolin, 6,4′-dihydroxy-3′-methoxyflavone-7-O-glucoside, 7-(methylthio)heptanenitrile, 7′,8′-dihydro-8′-hydroxycitraniaxanthin, 9,12-octadecadienoic acid, aloperine, argenteane, cassaidine, erythritol, glucosamine, glucose, glyceric acid, hexadecanoic acid, lactic acid, linoleic acid, lycoperoside D, malvidin, notoginsenoside R10, panaxydol linoleate, peonidin, phenethyl rutinoside, pipercitine, pyruvic acid, rhamnose, sinapoylspermine, sintaxanthin, tetradecanoic acid, and yiamoloside B) in different extracts (ethanol. Hexane and ethyl acetate) of CS obtained from the corn variety AG1051, with variations in the type and amount of metabolites between different extracts (da Hora *et al*., 2021). Analysis of aqueous extract of CS unveiled a total of 76 compounds, encompassing caffeic acid and nine of its derivatives, (E)-p-coumaric acid and two of its derivatives, ferulic acid and four of its derivatives, five flavones, along with various other metabolites (Wang *et al*., 2019). Apart from the type of solvent utilized, the phytochemical diversity of CS changes throughout the different growth stages of CS, affecting several different factors including the nutrient

composition, antioxidant and biological activity as well as mineral composition as depicted in Figure 7 (Singh *et al*., 2022b). Sarepoua *et al* (2013) reported variations in the total phenolic content, total flavonoid content and antioxidant activity of CS obtained from different corn varieties (Sarepoua *et al*., 2013). Rahman *et al*. (2014) reported differences in the total polyphenol content between three different extracts of CS (aqueous, ethanol and ethyl acetate) at two different growth stages (premature and mature) wherein ethanol and water were reported the highest total polyphenol content in premature and mature respectively whereas aqueous extract reported the highest total flavonoid content in both premature and mature CS (Rahman *et al*., 2014). Despite the growing interest in exploring the phytochemical composition of CS, this field remains underdeveloped, particularly in terms of systematically evaluating phytochemical profiles, investigating various types and varieties of corn, and establishing correlations between CS metabolites and reported biological activities. The constituents of CS offer a diverse array of advantages, making them valuable natural resources for industry and healthcare applications due to their extensive range of pharmacological properties including antioxidant, diuretic and kaliuretic effects, antidiabetic, anti-hyperlipidemic, antibacterial, anti-cancer, antihypertensive, and potential reduction of nephrotoxicity (Sabiu *et al*., 2019; Singh *et al.,* 2022; Kaur *et al.,* 2023).

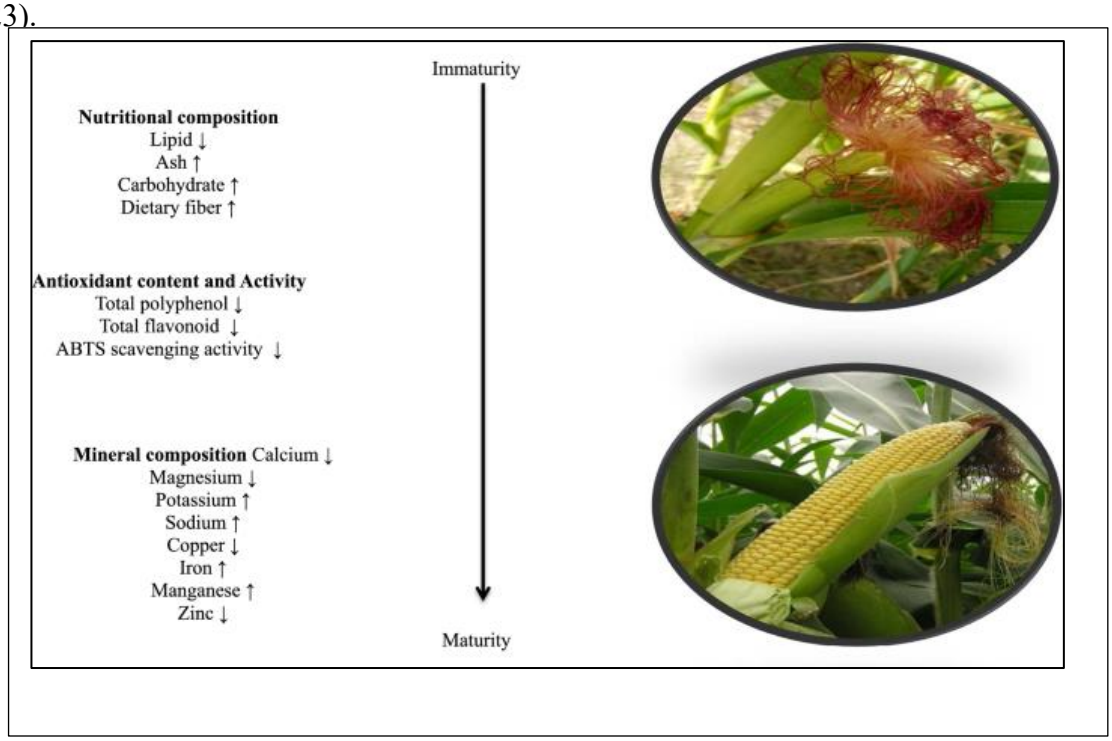

Figure 7: Variations that occur in biological activity, nutritional, phytochemical and mineral composition during the growth of corn silk from immature to mature (Singh *et al*., 2022b).

Arrow facing up indicates increase in content, composition or activity, whereas arrow facing down indicates decrease in content, composition or activity (Singh *et al*., 2022b)

3.7.4. Pharmacological properties of corn silk

Many cultures, such as Chinese, Korean, Turkish, French, and Native American, use CS as a traditional medicine to address a wide range of illnesses and diseases, such as cystitis, jaundice, kidney disorders (kidney stones), oedema, gout, rheumatism, arthritis prostate disorders, heart disorders, malaria, hyperglycaemia, bladder and urinary infections, psychological conditions (such as depression and anxiety), cancer, microbial and fungal infections, as well as obesity (Chen *et al*., 2013; Wang *et al*., 2019; Chaudhary *et al*., 2022). The possible therapeutic properties of CS have been explored in several research exploits which uncovered a range of beneficial properties such as diuretic, antihyperlipidemic, antihypertensive, anti-obesity, anti-microbial, neuroprotective, anti-cancer, anti-depressant, antioxidant, anti-inflammatory, and antidiabetic (Hasanudin *et al*., 2012; Chen *et al*., 2013; Chaiittianana *et al*., 2017; Shalihah *et al*., 2020), as detailed in Table 2.

Table 2: Selected biological activities of corn silk

Biological activity	Findings	Reference
Antioxidant	Aqueous-ethanol (1:1) extract of CS (1.6 mg/mL) exhibited 92.6% scavenging activity against 1,1-diphenyl-2-picryl hydrazyl (DPPH) radicals and 2 mg/mL of extract demonstrated chelating activity by interfering with the formation of ferrous and ferrozine complexes, indicating its ability to chelate metal ions. CS extract (522 mg/mL) reduced the production of antioxidant ions as well as had significant iron-reducing power at concentrations of 0.8 and 1.6 mg/mL. Moreover, CS extract 0.4 mg/mL inhibited lipid peroxidation, as determined by the ferric thiocyanate method.	Ebrahimzadeh *et al*. (2008)
	Kunming mice (fed normal diet and water) treated with 100 and 400 mg/kg of crude	Hu *et al*. (2011)

	flavonoids obtained from ethanolic (60%) extract of CS elevates exercise tolerance in the mice and provides protection against oxidative stress induced by exhaustive exercise by inhibiting lipid per-oxidation and increasing antioxidant enzymes levels.	
	Investigated fractions (N-butanol, petroleum, acetic ether and water) of CS showed potent total antioxidant activity. Petroleum ether fraction had the highest DPPH radical scavenging activity (307.75 µg/mL), reducing power (149 µg/mL) and iron chelating capacity (382.30 µg/mL) including in comparison to control at EC_{50} (ascorbic acid). isoorientin-2′″-O-α-l-rhamnoside and 3′-methoxymaysin were identified as two antioxidant compounds present in the N-butanol fraction of CS.	Liu *et al*. (2011)
	Ethanolic (80%) extract of CS relatively high total antioxidant activity (EC_{50}:102.4 µg/mL), reducing power (113.9 ± 11.0 µg/mL), greater DPPH reducing activity (116.2 ± 14.6 µg/mL) and higher hydroxyl radical scavenging activity (130.4 ± 8.7 µg/mL), in comparison to positive control (ascorbic acid: 0.22%).	Wang *et al*. (2019)
	Corn silk (CS) contains a high concentration of bioactive compounds, including phenolic acids, flavonoids (maysin, luteolin, quercetin etc.), polysaccharides, terpenoids, and steroids (sitosterol, stigmasterol etc.), many of which exhibit potent antioxidant potentials	Lapcik *et al*. (2023)
Antimicrobial	Extracts of CS [petroleum ether (1.1%), chloroform (1.2%) and methanol (6.5%)] and	Nessa *et al*. (2012).

	flavonoid glycosides [maysin and maysin-3′-methyl ether (2.0 mg/mL)] showed significantly ($p<0.05$) higher sensitivity against bacterial cultures *Bacillus cereus*, *Bacillus subtilis*, *Staphylococcus aureus*, *Pseudomonas aeruginosa*, *Enterobacter aerogenes*, *Salmonella typhi*, *Salmonella paratyphi*, *Escherichia coli*, *Shigella sonnei*, *Shigella flexneri*, *Proteus vulgaris* and *Proteus mirabilis* revealed using agar hole-plate diffusion method compared to gentamycin (5 µg/mL).	
	Most effective antibacterial activity of ethanolic extract of CS against urinary tract infection pathogens (*Proteus mirabilis*, *Klebsiella pneumoniae*, *Escherichia coli* and *Staphylococcus aureus*) was determined at 900 ug. Additionally, isolated fungi from spoiled vegetables (*Aspergillus niger*, *Aspergillus flavus*, *Aspergillus brasiliensis*) had 100% inhibition at 3 mg/20mL of CS extract.	Abirami *et al*. (2021)
	Ethanolic (80%) extract of corn silk exhibited significant inhibitory activity against against Gram-positive bacteria, including *Bacillus subtilis*, *Staphylococcus aureus*, and *Streptococcus* pyogenes in the agar well diffusion assay. 80% ethanol and methanol extracts from CS demonstrated substantial inhibitory activity against *Aspergillus flavus* ON470194 and *Aspergillus niger* (ATCC 16888) in fungal biomass method.	Sahana *et al*. (2023)
	Using agar plated diffusions and tube continuous dilution methods, *Staphylococcus aureus*, *Bacillus subtilis* and *Candida albicans*	Feng *et al*. (2011)

	were inhibited by aqueous extract of CS (500 mg/mL) when compared to *Andrographis paniculata*	
	Ethanolic extract of CS (500 mg/mL) inhibited microbial activity against bacterial microorganisms such as *Staphylococcus aureus*, *Pseudomonas aeruginosa*, *Bacillus cereus*, *Bacillus coli* and *Candida albicans* as determined by agar plated diffusion and tube continuous dilution methods.	Feng *et al*. (2012)
Anti-hyperlipidaemic effects	50 mg/kg BW, 100 mg/kg BW, and 150 mg/kg BW CS ethanolic (96%) extract administered to male wistar rats (fed high-fat diet and administered propylthiouracil for seven days to induce high cholesterol) significantly decreased cholesterol by 46-51%, reduced low density lipoprotein by 57-67%, decreased triglycerides by 60-67% and increased high density lipoprotein by 21-28%.	Nessa *et al*. (2023)
	Streptozotocin-induced diabetic mice were administered 500 mg/kg of ethanolic (80%) extract of CS for 28 days revealed reduction in total cholesterol, triacylglycerol and low-density lipoprotein cholesterol and increase in high density lipoprotein cholesterol level.	Zhang *et al*. (2015)
Diuretic effect	Malaysian aqueous CS extract showed a diuretic activity in elevating urine and sodium content at dosages 500-800 mg/kg in Sprague Dawley male adult rats.	Solihah *et al*. (2015)
Anti-cancer effect	Maysin isolated from methanolic extract of CS (obtained from Korean corn) dose-dependently reduced the PC-3 cell viability, with an 87%	Lee *et al*. (2014)

	reduction at 200 µg/mL. Maysin (150 and 200 µg/mL) significantly induced apoptotic cell death, DNA fragmentation, depolarization of MMP, and reduction in Bcl-2 and pro-caspase-3 expression levels	
	Aqueous extract of CS caused inhibition of cell proliferation, loss of mitochondrial membrane potential, release of calcium ions and release of cytochrome C from the mitochondria into the cytosol in LoVo and HT-29 human colon cancer cells and MGC-803 human gastric cancer cells.	Guo *et al*. (2017)
	Methanolic (80%) CS extract induced reactive oxygen species and lipid peroxidation, decreased glutathione resulting in cell apoptosis in MCF-7 cells. Effect of CS extract on matrix metalloproteinases (MMP) levels in MCF-7 cells was analysed using Rhodamine-123 fluorescence dye clearly showed a concentration-dependent decrease in the MMP levels in MCF-7 cells whereby a significant decrease of 10%, 35%, and 60% was found at 250, 500, and 1000 µg/mL of CS extract, respectively. In addition, CS extract (250-1000 µg/mL) upregulated the mRNA expression of p53, caspase-3, caspase-9, and Bax and downregulated the Bcl-2, which leads to apoptosis.	Al-Oqail *et al*. (2019)
	Polysaccharide CSP-S-2, derived from the ethanolic (95%) fraction of the aqueous extract of CS originating from Jilin province, China, demonstrated substantial inhibition of HeLa cell proliferation, indicative of its potential	Li *et al*. 2020

	anti-cancer activity. Maximum inhibition of HeLa cells was observed after 48 hours of treatment with CSP-S-2 at a concentration of 800 µg/mL.	

Key: EC_{50}: half maximal effective concentration; GAE: gallic acid equivalent; kg BW: kilogram body weight, ATCC: American Type Culture Collection, CS: corn silk.

3.7.5. Antidiabetic properties of corn silk

For decades, CS was employed as a traditional medicine for the treatment of various conditions due to its potential health benefits and medicinal properties, including as a therapeutic agent for the treatment of T2DM (Hasanudin *et al.,* 2012). Numerous studies propose that CS can regulate blood glucose levels, improve glucose tolerance, influence blood glucose uptake, stimulate insulin secretion and action, promote the recovery of damaged β-cells, and inhibit key enzymes (such as alpha-amylase and alpha-glucosidase), all of which are crucial for the regulation of glucose metabolism (Guo *et al.,* 2017; Chaudhary *et al.,* 2022; Singh *et al.,* 2022a; 2022b). Table 3 resents the results of some of the promising results reported by these studies.

Table 3: Studies investigating the antidiabetic effect of corn silk between 2009 and 2023

Study	Reported antidiabetic activity of CS	Reference
1	For 45 days, diabetic mice induced with alloxan (75 mg/kg) were treated with aqueous extracts of CS at doses of 2.0 and 4.0 g/kg. Compared to both the control group (saline) and the Xioke pill group (traditional Chinese medicine), mice treated with CS exhibited reduced levels of blood glucose and haemoglobin A1C. The study suggests that the hypoglycaemic effect of CS may be attributed to increased insulin levels and the regeneration of damaged β-cells.	Guo *et al*. (2009)
2	Polysaccharides extracted from the ethanolic fraction of CS were administered to streptozotocin-induced diabetic mice at a dosage of 500 mg/kg body weight for four weeks.	Zhao *et al*. (2012)

	The mice treated with CS exhibited significantly lower blood glucose levels compared to the control group (saline) and positive control (dimethyl biguanide). Administration of 400-500 mg/kg of CS polysaccharides showed improved glucose tolerance, evidenced by significantly lower glucose levels at 0, 30, and 120 minutes post-administration	
3	Crude CS polysaccharide obtained from aqueous extract of CS modified by carboxymethylation had alpha-amylase inhibitory potential when compared to acarbose.	Chen *et al*. (2013)
4	Five-week-old rabbits, fed normal diets, were administered aqueous and methanolic extracts of CS at a dosage of 400 mg/kg/day for three weeks showed significantly lower plasma glucose levels compared to the control group which was not treated with CS following 1 week of treatment.	Olaniyan *et al*. (2014)
5	Ethyl acetate (19.6%) fraction of CS reported antidiabetic bioactivity through preventing the formation of advanced glycation end products and through protection of insulin-secreting cells from glucotoxicity	Chang *et al*. (2016)
6	Aqueous extract of CS demonstrated strong inhibitory effects against α-amylase and moderate inhibitory effects against α-glucosidase at IC_{50} of 5.89 mg/mL and 0.93 mg/mL, respectively.	Sabiu *et al*. (2016)
7	Crude CS polysaccharide (PCS) isolated from aqueous extract inhibited carbohydrate-metabolizing enzyme alpha-amylase. Streptozotocin (90 mg/kg)-induced diabetic mice treated with PCS (200 mg/kg) reported lower fasting blood glucose after 120 minutes. Following PCS2 administration (200-800 mg/kg) the	Pan *et al*. (2017)

	levels of insulin in the serum were decreased compared with control group (rosiglitazone).	
8	Polysaccharides and phenolic compounds from an ethanolic (80%) fraction extracted from different varieties of CS using cold precipitation and vacuum solvent evaporation respectively. Subsequently, CS extracts (50 ul) (IC_{50} values ranging from 857 µg/mL - 38470 µg/mL) decreased the activity of α-glucosidases in contrast to acarbose (IC_{50}: 126 µg/mL). CS compounds maysin, methoxymaysin, apymaysin and luteolin reported higher negative docking scores in contract to acarbose and p-nitrophenyl-alpha-D-glucopyranoside and were recognized as potential inhibitors of alpha-glucosidase.	Alvarado-Díaz *et al*. (2019)
9	Non-toxic polysaccharides from CS (CSP: CSP1. CSP2 and CSP3) were investigated for their hypoglycaemic action. CSP2 reported higher inhibition of alpha-amylase and alpha-glucosidase with IC_{50} values of 0.13 mg/mL and 1.21 mg/mL, respectively, both of which were significantly higher when compared to acarbose. In contrast to the control (untreated) and metformin (positive control), 100, 300 µg/mL of CSP1 and CSP2 reported a higher percentage glucose uptake. The results from determining the effect of CSP on PI3K/Akt signalling pathway in L6 skeletal muscle myotube suggested that CSP1, CSP2 and CSP3 could regulate the PI3K/Akt signalling pathway and increase glucose uptake. In addition, CSP1, CSP2 and CSP3 promoted the GLUT4 translocation from intercellular vesicles to the plasma membrane.	Guo *et al*. (2019)
10	Ethanol extract derived from CS underwent liquid-liquid fractionation to yield distinct fractions	Wang *et al*. (2019)

	[petroleum ether fraction (PCS), ethyl acetate fraction (ECS), n-butanol fraction (BCS), and water fraction]. Both ECS and BCS demonstrated a noteworthy anti-hyperglycaemic effect by significantly inhibiting alpha-amylase and alpha-glucosidase in enzymatic assays. In the BSA-glucose model, ECS and BCS effectively impeded the formation of advanced glycation end products. Moreover, the assay assessing antidiabetic nephropathy activity showed that ethanolic extract of CS, ECS, and BCS significantly curtailed the production of collagen IV, fibronectin, and interleukin-6 in high-glucose-stimulated mesangial cells at a concentration of 200 μg/mL.	
11	The study examined the impact of crude flavonoids (CSFs) derived from the ethanolic extract of CS on streptozotocin-induced diabetic mice in at doses of 100, 300, and 500 mg/kg. Administration of 300 mg/kg and 500 mg/kg CSFs resulted in reduced blood glucose levels in diabetic mice and 500 mg/kg dose of CSFs offered protection against liver and kidney damage in diabetic mice in comparison to streptozotocin (positive control) and tap water (negative control).	Zhang *et al*. (2019)
12	Four polysaccharides' (CSP20, CSP40, CSP60 and CSP80) isolated from ethanolic fraction of CS inhibited alpha-glucosidase. CSP80 (obtained from 80% ethanolic CS) inhibited alpha-glucosidase at lowest IC_{50} (0.04 ± 0.01 mg/mL) compared to other polysaccharides and ascorbic acid (positive control).	Jia *et al*. (2021)
13	The antidiabetic potential of 26 bioactive compounds present in CS against therapeutic targets protein tyrosine phosphatase 1-B, glucose transporter-1, dipeptidyl peptidase-4, alpha-glucosidase, and alpha-amylase was accessed *in silico* using molecular	Chaudhary *et al*. (2022)

	docking analysis in which flavones, β-Carotene, gallotannins, 3-O-caffeoylquinic acid and stigmasterol were found to possess higher affinity towards the particular targets respectively.	
14	Ethanolic (80%) extract of CS displayed an IC_{50} value of 0.70 ± 0.02 and 0.71 ± 0.01 mg against α-amylase and α-glucosidase, respectively in comparison to their respective standards.	Sahana *et al*. (2023)

Key: IC_{50}: half-maximal inhibitory concentration.

Although the antidiabetic potential of CS is well documented, its precise mechanism of action remains incompletely understood, particularly its relationship with targets implicated in the pathogenesis of T2DM and its secondary complications .

3.8. Computational approaches in drug discovery

Understanding the different mechanisms of antidiabetic action of natural products, such as increased pancreatic secretion of insulin, insulin sensitization, inhibition of carbohydrate digestion, inhibition of intestinal glucose absorption, enhanced glucose uptake by the muscle and adipose tissues, antioxidant activity, anti-inflammatory activity, gluconeogenesis regulation and the inhibition of T2DM-related complication (Zaid *et al*., 2018), is crucial for treatment development, therapy optimization, efficacy and safety assessment, new drug targets identification, personalized medicine enablement, and healthcare providers and patients education (Shanak *et al*., 2019; Alam *et al*., 2022). This applies to the development of CS as a therapeutic agent for the treatment of T2DM (Sawangwong *et al*., 2024). The elucidation of mechanism of antidiabetic action of several natural products, including the plant species *Nigella sativa*, *Momordica charantia*, *Helicteres isora*, *Panax ginseng, Allium cepa*, *Azadiracta indica*, *Eugenia jambolana*, and *Medicago sativa*, has been contributed to the development of the abovementioned plants as antidiabetic therapeutic agents (Emeka *et al*., 2016). However, identifying and developing pharmacologically active natural products efficiently and systematically is challenging due to challenges in isolation and purification procedures, minimal available amounts of lead compounds, difficulty in synthesizing natural products with high structural complexity, and associated synthesis scale-up issues (Franco *et al*., 2021). In addressing these obstacles, a wide array of computational methodologies has emerged in recent times, with a rising trend

in utilizing these approaches to enhance and expedite the process of natural product-based drug discovery (Franco *et al*., 2021). These techniques include network pharmacology (Leung *et al*., 2013), molecular docking and molecular dynamics simulation (Hasan *et al*., 2022; Wang *et al*., 2022), which be discussed in detail further.

3.8.1. Network pharmacology

The recent application of cutting-edge technologies in analytical chemistry and chemical biology to characterize commonly used herbal medicine has facilitated the means to identify the active ingredients in traditional systems of medicine and their relationship with corresponding biological targets (Shao *et al*., 2013). In comparison to the expensive and time-consuming traditional drug discovery approaches (Shaker *et al*., 2021), network-based drug discovery is becoming an increasingly popular and promising approach that enables cost-effective drug development (Wu *et al*., 2008). Network pharmacology, an approach which combines systems biology, bioinformatics, high-throughput histology, pharmacology and information networks, can allows for the identification of drug leads, targets and biological systems on a network level (Zhan *et al*., 2018), in a time-efficient and cost-effective manner (Zhang *et al*., 2013; Chandan *et al*., 2017). Employing network pharmacology for the development of novel therapeutic agents offers several benefits, including regulation of signalling pathways through multiple channels, enhancing drug efficacy, minimizing side effects of drugs, improving the success rate of clinical trials, and lowering the costs associated with drug discovery (Zhang *et al*., 2013; Zhou *et al*., 2020). A field which has greatly benefited from the use of network pharmacology is traditional Chinese medicine systems in which the pharmacological effects of drugs on diseases and their mechanisms of action has been reported (Liu *et al*., 2017; Guo *et al*., 2019; Han *et al*., 2019). Several studies have elucidated the mechanism of antidiabetic action of several natural products, including plants such as *Potentilla discolor* bunge, *Lobelia chinensis, Duranta repens* L, *Caesalpinia sappan* L. Wood and *Rhizoma Coptidis*, using network pharmacology analysis (Wang *et al*., 2019; Adnan *et al*., 2020; Ge *et al*., 2020; An *et al*., 2021; Khanal *et al*., 2021). Using network pharmacology to identify the mechanism of action of CS as a therapeutic against several diseases, including Alzheimer's, obesity and gout has been reported (Oh *et al*., 2021; Zhang *et al*., 2022; Tao *et al*., 2023). However, the relationship between CS metabolites and therapeutic targets implicated in T2DM using network pharmacology analysis has not been elucidated to date. If network pharmacology was performed on CS, the identification of therapeutic targets implicated in T2DM and the

identification of the top lead drug candidates can be performed. This approach allows for a more comprehensive understanding of CS's potential in managing diabetes and highlights key bioactive components involved.

3.8.2. Molecular docking and molecular dynamics simulation analysis

In tandem with network pharmacology, computer-aided drug design (CADD) methodologies, including structure-based drug design, structure-based pharmacophore modelling, virtual screening, molecular docking, ligand-based drug design, quantitative structure–activity relationship models, ligand-based pharmacophore modelling, and molecular dynamics (MD) simulation, can be utilized to further investigate the correlation between targets and potential drug candidates (Xin *et al*., 2021; Hasan *et al*., 2022; Wang *et al.,* 2022). Through CADD, the identification and development of lead compounds are facilitated by employing theoretical calculations, simulations, and the prediction of interactions between drug candidates and target receptors, thereby expediting the drug discovery process (Gu *et al*., 2023; Sharma *et al*., 2023). Molecular docking is a cost-effective and fast computational tool utilized for predicting and analysing the interactions between a specific molecule and a macromolecular target (typically a protein) at an atomic level (Tran *et al*., 2022). This technique enables the examination of how small molecules behave within the binding sites of target proteins and aids in elucidating essential biochemical processes (McConkey *et al*., 2002). Molecular docking aids in understanding the binding mechanism, predicting the binding affinity, identifying potential drug candidates by screening large libraries of compounds against target proteins and optimizing drug leads, (Gaba *et al*., 2010; Eweas *et al*., 2014). Molecular docking analysis has been used previously to elucidate the mechanism of action of CS metabolites (Sawangwong *et al*., 2024), including targets implicated in T2DM (Alvarado *et al*., 2019; Chaudhary *et al*., 2022). Alvarado *et al*. (2019) and Chaudhary *et al*. (2022) investigated the relationship between CS metabolites, and therapeutic target enzymes implicated in T2DM (α-glucosidase, protein tyrosine phosphatase 1-B, dipeptidyl peptidase-4 and and α-amylase). Both studies reported good binding affinity between the therapeutic targets and CS metabolites, highlighting their value as modulators of the therapeutic targets (Alvarado *et al*., 2019; Chaudhary *et al*., 2022). Molecular docking can be integrated with molecular dynamic simulations, a powerful computational tool that allows one to explore the dynamic interactions within protein-ligand complexes (De Vivo *et al*., 2016; Agu *et al*., 2023). These simulations aid in comprehending the conformational changes induced by ligand binding

and assessing the stability of the complex (Agu *et al*., 2023). To date, molecular dynamics simulation serves as a modern-day tool to screen, determine and predict therapeutic agents against known druggable targets (Shode *et al*., 2022). Several studies have used molecular docking and molecular dynamics simulation to investigate the mechanism of antidiabetic action of natural plants such as *Aegle marmelos*, *Helianthus annuus* (sunflower) seed, *Momordica charantia*, *Englerophytum magalismontanum, Azadirachta indica, Aspalathus linearis* and *Trigonella foenum-graecum* (fenugreek) (Rampogu *et al*., 2018; Arif *et al*., 2021; Akoonjee *et al*., 2022; Olaokun *et al*., 2022; Sharma *et al*., 2022; Abdullah *et al*., 2023; Rampadarath *et al*., 2023) as well as plant compounds such as chlorogenic acid, luteolin and dihydropyrimidinone derivatives (Singh *et al*., 2021; Ilyas *et al*., 2022; Kahksha *et al*., 2023). Landeros-Martinez *et al*. (2023) used molecular docking and molecular dynamics simulation to investigate the potential inhibition of human sucrase-isomaltase by two CS flavonoid compounds (luteolin and maysin), to identity potential candidates as an alternative treatment against T2DM (Landeros-Martinez *et al*., 2023). In addition to molecular docking and MD simulation, density functional theory serves a valuable tool for assessing the antidiabetic properties of CS.

3.8.3. Density functional theory

Density functional theory (DFT) is a strong and affordable computational quantum mechanical modelling technique which is employed in physics, chemistry and materials science to study the electronic or nuclear structure (including the ground state) of many-body systems (system that consist of many interacting particles), such as atoms, molecules and condensed phases (Hohenberg *et al*., 1964; Assadi *et al*., 2013). The central concept of DFT is that the ground state energy and of a many-electron system can be uniquely determined by its electronic density instead of its wave function, which is a more complex entity (Hohenberg *et al*., 1964). Through the use of DFT, the ground state and properties of a many-electron system, including molecules, can be evaluated through the use of functionals (i.e. the functions of another function) (Kohn *et al*., 1965). The ground state energy functional is composed of three main components: the kinetic energy and potential energy, the interaction between nuclei and electrons along with the Coulomb interaction between electron distributions, and the exchange-correlation energy, which accounts for both exchange and correlation effects (Kohn *et al*., 1965). Density functional theory (DFT) is a powerful tool in the discovery and development of drugs, playing a crucial role in understanding molecular properties, interactions, and mechanisms at an atomic level, while

also providing essential information about the energetic properties of drug molecules (Zhu *et al*., 2019; Kim *et al*., 2020). There are numerous applications of DFT in drug discovery, such modelling drug-receptor interactions and mechanisms of drug action, optimizing molecular structure and geometry, predicting the chemical reactivity and spectroscopic properties of drug candidates, correlating structural features with drug activity, elucidating reaction mechanisms, and evaluating the various conformations of drug molecules (LaPointe *et al*., 2007; Adekoya *et al*., 2020). While there is limited information regarding the investigation of CS metabolites using DFT, Landeros-Martinez *et al*. (2023) employed DFT to investigate the interactions between human sucrase-isomaltase and the CS metabolites maysin and luteolin. The DFT analysis revealed that maysin and luteolin act as novel inhibitors of sucrase-isomaltase, suggesting them as potential alternative candidates for treating T2DM (Landoros-Martinez *et al*., 2023). In addition to DFT, network pharmacology, molecular docking and MD simulation can be used to elucidate the antidiabetic mechanism of action of CS metabolites, an area that is lacking at present that would greatly improve the development of CS as a therapeutic agent against T2DM.

3.9.Experimental validation of the antidiabetic activity of corn silk

Experimental validation, such as *in vitro* and *in vivo* validation, is imperative to ensure reliability, accuracy, efficacy and safety of potential drug candidates (Shalaby *et al*., 2014). Among the array of experimental validation approaches, employing mammalian cell lines stands out as a particularly robust method for assessing potential drug candidates. This approach offers valuable insights into the safety profiles and potential mechanisms of action of these candidates (Jaroch *et al*., 2018; Venkateswaran *et al*., 2020; Feraco *et al*., 2021). Despite numerous studies highlighting the anti-hyperglycaemic effects of CS in animal models (Zhao *et al*., 2012; Zhang *et al*., 2015; Pan *et al*., 2017; Han *et al*., 2019; Sheng *et al.,* 2021), there is a lack of information (limited number of published research) on using mammalian cell lines to investigate the impact of CS on the pathogenesis of T2DM and its associated complications. The toxicity analysis of CS obtained from two cultivars (yellow sweet corn silk and purple waxy corn silk) reported no effects on the viability of mouse 3T3-L1 pre-adipocytes at concentrations of 250-1000 parts per million, and was considered a safe therapeutic agent for obesity management (Chaiitianan *et al*., 2016). Chaiitianan *et al*. (2017) explored the cytotoxicity of purple CS, in which the CS demonstrated low to no toxicity at concentrations of 125-1000 µg/mL when tested on mouse 3T3-L1 pre-adipocytes. It was concluded that the purple CS was considered safe

and could be used for further experimentation (Chaiitianan *et al*., 2017). Maysin, abundant in CS, was isolated from Korean hybrid corn (Kwangpyeongok) and revealed increased viability of human neuroblastoma SK-N-MC cells following treatment of 5–50 μg/mL of maysin for 2 hours with doses (Choi *et al*., 2014). Cell line studies, including clonal rat pancreatic β-cell line, rat L6 skeletal muscle myotubes, rat mesangial cells and human umbilical vein endothelial cells, have been used to elucidate the mechanism of antidiabetic action of CS. These studies report that CS exerts its antidiabetic effects through various mechanisms, including beta-cell function restoration, mitigation of oxidative stress, inhibition of protein glycation, reduction of advanced glycation end product formation, extracellular matrix inhibition, glucose uptake induction, and enhancement of glucose transporter type 4 translocation (Chang *et al*., 2016; Guo *et al*., 2019; Wang *et al*., 2019). Although there is existing research on the antidiabetic action of CS using mammalian cell lines, there is currently a lack of studies confirming its antidiabetic potentials using the HepG2 cell line, which is a commonly employed human hepatoma cell line derived from foetal liver tumour cells and frequently utilized in diabetes-related studies (Liu *et al*., 2017). HepG2 cell line studies have been instrumental in exploring the relationship between various plants and their chemical constituents in T2DM pathogenesis and the prevention of associated complications (Huang *et al*., 2015; Mokashi *et al*., 2017; Chen *et al*., 2019; Aladejana *et al*., 2020; Bourebaba *et al*., 2021; Yarahmadi *et al*., 2021). For example. Bourebaba *et al*. (2021) demonstrated the potential action of *Laurus nobilis* ethanolic extract on enhancing insulin sensitivity and shielding liver cells from apoptosis, mitochondrial dysfunction, oxidative stress, and inflammation in HepG2 cells; all of which are considered as major changes that occur due to insulin resistance. It was revealed that the ethanolic extract of *Laurus nobilis* was an insulin sensitizing and hepatoprotective agent, which improved insulin sensitivity, reduced oxidative stress and inhibited caspases and had anti-apoptotic effects (Bourebaba *et al*., 2021). At present, there is a notable gap in knowledge regarding the validation of antidiabetic properties of CS in HepG2 cells, information that can be useful for the development of CS as a therapeutic agent against T2DM.

Generally, efforts about increasing the awareness on the severity of T2DM and its associated complications in communities and among health care professionals is crucial to better understand, manage and treat T2DM. Although there are many ways to effectively treat T2DM via medication, diet, exercise etc., however some of these components are not

always sustainable for most patients to effectively manage the disease. The present review highlights the importance of searching for novel antidiabetic therapeutic agents that can be used as an affordable, safe alternative and/or complementary aid against T2DM. Among many plants used in traditional South African herbal medicine systems against T2DM, CS remains an underutilized plant material with extensive therapeutic potentials for the treatment of many diseases and illnesses, including T2DM. The nutritional, functional, phytochemical and pharmacological aspects of CS have been well documented including its remarkable biological attributes highlighting the antidiabetic bioactivity of CS which. Although the antidiabetic potentials of CS are well reported, however, it's mechanism of action against T2DM is not yet well established, which identifies a grey area that may be further explored with computational techniques, such as network pharmacology, molecular docking and molecular dynamics simulation. Thereafter, the antidiabetic potential of CS can be experimentally validated through cell culture studies.

References:

Abdullah, A., Biswas, P., Sahabuddin, M., Mubasharah, A., Khan, D.A., Hossain, A., Roy, T., Rafi, N.M.R., Dey, D., Hasan, M.N. and Bibi, S. 2023. Molecular dynamics simulation and pharmacoinformatic integrated analysis of bioactive phytochemicals from *Azadirachta indica* (Neem) to treat diabetes mellitus. *Journal of Chemistry*, 2023. 1-19.

Abo, K.A., Fred-Jaiyesimi, A.A. and Jaiyesimi, A.E.A. 2008. Ethnobotanical studies of medicinal plants used in the management of diabetes mellitus in South-Western Nigeria. *Journal of Ethnopharmacology*, 115, 67-71

Abirami, S., Priyalakshmi, M., Soundariya, A., Samrot, A.V., Saigeetha, S., Emilin, R.R., Dhiva, S. and Inbathamizh, L. 2021. Antimicrobial activity, antiproliferative activity, amylase inhibitory activity and phytochemical analysis of ethanol extract of corn (*Zea mays* L.) silk. *Current Research in Green and Sustainable Chemistry*, 4, 100089.

Adekoya, O.C., Adekoya, G.J., Sadiku, E.R., Hamam, Y. and Ray, S.S. 2022. Application of DFT calculations in designing polymer-based drug delivery systems: An overview. *Pharmaceutics*, 14, 1972.

Adnan, M., Jeon, B.B., Chowdhury, M.H.U., Oh, K.K., Das, T., Chy, M.N.U. and Cho, D.H. 2022. Network pharmacology study to reveal the potentiality of a methanol extract of *Caesalpinia sappan* L. Wood against type-2 diabetes mellitus. *Life*, 12, 277.

Adnan, M., Siddiqui, A.J., Ashraf, S.A., Bardakci, F., Alreshidi, M., Badraoui, R., Noumi, E., Tepe, B., Sachidanandan, M. and Patel, M. 2023. Network pharmacology, molecular docking, and molecular dynamics simulation to elucidate the molecular targets and potential mechanism of *Phoenix dactylifera* (Ajwa Dates) against Candidiasis. *Pathogens*, 12, 1369.

Afolayan, A.J. and Sunmonu, T.O. 2010. *In vivo* studies on antidiabetic plants used in South African herbal medicine. *Journal of Clinical Biochemistry and Nutrition*, 47, 98-106.

Agamah, F.E., Mazandu, G.K., Hassan, R., Bope, C.D., Thomford, N.E., Ghansah, A. and Chimusa, E.R. 2020. Computational/in silico methods in drug target and lead prediction. *Briefings in Bioinformatics*, 21, 1663- 1675.

Ahmed, A.M. 2002. History of diabetes mellitus. *Saudi Medical Journal*, 23, 373-378.

Ahmed, S., Ali, M.C., Ruma, R.A., Mahmud, S., Paul, G.K., Saleh, M.A., Alshahrani, M.M., Obaidullah, A.J., Biswas, S.K. and Rahman, M.M. 2022. Molecular Docking and Dynamics Simulation of Natural Compounds from Betel Leaves (*Piper betle* L.) For Investigating the Potential Inhibition of Alpha-Amylase and Alpha-Glucosidase of Type 2 Diabetes. *Molecules*, 27, 4526.

Ahrén, B. 2011. GLP-1 for type 2 diabetes. *Experimental Cell Research*, 317, 1239-1245.

Akoonjee, A., Rampadarath, A., Aruwa, C.E., Ajiboye, T.A., Ajao, A.A.N. and Sabiu, S. 2022. Network pharmacology-and molecular dynamics simulation-based bioprospection of *Aspalathus linearis* for type-2 diabetes care. *Metabolites*, 12, 1013.

Aladejana, A.E., Bradley, G. and Afolayan, A.J. 2020. *In vitro* evaluation of the anti-diabetic potential of *Helichrysum petiolare* Hilliard and BL Burtt using HepG2 (C3A) and L6 cell lines. *F1000Research*, 9.

Alam, S., Sarker, M.M.R., Sultana, T.N., Chowdhury, M.N.R., Rashid, M.A., Chaity, N.I., Zhao, C., Xiao, J., Hafez, E.E., Khan, S.A. and Mohamed, I.N. 2022. Antidiabetic phytochemicals from medicinal plants: prospective candidates for new drug discovery and development. *Frontiers In Endocrinology*, 13, 800714.

Alimin, L. 2020. Effects of corn silk (*Stigma Maydis*) against blood glucose levels of type 2 diabetes mellitus patients. *Buletin Farmatera*, 202-207.

Al-Oqail, M.M., Al-Sheddi, E.S., Farshori, N.N., Al-Massarani, S.M., Al-Turki, E.A., Ahmad, J., Al-Khedhairy, A.A. and Siddiqui, M.A. 2019. Corn silk (*Zea mays* L.) induced apoptosis in human breast cancer (MCF-7) cells via the ROS-mediated mitochondrial pathway. *Oxidative Medicine and Cellular Longevity*, 2019.

Alvarado-Díaz, C.S., Gutiérrez-Méndez, N., Mendoza-López, M.L., Rodríguez-Rodríguez, M.Z., Quintero-Ramos, A., Landeros-Martínez, L.L., Rodríguez-Valdez, L.M., Rodríguez-Figueroa, J.C., Pérez-Vega, S., Salmeron-Ochoa, I. and Leal-Ramos, M.Y. 2019. Inhibitory effect of saccharides and phenolic compounds from maize silks on intestinal α-glucosidases. *Journal of Food Biochemistry*, 43, 12896.

American Diabetes Association. 2014. Diagnosis and classification of diabetes mellitus. *Diabetes Care*, 37 (Supplement 1), S1. 81-90.

American Diabetes Association. 2023. Health and wellness; insulin basics, retrieved from https://diabetes.org/healthy-living/medication-treatments/insulin-other-injectables/insulin-basics, accessed on 30/12/2023

An, W., Huang, Y., Chen, S., Teng, T., Shi, Y., Sun, Z. and Xu, Y. 2021. Mechanisms of *Rhizoma Coptidis* against type 2 diabetes mellitus explored by network pharmacology combined with molecular docking and experimental validation. *Scientific Reports*, 11, 20849.

Aribisala, J.O., Abdulsalam, R.A., Dweba, Y., Madonsela, K. and Sabiu, S. 2022. Identification of secondary metabolites from *Crescentia cujete* as promising antibacterial therapeutics targeting type 2A topoisomerases through molecular dynamics simulation. *Computers in Biology and Medicine*, 145, 105432.

Arif, R., Ahmad, S., Mustafa, G., Mahrosh, H.S., Ali, M., Tahir ul Qamar, M. and Dar, H.R. 2021. Molecular docking and simulation studies of antidiabetic agents devised from hypoglycemic polypeptide-P of *Momordica charantia*. *Biomed Research International*, 2021.

Assadi, M.H. and Hanaor, D.A. 2013. Theoretical study on copper's energetics and magnetism in TiO2 polymorphs. *Journal of Applied Physics*, 113, 233913

Aukkanit, N., Kemngoen, T. and Ponharn, N. 2015. Utilization of corn silk in low fat meatballs and its characteristics. *Procedia-Social and Behavioural Sciences*, 197, 1403-1410.

Bai, H., Hai, C., Xi, M., Liang, X. and Liu, R. 2010. Protective effect of maize silks (*Maydis stigma*) ethanol extract on radiation-induced oxidative stress in mice. *Plant Foods for Human Nutrition*, 65, 271-276.

Balogun, F.O., Tshabalala, N.T. and Ashafa, A.O.T. 2016. Antidiabetic medicinal plants used by the Basotho tribe of Eastern Free State: a review. *Journal of Diabetes Research*, 2016, 4602820.

Balogun, F.O., Naidoo, K., Aribisala, J.O., Pillay, C. and Sabiu, S. 2022. Cheminformatics identification and validation of dipeptidyl peptidase-iv modulators from shikimate pathway-derived phenolic acids towards interventive type-2 diabetes therapy. *Metabolites*, 12, 937.

Banwari, M., Kawathekar, N. and Jain, G. 2023. Pathophysiology and treatment of type 2 diabetes mellitus: A Review. *Journal of Coastal Life Medicine,* 11,1171-1193.

Blahova, J., Martiniakova, M., Babikova, M., Kovacova, V., Mondockova, V. and Omelka, R. 2021. Pharmaceutical drugs and natural therapeutic products for the treatment of type 2 diabetes mellitus. *Pharmaceuticals*, 14, 806.

Bourebaba, N., Kornicka-Garbowska, K., Marycz, K., Bourebaba, L. and Kowalczuk, A. 2021. *Laurus nobilis* ethanolic extract attenuates hyperglycemia and hyperinsulinemia-induced insulin resistance in HepG2 cell line through the reduction of oxidative stress and improvement of mitochondrial biogenesis–Possible implication in pharmacotherapy. *Mitochondrion*, 59, 190-213.

Bosenberg, L.H. and Van Zyl, D.G. 2008. The mechanism of action of oral antidiabetic drugs: A review of recent literature. *Journal of Endocrinology, Metabolism and Diabetes in South Africa*, 13, 80-88.

Buchanan, T.A. and Xiang, A.H. 2005. Gestational diabetes mellitus. *The Journal of Clinical Investigation*, 115, 485-491.

Cao, Z.Q., Wang, X.X., Lu, L., Xu, J.W., Li, X.B., Zhang, G.R., Ma, Z.J., Shi, A.C., Wang, Y. and Song, Y.J. 2019. β-Sitosterol and gemcitabine exhibit synergistic anti-pancreatic

cancer activity by modulating apoptosis and inhibiting epithelial–mesenchymal transition by deactivating Akt/GSK-3β signaling. *Frontiers in Pharmacology*, 9, 1525.

Chaachouay, N., Benkhnigue, O., El Ibaoui, H., El Ayadi, R. and Zidane, L. 2019. Medicinal plants used for diabetic problems in the Rif, Morocco. *Ethnobotany Research and Applications*, 18, 1-19.

Chaiittianan, R., Chayopas, P., Rattanathongkom, A., Tippayawat, P. and Sutthanut, K. 2016. Anti-obesity potential of corn silks: Relationships of phytochemicals and antioxidation, anti-pre-adipocyte proliferation, anti-adipogenesis, and lipolysis induction. *Journal of Functional Foods*, 23, 497-510.

Chaiittianan, R., Sutthanut, K. and Rattanathongkom, A. 2017. Purple corn silk: A potential anti-obesity agent with inhibition on adipogenesis and induction on lipolysis and apoptosis in adipocytes. *Journal of Ethnopharmacology*, 201, 9-16.

Chandler-Laney, P.C., Phadke, R.P., Granger, W.M., Fernández, J.R., Muñoz, J.A., Man, C.D., Cobelli, C., Ovalle, F. and Gower, B.A. 2011. Age-related changes in insulin sensitivity and β-cell function among European-American and African-American women. *Obesity*, 19, 528-535.

Chandran, U., Mehendale, N., Patil, S., Chaguturu, R. and Patwardhan, B. 2017. Network pharmacology. *Innovative Approaches in Drug Discovery*, 127.

Chang, C.C., Yuan, W., Roan, H.Y., Chang, J.L., Huang, H.C., Lee, Y.C., Tsay, H.J. and Liu, H.K. 2016. The ethyl acetate fraction of corn silk exhibits dual antioxidant and anti-glycation activities and protects insulin-secreting cells from glucotoxicity. *BMC Complementary and Alternative Medicine*, 16, 1-11.

Chaudhary, R.K., Karoli, S.S., Dwivedi, P.S. and Bhandari, R. 2022. Anti-diabetic potential of corn silk (*Stigma maydis*): an in-silico approach. *Journal of Diabetes and Metabolic Disorders,* 21, 445-454.

Chatterjee, S., Khunti, K. and Davies, M.J. 2017. Type 2 diabetes. *The Lancet*, 389, 2239-2251.

Chen, F.C., Shen, K.P., Ke, L.Y., Lin, H.L., Wu, C.C. and Shaw, S.Y. 2019. Flavonoids from *Camellia sinensis* (L.) O. Kuntze seed ameliorates TNF-α induced insulin resistance in HepG2 cells. *Saudi Pharmaceutical Journal,* 27, 507-516.

Chen, S., Chen, H., Tian, J., Wang, Y., Xing, L. and Wang, J. 2013. Chemical modification, antioxidant and α-amylase inhibitory activities of corn silk polysaccharides. *Carbohydrate Polymers*, 98, 428-437.

Chen, S.L., Yu, H., Luo, H.M., Wu, Q., Li, C.F. and Steinmetz, A. 2016. Conservation and sustainable use of medicinal plants: problems, progress, and prospects. *Chinese Medicine*, 11, 1-10.

Chen, L., Teng, H. and Cao, H. 2019. Chlorogenic acid and caffeic acid from *Sonchus oleraceus* Linn synergistically attenuate insulin resistance and modulate glucose uptake in HepG2 cells. *Food and Chemical Toxicology*, 127, 182-187.

Chen, L., Lin, X., Fan, X., Qian, Y., Lv, Q. and Teng, H. 2020. *Sonchus oleraceus* Linn extract enhanced glucose homeostasis through the AMPK/Akt/GSK-3β signaling pathway in diabetic liver and HepG2 cell culture. *Food and Chemical Toxicology*, 136, 111072.

Centre for Disease Control and Prevention, United States Department of Heath and Human Services. 2022. Gestational diabetes and pregnancy, retrieved from https://www.cdc.gov/pregnancy/diabetes-gestational.html#:~:text=Often%20gestational%20diabetes%20can%20be,diabetes%20must%20also%20take%20insulin, accessed on 30/12/2023.

Chiefari, E., Arcidiacono, B., Foti, D. and Brunetti, A. 2017. Gestational diabetes mellitus: an updated overview. *Journal of Endocrinological Investigation*, 40, 899-909.

Choi, D.J., Kim, S.L., Choi, J.W. and Park, Y.I. 2014. Neuroprotective effects of corn silk maysin via inhibition of H2O2-induced apoptotic cell death in SK-N-MC cells. *Life Sciences*, 109, 57-64.

Cole, J.B. and Florez, J.C. 2020. Genetics of diabetes mellitus and diabetes complications. *Nature Reviews Nephrology*, 16, 377-390.

da Hora, N.R., Santana, L.F., da Silva, V.D.A., Costa, S.L., Zambotti-Villela, L., Colepicolo, P., Ferraz, C.G. and Ribeiro, P.R. 2021. Identification of bioactive metabolites from corn silk extracts by a combination of metabolite profiling, univariate statistical analysis and chemometrics. *Food Chemistry*, 365, 130479.

Daneman, D. 2006. Type 1 diabetes. *The Lancet*, 367, 847-858.

Daryabor, G., Atashzar, M.R., Kabelitz, D., Meri, S. and Kalantar, K. 2020. The effects of type 2 diabetes mellitus on organ metabolism and the immune system. *Frontiers in Immunology,* 11, 546198.

Davids, D., Gibson, D. and Johnson, Q. 2016. Ethnobotanical survey of medicinal plants used to manage high blood pressure and type 2 diabetes mellitus in Bitterfontein, Western Cape Province, South Africa. *Journal of Ethnopharmacology*, 194, 755-766.

Deacon, C.F. 2020. Dipeptidyl peptidase 4 inhibitors in the treatment of type 2 diabetes mellitus. *Nature Reviews Endocrinology*, 16, 642-653.

Desmet, S., Saeys, Y., Verstaen, K., Dauwe, R., Kim, H., Niculaes, C., Fukushima, A., Goeminne, G., Vanholme, R., Ralph, J. and Boerjan, W. 2021. Maize specialized metabolome networks reveal organ-preferential mixed glycosides. *Computational and Structural Biotechnology Journal,* 19, 1127-1144.

Deutschländer, M.S., Lall, N. and Van De Venter, M. 2009. Plant species used in the treatment of diabetes by South African traditional healers: An inventory. *Pharmaceutical Biology,* 47, 348-365.

De Vivo, M., Masetti, M., Bottegoni, G. and Cavalli, A. 2016. Role of molecular dynamics and related methods in drug discovery. *Journal of Medicinal Chemistry*, 59, 4035-4061.

Diallo, A., Traore, M.S., Keita, S.M., Balde, M.A., Keita, A., Camara, M., Van Miert, S., Pieters, L. and Balde, A.M. 2012. Management of diabetes in Guinean traditional medicine: an ethnobotanical investigation in the coastal lowlands. *Journal of Ethnopharmacology*, 144, 353-361.

Di, S., Han, L., An, X., Kong, R., Gao, Z., Yang, Y., Wang, X., Zhang, P., Ding, Q., Wu, H. and Wang, H. 2021. *In silico* network pharmacology and in vivo analysis of berberine-related mechanisms against type 2 diabetes mellitus and its complications. *Journal of Ethnopharmacology*, 276, 114180.

Dludla, P.V., Muller, C.J., Louw, J., Mazibuko-Mbeje, S.E., Tiano, L., Silvestri, S., Orlando, P., Marcheggiani, F., Cirilli, I., Chellan, N. and Ghoor, S. 2020. The combination effect of aspalathin and phenylpyruvic acid-2-o-β-d-glucoside from rooibos against hyperglycemia-induced cardiac damage: an *in vitro* study. *Nutrients*, 12, 1151.

Dong, Y., Gong, L. J., Lu, J. L., Chen, P. L. 2009. Clinical trial of corn silk for the treatment of initial diagnosis of hypertension. *Chinese Journal of Integrative Medicine on Cardio-/Cerebrovascular Disease*. 7, 643.

Dong, W., Zhao, Y., Hao, Y., Sun, G., Huo, J. and Wang, W. 2022. Integrated molecular biology and metabonomics approach to understand the mechanism underlying reduction of insulin resistance by corn silk decoction. *Journal of Ethnopharmacology,* 284, 114756.

Emeka, P.M. and Badger-emeka, L.O.R.I.N.A. 2016. Mechanism of action of plants in relation to their medicinal properties. *Phytotherapeutic*s, 43, 471-484.

Erzse, A., Stacey, N., Chola, L., Tugendhaft, A., Freeman, M. and Hofman, K. 2019. The direct medical cost of type 2 diabetes mellitus in South Africa: a cost of illness study. *Global Health Action,* 12, 1636611

Eweas, A.F., Maghrabi, I.A. and Namarneh, A.I. 2014. Advances in molecular modeling and docking as a tool for modern drug discovery. *Der Pharma Chemica*, 6, 211-218.

Fougère, L., Zubrzycki, S., Elfakir, C. and Destandau, E. 2023. Characterization of corn silk extract using HPLC/HRMS/MS analyses and bioinformatic data processing. *Plants*, 12, 721.

Galicia-Garcia, U., Benito-Vicente, A., Jebari, S., Larrea-Sebal, A., Siddiqi, H., Uribe, K.B., Ostolaza, H. and Martín, C. 2020. Pathophysiology of type 2 diabetes mellitus. *International Journal of Molecular Sciences,* 21, 6275.

Ge, Q., Chen, L., Yuan, Y. and Chen, K. 2020. Network pharmacology-based dissection of the anti-diabetic mechanism of Lobelia chinensis. *Frontiers in Pharmacology*, 11, 489502.

Gaba, M., Gaba, P., Singh, S. and Gupta, G.D. 2010. An overview on molecular docking. *International Journal of Drug Development and Research*, 2, 219-231.

Ghada, M., Eltohami, M.S., Adurahman, H.N., Mahmoud, M.E. and Mudawi, I. 2014. *In vitro* study of the effect of corn silk on glucose uptake by isolated rat hemi-diaphragm. *World Journal of Pharmaceutical Research*, 3, 2190-2195.

Gilbert, M.P. and Pratley, R.E. (2020). GLP-1 analogs and DPP-4 inhibitors in type 2 diabetes therapy: review of head-to-head clinical trials. *Frontiers in Endocrinology*, 11, 178.

Glovaci, D., Fan, W. and Wong, N.D. 2019 Epidemiology of diabetes mellitus and cardiovascular disease. *Current Cardiology Reports*, 21, 1-19.

Gbolade, A.A. (2009). Inventory of antidiabetic plants in selected districts of Lagos State, Nigeria. *Journal of Ethnopharmacology*. 121, 135-139.

Gu, J., Gui, Y., Chen, L., Yuan, G., Lu, H.Z. and Xu, X. 2013. Use of natural products as chemical library for drug discovery and network pharmacology. *PloS One*, 8, 62839.

Gu, W. Z., Tan, C. F. 2015. 32 cases of H-type hypertension treated with modified corn silk tea and folicin. *Traditional Chinese Medicine Research*, 8, 27.

Guli, A. T., Liu, H., Jin, Y. 2017. Clinical analysis of corn silk used to mild and severe preeclampsia. *Journal of the Chinese Medical Association*, 33, 99.

Guo, J., Liu, T., Han, L. and Liu, Y. 2009. The effects of corn silk on glycaemic metabolism. *Nutrition and Metabolism*, 6, 1-6.

Guo, H., Guan, H., Yang, W., Liu, H., Hou, H., Chen, X., Liu, Z., Zang, C., Liu, Y. and Liu, J. 2017. Pro-apoptotic and anti-proliferative effects of corn silk extract on human colon cancer cell lines. *Oncology Letters*, 13, 973-978.

Guo, S.Y., Wu, J.R., Zhou, W., Jia, S.S., Zhang, J.Y. and Meng, Z.Q. 2019. Study on mechanism of safflower ruyi pills in treatment of gynecological diseases based on network pharmacology. *Evaluation and Analysis of Drug-Use in Hospitals of China*, 19, 257-264.

Haldar, S., Gan, L., Tay, S.L., Ponnalagu, S. and Henry, C.J. 2019. Postprandial glycemic and insulinemic effects of the addition of aqueous extracts of dried corn silk, cumin seed powder or tamarind pulp, in two forms, consumed with high glycemic index rice. *Foods*, 8, 437.

Haller, M.J., Atkinson, M.A. and Schatz, D. 2005. Type 1 diabetes mellitus: etiology, presentation, and management. *Pediatric Clinics*, 52, 1553-1578.

Hasanudin, K., Hashim, P. and Mustafa, S. 2012. Corn silk (*Stigma maydis*) in healthcare: a phytochemical and pharmacological review. *Molecules*, 17, 9697-9715.

Hasani-Ranjbar, S., Larijani, B. and Abdollahi, M. 2008. A systematic review of Iranian medicinal plants useful in diabetes mellitus. *Archives of Medical Science*, 4, 285-292.

Hassan, M.H., Salem, M.A. and Doweidar, M.M. 2021. Preparation and evaluation of healthy crackers by using flour mixes of different types of cereal. *Journal of Food and Dairy Sciences*, 12, 23-32.

Haslina, H., Praseptiangga, D., Bintoro, V.P. and Pujiasmanto, B. 2017. Chemical and phytochemical characteristics of local corn silk powder of three different varieties. *International Journal on Advanced Science, Engineering and Information Technology*, 7, 1957-1963.

Healthdirect. 2021. Type 2 diabetes, retrieved from https://www.healthdirect.gov.au/type-2-diabetes, accessed on 12/20/2023.

Helmstädter, J., Keppeler, K., Küster, L., Münzel, T., Daiber, A. and Steven, S. 2022. Glucagon-like peptide-1 (GLP-1) receptor agonists and their cardiovascular benefits—The role of the GLP-1 receptor. *British Journal of Pharmacology*, 179, 659-676.

Helmy, A., El-Shazly, M., Seleem, A., Abdelmohsen, U., Salem, M.A., Samir, A., Rabeh, M., Elshamy, A. and Singab, A.N.B. 2020. The synergistic effect of biosynthesized silver nanoparticles from a combined extract of parsley, corn silk, and gum arabic: *in vivo* antioxidant, anti-inflammatory and antimicrobial activities. *Materials Research Express*, 7, 025002.

Ho, T.Y., Li, C.C., Lo, H.Y., Chen, F.Y. and Hsiang, C.Y. 2017. Corn silk extract and its bioactive peptide ameliorated lipopolysaccharide-induced inflammation in mice via the nuclear factor-κB signaling pathway. *Journal of Agricultural and Food Chemistry*, 65, 759-768.

Hohenberg, P. and Kohn, W.J.P.R. 1964. Density functional theory (DFT). *Physical Review Letters*, 136, 864.

Hongsuwan, N. and Sutthanut, K. 2018. Comparison of chemical compositions, nutritional values, antioxidant and tyrosinase inhibition activities in corn silk of three different corn varieties. *Journal of Traditional Thai and Alternative Medicine*, 16, 362-371.

Hostettmann, K., Marston, A., Ndjoko, K. and Wolfender, J.L. 2000. The potential of African plants as a source of drugs. *Current Organic Chemistry*, 4, 973-1010.

Hsiang, C.Y., Lo, H.Y., Lu, G.L., Liao, P.Y. and Ho, T.Y. 2024. A novel heat-stable angiotensin-converting enzyme zinc-binding motif inhibitory peptide identified from corn silk. *Journal of Ethnopharmacology*, 320, 117435.

Hu, Q.L., Zhang, L.J., Li, Y.N., Ding, Y.J. and Li, F.L. 2010. Purification and anti-fatigue activity of flavonoids from corn silk. *International Journal of Physical Sciences*, 5, 321-326.

Huang, Q., Chen, L., Teng, H., Song, H., Wu, X. and Xu, M. 2015. Phenolic compounds ameliorate the glucose uptake in HepG2 cells' insulin resistance via activating AMPK: anti-diabetic effect of phenolic compounds in HepG2 cells. *Journal of Functional Foods*, 19, 487-494.

Ilyas, U., Nazir, B., Altaf, R., Muhammad, S.A., Zafar, H., Paiva-Santos, A.C., Abbas, M. and Duan, Y. 2022. Investigation of anti-diabetic potential and molecular simulation studies of dihydropyrimidinone derivatives. *Frontiers in Endocrinology*, 13, 1022623.

International Diabetes Federation (IDF), 2023, retrieved from https://idf.org/about-diabetes/type-2-diabetes/, accessed 05/08/2023

Ismael, R.H., Ahmed, S.A. and Mahmoud, S.S. 2017. Detection of rutin, kaepferol, and quercetin based crude from corn silk and studying their effects on the inhibition of pure urease enzyme and urease of *Klebsiella species*. *International Journal of Current Microbiology and Applied Sciences*, 6, 2676-2685.

International Diabetes Federation (IDF), 2021, retrieved from https://idf.org/our-network/regions-and-members/africa/members/south-africa/, accessed on 05/08/2023.

Jia, Y., Xue, Z., Wang, Y., Lu, Y., Li, R., Li, N., Wang, Q., Zhang, M. and Chen, H. 2021. Chemical structure and inhibition on α-glucosidase of polysaccharides from corn silk by fractional precipitation. *Carbohydrate Polymers*, 252, 117185.

Karamanou, M., Protogerou, A., Tsoucalas, G., Androutsos, G. and Poulakou-Rebelakou, E. 2016. Milestones in the history of diabetes mellitus: The main contributors. *World Journal of Diabetes*, 7, 1.

Katsila, T., Spyroulias, G.A., Patrinos, G.P. and Matsoukas, M.T. 2016. Computational approaches in target identification and drug discovery. *Computational and Structural Biotechnology Journal*, 14, 177-184.

Kaul, K., Tarr, J.M., Ahmad, S.I., Kohner, E.M. and Chibber, R. 2013. Introduction to diabetes mellitus. *Diabetes: An Old Disease, A New Insight*, 2013, 1-11.

Kaur, D., Kaur, D., Bains, N.A.V.P.R.E.E.T., Chopra, A.N.U.J.A. and Arora, P.O.O.N.A.M. 2015. Anti-anxiety evaluation of extracts of *Stigma maydis* (corn silk). *International Journal of Pharmacy and Pharmaceutical Sciences*, 8, 309-312.

Kaur, P., Singh, J., Kaur, M., Rasane, P., Kaur, S., Kaur, J., Nanda, V., Mehta, C.M. and Sowdhanya, D. 2023. Corn silk as an agricultural waste: a comprehensive review on its nutritional composition and bioactive potential. *Waste and Biomass Valorisation*, 14, 1413-1432.

Kautzky-Willer, A., Prager, R., Waldhäusl, W., Pacini, G., Thomaseth, K., Wagner, O.F., Ulm, M., Streli, C. and Ludvik, B. 1997. Pronounced insulin resistance and inadequate β-cell secretion characterize lean gestational diabetes during and after pregnancy. *Diabetes Care*, 20, 1717-1723.

Kasali, M.F., Mahano, A.O., Bwironde, F.M., Amani, A.C., Mangambu, J.D., Nyakabwa, D.S., Wimba, L.K., Tshibangu, D.S.T., Ngbolua, K.N., Kambale, J.K. and Mpiana, P.T. 2013. Ethnopharmacological survey of plants used against diabetes in Bukavu city (DR Congo). *The Journal of Ethnobiology and Traditional Medicine, Photon*, 119, 538-546.

Kasina, S.V.S.K., Baradhi, K.M. 2023. Dipeptidyl Peptidase IV (DPP IV) Inhibitors. StatPearls Publishing, retrieved from https://www.ncbi.nlm.nih.gov/books/NBK542331/, accessed on 30/12/2023.

Khanal, P. and Patil, B.M. 2021. Integration of network and experimental pharmacology to decipher the antidiabetic action of *Duranta repens* L. *Journal of Integrative Medicine*, 19, 66-77.

Kifle, Z.D., Yesuf, J.S. and Atnafie, S.A. 2020. Evaluation of *in vitro* and *in vivo* anti-diabetic, anti-hyperlipidemic and anti-oxidant activity of flower crude extract and solvent fractions of *Hagenia abyssinica* (rosaceae). *Journal of Experimental Pharmacology*, 151-167.

Kim, D.H., Kim, D.W., Jang, J.Y., Lee, N., Ko, Y.J., Lee, S.M., Kim, H.J., Na, K. and Son, S.U. 2020. Fe3O4@ void@ microporous organic polymer-based multifunctional drug

delivery systems: targeting, imaging, and magneto-thermal behaviors. *ACS Applied Materials and Interfaces*, 12, 37628-37636

Khan, A., Unnisa, A., Sohel, M., Date, M., Panpaliya, N., Saboo, S.G., Siddiqui, F. and Khan, S. 2022. Investigation of metabolites of *Enicostemma littorale* as potential glucokinase activators through molecular docking for the treatment of type 2 diabetes mellitus. *In Silico Pharmacology*, 10, 1.

Khan, M.A.B., Hashim, M.J., King, J.K., Govender, R.D., Mustafa, H. and Al Kaabi, J. 2020. Epidemiology of type 2 diabetes–global burden of disease and forecasted trends. *Journal of Epidemiology and Global Health*, 10, 107-111.

Khardori, R. and Griffing, G. 2023. Type 1 diabetes mellitus treatment and management. Medscape, retrieved from https://emedicine.medscape.com/article/117739-treatment?form=fpf#d10, accessed on 30/12/2023.

Kharroubi, A.T. and Darwish, H.M. 2015. Diabetes mellitus: The epidemic of the century. *World Journal of Diabetes*, 6, 850.

Kim, C., Newton, K.M. and Knopp, R.H. 2002. Gestational diabetes and the incidence of type 2 diabetes: a systematic review. *Diabetes Care*, 25, 1862-1868.

Kohn, W. and Sham, L.J. 1965. Self-consistent equations including exchange and correlation effects. *Physical Review*, 140, 1133.

Kokil, GR., Veedu, RN., Ramm, GA., Prins, JB. and Parekh, HS. 2015. Type 2 diabetes mellitus: limitations of conventional therapies and intervention with nucleic acid-based therapeutics. *Chemical Reviews*, 115. 4719-4743.

Koparde, A.A., Doijad, R.C. and Magdum, C.S. 2019. Natural products in drug discovery. *In Pharmacognosy-medicinal Plants*. IntechOpen.

Kahksha, Alam, O., Al-Keridis, L.A., Khan, J., Naaz, S., Alam, A., Ashraf, S.A., Alshammari, N., Adnan, M. and Beg, M.A. 2023. Evaluation of antidiabetic effect of luteolin in STZ induced diabetic rats: molecular docking, molecular dynamics, *in vitro* and *in vivo* studies. *Journal of Functional Biomaterials*, 14, 126.

Kaur, P., Singh, J., Kaur, M., Rasane, P., Kaur, S., Kaur, J., Nanda, V., Mehta, C.M. and Sowdhanya, D. 2023. Corn silk as an agricultural waste: A comprehensive review on its

nutritional composition and bioactive potential. *Waste and Biomass Valorization*, 14, 1413-1432.

Kirrella, A.A., Abdo, S.E., El-Naggar, K., Soliman, M.M., Aboelenin, S.M., Dawood, M.A. and Saleh, A.A. 2021. Use of corn silk meal in broiler diet: Effect on growth performance, blood biochemistry, immunological responses, and growth-related gene expression. *Animals*, 11, 1170.

Krusong, W., Sriphochanart, W., Suwapanich, R., Mekkerdchoo, O., Sriprom, P., Wipatanawin, A. and Massa, S. 2020. Healthy dried baby corn silk vinegar production and determination of its main organic volatiles containing antimicrobial activity. *Lwt*, 117, 108620.

Laeliocattleya, R.A., Prasiddha, I.J., Estiasih, T., Maligan, J.M. and Muchlisyiyah, J. 2014. The potential of bioactive compounds from corn silk (*Zea mays* L.) that result from gradual fractionation using organic solvents for the use as a natural sunscreen. *Jurnal Teknologi Pertanian,* 15.

Landeros-Martínez, L.L., Campos-Almazán, M.I., Sánchez-Bojorge, N.A., Flores, R., Palomares-Báez, J.P. and Rodríguez-Valdez, L.M. 2023. Theoretical studies for the discovery of potential sucrase-isomaltase inhibitors from maize silk phytochemicals: an approach to treatment of type 2 diabetes. *Molecules*, 28, 6778.

Langhans, S.A. 2018. Three-dimensional *in vitro* cell culture models in drug discovery and drug repositioning. *Frontiers in Pharmacology*, 9, 334617.

Lankatillake, C., Huynh, T. and Dias, D.A. 2019. Understanding glycaemic control and current approaches for screening antidiabetic natural products from evidence-based medicinal plants. *Plant Methods*, 15, 105.

LaPointe, S.M. and Weaver, D.F. 2007. A review of density functional theory quantum mechanics as applied to pharmaceutically relevant systems. *Current Computer-Aided Drug Design*, 3, 290-296.

Lebovitz, H.E. 2019. Thiazolidinediones: the forgotten diabetes medications. *Current Diabetes Reports,* 19, 151.

Lee, J., Kim, S.L., Lee, S., Chung, M.J. and Park, Y.I. 2014. Immunostimulating activity of maysin isolated from corn silk in murine RAW 264.7 macrophages. *BMB Reports*, 47, 382.

Lende, M. and Rijhsinghani, A. 2020. Gestational diabetes: overview with emphasis on medical management. *International Journal of Environmental Research and Public Health*, 17, 9573.

Leung, E.L., Cao, Z.W., Jiang, Z.H., Zhou, H. and Liu, L. 2013. Network-based drug discovery by integrating systems biology and computational technologies. *Briefings in Bioinformatics*, 14, 491-505.

Li, C.C., Lee, Y.C., Lo, H.Y., Huang, Y.W., Hsiang, C.Y. and Ho, T.Y. 2019. Antihypertensive effects of corn silk extract and its novel bioactive constituent in spontaneously hypertensive rats: the involvement of angiotensin-converting enzyme inhibition. *Molecules*, 24, 1886.

Li, Y., Hu, Z., Wang, X., Wu, M., Zhou, H. and Zhang, Y. 2020. Characterization of a polysaccharide with antioxidant and anti-cervical cancer potentials from the corn silk cultivated in Jilin province. *International Journal of Biological Macromolecules*, 155, 1105-1113.

Liang, H., Zhang, R., Zhou, L., Wu, X., Chen, J., Li, X., Chen, J., Shan, L. and Wang, H. (2024). Corn stigma ameliorates hyperglycemia in zebrafish and GK rats of type 2 diabetes. *Journal of Ethnopharmacology*, 325, 117746.

Limmatvapirat, C., Nateesathittarn, C., Dechasathian, K., Moohummad, T., Chinajitphan, P. and Limmatvapirat, S. 2020. Phytochemical analysis of baby corn silk extracts. *Journal of Ayurveda and Integrative Medicine*, 11, 344-351.

Liu, J., Wang, C., Wang, Z., Zhang, C., Lu, S. and Liu, J. 2011. The antioxidant and free-radical scavenging activities of extract and fractions from corn silk (*Zea mays* L.) and related flavone glycosides. *Food Chemistry*, 126, 261-269.

Liu, H., Jin, Y. 2017. The clinical effect of corn silk in the treatment of gestational hypertension. *China Rural Health*, 3 , 68-69.

Liu, X.K., Wu, J.R., Lin, M.J. and Zhang, X.M. 2017. Mechanism of Si Junzitang based on network pharmacology. *Chinese Journal of Experimental Traditional Medical Formulae*, 23, 194-202.

Macel, M., Visschers, I.G., Peters, J.L., Kappers, I.F., de Vos, R.C. and van Dam, N.M. 2019. Metabolomics of thrips resistance in pepper (*Capsicum spp*.) reveals monomer and

dimer acyclic diterpene glycosides as potential chemical defenses. *Journal of Chemical Ecology*, 45, 490-501.

Mane, P.B., Antre, R.V. and Oswal, R.J. (2012). Antidiabetic drugs: An overview. *International Journal of Pharmaceutical and Chemical Sciences*, 1, 301-306.

Marina, A.M., Rosli, W.W. and Neoh, S.L. 2014. Frying quality of virgin coconut oil as affected by *Zea mays* extract. Sains Malaysiana, 43, 1311-1315.

Masunda, A.T., Inkoto, C.L., Bongo, G.N., Wa Oloko, J.D., Ngbolua, K.N., Tshibangu, D.S.T., Tshilanda, D.D. and Mpiana, P.T. 2019. Ethnobotanical and ecological studies of plants used in the treatment of diabetes in Kwango, Kongo central and Kinshasa in the Democratic Republic of the Congo. *International Journal of Diabetes and Endocrinology*, 4, 18-25.

Mayosi, B.M., Flisher, A.J., Lalloo, U.G., Sitas, F., Tollman, S.M. and Bradshaw, D. 200). The burden of non-communicable diseases in South Africa. *The Lancet*, 374, 934-947.

McConkey, B.J., Sobolev, V. and Edelman, M. 2002. The performance of current methods in ligand–protein docking. *Current Science*, 845-856.

McGrew, Roderick. 1985. Encyclopaedia of medical history. 1st ed, London (United Kingdom). *McMillam Press*, 74.

McIntyre, H.D., Catalano, P., Zhang, C., Desoye, G., Mathiesen, E.R. and Damm, P. 2019. Gestational diabetes mellitus. *Nature Reviews Disease Primers*, 5, 47.

Mechchate, H., Es-safi, I., Bari, A., Grafov, A. and Bousta, D. 2020. Ethnobotanical survey about the management of diabetes with medicinal plants used by diabetic patients in region of FezMeknes, Morocco. *Journal of Ethnobotany Research and Applications*. 19, 1-28.

Meier, J.J. 2012. GLP-1 receptor agonists for individualized treatment of type 2 diabetes mellitus. *Nature Reviews Endocrinology*, 8, 728-742.

Meneses, M.J., Silva, B.M., Sousa, M., Sá, R., Oliveira, P.F. and Alves, M.G. 2015. Antidiabetic drugs: mechanisms of action and potential outcomes on cellular metabolism. *Current Pharmaceutical Design*, 21, 3606 -3620.

Michaelidou, M., Pappachan, J.M. and Jeeyavudeen, M.S. (2023). Management of diabesity: current concepts. *World Journal of Diabetes*, 14, 396-411.

Mobasseri, M., Shirmohammadi, M., Amiri, T., Vahed, N., Fard, H.H. and Ghojazadeh, M. 2020. Prevalence and incidence of type 1 diabetes in the world: a systematic review and meta-analysis. *Health Promotion Perspectives,* 10, 98-115.

Mohammed, A. and Tajuddeen, N. 2022. Antidiabetic compounds from medicinal plants traditionally used for the treatment of diabetes in Africa: A review update (2015–2020). *South African Journal of Botany*, 146, 585-602.

Mohammed, A. 2023. Hypoglycemic potential of African medicinal plants in diabetic and non-diabetic human subjects: a review. *Clinical Complementary Medicine and Pharmacology*, 3, 100081.

Moher, M. 2018. Diabetes mellitus, *Integrative Medicine*, 4, 334.

Mohlala, L.M., Bodunrin, M.O., Awosusi, A.A., Daramola, M.O., Cele, N.P. and Olubambi, P.A. 2016. Beneficiation of corncob and sugarcane bagasse for energy generation and materials development in Nigeria and South Africa: A short overview. *Alexandria Engineering Journal,* 55, 3025-3036.

Mohsin, S., Akhtar, N., Mahmood, T., Khan, H. and Mustafa, R. 2016. Formulation and stability of topical water in oil emulsion containing corn silk extract. *Tropical Journal of Pharmaceutical Research*, 15, 1115-1121.

Mokashi, P., Khanna, A., Pandita, N. 2017. Flavonoids from *Enicostema littorale* blume enhances glucose uptake of cells in insulin resistant human liver cancer (HepG2) cell line via IRS-1/PI3K/Akt pathway. *Biomedicine and Pharmacotherapy*, 90, 268-277.

Mthembu, S.X., Muller, C.J., Dludla, P.V., Madoroba, E., Kappo, A.P. and Mazibuko-Mbeje, S.E., 2021. Rooibos flavonoids, aspalathin, isoorientin, and orientin ameliorate antimycin A-induced mitochondrial dysfunction by improving mitochondrial bioenergetics in cultured skeletal muscle cells. *Molecules*, 26, 6289.

Mushtaq, S., Abbasi, B.H., Uzair, B. and Abbasi, R., 2018. Natural products as reservoirs of novel therapeutic agents. *EXCLI Journal*, 17, 420.

Msomi, N.Z., Shode, F.O., Pooe, O.J., Mazibuko-Mbeje, S. and Simelane, M.B. 2019. Iso-mukaadial acetate from *Warburgia salutaris* enhances glucose uptake in the L6 rat myoblast cell line. *Biomolecules*, 9, 520.

Nagahisa, T. and Saisho, Y. 2019. Cardiorenal protection: potential of SGLT2 inhibitors and GLP-1 receptor agonists in the treatment of type 2 diabetes. *Diabetes Therapy*, 10, 1733-1752.

Nathan, C. and Ding, A. (2010). Nonresolving inflammation. *Cell*, 140, 871-882.

National Kidney Foundation. 2023. Sodium-glucose cotransporter-2 (SGLT-2) inhibitors, retrieved from https://www.kidney.org/atoz/content/sglt2-inhibitors#, accessed 30/12/2023.

Nawaz, H., Muzaffar, S., Aslam, M. and Ahmad, S. 2018. Phytochemical composition: antioxidant potential and biological activities of corn. *Corn-production and Human Health in Changing Climate,* 10, 49-68.

Nawaz, H., Aslam, M. and Muntaha, S.T. 2019. Effect of solvent polarity and extraction method on phytochemical composition and antioxidant potential of corn silk. *Free Radicals and Antioxidants,* 9, 5-11.

Nurraihana, H., Wan Rosli, W.I., Sabreena, S. and Norfarizan-Hanoon, N.A. 2018. Optimisation extraction procedure and identification of phenolic compounds from fractional extract of corn silk (*Zea mays* hair) using LC-TOF/MS system. *Journal of Food Measurement and Characterization,* 12, 1852-1862.

eKonomics news team. 2023. Corn development and growth staging, Nutrien eKonomics, retrieved from https://nutrien-ekonomics.com/news/tissue-and-growth-model-corn/, accessed 31/12/2023.

Oguntibeju, O.O. 2019. Hypoglycaemic and anti-diabetic activity of selected African medicinal plants. *International Journal of Physiology, Pathophysiology and Pharmacology*, 11, 224-237.

Oh, K.K., Adnan, M. and Cho, D.H. 2020. Network pharmacology of bioactives from *Sorghum bicolor* with targets related to diabetes mellitus. *PLoS One*, 15, 0240873.

Oh, K.K., Adnan, M. and Cho, D.H. 2021. Elucidating drug-like compounds and potential mechanisms of corn silk (*Stigma Maydis*) against obesity: A network pharmacology study. *Current Issues In Molecular Biology*, 43, 1906-1936.

Okon, A.J., Etim, D.J., Daniel, A.I., Bobson, P.M. and Asuquo, A.E. 2018. Effect of ethanolic extracts of *Persea americana* seed and *Zea mays* silk on blood glucose levels,

body and organ weights of alloxan-induced hyperglycemic Albino wistar rats. *Global Journal of Pure and Applied Sciences*, 24, 153-168.

Olaokun, O.O., Manonga, S.A., Zubair, M.S., Maulana, S. and Mkolo, N.M. 2022. Molecular docking and molecular dynamics studies of antidiabetic phenolic compound isolated from leaf extract of *Englerophytum magalismontanum* (Sond.) TD Penn. *Molecules*, 27, 3175.

Odeyemi, S. and Bradley, G. 2018. Medicinal plants used for the traditional management of diabetes in the Eastern Cape, South Africa: pharmacology and toxicology. *Molecules*, 23, 2759.

Paddy, V., Van Tonder, JJ. and Steenkamp, V. (2014). The antidiabetic activity of a polyherbal tea mixture and its constituents *in vitro*. 17th World Congress of Basic and Clinical Pharmacology. 115, 151.

Padhi, S., Nayak, A.K. and Behera, A. 2020. Type II diabetes mellitus: a review on recent drug based therapeutics. *Biomedicine and Pharmacotherapy*, 131, 110708.

Palani, M., Devan, S., Arunkumar, R. and Vanisree, A.J. 2011. Frequency variations in the methylated pattern of p73/p21 genes and chromosomal aberrations correlating with different grades of glioma among south Indian population. *Medical Oncology*, 28, 445-452.

Paleontological Research Foundation. 2021. Earth@Home, Life cycles of maize, retrieved from https://evolution.earthathome.org/grasses/andropogoneae/maize-life-cycle/, accessed om 31/12/2023

Pan, L., Li, Z., Wang, Y., Zhang, B., Liu, G. and Liu, J. 2020. Network pharmacology and metabolomics study on the intervention of traditional Chinese medicine Huanglian Decoction in rats with type 2 diabetes mellitus. *Journal of Ethnopharmacology*, 258, 112842.

Parviainen, A., Härkönen, T., Ilonen, J., But, A., Knip, M. and Finnish Pediatric Diabetes Register. 2022. Heterogeneity of type 1 diabetes at diagnosis supports existence of age-related endotypes. *Diabetes Care*, 45, 871-879.

Patterson, C.C., Karuranga, S., Salpea, P., Saeedi, P., Dahlquist, G., Soltesz, G. and Ogle, G.D. (2019). Worldwide estimates of incidence, prevalence and mortality of type 1 diabetes

in children and adolescents: Results from the International Diabetes Federation Diabetes Atlas. *Diabetes Research and Clinical Practice*, 157, 107842.

Peumery, J.J., 1987. Histoire illustrée du diabète: de l'antiquité à nos jours. *Dacosta*.

Petry, C.J. 2023. Nutrients as risk factors and treatments for gestational diabetes. *Nutrients*, 15, 4716.

Pheiffer, C., Pillay-van Wyk, V., Joubert, J.D., Levitt, N., Nglazi, M.D. and Bradshaw, D. 2018. The prevalence of type 2 diabetes in South Africa: a systematic review protocol. *BMJ Open*, 8, 021029.

Pheiffer, C., Pillay-van Wyk, V., Turawa, E., Levitt, N., Kengne, A.P. and Bradshaw, D. 2021. Prevalence of type 2 diabetes in South Africa: a systematic review and meta-analysis. *International Journal of Environmental Research and Public Health*, 18, 5868.

Ponnulakshmi, R., Shyamaladevi, B., Selvaraj, J., Valli, G., Purushothaman, V., Alsawalha, M. and Mohan, S.K. (2019). Effect of chebulagic acid on apoptotic regulators in prostate cancer cell line-PC-3. *Drug Invention Today*, 12, 281-285.

Popoola, J.O. and Obembe, O.O. (2013). Local knowledge, use pattern and geographical distribution of *Moringa oleifera* Lam. (Moringaceae) in Nigeria. *Journal of Ethnopharmacology*, 150, 682-691.

Qi, J.H., Chen, P.Y., Cai, D.Y., Wang, Y., Wei, Y.L., He, S.P. and Zhou, W. 2023. Exploring novel targets of sitagliptin for type 2 diabetes mellitus: Network pharmacology, molecular docking, molecular dynamics simulation, and SPR approaches. *Frontiers in Endocrinology*, 13, 1096655.

Rahman, N.A. and Rosli, W.I.W. 2014. Nutritional compositions and antioxidative capacity of the silk obtained from immature and mature corn. *Journal of King Saud University-Science*, 26, 119-127.

Rampadarath, A., Balogun, F.O. and Sabiu, S. 2023. Insights into the mechanism of action of *Helianthus annuus* (sunflower) seed essential oil in the management of type-2 diabetes mellitus using network pharmacology and molecular docking approaches. *Endocrines*, 4, 327-349.

Rampogu, S., Parameswaran, S., Lemuel, M. and Lee, K. (2018). Exploring the therapeutic ability of fenugreek against type 2 diabetes and breast cancer employing molecular docking

and molecular dynamics simulations. *Evidence-based Complementary and Alternative Medicine*, 2018, 1943203.

Rao, A.D., Kuhadiya, N., Reynolds, K. and Fonseca, VA. (2008). Is the combination of sulfonylureas and metformin associated with an increased risk of cardiovascular disease or all-cause mortality? A meta-analysis of observational studies. *Diabetes Care*, 31, 1672-1678.

Ray, SD., Hussain, A., Niha,A., Krmic, M., Jalshgrari, A., Genis, D., Reji, J. (2023). Anti diabetic agents. *Encyclopaedia of Toxicology*, P. Wexler Academic Press, Oxford, 4, 573-589.

Rendell, M. 2004. The role of sulphonylureas in the management of type 2 diabetes mellitus. *Drugs*, 64, 1339-1358.

Ritz, E., Adamczak, M. and Wiecek, A. 2013. Chapter 2—carbohydrate metabolism in kidney disease and kidney failure. *Nutritional Management of Renal Disease*, 3, 17-30.

Rozan, M.A.A.G., El-Shshtawy, T. and Boriy, E.G. 2022. Nutritional value, antioxidant activity, cooking quality, and sensory attributes of pasta enriched with cornsilk. Egyptian *Journal of Food Science*, 50, 283-297.

Sabiu, S., O'Neill, FH. and Ashafa, AOT. 2016. Kinetics of α-amylase and α-glucosidase inhibitory potential of *Zea mays* Linnaeus (Poaceae), *Stigma maydis* aqueous extract: An *in vitro* assessment. *Journal of Ethnopharmacology*, 183, 1-8.

Sabiu, S., O'Neill, FH. and Ashafa, AOT. 2017. Toxicopathological evaluation of a 28-day repeated dose administration of *Zea mays* L. (Poaceae), *Stigma maydis* aqueous extract on key metabolic markers of Wistar rats. *Transactions of the Royal Society of South Africa*. 72, 225-233.

Sabiu, S., Madende, M., Ajao, A.A.N., Ogundeji, O.A., Lekena, N. and Alayande, K.A. 2019. The scope of phytotherapy in southern African antidiabetic healthcare. *Transactions of the Royal Society of South Africa*, 74, 1-18.

Sagbo, I.J. and Hussein, A.A. 2022. Antidiabetic Medicinal Plants Used in the Eastern Cape Province of South Africa: An Updated Review. *Processes*, 10, 1817.

Saisho, Y. 2020. SGLT2 inhibitors: the star in the treatment of type 2 diabetes?. *Diseases*, 8, 14.

Saleem, M., Nazir, M., Ali, M.S., Hussain, H., Lee, Y.S., Riaz, N. and Jabbar, A. 2010. Antimicrobial natural products: an update on future antibiotic drug candidates. *Natural Product Reports*, 27, 238-254.

Salehi, B., Ata, A., V. Anil Kumar, N., Sharopov, F., Ramírez-Alarcón, K., Ruiz-Ortega, A., Abdulmajid Ayatollahi, S., Valere Tsouh Fokou, P., Kobarfard, F., Amiruddin Zakaria, Z. and Iriti, M. 2019. Antidiabetic potential of medicinal plants and their active components. *Biomolecules*, 9, 551.

Sarepoua, E., Tangwongchai, R., Suriharn, B.O.R.O.N. and Lertrat, K. 2013. Relationships between phytochemicals and antioxidant activity in corn silk. *International Food Research Journal*, 20, 2073.

Sarepoua, E., Tangwongchai, R., Suriharn, B. and Lertrat, K. 2015. Influence of variety and harvest maturity on phytochemical content in corn silk. *Food Chemistry*, 169, 424-429.

Sarfare, S., Khan, S.I., Zulfiqar, F., Radhakrishnan, S., Ali, Z. and Khan, I.A. 2022. Undescribed C-glycosylflavones from corn silk and potential anti-inflammatory activity evaluation of isolates. *Planta Medica*, 88, 745-752.

Sawangwong, W., Kiattisin, K., Somwongin, S., Wongrattanakamon, P., Chaiyana, W., Poomanee, W. and Sainakham, M. 2024. The assessment of composition, biological properties, safety and molecular docking of corn silk (*Zea mays* L.) extracts from the valorization of agricultural waste products in Thailand. *Industrial Crops and Products*, 212, 118352.

Schmid-Schönbein, G.W. 2006. Analysis of inflammation. Annual Reviews of *Biomedical Engineering*, 8, 93-151.

Schiavonem, M., Putoto, G., Laterza, F. and Pizzol, D. 2016. Gestational diabetes: an overview with attention for developing countries. *Endocrine Regulations*, 50, 62-71.

Schneiderman, E.H. 2010. Gestational diabetes: an overview of a growing health concern for women. *Journal of Infusion Nursing*, 33, 48-54.

Senphan, T. (2019). Comparative studies on chemical composition and antioxidant activity of corn silk from two varieties of sweet corn and purple waxy corn as influenced by drying methods. *Food and Applied Bioscience Journal*, 7, 64-80.

Shalaby, N.M., Abd-Alla, H.I., Aly, H.F., Albalawy, M.A., Shaker, K.H. and Bouajila, J. 2014. Preliminary *in vitro* and *in vivo* evaluation of antidiabetic activity of *Ducrosia anethifolia* Boiss. and its linear furanocoumarins. *BioMed Research International*, 2014.

Shalihah, I.M., Pamela, V.Y. and Kusumasari, S. 2020. Cornsilk tea extract as antidiabetic: a review. *Food Science and Technology Journal*, 2202, 66-71.

Shanak, S., Saad, B. and Zaid, H. 2019. Metabolic and epigenetic action mechanisms of antidiabetic medicinal plants. *Evidence-Based Complementary and Alternative Medicine*, 2019.

Shao, L.I. and Zhang, B. 2013. Traditional Chinese medicine network pharmacology: theory, methodology and application. Chinese *Journal of Natural Medicines*, 11, 110-120.

Sharma, P., Joshi, T., Mathpal, S., Chandra, S. and Tamta, S. 2022. *In silico* identification of antidiabetic target for phytochemicals of *A. marmelos* and mechanistic insights by molecular dynamics simulations. *Journal of Biomolecular Structure and Dynamics*, 40, 10543-10560.

Sheng, L., Chen, Q., Di, L., and Li, N. 2020. Evaluation of anti-diabetic potential of corn silk in high-fat diet/streptozotocin- induced type 2 diabetes mice model. *Endocrine, Metabolic and Immune Disorders - Drug Targets*, 21, 131-138.

Shinkafi, T.S., Bello, L., Hassan, S.W. and Ali, S. 2015. An ethnobotanical survey of antidiabetic plants used by Hausa–Fulani tribes in Sokoto, Northwest Nigeria. *Journal of Ethnopharmacology*, 172, 91-99.

Shode, F.O., Uhomoibhi, J.O.O., Idowu, K.A., Sabiu, S. and Govender, K.K. 2022. Molecular dynamics study on selected bioactive phytochemicals as potential inhibitors of HIV-1 subtype C protease. *Metabolites*, 12, 1155.

Sifunda, S., Mbewu, A.D., Mabaso, M., Manyaapelo, T., Sewpaul, R., Morgan, J.W., Harriman, N.W., Williams, D.R. and Reddy, S.P., 2023. Prevalence and psychosocial correlates of diabetes mellitus in south africa: results from the South African National Health and Nutrition Examination Survey (SANHANES-1). *International Journal of Environmental Research and Public Health*, 20, 5798.

Singh, A. and Raghuvanshi, R.S. 2021. Development and evaluation of value-added fiber rich laddoo supplemented with processed corn silk. *International Journal of Research and Analytical Reviews,* 8, 909-922.

Singh, A.K., Rana, H.K., Singh, V., Yadav, T.C., Varadwaj, P. and Pandey, A.K. 2021. Evaluation of antidiabetic activity of dietary phenolic compound chlorogenic acid in streptozotocin induced diabetic rats: Molecular docking, molecular dynamics, *in silico* toxicity, *in vitro* and *in vivo* studies. *Computers in Biology and Medicine*, 134, 104462.

Singh, J., Inbaraj, B.S., Kaur, S., Rasane, P. and Nanda, V. 2022a. Phytochemical analysis and characterization of corn silk (*Zea mays*, G5417). *Agronomy,* 12, 777.

Singh, J., Rasane, P., Nanda, V. and Kaur, S. 2022b. Bioactive compounds of corn silk and their role in management of glycaemic response. *Journal of Food Science and Technology*, 60, 1695-1710.

Shakya, A.K. 2016. Medicinal plants: Future source of new drugs. International Journal of Herbal Medicine, 4, 59-64.

Snook, M.E., Widstrom, N.W., Wiseman, B.R., Bryne, P.F., Harwood, J.S. and Costello, C.E. 1995. New C-4''-hydroxyl derivatives of maysin and 3-'methoxymaysin isolated from corn silk (*Zea mays*). *Journal of Agricultural and Food Chemistry*, 43, 2740-2745.

Sofowora, A., Ogunbodede, E. and Onayade, A. 2013. The role and place of medicinal plants in the strategies for disease prevention. *African Journal of Traditional, Complementary and Alternative Medicines*, 10, 210-229.

Sohail, E., Ahsan, T., Ghaus, S. and Aijaz, W. 2021. SGLT 2 inhibitors; glycemic control, weight loss and safety profile in patients with type 2 diabetes, at Medicell Institute (MIDEM). *Pakistan Journal of Medical Sciences*, 37, 87-92.

Sola, D., Rossi, L., Schianca, G. P., Maffioli, P., Bigliocca, M., Mella, R., Corlianò, F., Fra, G. P., Bartoli, E. and Derosa, G. 2015. Sulfonylureas and their use in clinical practice. *Archives of Medical Science: AMS,* 11, 840-848.

Sorli, C. and Heile, M.K. 2014. Identifying and meeting the challenges of insulin therapy in type 2 diabetes. *Journal of Multidisciplinary Healthcare*, 267-282.

Soumyanath, A. 2005. Traditional medicines for modern times: antidiabetic plants. *CRC Press*. 1, 336.

Sulla, V. 2020. Poverty and equity brief: Sub-Saharan Africa: South Africa, World Bank Group, retrieved from https://databankfiles.worldbank.org/public/ddpext_download/poverty/33EF03BB-9722-4AE2-ABC7-AA2972D68AFE/Global_POVEQ_ZAF.pdf, accessed on 12/03/2024.

Süntar, I. 2020. Importance of ethnopharmacological studies in drug discovery: role of medicinal plants. *Phytochemistry Reviews*, 19, 1199-1209.

Stene, Lars C., Sami Oikarinen, Heikki Hyöty, Katherine J. Barriga, Jill M. Norris, Georgeanna Klingensmith, John C. Hutton, Henry A. Erlich, George S. Eisenbarth, and Marian Rewers. 2010. *Enterovirus* infection and progression from islet autoimmunity to type 1 diabetes: the Diabetes and Autoimmunity Study in the Young (DAISY). *Diabetes 59*, 12, 3174-3180.

Sukhikh, S., Babich, O., Prosekov, A., Kalashnikova, O., Noskova, S., Bakhtiyarova, A., Krol, O., Tsvetkova, E. and Ivanova, S. 2023. Antidiabetic properties of plant secondary metabolites. *Metabolites*, 13, 513.

Surya, C., Rajeshkumar, S., Lakshmi, T. and Roy, A. 2023. Antidiabetic activity of *Piper longum* and stevia herbal formulation. *Journal of Complementary Medicine Research*, 13, 29-32.

Taghvaei, S. and Saremi, L. 2022. Molecular Dynamics simulation and essential dynamics of deleterious proline 12 alanine single-nucleotide polymorphism in PPARγ2 associated with type 2 diabetes, cardiovascular disease, and nonalcoholic fatty liver disease. *PPAR Research*. 2022.

Tao, H., Chen, X., Du, Z. and Ding, K. 2020. Corn silk crude polysaccharide exerts anti-pancreatic cancer activity by blocking the EGFR/PI3K/AKT/CREB signaling pathway. *Food and Function*, 11, 6961-6970.

Tao, T.Z., Wang, L. and Liu, J. 2023. Role of corn silk for the treatment of Alzheimer's disease: A mechanism research based on network pharmacology combined with molecular docking and experimental validation. *Chemical Biology and Drug Design*, 102, 1231-1247.

Thoudam, B., Kirithika, T., Ramya, J. and Usha, K. 2011. Phytochemical constituents and antioxidant activity of various extracts of corn silk (*Zea mays* L). *Research Journal of Pharmaceutical, Biological and Chemical Sciences*, 2, 986-993.

Tian, S., Sun, Y. and Chen, Z. 2021. Extraction of flavonoids from corn silk and biological activities *in vitro*. *Journal of Food Quality*, 2021, 1-9.

Timmons, J.A. and Boyle, J. 2022. Sulfonylureas and meglitinides. *Diabetes Drug Notes*, 49-66.

Tran, M.N., and Lee, S. 2022. The molecular mechanisms of panax ginseng in treating type 2 diabetes mellitus: Network pharmacology analysis and molecular docking validation. *Evidence-based Complementary and Alternative Medicine: eCAM*, 2022.

Tyagi, A. and Pugazhenthi, S. 2021. Targeting insulin resistance to treat cognitive dysfunction. *Molecular Neurobiology*, 58, 2672-2691.

Ugochukwu, N.H. and Babady, N.E. 2002. Antioxidant effects of *Gongronema latifolium* in hepatocytes of rat models of non-insulin dependent diabetes mellitus. *Fitoterapia*, 73, 612-618.

Wallia, A. and Molitch, M.E. (2014). Insulin therapy for type 2 diabetes mellitus. *Jama*, 311, 2315-2325.

Wang, G.Q., Xu, T., Bu, X.M. and Liu, B.Y. 2012. Anti-inflammation effects of corn silk in a rat model of carrageenin-induced pleurisy. *Inflammation*, 35, 822-827.

Wang, X., Zhang, A., Yan, G., Sun, W., Han, Y. and Sun, H. 2013. Metabolomics and proteomics annotate therapeutic properties of geniposide: targeting and regulating multiple perturbed pathways. *PLoS One*, 8, 71403.

Wang, K.J. and Zhao, J.L. 2019. Corn silk (*Zea mays* L.), a source of natural antioxidants with α-amylase, α-glucosidase, advanced glycation and diabetic nephropathy inhibitory activities. *Biomedicine and Pharmacotherapy*, 110, 510-517.

Wang, Y., Liu, Q., Fan, S., Yang, X., Ming, L., Wang, H. and Liu, J. 2019. Rapid analysis and characterization of multiple constituents of corn silk aqueous extract using ultra-high-performance liquid chromatography combined with quadrupole time-of-flight mass spectrometry. *Journal of Separation Science*, 42, 3054-3066.

Wang, N., Zhu, F., Shen, M., Qiu, L., Tang, M., Xia, H., Chen, L., Yuan, Y., Ma, S. and Chen, K. 2019. Network pharmacology-based analysis on bioactive anti-diabetic compounds in *Potentilla discolor* bunge. *Journal of Ethnopharmacology*, 241, 111905.

Wharton, S., Davies, M., Dicker, D., Lingvay, I., Mosenzon, O., Rubino, D.M. and Pedersen, S.D. 2022. Managing the gastrointestinal side effects of GLP-1 receptor agonists in obesity: recommendations for clinical practice. *Postgraduate Medicine*, 134, 14-19.

World Health Organization. 2019. Cancer. WHO, retrieved from https://www.who.int/health-topics/cancer#tab=tab_1. accessed 04 August 2023

van de Venter, M., Roux, S., Bungu, L.C., Louw, J., Crouch, N.R., Grace, O.M., Maharaj, V., Pillay, P., Sewnarian, P., Bhagwandin, N. and Folb, P. 2008. Antidiabetic screening and scoring of 11 plants traditionally used in South Africa. *Journal of Ethnopharmacology,* 119, 81-86.

van Huyssteen, M., Milne, P.J., Campbell, E.E. and van de Venter, M. 2011. Antidiabetic and cytotoxicity screening of five medicinal plants used by traditional African health practitioners in the Nelson Mandela Metropole, South Africa. *African Journal of Traditional, Complementary and Alternative Medicines*, 8.

Van Wyk, B.E. and Wink, M. 2018. Medicinal plants of the world. Cabi.

Venkateswaran, M., Jayabal, S., Hemaiswarya, S., Murugesan, S., Enkateswara, S., Doble, M. and Periyasamy, S. (2021). Polyphenol-rich Indian ginger cultivars ameliorate GLUT4 activity in C2C12 cells, inhibit diabetes-related enzymes and LPS-induced inflammation: an in vitro study. *Journal of Food Biochemistry*, 45, 13600.

Vijitha, T.P. and Saranya, D. 2017. Corn silk-a medicinal boon. *International Jounral of ChemTech. Research*, 10. 129-137.

Xiao, E. and Luo, L. 2018. Alternative therapies for diabetes: a comparison of western and traditional Chinese medicine (TCM) approaches. *Current Diabetes Reviews*, 14, 487-496.

Xu, L., Zhang, Y., Zhang, P., Dai, X., Gao, Y., Lv, Y., Qin, S. and Xu, F. 2019. Integrated metabolomics and network pharmacology strategy-driven active traditional Chinese medicine ingredients discovery for the alleviation of cisplatin nephrotoxicity. *Chemical Research in Toxicology*, 32, 2411-2421.

Xu, M., Li, Z., Yang, L., Zhai, W., Wei, N., Zhang, Q., Chao, B., Huang, S. and Cui, H. 2020. Elucidation of the mechanisms and molecular targets of sanhuang xiexin decoction for type 2 diabetes mellitus based on network pharmacology. *BioMed Research International*, 2020.

Yagasaki, K. and Muller, C.J. 2022. The effect of phytochemicals and food bioactive compounds on diabetes. *International Journal of Molecular Sciences*, 23, 7765.

Yarahmadi, A., Sarabi, M.M., Sayahi, A. and Zal, F. 2021. Protective effects of quercetin against hyperglycemia-induced oxidative stress in hepatic HepG2 cell line. *Avicenna Journal of Phytomedicine*, 11, 269-280.

Yin, B., Bi, Y.M., Fan, G.J. and Xia, Y.Q. 2020. Molecular mechanism of the effect of Huanglian Jiedu decoction on type 2 diabetes mellitus based on network pharmacology and molecular docking. *Journal of Diabetes Research*, 2020.

Yucharoen, R., Srisuksomwong, P., Julsrigival, J., Mungmai, L., Kaewkod, T. and Tragoolpua, Y. (2023). Antioxidant, anti-tyrosinase, and anti-skin pathogenic bacterial activities and phytochemical compositions of corn silk extracts, and stability of corn silk facial cream product. *Antibiotics*, 12, 1443.

Zaid, H., Tamrakar, A.K., Razzaque, M.S. and Efferth, T. 2018. Diabetes and metabolism disorders medicinal plants: a glance at the past and a look to the future 2018. *Evidence-based Complementary and Alternative Medicine: eCAM*, 2018.

Zhan, L.L. and Su, H.H. 2018. Application of network pharmacology in the pharmacodynamics of traditional Chinese medicine. *Journal of Clinical Medical*, 5, 197.

Zhang, G.B., Li, Q.Y., Chen, Q.L. and Su, S.B. 2013. Network pharmacology: a new approach for Chinese herbal medicine research. *Evidence-based Complementary and Alternative Medicine,* 2013.

Zhang, Y., Wu, L., Ma, Z., Cheng, J. and Liu, J. 2015. Anti-diabetic, anti-oxidant and anti-hyperlipidemic activities of flavonoids from corn silk on STZ-induced diabetic mice. *Molecules*, 21, 7.

Zhang, W., Huai, Y., Miao, Z., Qian, A. and Wang, Y. (2019). Systems pharmacology for investigation of the mechanisms of action of traditional Chinese medicine in drug discovery. *Frontiers in Pharmacology*, 10, 743.

Zhang, H., Jiang, H., Zhao, M., Xu, Y., Liang, J., Ye, Y. and Chen, H. 2022. Treatment of gout with TCM using turmeric and corn silk: A concise review article and pharmacology network analysis. *Evidence-Based Complementary and Alternative Medicine*, 2022.

Zhao, W., Yin, Y., Yu, Z., Liu, J. and Chen, F. 2012. Comparison of anti-diabetic effects of polysaccharides from corn silk on normal and hyperglycemia rats. *International Journal of Biological Macromolecules*, 50, 1133-1137.

Zhou, Z., Chen, B., Chen, S., Lin, M., Chen, Y., Jin, S., Chen, W. and Zhang, Y. 2020. Applications of network pharmacology in traditional Chinese medicine research. *Evidence-Based Complementary and Alternative Medicine*, 2020.

Zhu, B., Cheng, B., Zhang, L. and Yu, J. 2019. Review on DFT calculation of s-triazine-based carbon nitride. Carbon Energy, 1, 32-56.

Žilić, S., Janković, M., Basić, Z., Vančetović, J. and Maksimović, V. 2016. Antioxidant activity, phenolic profile, chlorophyll and mineral matter content of corn silk (*Zea mays* L): comparison with medicinal herbs. *Journal of Cereal Science*, 69, 363-370.

Zou, Z., Xi, W., Hu, Y., Nie, C. and Zhou, Z. 2016. Antioxidant activity of *Citrus* fruits. *Food Chemistry,* 196, 885-896.

Chapter three

Metabolomics and computational bioprospection of corn silk against key enzymes implicated in type 2 diabetes mellitus and its complications

This chapter has been submitted in this format to the South African Journal of Botany (Impact Factor: 3.1)

Metabolomics and computational bioprospection of corn silk against key enzymes implicated in type 2 diabetes mellitus and its complications

Ayesha Akoonjee, Adedayo Ayodeji Lanrewaju and Saheed Sabiu*

Department of Biotechnology and Food Science, Faculty of Applied Sciences, Durban University of Technology, Durban 4000, South Africa

*Correspondence: sabius@dut.ac.za

Abstract

The rising prevalence of type-2 diabetes mellitus (T2DM) and the side effects associated with synthetic hypoglycaemic agents highlight the urgent need to explore new lead compounds with promising antidiabetic properties. Although corn silk (CS) has been proven to be antidiabetic, its mechanism of action remains unknown. This study investigated the potential of CS constituents in modulating six key enzymes [alpha-amylase (AA), alpha-glucosidase (AG), aldose reductase (AR), dipeptidyl peptidase-4 (DPP-4), protein tyrosine phosphatase 1B (PTP1B), and sorbitol dehydrogenase (SDH)] involved in T2DM pathogenesis and its complications using computer-aided drug design techniques. Using ultra-performance liquid chromatography-mass spectrometry, 128 metabolites were identified across three CS extracts (aqueous, hydro-ethanolic, and ethanolic) from two developmental (premature and mature) stages. The mature CS had higher relative abundance of most of the metabolites compared to premature CS. Among the extracts, the hydro-ethanolic extract of the mature CS had a higher relative abundance of most metabolites. Molecular docking of the identified metabolites against the six enzymes revealed top five compounds with the highest negative scores in each case. Further insight into the binding energy calculations over a 120-ns molecular dynamics (MD) simulation identified R-7-butyl-6,8-dihydroxy-3-[(3E)-pent-3-en-1-yl]-3,4-dihydroisochromen-1-one (BHP) (-40.30 kcal/mol) , 1-O-vanilloyl-beta-D-glucose (VBJ) (-34.17 kcal/mol), (-)-11-hydroxy-9,10-dihydrojasmonic acid 11-beta-D-glucoside (HDJ) (-44.13 kcal/mol), p-coumaroyl malic acid (CMA) (-34.40 kcal/mol), 2-hydroxydecanedioic acid (HDA) (-19.71 kcal/mol) and HDJ (-36.61) as having the highest negative binding free energy against AA, AG, AR, DPP-4, PTP1B, and SDH, respectively. Post-MD simulation analysis assessed the stability, flexibility, and compactness of the CS metabolites-enzyme complexes, confirming the formation of more thermodynamically stable final complexes in comparison to the respective reference standard-enzyme complexes and the unbound enzymes. A greater number of ligand-receptor interactions following a 120-ns simulation highlighted superior

binding between the CS metabolite-enzyme complexes, compared to the respective standard-enzyme complexes. The outcomes produced from this study highlight the ability of CS to modulate the activity of enzymes associated with T2DM pathogenesis and its secondary complications, allowing for the development of CS as an alternative agent to manage T2DM.

Keywords: Corn silk metabolites; Metabolomics; Molecular docking; Molecular dynamics simulation; Solvent variation; Type 2 diabetes mellitus

1. Introduction

Type 2 diabetes mellitus (T2DM), a major cause of morbidity and mortality globally, is a chronic metabolic disease characterized by impaired insulin production and/or insulin resistance resulting in high blood glucose levels (Pheiffer *et al*., 2018; Yagasaki *et al.*, 2022). Living with T2DM for prolonged period or inadequate management may culminate in severe secondary complications including kidney disease, ocular damage, cardiovascular disease, heart attacks, strokes, nerve damage, skin conditions, and foot ulcers (Yagasaki *et al.*, 2022) and eventual death in serious or severe cases (Xiao *et al*., 2019). Besides its secondary complications, T2DM imposes substantial physiological and psychological burdens on patients and exerts a significant financial strain on both public and private healthcare systems worldwide (Kharroubi *et al*., 2015; Lin *et al*., 2020). While T2DM is a non-communicable disease, its increasingly high prevalence irrespective of gender and age is a cause for concern (Animaw *et al*., 2017).

The consistent maintenance of blood glucose levels using lifestyle changes, such as a healthy diet, regular physical exercise, consistent blood glucose monitoring, regular medical check-ups and weight management is often unattainable for many patients. This has necessitated reliance on synthetic medications to effectively manage diabetes and its complications (Lankatillake *et al*., 2019). While the potency of the synthetic oral hypoglycaemic medications is undoubtable, the associated adverse side effects, compliance with complex dosing schedule and cost have undermined their application in clinical practice (Lankatillake *et al*., 2019; Singh *et al*., 2022a; Singh *et al*., 2022b). Therefore, the development of alternative or/and complementary therapeutics with promising antidiabetic potentials, is imperative.

The increased activity of alpha-amylase (AA) and alpha-glucosidase (AG) accelerates the breakdown of carbohydrates to simple sugars resulting in a rapid influx of glucose in the bloodstream, contributing to postprandial hyperglycaemia (Sabiu *et al*., 2021). Unlike AA

and AG, dipeptidyl peptidase-4 (DPP-4) plays a role in breaking down glucagon-like peptide-1, an incretin hormone that stimulates insulin release and inhibits glucagon release. These two hormones are essential in regulating blood glucose levels (Gilbert *et al*., 2020). Similarly, protein tyrosine phosphatase-1B (PTP1B) is involved in the dephosphorylation of insulin receptors and insulin receptor substrates, influencing the insulin signalling pathway (Thareja *et al*., 2012). In T2DM, elevated PTP1B activity hinders insulin signalling by excessively dephosphorylating insulin receptors, which results in decreased glucose uptake in cells, leading to elevated blood glucose levels (Balogun *et al*., 2023). On the other hand, aldose reductase (AR) and sorbitol dehydrogenase (SDH) play crucial roles in the polyol pathway, a metabolic route responsible for converting glucose into sorbitol and sorbitol to fructose, respectively (Ramana *et al*., 2011; Moemen *et al*., 2020). In T2DM, the activity of AR and SDH intensifies, resulting in the buildup of sorbitol and fructose respectively, within cells (Sabiu *et al*., 2017). Hence, accumulation of sorbitol and fructose can induce osmotic stress, causing cellular damage and dysfunction, thereby contributing to the development of secondary complications like neuropathy, nephropathy, and diabetic retinopathy (Tang *et al*., 2012; Omotosho *et al*., 2014). These six enzymes play crucial roles in the pathogenesis of T2DM or its related diabetic complications through various factors, not limited to glucose production and absorption, interference of insulin signalling, glucagon release, breakdown of glycogen, increasing of incretin concentration, accumulation of sorbitol among others (Oboh *et al*., 2014; Sharma *et al*., 2021; Thakur *et al*., 2021; Balogun *et al*., 2022). Therefore, the effective modulation of the specific activity of these enzymes is crucial in the discovery and development of novel antidiabetic compounds and emerging target-based therapies (Sabiu *et al*., 2021; Su *et al*., 2023).

Due to the rich and diverse presence of metabolites, medicinal plants serve as cogent source for the development of effective and culturally relevant therapeutic agents against several diseases including T2DM (Lankatillake *et al*., 2019; Sabiu *et al*., 2019). Corn silk (CS) is an underutilized plant material that consists of diverse phytochemicals, such as phenolic acids, flavonoids, carotenoids, sterols, tannins, volatile compounds, sugars, vitamins, minerals, polysaccharides, proteins, and peptides (Nawaz *et al*., 2019; Singh *et al.,* 2022a), many of which have contributed to its significant therapeutic properties (Wang *et al*., 2019; Shalihah *et al.,* 2020). Although CS is often discarded as a waste material (Hasanudin *et al*., 2012), it has several pharmacological properties including antioxidant, anti-inflammatory, diuretic, kaliuretic, anti-hyperlipidemic, anti-microbial, anti-cancer, anti-

hypertensive and antidiabetic (Kaur *et al.,* 2023), making it ethnopharmacologically relevant (Sabiu *et al*., 2019). Studies have shown the antidiabetic potential of CS (Guo *et al*., 2009; Zhao *et al*., 2012; Chang *et al*., 2016; Lee *et al.,* 2016; Sabiu *et al*., 2016; Vijitha *et al*., 2017; Haldar *et al*., 2019); however, there is limited information on the mechanism of action behind its antidiabetic therapeutic properties, particularly its relationship with the key enzymes implicated in T2DM pathogenesis.

Understanding the relationship between plant secondary metabolites, such as those present in CS, and enzymes implicated in the pathogenesis of T2DM can be useful for the development of targeted therapeutic approaches (Xu *et al*., 2019; Tran *et al*., 2020). This, will in turn, contribute to the development of novel antidiabetic therapeutics and the emerging field of target-based therapies, which expectedly will contribute to the effective management of T2DM (Tiwari *et al*., 2014). To this extent, the study explored metabolomic profiling and computational techniques in the identification of CS secondary metabolites and their molecular interactions with key enzymes implicated in T2DM and its complications in an effort to identify possible novel compounds with antidiabetic potentials.

2. Materials and methodology

2.1. Corn silk collection and processing for the preparation of extracts

Fresh CS of a commonly consumed South African commercial corn hybrid ILHYB22 was collected at two developmental stages [premature (collected 18/03/2022) and mature (collected 30/05/2022)] at the Cedara College of Agriculture, KwaZulu-Natal, South Africa. The processing and preparation of CS from both developmental stages to produce three extracts (aqueous, hydro-ethanolic, and ethanolic) were carried out as described in Figure 1 (Akoonjee *et al*., 2023). The powdered CS and the prepared extracts were stored (4°C) until needed (Taiwong, 2020).

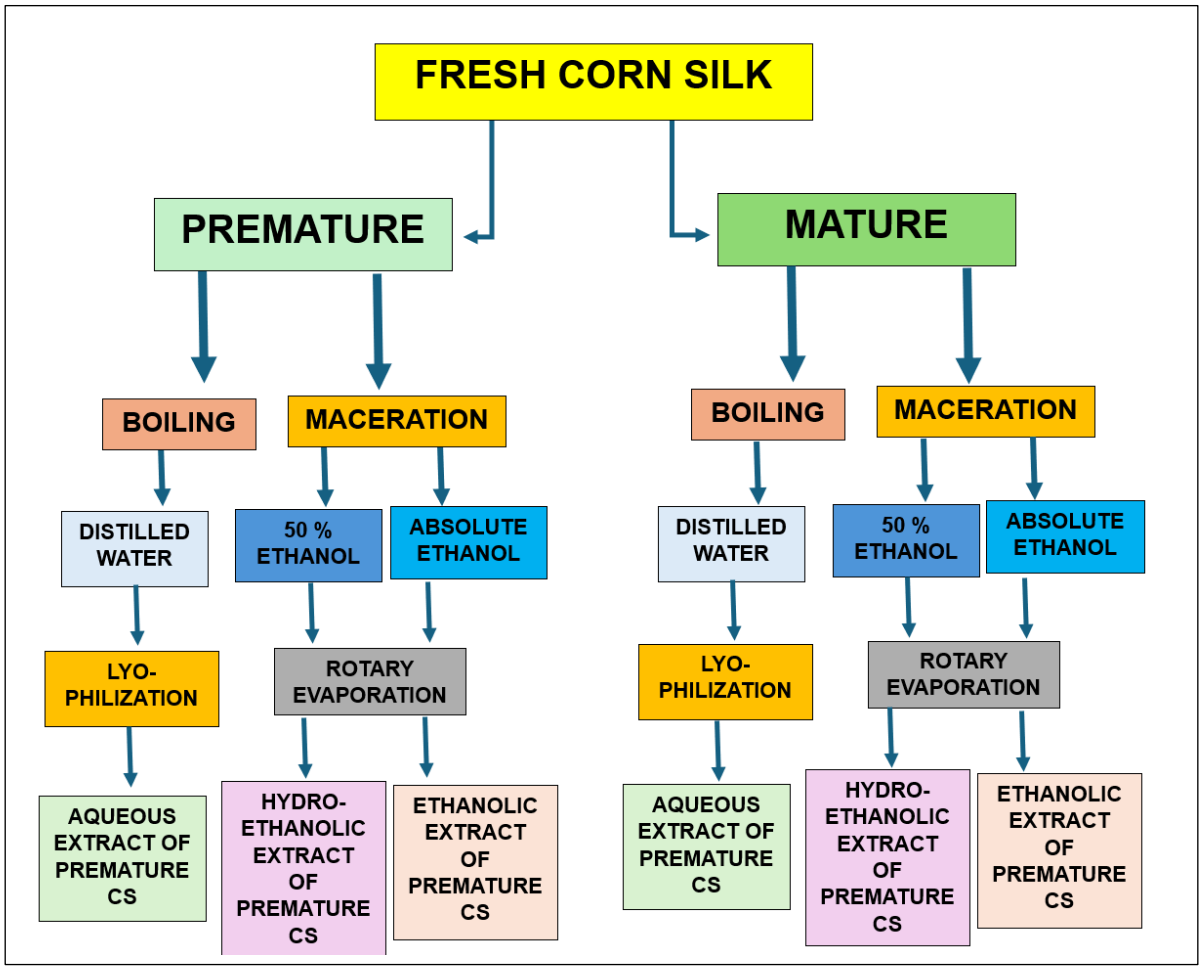

Figure 1: Preparation of aqueous, hydro-ethanolic and ethanolic extracts of mature and premature corn silk (CS)

2.2.Metabolomic profiling of corn silk

Ultra-performance liquid chromatography-mass spectrometry (UPLC-MS) analysis was performed on the raw (dried CS) and extracts (aqueous, hydro-ethanolic, and ethanolic) of mature and premature CS as previously reported (Magangana *et al*., 2021; Magangana *et al*., 2022). A Water Synapt G2 quadruple time-of-flight mass spectrometer connected to a Waters Acquity UPLC-combined with photo diode array detector (Milford, MA, United States of America) was used to analyze the samples. Briefly, 2 g of each sample was subjected to ultrasonic-assisted extraction (SS-6508T, Sunshine, India) using a solvent system of 50% methanol and 0.1% formic acid for 24 h at room temperature (Magangana *et al*., 2021). The samples were then centrifuged (mySPIN 12, Thermo Scientific, United States of America) for 5 min at 14 000 rpm and the resulting supernatant in each case was used for further analysis. Acquisition and confirmation of data were performed using Masslynx 4.1 while MS-DIAL and MS-FINDER 2.0 software (RIKEN Center for Sustainable Resource Science: Metabolome Informatics Research Team, Kanagawa,

Japan). Metaboanalyst (https://www.metaboanalyst.ca/MetaboAnalyst/) (accessed on 1 July 2022) was utilized for statistical analysis between the samples of CS where principal component analysis (PCA), partial-least squares discriminant analysis (PLS-DA), orthogonal partial-least squares discriminant analysis (OPLS-DA) and a hierarchal heat map were generated (Magangana *et al*., 2022). Relative abundance of the metabolites present in CS were performed based on peak height percentage (Macel *et al*., 2019).

2.3.Pharmacokinetics screening of corn silk metabolites

To identify orally bioavailable compounds, the drug-likeness properties of the metabolites present in CS were subjected to Lipinski's rule of five (Ro5) as previously described (Oh *et al*., 2020). The Simplified Molecular Input Line Entry System (SMILES) of the metabolites were obtained from the PubChem database (https://pubchem.ncbi.nlm.nih.gov/; accessed on 30 July 2022) and input into the SwissADME server (http://www.swissadme.ch/; accessed on 30 July 2022). Compounds with ≤ 2 violations of the Lipinski's rule (molecular weight ≤ 500 g/mol, < 5 hydrogen bond donors, ≤ 10 hydrogen bond acceptors and partition coefficient Log P < 5) were selected for subsequent analysis.

2.4.Molecular docking of corn silk metabolites against key enzymes implicated in T2DM

Following pharmacokinetic screening, the identified metabolites and selected enzymes were subjected to molecular docking. The X-ray crystal structures of the six enzymes namely: AA (protein data bank (PDB) ID 4W93), AG (3W37), AR (3RX3), DPP-4 (1WCY), PTP1B (1SUG), and SDH (1PL8), were obtained from Research Collaboratory for Structural Bioinformatics Protein (RSCB) Protein Data Bank (https://www.rcsb.org/; accessed 1 September 2022). The enzymes were prepared using USCF Chimera v 1.16 (Pettersen *et al*., 2004). The 3D conformers of the metabolites and the reference standards (acarbose for AA and AG,, epalrestat for AR, ursolic acid for PTP1B, sitaglpitin for DPP-4, and 4-[2-1R-hydroxy-ethyl)-pyrimidin-4-yl]piperazine-1-sulfonic acid dimethylamide for SDH) were obtained from PubChem (https://pubchem.ncbi.nlm.nih.gov/; accessed 1 September 2022) and subsequently optimized on USCF Chimera v 1.16 by addition of Gasteiger charges and non-polar hydrogen atoms (Balogun *et al*., 2022). Identification of grid box coordinates (x-y-z) and grid box side (x-y-z) of the native ligand for each enzyme was determined on UCSF Chimera v 1.16. These were then used to dock the CS metabolites

to the active site of the enzymes using the Autodock Vina Plugin on Chimera v 1.16 (Balogun *et al*., 2022). To prevent pseudo-positive binding conformations, the docking protocol was validated as previously detailed (Aribisala and Sabiu,2022), by measuring the root mean square deviation (RMSD) of docked ligands from the reference pocket bearing the native ligands in the co-crystal structures of AA (Figure 2a), AG (Figure 2b), AR (Figure 2c), DPP-4 (Figure 2d), PTP1B (Figure 2e) and SDH (Figure 2f), following optimal superimposition. The RMSD of the docked ligands from the native inhibitor in the 3D structures of all six enzymes was 0.5 Å which indicates similar binding orientation, ultimately validating the protocol employed.

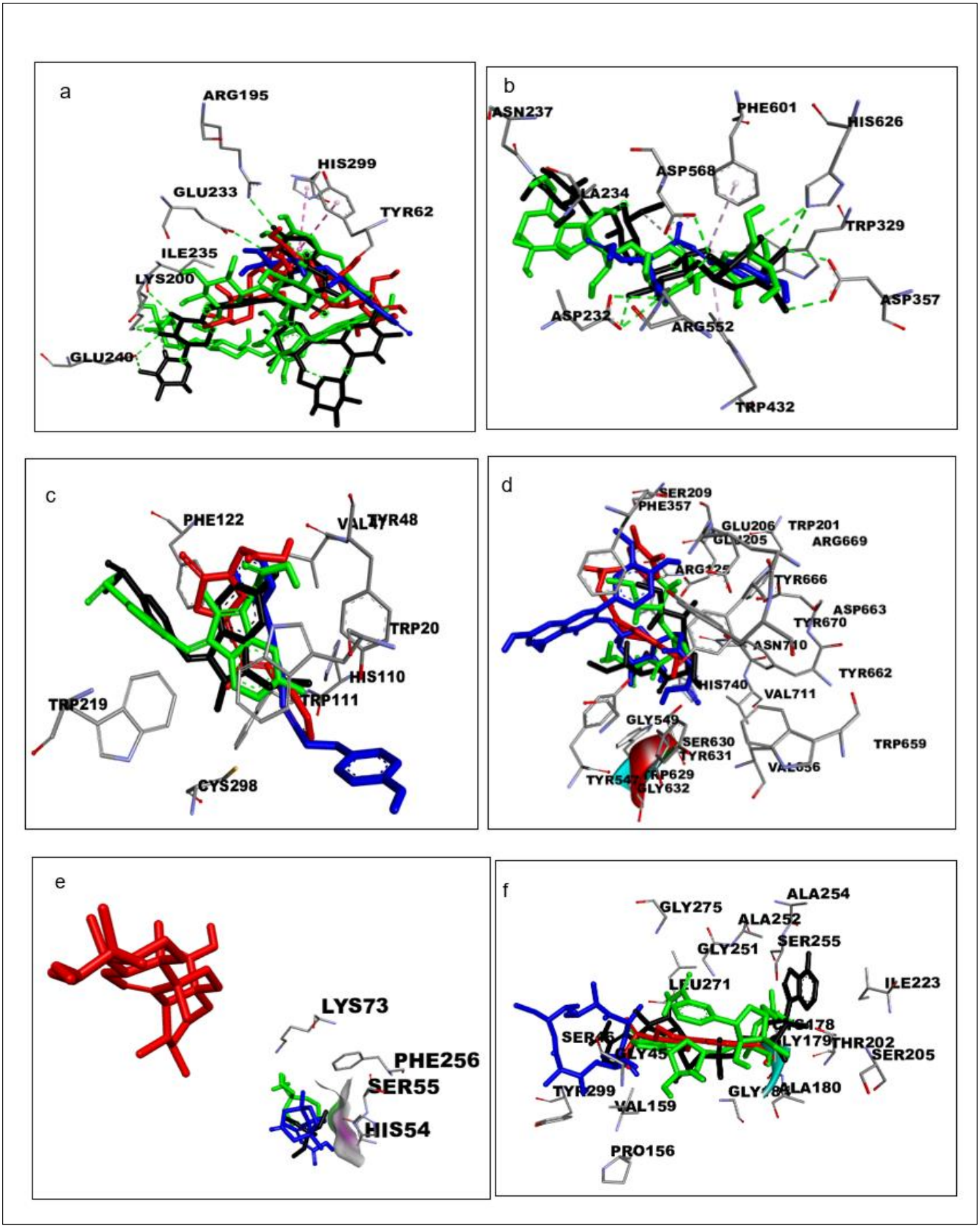

Figure 2. Superimposition on co-crystallized structure of a) alpha amylase: native ligand (black), superimposed docked native ligand (green), reference standard (red) and

compound with highest docking score (blue). Root Mean Square Deviation (RMSD) value of 0.5 Å. Grid box co-ordinates: centre (X = -11, Y = 4, Z = -22) and size (X = 20, Y = 18, Z = 13); b) alpha glucosidase: native ligand (black), superimposed docked native ligand and standard (green) and compound with highest docking score (blue). RMSD value of 0.5 Å. Grid box co-ordinates: centre (X = 0.2, Y = -3, Z = -23) and size (X = 11, Y = 22, Z = 12); c) aldose reductase: native ligand (black), superimposed docked native ligand (green), reference standard (red) and compound with highest docking score (blue). RMSD value of 0.5 Å. Grid box co-ordinates: centre (X = -10, Y = 9, Z = 17) and size (X = 11, Y = 22, Z = 12); d) dipeptidyl peptidase 4: native ligand (black), superimposed docked native ligand (green), reference standard (red) and compound with highest docking score (blue). RMSD value of 0.5 Å. Grid box co-ordinates: centre (X = 56, Y = 62, Z = 35) and size (X = 13, Y = 10, Z = 7); e) protein tyrosinase phosphatase-1B: native ligand (black), superimposed docked native ligand (green), reference standard (red) and compound with highest docking score (blue). RMSD value of 0.5 Å. Grid box co-ordinates: centre (X = 44, Y = -3, Z = -4) and size (X = 7, Y = 6, Z = 7) and f) sorbitol dehydrogenase: native ligand (black), superimposed docked native ligand (green), reference standard (red) and compound with highest docking score (blue). RMSD value of 0.5 Å. Grid box co-ordinates: centre (X = 97, Y = 31, Z = 26) and size (X = 9, Y = 15, Z = 13)

2.5. Molecular dynamics (MD) simulation of corn silk metabolites against the target enzymes

Following validation of the docking protocol, the top five complexes with the best pose (most negative docking score) against each enzyme were selected for further analysis through a 120-ns MD simulation, as detailed by Sabiu *et al*. (2022). The simulation was conducted using the GPU force field in AMBER 18 software in which the Force field 18SB variant of the AMBER force field was used. Using Restrained Electrostatic Potential (RESP) and the General Amber Force Field (GAFF) methods of the ANTECHAMBER, the atomic partial charges for the compounds were obtained. The leap module of AMBER 18 neutralized the system through the addition of hydrogen atoms and Na^+ and Cl^- counter ion. The residues were numbered 1–495, 1-913, 1-315, 1-729, 1-299 and 1-356 for AA, AG, AR, DPP-4, PTP1B and SDH, respectively. The system in each case was then lowered implicitly within an orthorhombic box of TIP3P water molecules such that all atoms were within 8Å of any box edge. The simulation was carried out with the Leap module SHAKE algorithm employed to constrict the expansion of all chemical bonding, such as hydrogen

atoms. The step size of each simulation was 2 fs, and an SPFP precision model was used. The simulations align with the isobaric-isothermal ensemble (NPT); having randomized seeding, Berendsen barostat maintains 1 bar constant pressure, 2 ps pressure-coupling constant, 300 K temperature and Langevin thermostat with a collision frequency of 1.0 ps. Using the CPPTRAJ module in the AMBER 18 suite, post-dynamics data [RMSD, root mean square fluctuation (RMSF), radius of gyration (RoG), solvent accessible surface (SASA) and number of hydrogen bonds] were computed (Aribisala *et al.,* 2021). The binding free energy (ΔG_{bind}) was calculated using the Molecular Mechanics/GB Surface Area (MM/GBSA) method wherein ΔG_{bind} was averaged over 100 000 snapshots extracted from the 120 ns trajectory (Ylilauri and Pentikäinen, 2013). The equations below represent the method for the calculation of the average ΔG_{bind} for each molecular species (complex, ligand, and protein):

$$\Delta G_{bind} = E_{gas} + G_{sol} - TS \quad [1]$$

$$\Delta G_{bind} = G_{complex} - G_{receptor} - G_{ligand} \quad [2]$$

$$E_{gas} = E_{int} + E_{vdw} + E_{ele} \quad [3]$$

$$G_{sol} = G_{GB} + G_{SA} \quad [4]$$

$$G_{SA} = \gamma SASA \quad [5]$$

The complexes' (ligand-receptor) interaction at the active site of each enzyme was examined at 0 ns, 60 ns and 120 ns using Discovery Studio version 21.1.1 (Biovia, 2021).

2.6.Quantum chemical calculations

The molecular characteristics of the lead compounds were predicted using Density Functional Theory (DFT) via quantum chemical calculations. The widely used 6-31 + G(d,p) basis set combined with the Becke3-Lee–Yang–Parr (B3LYP) method (Kruse *et al*., 2012) was adopted to optimize the lead compounds using the Gaussian 16 suite of the CHPC, Cape Town, South Africa and the resulting files were then visualized using GaussView 6 software V 6.0.16. The study assessed the conceptual DFT (cDFT), namely the frontier molecular orbitals comprising of the highest occupied molecular orbital (HOMO) and the lowest unoccupied molecular orbital (LUMO) (Calais, 1993), taking into consideration the Parr and Pearson interpretation of DFT and Koopmans theorem (Luo *et al*., 2006). The equations below were used to compute other chemical descriptors, including

energy gap (ΔE), ionization energy (I), electron affinity (A), chemical hardness (ŋ), softness (δ), electronegativity (χ), chemical potential (Cp), global electrophilicity (ω).

$$\Delta E = E_{LUMO} - E_{HOMO} \quad (1)$$

$$I = -E_{LUMO} \quad (2)$$

$$A = -E_{HOMO} \quad (3)$$

$$ŋ = \frac{\Delta E}{2} \quad (4)$$

$$\delta = \frac{1}{ŋ} \quad (5)$$

$$\chi = \frac{(I+A)}{2} \quad (6)$$

$$Cp = -\chi \quad (7)$$

$$\omega = \frac{\chi 2}{\Delta E} \quad (8)$$

3. Results

3.1.Metabolomic profiling of corn silk metabolites

The metabolites identified through UPLC-MS analysis (Supplementary Table S1) were confirmed on the chromatograms produced from MassLynx (Supplementary Figures S1-S4). Altogether, 128 metabolites (compounds C1 – 128) were identified in all the CS samples investigated. The highest amount of variation between the two developmental stages was 63.95 (41.1% in principal component 1 and 22.8% in principal component 2) with the compounds found to cluster majorly in two distinct positions (Figure 3a). The top 15 compounds responsible for the high chemical diversity between the different developmental stages are presented in Figure 3b. Thirteen out of the 15 metabolites were found to be highly present in the mature CS, whereas C103 (Pandangolide 1) and C74 (3-hydroxysebaic acid) were more prevalent in the premature CS (Supplementary Table S1). The use of different extraction solvent produced variation in the type of metabolites extracted in both the premature and mature CS. Between the different samples of CS, there was 62.4% quantitative and qualitative variation of metabolites (42.1% in principal component 1 and 20.3% in principal component 2) (Figure 4a). The top 15 metabolites responsible for the high chemical diversity between the eight samples of CS are presented in Figure 4b, where caffeoyl tartaric acid (C105) was the most variant between the samples.

The top 15 CS metabolites were less abundant in the aqueous extracts of CS while out of the 15 metabolites which contributed to the highest variation between the extracts, a total of 5, 1, 4, 2, and 3 metabolites were highly abundant in raw premature CS, raw mature CS, hydro-ethanolic extract of premature CS, hydro-ethanolic extract of mature CS, and ethanolic extract of mature CS, respectively (Figure 4b).

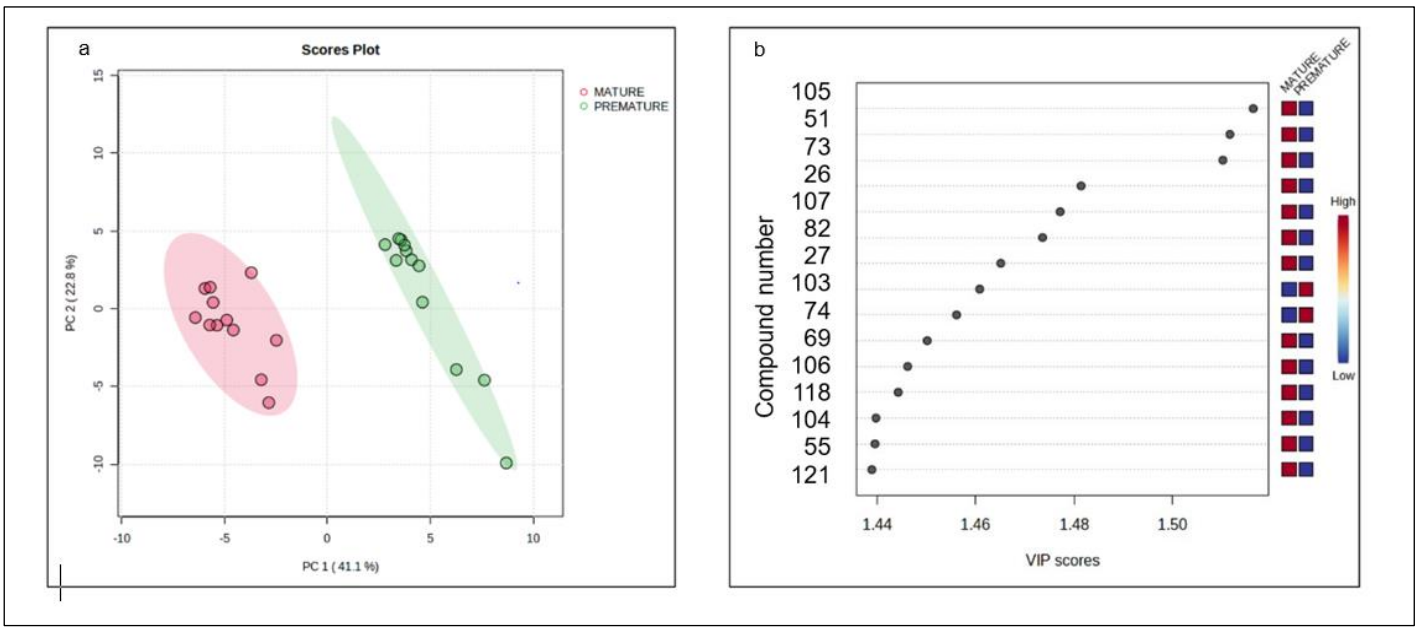

Figure 3. a) Principal component analysis (PCA) plot showing the percentage of chemical diversity of metabolites between the two different developmental growth stages [premature (light green) and mature (light red) of corn silk; b) Orthogonal partial least squares-discriminant analysis (OPLS-DA) loadings plot showing the top fifteen metabolites that were the most chemically diverse between the two different developmental growth stages (premature and mature) of corn silk with red showing high prevalence and blue showing low prevalence. PC: principal component, compound identities: C105: tetradecanedioic acid, C51: methyl geranate, C73: UNPD230015, C26: diaportinic acid, C107: genistin, C82: diaportinol, C27: benzyl-O-beta-D-glucopyranoside, C103: pandangolide 1a, C74: 3-hydroxysebacic acid, C69: dodecanedioic acid, C106: (R)-7-butyl-6,8-dihydroxy-3-[(3E)-pent-3-en-1-yl]-3,4-dihydroisochromen-1-one, C118: ginsenoyne E, C104: 4-hydroxynonenal, C55: daldiniapyrone and 1C21: UNPD205010

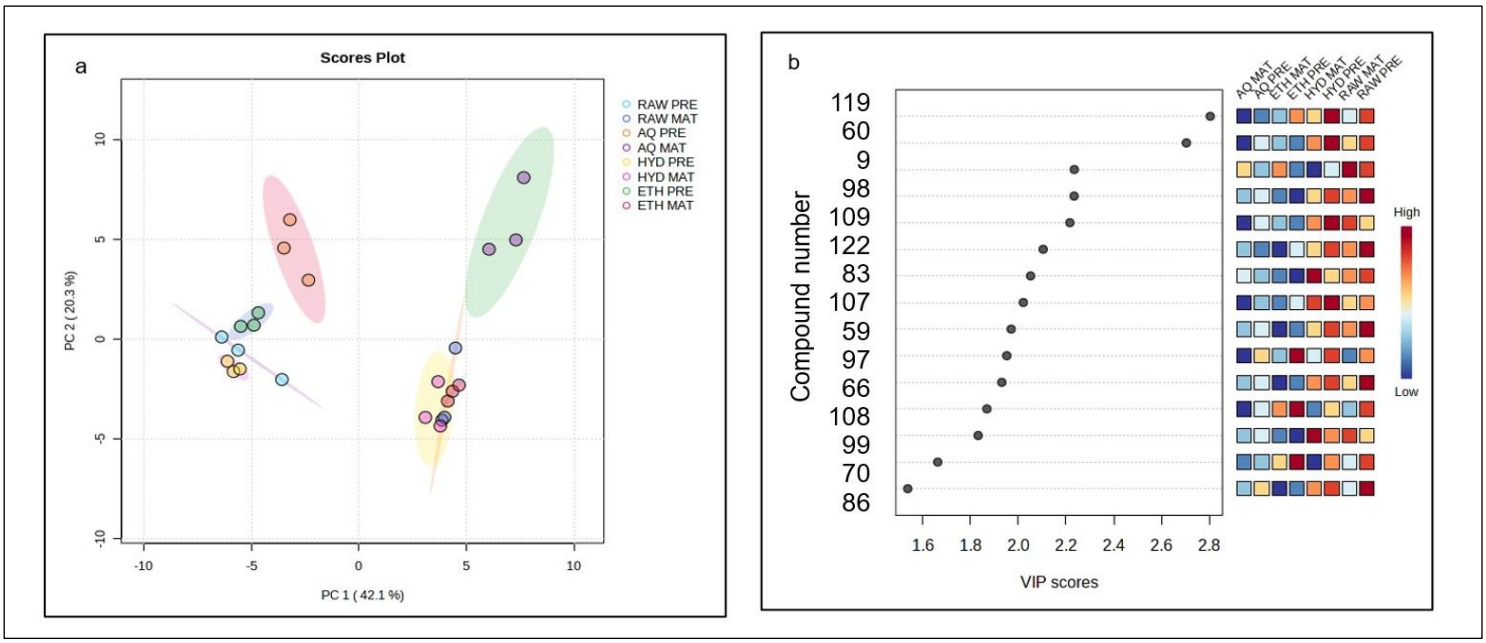

Figure 4: a). Principal component analysis (PCA) scores plot showing the percentage of chemical diversity of metabolites between eight samples of CS [raw extract of premature CS (light blue circle), raw extract of mature CS (dark blue circle), aqueous extract of premature CS (orange circle), aqueous extract of mature CS (purple circle), hydro-ethanolic extract of premature CS (yellow circle), hydro-ethanolic extract of mature CS (pink circle), ethanolic extract of premature CS (green circle) and ethanolic extract of mature CS (light red circle)]; b) Partial least squares-discriminant analysis (PLS-DA) loadings plot showing the top fifteen metabolites that were the most chemically diverse between the eight samples of CS [raw and three extracts (aqueous, hydro-ethanolic and ethanolic) at two different developmental stages (premature and mature)] with red showing high prevalence and blue showing low prevalence. PC: principal component AQ MAT: aqueous extract of mature CS, AQP; aqueous extract of premature CS, ETH MAT: ethanolic extract of mature CS, ETH PRE: ethanolic extract of premature CS, HYD MAT: hydro-ethanolic extract of mature CS, HYD PRE: hydro-ethanolic extract of premature CS, RAW MAT: raw extract of mature CS, RAW PRE: raw extract of premature CS. Compound identities: C119: caffeoyl tartaric acid, C60: quercitrin, C9: D-2-hydroxyglutaric acid, C98: 5,7,4'-trihydroxy-3'-methoxyflavone, C109: kaempferol 3-[2'''-acetyl-alpha-L-arabinopyranosyl-(1->6)-galactoside], C122: maysin 3'-methyl ether, C83: herbacetin 7-(6''-quinoylglucoside), C107: genistin, C59: apiin, C97: maysin, C66: UNPD19396, C108: p-coumaroyl malic acid, C99: quercetin 3-O-(6''-acetyl-glucoside), C70: kaempferitrin and C86: mirificin

The relative abundance of the metabolites in the different samples of CS are presented in Supplementary Figure S5 (compounds C1 – C65) and Supplementary Figure S6 (compounds C66 – C128) as well as Supplementary Table S2. Majority of the metabolites

were found to be more abundant in the hydro-ethanolic extract of mature CS except compounds C3, C8, C21, C32, C33, C38, C42, C58, C105, C124 (more abundant in aqueous extract of mature CS), compounds C1, C3, C8, C21, C32, C33, C92, C100, C102 (more abundant in aqueous extract of premature CS) C47, C48, C61, C76, C82, C88, C89, C99, C103, C106 (more abundant in ethanolic extract of mature CS), C36, C54, C70, C90, C96, C108, C125, C126, C127 (more abundant in ethanolic extract of premature CS), C5 (more abundant in hydro-ethanolic extract of premature CS) and C65 (more abundant in raw extract of premature CS). Percentage yield of the 128 metabolites between the different samples of CS (aqueous, hydro-ethanolic and ethanolic) extracts of premature and mature CS is presented in Supplementary Figure S7, in which the hydro-ethanolic extract of mature CS (37%) had the highest yield, followed by the hydro-ethanolic extract of premature CS (12%) and aqueous extract of premature CS (12%), with the raw sample of mature CS (5%) sample having the lowest yield.

3.2.Drug-likeness filtering of corn silk metabolites

Out of the 128 metabolites identified in the different samples of CS, 110 passed Lipinski's Ro5, while 18 compounds exhibited more than 2 violations and were excluded from further analysis (Supplementary Table S3).

3.3.Molecular docking of corn silk metabolites against enzyme targets

The results of the molecular docking analysis of the top five CS metabolites against the enzyme targets are presented in Table 1. Aesculin (AES), austricin (AUS), (6E)-1-(4-hydroxyphenyl)-7-phenylhepta-4,6-dien-3-one (HPH), (-)-11-hydroxy-9,10-dihydrojasmonic acid 11-beta-D-glucoside (HDJ), phaseic acid (PHA) and erythronolide B (ETB) had the highest negative docking scores against AA, AG, AR, DPP-4, PTP1B and SDH, respectively. The docking scores of the remaining 105 CS metabolites against the enzyme targets can be found in Supplementary Table S4.

Table 1. Molecular docking results of CS metabolites with the five highest negative docking score (best pose) and reference standards against each of the enzyme targets

Target enzymes	Compound number	Identity	Compound Abbreviation	Docking score (kcal/mol)
AA	C31	Aesculin	AES	-8.1
	C106	(R)-7-butyl-6,8-dihydroxy-3-[(3e)-pent-3-en-1-yl]-3,4-	BHP	-8.0

		dihydroisochromen-1-one		
	C88	Curvularol	CUR	-7.9
	C14	(6e)-1-(4-hydroxyphenyl)-7-phenylhepta-4,6-dien-3-one	HPH	-7.8
	C64	Austricin	AUS	-7.7
	-	Acarbose*	ACA	-6.9
AG	C64	Austricin	AUS	-7.8
	C12	Glutaric acid	GTA	-7.7
	C16	1-O-vanilloyl-beta-D-glucose	VBG	-7.5
	C51	Methyl geranate	MGN	-7.4
	C37	(-)-11-hydroxy-9,10-dihydrojasmonic acid 11-beta-D-glucoside	HDJ	-7.4
	-	Acarbose*	ACA	-7.3
AR	C14	(6E)-1-(4-hydroxyphenyl)-7-phenylhepta-4,6-dien-3-one	HPH	-9.9
	C106	(R)-7-butyl-6,8-dihydroxy-3-[(3E)-pent-3-en-1-yl]-3,4-dihydroisochromen-1-one	BHP	-8.6
	C31	Aesculin	AES	-8.5
	C64	Austricin	AUS	-8.5
	C37	(-)-11-hydroxy-9,10-dihydrojasmonic acid 11-beta-D-glucoside	HDJ	-8.5
	-	Epalrestat*	EPA	-6.3
DPP-4	C37	(-)-11-hydroxy-9,10-dihydrojasmonic acid 11-beta-D-glucoside	HDJ	-8.6
	C119	Caffeoyl tartaric acid	CTA	-8.0
	C106	(R)-7-butyl-6,8-dihydroxy-3-[(3E)-pent-3-en-1-yl]-3,4-dihydroisochromen-1-one	BHP	-7.8
	C81	Phaseic acid	PHA	-7.8
	C108	p-Coumaroyl malic acid	CMA	-7.7
	-	Sitagliptin*	SGT	-6.2
PTP1B	C81	Phaseic acid	PHA	-6.0
	C105	Tetradecanedioic acid	TDA	-5.8
	C52	2-Hydroxydecanedioic acid	HDA	-5.4
	C4	Methylisocitric acid	MCA	-5.2
	C69	Dodecanedioic acid	DCA	-5.2

	-	Ursolic acid*	URS	-5.2
SDH	C72	Erythronolide B	ETB	-9.2
	C111	(+)-Cnicin	CNI	-8.7
	C100	Blennin D	BLD	-8.5
	C37	(-)-11-hydroxy-9,10-dihydrojasmonic acid 11-beta-D-glucoside	HDJ	-8.4
	C106	(R)-7-butyl-6,8-dihydroxy-3-[(3E)-pent-3-en-1-yl]-3,4-dihydroisochromen-1-one	BHP	-8.3
	-	4-[2-1R-hydroxy-ethyl)-pyrimidin-4-yl]piperazine-1-sulfonic acid dimethylamide*	HPS	-5.0

*: reference standards against target enzyme. AA: alpha-amylase; AG: alpha-glucosidase; AR: aldose reductase; DPP-4: dipeptidyl peptidase-4; PTP1B: protein tyrosine phosphatase-1B; SDH: sorbitol dehydrogenase

3.4. Molecular dynamics simulation of identified CS metabolites against the target enzymes

The thermodynamic components of the top five CS compounds against each of the investigated enzyme following a 120-ns of MD simulation are presented in Table 2. The lowest change in Van der Waals energy (ΔEvdW) was observed for several CS compounds, including CUR, MGN, DCA, and BLD against AA, AG, PTB1B, and SDH following the 120 ns simulation. The lowest change in electrostatic energy (ΔE_{elec}) following the 120 ns simulation was observed for several CS compound-enzyme complexes, particularly AA-AUS, AG-MGN, AR-AUS, and SDH-BLD. Following the 120 ns simulation, AUS, MGN, DCA, and BLD exhibited the lowest changes in gas-phase energy (ΔG_{gas}) when bound to the enzyme targets AA, AG, PTP1B, and SDH. A lowest change in solvation free energy (ΔG_{solv}) was identified for multiple CS compounds interacting with enzyme targets, with the most notable complexes being AA-AUS, AG-MGN, AR-AUS, and PTP1B-DCA. Metabolites BHP, VBG, HDJ, CMA, HAD and HDJ had the highest negative ΔG_{bind} against AA, AG, AR, DPP-4, PTP1B and SDH, respectively. Except for AA-BHP complex (-40.30 ± 7.35 kcal/mol) which had lower negative ΔG_{bind} compared to AA-acarbose (49.08 ± 7.99 kcal/mol), others had higher negative ΔG_{bind} than their respective standards.

Table 2. Thermodynamic components of top 5 identified secondary metabolites present in CS against target enzymes

Thermodynamic energy components (kcal/mol)					
Complex	ΔE_{VdW}	ΔE_{elec}	ΔG_{gas}	ΔG_{solv}	ΔG_{bind}
Alpha-amylase					
AES	-28.64 ± 4.67	-38.73 ± 14.93	-67.37 ± 15.14	39.07 ± 8.41	-28.31 ± 8.24
BHP	-36.06 ± 3.95	-48.13± 14.03	-85.20 ± 14.41	45.17 ± 7.85	-40.30 ± 7.35
CUR	-24.89 ± 3.08	-27.14 ± 6.24	-52.03 ± 5.91	22.88 ± 3.75	-29.15 ± 3.74
HPH	-28.16 ± 4.81	-14.85 ± 6.56	-43.00 ± 6.46	19.40 ± 4.34	-23.55 ± 5.30
AUS	-24.98 ± 3.25	-10.72 ± 9.37	-35.69 ± 10.80	17.24 ± 7.93	-18.45 ± 4.04
ACA	-51.81 ± 5.29	-132.83 ± 15.05	-184.60 ± 14.87	135.57 ± 10.04	-49.08 ± 7.99
Alpha-glucosidase					
AUS	-24.10 ± 3.30	-44.02 ± 23.29	-68.12 ± 23.36	46.91 ± 18.00	-21.21 ± 7.72
GTA	-26.16 ± 4.32	-31.61 ± 22.53	-57.78 ± 23.27	35.19 ± 13.17	-22.57 ± 12.05
VBG	-23.42 ± 3.54	-72.98 ± 14.48	-96.40 ± 14.00	62.22 ± 8.84	-34.17 ± 6.08
MGN	-11.98 ± 9.58	-7.45 ± 8.63	-18.21 ± 16.09	11.29 ± 9.94	-6.92 ± 7.00
HDJ	-27.81 ± 4.45	-52.92 ± 14.77	-80.73 ± 13.48	52.10 ± 9.52	-28.63 ± 5.74
ACA	-31.64 ± 5.13	-161.95 ± 22.72	-193.60 ± 23.49	177.05 ± 20.09	-16.54 ± 6.71
Aldose reductase					
HPH	-35.06 ± 3.18	-25.23 ± 7.03	-60.30 ± 8.03	26.16 ± 3.87	-34.13 ± 5.05
BHP	-47.41 ± 2.95	-19.07 ± 4.47	-66.49 ± 5.16	25.64 ± 3.38	-40.85 ± 3.44
AES	-43.04 ± 5.01	-27.19 ± 9.85	-70.23 ± 11.30	33.01 ± 5.68	-37.22 ± 8.40
AUS	-35.07 ± 3.27	-13.42 ± 11.84	-48.50 ± 12.88	17.47 ± 7.66	-31.02 ± 5.99
HDJ	-58.97 ± 4.97	-33.08 ± 8.12	-92.06 ± 10.51	47.92 ± 5.78	-44.13± 6.75
EPA	-21.18 ± 5.82	-9.73 ± 8.05	-30.91 ± 9.94	15.80 ± 6.48	-15.10 ± 5.02
Dipeptidyl peptidase-4					
HDJ	-16.28 ± 12.70	-20.99 ± 25.20	-37.27 ± 33.50	25.26 ± 23.85	-12.00 ± 10.42
CTA	-23.08 ± 3.41	-49.31 ±16.10	-72.39 ± 15.32	55.70 ± 12.05	-16.69 ± 4.72
BHP	-36.40 ± 4.65	-46.36 ± 12.31	-82.77 ± 13.24	49.54 ± 8.24	-33.22 ± 6.24
PHA	-27.98 ± 3.30	-51.07 ± 8.92	-79.06 ± 8.45	57.26 ± 6.46	-21.79 ± 4.06

CMA	-18.45 ± 3.76	-77.1195 ± 8.25	-95.58 ± 7.62	61.16 ± 5.38	-34.40 ± 4.17
HDJ	-39.63 ± 4.59	-254.13 ± 12.21	-293.75 ± 12.39	262.99 ± 11.01	-30.77 ± 4.71
Protein tyrosine phosphatase B					
PHA	-16.47 ± 5.83	-11.47 ± 8.38	-27.94 ± 11.01	19.30 ± 8.62	-8.64 ± 3.49
TDA	-20.88 ± 6.79	-18.80 ± 13.35	-39.68 ± 16.18	21.95 ± 11.27	-17.72 ± 6.72
HDA	-21.31 ± 4.27	-20.75 ± 10.38	-42.07 ± 11.85	22.36 ± 7.68	-19.71 ± 5.86
MCA	-16.76 ± 3.66	-29.90 ± 14.68	-46.66 ± 16.42	33.19 ± 12.75	-13.47 ± 4.53
DCA	-13.54 ± 7.80	-13.76 ± 10.83	-27.30 ± 15.28	14.77 ± 8.80	-12.52 ± 8.06
URS	-30.78 ± 3.51	-13.01 ± 6.23	-36.19 ± 6.89	20.15 ± 5.79	-16.03 ± 4.03
Sorbitol dehydrogenase					
ETB	-28.90 ± 3.75	-23.10 ± 14.35	-52.01 ± 15.71	31.37 ± 10.29	-20.63 ± 7.06
CNI	-27.87 ± 5.69	-22.19 ± 14.26	-50.06 ± 14.79	27.99 ± 9.04	-22.06 ± 7.03
BLD	-23.54 ± 5.45	-12.27 ± 7.63	-35.82 ± 10.79	17.13 ± 6.44	-18.69 ± 7.07
HDJ	-40.01 ± 6.01	-56.06 ± 9.90	-96.08 ± 13.13	59.46 ± 7.41	-36.61 ± 7.39
BHP	-32.12 ± 4.05	-35.79 ± 8.64	-67.92 ± 9.72	40.60 ± 5.70	-27.31 ± 5.25
HPS	-36.62 ± 5.69	-12.81 ± 6.22	-44.43 ± 9.35	8.19 ± 5.02	-34.24 ± 9.18

Key: $\Delta E_{vdW:}$ Van der Waals energy; ΔE_{elec}: electrostatic energy; ΔE_{gas}: gas-phase free energy; ΔG_{solv} solvation free energy and ΔG_{bind}: total binding free energy. AES: aesculin; BHP: (R)-7-butyl-6,8-dihydroxy-3-[(3e)-pent-3-en-1-yl]-3,4-dihydroisochromen-1-one; CUR: curvularol; HPH: (6e)-1-(4-hydroxyphenyl)-7-phenylhepta-4,6-dien-3-one; AUS: austricin; ACA: acarbose; GTA: glutaric acid; VBG: 1-O-vanilloyl-beta-D-glucose; MGN: methyl geranate; HDJ: (6e)-1-(4-hydroxyphenyl)-7-phenylhepta-4,6-dien-3-one; EPA: epalrestat; CTA: caffeoyl tartaric acid; PHA: phaseic acid; CMA: p-coumaroyl malic acid; SGT: sitagliptin; TDA: tetradecanedioc acid; HDA: 2-hydroxydecanedioic acid; MCA: methylisocitric acid; DCA: dodecanedioc acid; URS: ursolic acid; ETB: erythronolide B; CNI: cnicin; BLD: blennin D; HPS: 4-[2-1R-hydroxy-ethyl)-pyrimidin-4- yl]piperazine-1-sulfonic acid dimethylamide

The alterations in structure and conformation resulting from the interactions of the top-ranked metabolites of CS with the enzymes during the simulation periods are presented in Tables 3 and Figures 5 – 10. All CS metabolites-AA complexes had higher average RMSD values than apo-AA (1.57 Å), except for AA-AES (1.52 Å) displaying the lowest average RMSD among the metabolite-AA complexes (Table 3). Following equilibration at 10 ns, RMSD of all AA complexes fluctuated between 1.10 Å and 2.25 Å throughout the remaining simulation, while AA-CUR fluctuated to 2.50 Å from 70 ns till the end of the simulation (Figure 5a). Conversely, both apo-AA (0.94 Å) and AA-ACA (0.97 Å) exhibited lower mean RMSF values than all AA

complexes, except for CUR (0.70 Å) (Table 3). Additionally, the complexes displayed random fluctuations in RMSF between 0.5 Å and 2.5 Å, with major fluctuations observed in various residues, including 120 – 140, 180 – 200, 240 – 320, 340 – 400, 405 – 410, and 450 – 495 swaying between 0.5 Å and 5.75 Å (Figure 5b). Similarly, all AA-complexes exhibited lower mean ROG values compared to apo-AA except CUR- (23.38 Å) and AUS- AA complexes (23.45 Å) (Table 3). After 5 ns, a stable ROG plot for all the bound complexes between 23.9 Å and 23.6 Å was observed except for ACA, which exhibited random fluctuations at 30, 80, and 100 ns (Figure 5c). A marginal increase in the mean number of hydrogen bonds formed in the CS metabolites complexes relative to the apo-enzyme was observed [BHP (266.49), CUR (267.01), and AES (267.39) compared to apo-AA (266.48)]. Interestingly, except for AUS (258.22), all AA complexes exhibited a higher mean number of hydrogen bonds than ACA (260.75) (Table 3). There was a slight fluctuation between 230 and 310 in number of hydrogen bonds formed during the 120 ns simulation period otherwise, no major fluctuations were observed (Figure 5d). Among the complexes, AA-AUS formed a greater number of hydrogen bonds compared to the other AA complexes (Figure 5d). Regarding SASA, an increase in the mean value was observed for all complexes compared to apo-AA (17130.45 Å) and ACA (17301.00 Å) (Table 3). Following a steady increase during the initial 5 ns of the simulation, all AA complexes exhibited a stable and continuous increase within the range of 16000 Å and 19000 Å (Figure 5e).

Table 3. Mean post-molecular dynamics parameters of top 5 identified metabolites of corn silk against the target enzymes

Complex	RMSD (Å)	RMSF (Å)	ROG (Å)	Number of H-Bonds	SASA (Å)
AA (apo-enzyme)	1.57 ± 0.15	0.94 ± 0.41	23.31 ± 0.09	266.48 ± 11.04	17130.45 ± 426.56
AA-AES	1.52 ± 0.14	1.01 ± 0.50	23.28 ± 0.09	267.39 ± 10.24	17547.30 ± 595.29
AA-BHP	1.89 ± 0.22	1.04 ± 0.68	23.20 ± 0.07	266.49 ± 10.61	17413.58 ± 411.68
AA-CUR	1.78 ± 0.30	0.70 ± 0.31	23.38 ± 0.11	267.01 ± 10.31	17492.10 ± 512.41
AA-HPH	1.67 ± 0.16	1.05 ± 0.56	23.27 ± 0.09	260.07 ± 10.67	17815.54 ± 514.36
AA-AUS	1.85 ± 0.25	1.20 ± 0.64	23.45 ± 0.14	258.22 ± 10.70	18410.21 ± 602.75
AA-ACA	1.82 ± 0.47	0.97 ± 0.25	23.28 ± 0.09	260.75 ± 10.62	17301.00 ± 421.52
AG (apo-enzyme)	1.61 ± 0.19	1.07 ± 0.55	27.77 ± 0.06	427.02 ± 12.77	29619.23 ± 477.95

AG-AUS	1.73 ± 0.18	0.85 ± 0.38	27.96 + 0.09	413.94 ± 13.26	30865.47 ± 658.70
AG-GTA	2.20 ± 0.23	1.03 ± 0.57	27.83 ± 0.06	410.42 ± 12.99	30623.51 ± 540.63
AG-VBG	1.95 ± 0.25	1.09 ± 0.63	27.76 ± 0.10	405.92 ± 13.50	29917.13 ± 566.38
AG-MGN	1.81 ± 0.19	1.09 ± 0.56	27.99 ± 0.11	411.04 ± 15.87	30951.06 ± 584.89
AG- HDJ	1.70 ± 0.12	1.06 ± 0.46	28.05 ± 0.09	415.38 ± 13.28	31439.30 ± 660.19
AG-ACA	1.65 ± 0.10	1.00 ± 0.44	27.84 ± 0.08	427.01 ± 13.66	29417.32 ± 532.42
AR (apo-enzyme)	1.59 ± 0.23	1.05 0.64±	19.33 ± 0.06	138.95 ± 8.05	13387.83 ± 284.35
AR-HPH	1.49 ± 0.22	1.07 ± 0.66	19.17 ± 0.09	142.29 ± 8.19	12864.95 ± 380.00
AR-BHP	1.24 ± 0.14	0.91 ± 0.51	19.11 ± 0.07	142.32 ± 7.87	12525.95 ± 307.21
AR-AES	1.57 ± 0.21	1.09 ± 0.59	19.27 ± 0.06	140.52 ± 7.99	12884.81 ± 275.19
AR-AUS	1.36 ± 0.14	1.03 ± 0.58	19.29 ± 0.09	134.74 ± 8.28	13134.07 ± 315.08
AR-HDJ	1.58 ± 0.29	0.76 ± 0.32	19.18 ± 0.06	143.24 ± 8.04	12661.33 ± 326.55
AR-EPA	2.00 ± 0.31	1.12 ± 0.73	19.45 ± 0.08	137.55 ± 7.96	13339.97 ± 304.39
DPP-4 (apo-enzyme)	1.81 ± 0.14	1.14 ± 0.59	27.04 ± 0.10	387.26 ± 12.43	29772.27 ± 407.99
DPP-4-HDJ	2.20 ± 0.42	1.30 ± 1.67	27.36 ± 0.21	380.75 ± 12.55	30518.02 ± 471.31
DPP-4-CTA	1.81 ± 0.18	1.23 ± 0.70	27.12 ± 0.09	376.11 ± 14.39	30495.52 ± 488.42
DPP-4-BHP	2.23 ± 0.33	1.30 ± 0.65	27.29 ± 0.11	387.35 ± 12.78	30644.12 ± 571.00
DPP-4-PHA	2.12 ± 0.28	1.14 ± 0.75	27.19 ± 0.10	383.89 ± 12.19	29588.14 ± 407.11
DPP-4-CMA	2.49 ± 0.23	1.14 ± 0.52	27.28 ± 0.12	382.29 ± 12.21	30372.92 ± 431.08
DPP-4-SGT	2.32 ± 0.32	1.23 ± 0.84	27.23 ± 0.14	385.80 ± 12.28	29879.51 ± 471.52
PTP1B (apo-enzyme)	1.47 ± 0.23	1.15 ± 0.54	19.37 ± 0.07	159.89 ± 8.32	13132.84 ± 295.15
PTP1B-PHA	1.44 ± 0.20	1.13 ± 0.88	19.49 ± 0.13	156.33 ± 9.00	13899.21 ± 563.67
PTP1B-TDA	1.39 ± 0.19	0.99 ± 0.53	19.36 ± 0.09	155.92 ± 8.78	13415.10 ± 338.21
PTP1B-HDA	1.15 ± 0.10	1.01 ± 0.52	19.33 ± 0.06	163.00 ± 8.44	13039.12 ± 293.12
PTP1B-MCA	1.14 ± 0.14	0.99 ± 0.54	19.25 ± 0.06	161.67 ± 8.17	13059.97 ± 422.08
PTP1B-DCA	1.70 ± 0.28	1.14 ± 1.55	19.47 ± 0.11	155.44 ± 8.57	13903.14 ± 284.06
PTP1B-URS	1.15 ± 0.10	1.00 ± 0.42	19.27 ± 0.06	159.76 ± 8.62	13136.17 ± 295.29

SDH (apo-enzyme)	2.48 ± 0.44	1.35 ± 1.01	20.72 ± 0.15	131.92 ± 7.41	12222.97 ± 332.44
SDH- ETB	2.41 ± 0.30	1.33 ± 0.99	21.16 ± 0.16	133.65 ± 7.69	12433.06 ± 250.00
SDH-CNI	3.15 ± 0.38	1.50 ± 1.25	21.22 ± 0.19	131.58 ± 7.58	12389.66 ± 331.358
SDH-BLD	2.42 ± 0.43	1.29 ± 0.81	21.02 ± 0.16	168.23 ± 8.86	14797.04 ± 277.96
SDH-HDJ	2.85 ± 0.51	1.44 ± 1.00	21.21 ± 0.22	133.37 ± 7.85	12145.93 ± 288.83
SDH-BHP	2.79 ± 0.28	1.37 ± 0.90	20.90 ± 0.12	161.22 ± 8.57	14975.50 ± 359.245
SDH-HPS	2.91 ± 0.55	1.35 ± 0.94	21.17 ± 0.19	166.34 ± 8.38	14759.29 ± 301.96

RMSD: root mean square deviation; RMSF: root mean square fluctuation; ROG: radius of gyration; H-bonds: hydrogen bonds; SASA; solvent accessible surface area; AA: alpha-amylase; AG: alpha-glucosidase; AR: aldose reductase; DPP-4: dipeptidyl peptidase-4; PTP1B: protein tyrosine phosphatase 1B; SDH: sorbitol dehydrogenase; AES: aesculin; BHP: (R)-7-butyl-6,8-dihydroxy-3-[(3e)-pent-3-en-1-yl]-3,4-dihydroisochromen-1-one; CUR: curvularol; HPH: (6e)-1-(4-hydroxyphenyl)-7-phenylhepta-4,6-dien-3-one; AUS: austricin; ACA: acarbose; GTA: glutaric acid; VBG: 1-O-vanilloyl-beta-D-glucose; MGN: methyl geranate; HDJ: (6e)-1-(4-hydroxyphenyl)-7-phenylhepta-4,6-dien-3-one; EPA: epalrestat; CTA: caffeoyl tartaric acid; PHA: phaseic acid; CMA: p-coumaroyl malic acid; SGT: sitagliptin; TDA: tetradecanedioc acid; HDA: 2-hydroxydecanedioic acid; MCA: methylisocitric acid; DCA: dodecanedioc acid; URS: ursolic acid; ETB: erythronolide B; CNI: cnicin; BLD: blennin D; HPS: 4-[2-1R-hydroxy-ethyl)-pyrimidin-4- yl]piperazine-1-sulfonic acid dimethylamide.

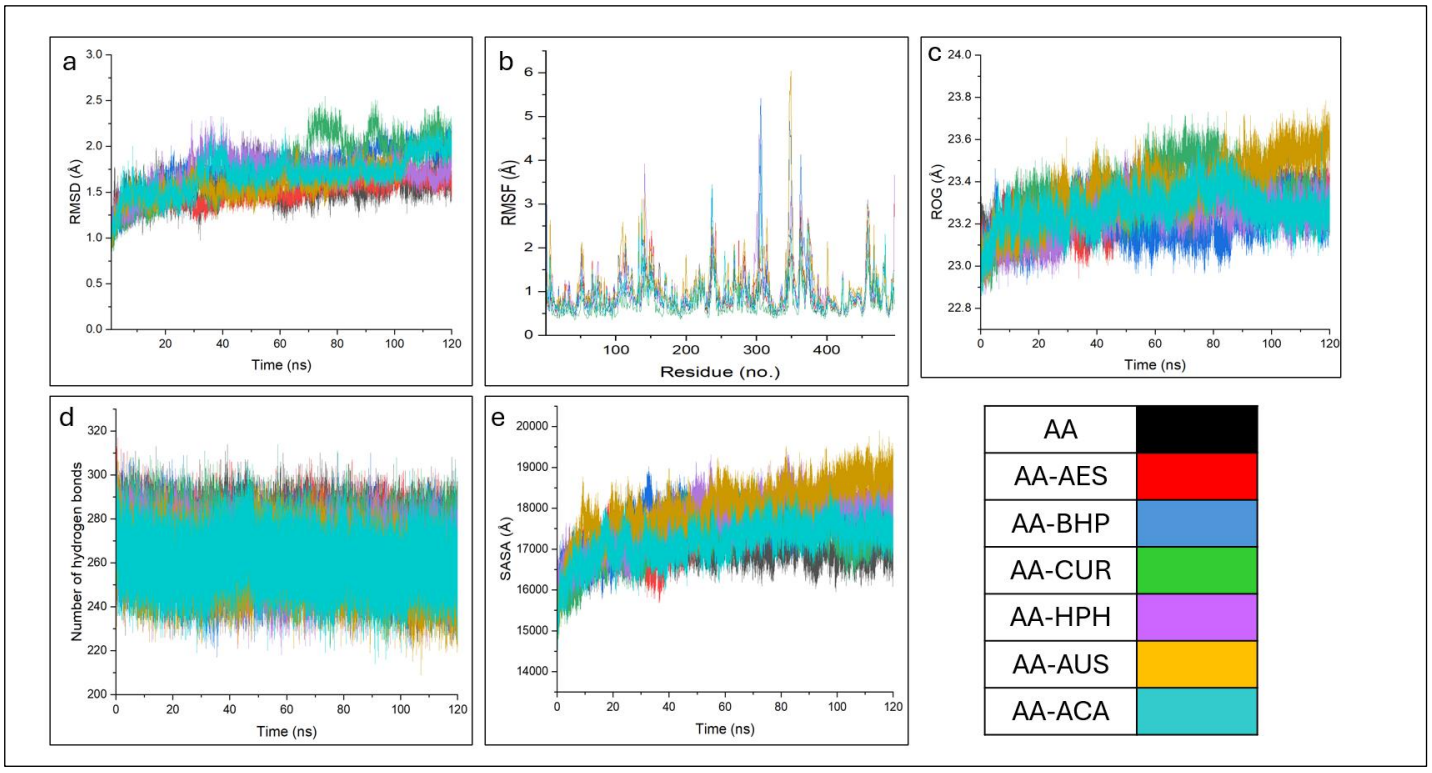

Figure 5: Post-dynamic component plots resulting from the binding of CS metabolites to AA presented as a) root mean square deviation (RMSD), b) root mean square fluctuation (RMSF),

c) radius of gyration (ROG), d) number of hydrogen bonds and e) solvent accessible area (SASA). AA: alpha-amylase; AES: aesculin; BHP: (R)-7-butyl-6,8-dihydroxy-3-[(3e)-pent-3-en-1-yl]-3,4-dihydroisochromen-1-one; CUR: curvularol; HPH: (6e)-1-(4-hydroxyphenyl)-7-phenylhepta-4,6-dien-3-one; AUS: austricin; ACA: acarbose

All AG complexes exhibited a higher average RMSD compared to both apo-AG (1.61 Å) and apo-ACA (1.65 Å) (Table 3). Following equilibration at 5 ns, fluctuations within the range of 0.75 Å to 2.5 Å persisted until the end of the simulation in all the bound complexes, (Figure 6a). The mean RMSF of apo-AG (1.07 Å) exceeded that of the AG-CS metabolites complexes apart from VBG (1.09 Å) and MGN (1.09 Å). Notably, the AG-AUS complex displayed the lowest average RMSF (0.85 Å) among all the complexes (Table 3). Upon binding to AG, all investigated compounds exhibited random fluctuations between 0.5 Å and 6 Å, with major fluctuations occurring sporadically across various amino acid residues (Figure 6b). Similarly, except for VBG (27.76 Å), all AG complexes demonstrated higher mean ROG values compared to apo-AG (27.77 Å), (Table 3). The ROG of all AG complexes fluctuated between 27.5 Å and 28.2 Å, with a decrease in ROG plot for VBG complex observed between 40 ns and 50 ns, as shown in Figure 6c. In contrast to apo-AG (427.02), a reduction in the mean number of hydrogen bonds was observed for all AG complexes (Table 3). Throughout the 120 ns simulation, the number of hydrogen bonds formed between AG complexes ranged from 360 to 470, showing no significant fluctuations in the plot (Figure 6d). However, higher average SASA values were observed for all AG complexes relative to apo-AG (29619.23 Å) and AG-ACA (29417.32 Å) (Table 3). After an equilibration in the SASA plot at 10 ns and 27 000 Å, all AG complexes fluctuated between 28000 Å and 32500 Å till the end of the simulation (Figure 6e).

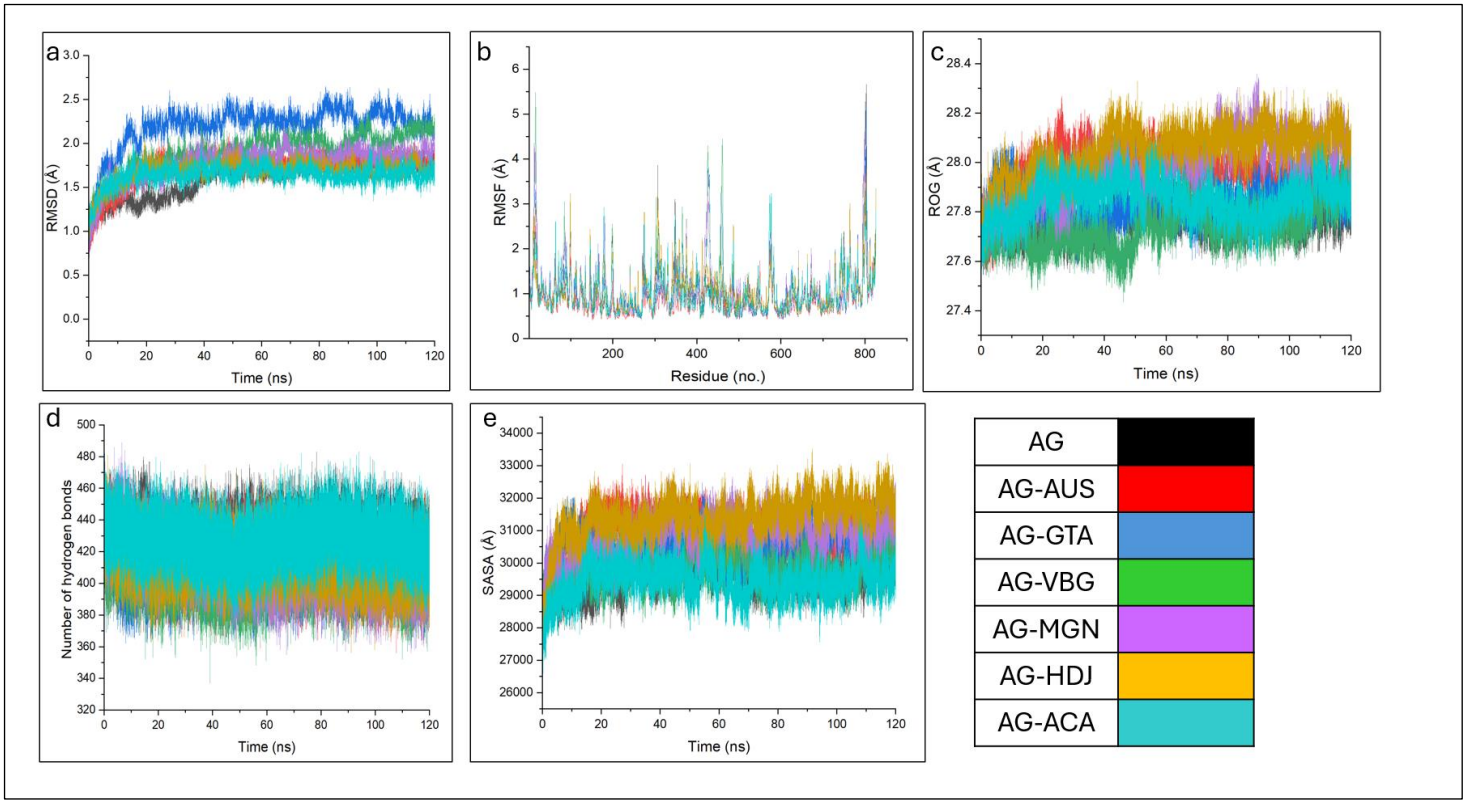

Figure 6: Post-dynamic component plots resulting from the binding of CS metabolites to AG presented as a) RMSD, b) RMSF, c) ROG, d) number of hydrogen bonds and e) SASA. AG: alpha-glucosidase; AUS: austricin; ; GTA: glutaric acid; VBG: 1-O-vanilloyl-beta-D-glucose; MGN: methyl geranate; HDJ: (6e)-1-(4-hydroxyphenyl)-7-phenylhepta-4,6-dien-3-one; ACA: acarbose

A decrease in the mean RMSD was noted for all AR complexes compared to the apo-AR (1.59 Å), except for EPA (2.00 Å), which exhibited an increase in the mean RMSD (Table 3). Following a steady rise in RMSD from 0.5 Å during the initial 5 ns of the simulation, the system reached equilibrium, and the RMSD of all AR complexes varied between 0.9 Å and 2.5 Å (Figure 7a). All examined AR complexes displayed a decline in the average RMSF, with HDJ exhibiting the lowest mean RMSF (0.76 Å) compared to apo-AR (1.05) and AR-EPA (1.12) (Table 3). After an initial decrease in RMSF during the first 5 ns of the simulation, all AR complexes fluctuated between 0.5 Å and 5 Å, with notable fluctuations observed in residues 25 – 50, 50 – 60, 75 – 90, 130 – 150, and 215 – 250 (Figure 7b). Similarly, all AR complexes demonstrated a decrease in their average ROG values compared to apo-AR (19.33), except for EPA, which exhibited an increase (19.45 Å) (Table 3). Throughout the simulation, the ROG fluctuated between 19.8 Å and 19.75 Å, with higher variations observed in EPA and AR-HDJ (Figure 7c). All AR complexes displayed a higher number of hydrogen bonds compared to apo-AR (138.95), except for AUS (134.74) (Table 3). The number of hydrogen bonds for all AR complexes ranged from 110 to 170, with no major fluctuations observed

(Figure 7d). In contrast to apo-AR (13387.83 Å), all AR complexes exhibited a decrease in mean SASA values, except for EPA (13339.97 Å) (Table 3). Following an initial increase in SASA during the first 5 ns, all AR complexes fluctuated between 11500 Å and 14500 Å, without significant variations (Figure 7e).

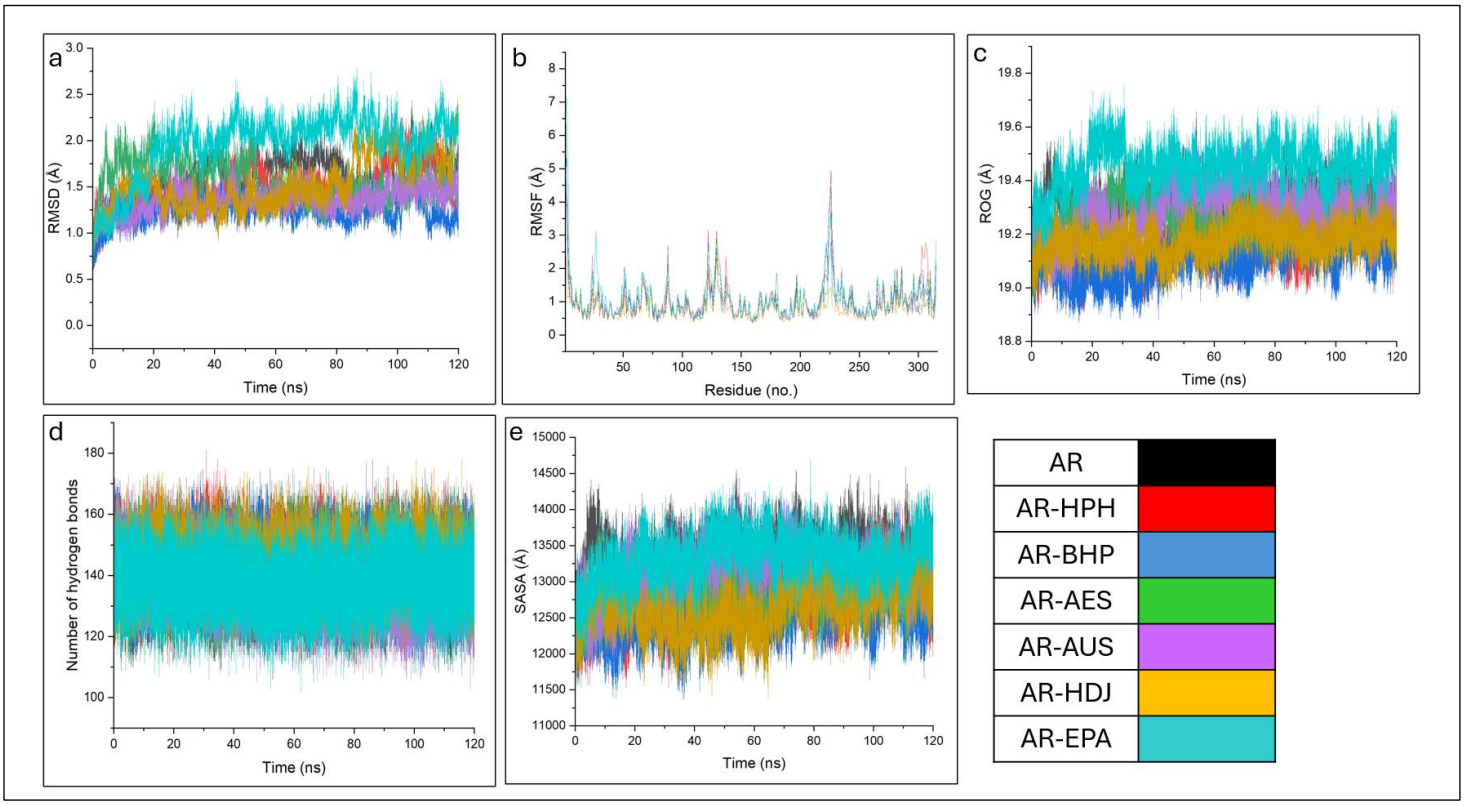

Figure 7. Post-dynamic component plots resulting from the binding of CS metabolites to AR presented as a) RMSD, b) RMSF, c) ROG, d) number of hydrogen bonds and e) SASA. AR: aldose reductase; HPH: (6e)-1-(4-hydroxyphenyl)-7-phenylhepta-4,6-dien-3-one; BHP: (R)-7-butyl-6,8-dihydroxy-3-[(3e)-pent-3-en-1-yl]-3,4-dihydroisochromen-1-one; AES: aesculin; AUS: austricin; HDJ: (6e)-1-(4-hydroxyphenyl)-7-phenylhepta-4,6-dien-3-one; EPA: epalrestat

All DPP-4 complexes exhibited higher average RMSD values relative to the apo-DPP-4 (1.81 Å) except for CTA (1.81 Å) which reported an equal value (Table 3). After an initial increase in RMSD from 0.5 Å, all DPP-4 complexes fluctuated between 1.25 Å and 3.5 Å with CMA and HDJ showing major fluctuations at 8 ns and 50 ns respectively (Figure 8a). In contrast to apo-DPP-4 (1.14 Å), all DPP-4 complexes had higher mean RMSF, except PHA(1.14 Å) and CMA (1.14 Å) with equal average RMSF value (Table 3). The RMSF of all DPP-4 complexes fluctuated between 0.5 – 3.5 Å, except for a major fluctuation increase to 8 Å between residues 200 – 240 (Figure 8b). All DPP-4 complexes showed an increase in mean ROG in comparison

to apo-DPP-4 (27.04 Å) (Table 3). After an increase in ROG from 26.6 Å during the first 5 ns, all DPP-4 complexes fluctuated between 26.8 Å and 27.3 Å except for HDJ and BHP which had increases ranging between 27.8 – 28.1 Å between 20 ns to 40 ns and 50 ns to 60 ns respectively (Figure 8c). All DPP-4 complexes showed a reduction in the mean number of hydrogen bonds in comparison to apo-DPP-4 (387.26), except for BHP (387.35) which had an increase (Table 3). The number of hydrogen bonds fluctuated between 320 and 440 throughout the 120 ns simulation (Figure 8d). In comparison to apo-DPP-4 (29772.27 Å), all DPP-4 complexes showed an increase in mean SASA except for PHA (29588.14 Å) (Table 3). Once the complexes equilibrated after 10 ns, the SASA of all DPP-4 complexes fluctuated between 28500 – 32500 Å (Figure 8e).

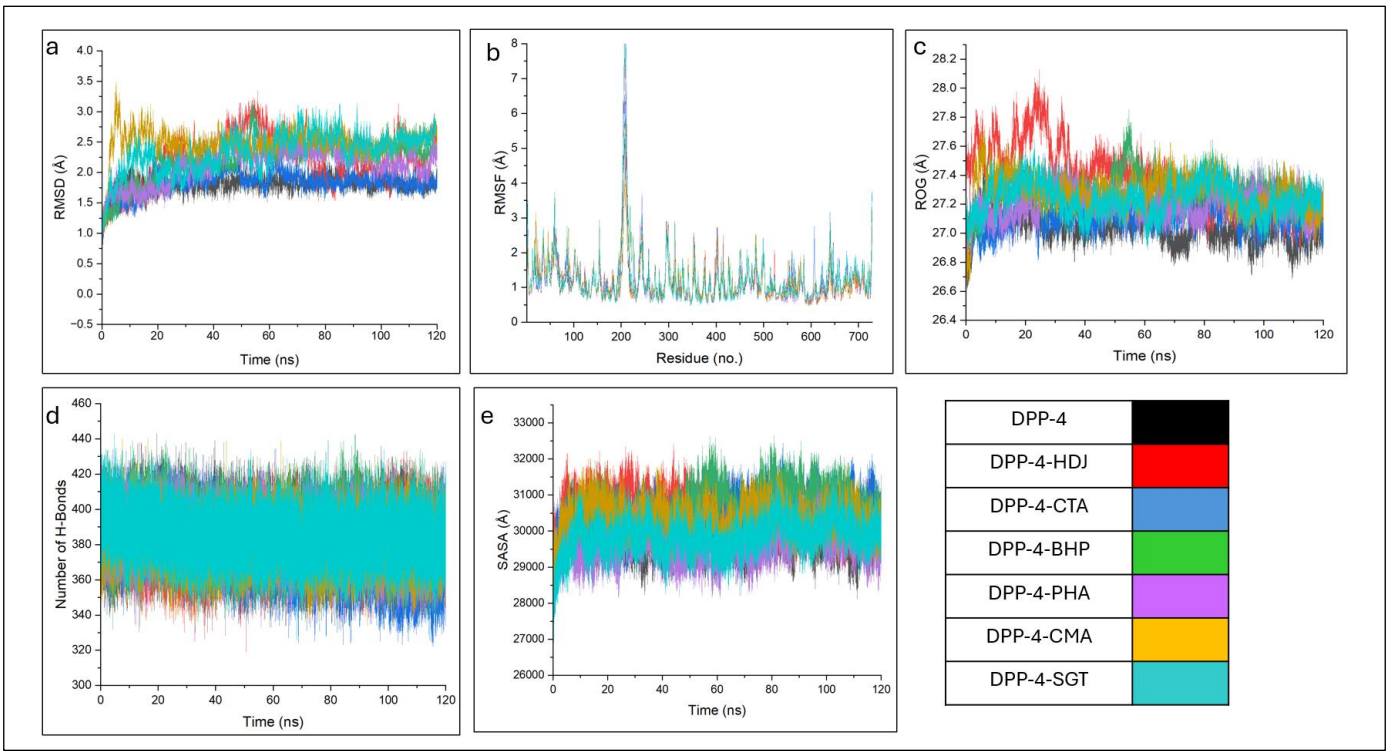

Figure 8. Post-dynamic component plots resulting from the binding of CS metabolites to DPP-4 presented as a) root mean square deviation (RMSD), b) root mean square fluctuation (RMSF), c) radius of gyration (ROG), d) number of hydrogen bonds and e) solvent accessible area (SASA). DPP-4: dipeptidyl peptidase-4; ; HDJ: (6e)-1-(4-hydroxyphenyl)-7-phenylhepta-4,6-dien-3-one; CTA: caffeoyl tartaric acid; ; BHP: (R)-7-butyl-6,8-dihydroxy-3-[(3e)-pent-3-en-1-yl]-3,4-dihydroisochromen-1-one; PHA: phaseic acid; CMA: p-coumaroyl malic acid; SGT: sitagliptin

When bound to PTP1B, all compounds exhibited a reduction in mean RMSD in comparison to apo-PTP1B (1.47 Å), except for DCA (1.70 Å). Notably, MCA displayed the lowest mean

RMSD of 1.14 Å when bound to PTP1B, lower than the PTP2B-URS complex (1.15 Å) (Table 3). Following an initial increase during the first 10 ns of the simulation, all PTP1B complexes exhibited fluctuations within the range of 0.75 – 2.00 Å, except for DCA, which fluctuated to 2.5 Å between 85 ns and 105 ns (Figure 9a). In comparison to the apo-PTP1B (1.15 Å), all PTP1B complexes had lower RMSF values, with MCA and TDA exhibiting the lowest mean RMSF of 0.99 ÅÅ, both notably comparable to URS (1.00 Å) (Table 3). The RMSF for all complexes varied within the range of 0.5 Å to 4.00 Å. Notably, DCA, TDA, and PHA displayed an increase in RMSF, ranging from 5.80 Å to 9.80 Å, specifically at residues 280 – 299. (Figure 9b). The mean ROG of all PTP1B complexes were comparably lower in comparison to apo-PTP1B (19.37 Å), with exception to PHA (19.49 Å) and DCA (19.47 Å). Interestingly, MCA (19.25 Å) exhibited the lowest mean RMSF, which was marginally less than URS (19.27 Å) (Table 3). During the 120 ns simulation the ROG of all PTP1B complexes fluctuated between 19.05 Å to 19.75 Å, except DCA, TDA and PHA with terminal fluctuations ranging from 19.90 Å to 20.10 Å between 110 – 120 ns (Figure 9c). The average number of hydrogen bonds formed between the PTP1B complexes compared to apo-PTP1B (159.89) decreased during the simulation, with exception to MCA (161.67) and HDA (163.67) which were comparably higher (Table 3). The number of hydrogen bonds formed between all the PTP1B complexes ranged between 120 – 190 during the 120 ns simulation (Figure 9d). All PTP1B complexes revealed a higher average SASA in contrast to apo-PTP1B (13132.84 Å), except for HDA (13039.12 Å) and MCA (13059.97 Å) which were notably lower (Table 3). After an increase in the SASA values during the initial 5 ns, all PTP1B complexes fluctuated between 12250 – 145000 Å with PHA and DCA increasing to 15250 Å during the final 20 ns of the simulation (Figure 9e).

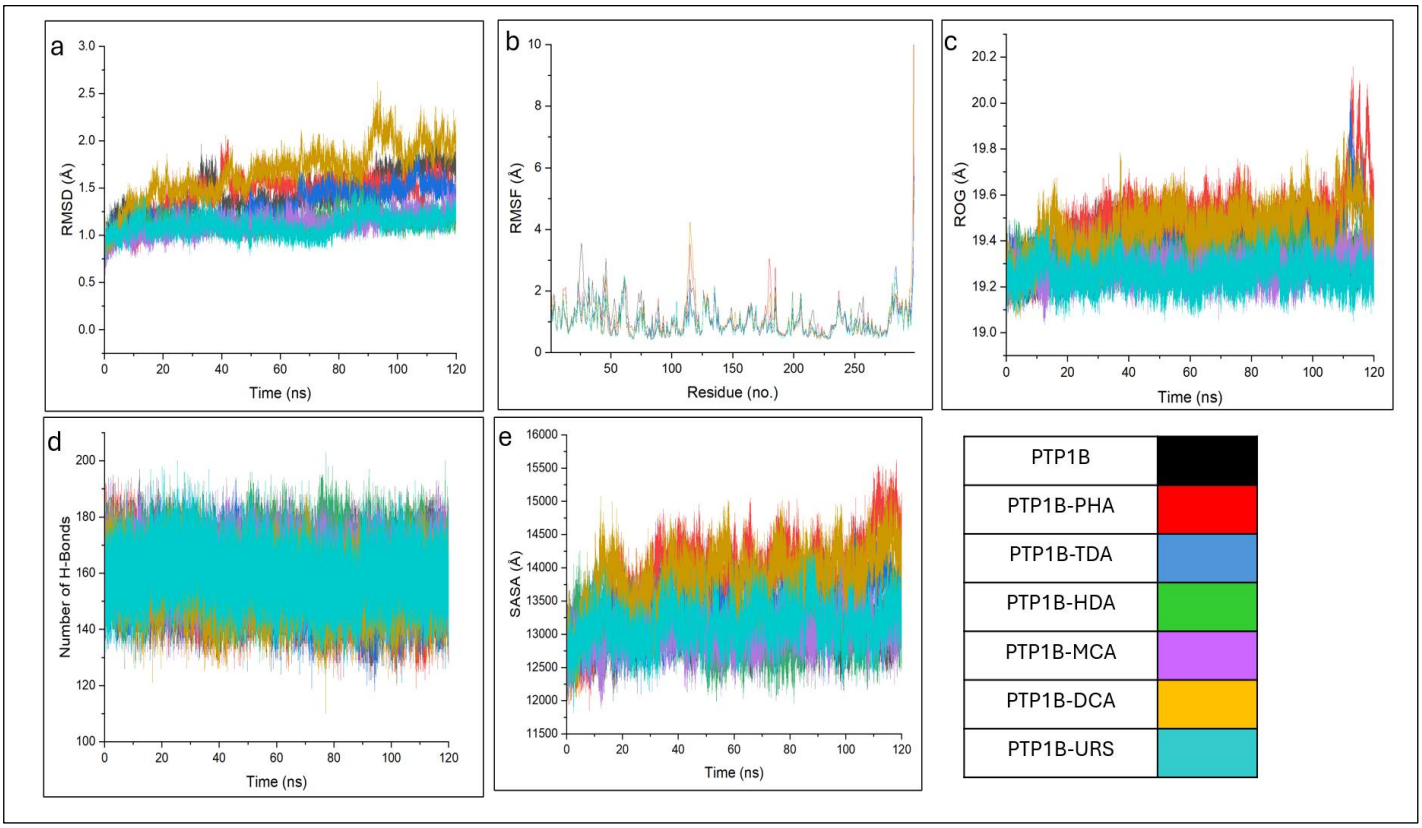

Figure 9. Post-dynamic component plots resulting from the binding of CS metabolites to PTP1B presented as a) root mean square deviation (RMSD), b) root mean square fluctuation (RMSF), c) radius of gyration (ROG), d) number of hydrogen bonds and e) solvent accessible area (SASA). PTP1B: protein tyrosine phosphatase 1B; PHA: phaseic acid; TDA: tetradecanedioc acid; HDA: 2-hydroxydecanedioic acid; MCA: methylisocitric acid; DCA: dodecanedioc acid; URS: ursolic acid

When bound to SDH, the investigated compounds displayed elevated mean RMSD values than apo-SDH (2.48 Å), with exception to ETB (2.41 Å) and BLD (2.45 Å), both of which exhibited lower values. In comparison to the AA-HPS (2.91 Å) (standard) complex, all SDH-CS complexes had lower mean RMSD, except for CNI (3.15 Å) (Table 3). The examined SDH complexes had RMSD values ranging from 1.00 Å to 4.00 Å during the simulation (Figure 10a). The mean RMSF of apo-SDH (1.35 Å) complex and SDH-HPS (1.35) complex were lower in comparison to the SDH-CS metabolite complexes, except for ETB (1.33 Å) and BLD (1.29 Å). Following a decline in the range of residues 0 – 10, the RMSF of the scrutinized SDH complexes exhibited fluctuations spanning from 0.50 Å to 3.00 Å at until residue 350. Pronounced variations were noted particularly between residues 40 – 75, 100 – 125, and 260 – 300, culminating in a significant surge in RMSF to 8.30 Å observed within residues 350 – 356 (Figure 10b). In comparison to apo-SDH (20.72 Å), the investigated SDH complexes

demonstrated higher mean ROG values. However, CS metabolites BHP (20.90 Å) and BLD (21.02 Å) had lower mean ROG when bound to SDH in comparison to the standard HPS (21.17 Å) (Table 3). Throughout the 120 ns simulation, fluctuations in ROG were observed, with the complexes showcasing a range between 20.30 Å and 22.10 Å (Figure 10c). Regarding the mean number of hydrogen bonds formed among the SDH complexes, all displayed an increase compared to apo-SDH (131.92), except CNI (131.58), which demonstrated a relatively similar number of hydrogen bonds. Interestingly, BLD (168.23) exhibited a higher number of hydrogen bonds in comparison to HPS (166.34) (Table 3). Throughout the 120 ns simulation, the number of hydrogen bonds exhibited fluctuations ranging between 100 and 200 for the SDH complexes. Notably, HPS and BLD stood out by displaying a higher number of hydrogen bonds when bound to SDH, as illustrated in Figure 10d. Among the SDH complexes, several displayed an increase in the mean SASA when compared to apo-SDH (12222.97 Å), except for HDJ (12145.93 Å) which showcased the lowest mean SASA value (Table 3). The SASA of all SDH complexes varied from 11250 to 16500, with the larger values attributed to BHP and HPS (Figure 10e).

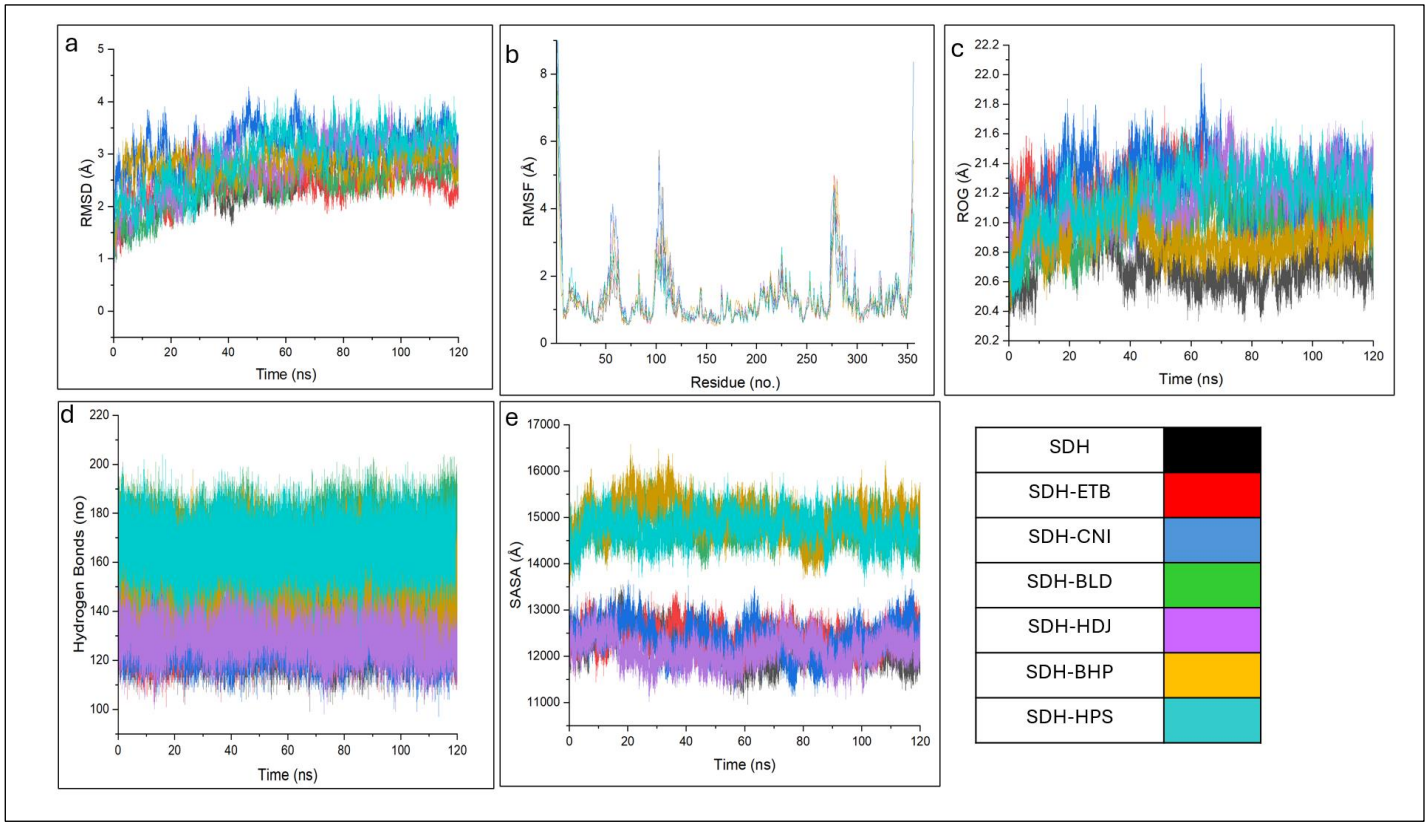

Figure 10: Post-dynamic component plots resulting from the binding of CS metabolites to SDH presented as a) root mean square deviation (RMSD), b) root mean square fluctuation (RMSF), c) radius of gyration (ROG), d) number of hydrogen bonds and e) solvent accessible area

(SASA). SDH: sorbitol dehydrogenase; cnicin; BLD: blennin D; HDJ: (6e)-1-(4-hydroxyphenyl)-7-phenylhepta-4,6-dien-3-one; BHP: (R)-7-butyl-6,8-dihydroxy-3-[(3e)-pent-3-en-1-yl]-3,4-dihydroisochromen-1-one; HPS: 4-[2-1R-hydroxy-ethyl)-pyrimidin-4- yl]piperazine-1-sulfonic acid dimethylamide

The 2D interaction plots of the top ranked CS compounds (highest negative ΔG_{bind} against their respective target enzymes over the 120 ns simulation showed various types of bonds namely hydrogen bonds (conventional and carbon), attractive charge, Van der Waals, pi-pi-stacked, pi-pi T-shaped, pi-cation, pi-anion, pi-alkyl, alky, halogen (fluoride), unfavorable acceptor–acceptor and donor–donor interactions (Figures 11 -17). The interactions between AA and BHP at 120 ns had 19 interactions [6 hydrogen (GLN 62, ASP 196, GLU 232, ASN 297, HIE 298 and ASP 299), 10 Van der Waals (TRP 57, TYR 61, HIE 100, THR 162, LEU 164, ARG 195, ALA 197, ILE 234, PHE 255, and ASN 300), 1 pi-pi stacked (TRP 58) 1 pi-pi T-shaped (TRP 58) and 1 pi-alkyl (TRP 58). (Figure 11a). The interactions formed between AA and ACA at the end of the stimulation resulted in 22 interactions [8 hydrogen bonds (HIE 100, THR 163, ASP 196, HID 200, HID 298, 2 at ASP 299 and HIP 300), 11 Van der Waals (TRP 57, TRP 58, TYR 61, GLN 62, VAL 97, TYR 150, ARG 194, ALA 197, LYS 199, ILE 234 and PHE 255), 2 pi-pi alkyl (LEU 161 and LEU 162) and 1 pi-anion (ASP 299)] after 120 ns (Figure 11b). Following 120 ns, the number of interactions formed between AG and VBG were 19 interactions consisting of 8 hydrogen bonds (2 at ASP 175, ILE 176, 2 at HIE 569, ASP 300 and 2 at 511), 6 Van der Waals (ALA 177, TRP 410, ARG 495, GLY 510, ASP 540 and ARG 567), 1 pi-anion (ASP 412), 1 pi-pi stacked (TRP 272) and 3 pi-alkyl (TRP 508, PHE 544 and HIE 569)] as shown in Figure 12a. At 120 ns, ACA formed 10 interactions when bound to AG [1 hydrogen bond (ARG 241), 8 Van der Waals (MET 200, GLY 240, THR 242, GLU 244, PRO 626, THR 642, ARG 642 and ASN 701) and 1 pi-anion (MET 245)] (Figure 12b). For aldose reductase at the end of the 120 ns stimulation, HDJ formed 22 interactions when bound to the enzyme, including 10 hydrogen bonds (TRP 23, 2 at HIE 113, TRP 114, TYR 219, PRO 221, VAL 300, CYS 301, ALA 302 and LEU 303), 7 Van der Waals (LYS 24, TYR 51, ASN 163, ARG 220, GLN 52, PHE 124 and LYS 224), 4 pi-alkyl (VAL 50, TRP 80, PHE 125 and LEU 304), 1 pi-pi stacked (TRP 222) (Figure 13a). In contrast, the binding of EPA to AR resulted in 20 interactions including 2 hydrogen bonds (TRP 23 and HIE 113), 10 Van der Waals interactions (LYS 24, ASP 46, VAL 50, LYS 80, TRP 114, SER162, ASN 163, GLN 186, ILE 263 and LEU 303), 3 pi-pi stacked (TYR 51, TRP 82, TYR 212), 3 pi-alkyl (HIE 113, TYR 212 and CYS 301) and 2 pi-sulfur (HIE 113, PHE 125) (Figure 13b). The binding of CMA to DPP-4 at 120 ns resulted in 13 interactions encompassing 5 hydrogen bonds (GLU

168, TYR 219, PRO 513, ASP 626 and ASN 673), 7 Van der Waals interactions (TRP 164, TYR 510, GLY 512, CYS 514, SER 593, TYR 625 and TYR 629) and 1 pi-pi T-shaped (PHE 320) (Figure 14a). In comparison, the binding of SGT at 120 ns to DPP-4 resulted in 16 interactions, including 3 hydrogen bonds (GLU 168, TYR 510 and ASN 673), 8 Van der Waals interactions (GLU 169, SER 172, PHE 320, ARG 321, SER 593, TYR 594, TRP 622 and VAL 674), 4 pi-pi alkyl (VAL 619, TYR 625, TYR 629 and HID 703) and 1 pi-anion (GLU 168) (Figure 14b). Additionally, the binding of HDA to PTP1B after 120 ns resulted in 11 interactions, including 2 hydrogen bonds (ARG 56 and LYS 58), 5 Van der Waals interactions (PHE 30, ASP53, SER 55, LYS 73 and LYS 255) and 3 pi-pi alkyl bonds (HIS 54, LEU 71 and 2 at PHE 256) (Figure 15a) while the bonding of URS to PTP1B at 120 ns resulted in 12 interactions encompassing 8 Van der Waals interactions (PRO 88, MET 113, ALA 121, GLN 122, GLN 126, MET 132, ILE 133 and ASP 136) and 4 pi-pi alkyl interactions (cys 91, LEU 118 and 2 at 134) (Figure 15b). Lastly, bound SDH-HDJ complex showed 22 interactions, including 5 hydrogen bonds (GLY 45, SER 46, 2 at THR 121 and ARG 298), 12 Van der Waals interactions (CYS 44, HIS 49, TYR 50, CYS 119, GLU 155, PRO 156, VAL 159, ILE 183, VAL 272, VAL 296, PHE 295 and TYR 299), 1 pi-pi stacked (PHE 59) and four pi-alkyl (ILE 56, HIS 69, PHE 119 and LEU 274) (Figure 16a). In comparison, HPS showed 9 interactions when bound to SDH encompassing 2 hydrogen bond (GLY 45 and THR 250), 5 Van der Waals interactions (CYS 44, SER 46, HIE 49, ILE 56 and CYS 249) and 2 pi-alkyl bonds (ILE 183 and LEU 274) (Figure 16b).

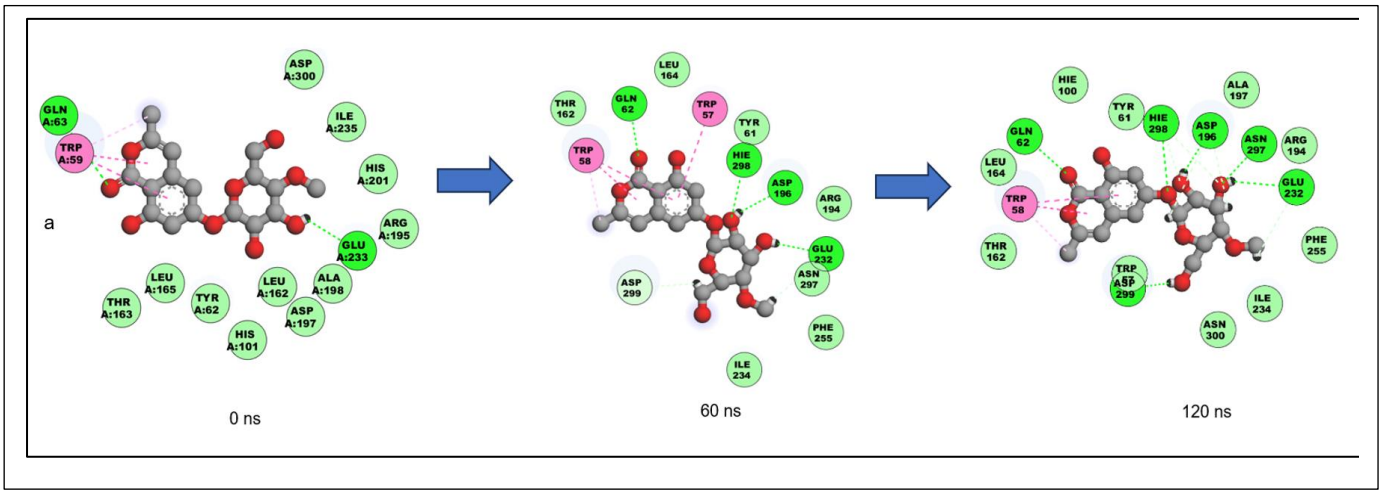

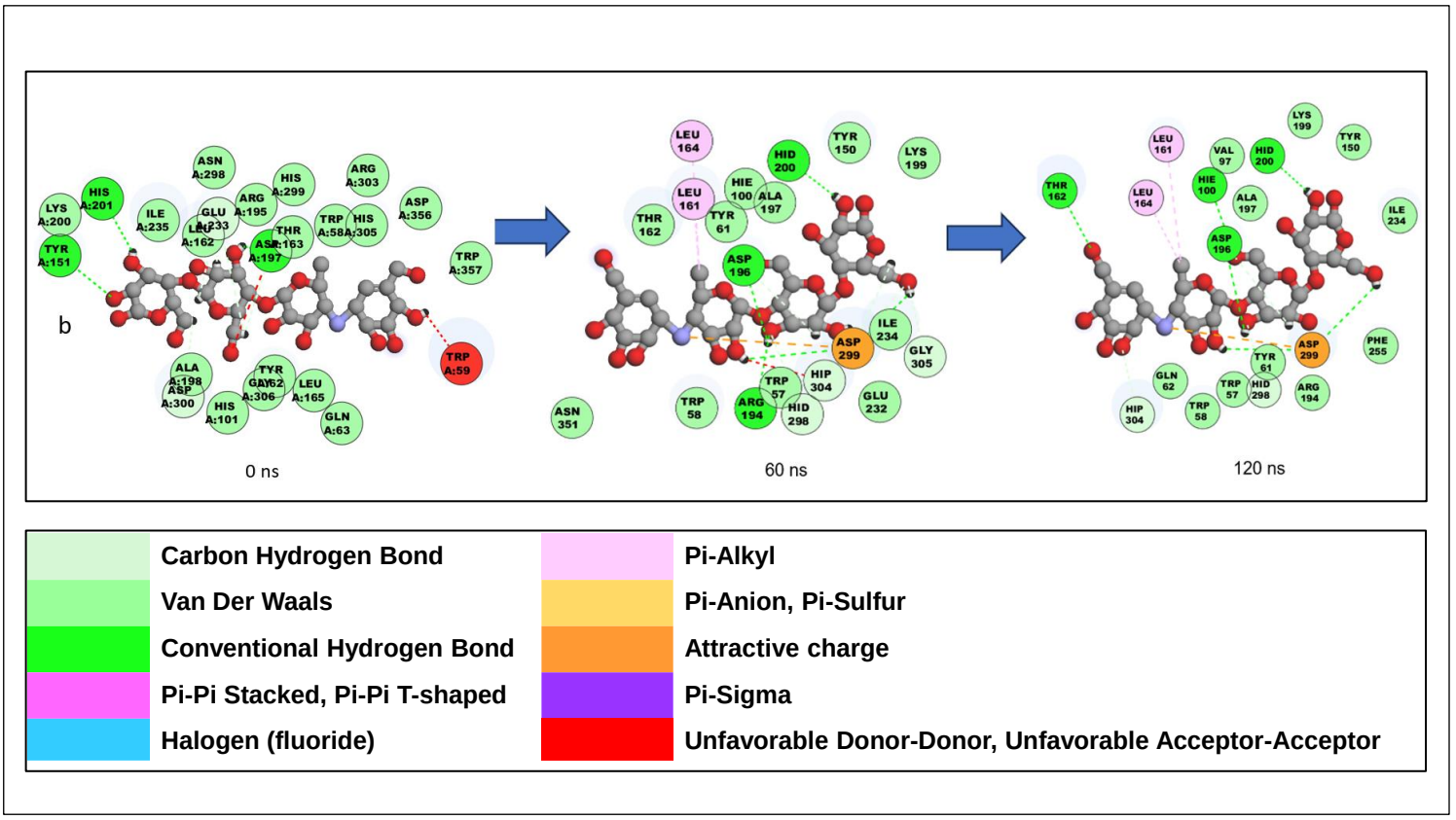

Figure 11: 2-D interaction plots following the binding of alpha-amylase (AA) to: (a) CS metabolite (R)-7-butyl-6,8-dihydroxy-3-[(3e)-pent-3-en-1-yl]-3,4-dihydroisochromen-1-one (BHP) and (b) reference standard acarbose (ACA), throughout the 120 ns simulation

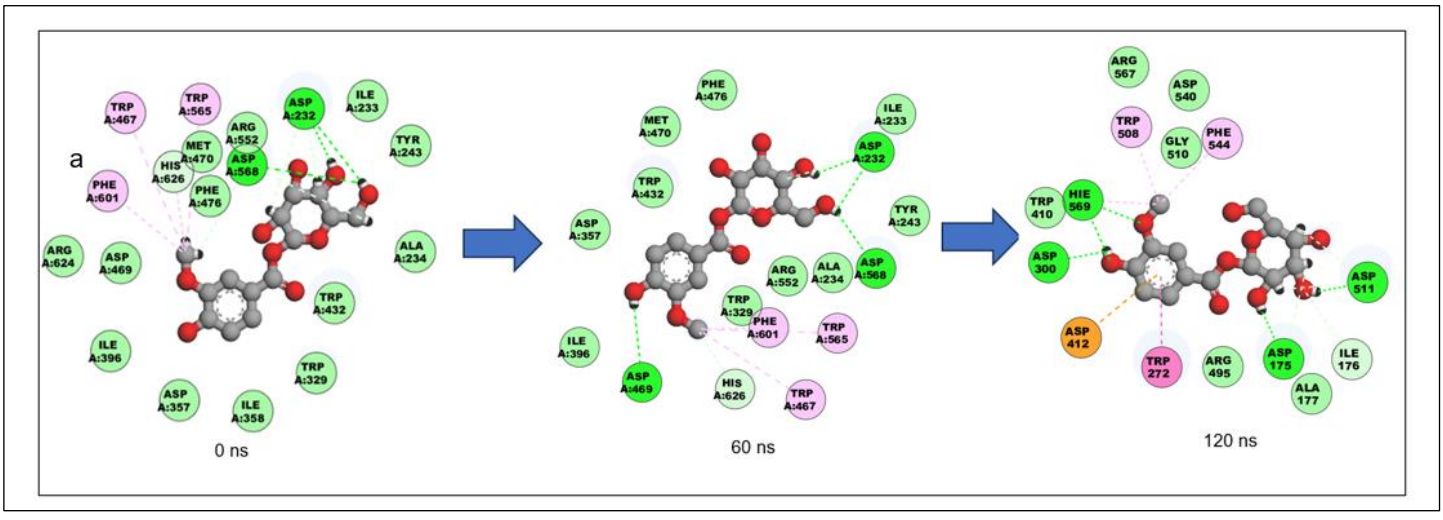

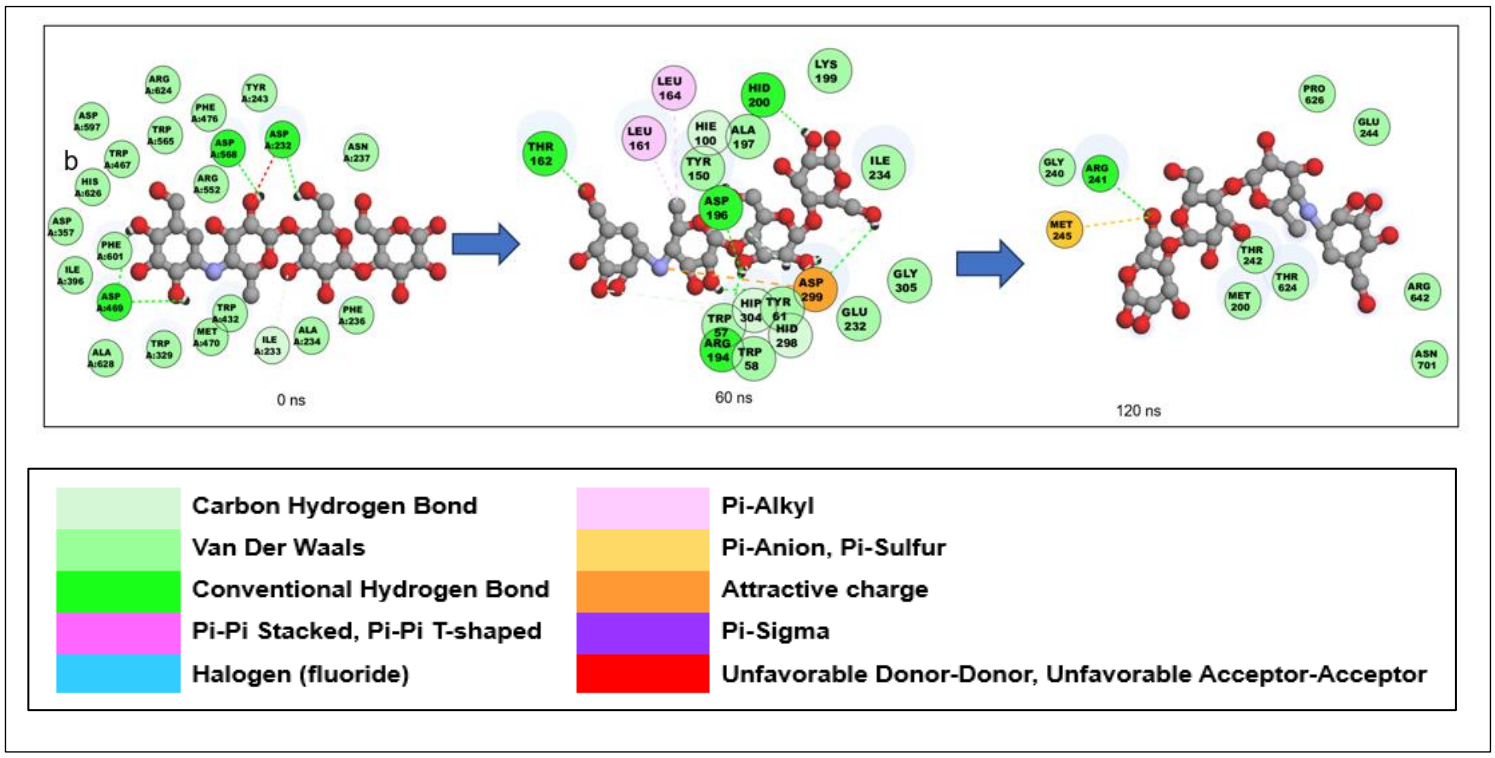

Figure 12: 2-D interaction plots following the binding of alpha-glucosidase (AG) to: (a) CS metabolite 1-O-vanilloyl-beta-D-glucose (VBG) and (b) reference standard acarbose (ACA), throughout the 120 ns simulation

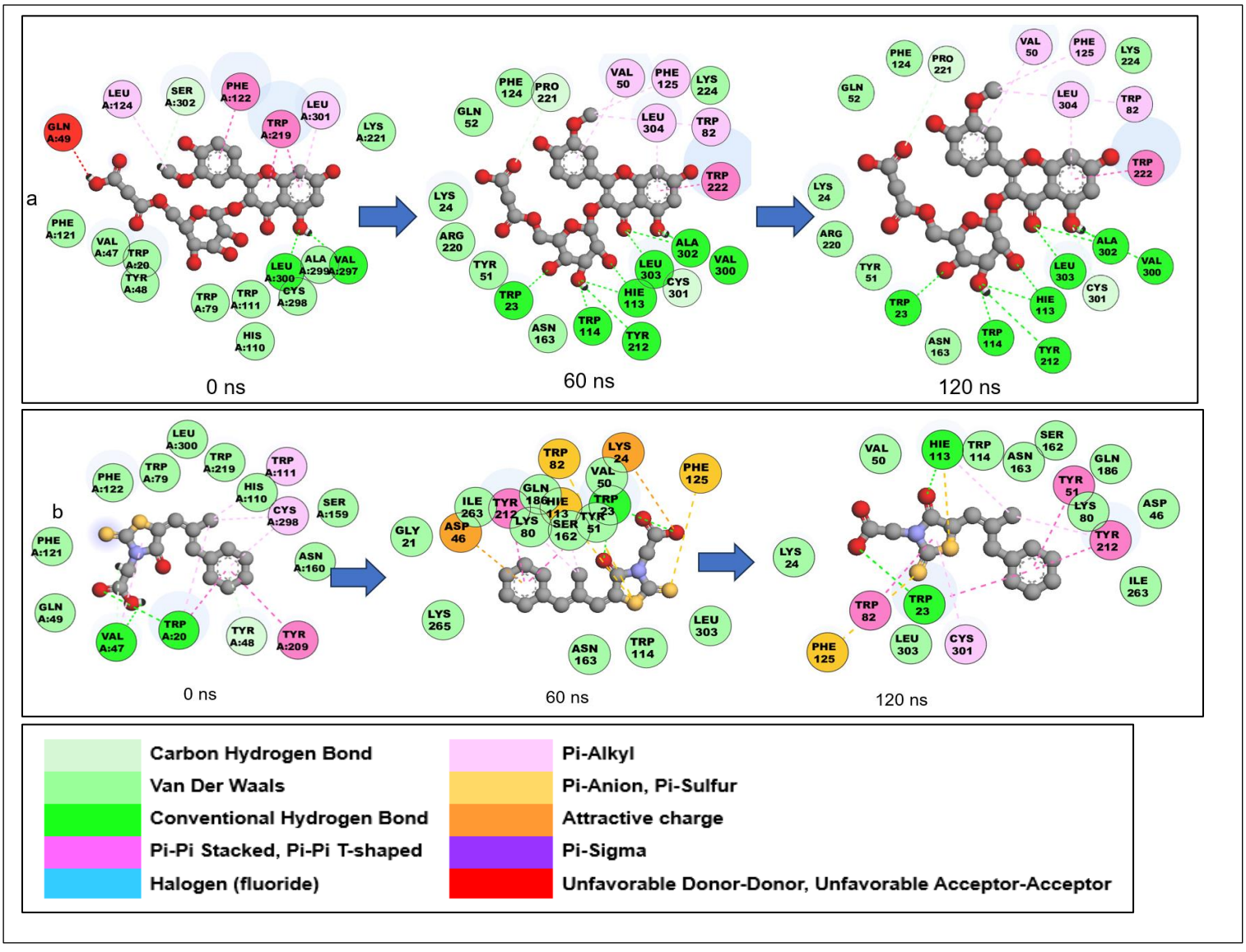

Figure 13: 2-D interaction plots following the binding of aldose reductase (AR) to (a) CS metabolite (6E)-1-(4-hydroxyphenyl)-7-phenylhepta-4,6-dien-3-one (HPH) and (b) reference standard epalrestat (EPA), throughout the 120 ns simulation

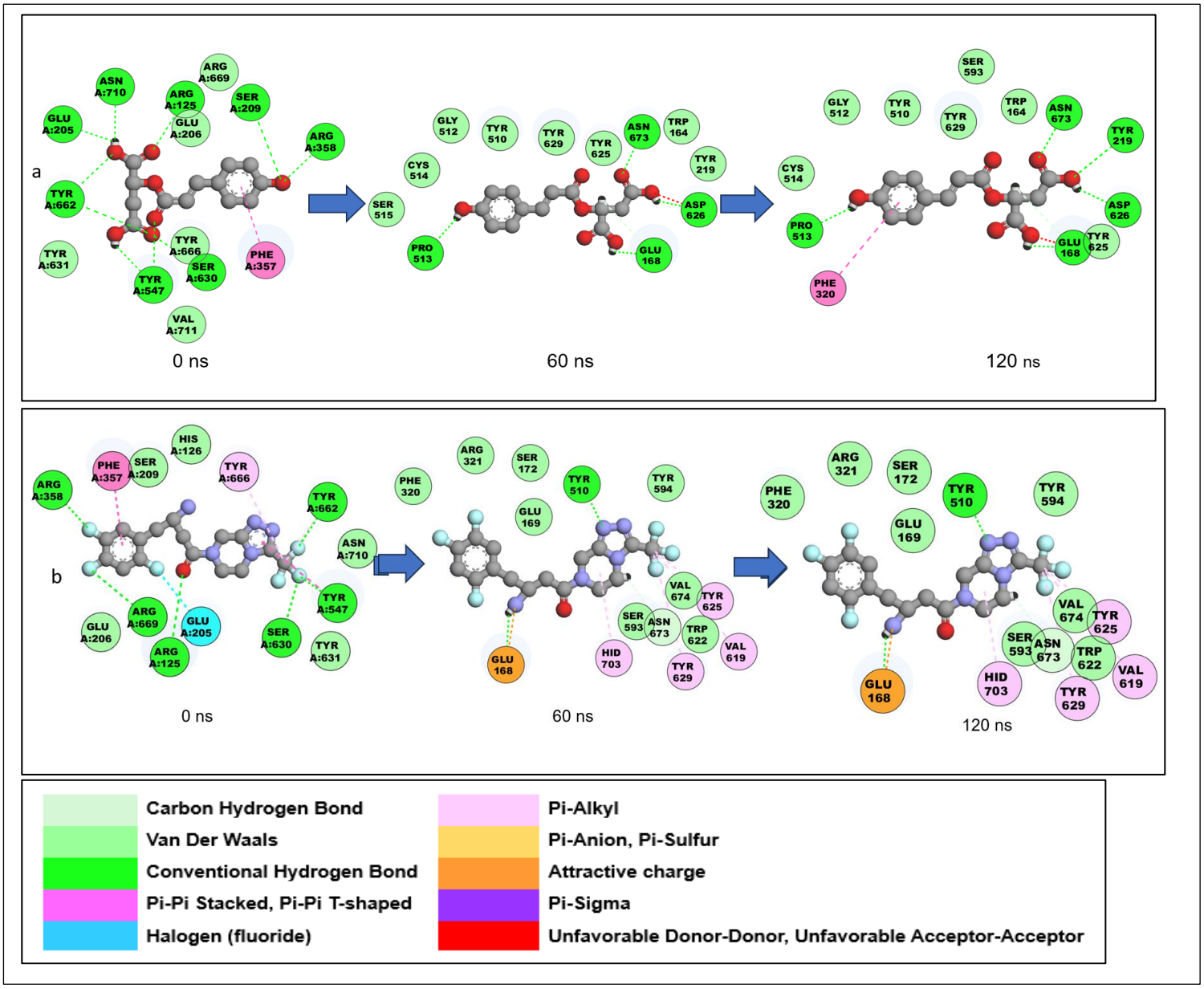

Figure 14: 2-D interaction plots following the binding of dipeptidyl peptidase-4 (DPP-4) to (a) CS metabolite p-coumaroyl malic acid (CMA) and (b) reference standard sitagliptin (SGT), throughout the 120 ns simulation

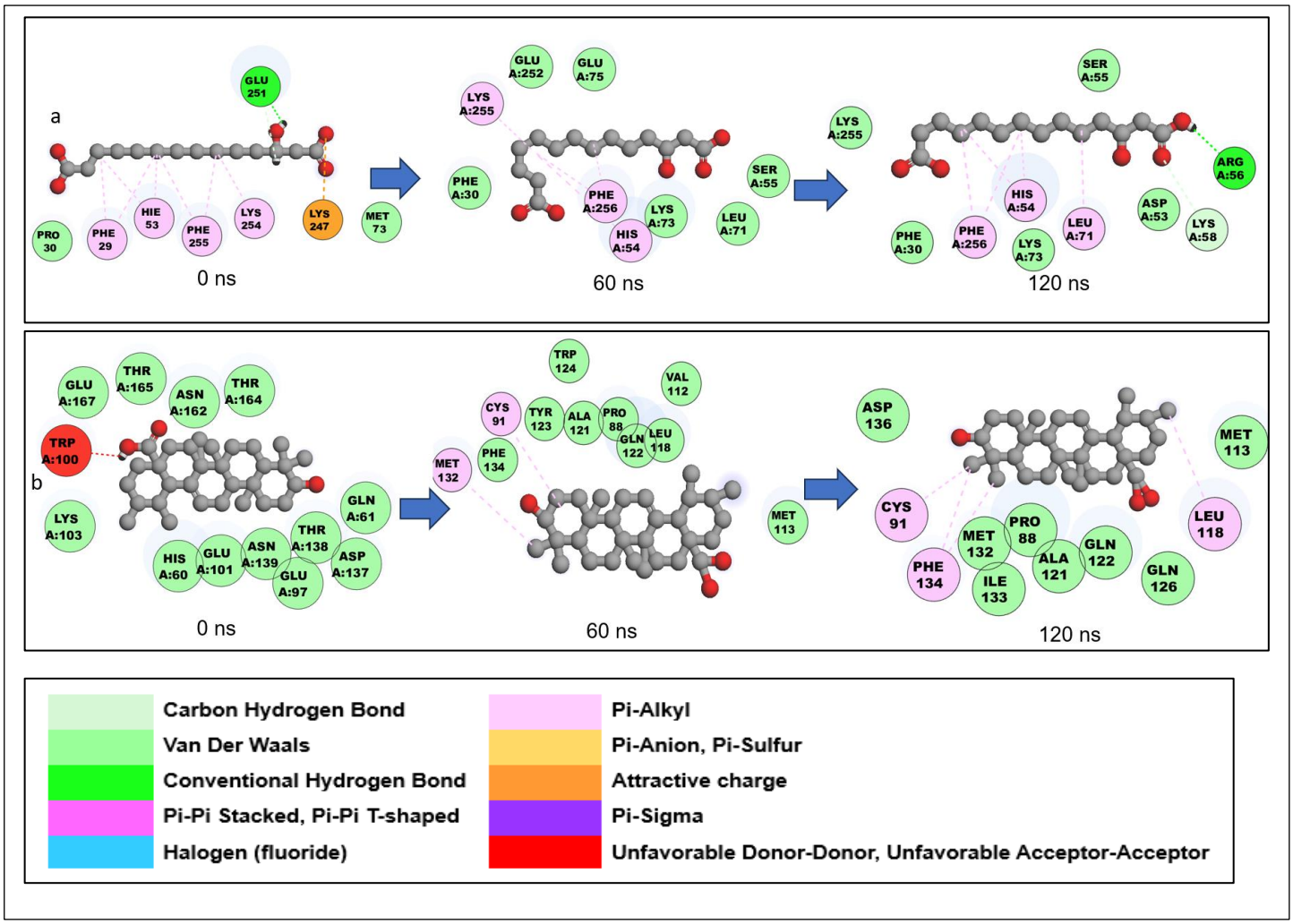

Figure 15. 2-D interaction plots of protein tyrosine phosphatase 1B (PTP1B) bound to a) CS metabolite 2-hydroxydecanedioic acid (HDA) and b) reference standard ursolic acid (URS), throughout the 120 ns simulation

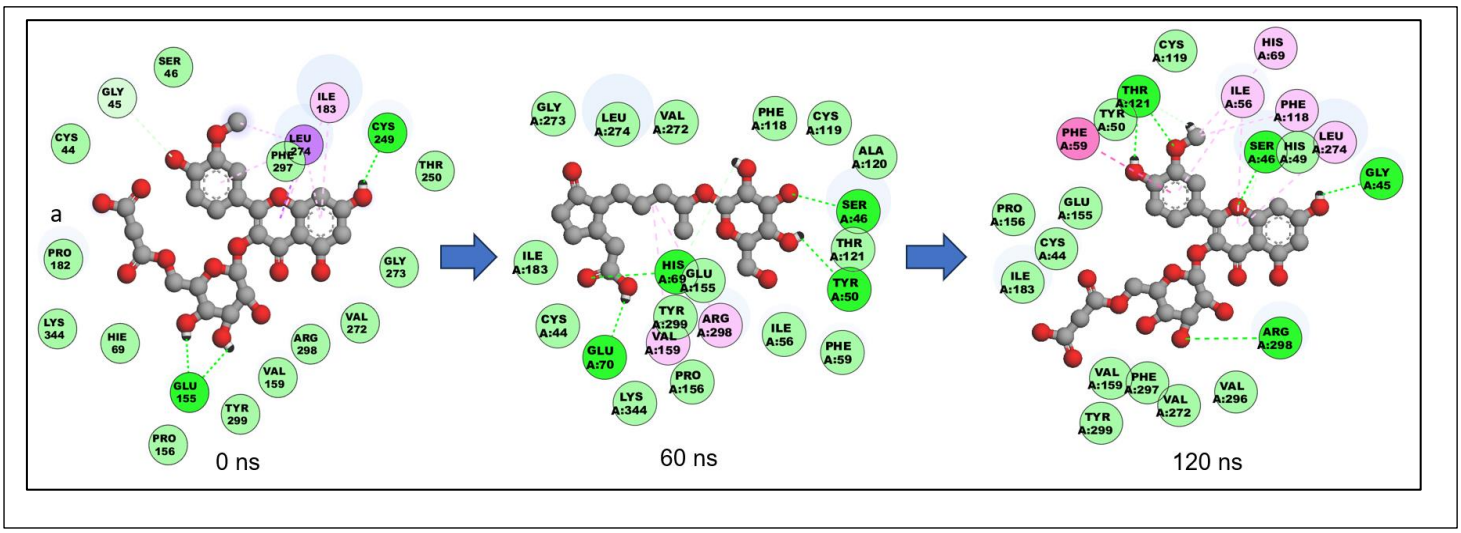

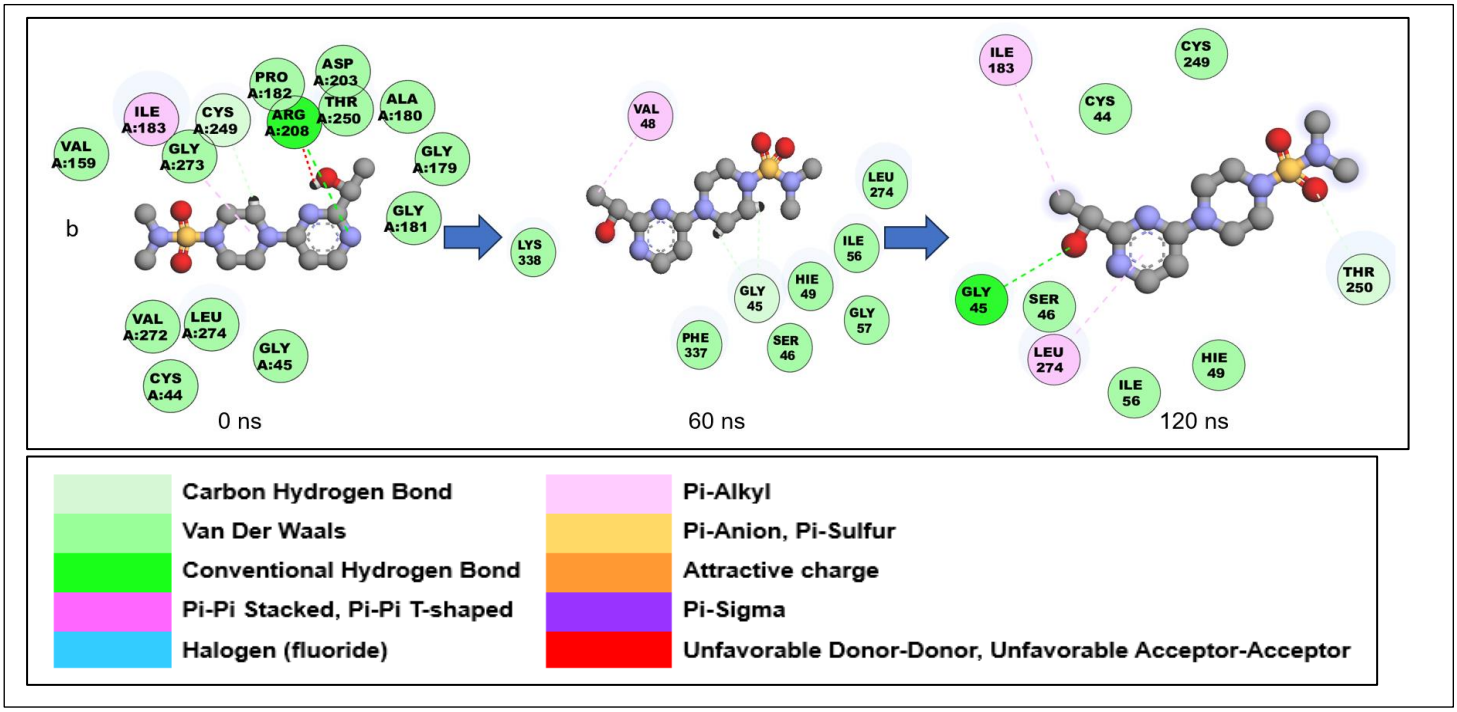

Figure 16. 2-D interaction plots of sorbitol dehydrogenase (SDH) bound to a) (-)-11-hydroxy-9,10-dihydrojasmonic acid 11-beta-D-glucoside (HDJ) and b) reference standard 4-[2-1R-hydroxy-ethyl)-pyrimidin-4- yl]piperazine-1-sulfonic acid dimethylamide (HPS), throughout the 120 ns simulation

3.5.Frontier molecular orbitals

The lead compounds had LUMO energies ranging between -5.92 and -0.22 eV, with the reference standards within the range except ACA (-0.89 eV) and URS (-0.24 eV) having higher values than the lead compounds' range. However, the HOMO energies of the standards fall within the range of the top-hit compounds (-5.85 and -7.72 eV) (Table 9 and Figure 17). The lowest energy gap among the top-ranked compounds was observed in HPH (3.61 eV), AUS (4.70 eV), HPH (3.61 eV), CTA (4.06 eV), PHA (4.41 eV) and CNI (4.46 eV) against AA, AG, AR, DPP-4, PTPIB and SDH respectively, however, a lower energy gap was observed in the two reference standards; EPA (3.21 eV) and HPS (4.39 eV) against AR and SDH respectively (Table 9, Supplementary file S4 and Figure 17). Consequently, these compounds exhibited the highest softness and lowest hardness values HPH (0.55 and 1.80 eV), AUS (0.43 and 2.35 eV), HPH (0.55 and 1.80 eV), CTA (0.50 and 2.03 eV), PHA (0.45 and 2.20 eV) and CNI (0.45 and 2.23 eV) against their respective targets. Notably, PHA had the highest ionization energy (2.30 eV), electronegativity (4.50 eV), electrophilicity index (4.59 eV) and the lowest chemical potential (-4.50 eV) while GTA had the highest electron affinity (7.72 eV) (Table 9). Summarily, the cDFT parameters of the top- ranked compounds taken for MD simulation and the reference standards are presented in Table 9, while those of DCA, TDA, MCA and PHA have been previously reported (Akoonjee *et al*., 2023).

Table 9. The cDFT parameters of the top-ranked compounds against enzymes implicated in T2DM

cDFT parameters (eV)										
Ligands	**LUMO**	**HOMO**	**Energy gap**	**Ionization energy**	**Electron affinity**	**Hardness**	**Softness**	**Electronegativity**	**Chemical potential**	**Global electrophilicity**
AA										
AES	-2.07	-6.42	4.35	2.07	6.42	2.17	0.46	4.24	-4.24	4.14
BHP	-1.19	-6.05	4.86	1.19	6.05	2.43	0.41	3.62	-3.62	2.70
CUR	-0.42	-6.43	6.01	0.42	6.43	3.01	0.33	3.43	-3.43	1.96
HPH	-2.24	-5.85	3.61	2.24	5.84	1.80	0.55	4.04	-4.04	4.53
AUS	-1.86	-6.56	4.70	1.86	6.56	2.35	0.43	4.21	-4.21	3.78
ACA	-0.89	-6.11	5.22	0.89	6.11	2.61	0.38	3.50	-3.50	2.35
AG										
AUS	-1.86	-6.56	4.70	1.86	6.56	2.35	0.43	4.21	-4.21	3.78
GTA	-0.44	-7.72	7.29	0.44	7.72	3.64	0.27	4.08	-4.08	2.29
VBG	-1.47	-6.18	4.71	1.47	6.18	2.36	0.42	3.83	-3.83	3.11
MGN	-1.10	-6.34	5.24	1.10	6.34	2.62	0.38	3.72	-3.72	2.64
HDJ	-1.17	-6.46	5.29	1.17	6.46	2.65	0.38	3.82	-3.82	2.75
ACA	-0.89	-6.11	5.22	0.89	6.11	2.61	0.38	3.50	-3.50	2.35
AR										
HPH	-2.24	-5.85	3.61	2.24	5.84	1.80	0.55	4.04	-4.04	4.53
BHP	-1.19	-6.05	4.86	1.19	6.05	2.43	0.41	3.62	-3.62	2.70

AES	-2.07	-6.42	4.35	2.07	6.42	2.17	0.46	4.24	-4.24	4.14
AUS	-1.86	-6.56	4.70	1.86	6.56	2.35	0.43	4.21	-4.21	3.78
HDJ	-1.17	-6.46	5.29	1.17	6.46	2.65	0.38	3.82	-3.82	2.75
EPA	-2.93	-6.13	3.21	2.93	6.13	1.60	0.62	4.53	-4.53	6.41
DPP-4										
HDJ	-1.17	-6.46	5.29	1.17	6.46	2.65	0.38	3.82	-3.82	2.75
CTA	-2.06	-6.12	4.06	2.06	6.12	2.03	0.50	4.09	-4.09	4.12
BHP	-1.19	-6.05	4.86	1.19	6.05	2.43	0.41	3.62	-3.62	2.70
PHA	-2.30	-6.70	4.41	2.30	6.70	2.20	0.45	4.50	-4.50	4.59
CMA	-1.86	-6.12	4.26	1.86	6.12	2.13	0.47	3.99	-3.99	3.74
SGT	-1.35	-6.65	5.30	1.35	6.65	2.65	0.38	4.00	-3.99	3.01
PTP1B										
HDA	-0.76	-7.42	6.66	0.76	7.42	3.33	0.30	4.08	-4.08	2.51
URS	-0.24	-6.10	5.85	0.24	6.10	2.93	0.34	3.17	-3.17	1.72
SDH										
ETB	-0.63	-6.48	5.85	0.63	6.48	2.92	0.34	3.55	-3.55	2.16
CNI	-2.12	-6.57	4.46	2.12	6.57	2.23	0.45	4.35	-4.35	4.23
BLD	-1.63	-7.34	5.72	1.63	7.34	2.86	0.35	4.49	-4.48	3.52
HDJ	-1.17	-6.46	5.29	1.17	6.46	2.65	0.38	3.82	-3.82	2.75
BHP	-1.19	-6.05	4.86	1.19	6.05	2.43	0.41	3.62	-3.62	2.70
HPS	-1.79	-6.17	4.39	1.79	6.17	2.19	0.46	3.98	-3.98	3.61

AA: alpha-amylase; AG: alpha-glucosidase; AR: aldose reductase; DPP-4: dipeptidyl peptidase-4; PTP1B: protein tyrosine phosphatase-1B; SDH: sorbitol dehydrogenase; HOMO: highest occupied molecular orbital; LUMO: lowest unoccupied molecular orbital; AA: alpha-amylase; AG: alpha-glucosidase; AR: aldose reductase; DPP-4: dipeptidyl peptidase-4; PTP1B: protein tyrosine phosphatase 1B; SDH: sorbitol dehydrogenase; AES: aesculin; BHP: (R)-7-butyl-6,8-dihydroxy-3-[(3e)-pent-3-en-1-yl]-3,4-dihydroisochromen-1-one; CUR: curvularol; HPH: (6e)-1-(4-hydroxyphenyl)-7-phenylhepta-4,6-dien-3-one; AUS: austricin; ACA: acarbose; GTA: glutaric acid; VBG: 1-O-vanilloyl-beta-D-glucose; MGN: methyl geranate; HDJ: (6e)-1-(4-hydroxyphenyl)-7-phenylhepta-4,6-dien-3-one; EPA: epalrestat; CTA: caffeoyl tartaric acid; PHA: phaseic acid; CMA: p-coumaroyl malic acid; SGT: sitagliptin; TDA: tetradecanedioc acid; HDA: 2-hydroxydecanedioic acid; MCA: methylisocitric acid; DCA: dodecanedioc acid; URS: ursolic acid; ETB: erythronolide B; CNI: cnicin; BLD: blennin D; HPS: 4-[2-1R-hydroxy-ethyl)-pyrimidin-4- yl]piperazine-1-sulfonic acid dimethylamide.

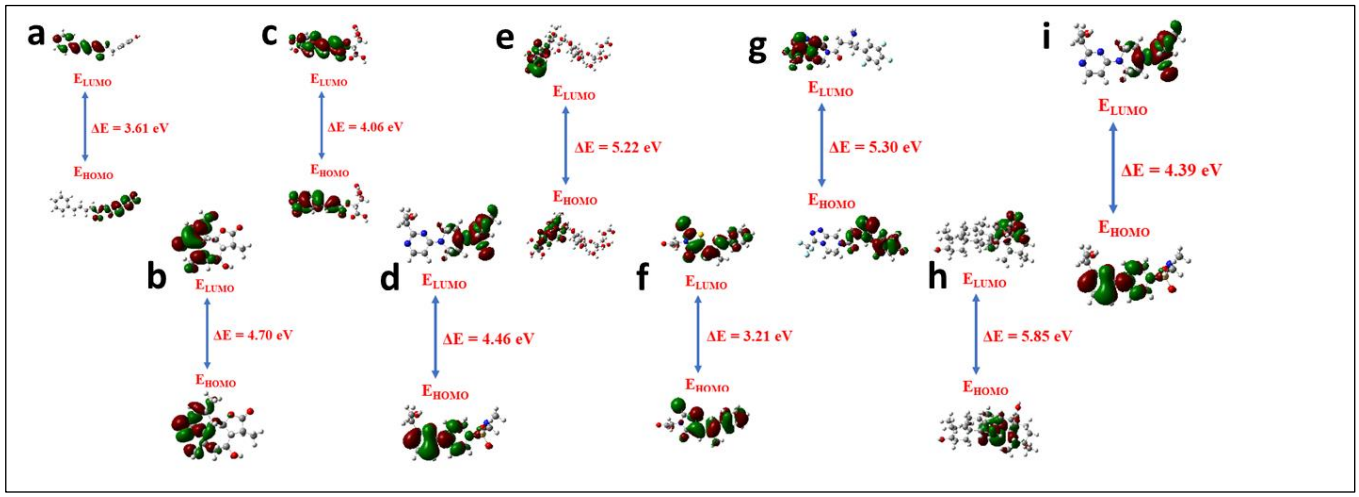

Figure 17. Frontier molecular orbitals for (a) HPH (b) AUS (c) CTA (d) CNI (e) ACA (f) EPA (g) STG (f) URS (g) HPS. HPH: (6e)-1-(4-hydroxyphenyl)-7-phenylhepta-4,6-dien-3-one; AUS: austricin; CTA: caffeoyl tartaric acid; ACA: acarbose; EPA: epalrestat; CNI: cnicin; ; SGT: sitagliptin; HPS: 4-[2-1R-hydroxy-ethyl)-pyrimidin-4- yl]piperazine-1-sulfonic acid dimethylamide; URS: ursolic acid

4. Discussion

Humanity has relied on nature to provide food, shelter, clothing, transportation, fertilizers, flavors and fragrances, and notably, medicinal resources among others (Petrovska, 2012). For centuries, plants with medicinal attributes have formed the basis of the traditional systems of medicine (Lankatillake *et al*., 2019), which is continuously developed to provide new remedies to treat and/or manage several diseases and illnesses (Petrovska, 2012), including T2DM (Zhang *et al*., 2015). For instance, despite being a waste material of *Zea mays*, CS has been identified as a possible therapeutic agent for T2DM management (Sabiu *et al*., 2019), and several other biological properties such as diuretic, antihyperlipidemic, antihypertensive, anti-obesity, anti-microbial, neuroprotective, anti-cancer, anti-depressant, antioxidant, anti-inflammatory, and antidiabetic (Hasanudin *et al*., 2012; Wang *et al*., 2019; Kaur *et al.,* 2023).

Amongst several factors that influences the phytochemical profile of therapeutically significant plants and plant materials (such as CS), determining the changes in chemical and bioactive components throughout the maturation process is crucial for identifying the optimal harvest time that ensures the highest level of therapeutic activity (Abeywardhana *et al*., 2014; Tremlová *et al*., 2021). The high concentration of metabolites profiled at the mature stage of CS relative to the premature stage suggests accumulation of the secondary metabolites during the maturation process of CS (Li *et al*., 2020). The observed variation in life or developmental cycle of a plant may be likened to the report of Sarepoua *et al*. (2015), wherein, despite the

presence of certain metabolites in abundance during the silking phase (premature), the milking stage (mature) exhibited the highest levels of secondary metabolites such as total phenolic content, total flavonoid content, total anthocyanin content and antioxidant capacity. Similarly, Abeywardhana *et al*. (2014) demonstrated that the therapeutic potential of *Ocimum sanctum* is more pronounced at the fully matured stage compared to premature stage. The increase in therapeutic potential at more mature phases of a plant or plant material may be attributed to a higher presence of therapeutic compounds (Singh *et al*., 2022b).

Aside from the influence of developmental (mature) stage contributing to the abundance of secondary metabolites, the processing conditions may also influence the composition and quantity of metabolites within CS (Kaur *et al*., 2023). In fact, the elevated abundance of various compounds, in the raw CS samples suggests that the processing of CS during extract preparation (such as drying, grinding, boiling and alcoholic solvent extraction) had an impact on the quantity of these metabolites in the processed CS samples (Oz and Kafkas, 2017). In traditional systems of medicine, the simplest and most popular methods for preserving the medicinal properties of CS involve aqueous, hydro-ethanolic, and ethanolic extractions (Hasanudin *et al*., 2012; Mihali *et al*., 2024). Interestingly, the type of solvent used for extraction plays a role in the types and amounts of phytoconstituents extracted (Nawaz *et al*., 2020). Among the CS samples, the hydro-ethanolic extract of mature CS displayed a higher abundance of most metabolites. Several of these metabolites, such as mirificin, maysin 3'-methyl ether, and D-2-hydroxyglutaric acid have been postulated to contribute to its pharmacological attributes of CS (Song *et al*., 2016; Singh *et al*., 2021a; Maciejewska-Turska *et al*., 2022), particularly its glucose-lowering effects (Kim *et al*., 2014). The higher concentration of metabolites present in the hydro-ethanolic extract of mature CS is attributed to the moderate polarity of hydro-ethanol, suggesting a majority of the metabolites present in CS are moderately polar (Nawaz *et al*., 2020; Bitwell *et al*., 2023).

The modulation of key enzymes implicated in the pathogenesis of T2DM and its related secondary complications by CS metabolites were explored through computational bioprospection, using tools such as molecular docking and molecular dynamics simulation. Molecular docking accessed the CS metabolites' docking scores at active sites of the investigated enzymes, with higher negative scores indicating stronger ligand attraction (Pagadala et al., 2017; Pantsar et al., 2018; Pellicani et al., 2023). The most negative docking scores of AES, AUS, HPH, HDJ, PHA and ETB compared to the reference standards against AA, AG, AR, DPP-4, PTP1B and SDH, respectively, indicates their better binding affinities,

interaction, superiority and their greater suitability or fitness as possible therapeutics (Agarwal *et al*., 2016; Gupta *et al*., 2018; Lanrewaju *et al*., 2023a). Although there are no studies that have previously explored the top-ranked CS metabolites to the investigated enzyme targets, Chaudhary *et al*. (2022) revealed that CS compounds gallotannin, 3-O-caffeoylquinic acid, stigmasterol and formononetin (7-hydroxy-4'-methoxyisoflavone) had higher negative docking scores against DPP-4 (-10.7 kcal.mol), AG (-8.9 kcal.mol), AA (-9.8 kcal.mol) and PTP1B (-8.7 kcal.mol), highlighting the ability of CS metabolites to modulate the activity of key enzymes implicated in the pathogenesis of T2DM. Similarly, Sabiu *et al*. (2021) demonstrated that phenolic compounds from *Carpobrotus edulis*, such as chlorogenic acid, luteolin-7-O-glucoside, epicatechin and isorhamnetin-3-O-rutinoside had commendable binding at the active site of AA, AG and AR. Interestingly, several of the compounds in the study of Sabiu *et al*. (2021) are present in CS, such as chlorogenic acid and analogues of luteolin-7-O-glucoside, isorhamnetin-3-O-rutinoside and epicatechin.

The combination of molecular docking and MD simulation provides a comprehensive understanding the molecular interactions and conformational changes that occur from the binding of a ligand to a target protein (Hollingsworth *et al*., 2018). The lowest change in ΔE_{VdW}, ΔE_{elec}, ΔG_{gas} and ΔG_{solv} observed for several CS compounds bound to enzyme targets emphasize the stability and favourable interactions of these complexes (Anazi *et al*., 2018; Hu *et al*., 2024). These findings demonstrate superior binding performance between the CS compounds and enzyme targets compared to reference standards and the apo-enzyme. Additionally, the MM/GBSA method calculates ΔG_{bind} for macromolecules by combining molecular mechanics calculations and continuum solvation models (Hou *et al*., 2011). Lower ΔG_{bind} values align with a higher binding affinity of a ligand to a given target (Hata *et al*., 2021), reflecting a more stable complex (Shunmugam *et al*., 2018). The high negative ΔG_{bind} values for BHP, VBG, HDJ, CMA, HDA, and HDJ indicate a greater binding affinity to AA, AG, AR, DPP-4, PTP1B, and SDH, respectively. This suggests stronger interactions between the CS metabolites and the enzymes compared to the reference standards, highlighting CS's potential to modulate enzyme activity. Specifically, the top-ranked CS metabolites' ability to inhibit AA, AG, AR, DPP-4, PTP1B, and SDH suggests CS can prevent carbohydrate and glucagon-like peptide 1 breakdown, enhance insulin signalling, and reduce sorbitol and fructose accumulation in cells. These effects contribute to CS's antidiabetic action by modulating enzymes involved in T2DM pathogenesis and its complications.

Additionally, MD simulation can be used to elucidate the extent of binding stability, flexibility, and compactness of a protein-ligand bound complex (Balogun *et al*., 2023). This is crucial due to the potential likelihood of an impending conformational or structural change that could occur after ligand binding to a receptor, which could potentially impact the biological activity of the enzyme (Salim *et al*., 2020; Lanrewaju *et al*., 2023b). The RMSD provides insight into the deviation or changes in the position of atoms over a simulation period and evaluates the stability of a protein-ligand complex (Muralidharan *et al*., 2020). A decrease in the RMSD value of a complex in comparison to the apo-enzyme throughout a simulation indicates enhanced stability (Childers *et al*., 2017). The lowest mean RMSD values observed in AA-AES, AR-BHP, DPP-CTA, PTP1B-MCA, and SDH-ETB complexes in comparison to their respective apo-enzyme and reference standard complexes, suggest that the binding of these CS metabolites formed stable complexes with the enzymes. Although, the average RMSD values of AES and AUS were greater than the apo enzymes (AA and AG, respectively), this finding did not indicate the formation of unstable complexes since, the values recorded were lower than the acceptable 3 Å, and hence depicting stable complexes formation (Rosenberg, 2009; Castro-Alvarez *et al*., 2017). It is noteworthy that the less stable complexes formed by the reference standards relative to the top-ranked metabolites against most of the targets in this study is in line with previous studies where compounds such as procyanidin, rutin, apigenin, chlorogenic acid, naringenin, luteolin and isoflavone bound systems exhibited lower mean RMSD values relative to their apo-enzymes and reference standards (Lukman *et al*., 2024; Balogun *et al*., 2023; Ramparadath *et al*., 2022; Sabiu *et al*., 2021).

The RMSF of a protein-ligand system signifies the effect of a bound compound on the behavior of active site residues (Hess *et al*., 2002), with lower or higher shifts in alpha (α)-carbon (C) indicating less or more flexible movements, respectively (Al-Khodairy *et al*., 2013). The low mean RMSF values of the AA-CUR, AG-AUS, AR-BHP, DPP-4-CMA, DPP-PHA, PTP1B-MCA, and SDH-BLD complexes compared to the apo-enzyme and reference standards suggest lesser flexible movements and, consequently, greater stability in the investigated complexes This finding is line with the study of Balogun *et al*., 2023 for some of the metabolites studied against AG and DPP-4.

The ROG measures the spatial distribution or compactness of a molecule (Alhadrami *et al*., 2020). It calculates the average distance of individual atoms (or groups of atoms) in a molecule from its center of mass, offering insights on how spread out or condensed a molecule is during

a simulation (Rampogu *et al*., 2022), with lower values indicating more compactness and thus more stability of the final complexes (S'thebe *et al.,* 2023). The CS metabolites bound to the investigated targets, specifically AA-BHP, AR-BHP, DPP-CTA, PTP1B-MCA, exhibited the lowest average ROG values suggesting a higher degree of compactness and, consequently, superior stability of the final complexes compared to the apo-enzyme and the respective standards). In tandem with this study, Sabiu *et al*. (2021), Rampadarath *et al*., 2022 and Eawsakul *et al*. (2023) previously reported that the binding of the CS metabolites to AA, PTP1B, and AG, respectively, resulted in lower mean ROG in comparison to the apo-enzyme and reference standard This observation further highlights the ability of CS metabolites to reduce the compactness and thus improve the stability of the final complexes,.

Hydrogen bonds are important interactions and are essential for molecular recognition, maintaining structural stability, facilitating enzyme catalysis, influencing drug partition, and permeability (Jairajpuri *et al*., 2021; S'thebe *et al.,* 2023). The increase in the average number of hydrogen bonds within the complexes AA-AES, AR-BHP, DPP-BHP, PTP1B-HDA and SDH-BLD, relative to the apo-enzyme and standard complexes, suggests the ability of CS compounds to occupy a portion of the proteins' intramolecular phase. resulting in the formation of more stable final complexes, This finding is in agreement with Sajal *et al.* (2020) and Rampadarath *et al*. (2022), in which the binding of plant metabolites, such as β-pinene, dehydro-p-cymene, -α-pinene, orientin, vitexin and apigenin, when bound to DPP-4 and PTP1B presented higher number of hydrogen bonds, in comparison to their reference standards. Hence, this suggests that CS metabolites have the potential to form a greater number of hydrogen bonds when bound to the enzyme targets better than the respective standards.

The SASA serves as a measure of thermodynamic stability, quantifying the surface area of a biomolecule available to solvent molecules (Mousavi *et al*., 2021), as well as changes in protein surface area (Ausaf Ali *et al*., 2014). High SASA values indicate expansion of the surface area, while lower SASA values suggest a reduction in protein volumes (S'thebe *et al.,* 2023). The low SASA values observed in: AG-VBJ, AR-BHP, DPP-4-PHA, PTP1B-MCA and SDH-HDJ complexes relative to the apo-enzymes and reference standard-complexes, depict higher degree of protein folding and consequently, the formation of more stable final complexes. Similar studies also reported a reduction in SASA upon the binding of plant metabolites to the apo-enzyme (Ahmad *et al*., 2022; Balogun *et al*., 2023; Lukman *et al*., 2024)

In addition, the nature and amount of interactions formed upon the binding of ligand and the amino acid residues of the target protein are crucial in determining the extent of the binding affinity (Balogun *et al*., 2022). The high number of interactions between AG-VBG, AR-HDJ and SDH-HDJ indicated stronger and more stable ligand–protein complexes, suggesting greater interaction between the CS metabolites and target enzymes. This suggests a higher degree of inhibition of the enzymes by the CS metabolites in comparison to the reference standards. The higher negative ΔG_{bind} could be attributed to the higher number of interactions occurring between the top-ranked CS metabolites and the enzyme targets, in comparison to the reference standards investigated. While BHP and CMA did not establish more interactions when bound to AA and DPP-4, respectively, the ΔG_{bind} of the complexes formed with the CS metabolites were lower when compared to the ΔG_{bind} of the standards. This suggests that despite a lower number of interactions within the CS metabolite and enzyme complexes, the interactions formed between the complexes resulted in greater binding affinity forming stable final complexes (Shunmugam *et al*., 2018). In contrast, the decrease in the number of interactions observed between PTP1B-HDA could contribute to the reduction in the ΔG_{bind} displayed by the complex in comparison to the URS.

The molecular characteristics of the top-ranked compounds were computed using cDFT parameters to explore their potential therapeutic importance. The HOMO and LUMO orbitals are generally recognized as important markers for forecasting the chemical and biological reactivity of chemical species (Aihara, 1999). The HOMO is the highest orbital that contains electrons from which electrons are transferred to the protein, forming a bond that obstructs the active site of the protein implicated in the disease condition pathogens. On the other hand, the LUMO refers to the lowest unoccupied orbital located in the innermost region that lacks electrons and functions as an electron acceptor or positive charge carrier, facilitating the transfer of these particles to larger components (Ahamed *et al*., 2023). Therefore, investigating the HOMO and LUMO energies of lead compounds may provide crucial insights into their mechanism of action, indicating a reactive site for structural alteration (Rampadarath *et al*., 2023).

The energy gap (ΔE) between the LUMO and HOMO is essential for comprehending the reactivity, kinetic stability, and chemical characteristics of a compound (Karabacak *et al*., 2012), with a wide energy gap suggesting firmness, low chemical reactivity and hardness, whereas a small energy gap indicates softness and high chemical reactivity (Esha *et al*., 2024). Unfortunately, the lower energy gaps, higher chemical softness, and lower chemical hardness

against each of the targets observed by some of the top-ranked compounds do not correlate with their free binding energy, and this could be due to the observed relative residue fluctuations and increased surface area of the targets upon ligand binding. This could have reduced the effect of the reactivity of each compound on the binding free energy. This observation contradicts our previous report (Akoonjee *et al*., 2023), where there is a correlation between a lower energy gap and higher negative binding free energy; however, it is consistent with Rampadarath *et al*. (2023), where lower energy gap of Formoxanthone B does not result in higher negative free binding energy upon binding for MMP1. The electrophilicity index quantifies the electrophilic reactivity of compounds. Molecules with values below 0.8 eV are categorized as weak electrophiles; values above 1.5 eV signify strong electrophiles, while between 0.8 and 1.5 eV suggest moderate electrophiles (Domingo and Pérez, 2011, Tananta *et al*., 2023). Remarkably, all the top-ranked compounds had electrophilicity index above 1.5 eV, suggesting they are strong electrophiles with a significant electrophile presence around the molecules.

5. Conclusion

The study established that the abundance and types of metabolites present in CS were influenced by growth stages, processing condition and solvent polarity with the mature CS and hydro-ethanolic extract of mature CS exhibiting higher metabolites' concentrations. The MD simulation of the metabolites over a 120-ns period against the respective enzymes profiled (R)-7-butyl-6,8-dihydroxy-3-[(3e)-pent-3-en-1-yl]-3,4-dihydroisochromen-1-one (BHP), 1-O-vanilloyl-beta-D-glucose (VBG), (-)-11-hydroxy-9,10-dihydrojasmonic acid 11-beta-D-glucoside (HDJ), p-coumaroyl malic acid (CMA), 2-hydroxydecanedioic acid (HDA) and (-)-11-hydroxy-9,10-dihydrojasmonic acid 11-beta-D-glucoside (HDJ) as promising candidates that could modulate the specific activity of alpha-amylase (AA), alpha-glucosidase (AG), aldose-reductase (AR), dipeptidyl peptidase-4 (DPP-4), protein tyrosine phosphatase 1B (PTP1B) and sorbitol dehydrogenase (SDH), respectively. These observations have lent scientific credence to understanding the antidiabetic mechanism of action of CS through modulation of the activity of the key enzymes involved in T2DM pathogenesis and its secondary complications, furthering the support of CS development as an antidiabetic therapeutic. Further studies, including *in vitro* enzymatic assays and *in vivo* experimentation, on the identified CS metabolites are highly suggested to enhance the development of CS for cost-effective management of T2DM and its complications.

Author Contribution: A.A. was involved in the methodology, formal analysis, data curation, and preparation of original draft; A.A.L. was involved in the software and data curation and S.S. conceptualized and administered the project, supervised, and provided funding. All authors have read and agreed to the published version of the manuscript.

Funding: The authors specially acknowledge the financial assistance of the Directorate of Research and Postgraduate Support, Durban University of Technology, the South African Medical Research Council (SAMRC) under a Self-Initiated Research Grant, the Technology Innovative Agency as well as the National Research Foundation's (NRF) Competitive Programme for Rated Researchers Support (SRUG2204193723) to S. Sabiu. The views and opinions expressed in this paper are those of the authors and do not necessarily represent the official views of the funders.

Institutional Review Board Statement: Not Applicable

Informed Consent Statement: Not Applicable

Acknowledgments: The assistance of the Directorate of Research and Postgraduate Support, Durban University of Technology, for the Master's Scholarship Scheme to A. Akoonjee is duly and thankfully acknowledged. The Centre for High Performance Computing (CHPC), Cape Town, South Africa is equally acknowledged for granting access to the computing software and modules used in this study.

Conflicts of Interest: The authors declared no known competing financial interests or personal relationships that could have appeared to influence the work reported in this paper.

References

Agarwal, S. and Mehrotra, R.J.J.C. 2016. An overview of molecular docking. *JSM Chemistry*, 4, 1024.

Ahamed, F. M., Chinnam, S., Challa, M., Kariyanna, G., Kumer, A., Jadoun, S., Salawi, A., G. Al-Sehemi, A., Chakma, U. and Mashud, M. A. A. 2023. Molecular Dynamics Simulation, QSAR, DFT, Molecular Docking, ADMET, and Synthesis of Ethyl 3-((5-Bromopyridin-2-yl) Imino) Butanoate Analogues as Potential Inhibitors of SARS-CoV-2. *Polycyclic Aromatic Compounds,* 1-19.

Ahmed, S., Ali, M.C., Ruma, R.A., Mahmud, S., Paul, G.K., Saleh, M.A., Alshahrani, M.M., Obaidullah, A.J., Biswas, S.K., Rahman, M.M. and Rahman, M.M. 2022. Molecular docking and dynamics simulation of natural compounds from betel leaves (*Piper betle* L.) for

investigating the potential inhibition of alpha-amylase and alpha-glucosidase of type 2 diabetes. *Molecules*, 27, 4526.

Aihara, J. I. 1999. Reduced HOMO− LUMO gap as an index of kinetic stability for polycyclic aromatic hydrocarbons. *The Journal of Physical Chemistry A*, 103, 7487-7495.

Akoonjee, A., Lanrewaju, A. A., Balogun, F. O., Makunga, N. P. and Sabiu, S. 2023. Waste to Medicine: Evidence from Computational Studies on the Modulatory Role of Corn Silk on the Therapeutic Targets Implicated in Type 2 Diabetes Mellitus. *Biology*, 12, 1509.

Al-Anazi, M., Al-Najjar, B.O. and Khairuddean, M. 2018. Structure-based drug design studies toward the discovery of novel chalcone derivatives as potential epidermal growth factor receptor (EGFR) inhibitors. *Molecules*, 23, 3203.

Alhadrami, H.A., Hamed, A.A., Hassan, H.M., Belbahri, L., Rateb, M.E. and Sayed, A.M. 2020. Flavonoids as potential anti-MRSA agents through modulation of PBP2a: A computational and experimental study. *Antibiotics*, 9, 562.

Al-Khodairy, F.M., Khan, M.K.A., Kunhi, M., Pulicat, M.S., Akhtar, S. and Arif, J.M. 2013. *In silico* prediction of mechanism of Erysolin-induced apoptosis in human breast cancer cell lines. *American Journal of Bioinformatics Research*, 3, 62.

Animaw, W. and Seyoum, Y. 2017. Increasing prevalence of diabetes mellitus in a developing country and its related factors. *PloS One*, 12, 0187670.

Aribisala, J.O. and Sabiu, S. 2022. Cheminformatics identification of phenolics as modulators of penicillin-binding protein 2a of *Staphylococcus aureus*: A structure–activity-relationship-based study. *Pharmaceutics*, 14, 1818.

Aribisala, J.O., Nkosi, S., Idowu, K., Nurain, I.O., Makolomakwa, G.M., Shode, F.O. and Sabiu, S. 2021. Astaxanthin-mediated bacterial lethality: evidence from oxidative stress contribution and molecular dynamics simulation. *Oxidative Medicine and Cellular Longevity*, 2021.

Ausaf Ali, S., Hassan, I., Islam, A. and Ahmad, F. 2014. A review of methods available to estimate solvent-accessible surface areas of soluble proteins in the folded and unfolded states. *Current Protein and Peptide Science*, 15, 456.

Balogun, F.O., Naidoo, K., Aribisala, J.O., Pillay, C. and Sabiu, S. 2022. Cheminformatics identification and validation of dipeptidyl peptidase-IV modulators from shikimate pathway-derived phenolic acids towards interventive type-2 diabetes therapy. *Metabolites*, 12, 937.

Balogun, F.O., Singh, K., Rampadarath, A., Akoonjee, A., Naidoo, K. and Sabiu, S. 2023. Cheminformatics identification of modulators of key carbohydrate-metabolizing enzymes from *C. cujete* for type-2 diabetes mellitus intervention. *Journal of Diabetes and Metabolic Disorders*, 22, 1299.

Biovia, D.S. 2021. Discovery Studio Visualizer v21. 1.0. 20298. San Diego: Dassault Systèmes.

Bitwell, C., Indra, S.S., Luke, C. and Kakoma, M.K. 2023. A review of modern and conventional extraction techniques and their applications for extracting phytochemicals from plants. *Scientific African*, 19, 01585.

Calais, J. L. 1993. Density-functional theory of atoms and molecules. RG Parr and W. Yang, Oxford University press, New York, Oxford, 1989. IX+ 333 pp. Price£ 45.00. *International Journal of Quantum Chemistry*, 47, 101-101.

Castro-Alvarez, A., Costa, A.M. and Vilarrasa, J. 2017. The performance of several docking programs at reproducing protein–macrolide-like crystal structures. *Molecules*, 22, 136.

Chang, C.C., Yuan, W., Roan, H.Y., Chang, J.L., Huang, H.C., Lee, Y.C., Tsay, H.J. and Liu, H.K. 2016. The ethyl acetate fraction of corn silk exhibits dual antioxidant and anti-glycation activities and protects insulin-secreting cells from glucotoxicity. *BMC Complementary and Alternative Medicine,* 16, 1.

Demir, Y., Ceylan, H., Türkeş, C. and Beydemir, Ş. 2022. Molecular docking and inhibition studies of vulpinic, carnosic and usnic acids on polyol pathway enzymes. *Journal of Biomolecular Structure and Dynamics,* 40, 12008.

Dias, R., de Azevedo, J. and Walter, F. 2008. Molecular docking algorithms. *Current Drug Targets*, 9, 1040.

Domingo, L. R. and Pérez, P. 2011. The nucleophilicity N index in organic chemistry. *Organic and Biomolecular Chemistry*, 9, 7168-7175.

Du, X., Li, Y., Xia, Y.L., Ai, S.M., Liang, J., Sang, P., Ji, X.L. and Liu, S.Q. 2016. Insights into protein–ligand interactions: mechanisms, models, and methods. *International Journal of Molecular Sciences*, 17, 144.

Eawsakul, K., Ongtanasup, T., Ngamdokmai, N. and Bunluepuech, K. 2023. Alpha-glucosidase inhibitory activities of astilbin contained in *Bauhinia strychnifolia* Craib. stems: an investigation by *in silico* and *in vitro* studies. *BMC Complementary Medicine and Therapies*, 23, 25.

Ebrahimie, M., Bahmani, M., Shirzad, H., Rafieian-Kopaei, M. and Saki, K. 2015. A review study on the effect of Iranian herbal medicines on opioid withdrawal syndrome. *Journal of Evidence-based Complementary and Alternative Medicine*, 20, 302.

Ebrahimzadeh, M.A., Pourmorad, F. and Hafezi, S. 2008. Antioxidant activities of Iranian corn silk. *Turkish Journal of Biology*, 32, 43.

Esha, N. J. I., Quayum, S. T., Saif, M. Z., Almatarneh, M. H., Rahman, S., Alodhayb, A., Poirier, R. A. and Uddin, K. M. 2024. Exploring the potential of fluoro-flavonoid derivatives as anti-lung cancer agents: DFT, molecular docking, and molecular dynamics techniques. *International Journal of Quantum Chemistry*, 124, e27274.

Guo, J., Liu, T., Han, L. and Liu, Y. 2009. The effects of corn silk on glycaemic metabolism. *Nutrition and Metabolism*, 6, 1.

Guo, L., Yan, Z., Zheng, X., Hu, L., Yang, Y. and Wang, J. 2014. A comparison of various optimization algorithms of protein–ligand docking programs by fitness accuracy. *Journal of Molecular Modeling*, 20, 1.

Gupta, M., Sharma, R. and Kumar, A. 2018. Docking techniques in pharmacology: How much promising?. *Computational Biology and Chemistry*, 76, 210.

Haldar, S., Gan, L., Tay, S.L., Ponnalagu, S. and Henry, C.J. 2019. Postprandial glycemic and insulinemic effects of the addition of aqueous extracts of dried corn silk, cumin seed powder or tamarind pulp, in two forms, consumed with high glycemic index rice. *Foods*, 8, 437.

Hasanudin, K., Hashim, P. and Mustafa, S. 2012. Corn silk (*Stigma maydis*) in healthcare: a phytochemical and pharmacological review. *Molecules*, 17, 9697.

Haslina, M, E. 2017. Extract corn silk with variation of solvents on yield, total phenolics, total flavonoids and antioxidant activity. *Indonesian Food and Nutrition Progress*. 14, 21.

Hata, H., Tran, D.P., Sobeh, M.M. and Kitao, A. 2021. Binding free energy of protein/ligand complexes calculated using dissociation Parallel Cascade Selection Molecular Dynamics and Markov state model. *Biophysics and Physicobiology*, 18, 305.

Hess, B. 2002. Convergence of sampling in protein simulations. *Physical Reviews*, 65, 031910.

Hollingsworth, S.A. and Dror, R.O. 2018. Molecular dynamics simulation for all. *Neuron*, 99, 1129.

Hou, T., Wang, J., Li, Y. and Wang, W. 2011. Assessing the performance of the MM/PBSA and MM/GBSA methods. 1. The accuracy of binding free energy calculations based on molecular dynamics simulations. *Journal of Chemical Information and Modeling*, 51, 69.

Jairajpuri, D.S., Hussain, A., Nasreen, K., Mohammad, T., Anjum, F., Rehman, M.T., Hasan, G.M., Alajmi, M.F. and Hassan, M.I. 2021. Identification of natural compounds as potent inhibitors of SARS-CoV-2 main protease using combined docking and molecular dynamics simulations. S*audi Journal of Biological Sciences*, 28, 2423.

Karabacak, M., Sinha, L., Prasad, O., Cinar, Z. and Cinar, M. 2012. The spectroscopic (FT-Raman, FT-IR, UV and NMR), molecular electrostatic potential, polarizability and hyperpolarizability, NBO and HOMO–LUMO analysis of monomeric and dimeric structures of 4-chloro-3, 5-dinitrobenzoic acid. *Spectrochimica Acta Part A: Molecular and Biomolecular Spectroscopy*, 93, 33-46.

Kaur, P., Singh, J., Kaur, M., Rasane, P., Kaur, S., Kaur, J., Nanda, V., Mehta, C.M. and Sowdhanya, D. 2023. Corn silk as an agricultural waste: a comprehensive review on its nutritional composition and bioactive potential. *Waste and Biomass Valorisation*, 14, 1413.

Kim, S.L., Kim, M.J., Lee, Y.Y., Jung, G.H., Son, B.Y., Lee, J.S., Kwon, Y.U. and Park, Y.I. 2014. Isolation and identification of flavonoids from corn silk. *The Korean Journal of Crop Science*, 59, 435.

Kruse, H., Goerigk, L. and Grimme, S. 2012. Why the standard B3LYP/6-31G* model chemistry should not be used in DFT calculations of molecular thermochemistry: understanding and correcting the problem. *The Journal of Organic Chemistry*, 77, 10824-10834.

Laeliocattleya, R.A. 2019. The potential of methanol and ethyl acetate extracts of corn silk (*Zea mays* L.) as sunscreen. In AIP Conference Proceedings (Vol. 2099, No. 1). AIP Publishing.

Lankatillake, C., Huynh, T. and Dias, D.A. 2019. Understanding glycaemic control and current approaches for screening antidiabetic natural products from evidence-based medicinal plants. *Plant Methods*, 15, 1.

Lanrewaju, A.A., Enitan-Folami, A.M., Nyaga, M.M., Sabiu, S. and Swalaha, F.M. 2023a. Metabolites profiling and cheminformatics bioprospection of selected medicinal plants against the main protease and RNA-dependent RNA polymerase of SARS-CoV-2. *Journal of Biomolecular Structure and Dynamics*, 1-21.

Lanrewaju, A.A., Enitan-Folami, A.M., Nyaga, M.M., Sabiu, S. and Swalaha, F.M. 2023b. Cheminformatics bioprospection of selected medicinal plants metabolites against trypsin cleaved VP4 (spike protein) of rotavirus A. *Journal of Biomolecular Structure and Dynamics*, 1-20.

Lee, J., Kim, S.L., Lee, S., Chung, M.J. and Park, Y.I. 2014. Immunostimulating activity of maysin isolated from corn silk in murine RAW 264.7 macrophages. *BMB reports*, 47, 382.

Li, Z., Feng, L., Wang, H., Zhang, L., Li, H., Li, Y., Niu, P., Tian, G., Yang, Y., Mei, X. and Peng, L. 2023. The impact of growth years on the medicinal material characteristics and metabolites of *Stellaria dichotoma* L. var. *lanceolata* Bge. reveals the optimal harvest age. *Plants (Basel)*. 12, 2286.

Lukman, H.Y., Aribisala, J.O., Akoonjee, A., Sulyman, A.O., Wudil, A.M. and Sabiu, S. 2024. Modulation of dipeptidyl peptidase by Rooibos tea metabolites towards type 2 diabetes care: Evidence from molecular dynamics simulation and density functional theory. *Scientific African*, 02173.

Li, Y., Kong, D., Fu, Y., Sussman, M.R. and Wu, H., 2020. The effect of developmental and environmental factors on secondary metabolites in medicinal plants. *Plant Physiology and Biochemistry*, 148, 80-89.

Li, R., Pan, Y., Li, N., Wang, Q., Chen, Y., Phisalaphong, M. and Chen, H. 2020. Antibacterial and cytotoxic activities of a green synthesized silver nanoparticles using corn silk aqueous extract. *Colloids and Surfaces A: Physicochemical and Engineering Aspects*, 598, 124827.

Lin, X., Xu, Y., Pan, X., Xu, J., Ding, Y., Sun, X., Song, X., Ren, Y. and Shan, P.F. 2020. Global, regional, and national burden and trend of diabetes in 195 countries and territories: an analysis from 1990 to 2025. *Scientific Reports*, 10, 14790.

Luo, J., Xue, Z. Q., Liu, W. M., Wu, J. L. and Yang, Z. Q. 2006. Koopmans' theorem for large molecular systems within density functional theory. *The Journal of Physical Chemistry A*, 110, 12005-12009.

Macel, M., Visschers, I.G., Peters, J.L., Kappers, I.F., de Vos, R.C. and van Dam, N.M. 2019. Metabolomics of thrips resistance in pepper (*Capsicum spp*.) reveals monomer and dimer acyclic diterpene glycosides as potential chemical defenses. *Journal of Chemical Ecology*, 45, 490.

Maciejewska-Turska, M., Pecio, Ł. and Zgórka, G. 2022. Isolation of mirificin and other bioactive isoflavone glycosides from the kudzu root lyophilisate using centrifugal partition and flash chromatographic techniques. *Molecules*, 27, 6227.

Magangana, T.P., Makunga, N.P., Amos Fawole, O. and Opara, U.L. 2021. Effect of solvent extraction and blanching pre-treatment on phytochemical, antioxidant properties, enzyme inactivation and antibacterial activities of 'Wonderful' pomegranate peel extracts. *Processes*, 9, 1012.

Magangana, T.P., Makunga, N.P., Fawole, O.A., Stander, M.A. and Opara, U.L. 2022. Antioxidant, antimicrobial, and metabolomic characterization of blanched pomegranate peel extracts: Effect of cultivar. *Molecules*, 27, 2979.

Maphetu, N., Unuofin, J.O., Masuku, N.P., Olisah, C. and Lebelo, S.L. 2022. Medicinal uses, pharmacological activities, phytochemistry, and the molecular mechanisms of *Punica granatum* L. (pomegranate) plant extracts: A review. *Biomedicine and Pharmacotherapy*, 153, 113256.

Michaelidou, M., Pappachan, J.M. and Jeeyavudeen, M.S. 2023. Management of diabesity: current concepts. *World Journal of Diabetes*, 14, 396.

Mihali, C., Frumuzachi, O., Nicolescu, A., Babotă, M., Păltinean, R., Tanase, C. and Mocan, A. 2024. Valorization of corn silk as an agricultural by-product through the optimization of ultrasound-assisted extraction. *Applied Sciences*, 14, 1516.

Moemen, L.A., Abdel Hamid, M.A., Wahab, S.A., Kenawy, M.K.M., Abuelela, M.H., Hassanin, O.A., Fouly, M.A., Abdelazeem, A.A., Noweir, S.R., Ismail, S.M. and Abdel Gawad, Y.H.E.R. 2020. Role of advanced glycation end products and sorbitol dehydrogenase in the pathogenesis of diabetic retinopathy. *Bulletin of the National Research Centre*, 44, 1.

Mousavi, S.S., Karami, A., Haghighi, T.M., Tumilaar, S.G., Fatimawali, Idroes, R., Mahmud, S., Celik, I., Ağagündüz, D., Tallei, T.E. and Emran, T.B. 2021. *In silico* evaluation of Iranian medicinal plant metabolites as inhibitors against main protease and the receptor-binding domain of SARS-CoV-2. *Molecules*, 26, 5724.

Haq Nawaz, Muhammad Aslam Shad, Najiha Rehman, Hina Andaleeb, Najeeb Ullah. 2020. Effect of solvent polarity on extraction yield and antioxidant properties of phytochemicals from bean (Phaseolus vulgaris) seeds. *Brazilian Journal of Pharmaceutical Sciences*, 56, 17129.

Hu, X., Jiang, C., Gu, Y. and Xue, X. 2024. Exploring the conformational dynamics and key amino acids in the CD26-caveolin-1 interaction and potential therapeutic interventions. *Medicine*, 103, 38367.

Nawaz, H., Aslam, M. and Muntaha, S.T. 2019. Effect of solvent polarity and extraction method on phytochemical composition and antioxidant potential of corn silk. *Free Radicals and Antioxidants*, 9, 5.

Oboh, G., Isaac, A.T., Akinyemi, A.J. and Ajani, R.A. 2014. Inhibition of key enzymes linked to type 2 diabetes and sodium nitroprusside induced lipid peroxidation in rats' pancreas by phenolic extracts of avocado pear leaves and fruit. *International Journal of Biomedical Science: IJBS*, 10, 208.

Oh, K.K., Adnan, M. and Cho, D.H. 2020. Network pharmacology of bioactives from *Sorghum bicolor* with targets related to diabetes mellitus. *PLoS One*, 15, 0240873.

Omotosho, I.O., Obisesan, O.B. and Oluleye, O. 2014. Sorbitol dehydrogenase activity in diabetes mellitus and cataract patients. *Journal of Applied Medical Science*, 3, 61.

Oz AT, Kafkas E. 2017. Phytochemicals in fruits and vegetables. *Waisundara V. Superfood and Functional Food. London: IntechOpen*, 175-184.

Paddy, V., Van Tonder, JJ. and Steenkamp, V. 2014. The antidiabetic activity of a polyherbal tea mixture and its constituents *in vitro*. *17th World Congress of Basic and Clinical Pharmacology*. 13.

Pagadala, N.S., Syed, K. and Tuszynski, J. 2017. Software for molecular docking: a review. *Biophysical Reviews*, 9, 91.

Pantsar, T. and Poso, A. 2018. Binding affinity via docking: fact and fiction. *Molecules*, 23, 1899.

Pellicani, F., Dal Ben, D., Perali, A. and Pilati, S. 2023. Machine learning scoring functions for drug discovery from experimental and computer-generated protein–ligand structures: towards per-target scoring functions. *Molecules*, 28, 1661.

Petrovska, B.B. 2012. Historical review of medicinal plants' usage. *Pharmacognosy Reviews*, 6, 1.

Pheiffer, C., Pillay-van Wyk, V., Joubert, J.D., Levitt, N., Nglazi, M.D. and Bradshaw, D. 2018. The prevalence of type 2 diabetes in South Africa: a systematic review protocol. *BMJ Open*, 8, 021029.

Rahman, N.A. and Rosli, W.I.W. 2014. Nutritional compositions and antioxidative capacity of the silk obtained from immature and mature corn. *Journal of King Saud University-Science*, 26, 119.

Ramana, K.V. 2011. Aldose reductase: new insights for an old enzyme. *Biomolecular Concepts*, 2, 103.

Rampadarath, A., Balogun, F.O., Pillay, C. and Sabiu, S. 2022. Identification of flavonoid C-glycosides as promising antidiabetics targeting protein tyrosine phosphatase 1B. *Journal of Diabetes Research*, 2022.

Rampadarath, A., Balogun, F.O., Pillay, C. and Sabiu, S. 2022. Identification of flavonoid C-glycosides as promising antidiabetics targeting protein tyrosine phosphatase 1B. *Journal of Diabetes Research,* 2022.

Rampadarath, A., Aribisala, J.O., Makunga, N.P., Mazibuko-Mbeje, S. and Sabiu, S. 2023. Molecular bioprospection of *Helianthus annuus* L.(sunflower) cypsela for antidiabetic therapeutics through network pharmacology, density functional theory and molecular dynamics simulation. South *African Journal of Botany*, 162, 72-95.

Rampogu, S., Lee, G., Park, J.S., Lee, K.W. and Kim, M.O. 2022. Molecular docking and molecular dynamics simulations discover curcumin analogue as a plausible dual inhibitor for SARS-CoV-2. *International Journal of Molecular Sciences*, 23, 1771.

Rosenberg, M.S. *Sequence Alignment: Methods, Models, Concepts and Strategies*; University of California Press: CA, USA, 2009 retrieved from https://doi.org/10.1525/9780520943742, accessed on 01/04/2024.

S'thebe, N.W., Aribisala, J.O. and Sabiu, S. 2023. Cheminformatics bioprospection of sunflower seeds' oils against quorum sensing system of *Pseudomonas aeruginosa*. *Antibiotics*, 12, 504.

Sabiu, S., O'Neill, FH. and Ashafa, AOT. 2016. Kinetics of α-amylase and α-glucosidase inhibitory potential of *Zea mays Linnaeus* (Poaceae), *Stigma maydis* aqueous extract: An *in vitro* assessment. *Journal of Ethnopharmacology*. 183, 1.

Sabiu, S., Ajani, E.O., Sunmonu, T.O. and Ashafa, A.O.T. 2017. Kinetics of modulatory role of *Cyperus esculentus* L. on the specific activity of key carbohydrate metabolizing enzymes. *African Journal of Traditional, Complementary and Alternative Medicines*, 14, 46.

Sabiu, S., Madende, M., Ajao, A.A.N., Ogundeji, O.A., Lekena, N. and Alayande, K.A. 2019. The scope of phytotherapy in southern African antidiabetic healthcare. *Transactions of the Royal Society of South Africa*, 74, 1.

Sabiu, S., Balogun, F.O. and Amoo, S.O. 2021. Phenolics profiling of *Carpobrotus edulis* (L.) NE Br. and insights into molecular dynamics of their significance in type 2 diabetes therapy and its retinopathy complication. *Molecules*, 26, 4867.

Sabiu, S., and Idowu, K. 2022. An insight on the nature of biochemical interactions between glycyrrhizin, myricetin and CYP3A4 isoform. *Journal of Food Biochemistry*, 46. 13831.

Sajal, H., Patil, S.M., Raj, R., Shbeer, A.M., Ageel, M. and Ramu, R. 2022. Computer-aided screening of metabolites from *Ocimum tenuiflorum* against diabetes mellitus targeting DPP4 inhibition: A combination of molecular docking, molecular dynamics, and pharmacokinetics approaches. *Molecules*, 27, 5133.

Salim, B., Said, G., Kambouche, N. and Kress, S. 2020. Identification of phenolic compounds from Nettle as new candidate inhibitors of main enzymes responsible on type-II diabetes. *Current Drug Discovery Technologies*, 17, 197.

Shalihah, I.M., Pamela, V.Y. and Kusumasari, S. 2020. Cornsilk tea extract as antidiabetic: a review. *Food Science and Technology Journal*, 2202, 66.

Sharma, P., Joshi, T., Joshi, T., Chandra, S. and Tamta, S. 2021. Molecular dynamics simulation for screening phytochemicals as α-amylase inhibitors from medicinal plants. *Journal of Biomolecular Structure and Dynamics*, 39. 6524.

Sharma, P., Singh, S., Thakur, V., Sharma, N. and Grewal, A.S. 2021. Novel and emerging therapeutic drug targets for management of type 2 diabetes mellitus. *Obesity Medicine*, 23, 100329.

Shode, F.O., Uhomoibhi, J.O.O., Idowu, K.A., Sabiu, S. and Govender, K.K. 2022. Molecular dynamics study on selected bioactive phytochemicals as potential inhibitors of HIV-1 Subtype C protease. *Metabolites*, 12, 1155.

Shunmugam, L. and Soliman, M.E. 2018. Targeting HCV polymerase: a structural and dynamic perspective into the mechanism of selective covalent inhibition. *RSC Advances*, 8, 42210.

Singh, J., Inbaraj, B.S., Kaur, S., Rasane, P. and Nanda, V. 2022a. Phytochemical analysis and characterization of corn silk (*Zea mays*, G5417). *Agronomy*, 12, 777.

Singh, J., Rasane, P., Nanda, V. and Kaur, S. 2022b. Bioactive compounds of corn silk and their role in management of glycaemic response. *Journal of Food Science and Technology*, 1.

Sola, D., Rossi, L., Schianca, G. P., Maffioli, P., Bigliocca, M., Mella, R., Corlianò, F., Fra, G. P., Bartoli, E. and Derosa, G. 2015. Sulfonylureas and their use in clinical practice. *Archives of Medical Science: AMS*, 11, 840.

Song, Y., Wu, F. and Wu, J. 2016. Targeting histone methylation for cancer therapy: enzymes, inhibitors, biological activity and perspectives. *Journal of Haematology and Oncology*, 9, 1.

Su, J., Luo, Y., Hu, S., Tang, L. and Ouyang, S. 2023. Advances in research on type 2 diabetes mellitus targets and therapeutic agents. International Journal of Molecular Sciences, 24, 13381.

Süntar, I. 2020. Importance of ethnopharmacological studies in drug discovery: role of medicinal plants. *Phytochemistry Reviews*, 19, 1199.

Taiwong, N. 2020. Drying temperature of corn silk tea: Physical properties, total phenolic content, antioxidant activity and flavonoid content. *Food and Applied Bioscience Journal*. 8, 38,

Tananta, V. L., Costa, E. V., Mary, Y. S., Mary, Y. S., S. Al-Otaibi, J. and Costa, R. A. 2023. DFT, ADME studies and evaluation of the binding with HSA and MAO-B inhibitory potential of protoberberine alkaloids from *Guatteria friesiana*: theoretical insights of promising candidates for the treatment of Parkinson's disease. *Journal of Molecular Modeling*, 29, 353.

Tang, W.H., Martin, K.A. and Hwa, J. 2012. Aldose reductase, oxidative stress, and diabetic mellitus. *Frontiers in Pharmacology*, 3, 87.

Thakur, S., Gupta, S.K., Ali, V., Singh, P. and Verma, M. 2021. Aldose Reductase: A cause and a potential target for the treatment of diabetic complications. *Archives of Pharmacal Research*, 44, 655.

Thareja, S., Aggarwal, S., Bhardwaj, T.R. and Kumar, M. 2012. Protein tyrosine phosphatase 1B inhibitors: a molecular level legitimate approach for the management of diabetes mellitus. *Medicinal Research Reviews*, 32. 459.

Tian, S., Sun, Y. and Chen, Z. 2021. Extraction of flavonoids from corn silk and biological activities *in vitro*. *Journal of Food Quality*, 2021, 1.

Tiwari, N., Thakur, A.K., Kumar, V., Dey, A. and Kumar, V. 2014. Therapeutic targets for diabetes mellitus: an update. *Clinical Pharmacology and Biopharmaceutics*, 3, 1.

Tiwari, S.P., Srivastava, R., Singh, C.S., Shukla, K., Singh, R.K., Singh, P., Singh, R., Singh, N.L. and Sharma, R. (2015). Amylases: an overview with special reference to alpha amylase. *Journal of Global Biosciences*, 4, 1886.

Tran, N., Pham, B. and Le, L. 2020. Bioactive compounds in anti-diabetic plants: From herbal medicine to modern drug discovery. *Biology*, 9, 252.

Tremlová, B., Mikulášková, H.K., Hajduchová, K., Jancikova, S., Kaczorová, D., Ćavar Zeljković, S. and Dordevic, D. 2021. Influence of technological maturity on the secondary metabolites of hemp concentrate (*Cannabis sativa* L.). *Foods*, 10, 1418.

Tyagi, A. and Pugazhenthi, S. 2021. Targeting insulin resistance to treat cognitive dysfunction. *Molecular Neurobiology*, 58, 2672.

Verpoorte, R. 1998. Exploration of nature's chemodiversity: the role of secondary metabolites as leads in drug development. Drug Discovery Today, 3, 232.

Vijitha, T.P. and Saranya, D. 2017. Corn silk-a medicinal boon. *International Journal of ChemTech.* Research, 10. 129.

Wang, K.J. and Zhao, J.L. 2019. Corn silk (*Zea mays* L.), a source of natural antioxidants with α-amylase, α-glucosidase, advanced glycation and diabetic nephropathy inhibitory activities. *Biomedicine and Pharmacotherapy*, 110, 510.

Wu, Y., Pan, L., Chen, Z., Zheng, Y., Diao, X. and Zhong, D. 2021. Metabolite identification in the preclinical and clinical phase of drug development. *Current Drug Metabolism*, 22, 838.

Xiao, E. and Luo, L. 2018. Alternative therapies for diabetes: a comparison of western and traditional Chinese medicine (TCM) approaches. *Current Diabetes Reviews*, 14, 487.

Xu, Q., Wang, L., Luo, J. and Shi, D. 2018. The hot and potential targets of type 2 diabetes mellitus treatment in recent decade. *Current Drug Targets*, 19, 55.

Yagasaki, K. and Muller, C.J. 2022. The effect of phytochemicals and food bioactive compounds on diabetes. *International Journal of Molecular Sciences*, 23, 7765.

Ylilauri, M., and Pentikäinen, O. T. 2013. MMGBSA as a tool to understand the binding affinities of filamin-peptide interactions. *Journal of Chemical Information and Modeling*, 53, 2626.

Zeng, X., Zhao, M. and Yao, H. 2023. Anti-lung cancer, anti-microbial, anti-α-glucosidase, anti-sorbitol dehydrogenase, and *in silico* studies of wogonoside and isoliquiritigenin as natural compounds. *Journal of Oleo Science*, 72, 919.

Zhao, W., Yin, Y., Yu, Z., Liu, J. and Chen, F. 2012. Comparison of anti-diabetic effects of polysaccharides from corn silk on normal and hyperglycemia rats. *International Journal of Biological Macromolecules,* 50, 1133.

Zhong, Z., Chen, Z., Liu, J., Hirad, A.H. and Sun, J. 2023. *In silico* studies, anti-oxidant properties, antisorbitol dehydrogenase, anti-alpha amylase and anti-gastrointestinal cancer potential of violanthin as a natural compound. *Journal of Oleo Science*, 72, 1015.

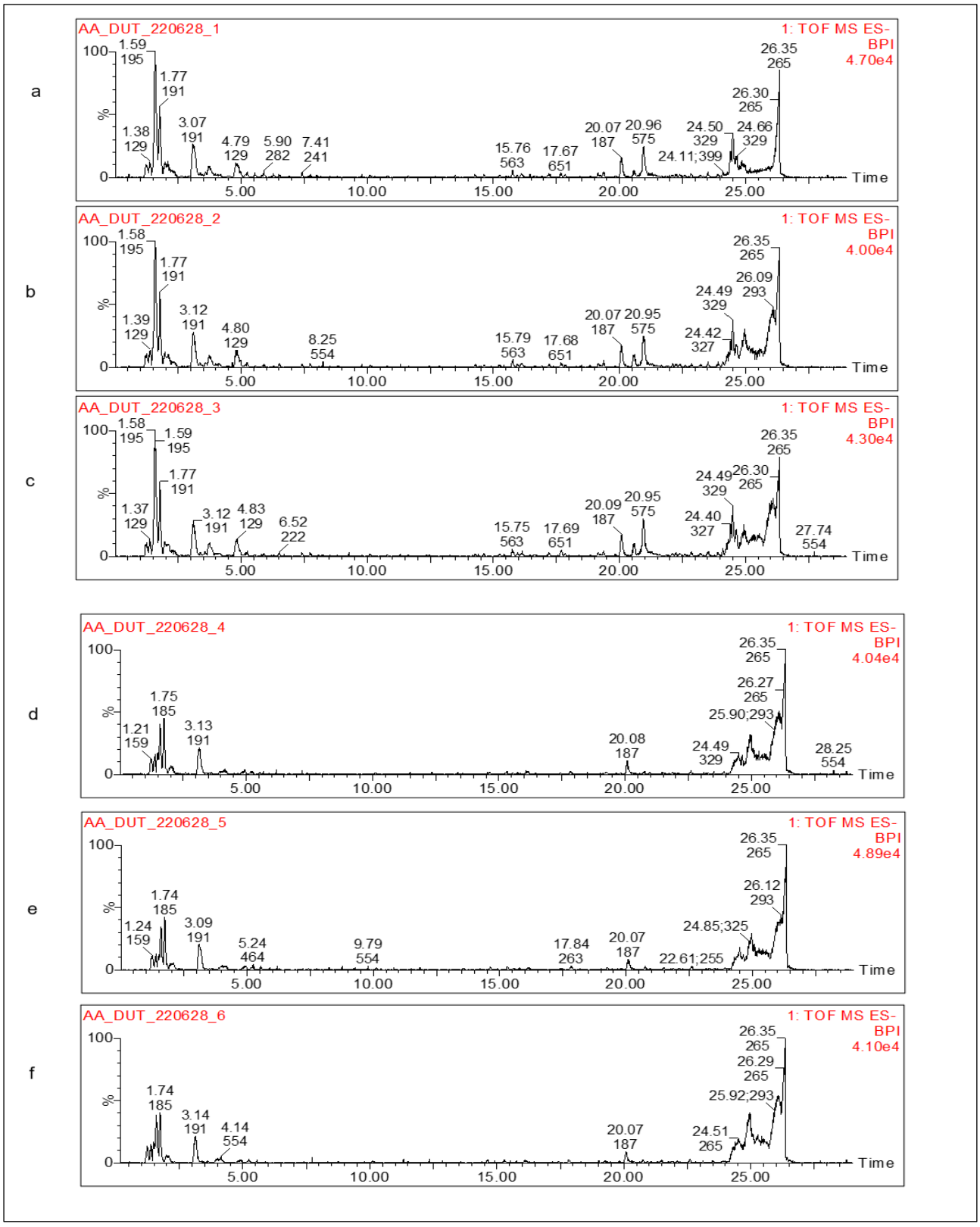

Supplementary materials:

Figure S1: Chromatograms produced showing mass-to-charge ratio and retention times of a CS metabolites found in replicates of raw CS: a) raw premature CS 1, b) raw premature CS 2.

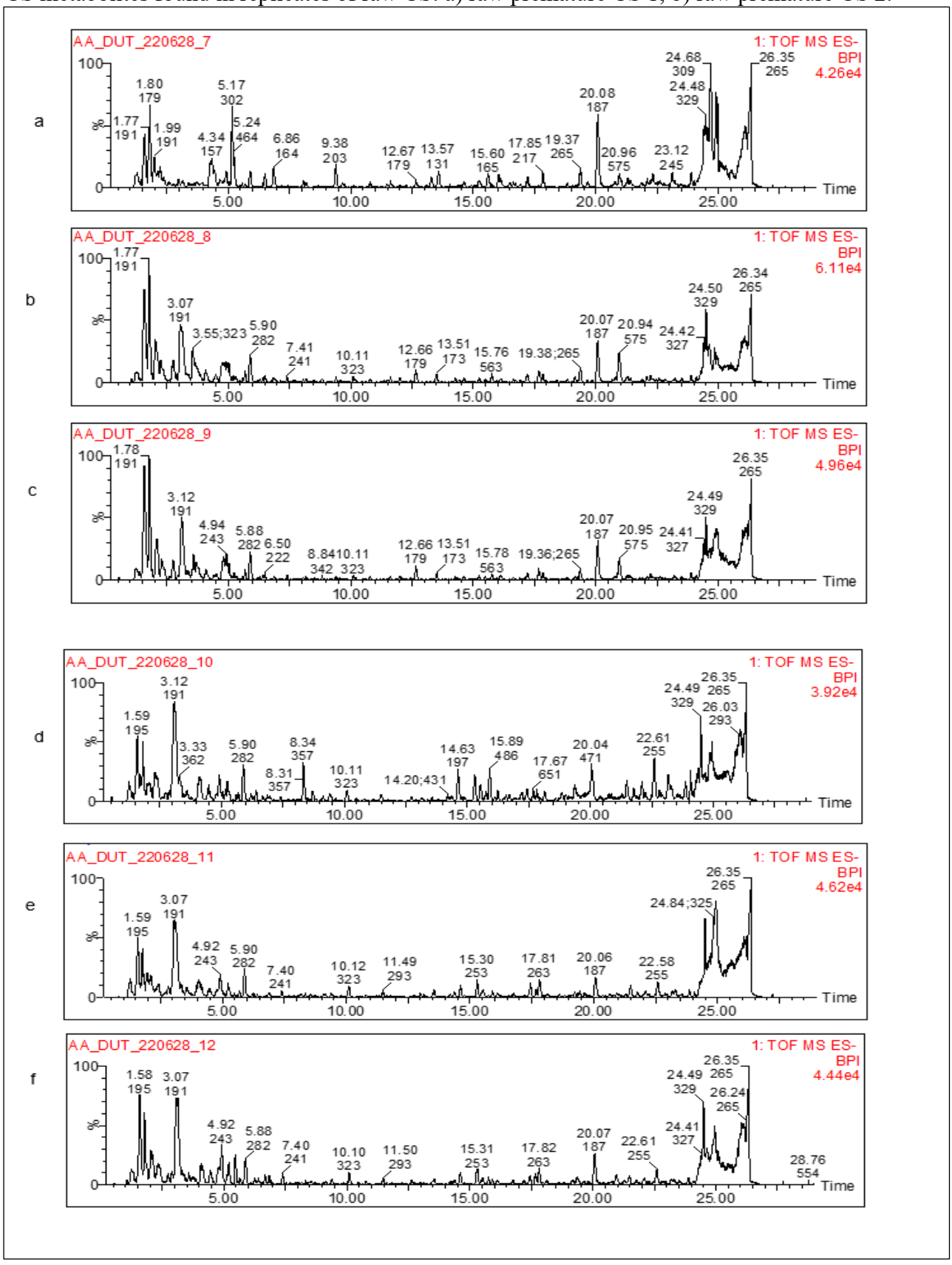

Figure S2: Chromatograms produced showing mass-to-charge ratio and retention times of a CS metabolites found in replicates of aqueous extracts of CS: a) aqueous extract of premature CS 1, b) aqueous extract of premature CS 2. C) aqueous extract of premature CS 3, d) aqueous extract of mature CS 1, e) aqueous extract of mature CS 2 and f) aqueous extract of mature CS 3.

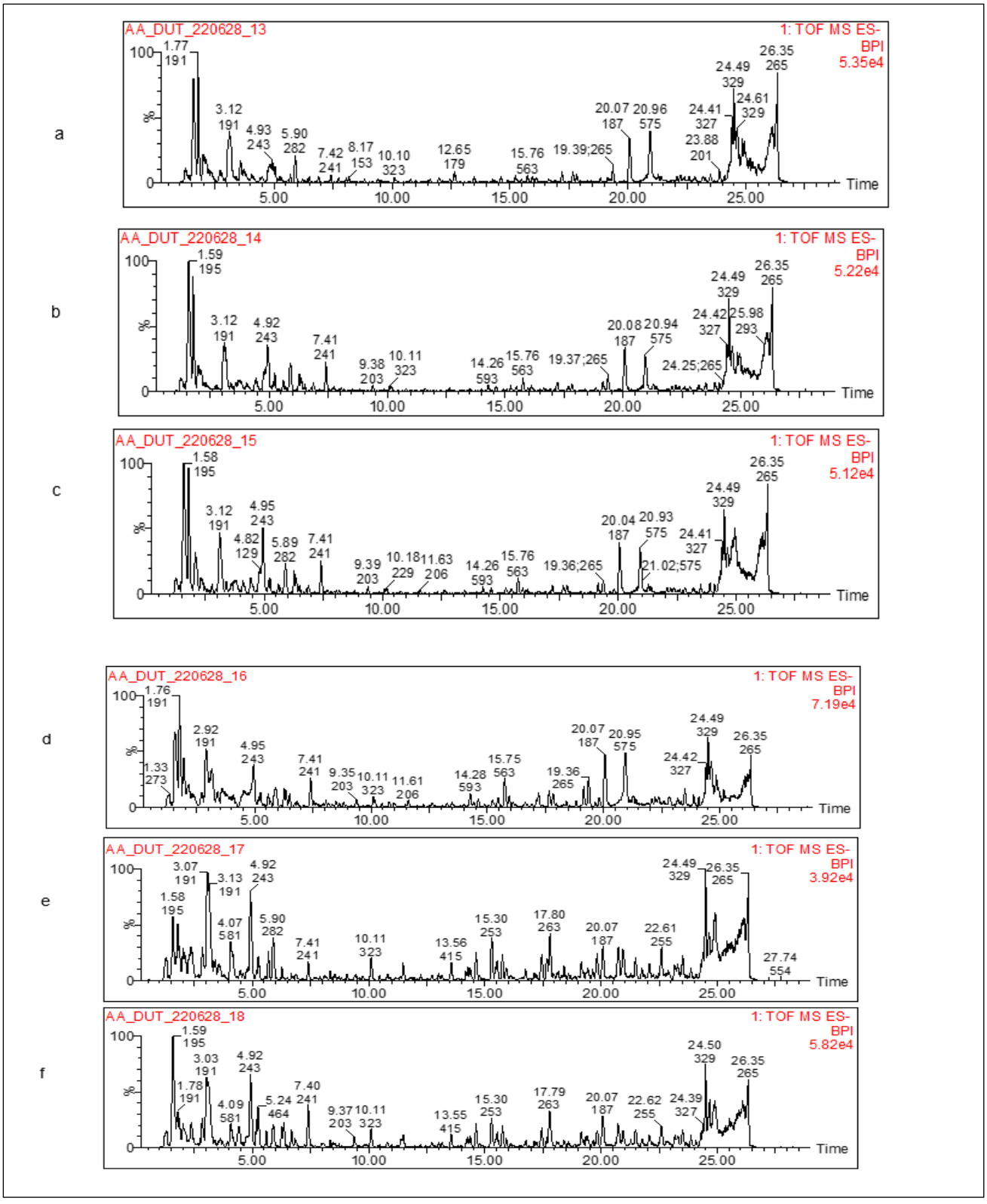

Figure S3: Chromatograms produced showing mass-to-charge ratio and retention times of a CS metabolites found in replicates of hydro-ethanolic extracts of extract of CS: a) hydro-ethanolic extract of premature CS 1, b) hydro-ethanolic extract of premature CS 2. C) hydro-ethanolic extract of premature CS, d) hydro-ethanolic extract of mature CS 1, e) hydro-ethanolic extract of mature CS 2 and f) hydro-ethanolic extract of mature CS.

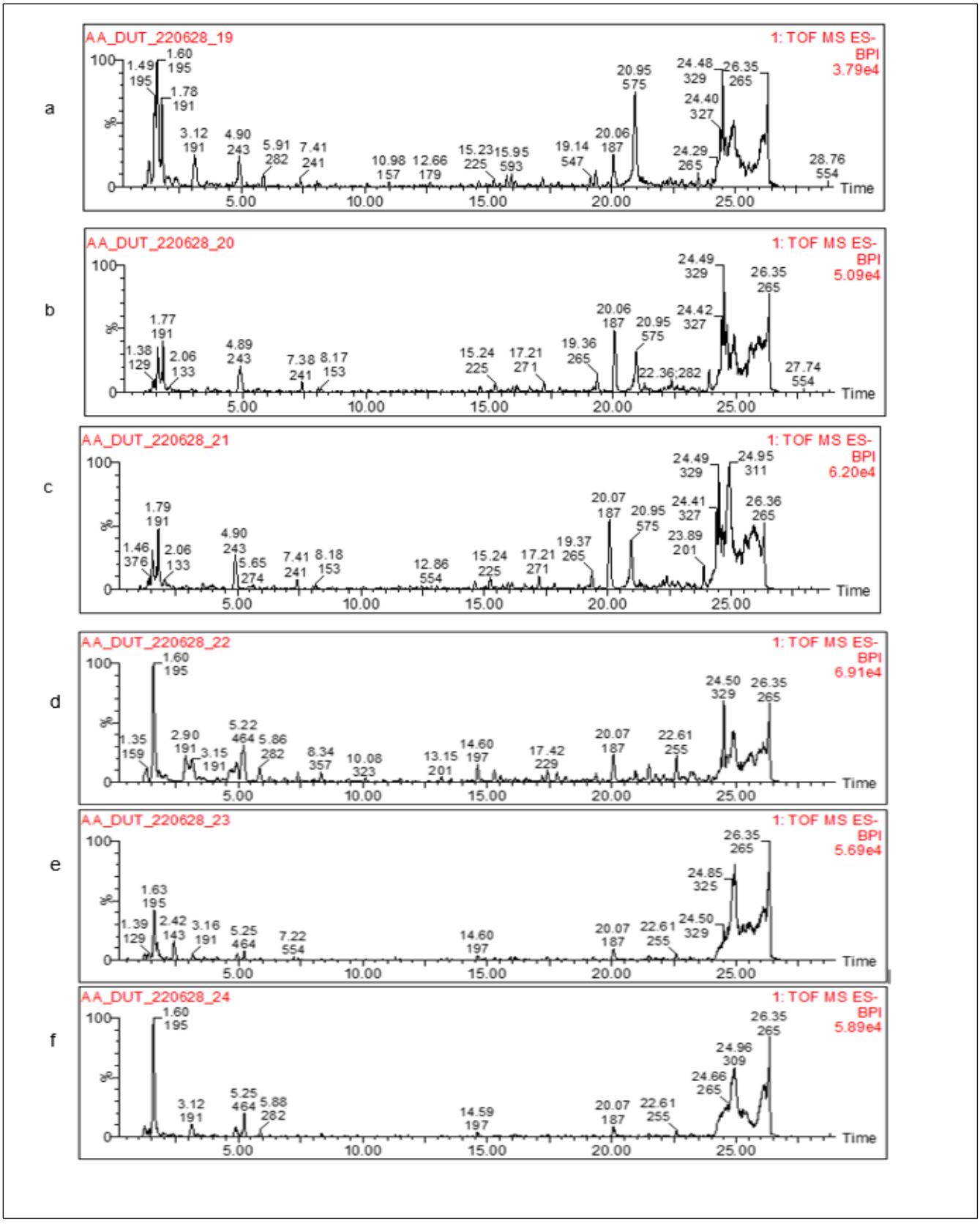

Figure S4: Chromatograms produced showing mass-to-charge ratio and retention times of a CS metabolites found in replicates of ethanolic extracts of CS: a) ethanolic extracts of premature CS 1, b) ethanolic extracts of premature CS 2. C) ethanolic extracts of premature CS 3, d) ethanolic extracts of mature CS 1, e) ethanolic extracts of mature CS 2 and f) ethanolic extracts of mature CS

Table S1: Secondary metabolites identified in various extracts corn silk through ultra-performance liquid chromatography-mass spectrometry analysis showing average retention times and mass-to-charge (m/z) ratio.

Compound number	Identity	Average retention time (minute)	m/z [M - H]-
C1	(7'R)-(+)-Lyoniresinol 9'-glucoside	4. 07	581. 22
C2	Estriol-16-Glucuronide	4.15	509.20
C3	Ascorbic acid	4.31	175.02
C4	Methylisocitric acid	4.39	205.03
C5	Citraconic acid	4.52	129.02
C6	Oxalosuccinic acid	4.98	189.01
C7	Pinocembrin 7-apiosyl-(1->5)-apiosyl-(1->2)-glucoside;5,7-Dihydroxyflavanone 7-apiosyl-(1->5)-apiosyl-(1->2)-glucoside	4.99	681.21
C8	Mevalonic acid	5.09	147.07
C9	D-2-Hydroxyglutaric acid	5.18	147.03
C10	(2R,3S)-2,3-dimethylmalic acid	5.24	161.04
C11	UNPD109129	6.35	251.08
C12	Glutaric acid	6.15	131.03
C13	Cinnamic acid	6.85	147.04
C14	(6E)-1-(4-hydroxyphenyl)-7-phenylhepta-4,6-dien-3-one	8.45	277.13
C15	Vanillic acid	8.55	167.03
C16	1-O-vanilloyl-beta-D-glucose	8.55	329.09
C17	Isorhamnetin 3-(6"-malonylglucoside)	8.64	563.10
C18	Saccharumoside C	9.08	461.13
C19	7-hydroxy-4-{3-oxo-3H-benzo[f]chromen-2-yl}-2H-chromen-2-one	9.14	355.06
C20	Sarmentose	9.45	161.08
C21	CNP0447999	9.57	353.08
C22	1-O-Caffeoylglucose	9.75	341.09
C23	1-O-Galloylglycerol	10.05	243.05
C24	C00051555	10.11	323.13
C25	3-Isopropylmalate	10.79	175.06
C26	Diaportinic acid	10.82	279.05

C27	Benzyl beta-D-glucopyranoside;(-)-Benzyl-O-beta-D-glucopyranoside	11.15	269.10
C28	Domesticoside	11.35	343.10
C29	Dihydrophaseic acid 4'-O-beta-D-glucopyranoside	11.37	443.19
C30	Ketoleucine	11.47	129.05
C31	Aesculin	11.47	339.07
C32	Chlorogenic acid	12.00	353.09
C33	Quinic acid	12.00	191.06
C34	Cudraphenone A	12.23	363.16
C35	Pimelic acid	12.26	159.07
C36	(-)-6-((2S,3R,4R,5S,6R)-3,4-dihydroxy-6-(hydroxymethyl)-5-methoxytetrahydro-2H-pyran-2-yloxy)-8-hydroxy-3-methyl-1H-isochromen-1-one	12.46	367.10
C37	(-)-11-hydroxy-9,10-dihydrojasmonic acid 11-beta-D-glucoside	12.52	389.18
C38	Caffeic acid	12.65	179.03
C39	5-Carboxyvanillic acid	12.73	211.02
C40	Phellodendric acid A;(+)-Phellodendric acid A	12.75	203.09
C41	(-)-Epigallocatechin	13.27	305.07
C42	D-Leucic acid	13.29	131.07
C43	cis-Aconitic acid	13.50	173.01
C44	MINEs-320976	14.20	431.19
C45	Loganic acid	14.25	375.13
C46	Astragalin 7-rhamnoside	14.27	593.15
C47	Quing hau sau; quinghaosu; artemisinin	14.35	281.14
C48	3-Hydroxy-4-butanolide	14.43	263.08
C49	Annularin A;(+)-Annularin A	14.62	197.08
C50	Traumatic acid	14.78	227.13
C51	Methyl geranate	14.87	181.12
C52	3-Hydroxytetradecanedioic acid	14.87	273.17
C53	Dihydrophaseic acid	14.94	281.14
C54	Tuberonic acid	15.24	225.11
C55	Daldiniapyrone	15.29	253.11
C56	4-Hydroxycinnamic acid	15.48	163.04
C57	Monascusone A	15.54	253.11
C58	Acetovanillone;Apocynin	15.60	165.05
C59	Apiin	15.76	563.14
C60	Quercitrin	15.95	447.09
C61	2-Hydroxydecanedioic acid	16.18	217.11
C62	UNPD221406	16.24	241.11
C63	Cichorioside M;(+)-Cichorioside M	16.62	427.19
C64	Austricin; 8-Deacetylmatricarin; Desacetylmatricarin	16.71	261.12

C65	trans-Ferulic acid	17.09	193.05
C66	UNPD19396	17.12	577.15
C67	UNPD77208	17.21	271.15
C68	Nepetaside	17.24	345.16
C69	Dodecanedioic acid	17.42	229.14
C70	Kaempferitrin	17.55	577.15
C71	Chrysoeriol 4',7-diglucuronide	17.68	651.12
C72	Erythronolide B	17.73	401.25
C73	UNPD230015	17.82	263.06
C74	3-Hydroxysebacic acid	17.84	217.11
C75	Tricin 7-diglucuronoside	17.96	681.13
C76	Esculetin	18.08	177.02
C77	ethyl 5-[(2,5-dimethylphenyl)methoxy]-2-phenyl-1-benzofuran-3-carboxylate	18.09	399.16
C78	xi-2,2,6-Trimethyl-1,4-cyclohexanedione	18.25	153.09
C79	Quercetin 3-(2",3",4"-triacetylgalactoside)	18.31	589.12
C80	[4]-Gingerol	18.84	265.14
C81	Phaseic acid	18.56	279.12
C82	Diaportinol	18.60	265.07
C83	Herbacetin 7-(6"-quinoylglucoside)	18.68	637.14
C84	12-deoxyerythronolide A	19.05	401.25
C85	UNPD156113	19.09	605.12
C86	Mirificin	19.15	547.14
C87	Phaseolic acid	19.24	261.13
C88	Curvularol	19.37	265.14
C89	(+)-(S)-Carvone	19.65	149.10
C90	Kaempferol 3-rhamnoside 7-galacturonide	19.87	607.13
C91	Azelaic acid	20.07	187.10
C92	(3R,4S,6S)-3,4,5-trihydroxy-6-[5-hydroxy-2-(4-hydroxyphenyl)-4-oxo-3-[(2S,3S,5R)-3,4,5-trihydroxy-6-methyloxan-2-yl]oxychromen-7-yl]oxyoxane-2-carboxylic acid	20.29	607.13
C93	Stagonolide F;(-)-Stagonolide F	20.68	183.10
C94	Isowertin 2"-rhamnoside	20.73	1183.34
C95	UNPD223815	20.86	255.16
C96	9-hydroxynonanoic acid	20.89	173.12
C97	Maysin	20.94	1151.29
C98	5,7,4'-Trihydroxy-3'-methoxyflavone	21.01	475.09
C99	Quercetin 3-O-(6"-acetyl-glucoside)	21.14	505.10
C100	Blennin D	21.15	265.14

C101	10-Deoxygeniposidic acid	21.27	357.12
C102	Gallicynoic acid F;(-)-Gallicynoic acid F	21.41	343.21
C103	Pandangolide 1a;(-)-Pandangolide 1a	21.46	243.12
C104	4-Hydroxynonenal	21.57	155.11
C105	Tetradecanedioic acid	21.76	257.17
C106	(R)-7-butyl-6,8-dihydroxy-3-[(3E)-pent-3-en-1-yl]-3,4-dihydroisochromen-1-one	21.82	303.16
C107	Genistin	21.82	431.10
C108	p-Coumaroyl malic acid	20.85	282.11
C109	Kaempferol 3-[2'''-acetyl-alpha-L-arabinopyranosyl-(1->6)-galactoside]	21.94	621.14
C110	Cyperine	22.09	259.10
C111	(+)-Cnicin; Cnicin	22.11	377.16
C112	(S)-Abscisic acid	22.20	263.13
C113	Sydnic acid; Sydonic acid	22.23	265.14
C114	Gallicynoic acid A;(+)-Gallicynoic acid A	22.81	253.14
C115	Apigenin 7-O-(6''-O-acetylglucoside)	22.85	473.11
C116	UNPD127537	23.18	255.16
C117	Olivetol	23.21	179.11
C118	Ginsenoyne E	23.29	303.16
C119	Caffeoyl tartaric acid	23.33	312.12
C120	Luteolin 3'-methyl ether 7-glucuronide	23.48	265.14
C121	UNPD205010	23.48	343.17
C122	Maysin 3'-methyl ether	23.51	589.15
C123	Artemin	23.66	265.15
C124	Gallicynoic acid B	23.69	267.16
C125	Aspergillide A	23.80	253.14
C126	(S)-Oleuropeic acid	23.89	183.10
C127	Sebacic acid	23.89	201.11
C128	7-Acetoxy-5,6-dimethoxycoumarin	17.82	263.06

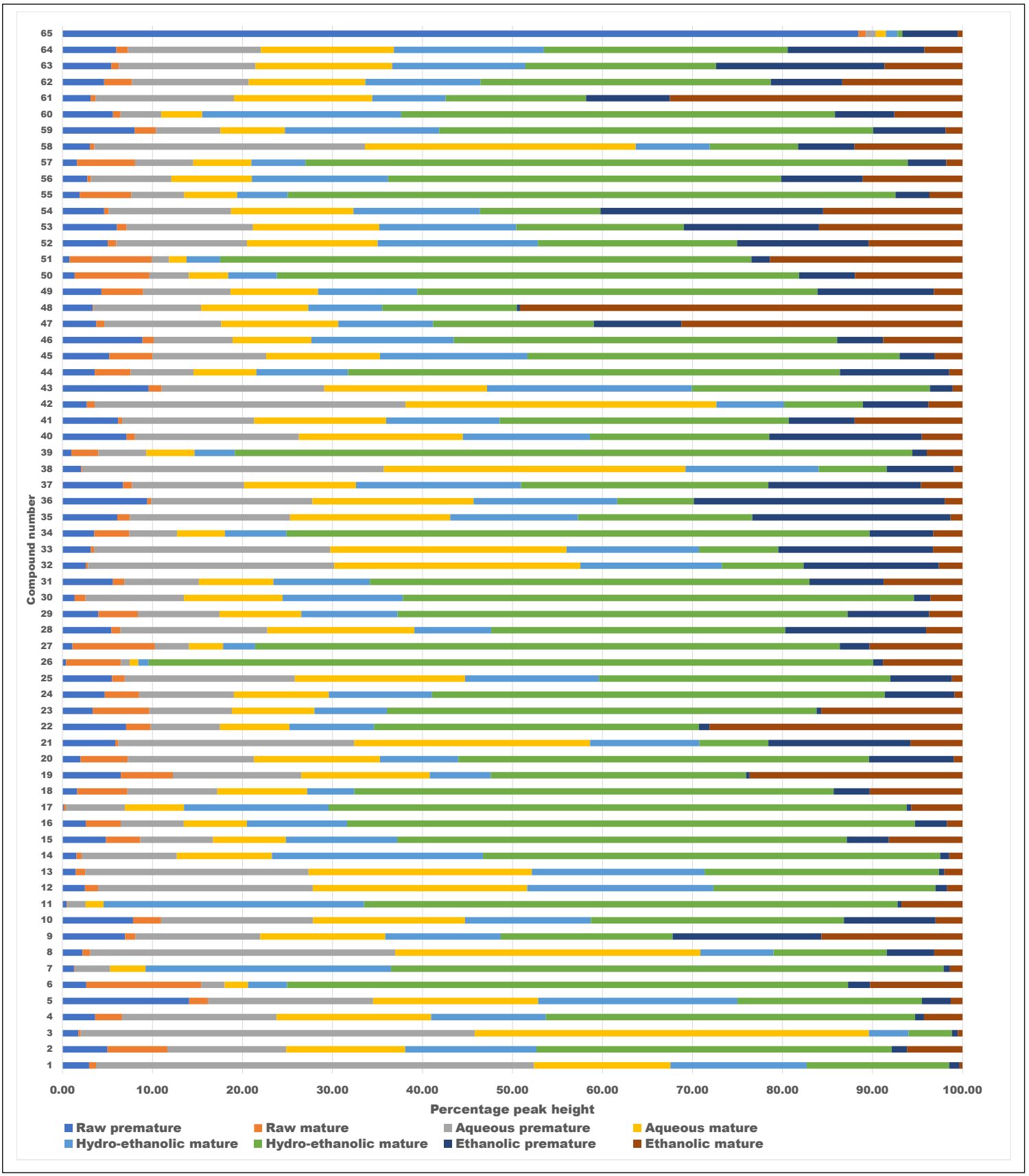

Figure S5: Stacked bar chart showing relative abundance of CS metabolites 1-65 in different extracts of CS

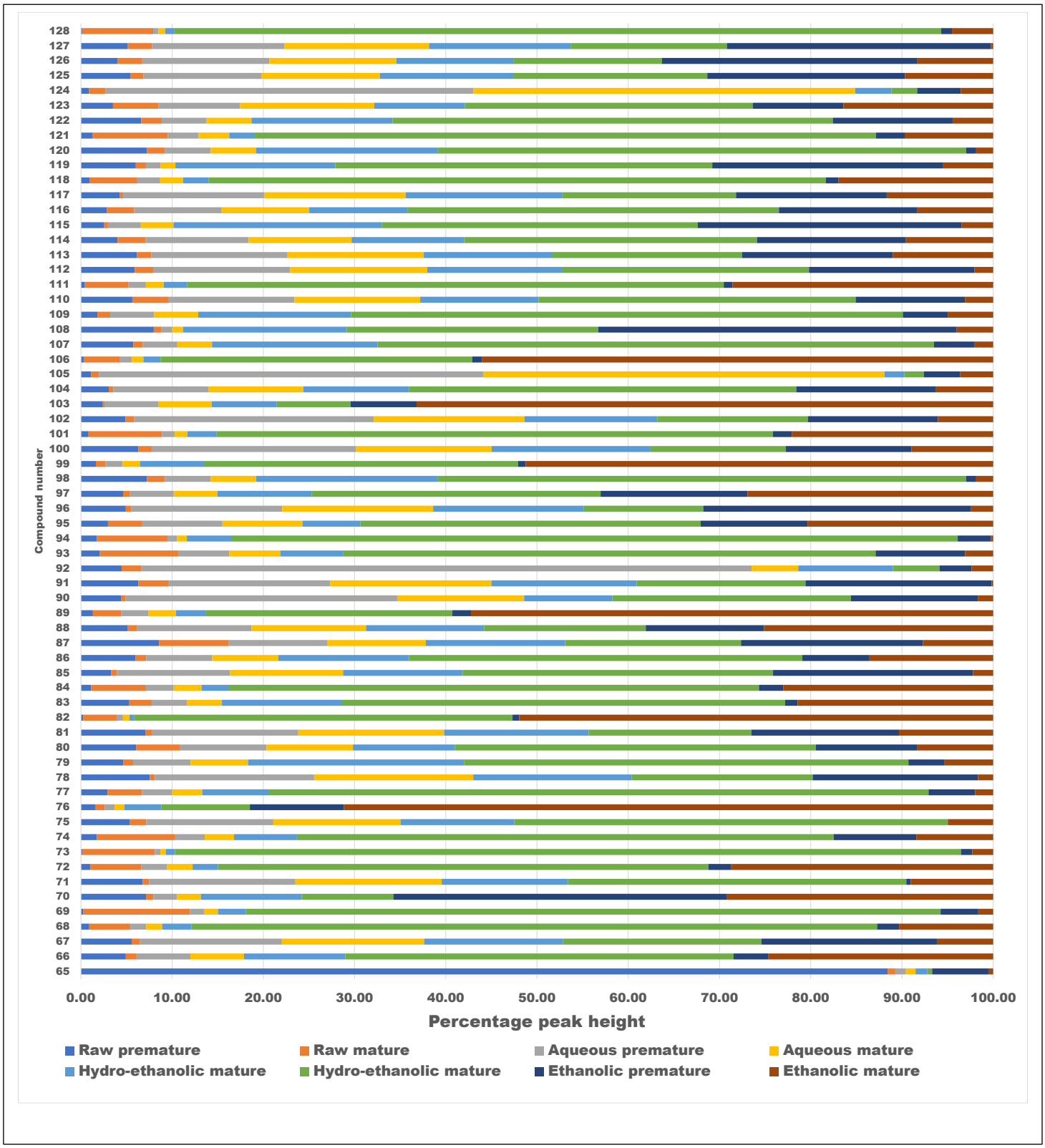

Figure S6: Stacked bar chart showing relative abundance of CS metabolites 66-128 in different extracts of CS.

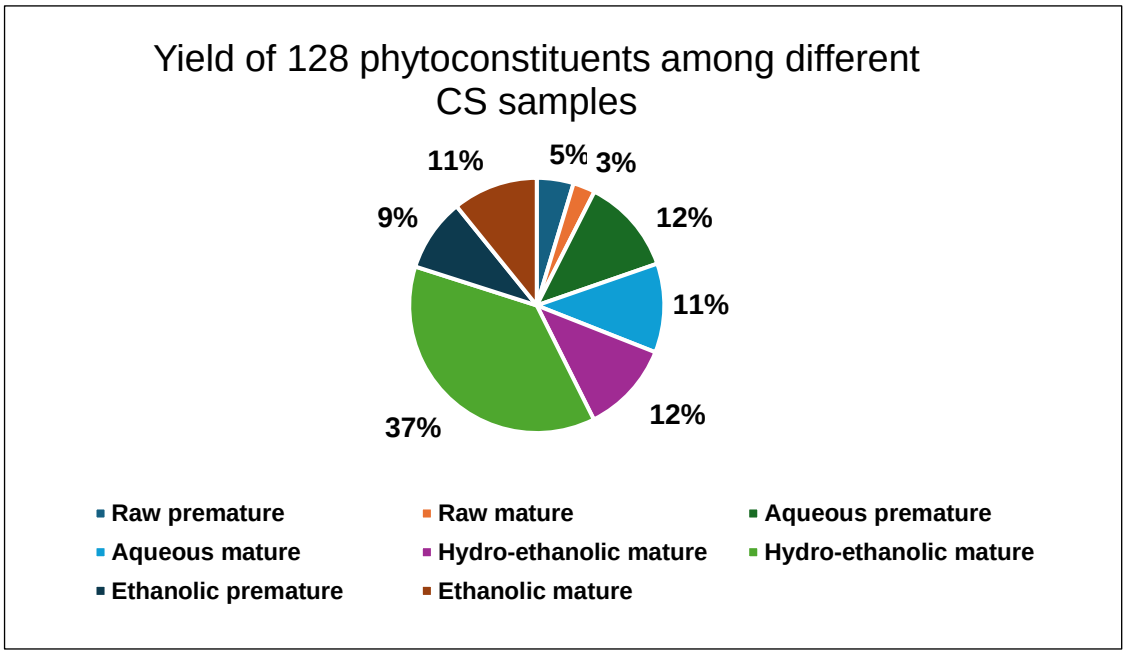

Figure S7: Yield (%) of the 128 metabolites identified in corn silk among the different extracts (aqueous, hydro-ethanolic and ethanolic) at two different developmental growth stages (premature and mature)

Table S2: Percentage relative abundance of CS metabolites identified in different samples of CS based on peak height percentage

Compound number	Raw premature CS	Raw mature CS	Aqueous extract of premature CS	Aqueous extract of mature CS	Hydro-ethanolic extract of premature CS	Hydro-ethanolic extract of mature CS	Ethanolic extract of premature CS	Ethanolic extract of mature CS
C1	2.96	0.77	48.65	15.15	15.15	15.83	1.16	0.32
C2	5.00	6.65	13.21	13.21	14.58	39.47	1.71	6.16
C3	1.78	0.25	43.79	43.79	4.40	4.83	0.66	0.51
C4	3.64	2.98	17.17	17.17	12.75	41.02	0.99	4.27
C5	14.08	2.08	18.34	18.34	22.16	20.49	3.20	1.31
C6	2.65	12.75	2.61	2.61	4.35	62.32	2.44	10.27
C7	1.28	0.07	3.94	3.94	27.29	61.39	0.71	1.38
C8	2.23	0.85	33.90	33.90	8.11	12.59	5.28	3.13
C9	6.95	1.14	13.89	13.89	12.83	19.10	16.52	15.68
C10	7.85	3.11	16.88	16.88	13.98	28.12	10.18	2.99
C11	0.49	0.10	1.99	1.99	28.93	59.28	0.44	6.78
C12	2.50	1.46	23.85	23.85	20.67	24.67	1.31	1.70
C13	1.47	1.06	24.81	24.81	19.20	26.04	0.60	2.01
C14	1.56	0.57	10.57	10.57	23.46	50.79	1.00	1.47
C15	4.83	3.81	8.09	8.09	12.38	49.95	4.66	8.19
C16	2.60	3.89	7.00	7.00	11.15	63.10	3.56	1.70
C17	0.14	0.25	6.56	6.56	16.07	64.23	0.49	5.70
C18	1.65	5.58	9.98	9.98	5.25	53.26	4.00	10.31
C19	6.48	5.78	14.27	14.27	6.78	28.35	0.42	23.64
C20	2.00	5.27	14.01	14.01	8.71	45.62	9.40	0.98
C21	5.87	0.35	26.21	26.21	12.14	7.67	15.78	5.78

C22	7.08	2.72	7.71	7.71	9.40	36.10	1.16	28.12
C23	3.36	6.29	9.17	9.17	8.06	47.74	0.52	15.69
C24	4.70	3.81	10.54	10.54	11.47	50.32	7.73	0.89
C25	5.50	1.41	18.91	18.91	14.88	32.37	6.84	1.17
C26	0.39	6.10	0.97	0.97	1.15	80.51	1.08	8.83
C27	1.10	9.18	3.78	3.78	3.56	64.97	3.31	10.32
C28	5.44	0.98	16.35	16.35	8.53	32.68	15.65	4.03
C29	3.98	4.40	9.08	9.08	10.69	50.01	9.06	3.70
C30	1.35	1.20	10.95	10.95	13.39	56.77	1.84	3.55
C31	5.62	1.26	8.29	8.29	10.72	48.83	8.25	8.76
C32	2.59	0.25	27.35	27.35	15.72	9.08	15.04	2.62
C33	3.15	0.36	26.25	26.25	14.73	8.80	17.20	3.27
C34	3.53	3.90	5.31	5.31	6.85	64.79	7.09	3.23
C35	6.09	1.41	17.80	17.80	14.19	19.37	22.03	1.32
C36	9.43	0.42	17.91	17.91	15.98	8.50	27.88	1.97
C37	6.72	1.02	12.44	12.44	18.33	27.49	16.96	4.61
C38	2.08	0.11	33.52	33.52	14.81	7.55	7.45	0.96
C39	1.00	2.98	5.34	5.34	4.48	75.28	1.61	3.96
C40	7.14	0.92	18.22	18.22	14.12	19.92	16.94	4.53
C41	6.18	0.45	14.66	14.66	12.62	32.12	7.32	11.98
C42	2.71	0.87	34.54	34.54	7.52	8.76	7.27	3.79
C43	9.58	1.44	18.08	18.08	22.77	26.44	2.53	1.09
C44	3.58	3.99	6.99	6.99	10.19	54.64	12.15	1.47
C45	5.19	4.81	12.64	12.64	16.39	41.34	3.92	3.07
C46	8.89	1.25	8.76	8.76	15.82	42.59	5.10	8.82
C47	3.77	0.88	13.00	13.00	10.53	17.86	9.73	31.24
C48	3.37	0.10	11.92	11.92	8.21	14.95	0.36	49.17
C49	4.33	4.65	9.71	9.71	11.03	44.46	12.92	3.19
C50	1.35	8.32	4.37	4.37	5.41	58.03	6.20	11.94
C51	0.78	9.13	1.94	1.94	3.74	59.03	2.05	21.40
C52	5.03	0.94	14.53	14.53	17.80	22.13	14.61	10.43
C53	6.06	1.08	14.04	14.04	15.22	18.62	15.01	15.94
C54	4.63	0.50	13.60	13.60	14.06	13.38	24.74	15.49
C55	1.92	5.72	5.88	5.88	5.63	67.53	3.78	3.67
C56	2.77	0.38	8.95	8.95	15.14	43.68	9.06	11.07
C57	1.62	6.44	6.47	6.47	6.00	66.93	4.26	1.81
C58	3.05	0.48	30.08	30.08	8.23	9.81	6.26	12.00
C59	8.01	2.38	7.16	7.16	17.15	48.22	8.04	1.87
C60	5.62	0.83	4.54	4.54	22.12	48.19	6.59	7.57
C61	3.13	0.54	15.38	15.38	8.14	15.62	9.31	32.51
C62	4.63	3.11	12.96	12.96	12.78	32.26	7.94	13.35
C63	5.43	0.85	15.18	15.18	14.81	21.17	18.73	8.66
C64	5.98	1.30	14.77	14.77	16.67	27.09	15.18	4.24
C65	88.42	0.85	1.11	1.11	1.31	0.52	6.16	0.52
C66	4.93	1.18	5.89	5.89	11.10	42.56	3.78	24.67
C67	5.57	0.87	15.60	15.60	15.21	21.75	19.24	6.17
C68	0.93	4.50	1.74	1.74	3.21	75.17	2.41	10.31
C69	0.28	11.69	1.53	1.53	3.08	76.14	4.13	1.63

C70	7.14	0.82	2.60	2.60	11.05	10.05	36.51	29.23
C71	6.77	0.71	16.03	16.03	13.86	37.08	0.50	9.03
C72	1.05	5.56	2.82	2.82	2.79	53.76	2.46	28.74
C73	0.15	7.97	0.60	0.60	0.99	86.16	1.22	2.30
C74	1.75	8.60	3.22	3.22	6.90	58.83	9.06	8.42
C75	5.34	1.82	13.93	13.93	12.50	47.47	0.06	4.95
C76	1.56	1.07	1.07	1.07	4.07	9.68	10.32	71.16
C77	2.94	3.77	3.30	3.30	7.34	72.28	5.11	1.97
C78	7.55	0.57	17.44	17.44	17.39	19.83	18.11	1.67
C79	4.67	1.05	6.30	6.30	23.67	48.72	3.92	5.37
C80	6.08	4.81	9.47	9.47	11.16	39.58	11.08	8.36
C81	7.10	0.73	15.99	15.99	15.84	17.84	16.19	10.32
C82	0.25	3.67	0.70	0.70	0.49	41.50	0.74	51.95
C83	5.31	2.44	3.85	3.85	13.17	48.57	1.37	21.43
C84	1.13	6.00	3.05	3.05	3.01	58.08	2.66	23.02
C85	3.31	0.65	12.39	12.39	13.11	34.03	21.93	2.20
C86	6.00	1.15	7.24	7.24	14.34	43.11	7.35	13.56
C87	8.57	7.61	10.82	10.82	15.27	19.28	19.96	7.68
C88	5.15	1.03	12.54	12.54	12.94	17.72	12.95	25.13
C89	1.33	3.08	3.01	3.01	3.22	27.08	2.03	57.24
C90	4.40	0.48	29.80	13.91	9.66	26.16	13.91	1.68
C91	6.31	3.32	17.69	17.69	15.91	18.50	20.41	0.17
C92	4.46	2.13	66.92	5.12	10.37	5.12	3.50	2.38
C93	2.09	8.59	5.59	5.59	6.86	58.39	9.81	3.07
C94	1.74	7.76	1.06	1.06	4.94	79.57	3.63	0.25
C95	2.98	3.76	8.78	8.78	6.33	37.31	11.71	20.36
C96	4.93	0.58	16.56	16.56	16.51	13.09	29.35	2.42
C97	4.62	0.77	4.78	4.78	10.32	31.68	16.10	26.94
C98	7.24	1.99	5.00	5.00	19.91	57.90	1.10	1.85
C99	1.65	1.06	1.88	1.88	7.01	34.43	0.86	51.23
C100	6.30	1.47	22.41	14.85	17.41	14.85	13.75	8.96
C101	0.83	8.06	1.39	1.39	3.22	60.96	2.07	22.08
C102	4.88	0.96	26.27	16.52	14.55	16.52	14.25	6.05
C103	2.41	0.18	5.88	5.88	7.12	8.08	7.23	63.21
C104	3.06	0.48	10.43	10.43	11.56	42.47	15.26	6.32
C105	1.12	0.87	42.09	44.02	2.14	2.14	4.00	3.62
C106	0.31	4.00	1.27	1.27	1.88	34.17	1.09	56.01
C107	5.74	1.03	3.80	3.80	18.14	60.99	4.46	2.02
C108	7.99	0.85	1.19	1.19	17.93	27.59	39.28	3.99
C109	1.81	1.40	4.82	4.82	16.74	60.50	4.92	4.98
C110	5.64	3.99	13.78	13.78	12.99	34.76	11.97	3.10
C111	0.45	4.75	1.94	1.94	2.56	58.84	0.97	28.56
C112	5.91	2.01	15.02	15.02	14.75	27.09	18.12	2.06
C113	6.14	1.58	14.94	14.94	14.02	20.85	16.54	10.99
C114	4.03	3.08	11.28	11.28	12.36	32.08	16.33	9.56
C115	2.56	0.42	3.59	3.59	22.80	34.66	28.94	3.44
C116	2.86	2.98	9.59	9.59	10.81	40.67	15.13	8.35
C117	4.25	0.40	15.47	15.47	17.19	19.03	16.53	11.66

C118	0.93	5.25	2.51	2.51	2.79	67.69	1.35	16.98
C119	6.02	1.11	1.62	1.62	17.52	41.33	25.31	5.47
C120	7.24	1.99	5.00	5.00	19.91	57.90	1.10	1.85
C121	1.30	8.24	3.37	3.37	2.72	68.18	3.13	9.70
C122	6.61	2.25	4.92	4.92	15.46	48.27	13.13	4.44
C123	3.52	5.01	8.92	14.71	9.95	31.56	9.93	16.41
C124	0.91	1.78	40.34	41.84	4.00	2.80	4.77	3.58
C125	5.46	1.41	12.95	12.95	14.61	21.28	21.68	9.66
C126	4.04	2.69	13.93	13.93	12.80	16.31	27.95	8.35
C127	5.14	2.66	14.50	15.86	15.52	17.14	28.93	0.25
C128	0.14	7.78	0.59	0.73	0.96	84.09	1.19	4.51

Table S3: Drug-likeness filtering of corn silk metabolites based on Lipinksi's rule of five

Compound number	Formula	Molecular weight (g/mol)	#H-bond acceptors	#H-bond donors	iLOGP (octanol/ water partition coefficient)	Lipinski #violations
C1	$C_{28}H_{38}O_{13}$	582.59	13	7	4.71	3
C2	C24H32O9	464.51	9	6	1.67	1
C3	$C_6H_8O_6$	176.12	6	4	0.39	0
C4	$C_7H_{10}O_7$	206.15	7	4	-0.94	0
C5	$C_5H_6O_4$	130.10	4	2	0.46	0
C6	$C_6H_6O_7$	190.11	7	3	-0.71	0
C7	$C_{31}H_{38}O_{17}$	682.62	17	9	2.27	3
C8	$C_6H_{12}O_4$	148.16	4	3	0.39	0
C9	$C_5H_8O_5$	148.11	5	3	0.18	0
C10	$C_6H_{10}O_5$	162.14	5	3	0.34	0
C11	$C_9H_{16}O_8$	252.22	8	5	0.37	0
C12	$C_5H_8O_4$	132.11	4	2	0.45	0
C13	$C_9H_8O_2$	148.16	2	1	1.55	0
C14	$C_{19}H_{18}O_2$	278.35	2	1	2.79	0
C15	$C_8H_8O_4$	168.15	4	2	1.40	0
C16	$C_{14}H_{18}O_9$	330.29	9	5	1.88	0
C17	$C_{25}H_{24}O_{15}$	564.45	15	7	1.77	3
C18	$C_{19}H_{26}O_{13}$	462.40	13	7	1.35	2
C19	$C_{22}H_{12}O_5$	356.33	5	1	2.52	0
C20	$C_7H_{14}O_4$	162.18	4	2	0.94	0
C21	$C_{23}H_{14}O_4$	354.35	4	1	2.41	0
C22	$C_{15}H_{18}O_9$	342.30	9	6	0.23	1
C23	$C_{10}H_{12}O_7$	244.20	7	5	0.63	0
C24	$C_{13}H_{24}O_9$	324.32	9	5	1.95	0
C25	$C_7H_{12}O_5$	176.17	5	3	0.24	0
C26	$C_{13}H_{12}O_7$	280.23	7	3	1.54	0
C27	$C_{13}H_{18}O_6$	270.28	6	4	1.60	0
C28	$C_{15}H_{20}O_9$	344.31	9	5	2.05	0
C29	$C_{21}H_{32}O_{10}$	444.47	10	6	1.89	1

C30	$C_6H_{10}O_3$	130.14	3	1	1.06	0
C31	$C_{15}H_{16}O_9$	340.28	9	5	1.04	0
C32	$C_{16}H_{18}O_9$	354.31	9	6	0.96	1
C33	$C_7H_{12}O_6$	192.17	6	5	-0.12	0
C34	$C_{23}H_{24}O_4$	364.43	4	2	3.70	0
C35	$C_7H_{12}O_4$	160.17	4	2	0.94	0
C36	$C_{17}H_{20}O_9$	368.34	9	4	2.54	0
C37	$C_{18}H_{30}O_9$	390.43	9	5	2.35	0
C38	$C_9H_8O_4$	180.16	4	3	0.97	0
C39	$C_9H_8O_6$	212.16	6	3	0.24	0
C40	$C_9H_{16}O_5$	204.22	5	2	1.55	0
C41	$C_{15}H_{14}O_7$	306.27	7	6	0.98	1
C42	$C_6H_{12}O_3$	132.16	3	2	1.17	0
C43	$C_6H_6O_6$	174.11	6	3	-0.13	0
C44	$C_{20}H_{32}O_{10}$	432.46	10	6	1.57	1
C45	$C_{16}H_{24}O_{10}$	376.36	10	6	1.26	1
C46	$C_{27}H_{30}O_{15}$	594.52	15	9	1.80	3
C47	$C_{15}H_{22}O_5$	282.33	5	0	2.75	0
C48	$C_{10}H_{16}O_8$	264.23	8	4	0.97	0
C49	$C_{10}H_{14}O_4$	198.22	4	1	2.32	0
C50	$C_{12}H_{20}O_4$	228.28	4	2	2.04	0
C51	$C_{11}H_{18}O_2$	182.26	2	0	3.05	0
C52	$C_{14}H_{26}O_5$	274.35	5	3	2.34	0
C53	$C_{15}H_{22}O_5$	282.33	5	3	2.09	0
C54	$C_{12}H_{18}O_4$	226.27	4	2	1.46	0
C55	$C_{13}H_{18}O_5$	254.28	5	0	3.07	0
C56	$C_9H_8O_3$	164.16	3	2	0.95	0
C57	$C_{13}H_{18}O_5$	254.28	5	3	1.82	0
C58	$C_9H_{10}O_3$	166.17	3	1	1.77	0
C59	$C_{26}H_{28}O_{14}$	564.49	14	8	2.11	3
C60	$C_{21}H_{20}O_{11}$	448.38	11	7	1.27	2
C61	$C_{10}H_{18}O_5$	218.25	5	3	0.96	0
C62	$C_{12}H_{18}O_5$	242.27	5	2	1.81	0
C63	$C_{21}H_{32}O_9$	428.47	9	5	1.97	0
C64	$C_{15}H_{18}O_4$	262.30	4	1	2.03	0
C65	$C_{10}H_{10}O_4$	194.18	4	2	1.62	0
C66	$C_{34}H_{26}O_9$	578.56	9	6	3.45	2
C67	$C_{14}H_{24}O_5$	272.34	5	1	2.71	0
C68	$C_{16}H_{26}O_8$	346.37	8	4	2.06	0
C69	$C_{12}H_{22}O_4$	230.30	4	2	1.83	0
C70	$C_{27}H_{30}O_{14}$	578.52	14	8	1.89	3
C71	$C_{28}H_{28}O_{18}$	652.51	18	9	0.94	3
C72	$C_{21}H_{38}O_7$	402.52	7	4	2.83	0
C73	$C_{13}H_{12}O_6$	264.23	6	3	1.70	0
C74	$C_{10}H_{18}O_5$	218.25	5	3	1.32	0
C75	$C_{29}H_{30}O_{19}$	682.54	19	9	1.95	3
C76	$C_9H_6O_4$	178.14	4	2	1.25	0
C77	$C_{26}H_{24}O_4$	400.47	4	0	4.45	1

C78	$C_9H_{14}O_2$	154.21	2	0	1.63	0
C79	$C_{27}H_{26}O_{15}$	590.49	15	5	1.94	2
C80	$C_{15}H_{22}O_4$	266.33	4	2	2.38	0
C81	$C_{15}H_{20}O_5$	280.32	5	2	1.76	0
C82	$C_{13}H_{14}O_6$	266.25	6	3	2.33	0
C83	$C_{28}H_{30}O_{17}$	638.53	17	11	1.81	3
C84	$C_{21}H_{38}O_7$	402.52	7	4	2.83	0
C85	$C_{27}H_{26}O_{16}$	606.49	16	9	2.59	3
C86	$C_{26}H_{28}O_{13}$	548.49	13	8	0.66	3
C87	$C_{12}H_{22}O_6$	262.30	6	4	1.32	0
C88	$C_{15}H_{22}O_4$	266.33	4	2	2.35	0
C89	$C_{10}H_{14}O$	150.22	1	0	2.27	0
C90	$C_{27}H_{28}O_{16}$	608.50	16	9	1.66	3
C91	$C_9H_{16}O_4$	188.22	4	2	1.44	0
C92	$C_{27}H_{28}O_{16}$	608.50	16	9	1.66	3
C93	$C_{10}H_{16}O_3$	184.23	3	1	2.03	0
C94	$C_{28}H_{32}O_{14}$	592.55	14	8	0.80	3
C95	$C_{14}H_{24}O_4$	256.34	4	1	3.26	0
C96	$C_9H_{18}O_3$	174.24	3	2	1.83	0
C97	$C_{27}H_{28}O_{14}$	576.50	14	8	1.95	3
C98	$C_{22}H_{20}O_{12}$	476.39	12	6	2.02	2
C99	$C_{23}H_{22}O_{13}$	506.41	13	7	1.61	3
C100	$C_{15}H_{22}O_4$	266.33	4	2	2.46	0
C101	$C_{16}H_{22}O_9$	358.34	9	5	1.24	0
C102	$C_{18}H_{32}O_6$	344.44	6	5	2.95	0
C103	$C_{12}H_{20}O_5$	244.28	5	2	1.91	0
C104	$C_9H_{16}O_2$	156.22	2	1	2.15	0
C105	$C_{14}H_{26}O_4$	258.35	4	2	2.49	0
C106	$C_{18}H_{24}O_4$	304.38	4	2	3.45	0
C107	$C_{21}H_{20}O_{10}$	432.38	10	6	2.11	1
C108	$C_{13}H_{12}O_7$	280.23	7	3	0.62	0
C109	$C_{28}H_{30}O_{16}$	622.53	16	8	1.81	3
C110	$C_{15}H_{16}O_4$	260.29	4	2	2.73	0
C111	$C_{20}H_{26}O_7$	378.42	7	3	1.97	0
C112	$C_{15}H_{20}O_4$	264.32	4	2	1.97	0
C113	$C_{15}H_{22}O_4$	266.33	4	3	2.59	0
C114	$C_{14}H_{22}O_4$	254.32	4	3	2.19	0
C115	$C_{23}H_{22}O_{11}$	474.41	11	5	2.31	1
C116	$C_{14}H_{24}O_4$	256.34	4	2	2.66	0
C117	$C_{11}H_{16}O_2$	180.24	2	2	2.04	0
C118	$C_{17}H_{22}O_2$	258.36	2	0	4.10	0
C119	$C_{13}H_{12}O_9$	312.23	9	5	0.55	0
C120	$C_{28}H_{30}O_{16}$	622.50	4	3	2.59	1
C121	$C_{17}H_{28}O_7$	344.40	7	2	2.59	0
C122	$C_{28}H_{30}O_{14}$	590.53	14	7	1.76	3
C123	$C_{15}H_{22}O_4$	266.33	4	2	2.19	0
C124	$C_{15}H_{24}O_4$	268.35	4	3	2.87	0
C125	$C_{14}H_{22}O_4$	254.32	4	1	2.59	0

C126	$C_{10}H_{16}O_3$	184.23	3	2	1.65	0
C127	$C_{10}H_{18}O_4$	202.25	4	2	1.77	0
C128	$C_{13}H_{12}O_6$	264.23	6	3	1.70	1

Table S4: Molecular docking analysis of corn silk metabolites against enzyme targets

Compound number	Identity	AA	AG	AR	DPP-4	PTP1B	SDH
2	Estriol-16-Glucuronide	-6.8	-6.7	-7.2	-6.2	-4.8	-7.5
3	Ascorbic acid	-6.1	-5.6	-6.8	-7.2	-4.5	-6.3
4	Methylisocitric acid	-6.9	-5.8	-7.8	-6.8	-5.2	-7.1
5	Citraconic acid	-5.7	-7.2	-5.6	-6.4	-4.9	-5.9
6	Oxalosuccinic acid	-6.2	-6.3	-7.1	-6.7	-4.7	-6.8
8	Mevalonic acid	-7.2	-5.4	-6.3	-7.4	-4.4	-7.3
9	D-2-Hydroxyglutaric acid	-5.8	-6.1	-7.5	-6.1	-4.8	-5.7
10	(2R,3S)-2,3-dimethylmalic acid	-6.5	-7.1	-6.9	-5.7	-4.5	-6.1
11	UNPD109129	-6.7	-6.9	-7.3	-6.9	-4.6	-6.9
12	Glutaric acid	-6.3	-7.7	-6	-6	-4.9	-6.5
13	Cinnamic acid	-5.3	-5.3	-5.4	-7	-4.7	-7.7
14	(6E)-1-(4-hydroxyphenyl)-7-phenylhepta-4,6-dien-3-one	-7.8	-7.0	-9.9	-5.8	-4.4	-7
15	Vanillic acid	-5.6	-6.2	-8	-6.3	-4.8	-5.4
16	1-O-vanilloyl-beta-D-glucose	-6.4	-7.5	-5.8	-5.9	-4.5	-6.2
18	Saccharumoside C	-6.0	-7	-6.5	-7.3	-4.6	-8
19	7-hydroxy-4-{3-oxo-3H-benzo[f]chromen-2-yl}-2H-chromen-2-one	-6.9	-5.9	-7.4	-6.6	-4.9	-7.8
20	Sarmentose	-7.1	-6.6	-6.2	-6.5	-4.7	-6.6
21	CNP0447999	-5.9	-6.4	-7	-5.6	-4.4	-5.2
22	1-O-Caffeoylglucose	-6.8	-5.7	-5.2	-7.5	-4.8	-6.4
23	1-O-Galloylglycerol	-6.2	-7.3	-7.9	-5.3	-4.5	-7.4
24	C00051555	-5.4	-6.8	-6.6	-7.1	-4.6	-6.7
25	3-Isopropylmalate	-6.7	-5.2	-7.7	-7.6	-4.9	-5.5
26	Diaportinic acid	-6.5	-6.7	-5.9	-6.2	-4.7	-7.2
27	Benzyl beta-D-glucopyranoside;(-)-Benzyl-O-beta-D-glucopyranoside	-5.7	-5.6	-6.1	-6.8	-4.4	-6
28	Domesticoside	-6.3	-6.1	-8.1	-6.4	-4.8	-7.9
29	Dihydrophaseic acid 4'-O-beta-D-glucopyranoside	-5.5	-7.4	-5.3	-7.4	-4.5	-6.3
30	Ketoleucine	-6.0	-6.3	-7.6	-6.7	-4.6	-5.9
31	Aesculin	-8.1	-5.4	-8.5	-5.7	-4.9	-7
32	Chlorogenic acid	-5.2	-6.9	-7.2	-7.2	-4.7	-6.8
33	Quinic acid	-6.4	-6	-5.7	-6.1	-4.4	-5.6
34	Cudraphenone A	-5.6	-5.3	-6.3	-5.9	-4.8	-8.1
35	Pimelic acid	-6.1	-6.5	-8.2	-6.9	-4.5	-6.5
36	(-)-6-((2S,3R,4R,5S,6R)-3,4-dihydroxy-6-(hydroxymethyl)-5-methoxytetrahydro-2H-pyran-2-yloxy)-8-hydroxy-3-methyl-1H-isochromen-1-one	-7.0	-5.8	-5.5	-6	-4.6	-7.3
37	(-)-11-hydroxy-9,10-dihydrojasmonic acid 11-beta-D-glucoside	-6.6	-7.4	-8.5	-8.6	-4.9	-8.4
38	Caffeic acid	-5.8	-6.2	-6.8	-5.8	-4.7	-5.8
39	5-Carboxyvanillic acid	-6.9	-5.5	-5	-6.3	-4.4	-7.6
40	Phellodendric acid A;(+)-Phellodendric acid A	-5.3	-7.1	-7	-7.3	-4.8	-6.1
41	(-)-Epigallocatechin	-6.2	-6.6	-6.6	-6.6	-4.5	-7.7
42	D-Leucic acid	-6.8	-5.7	-8.3	-6.5	-4.6	-6.4
43	cis-Aconitic acid	-5.4	-6.4	-5.2	-5.6	-4.9	-5.2

44	MINEs-320976	-6.5	-6.8	-6.9	-7.5	-4.7	-6.9
45	Loganic acid	-6.7	-5.9	-7.1	-5.3	-4.4	-6.6
47	Quing hau sau; quinghaosu; artemisinin	-5.9	-7	-5.4	-7.1	-4.8	-8.2
48	3-Hydroxy-4-butanolide	-6.3	-6.1	-6.5	-7.6	-4.5	-5.4
49	Annularin A;(+)-Annularin A	-7.2	-5.2	-7.4	-6.2	-4.6	-7.1
50	Traumatic acid	-5.7	-6.7	-6.2	-6.8	-4.9	-5.7
51	Methyl geranate	-6.4	-7.4	-7.8	-6.4	-4.7	-6.3
52	3-Hydroxytetradecanedioic acid	-5.5	-6.3	-5.6	-7.4	-4.4	-8
53	Dihydrophaseic acid	-6.0	-7.4	-7.5	-6.7	-4.8	-7.8
54	Tuberonic acid	-6.6	-5.4	-6	-5.7	-4.5	-6
55	Daldiniapyrone	-7.1	-6.5	-6.3	-7.2	-4.6	-5.6
56	4-Hydroxycinnamic acid	-5.2	-6	-8	-6.1	-4.9	-6.8
57	Monascusone A	-6.9	-5.3	-5.8	-5.9	-4.7	-7.5
58	Acetovanillone;Apocynin	-5.3	-7.3	-6.7	-6.9	-4.4	-6.2
60	Quercitrin	-6.1	-6.2	-7.2	-6	-4.8	-7.4
61	2-Hydroxydecanedioic acid	-6.8	-5.5	-5.9	-7	-5.4	-5.5
62	UNPD221406	-5.4	-6.9	-7.9	-5.8	-4.6	-7.2
63	Cichorioside M;(+)-Cichorioside M	-6.2	-6.4	-6.4	-6.3	-4.9	-6.7
64	Austricin;8-Deacetylmatricarin;Desacetylmatricarin	-7.7	-7.8	-8.5	-7.3	-4.7	-5.9
65	trans-Ferulic acid	-6.7	-7.2	-5.3	-6.6	-4.4	-6.4
66	UNPD19396	-6.5	-6.8	-8.1	-6.5	-4.8	-8.1
67	UNPD77208	-5.7	-5.2	-6.1	-5.6	-4.5	-6.6
68	Nepetaside	-6.3	-6.7	-7.6	-7.5	-4.6	-5.2
69	Dodecanedioic acid	-7.0	-5.6	-5.5	-5.3	-5.2	-7.9
72	Erythronolide B	-5.9	-6.1	-6.2	-7.1	-4.7	-9.2
73	UNPD230015	-6.0	-7.4	-8.2	-7.6	-4.4	-7
74	3-Hydroxysebacic acid	-6.4	-6.3	-5.7	-6.2	-4.8	-5.8
76	Esculetin	-7.2	-5.4	-7.3	-6.8	-4.5	-7.3
77	ethyl 5-[(2,5-dimethylphenyl)methoxy]-2-phenyl-1-benzofuran-3-carboxylate	-6.6	-6.9	-6.8	-6.4	-4.6	-6.1
78	xi-2,2,6-Trimethyl-1,4-cyclohexanedione	-5.5	-6	-5	-7.4	-4.9	-7.7
79	Quercetin 3-(2",3",4"-triacetylgalactoside)	-6.8	-5.3	-7	-6.7	-4.7	-6.5
80	[4]-Gingerol	-5.8	-6.5	-6.6	-5.7	-4.4	-5.4
81	Phaseic acid	-6.1	-5.8	-8.3	-7.8	-6	-6.2
82	Diaportinol	-7.1	-7.1	-5.2	-6.1	-4.5	-8.2
84	12-deoxyerythronolide A	-5.3	-6.2	-6.9	-5.9	-4.6	-7.1
87	Phaseolic acid	-6.9	-5.5	-7.1	-6.9	-4.9	-5.7
88	Curvularol	-7.9	-7	-5.4	-6	-4.7	-6.9
89	(+)-(S)-Carvone	-5.4	-6.6	-6.5	-7	-4.4	-6
91	Azelaic acid	-6.7	-5.7	-7.4	-5.8	-4.8	-7.8
93	Stagonolide F;(-)-Stagonolide F	-6.5	-6.4	-6.2	-6.3	-4.5	-6.4
95	UNPD223815	-5.7	-6.8	-7.8	-7.3	-4.6	-5.6
96	9-hydroxynonanoic acid	-6.3	-5.9	-5.6	-6.6	-4.9	-7.5
98	5,7,4'-Trihydroxy-3'-methoxyflavone	-6.0	-7.2	-7.5	-6.5	-4.7	-6.2
100	Blennin D	-7.3	-6.1	-6	-5.6	-4.4	-8.5
101	10-Deoxygeniposidic acid	-5.6	-5.2	-6.3	-7.5	-4.8	-5.5
102	Gallicynoic acid F;(-)-Gallicynoic acid F	-6.4	-6.7	-8	-5.3	-4.5	-7.2
103	Pandangolide 1a;(-)-Pandangolide 1a	-6.6	-5.6	-5.8	-7.1	-4.6	-6.7
104	4-Hydroxynonenal	-5.9	-6.3	-6.7	-7.6	-4.9	-5.9
105	Tetradecanedioic acid	-6.8	-7.4	-7.2	-6.2	-5.8	-6.3
106	(R)-7-butyl-6,8-dihydroxy-3-[(3E)-pent-3-en-1-yl]-3,4-dihydroisochromen-1-one	-8.0	-5.4	-8.6	-7.8	-4.4	-8.3
107	Genistin	-5.5	-6.5	-7.9	-6.4	-4.8	-7.6
108	p-Coumaroyl malic acid	-6.2	-6	-6.4	-7.7	-4.5	-6.1
110	Cyperine	-5.8	-5.3	-7.7	-6.7	-4.6	-7.9
111	(+)-Cnicin; Cnicin	-6.1	-7.3	-5.3	-5.7	-4.9	-8.7
112	(S)-Abscisic acid	-6.9	-6.2	-8.1	-7.2	-4.7	-5.2

113	Sydnic acid; Sydonic acid	-5.3	-5.5	-6.1	-6.1	-4.4	-7.3
114	Gallicynoic acid A;(+)-Gallicynoic acid A	-6.7	-6.9	-7.6	-5.9	-4.8	-6.8
115	Apigenin 7-O-(6"-O-acetylglucoside)	-6.5	-6.4	-5.5	-6.9	-4.5	-5.4
116	UNPD127537	-5.7	-5.7	-6.2	-6	-4.6	-6.5
117	Olivetol	-6.3	-7.2	-8.2	-7	-4.9	-7
118	Ginsenoyne E	-6.0	-6.8	-5.7	-5.8	-4.7	-5.8
119	Caffeoyl tartaric acid	-7.2	-5.2	-7.3	-8	-4.4	-7.1
120	Luteolin 3'-methyl ether 7-glucuronide	-5.6	-6.7	-6.8	-7.3	-4.8	-6.2
121	UNPD205010	-6.4	-5.6	-5	-6.6	-4.5	-8.1
123	Artemin	-6.8	-6.1	-7	-6.5	-4.6	-6.4
124	Gallicynoic acid B	-5.9	-7.4	-6.6	-5.6	-4.9	-5.6
125	Aspergillide A	-6.6	-6.3	-8.3	-7.5	-4.7	-7.7
126	(S)-Oleuropeic acid	-7.1	-5.4	-5.2	-5.3	-4.4	-6.3
127	Sebacic acid	-5.2	-6.9	-6.9	-7.1	-4.8	-5.9
128	7-Acetoxy-5,6-dimethoxycoumarin	-6.1	-6	-7.1	-7.6	-4.5	-6

Table S5: Frontier molecular orbitals of the top-ranked compounds against enzymes implicated in T2DM

Compound	**LUMO**	**HOMO**	**Energy gap (eV)**
AA			
Aesculin	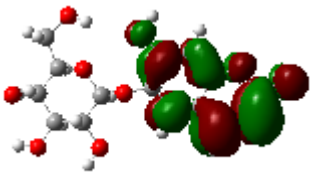	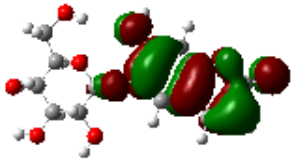	4.35
(R)-7-butyl-6,8-dihydroxy-3-[(3e)-pent-3-en-1-yl]-3,4-dihydroisochromen-1-one	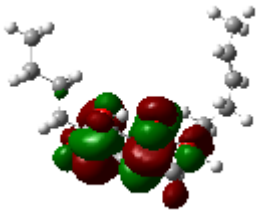	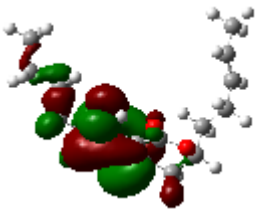	4.86
Curvularol	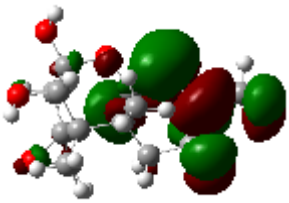	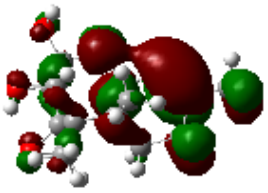	6.01
(4E,6E)-1-(4-hydroxyphenyl)-7-phenylhepta-4,6-dien-3-one	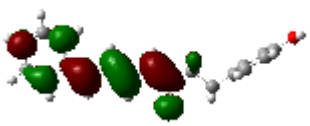	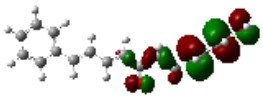	3.61

Austricin	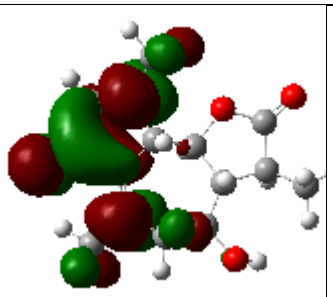	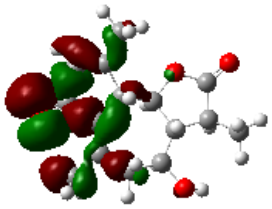	4.70
Acarbose		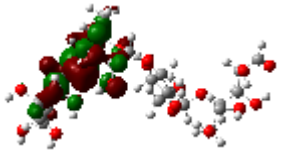	5.22
AG			
Austricin	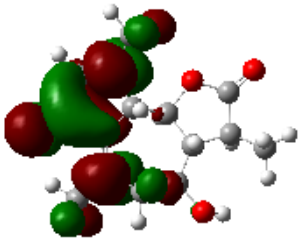	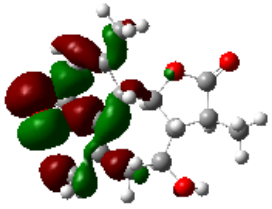	4.70
Glutaric acid	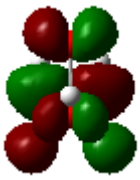	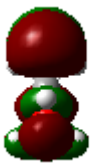	7.29
1-O-vanilloyl-beta-D-glucose	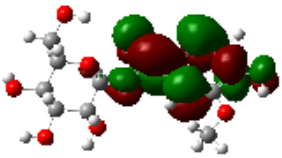	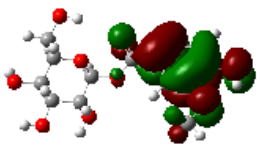	4.71
Methyl geranate	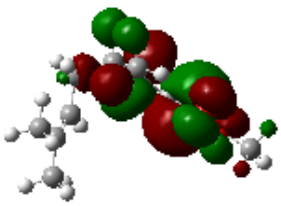	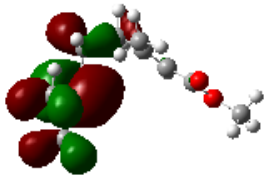	5.24
(-)-11-hydroxy-9,10-dihydrojasmonic acid 11-beta-D-glucoside	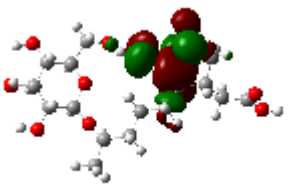	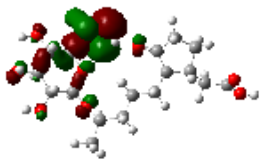	5.29
Acarbose		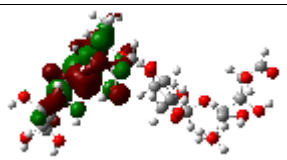	5.22

AR			
(4E,6E)-1-(4-hydroxyphenyl)-7-phenylhepta-4,6-dien-3-one	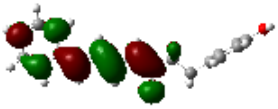	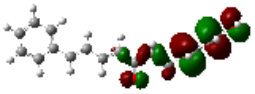	3.61
(R)-7-butyl-6,8-dihydroxy-3-[(3E)-pent-3-en-1-yl]-3,4-dihydroisochromen-1-one	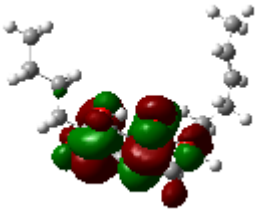	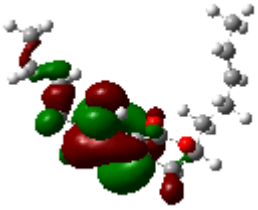	4.86
Aesculin	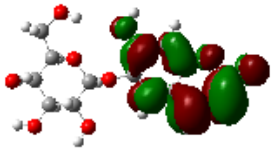	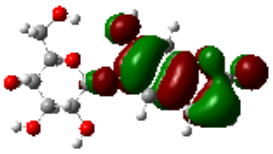	4.35
Austricin	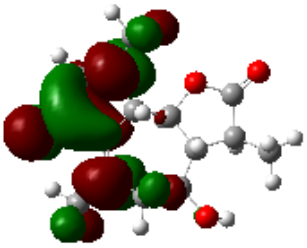	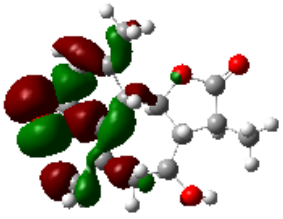	4.70
-(-)-11-hydroxy-9,10-dihydrojasmonic acid 11-beta-D-glucoside	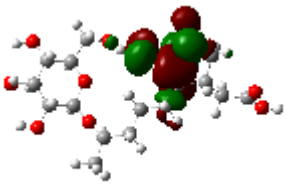	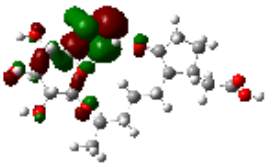	5.29
Epalrestat	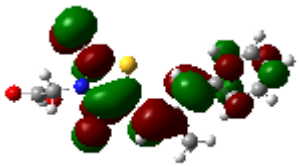	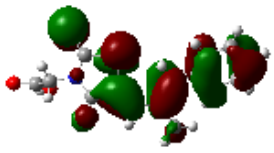	3.21
DPP-4			
(-)-11-hydroxy-9,10-dihydrojasmonic acid 11-beta-D-glucoside	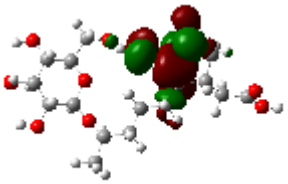	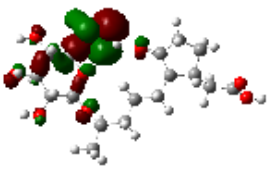	5.29
caffeoyl tartaric acid	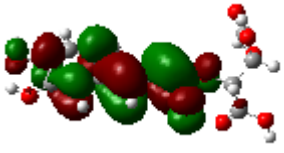	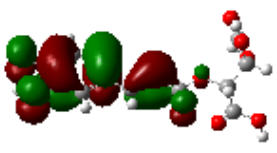	4.06

(R)-7-butyl-6,8-dihydroxy-3-[(3E)-pent-3-en-1-yl]-3,4-dihydroisochromen-1-one	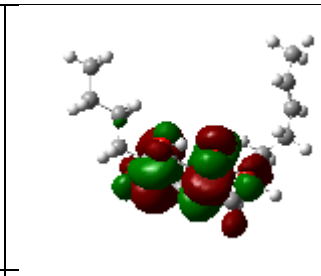	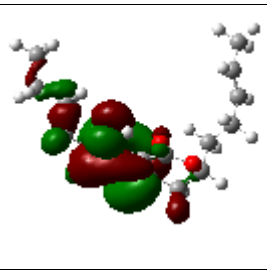	4.86
p-coumaroyl malic acid		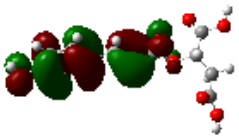	4.26
sitagliptin	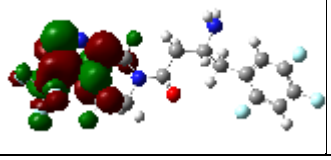	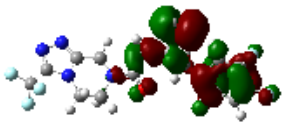	5.30
PTP1B			
2-hydroxydecanedioic acid	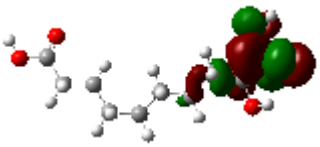	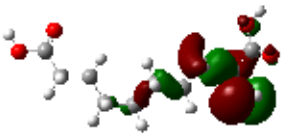	6.66
Ursolic acid	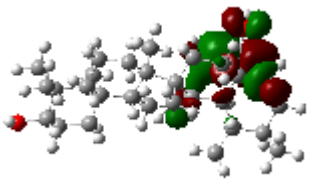	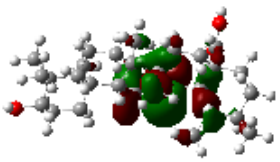	5.85
SDH			
Erythronolide B	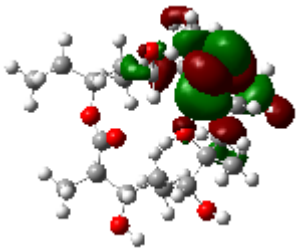	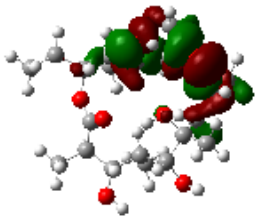	5.85
Cnicin	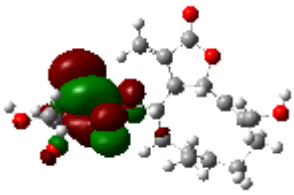	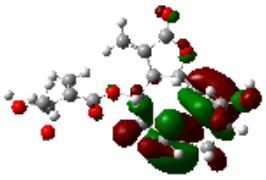	4.46
(+)-blennin D	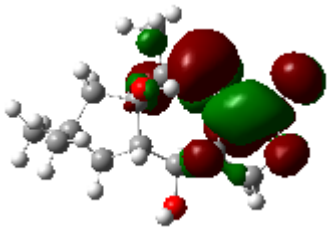	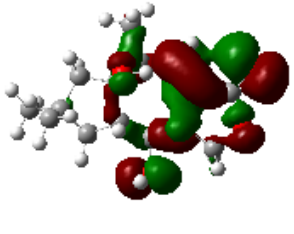	5.72

(-)-11-hydroxy-9,10-dihydrojasmonic acid 11-beta-D-glucoside	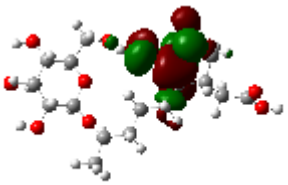	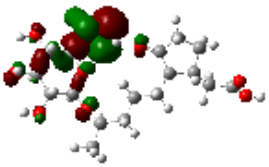	5.29
(R)-7-butyl-6.8-dihydroxy-3-[(3E)-pent-3-en-1-yl]-3.4-dihydroisochromen-1-one	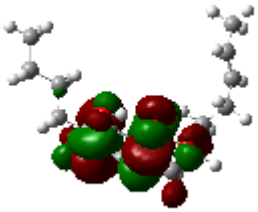	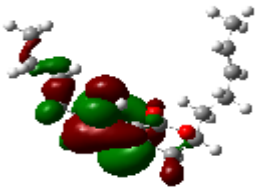	4.86
4-[2-1R-hydroxy-ethyl)-pyrimidin-4-yl] piperazine-1-sulfonic acid dimethylamide	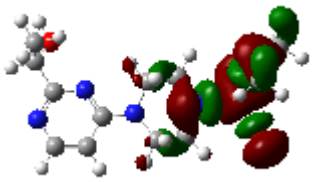	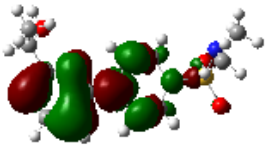	4.39

Chapter four

Waste to medicine: Evidence from computational studies on the modulatory role of corn silk on the therapeutic targets implicated in type 2 diabetes mellitus

This chapter was published in *Biology* (Impact Factor: 3.6)

biology

MDPI

Article

Waste to Medicine: Evidence from Computational Studies on the Modulatory Role of Corn Silk on the Therapeutic Targets Implicated in Type 2 Diabetes Mellitus

Ayesha Akoonjee [1], Adedayo Ayodeji Lanrewaju [1], Fatai Oladunni Balogun [1], Nokwanda Pearl Makunga [2] and Saheed Sabiu [1,*]

[1] Department of Biotechnology and Food Science, Faculty of Applied Sciences, Durban University of Technology, Durban 4000, South Africa; 22290008@dut4life.ac.za (A.A.); 22172511@dut4life.ac.za (A.A.L.); fataib@dut.ac.za (F.O.B.)
[2] Department of Botany and Zoology, Stellenbosch University, Private Bag X1, Matieland, Stellenbosch 7602, South Africa; makunga@sun.ac.za
* Correspondence: sabius@dut.ac.za; Tel.: +27-313735330

Simple Summary: Type 2 diabetes mellitus (T2DM) is characterized by insulin resistance and/or defective insulin production in the human body. Corn silk (CS), an abundant, readily available and affordable waste product of corn cultivation, has extensive therapeutic applications against various diseases including T2DM. Although the antidiabetic potential of CS is well-established, the understanding of the mechanism of action (MoA) behind its reported antidiabetic potentials is lacking. Hence, determining its MoA may provide laudable insight contributing towards developing an effective drug candidate for combating the ill effects of T2DM.

Abstract: Type 2 diabetes mellitus (T2DM) is characterized by insulin resistance and/or defective insulin production in the human body. Although the antidiabetic action of corn silk (CS) is well-established, the understanding of the mechanism of action (MoA) behind this potential is lacking. Hence, this study aimed to elucidate the MoA in different samples (raw and three extracts: aqueous, hydro-ethanolic, and ethanolic) as a therapeutic agent for the management of T2DM using metabolomic profiling and computational techniques. Ultra-performance liquid chromatography-mass spectrometry (UP-LCMS), in silico techniques, and density functional theory were used for compound identification and to predict the MoA. A total of 110 out of the 128 identified secondary metabolites passed the Lipinski's rule of five. The Kyoto Encyclopaedia of Genes and Genomes pathway enrichment analysis revealed the cAMP pathway as the hub signaling pathway, in which *ADORA1*, *HCAR2*, and *GABBR1* were identified as the key target genes implicated in the pathway. Since gallicynoic acid (−48.74 kcal/mol), dodecanedioc acid (−34.53 kcal/mol), and tetradecanedioc acid (−36.80 kcal/mol) interacted well with *ADORA1*, *HCAR2*, and *GABBR1*, respectively, and are thermodynamically stable in their formed compatible complexes, according to the post-molecular dynamics simulation results, they are suggested as potential drug candidates for T2DM therapy via the maintenance of normal glucose homeostasis and pancreatic β-cell function.

Keywords: *ADORA1*; cAMP signaling pathway; chromatography; corn silk; *GABBR1*; *HCAR2*; in silico techniques; systems biology; African traditional medicine; type 2 diabetes mellitus

Citation: Akoonjee, A.; Lanrewaju, A.A.; Balogun, F.O.; Makunga, N.P.; Sabiu, S. Waste to Medicine: Evidence from Computational Studies on the Modulatory Role of Corn Silk on the Therapeutic Targets Implicated in Type 2 Diabetes Mellitus. *Biology* **2023**, *12*, 1509. https://doi.org/10.3390/biology12121509

Academic Editor: Daniel G. Peterson

Received: 5 November 2023
Revised: 2 December 2023
Accepted: 5 December 2023
Published: 11 December 2023

1. Introduction

Diabetes mellitus (DM), a chronic, uncurable metabolic disease characterized by elevated blood glucose levels, is a significant contributor to morbidity, mortality, and health costs worldwide [1]. In 2021, an estimated 24 million adults (20–79 years old) in Africa were living with DM and approximately 13 million of these adults remain undiagnosed [2]. The International Diabetes Federation (IDF) stipulated that, in 2021, around

4,234,000 South African adults had DM out of a total adult population of 37,416,800, indicating a prevalence of 1 in 11 adults [3]. Type 2 diabetes mellitus (T2DM) is the most prevalent type of diabetes, constituting roughly 90% of all DM cases [4], and, if left untreated, can result in severe complications, including kidney disease, ocular damage, cardiovascular diseases (e.g., stroke and heart attack), increased risk of bone fracture, nerve damage, skin conditions, and hearing impairment [5]. The pathogenesis of T2DM lies in defective insulin production by β-cells and/or insulin resistance in insulin-sensitive cells [5]. Although the efficacy of many synthetic hypoglycaemic drugs such as sulfonyl ureas, biguanides, alpha-glucosidase inhibitors, thiazolidinediones, and non-sulfonyl urea secretagogues are undoubtedly potent in the management of T2DM [6], their limitations, including long-term regimens, high cost, efficacy and individual variability as well as the elicitation of considerable side effects (nausea, weight gain or loss, cardiovascular complications, and gastrointestinal discomforts) have undermined their application in clinical practice [7]. Consequently, cost-effective therapeutic agents with significant antidiabetic activity and little or no toxic effects are highly sought out as alternative T2DM therapeutics [8].

Medicinal plants (MPs) have been utilized in traditional medicine systems for centuries, offering a wealth of knowledge and therapeutic possibilities for the treatment of various ailments, including T2DM [7]. Currently, over 1200 species of plants have been traditionally used as natural antidiabetics globally, many of which are being explored for their potential hypoglycaemic properties [8]. For example, corn silk (CS) is an abundant waste plant material of corn, *Zea mays* (L.) which has been used in traditional medicine for several applications, including as a potential remedy for T2DM [9,10]. Corn silk is described as pale green, yellow, or light brown thread-like strands, crucial for the successful pollination of corn kernels [11]. A considerable number of phytochemicals have been identified in CS, including phenolic acids, flavonoids, carotenoids, tannins, sterols, volatile compounds, sugars, vitamins, minerals, polysaccharides, proteins, and peptides responsible for a diverse range of promising pharmacological properties not limited to antioxidant, anti-hyperlipidemic, antibacterial, anti-cancer, antihypertensive, antidiabetic, diuretic, and kaliuretic [7,8,12], making CS a valuable natural resource for healthcare applications [12,13]. Although numerous studies have reported the promising antidiabetic action of CS [11,14–19], additional research is needed to establish the mechanism of antidiabetic action for it to be considered as a possible therapeutic agent in the management of T2DM [20].

With the rapid development in technology, the field of drug discovery has been revolutionized, accelerating the discovery and development of therapeutic drugs [21]. This expands the possibilities of quickly identifying, designing, optimizing, and developing new therapeutic agents [22]. The use of computational techniques such as network pharmacology (NP), molecular docking, and molecular dynamics (MD) simulation is essential in drug discovery, allowing for the understanding of interactions between drugs and their target proteins at different biological levels [23]. Network pharmacology (NP) integrates systems biology, network science, and pharmacology to provide a comprehensive understanding of the mechanisms of drug action, the prediction of drug targets, the pathogenesis of diseases, and the optimization of therapeutic outcomes [24]. The interaction between drug targets and multiple components such as proteins, genes, and signaling pathways in a biological system are better explored using NP analysis [25], providing a unique perspective on drug action and disease mechanisms by considering the complexity of biological systems in order to provide insights into drug development and optimization [26]. Interestingly, there have been numerous studies that have investigated the antidiabetic mechanism of action (MoA) of natural products, plants, or plant fractions using NP [19,27–30]. Molecular docking is a cost-effective, fast, and reliable computational method, employed in drug discovery, medicinal chemistry, and structural biology, to examine the interactions between a small molecule (ligand) and a target biomolecule, typically a protein [31]. Natural products, plants, and plant fractions may be assessed against different targets implicated in disease emergence (and in this case, T2DM), such as key enzymes and genes, thus allowing

for a comprehensive understanding of the antidiabetic potentials of CS typically against these targets through this approach [23,29]. Molecular dynamics (MD) simulation on the other hand, being a powerful computational technique, is used to the study the behaviour and interactions of atoms and molecules over time [32,33]. The approach similarly provides insight into protein–ligand interactions and the MoA of therapeutic agents, which can prove useful in the discovery and development of therapeutic agents, particularly T2DM [33–36]. The integration of various technologies, particularly NP, molecular docking, and MD simulation, as adopted in this study, should provide information towards identifying novel therapeutic agents from CS, which can be discovered and/or developed as alternative agents for the management of T2DM [37]. The present study is thus aimed at studying the antidiabetic MoA of secondary metabolites in various extracts of CS, with key targets implicated in T2DM through metabolomic profiling, NP, molecular docking, and MD simulation for the discovery and development of novel therapeutic agents for the management of T2DM.

2. Materials and Methods

2.1. Silk Collection, Processing and Extract Preparation

Fresh CS of the commercial hybrid ILHYB22, a commonly consumed cultivar in South Africa, was harvested at the Cedara College of Agriculture in KwaZulu Natal, South Africa. The CS was washed with water to remove dirt and other contaminants before being air-dried for three days [38]. The dried CS was then powdered to a constant weight using an electric grinder (SM-450, Mills, MRC Laboratory Instruments, Twickenham, UK) [39]. The powdered materials were used for the preparation of extracts (aqueous, hydro-ethanol, and ethanol). Briefly, for the preparation of the aqueous extract, 150 g of CS powder was boiled at 100 °C in 1.5 L distilled water for 30 min [39,40], followed by filtration (Whatman No.1 filter paper) and lyophilization (Telstar Lyoquest Arctic, Tokyo, Japan) [10]. The hydro-ethanol and ethanol extracts were prepared by macerating approximately 100 g each of CS powder in 1 L of 50% ethanol and absolute ethanol, respectively, at 150 rpm, using an orbital shaker (Labnet Orbit LS, Edison, NJ, USA) for three days, followed by filtration (Whatman No.1 filter paper) [39]. The filtrates were concentrated using a rotary evaporator (HEI-VAP Core, 571-01310-00, Heidolph, Schwabach, Germany) and the leftover water from the hydro-ethanol filtrate was subsequently lyophilized to complete the extract preparation [39]. All the extracts were refrigerated at 4 °C until needed [10].

2.2. Ultra-Performance Liquid Chromatography-Mass Spectrometry Analysis

Four samples of CS [raw and three extracts (aqueous, hydro-ethanolic, and ethanolic)] were used for identification of the phytoconstituents present in CS through ultra-performance liquid chromatography-mass spectrometry (UPLC-MS) analysis according to the methods of Mangana et al. [41] and Mangana et al. [42]. Analysis of the CS samples was performed by utilizing a Water Synapt G2 quadruple time-of-flight mass spectrometer which was connected to a Waters Acquity UPLC-combined photo diode array detector (Milford, Massachusetts, United States of America). Extraction of the sample was performed with 2 g of each sample by employing a solvent system containing 50% methanol and 0.1% formic acid for 24 h at room temperature. The samples were then vortexed (model VX-200 S0200, Labnet, Edison, NJ, USA) for 1 min and extraction was performed using an ultrasonic bath (SS-6508T, Sunshine Scientific Equipment, Delhi, India) for 1 h. A volume of 1 mL of the residue was then withdrawn and centrifuged (mySPIN 12, Thermo Scientific, Waltham, MA, USA) at 14,000× *g* rpm 5 min. Ionization was accomplished using an electrospray source using a cone voltage of 15 V and capillary voltage of 2.5 kV, wherein only the negative mode was employed. Nitrogen was employed as the desolvation gas at 650 L h^{-1} and the desolvation temperature was set to 275 °C. A Waters UPLC BEH C18 column (2.1 × 100 mm^2, 1.7 µm particle size) was utilized and 2 µL was injected for analysis. The gradient commenced at 95%, consisting of 0.1% (*v*/*v*) formic acid (solvent A) and 5% acetonitrile (solvent B). This was followed by a gradient of 60%, consisting

of 0.1% solvent A and 40% solvent B at 9 min; 30% solvent A and 70% solvent B over 9.1 min; 100% solvent B at 14 min; and 95% solvent A and 5% solvent B at 14.01 min. The conditions thereafter remained constant to a total run time of 15 min, with solvent A at 95% and solvent B at 5%. Acquisition of data was performed through employment of MassLynx4.1 software. The detection and confirmation of compounds were processed using the MS-DIAL and MS-FINDER software 2.0 (RIKEN Center for Sustainable Resource Science: Metabolome Informatics Research Team, Kanagawa, Japan). Principal component analysis (PCA) scores plot was applied as previously discussed by [42] using the database Metaboanalyst (https://www.metaboanalyst.ca/MetaboAnalyst/) (accessed on 1 July 2022).

2.3. Network Pharmacology

2.3.1. Pharmacokinetic Properties of Corn Silk Phytoconstituents

The pharmacokinetic properties of the UPLC-MS identified secondary metabolites of CS were evaluated using Lipinski's rule of five (Ro5) on the SwissADME server (http://www.swissadme.ch/; accessed on 30 July 2022) to predict their drug-likeness property [25]. The Simplified Molecular Input Line Entry System (SMILES) of the CS secondary metabolites were obtained from PubChem website (https://pubchem.ncbi.nlm.nih.gov/; accessed on 30 July 2022) to identify orally bioavailable compounds [25]. Compounds with 2 or less violations (<5 hydrogen bond donors; ≤10 hydrogen bond acceptors; molecular weight ≤ 500 g/mol and partition co-efficient < 5) were considered to pass the pharmacokinetics analysis [43].

2.3.2. Acquisition of CS Phytoconstituents and T2DM-Associated Targets

The acquisition of therapeutic targets related to phytoconstituents of CS and T2DM was achieved as previously reported by Akoonjee et al. [29]. Identification of target genes related to CS secondary metabolites was performed through employing both Swiss Target Prediction (STP) (http://www.swisstargetprediction.ch/; accessed on 1 August 2022) and Similarity Ensemble Approach (SEA) (https://sea.bkslab.org/; accessed on 1 August 2022) databases to avoid biases, while the T2DM-related target genes were identified from GeneCards database (https://www.genecards.org/; accessed on 1 August 2022). Subsequently, Venny 2.1 (https://bioinfogp.cnb.csic.es/tools/venny/; accessed on 10 August 2022) was employed to identify and characterize the overlapping targets between CS secondary metabolites and T2DM target genes [30].

2.3.3. Protein–Protein Interaction Network Construction and Analyses of KEGG Enrichment Pathway, Gene Ontology, and Compound–Target Pathway of Overlapping Target Genes

The Search Tool for the Retrieval of Interacting Genes/Proteins (STRING) database (https://string-db.org/; accessed on 1 September 2022) was utilized to correlate the network analysis of the overlapping T2DM target genes related to CS secondary metabolites and Kyoto Encyclopaedia of Genes and Genomes (KEGG) pathway enrichment analysis to identify key T2DM-related signaling pathways associated with the overlapping genes [28]. The Database for Annotation, Visualization and Integrated Discovery (DAVID) (https://david.ncifcrf.gov/tools.jsp; accessed on 11 November 2022) was adopted to execute gene ontology analysis related to this study, while the software Cytoscape 3.6.0 with the built-in merger algorithm was employed to correlate and visualize compound–target network pathways and gene–compound interaction networks [29].

2.4. Molecular Docking and MD Simulation of T2DM-Related Target Genes with CS Secondary Metabolites

Following NP analysis, the key CS secondary metabolites and targets identified were subjected to molecular docking, as previously reported [44,45]. Briefly, the X-ray crystal structures of the identified key T2DM-related target genes such as adenosine receptor A1 (*ADORA1*) (PDB ID: 5UEN) and gamma-aminobutyric acid type B recep-

tor subunit (*GABBR1*) (PDB ID: 4MQF) were obtained from RSCB Protein Data Bank (https://www.rcsb.org/; accessed on 1 September 2022), while the X-ray crystal structure of the target gene hydroxycarboxylic acid receptor 2 (*HCAR2*) (AlphaFold ID: Q8TDS4) was obtained from AlphaFold protein structural database (https://alphafold.ebi.ac.uk/; accessed on 1 September 2022). Preparation of the T2DM-related target genes was performed using USCF Chimera v 1.16 through the removal of water molecules and protein residue connectivity [44]. Three-dimensional (3D) conformers of the CS secondary metabolites as well as the reference standards metformin and resveratrol were obtained from PubChem (https://pubchem.ncbi.nlm.nih.gov/; accessed on 1 September 2022) as previously reported [30]. The addition of Gasteiger charges and non-polar hydrogen atoms was performed on USCF Chimera v 1.16 for optimization of the 3D conformers [45]. Thereafter, the optimized secondary metabolites were individually docked at the active site of their respective T2DM-related target genes (*ADORA1*, *HCAR2*, and *GABBR1*) using Autodock Vina Plugin on Chimera v 1.16 [44]. The docking of the CS phytoconstituents at the active sites of the therapeutic targets was performed through the adjustment of the grid box coordinates to match the established x, y, and z coordinates of the native ligand obtained with Discovery Studio version 21.1.0. Docking protocol validation was carried out to prevent pseudo-positive binding conformations [45] by measuring root mean square deviation (RMSD) of docked ligands from the reference pocket bearing the native ligands in the experimental co-crystal structures of *ADORA1* (Figure 1a), *HCAR2* (Figure 1b), and *GABBR1* (Figure 1c), following optimal superimposition [45]. The RMSD values (0.5 Å) obtained between the docked ligands from the native inhibitor in the 3D structures of *ADORA1*, *HCAR2*, and *GABBR1* indicated the same binding orientation, ultimately validating the protocol adopted [45]. Based on the docking scores, the five complexes with the best pose (most negative docking score) against each target was selected for further analysis through a 120 ns MD simulation, as detailed by Sabiu et al. [46].

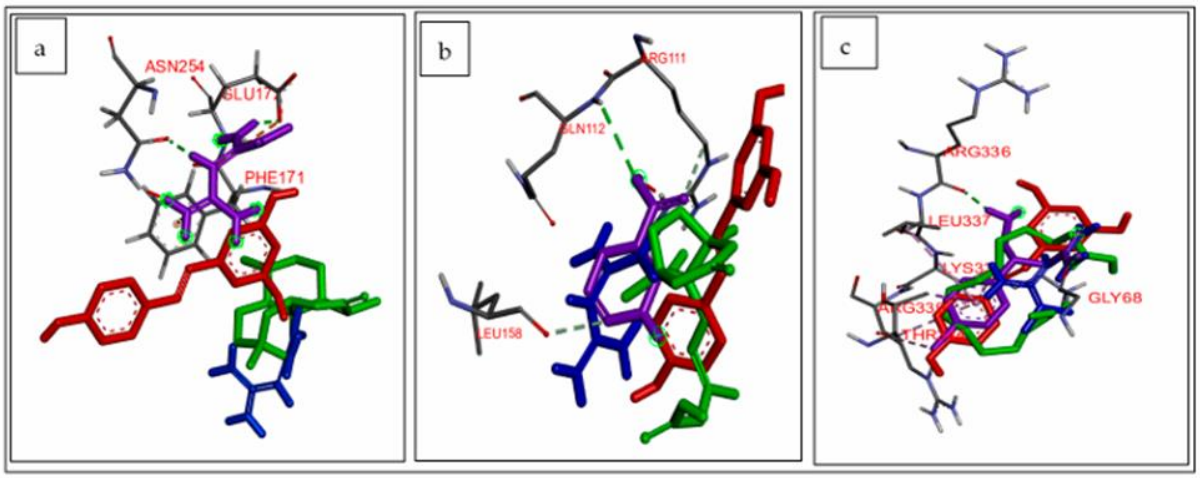

Figure 1. Superimposed structure of (**a**) *ADORA1* (grey) with native inhibitor (purple), metformin (blue), resveratrol (red), and ligand with highest docking score (green); (**b**) *HCAR2* (grey) with native inhibitor (purple), metformin (blue), resveratrol (red), and ligand with highest docking score (green); (**c**) *GABBR1* (grey) with native inhibitor (purple), metformin (blue), resveratrol (red), and ligand with highest docking score (green).

The GPU version with the AMBER 18 package (Centre for High Performance and Computing) system with the FF18SB variant of the AMBER force field was used for the MD simulation analysis. To generate atomic partial charges for the CS compounds, ANTECHAMBER was utilized, employing the restrained electrostatic potential (RESP) and the general amber force field (GAFF) procedures. The Leap module of AMBER 18 was used to

add hydrogen atoms and Na+ and Cl- counterions to neutralize all systems. These systems were then placed in orthorhombic boxes filled with TIP3P water molecules, ensuring that all atoms were within 8 Å of any box edge. An initial minimization of 2000 steps was conducted, applying a restraint potential of 500 kcal/mol to both solutes. This minimization included 1000 steps using the steepest descent method, followed by 1000 steps using the conjugate gradients method. Subsequently, a full minimization of 1000 steps was performed using the conjugate gradient algorithm without any restraint. Gradual heating from 0 K to 300 K was carried out for 50 ps, ensuring all systems maintained a consistent number of atoms and volume. During this process, a potential harmonic restraint of 10 kcal/mol and a collision frequency of 1.0 ps were applied to the solutes within the systems. Following heating, an equilibration estimating 500 ps of each system was carried out wherein the operating temperature and pressure were kept consistent at 300 K and 1 bar, respectively, for simulation of an isobaric–isothermal ensemble [46]. Furthermore, additional features, such as several atoms and the pressure were kept constant, mimicking an isobaric–isothermal ensemble. The system's pressure was maintained at 1 bar, employing the Berendsen's barostat, while the MD simulation lasted for 120 ns. In each simulation, the SHAKE algorithm was employed to constrict the bonds of the hydrogen atoms. The step size of each simulation was 2 fs and an SPFP precision model was used. The simulations coincided with the isobaric–isothermal ensemble (NPT), with randomized seeding, the constant pressure of 1 bar maintained by a pressure-coupling constant of 2 ps, a temperature of 300 K, and Langevin thermostat with a collision frequency of 1.0 ps [46]. The post-dynamics data were examined as previously described by Aribisala et al. [44]. Post-MDS parameters such as root mean square deviation (RMSD), root mean square fluctuation (RMSF), radius of gyration (RoG), solvent accessible surface (SASA), and number of hydrogen bonds were investigated using the CPPTRAJ module incorporated in the AMBER 18 suite. The free binding energy of the formed complexes were calculated using the Molecular Mechanics/GB Surface Area (MM/GBSA) method, as detailed by Sabiu et al. [46]. The average binding free energy was calculated over 100,000 snapshots obtained from the 120 ns trajectory. The free binding energy (ΔG) for each molecular species (complex, ligand, and protein) was calculated using the expressions [(1)–(5)] below:

$$\Delta G_{bind} = E_{gas} + G_{sol} - TS \quad (1)$$

$$\Delta G_{bind} = G_{complex} - G_{receptor} - G_{ligand} \quad (2)$$

$$E_{gas} = E_{int} + E_{vdw} + E_{ele} \quad (3)$$

$$G_{sol} = G_{GB} + G_{SA} \quad (4)$$

$$G_{SA} = \gamma SASA \quad (5)$$

The ligand–receptor complexes' interaction at the active sites in each treatment case was identified with post-MDS and visualized using Discovery Studio version 21.1.0 [44].

2.5. Quantum Chemical Calculations

The electronic properties of the compounds were investigated using the density functional theory (DFT) method available in the Gaussian 16 suite while Gauss View v 6.0 to view the output files [47]. The functional Becke3-Lee–Yang–Parr (B3LYP) method combined with the 6–31 + G(d,p) basis set was employed for the geometry optimization of the compounds [47]. The study assessed the conceptual DFT (cDFT); namely, the energies of the lowest unoccupied molecular orbital (E_{LUMO}) and the highest occupied molecular orbital (E_{HOMO}). Thereafter, other chemical descriptors such as energy gap (ΔE), ionization energy (I), electron affinity (A), chemical hardness (η), softness (δ), electronegativity (χ), chemical

potential (Cp), global electrophilicity (ω) were calculated using the equations below, as described previously [47].

$$\Delta E = E_{LUMO} - E_{HOMO} \quad (6)$$

$$I = -E_{LUMO} \quad (7)$$

$$A = -E_{HOMO} \quad (8)$$

$$\eta = (\Delta E)/2 \quad (9)$$

$$\delta = 1/(\eta) \quad (10)$$

$$\chi = (I + A)/2 \quad (11)$$

$$Cp = -\chi \quad (12)$$

$$\omega = \chi^2/(\Delta E) \quad (13)$$

3. Results

3.1. Metabolomic Profiling

3.1.1. Ultra-Performance Liquid Chromatography-Mass Spectrometry

The data obtained with respect to the 128 identified phytoconstituents from the metabolites of the investigated CS extracts by UPLC-MS analysis is presented in Supplementary Table S1 and was confirmed on the chromatograms produced from MassLynx (Supplementary Figure S1).

3.1.2. Principal Component Analysis

The principal component analysis results, which indicated the presence of differences (qualitative and quantitative) between the various samples of the CS, are presented in Supplementary Figure S2a. The highest amount of variance between the raw CS and various extracts (aqueous, hydro-ethanolic, and ethanolic) was 67% (46.8% observed in principal component 1 and 20.2% between the samples in principal component 2). Among the samples investigated, the aqueous, hydro-ethanol, and raw CS samples showed more similarity in the chemical diversity of the phytoconstituents in comparison to the ethanolic CS. There were variations in the amount of secondary metabolites present in the different samples of CS, as observed in Supplementary Figure S2b.

3.2. Drug Candidate Filtering/ADME Property Analysis

A total number of 110 phytocompounds from the 128 identified from the UPLC-MS analysis passed the Lipinski's Ro5, while 18 compounds, which revealed more than one violation of the rules, were excluded (Supplementary Table S2).

3.3. Identification of Overlapping Targets of Secondary Metabolites within SEA and STP Databases

In total, 1040 targets from the STP database and 843 targets arising from the SEA database were obtained. The result of the Venn diagram analysis disclosed the presence of 20.6% (322 genes) of the prevalent overlapping targets being common to the two databases (Figure 2).

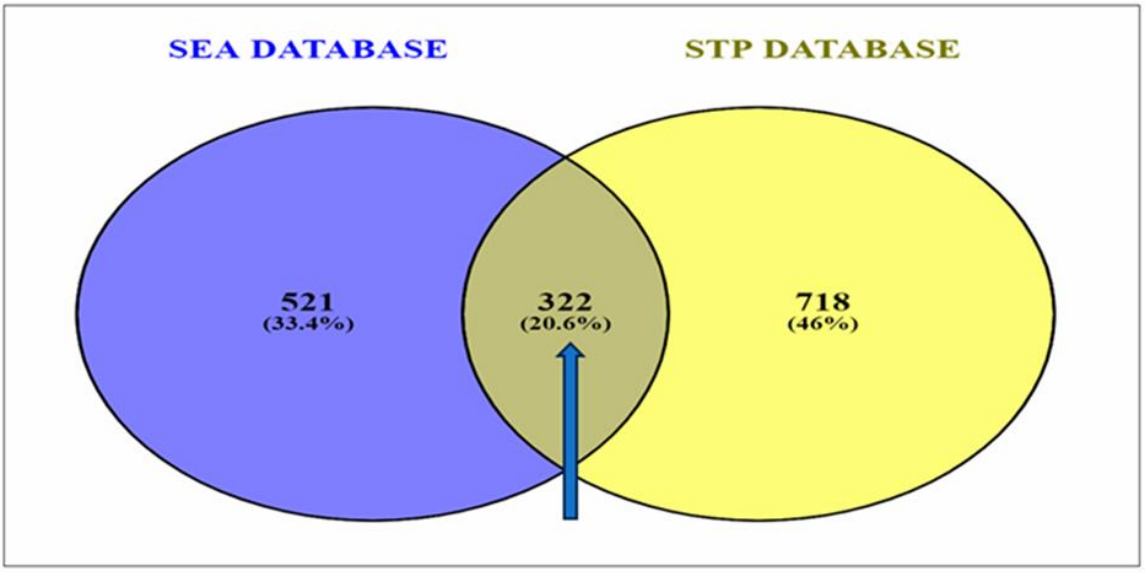

Figure 2. Identification of overlapping targets linked to secondary metabolites present in corn silk between SEA and STP databases [SEA: similarity ensemble approach; STP: Swiss target prediction].

A total number of 13,395 targets were identified via the GeneCards predictions based on the findings of the retrieval of the T2DM gene targets from the related databases. Mapping the 322 compound-related targets to the CS secondary metabolites revealed 274 (2%) common targets directly related to T2DM (Figure 3).

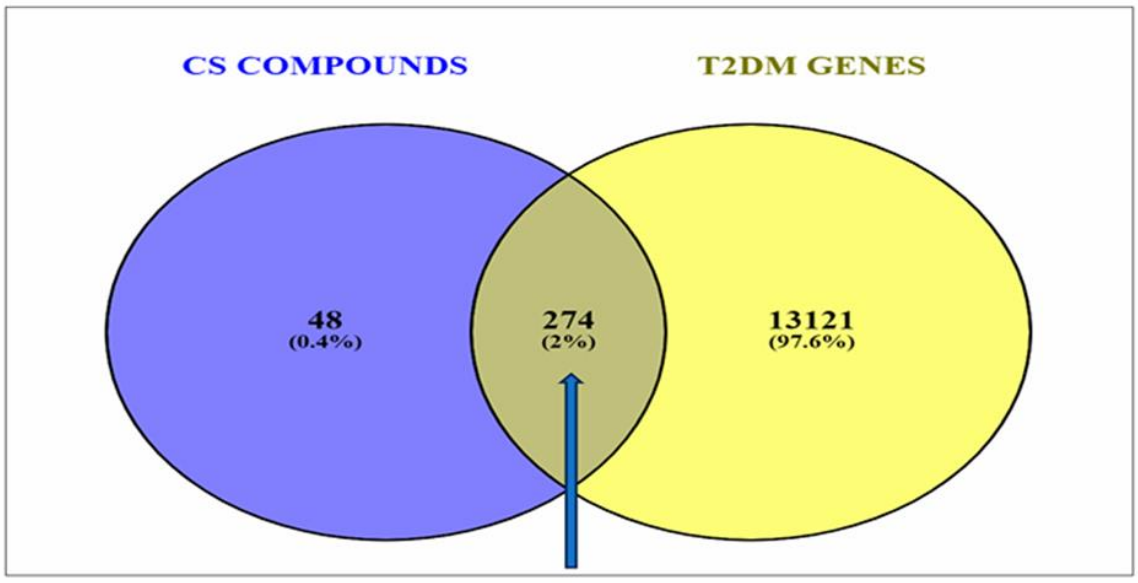

Figure 3. Venn diagram showing the overlapping genes common to the corn silk phytoconstituents and the T2DM-related target genes.

3.4. PPI Network Analysis

The 274 CS-T2DM overlapped genes arising from the STRING algorithm revealed 274 nodes connected to a network, with 2011 edges. The average node degree was 14.7, while the average local clustering coefficient and the PPI enrichment *p*-value were 0.448

and <1.0×10^{-16}, respectively. While the edges are characterized by the number of degrees for each target (with the highest number of degrees meaning the best network); however, five targets, *SLC37A*, *HPSE*, *MLNR*, *GABBR1*, and *PTAFR* (circled in Figure 4), had no interaction with any (Figure 4).

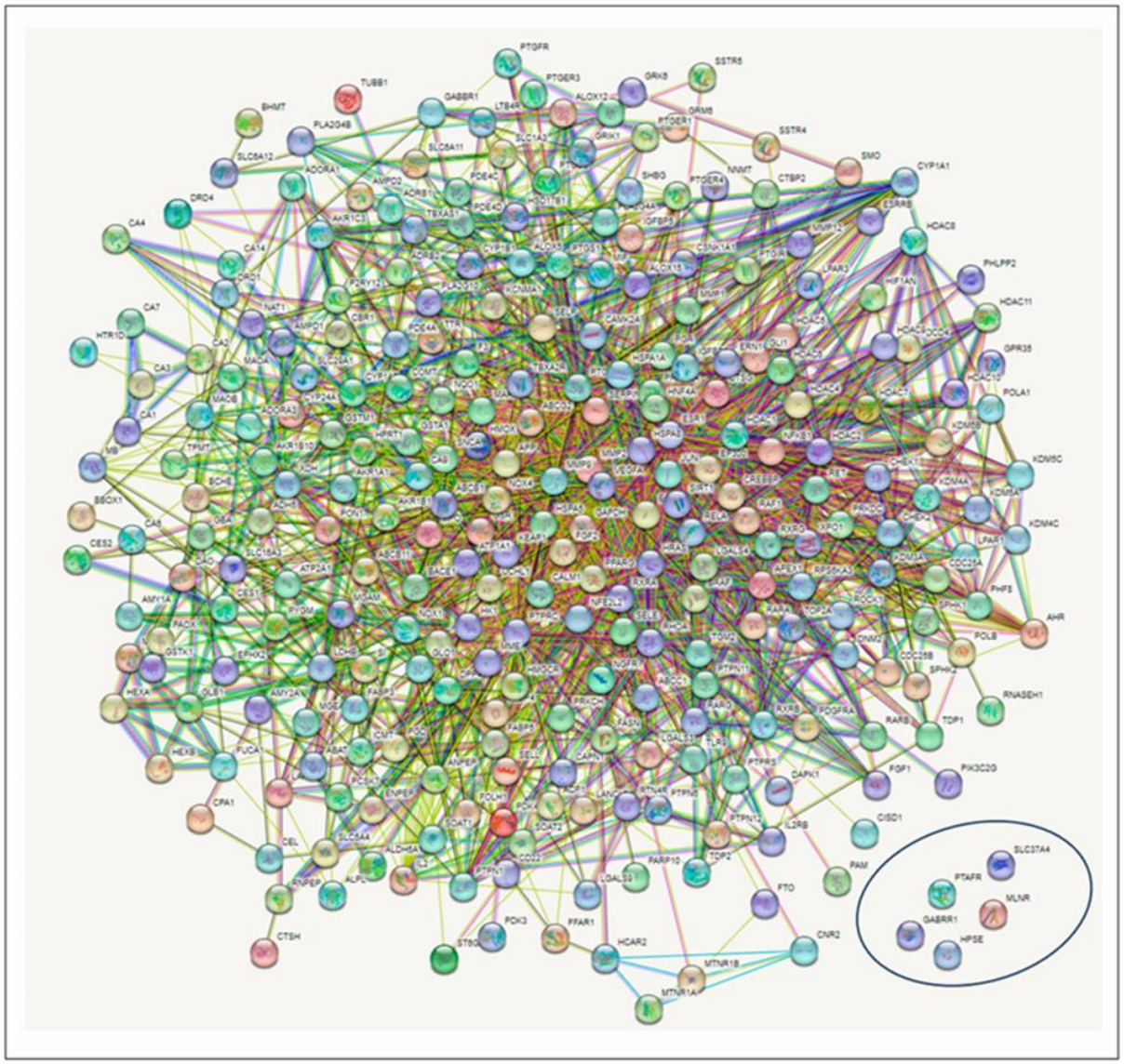

Figure 4. Protein–protein interaction (PPI) network showing the intersecting targets between the secondary metabolites in corn silk and type 2 diabetes mellitus. (Circled target genes showed no interactions with any nodes).

KEGG Pathway Enrichment Analysis

The results of the KEGG pathway enrichment analysis on the 274 intersecting targets using the STRING database revealed 13 signaling pathways implicated in T2DM associated with the genes related to the CS constituents (Table 1). The identification of the different signaling pathways implicated in T2DM related to the identified genes of the CS phytoconstituents and T2DM target genes were performed through the use of a bubble chart (Figure 5). The bigger the bubble, the lower the false discovery rate of the signaling

pathway and the more significant. Thus, the cAMP pathway was the key signaling pathway with the highest significant degree (26), a good strength score (0.95), and the lowest false discovery rate of 1.88×10^{-14}. A PPI network of the 26 target genes in the cAMP pathway is shown in Figure 6 and there were 54 reported interactions between these 26 nodes, in which the average node degree and average local clustering coefficient are 4.15 and 0.421, respectively. The PPI enrichment *p*-value of the 26 target genes in the cAMP pathway was 2.34×10^{-11}. However, 4 (*HTR1A*, *PTGER3*, *HCAR2*, *PTGER2*) of the 26 target genes had no interactions with the remaining 22 genes, indicating no connectivity to the network (Figure 6).

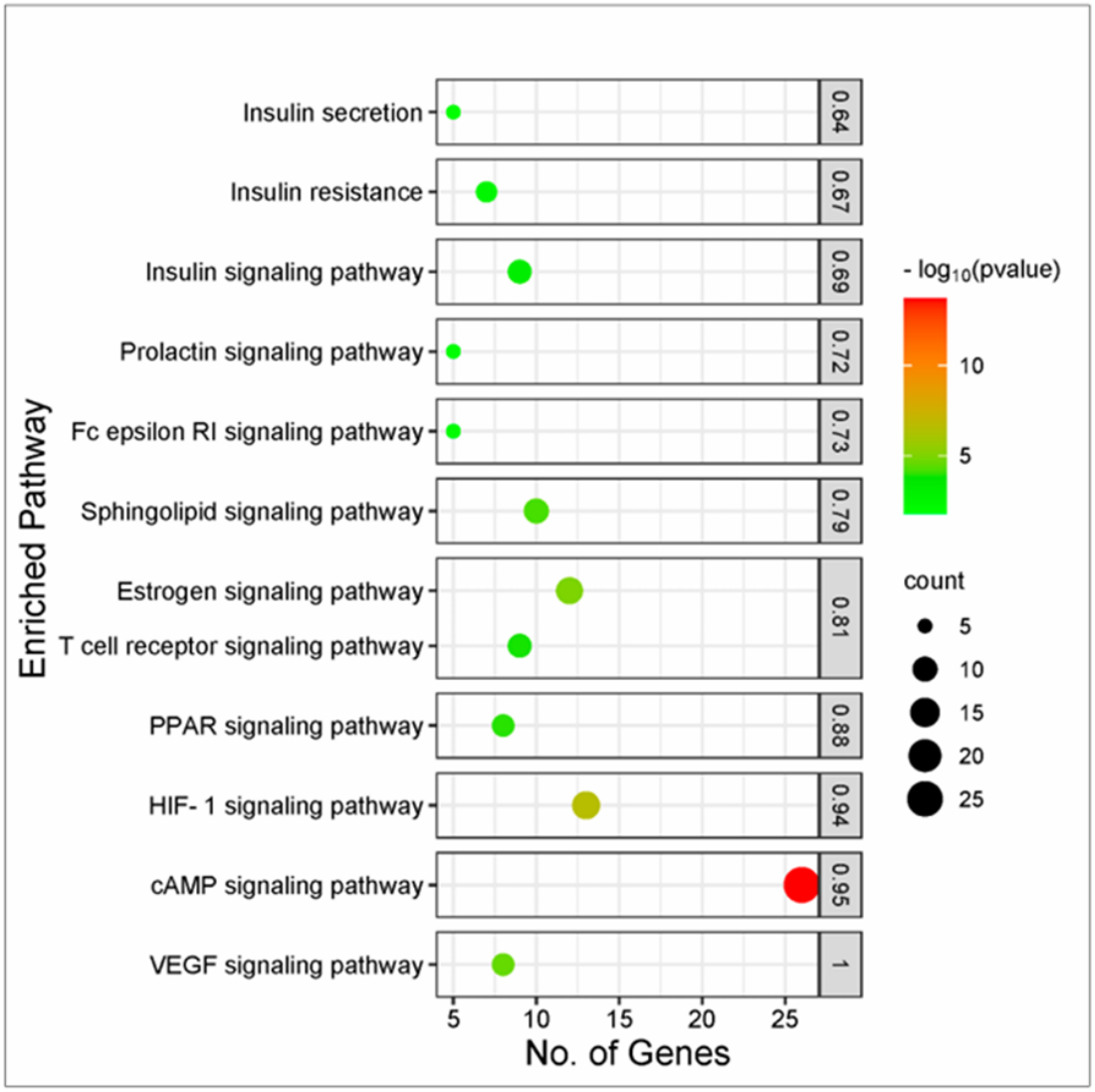

Figure 5. Bubble plot of KEGG pathway enrichment analysis of 274 intersecting targets related to CS secondary metabolites and T2DM.

Table 1. Pathway enrichment analysis results of the 274 intersecting targets involved in 13 signaling pathways implicated in T2DM.

Pathway Code	Description	Degree	Total	Strength	False Discovery Rate	Genes
hsa04933	AGE-RAGE signaling pathway in diabetic complications	11	98	0.91	4.88×10^{-6}	*MMP2, SERPINE1, NOX4, F3, JUN, NOX1, RELA, HRAS, VEGFA*
hsa04917	Prolactin signaling pathway	5	69	0.72	8.80×10^{-3}	*NFKB1, RAF1, RELA, ESR1, HRAS*
hsa04915	Estrogen signaling pathway	12	133	0.81	1.08×10^{-5}	*MMP2, RAF1, RARA, EGFR, PRKACA, PGR, JUN, MMP9, GABBR1, ESR1, HRAS, HSPA8*
hsa04664	Fc epsilon RI signaling pathway	5	66	0.73	7.50×10^{-3}	*RAF1, PLA2G4A, ALOX5, PLA2G4B, HRAS*
hsa04660	T cell receptor signaling pathway	9	101	0.81	1.30×10^{-4}	*NFKB1, IL2, RAF1, JUN, RELA, PTPN6, RHOA, HRAS, PTPRC*
hsa04370	VEGF signaling pathway	8	57	1.00	2.77×10^{-5}	*SPHK2, RAF1, SPHK1, PLA2G4A, PTGS2, PLA2G4B, HRAS, VEGFA*
hsa04071	Sphingolipid signaling pathway	10	116	0.79	6.82×10^{-5}	*NFKB1, SPHK2, RAF1, SPHK1, ADORA1, ABCC1, ROCK1, RELA, RHOA, HRAS*
hsa04910	Insulin signaling pathway	9	133	0.69	7.50×10^{-4}	*PYGM, RAF1, BRAF, HK2, FASN, PRKACA, PTPN1, HK1, HRAS*
hsa04911	Insulin secretion	5	82	0.64	1.59×10^{-2}	*FFAR1, KCNMA1, PRKACA, CAMK2A, ATP1A1*
hsa04931	Insulin resistance	7	107	0.67	3.10×10^{-3}	*PYGM, NFKB1, PTPN11, MGEA5, PTPN1, RPS6KA3, RELA*
hsa04024	cAMP signaling pathway	26	208	0.95	1.88×10^{-14}	*NFKB1, GLI1, RAF1, CREBBP, EP300, BRAF, SSTR5, ADRB2, PRKACA, PDE4D, PDE4C, PTGER3, ATP2A1, ADORA1, ADRB1, JUN, HTR1D, GABBR1, PDE4A, HCAR2, DRD1, CAMK2A, ROCK1, RELA, RHOA, ATP1A1*
hsa03320	PPAR signaling pathway	8	75	0.88	1.11×10^{-4}	*FABP4, PPARG, FABP5, MMP1, RXRG, FABP3, RXRB, RXRA*
hsa04066	HIF-1 signaling pathway	13	106	0.94	2.63×10^{-7}	*HMOX1, SERPINE1, NFKB1, GAPDH, CREBBP, EP300, EGFR, HK2, LDHB, CAMK2A, RELA, HK1, VEGFA*

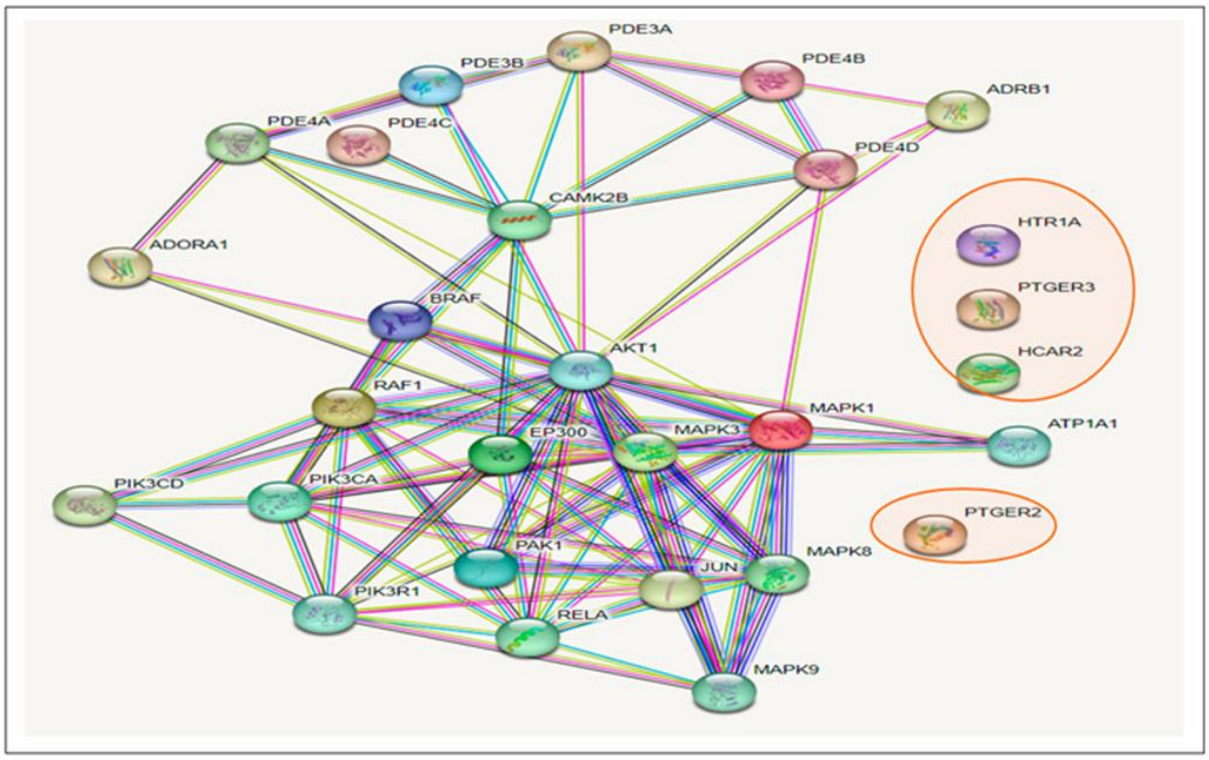

Figure 6. Gene–gene interactions amongst 26 T2DM target genes in the cAMP pathway related to CS secondary metabolites (The 4 target genes not connected to the 22 other genes are circled in red).

3.5. Gene Ontology Analysis

The gene ontology analysis performed on the 274 intersecting targets of the secondary metabolites present in the CS and T2DM revealed 494 biological processes, 75 cellular components, and 296 molecular functions. Out of the 494 biological processes reported, the top 10 were identified (Figure 7a), where drug response reported a degree of 30 with the lowest *p*-value of 1.3×10^{-16}. Additionally, of the 74 cellular components reported, the top 10 components were identified (Figure 7b) and an extracellular exosome was observed with a degree of 78 with the lowest *p*-value of 7.7×10^{-16}. Similarly, from the 296 molecular functions, ion binding was among the top 10 functions, having a degree of 174 and the lowest *p*-value of 2.8×10^{-18} (Figure 7c).

3.6. Compound–Target Pathway Network Analysis

Compound–target pathway network analysis revealed 63 nodes (26 related to the cAMP signaling pathway and 37 related to the secondary metabolites present in the CS) interacting with one another through 87 edges (Figure 8a). Additionally, it was revealed that the target *ATP1A1* had no interactions with any of the compounds or metabolites and was excluded from further analysis (Figure 8a). The gene–compound interaction networks revealed that adenosine A1 receptor (*ADORA1*) (Figure 8b), hydroxycarboxylic acid receptor 2 (*HCAR2*) (Figure 8c), and gamma-aminobutyric acid type B receptor subunit 1 (*GABBR1*) (Figure 8d) target genes connected to the highest number of bioactive secondary CS metabolites (15, 11, and 8, respectively).

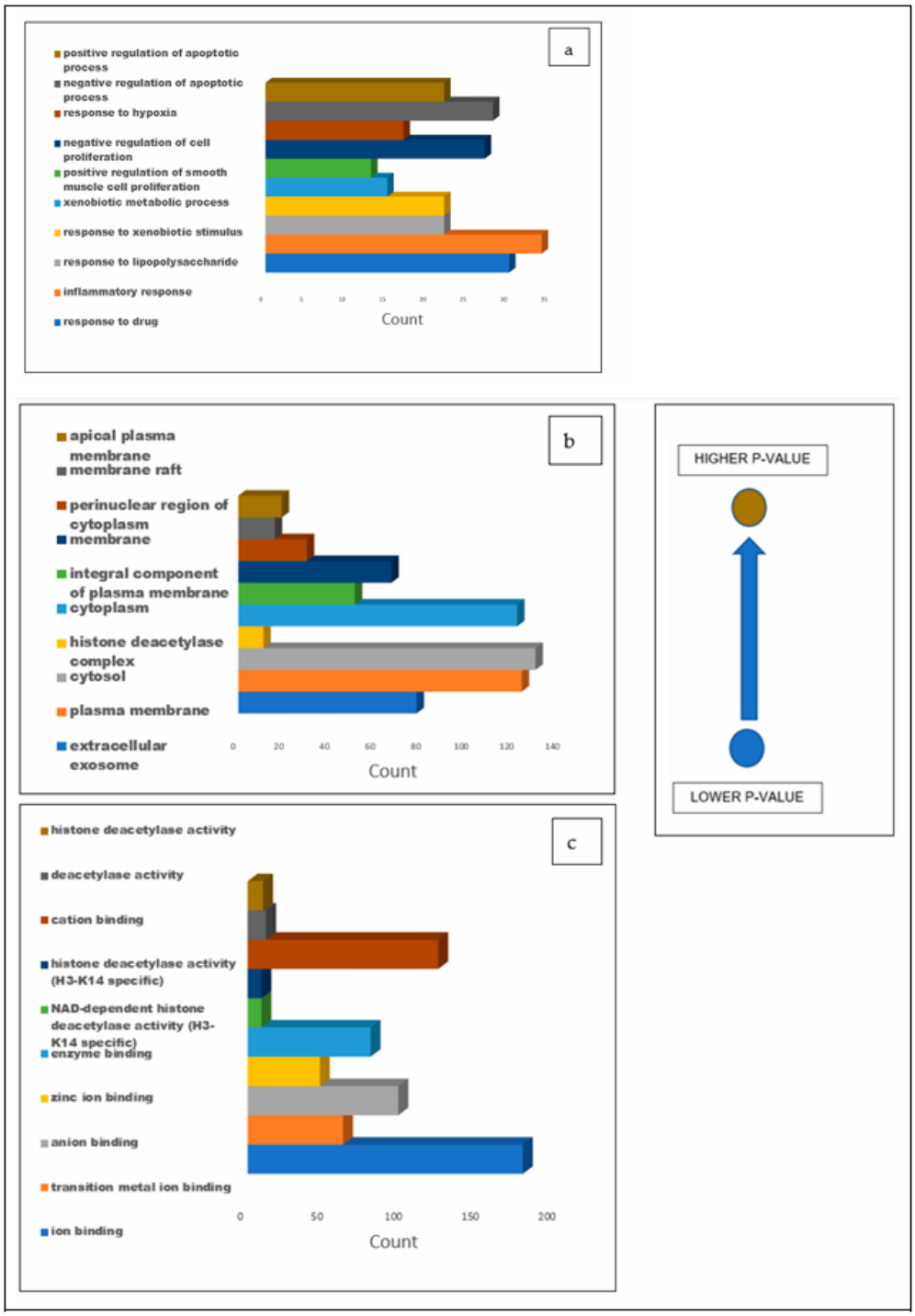

Figure 7. Bar graphs illustrating the GO analysis of the 274 common targets between T2DM and CS secondary metabolites for (**a**) biological processes, (**b**) cellular components, and (**c**) molecular functions with blue representing the lowest *p*-value and light brown representing the higher *p*-value.

3.7. Molecular Docking Analysis of Identified Secondary Metabolites Present in CS against ADORA1, HCAR2, and GABBR1 in the cAMP Signaling Pathway

The results of the molecular docking analysis for the identified phytoconstituents present in the CS against adenosine A1 receptor (*ADORA1*), hydroxycarboxylic acid receptor 2 (*HCAR2*), and gamma-aminobutyric acid type B receptor subunit 1 (*GABBR1*) targets arising from the NP analysis are presented in Table 2. Quing hau sau, phaseic acid, and tetradecanedioc acid reported the highest negative docking scores against *ADORA1*, *HCAR2*, and *GABBR1*, respectively. All the secondary metabolites present in the CS had higher or equal negative docking scores against *ADORA1*, *HCAR2*, and *GABBR1* compared to metformin (reference standard), except glutaric acid against *HCAR2*. Quing hau sau and phaseic acid as well as caffeic acid were also found to have the highest negative docking scores as compared to resveratrol (reference standard) against *ADORA1* and *HCAR2*, respectively. While the gene agonists 2-Chloro-n6-cyclopentyladenosine, butyric acid, and baclofen were docked against *ADORA1*, *HCAR2*, and *GABBR1*, respectively, quing hau sau and cyperine were observed to reveal most negative docking scores against *ADORA1*. This is in comparison to 2-Chloro-n6-cyclopentyladenosine, with all the compounds exhibiting higher docking scores against *HCAR2* relative to the gene agonist, butyric acid, and an observed reversed trend against *GABBR1* (Table 2).

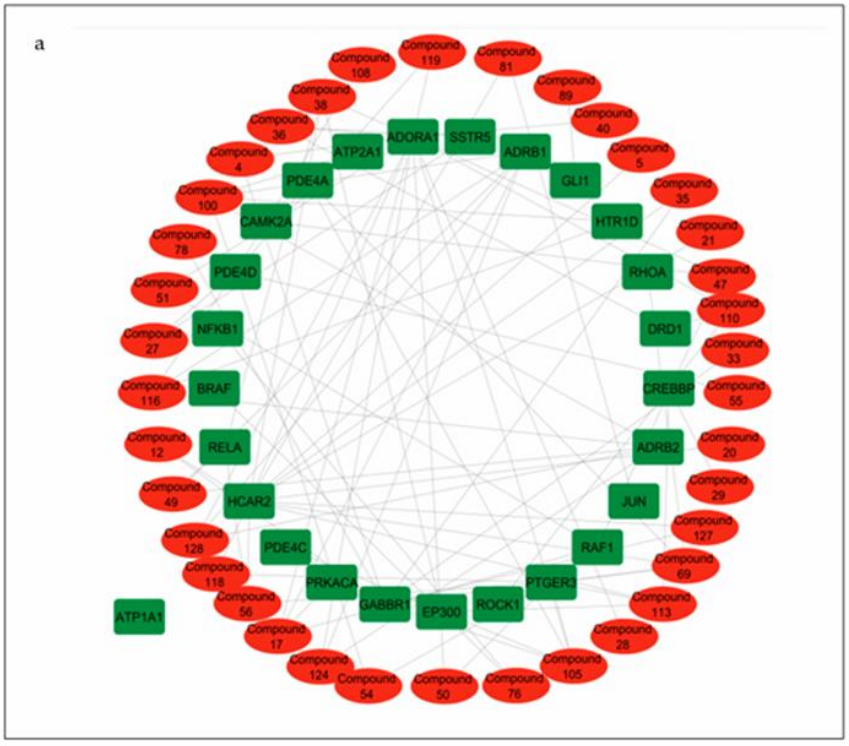

Figure 8. *Cont.*

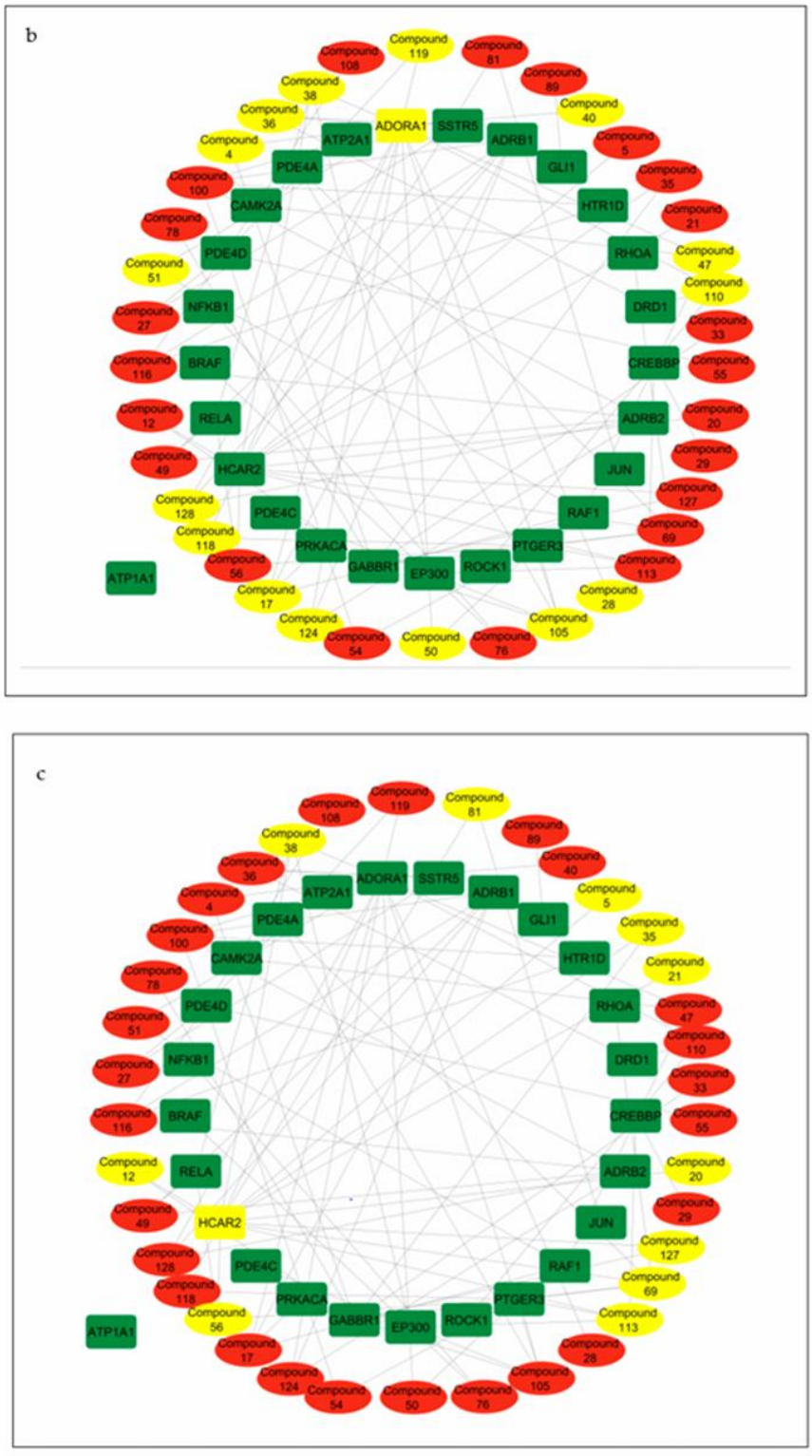

Figure 8. *Cont.*

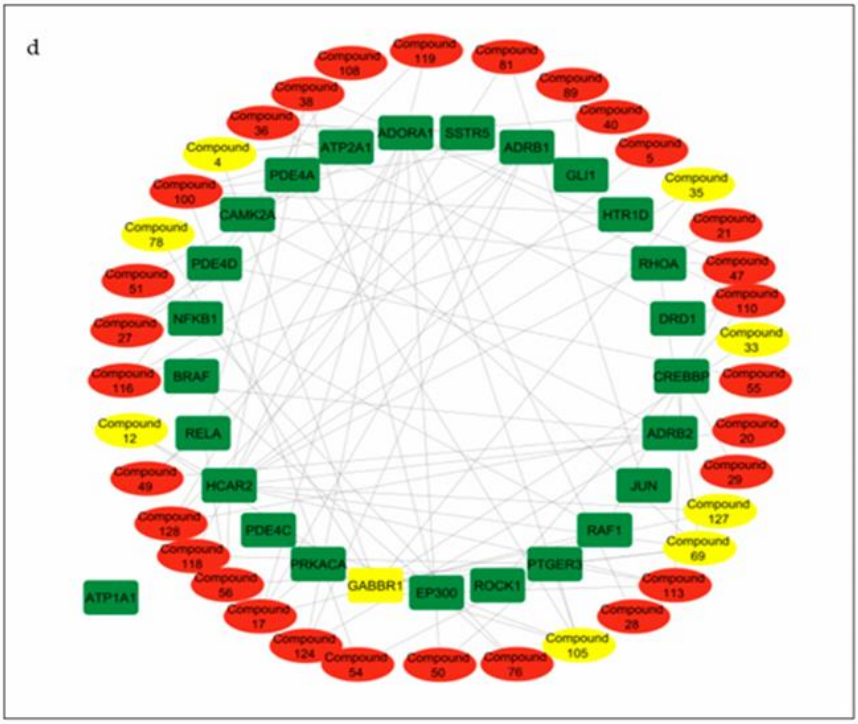

Figure 8. (**a**) Pathway of compound–target interaction network illustrating 37 CS secondary metabolites (red) interacting with 26 T2DM target genes implicated in the cAMP pathway (green); CS secondary metabolites (yellow) interacting with cAMP pathway genes (**b**) *ADORA1* (yellow rectangle); (**c**) *HCAR2* (yellow rectangle); (**d**) *GABBR1* (yellow rectangle).

Table 2. Molecular docking scores of identified secondary metabolites against cAMP pathway genes (*ADORA1*, *HCAR2*, and *GABBR1*).

Target	Compounds	Docking Score (kcal/mol)
ADORA1	Quing hau sau	−8.5
	Cyperine	−7.9
	Domesticoside	−6.9
	Gallicynoic acid B	−6.4
	Ginsenoyne e	−6.3
	Caffeic acid	−6.3
	Caffeoyl tartaric acid	−6.3
	Methyl geranate	−6.1
	Tetradecanedioic acid	−5.7
	Traumatic acid	−5.6
	7-acetoxy-5,6-dimethoxycoumarin	−5.6
	Methylisocitric acid	−4.9
	(-)-6-((2S,3R,4R,5S,6R)-3,4-dihydroxy-6-(hydroxymethyl)-5-methoxytetrahydro-2H-pyran-2-yloxy)-8-hydroxy-3-methyl-1H-isochromen-1-one	−4.8
	Isorhamnetin 3–6 malonyl glycoside	−4.8
	Phellodendric acid	−4.7
	Metformin	−4.6
	Resveratrol	−8.0
	2-Chloro-n6-cyclopentyladenosine (gene agonist)	−7.3

Table 2. *Cont.*

Target	Compounds	Docking Score (kcal/mol)
HCAR2	Phaseic acid	−6.9
	Caffeic acid	−6.6
	4-hydoxycinnamic acid	−6.2
	Dodecanedioc acid	−5.6
	Sebaic acid	−4.9
	Citraconic acid	−4.8
	CNPD0447999	−4.7
	Pimelic acid	−4.7
	Sarmentose	−4.7
	Syndic acid	−4.7
	Glutaric acid	−4.6
	Metformin	−4.7
	Resveratrol	−6.5
	Butyric acid (gene agonist)	−3.4
GABBR1	Tetradecanedioc acid	−5.8
	Dodecanedioc acid	−5.7
	Methylisocitric acid	−5.6
	Quinic acid	−5.5
	xi-2,2,6-Trimethyl-1,4-cyclohexanedione	−5.4
	Sebaic acid	−5.1
	Pimelic acid	−5.0
	Glutaric acid	−4.7
	Metformin	−4.6
	Resveratrol	−6.4
	Baclofen (gene agonist)	−5.9

3.8. Molecular Dynamics (MD) Simulation of Identified Secondary Metabolites against ADORA1, HCAR2, and GABBR1 Genes from the cAMP Signaling Pathway

The free binding energies of the top five CS compounds against each of the investigated targets following a 120 ns of MD simulation is presented in Table 3. Against *ADORA1*, all the top five compounds have higher binding free energy compared to the reference standards. Conversely, only 4-hydoxycinnamic acid had lesser free binding energy relative to the standards against *HCAR2*. A partly similar trend was observed in *GABBR1*, with quinic acid and Xi-2,2,6, trimethyl-1,4-cyclohexanedione having lesser binding free energy than the reference standards. In summary, gallicynoic acid B (−48.74 kcal/mol), dodecanedioc acid (−34.53 kcal/mol), and tetradecanedioc acid (−36.80 kcal/mol) had the highest binding affinities for *ADORA1*, *HCAR2*, and *GABBR1*, respectively (Table 3).

The structural and conformational alterations resulting from the binding of the CS phytoconstituents to the elucidated targets were evaluated by the different thermodynamic parameters (Table 4). The average RMSD (4.10 Å) of the apo-gene *ADORA1* was lower compared to the *ADORA1* complexes (standards and compounds) except ginsenoyne E (3.48 Å) and Quing hau sau (4.06 Å) (Table 4). Additionally, after 5 ns of simulation, when the atoms in each system had equilibrated, the fluctuation began thereafter within 2 Å and 7.5 Å till the end of the simulation (Figure 9a). With respect to *HCAR2*, the bound systems of some CS phytocompounds revealed hyped average RMSD values relative to the apo–*HCAR2* (9.64 Å) except phaseic acid–*HCAR2* (7.08 Å), dodecanedioc acid–*HCAR2* (7.80 Å) and 4-hydoxycinnamic acid–*HCAR2* (9.46 Å); in fact, the RMSD values of these three compounds were lower compared to metformin (9.54 Å) and resveratrol (9.10 Å), which was lower compared to the latter compound (Table 4). There was a significant fluctuation in the *HCAR2* system relative to the other genes, with caffeic acid contributing to most of the observed fluctuation between 10 Å and 12.5 Å (Figure 9b). Against *GABBR1*, the unbound system (1.97 Å) was lower compared to the bound systems of the CS phytocompounds and standards, except tetradecanedioc acid (1.54 Å) and quinic acid (1.69 Å) (Table 4). The system fluctuates between 1 Å and 3.5 Å after equilibrating at 16 ns, while the lowest and highest fluctuation in the *GABBR1* system was observed in tetradecanedioc acid and dodecanedioc acid, respectively (Figure 9c).

Table 3. Thermodynamic components of identified secondary metabolites present in CS against target genes in cAMP pathway.

	Energy Components (kcal/mol)				
Compound	**ΔE_{VdW}**	**ΔE_{elec}**	**ΔG_{gas}**	**ΔG_{solv}**	**ΔG_{bind}**
ADORA1					
Cyperine	−34.29 ± 3.40	−12.89 ± 3.14	−47.18 ± 4.44	15.34 ± 2.60	−31.84 ± 3.68
Domesticoside	−42.99 ± 3.22	−19.59 ± 7.79	−62.58 ± 7.48	28.53 ± 6.08	−34.05 ± 3.72
Gallicynoic acid B	−47.88 ± 3.06	−18.32 ± 8.06	−66.20 ± 8.19	17.47 ± 4.65	−48.74 ± 4.86
Ginsenoyne e	−52.55 ± 3.32	−5.20 ± 2.36	−57.75 ± 4.24	9.87 ± 1.94	−34.05 ± 3.72
Quing hau sau	−40.15 ± 2.20	−5.63 ± 3.60	−45.78 ± 4.38	13.74 ± 3.58	−32.04 ± 2.56
Metformin	−2.78 ± 3.10	−93.28 ± 110.41	−96.05 ± 111.67	85.26 ± 104.62	−10.80 ± 7.76
Resveratrol	−6.80 ± 6.62	−8.12 ± 9.86	−14.92 ± 14.89	9.61 ± 9.82	−5.31 ± 5.62
HCAR2					
Caffeic acid	−17.94 ± 3.06	−37.51 ± 10.87	−55.45 ± 10.01	28.61 ± 8.60	−26.83 ± 3.60
Dodecanedioc acid	−36.58 ± 3.16	−31.29 ± 8.71	−67.87 ± 8.55	33.34 ± 6.29	−34.53 ± 4.21
4-hydoxycinnamic acid	−21.38 ± 2.04	−15.31 ± 9.12	−36.69 ± 8.70	22.11 ± 5.79	−14.50 ± 4.1
Phaseic acid	−29.88 ± 3.78	−8.14 ± 7.54	−34.80 ± 7.20	17.40 ± 6.55	−17.40 ± 3.90
Sebaic acid	−24.65 ± 3.89	−29.39 ± 15.43	−54.04 ± 13.34	32.12 ± 11.32	−21.92 ± 4.24
Metformin	−0.01 ± 0.15	107.28 ± 28.17	107.28 ± 28.15	−107.27 ± 28.14	0.01 ± 0.07
Resveratrol	−23.40 ± 5.18	−8.87 ± 4.24	−32.27 ± 5.84	15.97 ± 3.94	−16.31 ± 4.25
GABBR1					
Dodecanedioc acid	−31.61 ± 4.00	−43.03 ± 14.45	−74.64 ± 15.77	40.17 ± 11.38	−34.46 ± 5.56
Methylisocitric acid	−14.85 ± 3.36	−32.17 ± 14.21	−47.01 ± 13.67	29.01 ± 9.53	−18.00 ± 5.52
Quinic acid	−10.90 ± 4.99	−33.92 ± 20.44	−44.82 ± 22.61	31.78 ± 16.50	−13.04 ± 6.99
Tetradecanedioc acid	−28.26 ± 3.79	−45.28 ± 15.18	−73.54 ± 13.64	36.73 ± 9.51	−36.80 ± 5.25
Xi-2,2,6, trimethyl-1,4-cyclohexanedione	−15.51 ± 5.75	−5.03 ± 4.48	−20.55 ± 8.63	8.81 ± 4.35	−11.74 ± 5.15
Metformin	−2.53 ± 2.66	−273.87 ± 95.97	−276.40 ± 96.89	271.81 ± 93.74	−4.59 ± 4.68
Resveratrol	−28.78 ± 2.12	−11.87 ± 4.09	−40.65 ± 4.81	22.55 ± 2.82	−18.09 ± 2.87

ΔE_{vdW}: van der Waals energy; ΔE_{elec}: electrostatic energy; ΔE_{gas}: gas-phase free energy; ΔG_{solv} solvation free energy and ΔG_{bind}: total binding free energy.

The top five compounds and resveratrol in complex with *ADORA1* had higher average RMSF values than the unbound *ADORA1* (1.93 Å) and metformin–*ADORA1* (1.88 Å) (Table 4). The compounds under investigation exhibited random fluctuations upon binding to *ADORA1*, with noticeable fluctuations at residues 230–270 between 1.0 Å and 6.5 Å (Figure 10a). The bound systems decreased, with fluctuations between 1 Å and 5.8 Å until amino acid residue 25, before a major increase above 12 Å after residue 350. Contrary to the trend in *ADORA1*, the average RMSF of the apo gene (*HCAR2*) was higher (2.57 Å) compared to the bound systems (CS compounds and resveratrol) except 4-hydoxycinnamic acid–*HCAR2* (2.85 Å) and metformin (2.63 Å) had higher mean RMSF values compared to the apo–*HCAR2* (2.57 Å). Most of the CS compounds revealed reduced RMSF values compared with resveratrol. Minimal fluctuation was observed in the RMSF plot between 1 Å and 5 Å until residue 300 till the end of the simulation, with increased fluctuation between 8 Å to 15 Å (Figure 10b). Similarly, the unbound *GABBR1* (1.29 Å) had lower average RMSF values relative to the bound GABBR1 complexes [dodecanedioc acid–*GABBR1* (1.49 Å), quinic acid–*GABBR1* (1.34 Å), xi-2,2,6, trimethyl-1,4-cyclohexanedione–*GABBR1* (1.58 Å) and metformin–*GABBR1* (1.63 Å)] except methylisocitric acid–*GABBR1* (1.27 Å), tetradecanedioc acid–*GABBR1* (1.25 Å), and *GABBR1*–reservatrol (1.22 Å).There was a reduced swaying between residues 0 and 225, fluctuating in the range of 0.75 Å to 3 Å, while higher fluctuations were noticed around residues 225, 250, 280, and 310 from 0.5 Å to 3.5 Å (Figure 10c).

Table 4. Post-molecular dynamics parameters of identified metabolites of CS against targets of cAMP pathway.

Compound	RMSD (Å)	RMSF (Å)	ROG (Å)	Number of H-bonds	SASA (Å)
			ADORA1		
ADORA1	4.10 ± 0.60	1.93 ± 0.86	28.64 ± 0.39	173.53 ± 9.20	22,151.21 ± 602.21
Cyperine	5.93 ± 1.04	2.18 ± 1.16	29.04 ± 0.26	167.97 ± 9.25	22,745.86 ± 336.02
Domesticoside	4.81 ± 0.90	2.29 ± 1.43	28.55 ± 0.32	162.94 ± 9.61	22,760.33 ± 405.56
Gallicynoic acid B	6.71 ± 1.10	2.12 ± 1.59	28.39 ± 0.27	171.58 ± 9.69	21,996.14 ± 357.48
Ginsenoyne e	3.48 ± 0.53	2.12 ± 1.55	28.59 ± 0.27	170.93 ± 9.60	21,484.73± 426.66
Quing hau sau	4.06 ± 0.48	2.06 ± 0.98	28.51 ± 0.27	170.30 ± 9.68	22,366.55 ± 398.10
Metformin	6.26 ± 0.77	1.88 ± 0.86	28.39 ± 0.36	136.77 ± 8.90	17,546.87 ± 446.41
Resveratrol	4.10 ± 0.66	2.11 ± 1.02	29.16 ± 0.39	143.60 ± 8.90	18,462.50 ± 314.93
			HCAR2		
HCAR2	9.64 ± 1.13	2.57 ± 2.39	24.24 ± 0.74	158.21 ± 10.58	20,865.81 ± 899.36
Caffeic acid	11.37 ± 1.67	2.25 ± 1.68	22.98 ± 0.63	166.40 ± 9.39	19,469.28 ± 645.20
Dodecanedioc acid	7.80 ± 0.80	2.21 ± 1.76	24.06 ± 0.33	160.98 ± 9.42	20,231.01 ± 515.88
4-hydoxycinnamic acid	9.46 ± 1.30	2.85 ± 2.29	23.70 ± 0.86	163.67 ± 9.43	20,516.00 ± 677.56
Phaseic acid	7.08 ± 0.53	2.07± 1.30	23.17 ± 0.27	158.70 ± 9.61	20,100.35 ± 631.16
Sebaic acid	9.73 ± 9.73	2.13 ± 1.55	23.20 ± 0.60	160.16 ± 9.14	20,546.94 ± 553.95
Metformin	9.54 ± 1.09	2.63 ± 1.91	24.70 ± 0.44	156.60 ± 9.51	20,894.76 ± 554.19
Resveratrol	9.10 ± 1.00	2.25 ± 1.96	23.79 ± 0.43	168.97 ± 10.01	20,736.27 ± 550.78
			GABBR1		
GABBR1	1.97 ± 0.37	1.29 ± 0.50	23.11 ± 0.18	203.89 ± 9.56	17,313.73 ± 317.08
Dodecanedioc acid	2.21 ± 0.46	1.49± 0.57	23.49 ± 0.24	205.08 ± 9.77	17,372.46 ± 384.40
Methylisocitric acid	2.23 ± 0.39	1.27 ± 0.52	22.73 ± 0.18	205.83 ± 9.77	17,499.85 ± 327.27
Quinic acid	1.69 ± 0.28	1.34 ± 0.96	23.41 ± 0.19	211.12 ± 9. 11	17,117.23 ± 356.12
Tetradecanedioc acid	1.54 ± 0.24	1.25 ± 0.48	23.35 ± 0.17	211.77 ± 9.96	17,361.58 ± 314.41
Xi-2,2,6, trimethyl-1,4-cyclohexanedione	2.06 ± 0.38	1.58 ± 0.93	23.50 ± 0.25	207.06 ± 9.60	17,688.30 ± 388.06
Metformin	2.15 ± 0.47	1.63 ± 1.29	23.53 ± 0.22	207.00 ± 9.78	17,616.59 ± 385.58
Resveratrol	2.21 ± 0.35	1.22 ± 0.46	22.69 ± 0.14	205.87 ± 9.81	16,994.73 ± 319.80

RMSD: root mean square deviation, RMSF: root mean square fluctuation, ROG: radius of gyration: SASA: solvent accessible surface, H-bonds: hydrogen bonds.

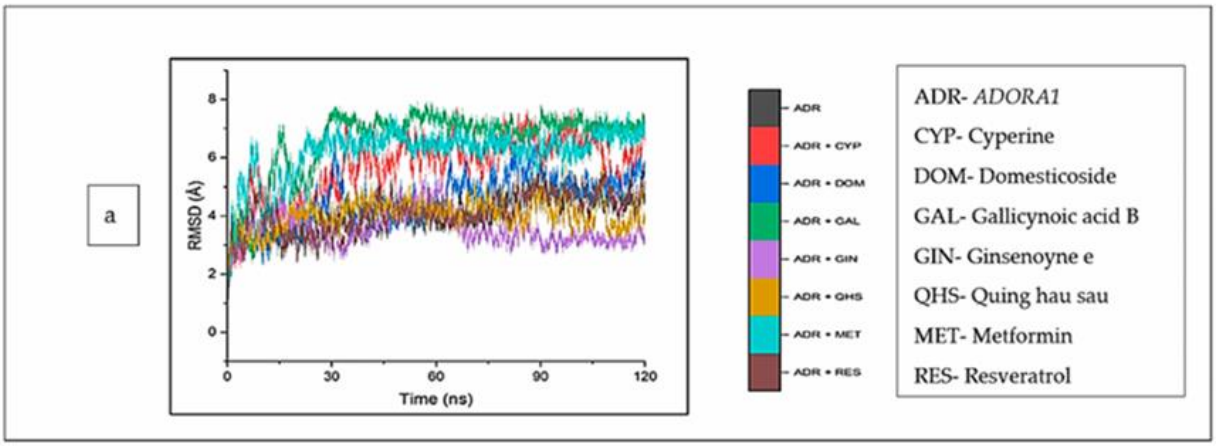

Figure 9. *Cont.*

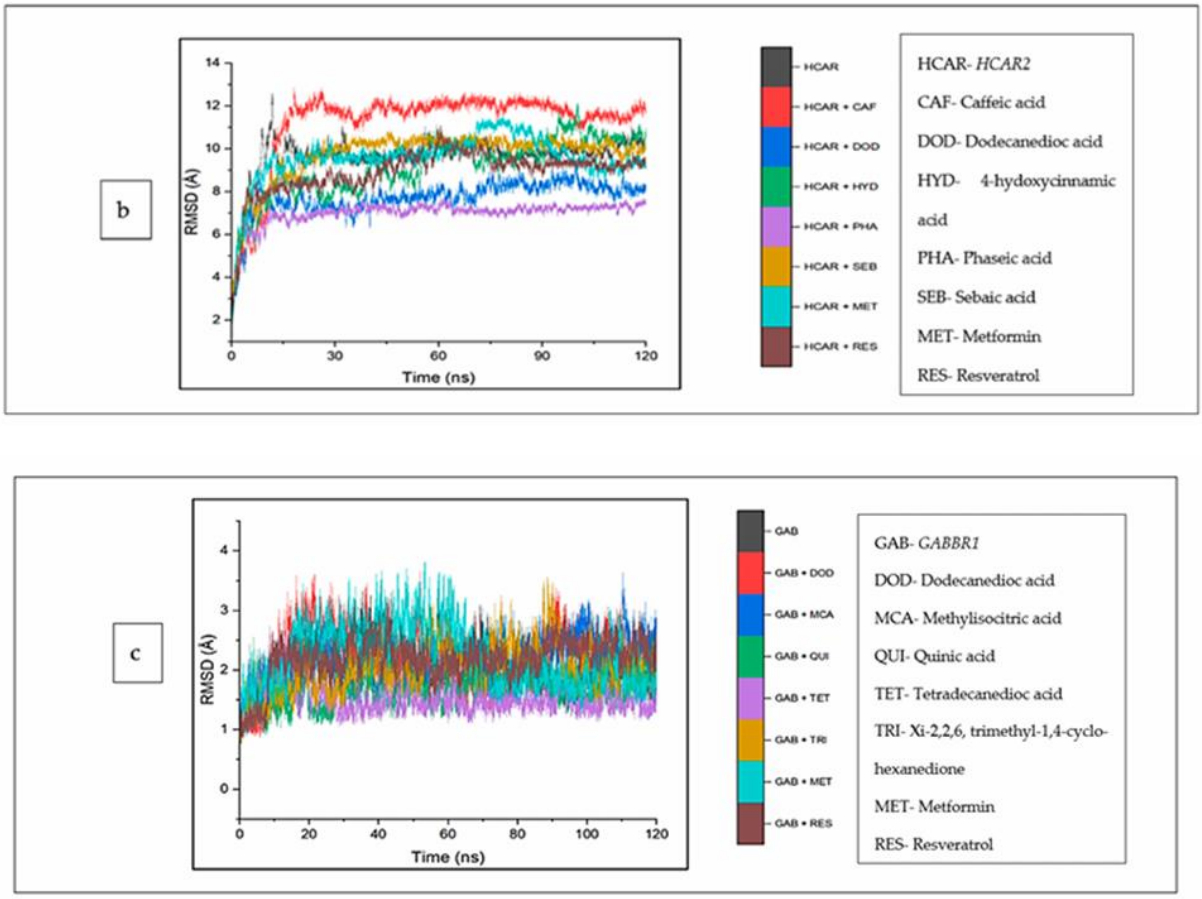

Figure 9. Root mean square deviations plots of comparison between CS phytocompounds, standards and target genes (**a**) *ADORA1*, (**b**) *HCAR2*, and (**c**) *GABBR1* determined over 120 ns simulation.

The mean RoG values of the cyperine–*ADORA1* (29.04 Å) and reservatrol–*ADORA1* (29.16 Å) complexes was higher than the apo-gene (28.64 Å). However, the other bound complexes and metformin revealed RoG values lower than those of *ADORA1* (Table 4). An inconsistency in the stability of all the systems was observed for the initial 30 ns, after this time, the stabilities of the individual systems, particularly metformin, appear to tend towards 120 ns, except ginsenoyne E (Figure 11a). In the same vein, against *HCAR2*, the RoG values of the bound systems of the CS compounds (including dodecanedioc acid, which was marginally lower) and resveratrol were reduced, compared with *HCAR2* (24.24). Caffeic acid (22.98 Å) was the lowest among the co-compounds and resveratrol (23.79 Å). A reduced trend in the stabilities of the systems at around 20 ns was observed, which was then stable throughout the rest of the simulation (Figure 11b). Against GABBR1, the RoG values of all the CS compounds and metformin were higher than the apo-gene (23.11 Å), and resveratrol (22.69 Å) was the lowest (Figure 11c).

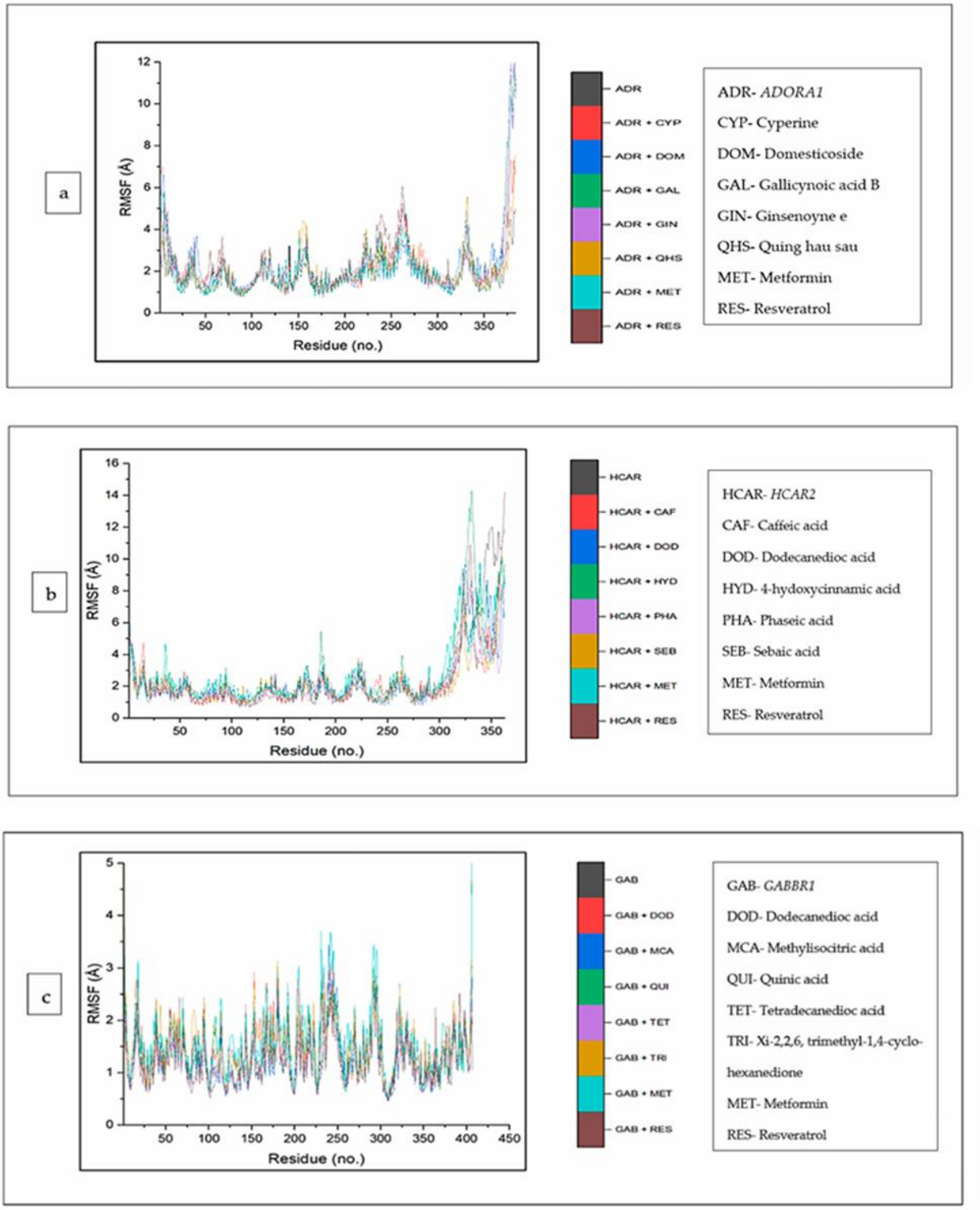

Figure 10. Root mean square fluctuation plots of comparison between CS phytocompounds, standards and target genes (**a**) *ADORA1*, (**b**) *HCAR2*, and (**c**) *GABBR1*, determined over 120 ns simulation.

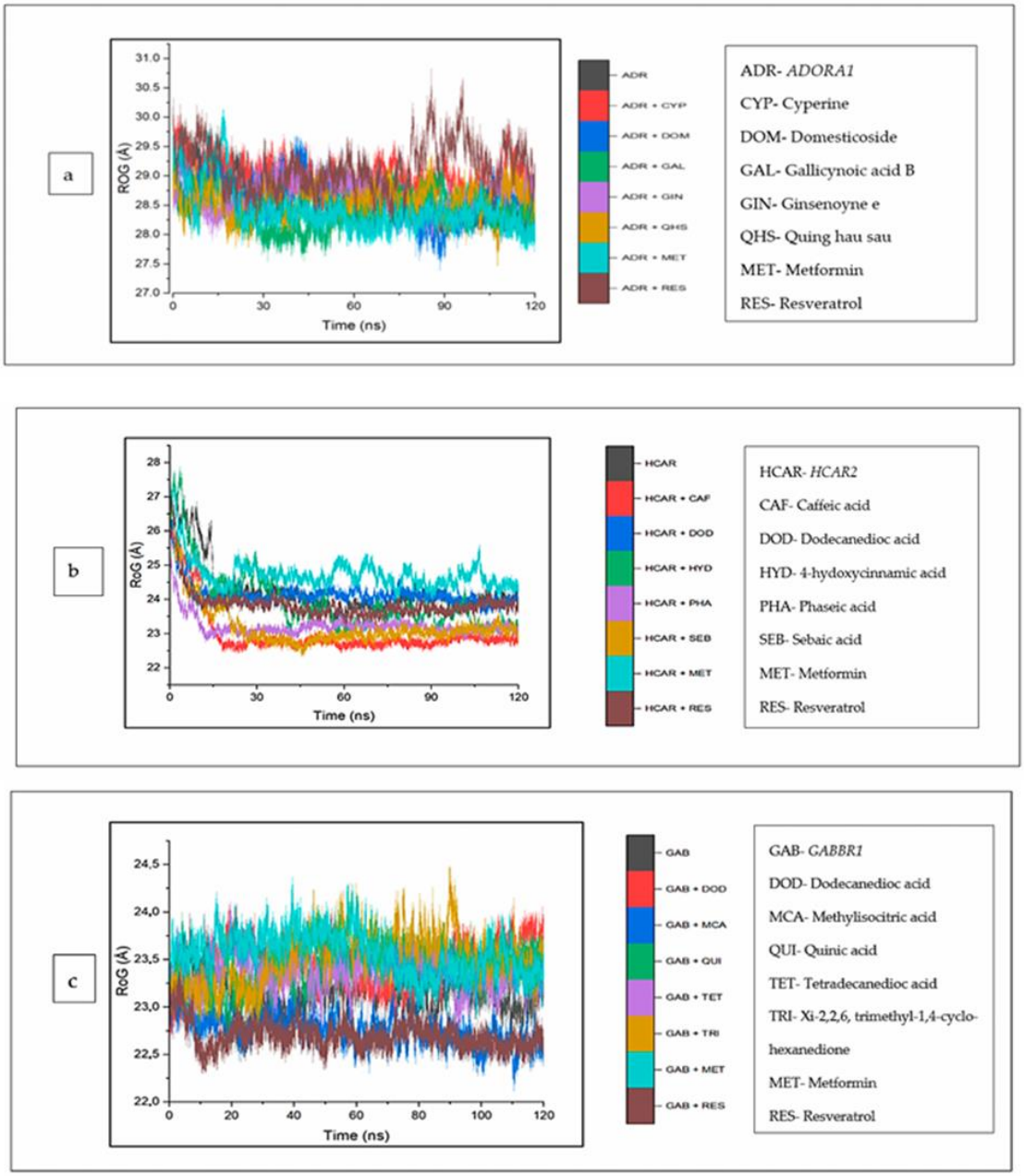

Figure 11. Radius of gyration plots of comparison between CS phytocompounds, standards and target genes (**a**) *ADORA1*, (**b**) *HCAR2*, and (**c**) *GABBR1*, determined over 120 ns simulation.

The intramolecular hydrogen bonds formed between the complexes were analyzed and are depicted in (Figure 12a–c). Typically, against *ADORA1*, a reduction in the number of hydrogen bonds formed was observed across all the complexes, including cyperine (167.97), domesticoside (162.94), gallicynoic acid B (171.58), ginsenoyne E (170.93), and quing hau sau (170.30), relative to apo–*ADORA1*, with the highest average number of hydrogen bonds (173.53). The lowest number of hydrogen bonds was observed in metformin (136.77) and resveratrol (143.60) (Figure 12a). On the contrary, for *HCAR2*, there was an increase in the number of hydrogen bonds in the bound systems of the CS compounds relative to

the unbound *HCAR2* (158.21); this was also observed for the reference standards, except metformin (156.60) (Figure 12b). The increase in the number of hydrogen bonds was expressed in this order: phaseic acid (158.70) < sebaic acid (160.16) < dodecanoic acid (160.98) < 4-hydoxycinnamic acid (163.67) < caffeic acid (166.40) (Table 4). A similar trend was observed with *GABBR1* when the bound systems of *GABBR1* and the CS compounds and standards were higher compared to the apo-gene (203.89) (Figure 12c).

The investigation of the complexes was extended to include an analysis of the solvent accessibility and surface area (SASA). Against *ADORA1*, the mean SASA values of cyperine (22,745.86 Å), domesticoside (22,760.33 Å), and quing hau sau (22,366.55 Å) are marginally higher compared to the unbound *ADORA1* (22,151.21 Å), though gallicynoic acid B-*ADORA1* (21,996.14 Å) and ginsenoyne E-*ADORA1* (21,484.73 Å) had the lowest SASA values among the CS compounds. However, the mean SASA value observed for the reference standards, and the metformin–*ADORA1* (17,546.87 Å) and resveratrol–*ADORA1* (18,462.50 Å) complexes are lesser compared to apo–*ADORA1* (Figure 13a). Furthermore, for *HCAR2*, the CS compound bound complexes reflected reduced SASA values relative to the apo-gene (20,865.81 Å). While the SASA values of the reference standards [metformin (20,894.76 Å), resveratrol (20,736.21 Å)] are marginally lower than the apo-gene, caffeic acid (19,469.68 Å) depicted the lowest SASA values. A downward trend around 15 ns was observed for all the systems, which became stable until the end of the simulation period (Figure 13b). Similarly, the complexes of the CS compounds and standards were higher compared with the apo-gene (17,313.17 Å), except for quinic acid (17,117.23 Å). An inconsistency of all the systems was witnessed throughout the simulation period (Figure 13c).

The data obtained regarding the interaction plots of the investigated CS metabolites (based on the results of the thermodynamics profiles) against each of the established target genes (*ADORA1*, *HCAR2*, and *GABBR1*) revealed diverse bond types such as hydrogen bonds (conventional, carbon, and π-donor), attractive charge, van der Waals, amide π-stacked, π-sigma, π-cation, π-anion, π-alkyl, alky, π-sulphur, salt bridge, unfavorable acceptor–acceptor and donor–donor interactions (Figures 14–16; Supplementary Figures S3–S5). Specifically, the binding of gallicynoic acid B with *ADORA1* after a 120 ns simulation period showed 20 interactions, consisting of 2 hydrogen bonds (PHE168 and HIE346), 2 carbon hydrogen bonds (GLU167 and THR345), 12 van der Waal (ILE60, ASN67, VAL80, ALA81, VAL84, THR88, CYS166, GLU169, TRP315, LEU318, HIE319 and ILE342), 3 alkyl (ALA63, ILE64 and LEU84), and 1 π-anion interaction (TYR339) (Figure 14a). The metformin–*ADORA1* complex had eight interactions (with six amino acid residues), including one hydrogen bond interaction (GLU160), two carbon–hydrogen bonds (GLY160 and GLU161), three van der Waal interactions (LEU 146, TRP153 and PRO162) and two salt bridges with attractive charge interactions (GLU160 and GLU161) (Figure 14b). At the end of the 120 ns simulation period, resveratrol was unbound to *ADORA1*, and thus, displayed no interaction (Figure 14c). The binding of dodecanedioc acid to *HCAR2* following the 120 ns simulation period revealed 20 interactions which consisted of 5 hydrogen bonds (TYR87, 2 SER179, LEU280, and TYR284), 11 van der Waal forces (LEU83, LEU104, ASN110, ARG111, LEU162, SER181, PHE193, ARG251, PHE277, SER281, and THR283), 2 alkyl groups (LEU107 and ALA108) and 2 π-cation interactions with attractive charges (PHE180 and GLU190) (Figure 15a). While, at 60 ns and 120 ns, metformin had no interaction with *HCAR2* as the ligand was unbound (Figure 15b), resveratrol bound to *HCAR2* had eight interactions including five van der Waals (TRP50, PHE54, HIE55, LEU308, and GLY340), two π-alkyl (ALA341 and PRO342) and one π-cation interaction (ARG339) (Figure 15c). Tetradecanedioc acid and *GABBR1* bound presented 13 interactions consisting of 3 hydrogen bonds (ALA126, ARG133, and GLU204), 5 van der Waals (SER106, THR127, THR158, TYR203, and ILE229), 2 alkyl (VAL154 and PHE155), 1 π-sigma (TRP231) and 2 π-anion with salt bridge interactions (HIE129 and ARG133) (Figure 16a). At the end of the 120 ns simulation, metformin was unbound and had no interaction with GABBR1 (Figure 16b). However, resveratrol was bound to *GABBR1* through 12 interactions containing 8 van der Waals (TRP18, SER106,

HIE123, HIE129, GLN150, GLN152, THR158, and TRP231), 2 π-alkyl (ALA126 and VAL154) and 2 π-π-stacked interactions (PHE155 and TYR203) (Figure 16c).

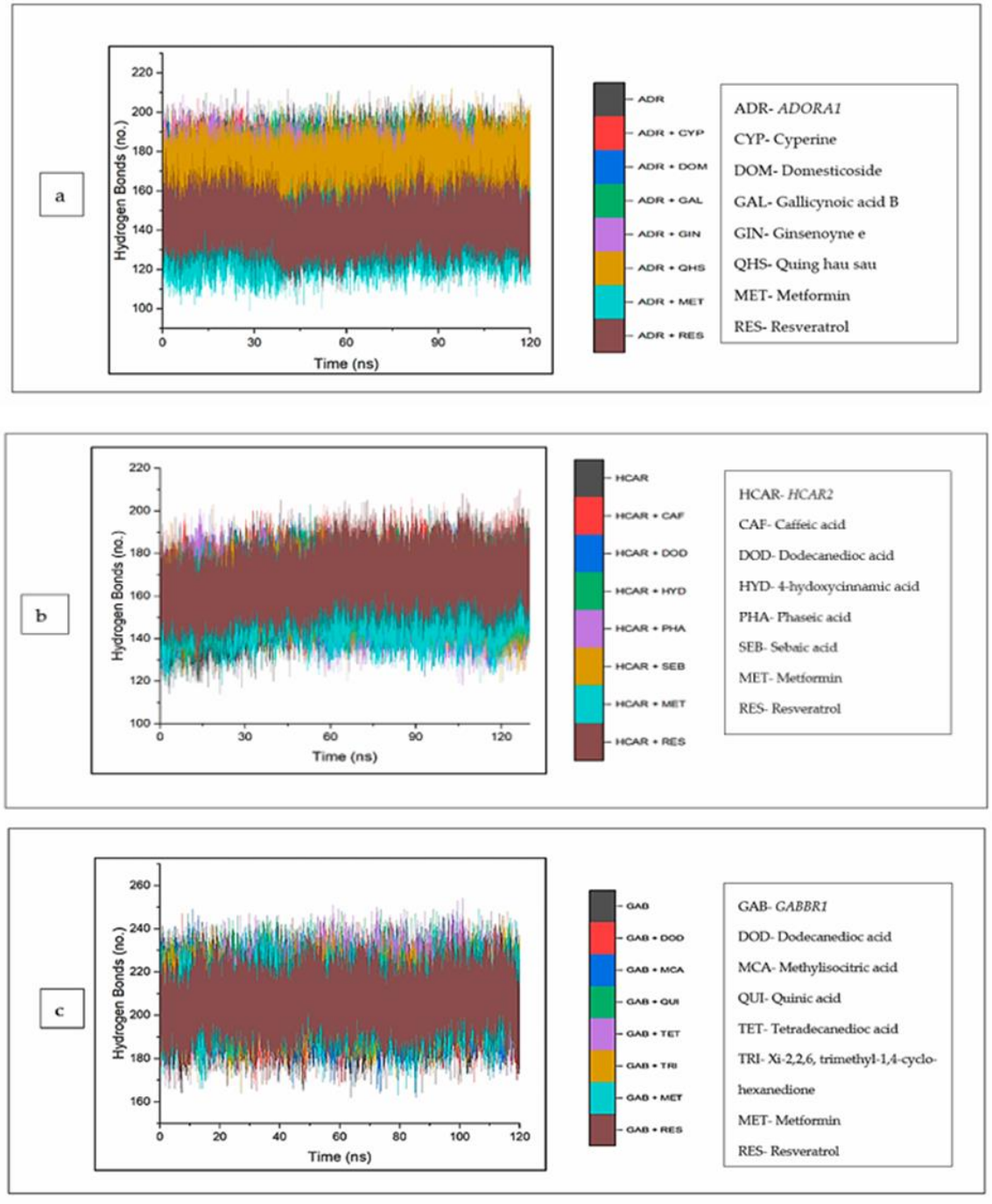

Figure 12. Backbone hydrogen bonding trajectory between CS phytocompounds, standards, and target genes (**a**) *ADORA1*, (**b**) *HCAR2*, and (**c**) *GABBR1* determined over 120 ns simulation.

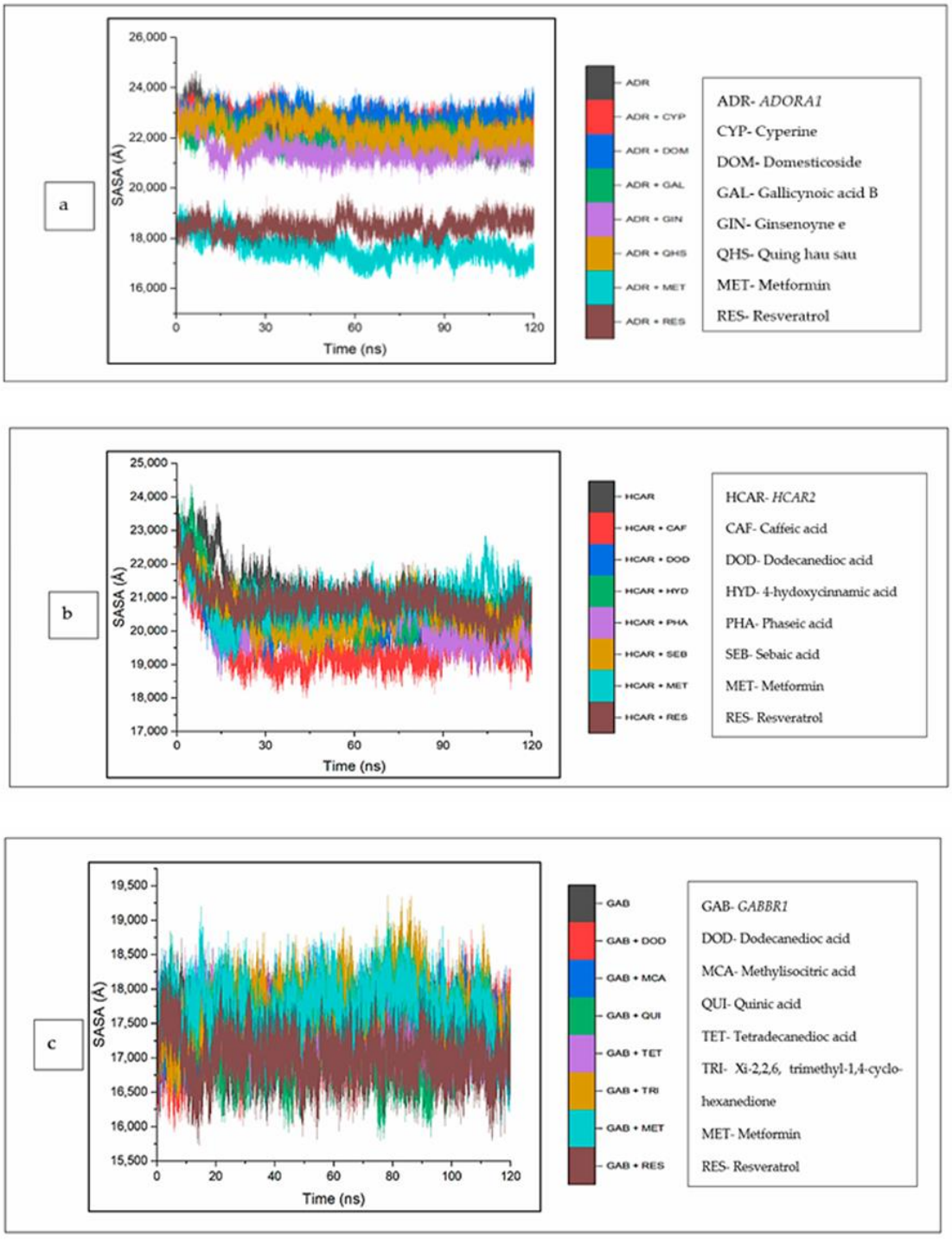

Figure 13. Solvent accessible surface area plots of comparison between CS phytocompounds, standards, and target genes (**a**) *ADORA1*, (**b**) *HCAR2*, and (**c**) *GABBR1*, determined over 120 ns simulation.

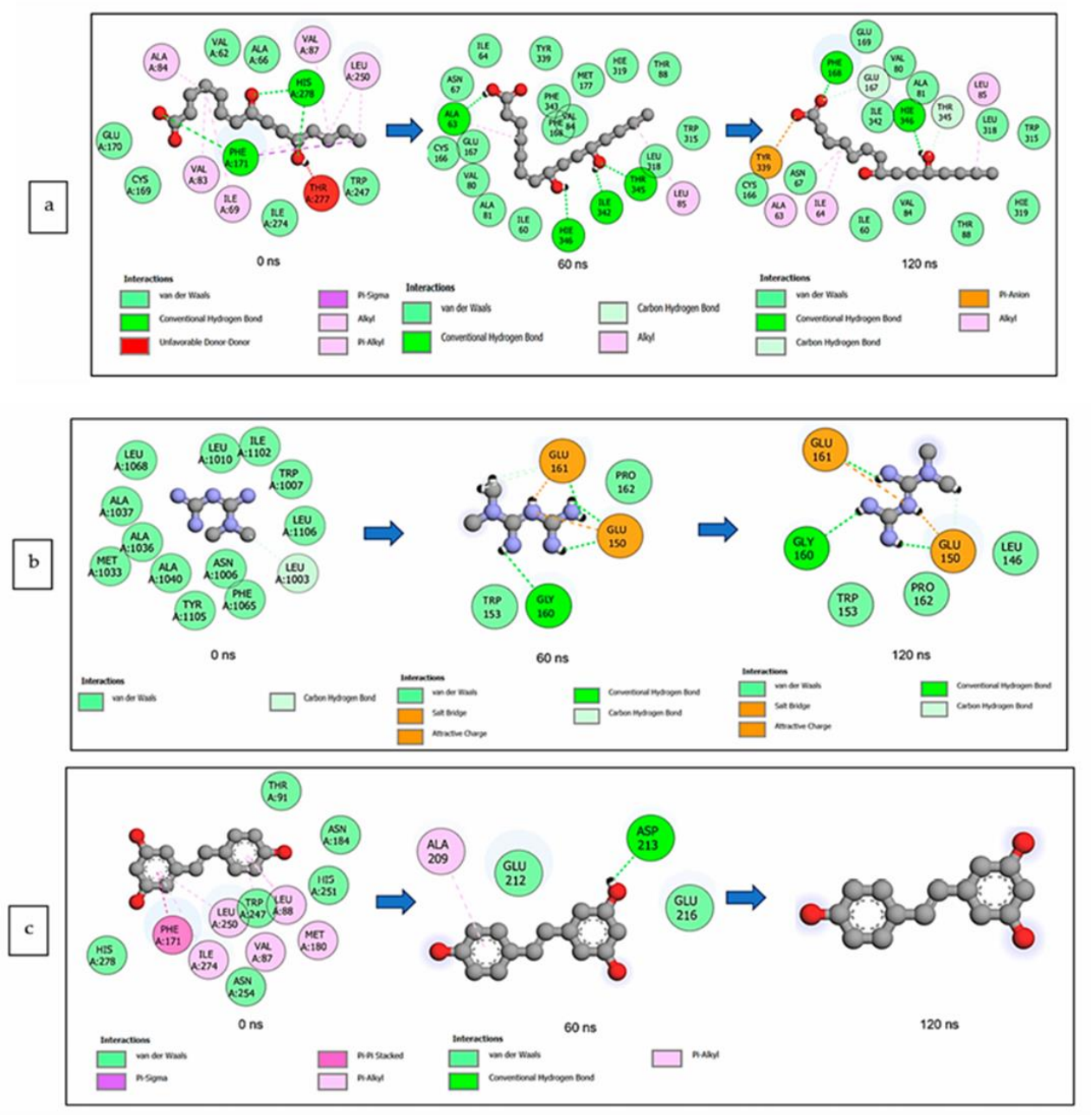

Figure 14. 2-D interaction plots of *ADORA1* with (**a**) gallicynoic acid B, (**b**) metformin, and (**c**) resveratrol at 0, 60 and 120 ns.

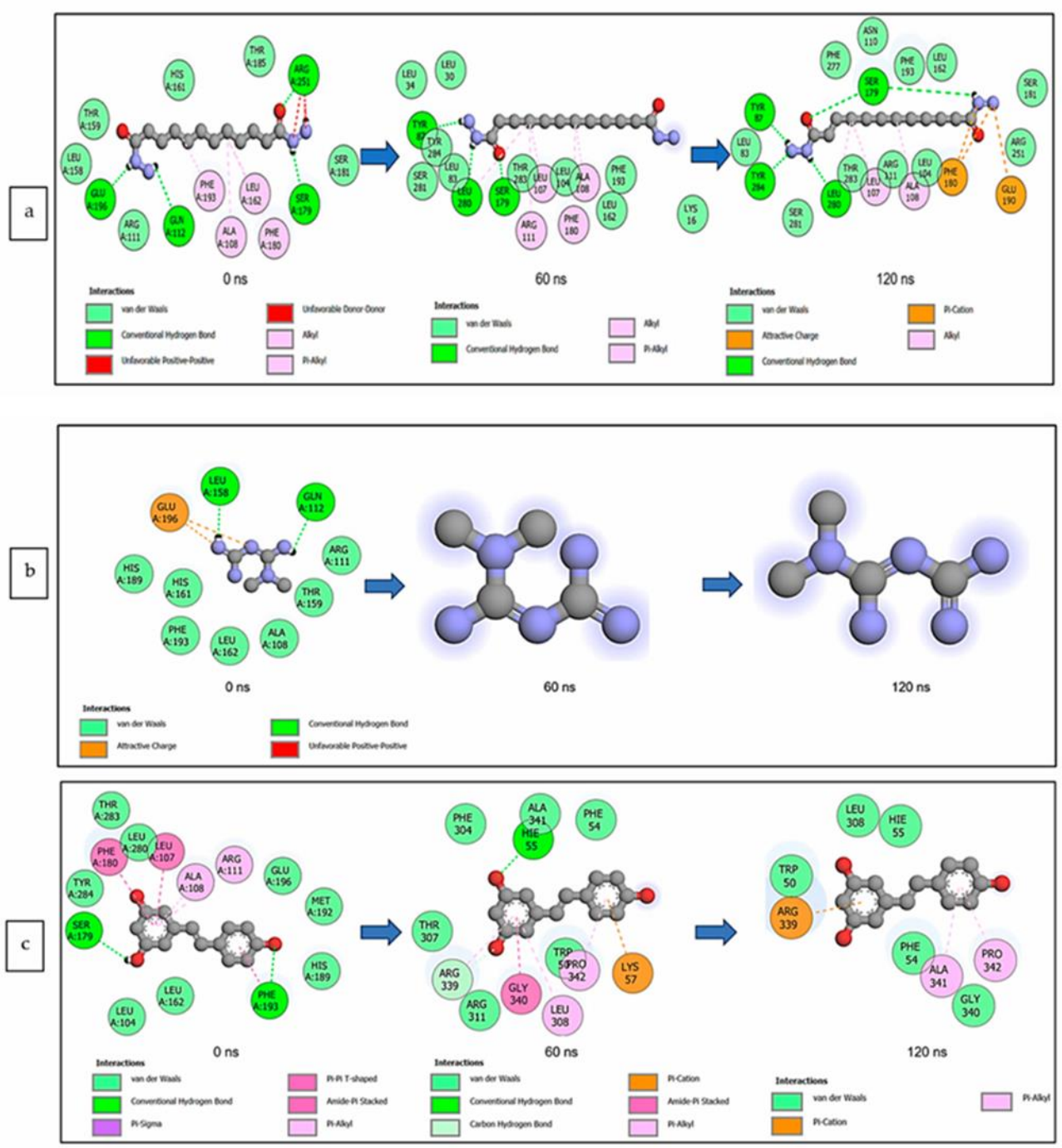

Figure 15. 2-D interaction plots of target gene *HCAR2* with (**a**) dodecanedioc acid and standards, (**b**) metformin, and (**c**) resveratrol at 0, 60, and 120 ns.

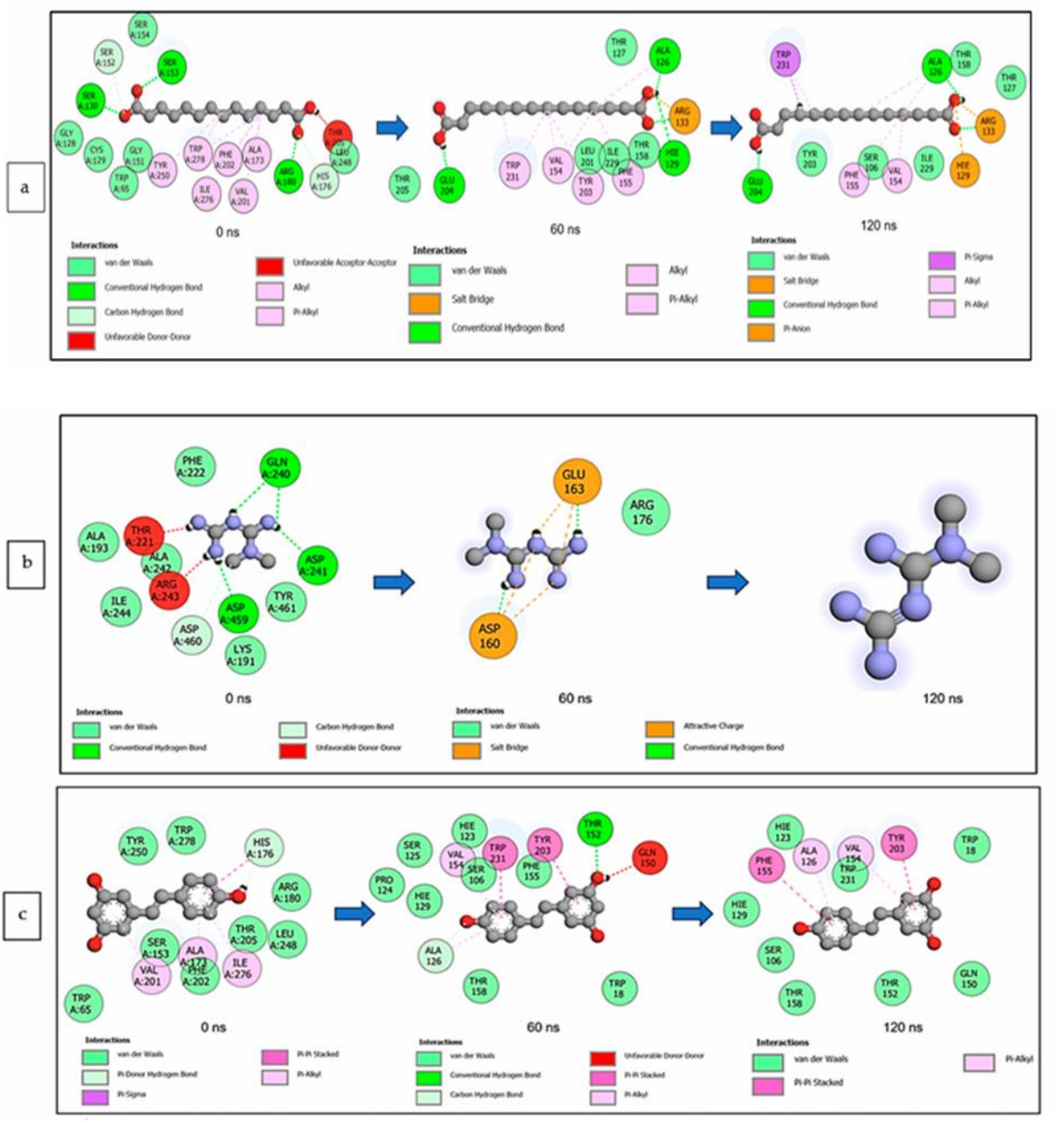

Figure 16. 2-D interaction plots of *GABBR1* with (**a**) tetradecanedioc acid, (**b**) metformin, and (**c**) resveratrol at 0, 60, and 120 ns.

3.9. Molecular Orbital Properties

A detailed analysis of the top-scoring compounds' structural and chemical reactivity properties was generated using DFT (Table 5). Apart from resveratrol (4.06 eV), which recorded the lowest energy gap across the three targets, and metformin (5.26 eV), which was second to the lowest against *GABBR1*, ginsenoyne E (4.43 eV), caffeic acid (4.14 eV), and quinic acid (5.51 eV) exhibited the lowest energy gap against *ADORA1*, *HCAR2*, and *GABBR1*, respectively (Figure 17). Consequently, ginsenoyne E (0.45 eV), caffeic acid

(0.48 eV), and quinic acid (0.36 eV) exhibited the highest chemical softness in a similar manner, with the energy gap from xi-2,2,6-trimethyl-1,4-cyclohexanedione also having the lowest chemical softness against *GABBR1*, the same as quinic acid. However, the highest chemical hardness value was observed in quing hau sau (3.03 eV), sebaic acid (3.70 eV), and tetradecanedioc acid (3.70 eV). Furthermore, the highest electronegativity value was observed in ginsenoyne E (4.80 eV), phaseic acid (4.50 eV), and methylisocitric acid (4.21 eV) against *ADORA1*, *HCAR2*, and *GABBR1*, respectively, while dodecanedioc acid (1.38 eV) exhibited the lowest electrophilicity value against *HCAR2* and *GABBR1*, with cyperine (1.47 eV) showing the lowest against *ADORA1*.

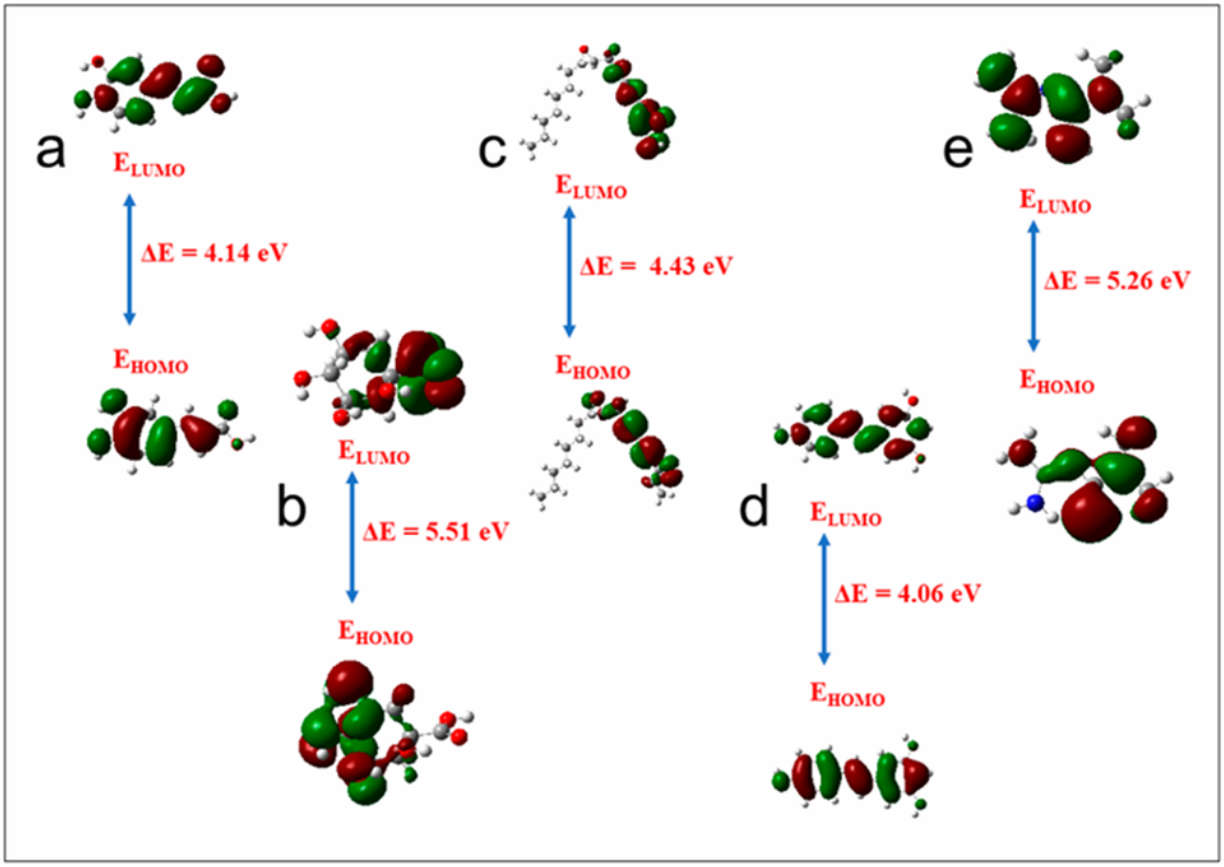

Figure 17. Frontier molecular orbitals for (**a**) caffeic acid, (**b**) quinic acid, (**c**) ginsenoyne, (**d**) reservatrol, (**e**) metformin (E_{LUMO}: energy of the lowest unoccupied molecular orbital; E_{HOMO}: energy of the highest occupied molecular orbital).

Table 5. The cDFT parameters of the top-hit compounds against target genes in the cAMP pathway.

					cDFT Parameters (eV)					
Ligands	**LUMO**	**HUMO**	**EA**	**IE**	**EA**	**Hardness**	**Softness**	**EN**	**CP**	**GE**
ADORA1										
Cyperine	−0.04	−5.75	5.71	0.04	5.75	2.85	0.35	2.89	−2.89	1.47
Domesticoside	−1.41	−6.29	4.88	1.41	6.29	2.44	0.41	3.85	−3.85	3.04
Gallicynoic acid B	−0.80	−6.63	5.83	0.80	6.63	2.91	0.34	3.72	−3.72	2.37
Ginsenoyne E	−2.58	−7.01	4.43	2.58	7.01	2.22	0.45	4.80	−4.80	5.19
Quing hau sau	−1.07	−7.13	6.06	1.07	7.13	3.03	0.33	4.10	−4.10	2.77
Metformin	−0.91	−6.17	5.26	0.91	6.17	2.63	0.38	3.54	−3.54	2.38
Reservatrol	−1.38	−5.44	4.06	1.38	5.44	2.03	0.49	3.41	−3.41	2.86
HCAR2										
Caffeic acid	−1.91	−6.05	4.14	1.91	6.05	2.07	0.48	3.98	−3.98	3.82
Dodecanedioc acid	0.45	−6.77	7.22	−0.45	6.77	3.61	0.28	3.16	−3.16	1.38
4-Hydroxycinnamic acid	−1.90	−6.17	4.27	1.90	6.17	2.14	0.47	4.03	−4.03	3.81
Phaseic acid	−2.30	−6.70	4.41	2.30	6.70	2.20	0.45	4.50	−4.50	4.59
Sebaic acid	−0.24	−7.65	7.41	0.24	7.65	3.70	0.27	3.94	−3.94	2.10
Metformin	−0.91	−6.17	5.26	0.91	6.17	2.63	0.38	3.54	−3.54	2.38
Reservatrol	−1.38	−5.44	4.06	1.38	5.44	2.03	0.49	3.41	−3.41	2.86
GABBR1										
Dodecanedioc acid	0.45	−6.77	7.22	−0.45	6.77	3.61	0.28	3.16	−3.16	1.38
Methylisocitric acid	−0.89	−7.54	6.65	0.89	7.54	3.33	0.30	4.21	−4.21	2.67
Quinic acid	−1.27	−6.78	5.51	1.27	6.78	2.76	0.36	4.03	−4.03	2.94
Tetradecanedioc acid	−0.22	−7.63	7.41	0.22	7.63	3.70	0.27	3.92	−3.92	2.08
Xi-2,2,6-Trimethyl-1,4-Cyclohexanedione	−1.25	−6.85	5.60	1.25	6.85	2.80	0.36	4.05	−4.05	2.93
Metformin	−0.91	−6.17	5.26	0.91	6.17	2.63	0.38	3.54	−3.54	2.38
Reservatrol	−1.38	−5.44	4.06	1.38	5.44	2.03	0.49	3.41	−3.41	2.86

cDFT: conceptual density functional theory; LUMO: lowest unoccupied molecular orbital; HOMO: highest occupied molecular orbital; EG: energy gap; IE: ionization energy; EA: electron effinity; EN: electronegativity; CP: chemical potentials; GE: global electropilicity.

4. Discussion

Historically, medicinal plants, for many centuries, have continued to be employed in traditional medicine systems for the provision of knowledge and relieve and/or cure numerous diseases and illnesses [4], most especially T2DM [7,10]. Corn silk, for example, despite being an abundant waste material, is a potential remedy for T2DM [8,10] and established in many studies, including antioxidant and anti-inflammatory activities [11,16–18,48].

While the therapeutic significance of medicinal plants (such as CS) is due to be endowed with key phytochemicals, if the development of novel drugs [49] is to be warranted, it is crucial, therefore, to begin the screening of plants of potential therapeutic significance to determine their metabolite profiles [41]. However, it must be noted that the type of solvents utilized in the extraction of medicinal plants and/or natural products is critical in determining the type of the composition and concentration of phytoconstituents [50]. The choice of polar solvents in the study, though majorly used in indigenous medicine for the extraction and preparation of formulations, is based on established literature reports of a possible high extraction yield [50,51]. However, there are reports of moderate apolar (ethyl acetate) and non-polar solvents (acetone and hexane) in addition to the polar solvents used on CS [50–54].

The high abundance of (7′R)-(+)-Lyoniresinol 9′-glucoside, cnicin, methyisocitric acid, chrysoeriol 4′,7-diglucoronide, and 3-isopropylmalatte in the aqueous extract and D-leucic acid, dodecanedioc acid, quercetin-3-(2″,3″,4″-triacetylgalactoside), sebacic acid, and p-coumaroyl malic acid in the ethanolic extract and vice versa could be attributed to the degree of polarity of the extracting medium [55] and may explain or buttress the variation

(46.8%) in the types and amounts of phytoconstituents (generally) as identified based on UPLC-MS analysis. While the use of this technique is adequate and reliable, as buttressed in the work of Fougre et al. [56], adopting a related tool, the high abundance of phytoconstituents, namely, azealic acid, isowertin 2″-rhamnoside, D-2-hydrozyglutaric acid, citraconic acid, 3-p-courmaroylquinic acid, cis-aconitic acid, UNPD129404, caffeic acid ethyl ester, and myricitrin, particularly in the raw CS sample, may be suggested to contribute to the pharmacological attributes (glucose lowering) of CS, since the concentration of bioactive ingredients within a medicinal sample is well-established to influence the pharmacological effectiveness. In fact, compounds or their derivatives such as azealic acid, 3-p-coumaroylquinic acid, caffeic acid, and myricitrin identified in CS have also been detected in several other plants exhibiting an antihyperglycaemic effect [57–60].

The network pharmacology approach provides avenues for new drug candidates or secondary metabolites, genetic target profiles, and connected signaling pathways linked to diseases, including infectious and non-infectious ones [30,61], achieved by a number of analyses [25,27,28,30,31]. While the five targets not connected in the PPI network may indicate their lack of involvement in the connectivity of the network, suggesting that they may not necessarily or unlikely be involved in any metabolic pathway or offer any molecular function, the cAMP as a key second messenger in signaling pathways has been reported, particularly in drug development [62], particularly against T2DM [25]. cAMP maintains glucose homeostasis in many ways, including insulin and glucagon secretion, glucose uptake, glycogen synthesis and breakdown, gluconeogenesis, the maintenance of β-cell differentiation, and the neural control of glucose homeostasis [63]. The establishment of cAMP as the best signaling pathway in this study buttresses it as an important signaling pathway to consider if deciphering the MoA of the CS in alleviating the negative effect of hyperglycaemia is to be completely elucidated [64].

The gene ontology analysis of the 274 intersecting targets between the CS phytoconstituents and T2DM targets revealed the regulation of the drug response, exosomes, and ion binding as the most significant biological process, cellular component, and molecular function. The regulation of the drug response modulates the frequency, rate, or extent of the drug response and refers to the regulation of drug resistance and determines the response and side effects a drug has on the body [65–68]. Exosomes are delivery vehicles for different signaling molecules (lipids, proteins, and nucleic acids) and serve as important mediators of intracellular communication [66]. Extracellular exosomes play a role in the regulation of inflammation, the stimulation of glycogen accumulation, and the regulation of GLUT4 metabolism, all of which are implicated in T2DM [69,70]. Ions are involved in the folding of proteins and nucleic acids, enzyme catalysis, and numerous cellular signaling processes, and thus, ion binding has a significant role in the normal functioning of processes in the human body [65,71]. A change in the binding of ions in the human body can affect many processes involved in glucose metabolism, including insulin signaling, secretion, and β-cell functioning [71]. Several studies have previously explored the role that the regulation of drug response, exosomes, and ion binding plays in the pathogenesis of T2DM [66,69,70,72,73].

Compound–target pathway network analysis is important for the discovery of therapeutic targets as well as lead compounds [74]. The association of many of the CS compounds to cAMP targets such as *ADORA1*, *HCAR2*, and *GABBR1* highlighted them among the genes in the cAMP pathway. Adenosine A1 receptor (*ADORA1*), a G protein-coupled receptor, inhibits the enzyme adenylate cyclase and plays a role in the regulation of cell metabolism and gene transcription, and therefore, has been identified as an important drug target for the treatment of various diseases and illnesses [75,76], including T2DM via glucose homeostasis and glucagon secretion regulation [77]. The identification of *ADORA1* as a key target for T2DM and related complications (e.g., nephropathy) therapy buttresses previous studies (on morusin, kuwanon C, and morusyunnansin) from *Morus alba* (leaves) and *Salvia miltiorhiza* through NP and molecular docking analyses [77,78]. Hydroxycarboxylic acid receptor 2 (*HCAR2*) is a G-protein-coupled receptor responsible for mediating

the antilipolytic actions of niacin and the lowering of blood lipid levels [79]. The expression of *HCAR2* in cells affects the regulation of inflammatory factors, inhibition of lipolysis, and glucose homeostasis [79,80]. G-protein-coupled receptors (GPCRs), including *GABBR1* are transmembrane signaling molecules involved in a wide variety of physiological processes such as the modulation of insulin secretion and the regulation of islet function, making them potential targets for antidiabetic compounds [81]. Previous reports of their involvement as a therapeutic target for treating various diseases such as T1DM, cancer, etc., have been well-established [81–85]. Typically, studies have demonstrated that, in human beta cells, signaling through *GABBR* participates in an autocrine feedback inhibition loop that regulates beta cell-specific gene expression and insulin secretion [84]. Although *GABBR1* was among the five non-target genes of the PPI network, the compound–target pathway network analysis revealed its importance as a therapeutic target, having the third highest number of CS phytoconstituents related to it [25,29].

Molecular docking, a structure-based drug design approach, is a preliminary screening tool for the identification of a suitable ligand (say, secondary metabolites) based on its binding free energy (docking score) at the active site of the target gene that could be developed as a probable candidate [86]. The most negative docking score of Quing hau sau, phaseic acid, and tetradecanoic acid, arising from their binding at the active sites of *ADORA1*, *HCAR2*, and *GABBR1*, respectively, suggests their binding affinities and superiority (particularly the former two) compared to the reference standards. This is because the higher the negative binding free energy, the better the fitness of that bioactive compound [86,87], and thus suggests an attraction between the CS secondary metabolites and the target genes [30]. While no related report of the possible stability of phytocompounds with the studied targets (particularly) *ADORA1* and/or superiority over reference standards against the target of concern, the overall findings of the molecular docking analysis provide an insight into the further investigation of CS bioactive metabolites as possible lead antidiabetic compounds.

Since molecular docking only predicts a metabolite's fitness at a protein active site [35], which limits its consideration as a measure of stability, binding free energy value calculations and MD simulation were employed to evaluate the compound-to-protein target systems and binding conformation data [45]. The highest negative ΔG_{bind} reported for gallicynoic acid B, dodecanedioc acid, and tetradecanedioc acid is indicative of significant binding affinity to *ADORA1*, *HCAR2*, and *GABBR1*, respectively, and could represent greater interactions with the targets compared to other investigated metabolites and standards. The observed lower binding free energy of some top-ranked metabolites against *ADORA1*, *HCAR2*, and *GABBR1* compared to metformin and resveratrol indicates their better potential to inhibit the respective targets relative to the standards used.

The binding of ligands (say CS phytoconstituents) may constitute structural or conformational changes in the respective targets, which could ultimately alter their biological activities [45,61]. The post-dynamics simulation evaluates the likely conformational changes of the protein as a result of the binding of the ligand, which are mostly determined by parameters such as RMSD (stability), RMSF (flexibility), RoG (compactness), SASA (degree of hydrophobic interactions), and intermolecular H bonding [88–90]. The revealed post-MDS analysis of the bound and unbound complex systems for the CS metabolites against *ADORA1*, *HCAR2*, and *GABBR1* targets in terms of the average RMSD (value) expresses the degree of convergence, stability, or deviations produced by a protein in a simulation system [91]. The lowest average RMSD values observed in ginsenoyne E–*ADORA1*, dodecanedioc acid–*HCAR2* and tetradecanedioc acid–*GABBR1* complexes are suggestive of the ability of the phytocompounds to enhance the stability of the target. Although the increased mean RMSD values observed in this study for most of the compounds including the reference standards, particularly against *ADORA1* and *HCAR2*, were above the satisfactory or acceptable 3.0 Å [89,92]. However, the average RMSD values of several phytoconstituents lower than or comparable to the respective standards may indicate that the abovementioned CS phytoconstituents may have better potential in promoting the structural stability of the genes [93,94], though an RMSD value above may suggest an unstable complex and

the inability of the compounds to inhibit the target protein (and, in this case, *ADORA1* and *HCAR2*) [88]. Meanwhile, the mean RMSD values of CS phytoconstituent–GABBR1 were less than 3.0 Å, suggestive of the good structural stability and compatibility of the metabolites with the gene [30,43,90,95].

The average RMSF (value) indicates the effect the bound compound has on active site residue behavior, with lower or higher alpha (α)-carbon (C) shifts indicating less or more flexible movements, respectively [94,96,97]. A lower RMSF value indicates that the created intra- and intermolecular bonds are more stable [97]. The reduced RMSF of quing hau sau against *ADORA1* compared to other phytocompounds with increased RMSF relative to resveratrol indicates lesser flexible movements, and thus, the greater stability of the complex [29]. Except for 4-hydroxycinnamic acid, the lesser average RMSF values observed in all the investigated phytocompounds against *HCAR2* compared to the standard *HCAR2* complexes indicated less flexible movements. This observation suggests the lesser flexibility of *HCAR2* amino acid residues, following the binding of the top-ranked metabolites, revealing their stronger attraction and ability to promote *HCAR2* amino acid residue stability [97–99]. Similarly, the reduced RMSF of methylisocitric acid and tetradecanedioc acid bound to *GABBR1* compared to metformin suggests less flexibility and stability (of the complexes) [35,44,93,95].

The RoG (value) evaluates the overall structural compactness of molecule–target complex systems, which may affect the biological properties due to induced changes from the ligand binding to a target [46,94,100,101]. The lowest or comparable average RoG values of the CS compounds (particularly, gallicynoic acid B, caffeic acid, and methylisocitric acid) against *ADORA1* and *HCAR2* relative to the standards, respectively, is indicative of a greater stability [30]. Typically, the lower RMSD of a ligand (such as CS compounds excluding cyperine) compared to resveratrol against *ADORA1* is suggestive of a superior stability compared to the latter.

During a simulation, the number of hydrogen bonds in a protein may be calculated, thus, providing insight into how ligand binding affects the protein's stability [90,94,102,103]. The observed reduction (for this study) in the number of H bonds in the CS compounds (most importantly, domesticoside) and reference standards against *ADORA1* following complex formation may be due to an intramolecular breakage of these bonds [94]. This observation is coherent with S'thebe et al.'s [97] report, in which ligand binding to the investigated protein resulted in the reduction in the intramolecular hydrogen bonding. However, the increased number of hydrogen bonds of the bound systems of the CS compounds (especially caffeic acid, tetradecanedioc acid, and resveratrol) against *HCAR2* and *GABBR1* (respectively), as observed in this study, may suggest that the ligands occupy part of the proteins' intramolecular space. This finding is in tandem with Aribisala and Sabiu's [45] report, in which ligand binding resulted in an increased number of hydrogen bonds [45].

Protein folding and variations in the surface area are analyzed using the solvent-accessible surface area (SASA), with higher values indicating more surface area and lower values suggesting less protein volume as the simulation progresses [30,44,104]. The lower average SASA values of gallicynoic acid B and ginsenoyne E following binding to *ADORA1* relative to the unbound system indicates the compactness and stability of the complexes, as it shows that more residues in the unbound state are exposed to the solvent [104,105]. The lowest SASA values as observed with the reference standards depicted the inferiority of the CS compounds in terms of their compactness and stability. While the superior compactness and stability of the CS compounds (especially caffeic and phaseic acids) were also confirmed against *HCAR2*, interestingly, the reference standards were inferior to these phytocompounds in terms of stability and compactness, owing to the high SASA values displaced. The reports of phytocompounds exhibiting better stability above the studied standard are well-established [30,61,98]. The comparable SASA values of quinic acid and resveratrol against *GABBR1*, which were the lowest relative to the unbound system and other bound systems, reflects the compactness and stability of the protein–ligand

complex [98]. While it is established that ligand–protein interactions may have a major effect on the SASA value [92], the SASA results may be seen to correspond with the findings from other studies, where the binding of the ligands enhanced the thermodynamic stability of the drug targets [29,30]. Above all, the findings (SASA) may be observed to be consistent with the revelations from other thermodynamic parameters (RMSD, ROG, and RMSF).

Various ligand–protein interactions were observed over the 120 ns MD simulation. The hydrogen bonds formed between a ligand and the protein target receptor determine the protein–ligand complex's stability [45,94,99]. Additionally, hydrogen bonds are indicative of a drug's specificity, metabolism, and adsorption [89]. Notwithstanding the aforementioned, other significant interactions like van der Waals and π-alkyl also contribute to the stability of the investigated complexes [29]. Although van der Waals interactions are weak in comparison to hydrogen bonds, when combined, the strength of the interaction increases significantly [104]. Interestingly, these major bonds form the backbone, contributing to the stability witnessed between CS compounds such as gallicynoic acid B, dodecanedioc acid, and tetradecanedioc acid and their respective target genes (*ADORA1*, *HCAR2*, and *GABBR1*) as compared to the reference standards. In fact, the lack of interaction between resveratrol and *ADORA1* and with *GABBR1* alludes to the structural instability of the complexes, which contributed to the observed low binding free energy of the respective complexes. Since it is a known fact the stability of a drug and/or ligand–protein complex contributes positively to the eventual pharmacological effect of the drug [105], the contribution of these bonds or interactions to the stability of gallicynoic acid B–, dodecanedioc acid–, and tetradecanedioc acid–target complexes highlights the possible superior therapeutic advantage of these CS compounds over the already available standard drug.

The lead compounds were characterized using quantitative chemical parameters to probe into their potential molecular properties of therapeutic importance. Frontier molecular orbitals, namely, the LUMO and HOMO, are critical for identifying the chemical reaction of a system [106]. The energy gap between a molecule's HOMO and LUMO influences its chemical reactivity, kinetic stability, optical polarizability, and chemical hardness–softness [99,107]. In particular, the reactivity of a molecule exhibits a direct correlation with its energy gap, indicating that a molecule with smaller dimensions possesses a higher propensity to react with other molecular entities, such as proteins and enzymes [107]. The lower energy gap observed in ginsenoyne E, caffeic acid, and quinic acid against *ADORA1*, *HCAR2*, and *GABBR1*, respectively, suggests their high reactivities relative to other CS metabolites' reactivity (Table 4). Furthermore, molecules characterized by a larger energy gap tend to display enhanced hardness, reducing their reactivity [99,108]. The chemical hardness serves as a robust metric for evaluating the chemical stability of a molecule and plays a crucial role in investigations pertaining to drug design elucidations [36,99]. Soft molecules are characterized by an elevated level of polarizability compared to hard molecules, primarily because of their reduced energy demand for excitation [108]. Expectedly, the high reactivity of ginsenoyne E, caffeic acid, and quinic acid against *ADORA1*, *HCAR2*, and *GABBR1*, respectively, could equally be linked to their high chemical softness value. On the contrary, the highest chemical hardness value exhibited by quing hau sau, dodecanedioc acid, and tetradecanedioc acid against *ADORA1*, *HCAR2*, and *GABBR1*, respectively, suggest their resistance to charge transfer and are the least reactive, as evidenced by their relatively high energy gap (Table S3). In addition, the observed reduced value of the chemical potential across all the compounds implies that the molecules exhibit diminished polarization. As a result, this molecule displays heightened resilience against electronic deformation when exposed to minor perturbations during a chemical reaction. A negative chemical potential value further supports the molecule's stability by inhibiting spontaneous decomposition [107,109]. Another cDFT descriptor is electronegativity, a fundamental metric that quantifies electron distribution within a given molecular entity [105]. The top-scoring compounds' readiness to accept electrons is revealed in their high electronegativity values against the investigated targets [109]. Moreover, the electrophilicity index quantifies a molecule's propensity to accept electrons from the surrounding environ-

ment, thus indicating its inherent capability to act as an electrophile [108]. A molecule may be categorized as a low electrophile if its electrophilicity value falls below 0.8 eV, while a moderate electrophile is characterized by an electrophilicity value ranging from 0.8 to 1.5 eV, and a molecule is deemed a heavy electrophile when its electrophilicity value exceeds 1.5 eV [36,109]. Interestingly, the electrophilicity index of the top-scoring compounds suggests a significant electrophile presence around the molecules except in cyperine, and dodecanedioc acid with a moderate electrophile presence.

5. Conclusions

The metabolomic profiling identified 128 secondary metabolites in various samples of CS (raw and three extracts) with qualitative and quantitative variance in the type and amounts of secondary metabolites. This is attributed to the polarity of the solvents, namely, water, hydro-ethanol, and ethanol, used for the extractions. The network pharmacology analysis identified 274 common overlapping target genes related to the CS phytoconstituents and T2DM. The top-scoring metabolites identified in the various extracts of CS are majorly involved in the modulation of the cAMP signaling pathway, which is implicated in glucose metabolism and homeostasis. The therapeutic target genes *ADORA1*, *HCAR2*, and *GABBR1* in the cAMP pathway were related to most of the CS phytoconstituents, with *ADORA1* being related to more than the others. This suggests the CS phytoconstituents modulate the activity of *ADORA1*, *HCAR2*, and *GABBR1* in the cAMP pathway. The molecular docking analysis identified several CS phytoconstituents as inhibitors of the target genes (*ADORA1*, *HCAR2*, and *GABBR1*) from the cAMP pathway. Based on the structural stability and affinity of several CS phytoconstituent–target gene complexes: gallicynoic acid B–*ADORA1*, dodecanedioc acid–*HCAR2* and tetradecanedioc acid—*GABBR1*, these abovementioned phytoconstituents have been identified as the key components of CS that behave as agonists of the cAMP signaling pathway. It is deduced that through the modulation of the therapeutic target genes *ADORA1*, *HCAR2*, and *GABBR1*, present in the cAMP signaling pathway, phytoconstituents present in CS could contribute to the maintenance of glucose homeostasis, the proper functioning of pancreas and pancreatic beta-cells, as well as the prevention of T2DM-associated secondary complications. Therefore, this study contributes to the use of CS as a therapeutic agent for the management of T2DM. Further in vitro and in vivo studies are recommended to validate the findings, and, interestingly, efforts are ongoing in this direction.

Supplementary Materials: The following supporting information can be downloaded at https://www.mdpi.com/article/10.3390/biology12121509/s1, Figure S1: Chromatograms produced (in duplicate) showing mass to charge and retention times of compounds, (a) raw premature CS extract, (b) raw mature CS extract, (c) aqueous premature CS extract, (d) aqueous mature CS extract, (e) hydroethanolic premature extract CS, (f) hydroethanolic mature CS extract, (g) ethanolic premature CS extract and (h) ethanolic mature CS extract; Figure S2: (a) Principal component analysis scores plot showing variance in CS secondary metabolites between the four extracts; (b) partial least square discriminant analysis (PLS-DA) loadings plot showing the differences in the amount of secondary metabolites present in the four samples of CS; Figure S3: Two-dimensional interaction plots of target gene *ADORA1* with bioactive constituents present in CS: (a) domesticoside, (b) quing hau sau, (c) cyperine, and (d) ginsenoyne E, over a 120 ns simulation; Figure S4: Two-dimensional interaction plots of target gene *HCAR2* with bioactive constituents present in CS: (a) 4-hydroxycinnamic acid, (b) sebacic acid, (c) phaseic acid, and (d) caffeic acid over a 120 ns simulation; Figure S5: Two-dimensional interaction plots of target gene *GABBR1* with bioactive constituents present in CS: (a) methylisocitric acid, (b) dodecanedioc acid, (c) xi-2,2,6,trimethyl-1,4-cyclohexanedione, and (d) quinic acid, over a 120 ns simulation. Table S1: Bioactive secondary metabolites identified in various extracts of CS through UPLC-MS analysis; Table S2: Result of CS bioactive compounds following Lipinski's rule of 5 experimentation; Table S3: Frontier molecular orbitals for the top-scoring compounds against *ADORA1*, *HCAR2*, *GABBR1*.

Author Contributions: A.A. was involved in the methodology, formal analysis, data curation, and preparation of original draft; A.A.L. was involved in the software and data curation; F.O.B. was

involved in the review and editing of the draft; N.P.M. was involved in the experimentation co-supervision and S.S. conceptualized and administered the project, supervised, and provided funding. All authors have read and agreed to the published version of the manuscript.

Funding: The authors especially acknowledge the financial assistance of the Directorate of Research and Postgraduate Support, Durban University of Technology, the South African Medical Research Council (SAMRC) under a Self-Initiated Research Grant, the Technology Innovative Agency as well as the National Research Foundation (NRF) Research Development Grant for Rated Researchers (Grant number 120433) and the Competitive Programme for Rated Researchers Support (SRUG2204193723) to S. Sabiu. The views and opinions expressed in this paper are those of the authors and do not necessarily represent the official views of the funders.

Institutional Review Board Statement: Not applicable.

Informed Consent Statement: Not applicable.

Data Availability Statement: The data relating to the article are within the manuscript and in the supplementary files.

Acknowledgments: The assistance of the Directorate of Research and Postgraduate Support, Durban University of Technology, for the Master's Scholarship Scheme to A. Akoonjee is duly and thankfully acknowledged. The Centre for High Performance Computing (CHPC), Cape Town, South Africa is equally acknowledged for granting access to the computing software and modules used in this study.

Conflicts of Interest: The authors declared no known competing financial interest or personal relationship that could have appeared to influence the work reported in this paper.

References

1. Pheiffer, C.; Wyk, V.P.-V.; Joubert, J.D.; Levitt, N.; Nglazi, M.D.; Bradshaw, D. The prevalence of type 2 diabetes in South Africa: A systematic review protocol. *BMJ Open* **2018**, *8*, e021029. [CrossRef] [PubMed]
2. International Diabetes Federation (IDF). 2022. Available online: https://idf.org/about-diabetes/type-2-diabetes/ (accessed on 5 August 2023).
3. International Diabetes Federation (IDF). 2021. Available online: https://idf.org/our-network/regions-and-members/africa/members/south-africa/ (accessed on 5 August 2023).
4. Lankatillake, C.; Huynh, T.; Dias, D.A. Understanding glycaemic control and current approaches for screening antidiabetic natural products from evidence-based medicinal plants. *Plant Methods* **2019**, *15*, 105. [CrossRef] [PubMed]
5. Yagasaki, K.; Muller, C.J. The effect of phytochemicals and food bioactive compounds on diabetes. *Int. J. Mol. Sci.* **2022**, *23*, 7765. [CrossRef] [PubMed]
6. Paddy, V.; Van Tonder, J.J.; Steenkamp, V. The antidiabetic activity of a polyherbal tea mixture and its constituents in vitro. In Proceedings of the 17th World Congress of Basic and Clinical Pharmacology, Cape Town, South Africa, 13–18 July 2014; p. 13.
7. Sabiu, S.; O'Neill, F.H.; Ashafa, A.O.T. Toxicopathological evaluation of a 28-day repeated dose administration of *Zea mays* L. (Poaceae), *Stigma maydis* aqueous extract on key metabolic markers of Wistar rats. *Trans. R. Soc. S. Afr.* **2017**, *72*, 225–233. [CrossRef]
8. Hasanudin, K.; Hashim, P.; Mustafa, S. Corn silk (*Stigma maydis*) in healthcare: A phytochemical and pharmacological review. *Molecules* **2012**, *17*, 9697. [CrossRef] [PubMed]
9. Zhang, Y.; Wu, L.; Ma, Z.; Cheng, J.; Liu, J. Anti-diabetic, anti-oxidant and anti-hyperlipidemic activities of flavonoids from corn silk on STZ-induced diabetic mice. *Molecules* **2015**, *21*, 7. [CrossRef] [PubMed]
10. Sabiu, S.; O'Neill, F.H.; Ashafa, A.O.T. Kinetics of alpha amylase and alpha glucosidase inhibitory potentials of Zea mays Linnaeus (Poaceae), Stigma maydis aqueous extract: An in vitro assessment. *J. Ethnopharmacol.* **2016**, *183*, 1–8. [CrossRef] [PubMed]
11. Wang, K.J.; Zhao, J.L. Corn silk (*Zea mays* L.), a source of natural antioxidants with α-amylase, α-glucosidase, advanced glycation and diabetic nephropathy inhibitory activities. *Biomed. Pharmacother.* **2018**, *110*, 510–517. [CrossRef]
12. Singh, J.; Rasane, P.; Nanda, V.; Kaur, S. Bioactive compounds of corn silk and their role in management of glycaemic response. *J. Food Sci. Technol.* **2022**, *60*, 1695–1710. [CrossRef]
13. Shalihah, I.M.; Pamela, V.Y.; Kusumasari, S. Cornsilk tea extract as antidiabetic: A review. *Food Sci. Technol. J.* **2020**, *2202*, 66.
14. Pan, Y.; Wang, C.; Chen, Z.; Li, W.; Yuan, G.; Chen, H. Physicochemical properties and antidiabetic ef, fects of a polysaccharide from corn silk in high-fat diet and streptozotocin-induced diabetic mice. *Carbohydr. Polym.* **2017**, *164*, 370. [CrossRef]
15. Vijitha, T.P.; Saranya, D. Corn Silk-A medicinal boon. *Int. J. ChemTech. Res.* **2017**, *10*, 129.
16. Haldar, S.; Gan, L.; Tay, S.L.; Ponnalagu, S.; Henry, C.J. Postprandial glycemic and insulinemic effects of the addition of aqueous extracts of dried corn silk, cumin seed powder or tamarind pulp, in two forms, consumed with high glycemic index rice. *Foods* **2019**, *8*, 437. [CrossRef] [PubMed]

17. Guo, Q.; Chen, Z.; Santhanam, R.K.; Xu, L.; Gao, X.; Ma, Q.; Xue, Z.; Chen, H. Hypoglycemic effects of polysaccharides from corn silk (*Maydis stigma*) and their beneficial roles via regulating the PI3K/Akt signaling pathway in L6 skeletal muscle myotubes. *Int. J. Biol. Macromol.* **2019**, *121*, 981. [CrossRef]
18. Jia, Y.; Xue, Z.; Wang, Y.; Lu, Y.; Li, R.; Li, N.; Wang, Q.; Zhang, M.; Chen, H. Chemical structure and inhibition on α-glucosidase of polysaccharides from corn silk by fractional precipitation. *Carbohydr. Polym.* **2021**, *252*, 117185. [CrossRef] [PubMed]
19. Chaudhary, R.K.; Karoli, S.S.; Dwivedi, P.S.; Bhandari, R. Anti-diabetic potential of corn silk (*Stigma maydis*): An in-silico approach. *J. Diabetes Metab. Disord.* **2022**, *21*, 445. [CrossRef]
20. Alimin, L. Effects of corn silk (Stigma Maydis) against blood glucose levels of type 2 diabetes mellitus patients. *Bul. Farmatera* **2020**, *5*, 202. [CrossRef]
21. Agamah, F.E.; Mazandu, G.K.; Hassan, R.; Bope, C.D.; Thomford, N.E.; Ghansah, A.; Chimusa, E.R. Computational/in silico methods in drug target and lead prediction. *Brief. Bioinform.* **2020**, *21*, 1663. [CrossRef]
22. Koparde, A.A.; Doijad, R.C.; Magdum, C.S. Natural Products in Drug Discovery. In *Pharmacognosy-Medicinal Plants*; IntechOpen: London, UK, 2019.
23. Yin, B.; Bi, Y.M.; Fan, G.J.; Xia, Y.Q. Molecular mechanism of the effect of Huanglian Jiedu decoction on type 2 diabetes mellitus based on network pharmacology and molecular docking. *J. Diabetes Res.* **2020**, *2020*, 1–24. [CrossRef] [PubMed]
24. Shaker, B.; Ahmad, S.; Lee, J.; Jung, C.; Na, D. In silico methods and tools for drug discovery. *Comput. Biol. Med.* **2021**, *137*, 104851. [CrossRef]
25. Oh, K.K.; Adnan, M.; Cho, D.H. Network pharmacology of bioactives from *Sorghum bicolor* with targets related to diabetes mellitus. *PLoS ONE* **2020**, *15*, 0240873. [CrossRef] [PubMed]
26. An, W.; Huang, Y.; Chen, S.; Teng, T.; Shi, Y.; Sun, Z.; Xu, Y. Mechanisms of *Rhizoma Coptidis* against type 2 diabetes mellitus explored by network pharmacology combined with molecular docking and experimental validation. *Sci. Rep.* **2021**, *11*, 20849. [CrossRef] [PubMed]
27. Di, S.; Han, L.; An, X.; Kong, R.; Gao, Z.; Yang, Y.; Wang, X.; Zhang, P.; Ding, Q.; Wu, H.; et al. In silico network pharmacology and in vivo analysis of berberine-related mechanisms against type 2 diabetes mellitus and its complications. *J. Ethnopharmacol.* **2021**, *276*, 114180. [CrossRef] [PubMed]
28. Adnan, M.; Jeon, B.B.; Chowdhury, M.H.U.; Oh, K.K.; Das, T.; Chy, M.N.U.; Cho, D.H. Network pharmacology study to reveal the potentiality of a methanol extract of *Caesalpinia sappan* L. Wood against type-2 diabetes mellitus. *Life* **2022**, *12*, 277. [CrossRef] [PubMed]
29. Akoonjee, A.; Rampadarath, A.; Aruwa, C.E.; Ajiboye, T.A.; Ajao, A.A.N.; Sabiu, S. Network pharmacology-and molecular dynamics simulation-based bioprospection of *Aspalathus linearis* for type-2 diabetes care. *Metabolites* **2022**, *12*, 1013. [CrossRef] [PubMed]
30. Rampadarath, A.; Balogun, F.O.; Sabiu, S. Insights into the mechanism of action of *Helianthus annuus* (sunflower) seed essential oil in the management of type-2 diabetes mellitus using network pharmacology and molecular docking approaches. *Endocrines* **2023**, *4*, 327. [CrossRef]
31. Tran, M.N.; Lee, S. The molecular mechanisms of panax ginseng in treating type 2 diabetes mellitus: Network pharmacology analysis and molecular docking validation. *Evid.-Based Complement. Altern. Med.* **2022**, *2022*, 3082109. [CrossRef] [PubMed]
32. De Vivo, M.; Masetti, M.; Bottegoni, G.; Cavalli, A. Role of molecular dynamics and related methods in drug discovery. *J. Med. Chem.* **2016**, *59*, 4035. [CrossRef]
33. Abdullah, A.; Biswas, P.; Sahabuddin, M.; Mubasharah, A.; Khan, D.A.; Hossain, A.; Roy, T.; Rafi, N.M.R.; Dey, D.; Hasan, M.N.; et al. Molecular Dynamics simulation and pharmacoinformatic integrated analysis of bioactive phytochemicals from *Azadirachta indica* (Neem) to treat diabetes mellitus. *J. Chem.* **2023**, *2023*, 4170703. [CrossRef]
34. Rampogu, S.; Parameswaran, S.; Lemuel, M.; Lee, K. Exploring the therapeutic ability of fenugreek against type 2 diabetes and breast cancer employing molecular docking and molecular dynamics simulations. *Evid.-Based Complement. Altern. Med.* **2018**, *2018*, 1943203. [CrossRef]
35. Shode, F.O.; Uhomoibhi, J.O.O.; Idowu, K.A.; Sabiu, S.; Govender, K.K. Molecular dynamics study on selected bioactive phytochemicals as potential inhibitors of HIV-1 subtype C protease. *Metabolites* **2022**, *12*, 1155. [CrossRef] [PubMed]
36. Lanrewaju, A.A.; Enitan-Folami, A.M.; Nyaga, M.M.; Sabiu, S.; Swalaha, F.M. Metabolites profiling and cheminformatics bioprospection of selected medicinal plants against the main protease and RNA-dependent RNA polymerase of SARS-CoV-2. *J. Biomol. Struct. Dyn.* **2023**, 1–21, *Online ahead of print*. [CrossRef] [PubMed]
37. Ahmed, S.; Ali, M.C.; Ruma, R.A.; Mahmud, S.; Paul, G.K.; Saleh, M.A.; Alshahrani, M.M.; Obaidullah, A.J.; Biswas, S.K.; Rahman, M.M. Molecular Docking and dynamics simulation of natural compounds from betel leaves (*Piper betle* L.) for investigating the potential inhibition of alpha-amylase and alpha-glucosidase of type 2 diabetes. *Molecules* **2022**, *27*, 4526. [CrossRef] [PubMed]
38. Azevedo, A.S.D.; Seibert, J.B.; Amparo, T.R.; Antunes, A.D.S.; Sousa, L.R.D.; Souza, G.H.B.D.; Teixeira, L.F.M.; Vieira, P.M.D.A.; Santos, V.M.R.D.; Nascimento, A.M.D.; et al. Chemical constituents, antioxidant potential, antibacterial study and photoprotective activity of Brazilian corn silk extract. *Food Sci. Technol.* **2022**, *42*, e98421. [CrossRef]
39. El-Ghorab, A.; El-Massry, K.F.; Shibamoto, T. Chemical composition of the volatile extract and antioxidant activities of the volatile and nonvolatile extracts of Egyptian corn silk (*Zea mays* L.). *J. Agric. Food Chem.* **2007**, *55*, 9124. [CrossRef] [PubMed]
40. Tian, S.; Sun, Y.; Chen, Z. Extraction of flavonoids from corn silk and biological activities in vitro. *J. Food Qual.* **2021**, *2021*, 7390425. [CrossRef]

41. Magangana, T.P.; Stander, M.; Makunga, N.P. Effect of nitrogen and phosphate on in vitro growth and metabolite profiles of *Stevia rebaudiana* Bertoni (Asteraceae). *Plant Cell Tissue Organ Cult.* **2022**, *134*, 141. [CrossRef]
42. Magangana, T.P.; Makunga, N.P.; Fawole, O.A.; Stander, M.A.; Opara, U.L. Antioxidant, antimicrobial, and metabolomic characterization of blanched pomegranate peel extracts: Effect of cultivar. *Molecules* **2022**, *27*, 2979. [CrossRef]
43. Qian, L.; Xia, Z.; Zhang, M.; Han, Q.; Hu, D.; Qi, S.; Xing, D.; Chen, Y.; Zhao, X. Integrated bioinformatics-based identification of potential diagnostic biomarkers associated with diabetic foot ulcer development. *J. Diabetes Res.* **2021**, *2021*, 5445349. [CrossRef]
44. Aribisala, J.O.; Nkosi, S.; Idowu, K.; Nurain, I.O.; Makolomakwa, G.M.; Shode, F.O.; Sabiu, S. Astaxanthin-mediated bacterial lethality: Evidence from oxidative stress contribution and molecular dynamics simulation. *Oxidative Med. Cell. Longev.* **2021**, *2021*, 7159652. [CrossRef]
45. Aribisala, J.O.; Sabiu, S. Cheminformatics identification of phenolics as modulators of penicillin-binding protein 2a of *Staphylococcus aureus*: A structure-activity-relationship-based study. *Pharmaceutics* **2022**, *14*, 1818. [CrossRef] [PubMed]
46. Sabiu, S.; Idowu, K. An insight on the nature of biochemical interactions between glycyrrhizin, myricetin and CYP3A4 isoform. *J. Food Biochem.* **2022**, *46*, 13831. [CrossRef] [PubMed]
47. Ibeji, C.U.; Akintayo, D.C.; Oluwasola, H.O.; Akintemi, E.O.; Onwukwe, O.G.; Eziomume, O.M. Synthesis, experimental and computational studies on the anti-corrosion performance of substituted Schiff bases of 2-methoxybenzaldehyde for mild steel in HCl medium. *Sci. Rep.* **2023**, *13*, 3265. [CrossRef] [PubMed]
48. Zhong, Y.; Song, B.; Zheng, C.; Zhang, S.; Yan, Z.; Tang, Z.; Kong, X.; Duan, Y.; Li, F. Flavonoids from mulberry leaves alleviate lipid dysmetabolism in high fat diet-fed mice: Involvement of gut microbiota. *Microorganisms* **2020**, *8*, 860. [CrossRef] [PubMed]
49. Azwanida, N.N. A review on the extraction methods use in medicinal plants, principle, strength and limitation. *Med. Aromat. Plants* **2015**, *4*, 2167.
50. Nawaz, H.; Aslam, M.; Muntaha, S.T. Effect of solvent polarity and extraction method on phytochemical composition and antioxidant potential of corn silk. *Fee Radic. Antioxid.* **2019**, *9*, 5. [CrossRef]
51. Nurhanan, A.R.; Wi, W.R. Evaluation of polyphenol content and antioxidant activities of some selected organic and aqueous extracts of cornsilk (*Zea Mays* Hairs). *J. Med. Bioeng.* **2012**, *1*, 48–51.
52. Liu, J.; Wang, C.; Wang, Z.; Zhang, C.; Lu, S.; Liu, J. The antioxidant and free-radical scavenging activities of extract and fractions from corn silk (*Zea mays* L.) and related flavone glycosides. *Food Chem.* **2011**, *126*, 261. [CrossRef]
53. Min, O.J.; Sharma, B.R.; Park, C.M.; Rhyu, D.Y. Effect of myadis stigma water extract on adipogenesis and blood glucose in 3T3-L1 adipocytes and db/db mice. *Korean J. Pharmacogn.* **2011**, *2011*, 9.
54. Borhan, M.Z.; Ahmad, R.; Rusop, M.; Abdullah, S. Impact of nanopowders on extraction yield of *Centella asiatica*. *Adv. Mater. Res.* **2013**, *667*, 246. [CrossRef]
55. Haslina, M.E. Extract corn silk with variation of solvents on yield, total phenolics, total flavonoids and antioxidant activity. *Indones. Food Nutr. Prog.* **2017**, *14*, 21. [CrossRef]
56. Fougère, L.; Zubrzycki, S.; Elfakir, C.; Destandau, E. Characterization of corn silk extract using HPLC/HRMS/MS analyses and bioinformatic data processing. *Plants* **2023**, *12*, 721. [CrossRef] [PubMed]
57. Eid, H.M.; Thong, F.; Nachar, A.; Haddad, P.S. Caffeic acid methyl and ethyl esters exert potential antidiabetic effects on glucose and lipid metabolism in cultured murine insulin-sensitive cells through mechanisms implicating activation of AMPK. *Pharm. Biol.* **2017**, *55*, 2026. [CrossRef] [PubMed]
58. Omidi, M.; Ahangarpour, A.; Khorsandi, L.; Ramezani-AliAkbari, F. The antidiabetic and hepatoprotective effects of myricitrin on aged mice with D-galactose. *Gastroenterol. Hepatol. Bed Bench* **2020**, *13*, 247. [PubMed]
59. Streeper, R.T.; Louden, C.; Izbicka, E. Oral azelaic acid ester decreases markers of insulin resistance in overweight human male subjects. *In Vivo* **2020**, *34*, 1173. [CrossRef] [PubMed]
60. Abdel Hakam, A.; Khowailed, A.; Mohammed, M. Protective effect of p-coumaric acid on fructose induced- insulin resistance in albino rats. *Minia J. Med. Res.* **2021**, *32*, 1. [CrossRef]
61. Balogun, F.O.; Naidoo, K.; Aribisala, J.O.; Pillay, C.; Sabiu, S. Cheminformatics Identification and validation of dipeptidyl peptidase-iv modulators from shikimate pathway-derived phenolic acids towards interventive type-2 diabetes therapy. *Metabolites* **2023**, *12*, 937. [CrossRef] [PubMed]
62. Yang, H.; Yang, L. Targeting cAMP/PKA pathway for glycemic control and type 2 diabetes therapy. *J. Mol. Endocrinol.* **2016**, *52*, 93. [CrossRef]
63. Deb, D.K.; Bao, R.; Li, Y.C. Critical role of the cAMP-PKA pathway in hyperglycemia-induced epigenetic activation of fibrogenic program in the kidney. *FASEB J.* **2017**, *31*, 2065. [CrossRef]
64. Chen, P.C.; Kryukova, Y.N.; Shyng, S.L. Leptin regulates KATP channel trafficking in pancreatic beta-cells by a signaling mechanism involving AMP-activated protein kinase (AMPK) and cAMP-dependent protein kinase (PKA). *J. Biol. Chem.* **2013**, *288*, 34098. [CrossRef]
65. Rhee, S.; Wood, V.; Dolinski, K.; Draghici, S. Use and misuse of the gene ontology annotations. *Nat. Rev. Genet.* **2008**, *9*, 50.
66. Huang-Doran, I.; Zhang, C.Y.; Vidal-Puig, A. Extracellular vesicles: Novel mediators of cell communication in metabolic disease. *Trends Endocrinol. Metaolism* **2017**, *28*, 3. [CrossRef] [PubMed]
67. Blake, J.A.; Baldarelli, R.; Kadin, J.A.; Richardson, J.E.; Smith, C.L.; Bult, C.J.; Mouse Genome Database Group. Mouse Genome Database (MGD): Knowledgebase for mouse-human comparative biology. *Nucleic Acids Reserves* **2021**, *2021*, 981. [CrossRef] [PubMed]

68. Li, C.; Yang, W.; Meng, Y.; Feng, L.; Sun, L.; Li, Z.; Liu, X.; Li, M. Exploring the therapeutic mechanism of Banxia Xiexin decoction in mild cognitive impairment and diabetes mellitus: A netwrk pharmacology approach. *Metab. Brain Dis.* **2023**, *38*, 2315–2325. [CrossRef] [PubMed]
69. Keerthikumar, S.; Chisanga, D.; Ariyaratne, D.; Al Saffar, H.; Anand, S.; Zhao, K.; Samuel, M.; Pathan, M.; Jois, M.; Chilamkurti, N.; et al. ExoCarta: A web-based compendium of exosomal cargo. *J. Mol. Biol.* **2016**, *428*, 688. [CrossRef] [PubMed]
70. Pardo, F.; Villalobos-Labra, R.; Sobrevia, B.; Toledo, F.; Sobrevia, L. Extracellular vesicles in obesity and diabetes mellitus. *Mol. Asp. Med.* **2018**, *60*, 81. [CrossRef] [PubMed]
71. Jacobson, D.; Shyng, S. Ion channels of the islets in type 2 diabetes. *J. Mol. Biol.* **2019**, *432*, 1326. [CrossRef] [PubMed]
72. Liang, W.; Sun, F.; Zhao, Y.; Shan, L.; Lou, H. Identification of susceptibility modules and genes for cardiovascular disease in diabetic patients using WGCNA analysis. *J. Diabetes Res.* **2020**, *2020*, 4178639. [CrossRef]
73. Zhang, M.; Wang, L.; Chen, Z. Research progress of extracellular vesicles in type 2 diabetes and its complications. *Diabet. Med.* **2022**, *39*, 14865. [CrossRef]
74. Haisu, M.; Hongvu, Z. Drug target inference through pathway analysis of genomics data. *Adv. Drug Deliv. Rev.* **2013**, *65*, 966–972.
75. Liu, S.N.; Liu, Q.; Sun, S.J.; Li, C.N.; Huan, Y.; Chen, Y.T.; Wang, R.Y.; Xia, X.J.; Liu, Z.H.; Liu, Y.L.; et al. Anti-diabetic effects of the fraction of alkaloids from *Ramulus Mori*, an innovative Sangzhi alkaloids as an α-glucosidase inhibitor. *Acta Pharm. Sin.* **2019**, *12*, 1225–1233.
76. Hu, S.; Chen, S.; Li, Z.; Wang, Y.; Wang, Y. Research on the potential mechanism of Chuanxiong Rhizoma on treating diabetic nephropathy based on network pharmacology. *Int. J. Med. Sci.* **2020**, *17*, 2240. [CrossRef] [PubMed]
77. Lv, Q.; Lin, J.; Wu, X.; Pu, H.; Guan, Y.; Xiao, P.; He, C.; Jiang, B. Novel active compounds and the anti-diabetic mechanism of mulberry leaves. *Front. Pharmacol.* **2022**, *13*, 986931. [CrossRef]
78. Zhang, L.; Han, L.; Wang, X.; Wei, Y.; Zheng, J.; Zhao, L.; Tong, X. Exploring the mechanisms underlying the therapeutic effect of *Salvia miltiorrhiza* in diabetic nephropathy using network pharmacology and molecular docking. *Biosci. Rep.* **2021**, *41*, BSR20203520. [CrossRef] [PubMed]
79. Newman, J.C.; Verdin, E. β-hydroxybutyrate: Much more than a metabolite. *Diabetes Res. Clin. Pract.* **2014**, *106*, 173. [CrossRef]
80. Yip, L.; Taylor, C.; Whiting, C.C.; Fathman, C.G. Diminished adenosine A1 receptor expression in pancreatic α-cells may contribute to the pathology of type 1 diabetes. *Diabetes* **2013**, *62*, 4208. [CrossRef] [PubMed]
81. Dobbins, R.L.; Shearn, S.P.; Byerly, R.L.; Gao, F.F.; Mahar, K.M.; Napolitano, A.; Nachbaur, G.J.; Le Monnier de Gouville, A.C. GSK256073, a selective agonist of G-protein coupled receptor 109A (GPR109A) reduces serum glucose in subjects with type 2 diabetes mellitus. *Diabetes Obes. Metab.* **2013**, *15*, 1013. [CrossRef]
82. Gambhir, D.; Ananth, S.; Veeranan-Karmegam, R.; Elangovan, R.; Hester, S.; Jennings, E.; Offermanns, S.; Nussbaum, J.J.; Smith, S.B.; Thangaraju, M.; et al. GPR109A as an anti-inflammatory receptor in retinal pigment epithelial cells and its relevance to diabetic retinopathy. *Retin. Cell Biol.* **2012**, *53*, 2208. [CrossRef]
83. Liu, F.; Fu, Y.; Wei, C.; Chen, Y.; Ma, S.; Xu, W. The expression of GPR109A, NF-kB and IL-1β in peripheral blood leukocytes from patients with type 2 diabetes. *Ann. Clin. Lab. Sci.* **2014**, *44*, 443.
84. Rachdi, L.; Maugein, A.; Pechberty, S.; Armanet, M.; Hamroune, J.; Ravassard, P.; Marullo, S.; Albagli, O.; Scharfmann, R. Regulated expression and function of the GABAB receptor in human pancreatic beta cell line and islets. *Sci. Rep.* **2020**, *10*, 13469. [CrossRef]
85. Lyu, Z.; Zhao, M.; Atanes, P.; Persuad, S.J. Quantification of changes in human islet G protein-coupled receptor mRNA expression in obesity. *Diabet. Med.* **2022**, *39*, 14974. [CrossRef]
86. Fan, J.; Fu, A.; Zhang, L. Progress in molecular docking. *Quant Biol.* **2019**, *7*, 80–83. [CrossRef]
87. Alvarado-Díaz, C.S.; Gutiérrez-Méndez, N.; Mendoza-López, M.L.; Rodríguez-Rodríguez, M.Z.; Quintero-Ramos, A.; Landeros-Martínez, L.L.; Rodríguez-Valdez, L.M.; Rodríguez-Figueroa, J.C.; Pérez-Vega, S.; Salmeron-Ochoa, I.; et al. Inhibitory effect of saccharides and phenolic compounds from maize silks on intestinal α-glucosidases. *J. Food Biochem.* **2019**, *43*, 12896. [CrossRef]
88. Rosenberg, M.S. *Sequence Alignment: Methods, Models, Concepts and Strategies*; University of California Press: Oakland, CA, USA, 2009. [CrossRef]
89. Du, X.; Li, Y.; Xia, Y.L.; Ai, X.M.; Liang, J.; Sang, P.; Ji, X.L.; Liu, S.Q. Insights into Protein-Ligand Interactions: Mechanisms, Models, and Methods. *Int. J. Mol. Sci.* **2016**, *17*, 144. [CrossRef] [PubMed]
90. Nayak, C.; Chandra, I.; Singh, S.K. An in silico pharmacological approach toward the discovery of potent inhibitors to combat drub resistant HIV-1 proteas variants. *J. Cell. Biochem.* **2018**, *120*, 9063–9081. [CrossRef] [PubMed]
91. Perelson, A.S. Modelling viral and immune system dynamics. *Nat. Rev. Immunol.* **2002**, *2*, 28–36. [CrossRef] [PubMed]
92. Ramírez, D.; Caballero, J. Is it reliable to use common molecular docking methods for comparing the binding affinities of enantiomer pairs for their protein target? *Int. J. Mol. Sci.* **2016**, *17*, 525. [CrossRef] [PubMed]
93. Hess, B. Convergence of sampling in protein simulations. *Phys. Rev.* **2002**, *65*, 031910. [CrossRef]
94. Fahad, M.; Al-Khodairy, M.; Kalim, A.; Khan, M.K.; Manogaran, S.P.; Salman, A.; Jamal, M.A. In Silico Prediction of Mechanism of Erysolin-induced Apoptosis in Human Breast Cancer Cell Lines. *Am. J. Bioinform.* **2013**, *3*, 62.
95. Murali, M.; Ahmed, F.; Gowtham, H.G.; Aribisala, J.O.; Abdulsalam, R.A.; Shati, A.A.; Alfaifi, M.Y.; Sayyed, R.Z.; Sabiu, S.; Amruthesh, K.N.; et al. Exploration of CviR-mediated quorum sensing inhibitors from *Cladosporium spp.* against *Chromobacterium violaceum* through computational studies. *Sci. Rep.* **2023**, *13*, 15505. [CrossRef] [PubMed]

96. Mandal, S.K.; Kumar, B.K.; Sharma, P.K.; Murugesan, S.; Deepa, P.R. In silico and in vitro analysis of PPAR–α/γ dual agonists: Comparative evaluation of potential phytochemicals with anti-obesity drug orlistat. *Comput. Biol. Med.* **2022**, *147*, 105796. [CrossRef]
97. S'thebe, N.W.; Aribisala, J.O.; Sabiu, S. Cheminformatics bioprospection of sunflower seeds' oils against quorum sensing system of *Pseudomonas aeruginosa*. *Antibiotics* **2023**, *12*, 504. [CrossRef] [PubMed]
98. Sabiu, S.; Balogun, F.O.; Amoo, O. Phenolics profiling of *Carpobrotus edulis* (L.) NE Br. and insights into molecular dynamics of their significance in type 2 diabtes therapy and its retinopathy complication. *Molecules* **2021**, *26*, 4867. [CrossRef] [PubMed]
99. Rampadarath, A.; Aribisala, J.O.; Makunga, N.P.; Mazibuko-Mbeje, S.; Sabiu, S. Molecular bioprospection of *Helianthus annuus* L. (sunflower) cypsela for antidiabetic therapeutics through network pharmacology, density functional theory and molecular dynamics simulation. *S. Afr. J. Bot.* **2023**, *162*, 72. [CrossRef]
100. Joshi, T.; Sharma, P.; Joshi, T.; Pundir, H.; Mathpal, S.; Chandra, S. Structure-based screening of novel lichen compounds against SARS Coronavirus main protease (Mpro) as potentials inhibitrs of COVID-19. *Mol. Divers.* **2021**, *25*, 1665. [CrossRef] [PubMed]
101. Kehinde, I.; Ramharack, P.; Nlooto, M.; Gordon, M. The pharmacokinetic properties of HIV-1 protease inhibitors: A computational perspective on herbal phytochemicals. *Heliyon* **2019**, *5*, 02565. [CrossRef] [PubMed]
102. Jairajpuri, D.S.; Hussain, A.; Nasreen, K.; Mohammad, T.; Anjum, F.; Rehman, M.T.; Hasan, G.M.; Alajmi, M.F.; Hassan, M.I. Identification of natural compounds as potent inhibitors of SARS-CoV-2 main protease using combined docking and molecular dynamics simulations. *Saudi J. Biol. Sci.* **2021**, *28*, 2423. [CrossRef] [PubMed]
103. Mousavi, S.S.; Karami, A.; Haghighi, T.M.; Tumilaar, S.G.; Fatimawali, I.R.; Mahmud, S.; Celik, I.A.; Agagündüz, D.; Tallei, T.E.; Emran, T.B. In Silico evaluation of iranian medicinal plant phytoconstituents as inhibitors against main protease and the receptor-binding domain of SARS-CoV-2. *Molecules* **2021**, *26*, 5724. [CrossRef]
104. Santra, B.; Klimeš, J.; Alfe, D.; Tkatchenko, A.; Slater, B.; Michaelides, A.; Car, R.; Scheffler, M. Hydrogen bonds and van der Waals forces in ice at ambient and high pressures. *Phys. Rev. Lett.* **2011**, *107*, 185701. [CrossRef]
105. Munnangi, S.R.; Youssef, A.A.A.; Narala, N.; Lakkala, P.; Narala, S.; Vemula, S.K.; Repka, M. Drug complexes: Perspective from academic research and pharmaceutical market. *Pharm. Res.* **2023**, *40*, 1519–1540. [CrossRef]
106. Prasad, O.; Sinha, L.; Misra, N.; Narayan, V.; Kumar, N.; Pathak, J. Molecular structure and vibrational study on 2, 3-dihydro-1H-indene and its derivative 1H-indene-1, 3 (2H)-dione by density functional theory calculations. *J. Mol. Struct. Theochem* **2010**, *940*, 82. [CrossRef]
107. Akintemi, E.O.; Govender, K.K.; Singh, T. A DFT study of the chemical reactivity properties, spectroscopy and bioactivity scores of bioactive flavonols. *Comput. Theor. Chem.* **2022**, *1210*, 113658. [CrossRef]
108. Mountessou, B.Y.G.; Ngouonpe, A.W.; Mbobda, A.S.W.; Akintemi, E.O.; Stammler, H.-G.; Kouam, S.F.; Tchouankeu, J.C.; Lenta, B.N.; Sewald, N.; Singh, T. Structural analysis and molecular docking study of pachypodostyflavone: A potent anti-onchocerca. *J. Mol. Struct.* **2023**, *2023*, 136003. [CrossRef]
109. Lakhera, S.; Devlal, K.; Ghosh, A.; Chowdhury, P.; Rana, M. Modelling the DFT structural and reactivity study of feverfew and evaluation of its potential antiviral activity against COVID-9 using molecular docking and MD simulations. *Chem. Pap.* **2022**, *76*, 2759. [CrossRef]

Supplementary materials

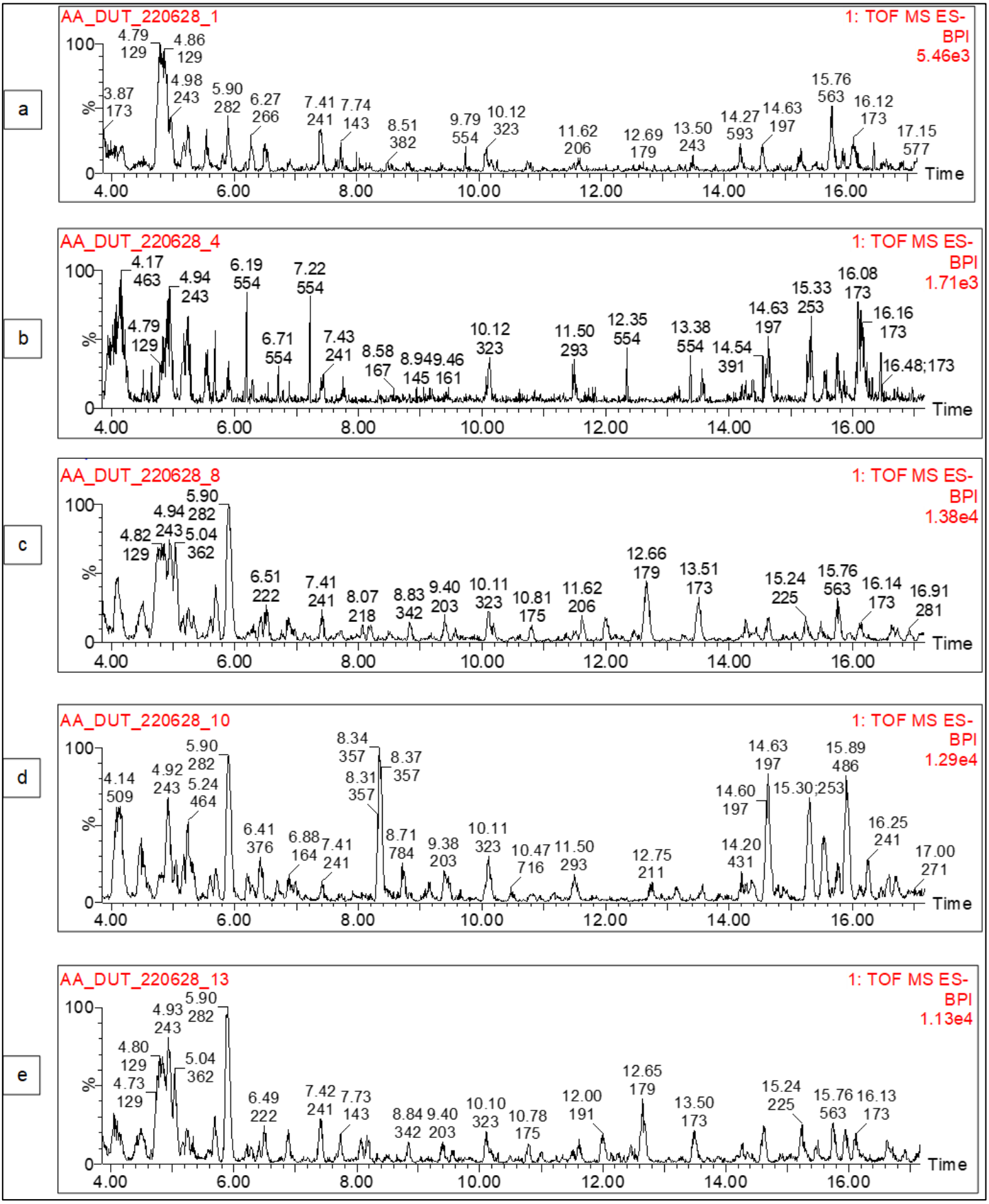

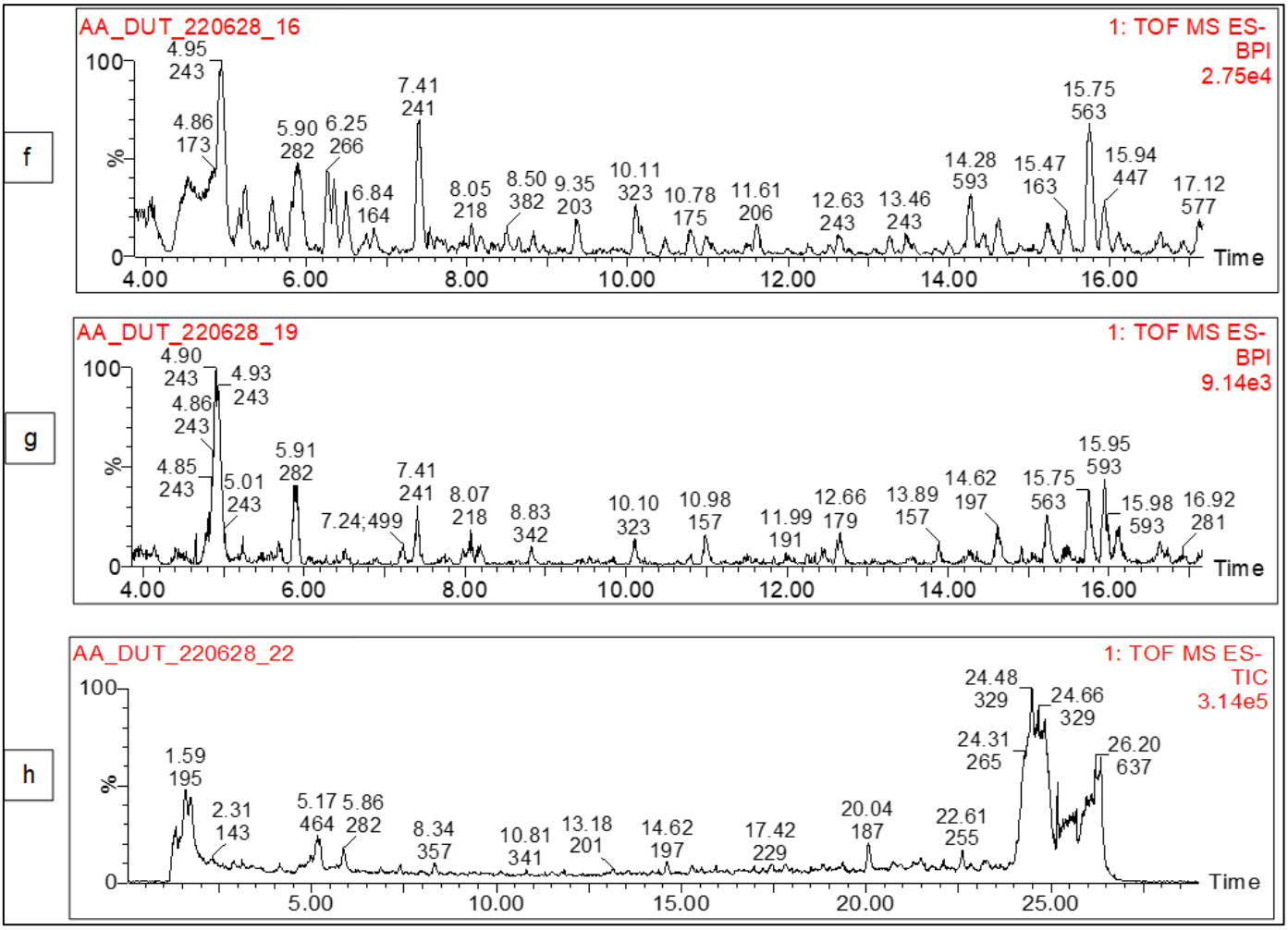

Figure S1: Examples of chromatograms produced showing mass to charge and retention times of compounds found in a) raw premature CS, b) raw mature CS as well as CS extracts; c) aqueous extract of premature CS, d) aqueous extract of mature CS, e) hydroethanolic extract of premature CS, f) hydroethanolic extract of mature CS, g) ethanolic extract of premature CS and h) ethanolic extract of mature CS

Table 1: Bioactive secondary metabolites identified in various extracts of CS through UPLC-MS analysis

Compound number	Identity	Average retention time (minute)	m/z [M - H]$^-$
1	(7'R)-(+)-Lyoniresinol 9'-glucoside	4.07	581.22
2	Estriol-16-Glucuronide	4.15	509.20
3	Ascorbic acid	4.31	175.02
4	Methylisocitric acid	4.39	205.03
5	Citraconic acid	4.52	129.02
6	Oxalosuccinic acid	4.98	189.01
7	Pinocembrin 7-apiosyl-(1->5)-apiosyl-(1->2)-glucoside;5,7-Dihydroxyflavanone 7-apiosyl-(1->5)-apiosyl-(1->2)-glucoside	4.99	681.21
8	Mevalonic acid	5.09	147.07
9	D-2-Hydroxyglutaric acid	5.18	147.03
10	(2R,3S)-2,3-dimethylmalic acid	5.24	161.04
11	UNPD109129	6.35	251.08

12	Glutaric acid	6.15	131.03
13	Cinnamic acid	6.85	147.04
14	(6E)-1-(4-hydroxyphenyl)-7-phenylhepta-4,6-dien-3-one	8.45	277.13
15	Vanillic acid	8.55	167.03
16	1-O-vanilloyl-beta-D-glucose	8.55	329.09
17	Isorhamnetin 3-(6"-malonylglucoside)	8.64	563.10
18	Saccharumoside C	9.08	461.13
19	7-hydroxy-4-{3-oxo-3H-benzo[f]chromen-2-yl}-2H-chromen-2-one	9.14	355.06
20	Sarmentose	9.45	161.08
21	CNP0447999	9.57	353.08
22	1-O-Caffeoylglucose	9.75	341.09
23	1-O-Galloylglycerol	10.05	243.05
24	C00051555	10.11	323.13
25	3-Isopropylmalate	10.79	175.06
26	Diaportinic acid	10.82	279.05
27	Benzyl beta-D-glucopyranoside;(-)-Benzyl-O-beta-D-glucopyranoside	11.15	269.10
28	Domesticoside	11.35	343.10
29	Dihydrophaseic acid 4'-O-beta-D-glucopyranoside	11.37	443.19
30	Ketoleucine	11.47	129.05
31	Aesculin	11.47	339.07
32	Chlorogenic acid	12.00	353.09
33	Quinic acid	12.00	191.06
34	Cudraphenone A	12.23	363.16
35	Pimelic acid	12.26	159.07
36	(-)-6-((2S,3R,4R,5S,6R)-3,4-dihydroxy-6-(hydroxymethyl)-5-methoxytetrahydro-2H-pyran-2-yloxy)-8-hydroxy-3-methyl-1H-isochromen-1-one	12.46	367.10
37	(-)-11-hydroxy-9,10-dihydrojasmonic acid 11-beta-D-glucoside	12.52	389.18
38	Caffeic acid	12.65	179.03
39	5-Carboxyvanillic acid	12.73	211.02
40	Phellodendric acid A;(+)-Phellodendric acid A	12.75	203.09
41	(-)-Epigallocatechin	13.27	305.07
42	D-Leucic acid	13.29	131.07
43	cis-Aconitic acid	13.50	173.01
44	MINEs-320976	14.20	431.19
45	Loganic acid	14.25	375.13
46	Astragalin 7-rhamnoside	14.27	593.15
47	Quing hau sau; quinghaosu; artemisinin	14.35	281.14
48	3-Hydroxy-4-butanolide	14.43	263.08
49	Annularin A;(+)-Annularin A	14.62	197.08
50	Traumatic acid	14.78	227.13
51	Methyl geranate	14.87	181.12
52	3-Hydroxytetradecanedioic acid	14.87	273.17
53	Dihydrophaseic acid	14.94	281.14
54	Tuberonic acid	15.24	225.11
55	Daldiniapyrone	15.29	253.11

56	4-Hydroxycinnamic acid	15.48	163.04
57	Monascusone A	15.54	253.11
58	Acetovanillone;Apocynin	15.60	165.05
59	Apiin	15.76	563.14
60	Quercitrin	15.95	447.09
61	2-Hydroxydecanedioic acid	16.18	217.11
62	UNPD221406	16.24	241.11
63	Cichorioside M;(+)-Cichorioside M	16.62	427.19
64	Austricin;8-Deacetylmatricarin;Desacetylmatricarin	16.71	261.12
65	trans-Ferulic acid	17.09	193.05
66	UNPD19396	17.12	577.15
67	UNPD77208	17.21	271.15
68	Nepetaside	17.24	345.16
69	Dodecanedioic acid	17.42	229.14
70	Kaempferitrin	17.55	577.15
71	Chrysoeriol 4',7-diglucuronide	17.68	651.12
72	erythronolide B	17.73	401.25
73	UNPD230015	17.82	263.06
74	3-Hydroxysebacic acid	17.84	217.11
75	Tricin 7-diglucuronoside	17.96	681.13
76	Esculetin	18.08	177.02
77	ethyl 5-[(2,5-dimethylphenyl)methoxy]-2-phenyl-1-benzofuran-3-carboxylate	18.09	399.16
78	xi-2,2,6-Trimethyl-1,4-cyclohexanedione	18.25	153.09
79	Quercetin 3-(2",3",4"-triacetylgalactoside)	18.31	589.12
80	[4]-Gingerol	18.84	265.14
81	Phaseic acid	18.56	279.12
82	Diaportinol	18.60	265.07
83	Herbacetin 7-(6"-quinoylglucoside)	18.68	637.14
84	12-deoxyerythronolide A	19.05	401.25
85	UNPD156113	19.09	605.12
86	Mirificin	19.15	547.14
87	Phaseolic acid	19.24	261.13
88	Curvularol	19.37	265.14
89	(+)-(S)-Carvone	19.65	149.10
90	Kaempferol 3-rhamnoside 7-galacturonide	19.87	607.13
91	Azelaic acid	20.07	187.10
92	Kaempferol 3-rhamnoside 7-galacturonide	20.29	607.13
93	Stagonolide F;(-)-Stagonolide F	20.68	183.10
94	Isowertin 2"-rhamnoside	20.73	1183.34
95	UNPD223815	20.86	255.16
96	9-hydroxynonanoic acid	20.89	173.12
97	Maysin	20.94	1151.29
98	5,7,4'-Trihydroxy-3'-methoxyflavone; Luteolin 3'-methyl ether 7-glucuronide	21.01	475.09
99	Quercetin 3-O-(6"-acetyl-glucoside)	21.14	505.10
100	Blennin D	21.15	265.14

101	10-Deoxygeniposidic acid	21.27	357.12
102	Gallicynoic acid F;(-)-Gallicynoic acid F	21.41	343.21
103	Pandangolide 1a;(-)-Pandangolide 1a	21.46	243.12
104	4-Hydroxynonenal	21.57	155.11
105	Tetradecanedioic acid	21.76	257.17
106	(R)-7-butyl-6,8-dihydroxy-3-[(3E)-pent-3-en-1-yl]-3,4-dihydroisochromen-1-one	21.82	303.16
107	Genistin	21.82	431.10
108	p-Coumaroyl malic acid	20.85	282.11
109	Kaempferol 3-[2'''-acetyl-alpha-L-arabinopyranosyl-(1->6)-galactoside]	21.94	621.14
110	Cyperine	22.09	259.10
111	(+)-Cnicin; Cnicin	22.11	377.16
112	(S)-Abscisic acid	22.20	263.13
113	Sydnic acid; Sydonic acid	22.23	265.14
114	Gallicynoic acid A;(+)-Gallicynoic acid A	22.81	253.14
115	Apigenin 7-O-(6''-O-acetylglucoside)	22.85	473.11
116	UNPD127537	23.18	255.16
117	olivetol	23.21	179.11
118	Ginsenoyne E	23.29	303.16
119	Caffeoyl tartaric acid	23.33	312.12
120	Luteolin 3'-methyl ether 7-glucuronide	23.48	265.14
121	UNPD205010	23.48	343.17
122	Maysin 3'-methyl ether	23.51	589.15
123	Artemin	23.66	265.15
124	Gallicynoic acid B	23.69	267.16
125	Aspergillide A	23.80	253.14
126	(S)-Oleuropeic acid	23.89	183.10
127	Sebacic acid	23.89	201.11
128	7-Acetoxy-5,6-dimethoxycoumarin	17.82	263.0574

a

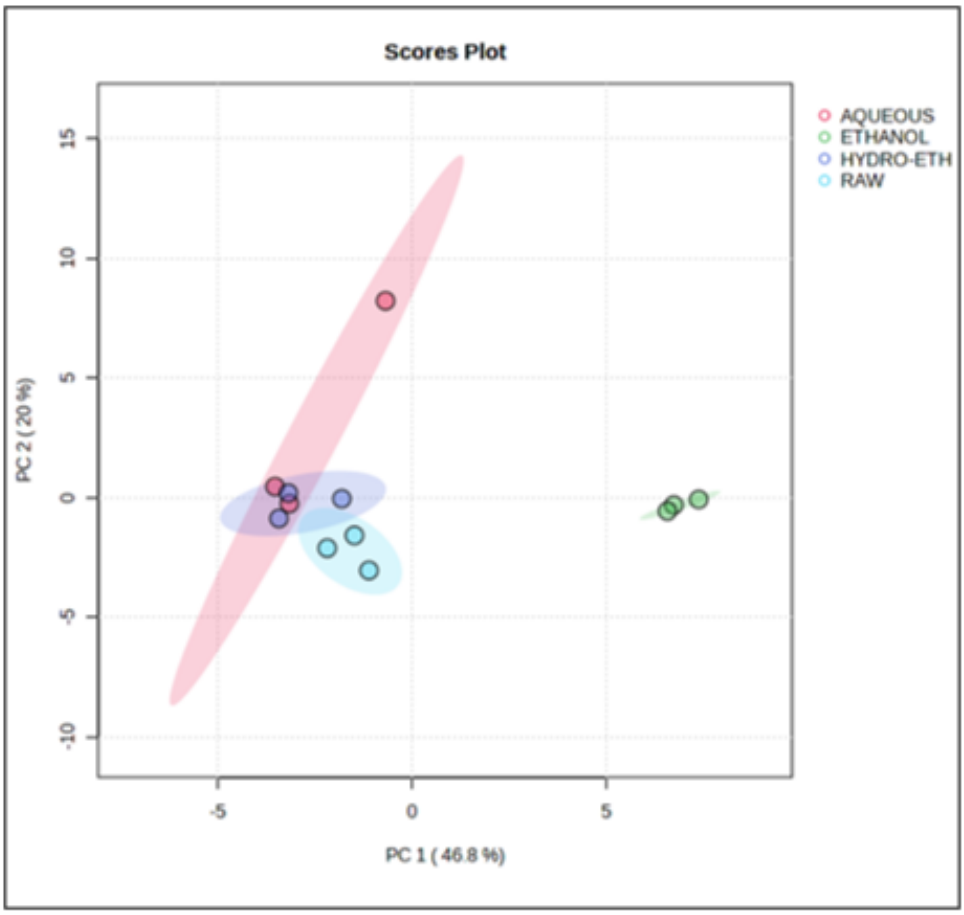
Scores Plot
AQUEOUS
ETHANOL
HYDRO-ETH
RAW
PC 2 (20 %)
PC 1 (46.8 %)
15
10
5
0
-5
-10
-5
0
5

b

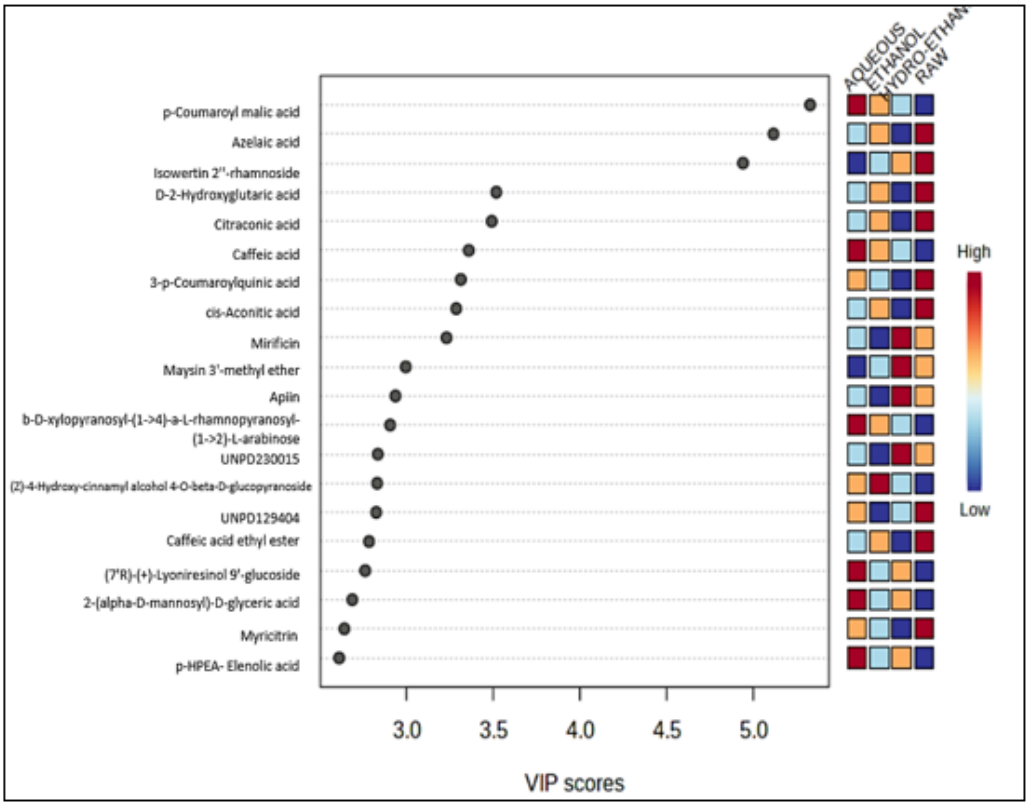
p-Coumaroyl malic acid
Azelaic acid
Isowertin 2''-rhamnoside
D-2-Hydroxyglutaric acid
Citraconic acid
Caffeic acid
3-p-Coumaroylquinic acid
cis-Aconitic acid
Mirificin
Maysin 3'-methyl ether
Apiin
b-D-xylopyranosyl-(1->4)-a-L-rhamnopyranosyl-(1->2)-L-arabinose
UNPD230015
(Z)-4-Hydroxy-cinnamyl alcohol 4-O-beta-D-glucopyranoside
UNPD129404
Caffeic acid ethyl ester
(7'R)-(+)-Lyoniresinol 9'-glucoside
2-(alpha-D-mannosyl)-D-glyceric acid
Myricitrin
p-HPEA- Elenolic acid
AQUEOUS
ETHANOL
HYDRO-ETHAN
RAW
High
Low
3.0
3.5
4.0
4.5
5.0
VIP scores

Figure S2: a) Principal component analysis scores plot showing variance in CS secondary metabolites between the four extracts; b) Partial least square discriminant analysis (PLS-DA) loadings plot showing the differences in the amount of secondary metabolites present in the four samples of CS. Red indicates high prevalence and blue indicates low prevalence.

Table S2: Number of Lipinski's violations of CS bioactive compounds

Compound number	Formula	Molecular weight (g/mol)	#H-bond acceptors	#H-bond donors	iLOGP (octanol/ water partition coefficient)	Lipinski #violations
1	$C_{28}H_{38}O_{13}$	582.59	13	7	4.71	3
2	$C24H32O_9$	464.51	9	6	1.67	1
3	$C_6H_8O_6$	176.12	6	4	0.39	0
4	$C_7H_{10}O_7$	206.15	7	4	-0.94	0
5	$C_5H_6O_4$	130.10	4	2	0.46	0
6	$C_6H_6O_7$	190.11	7	3	-0.71	0
7	$C_{31}H_{38}O_{17}$	682.62	17	9	2.27	3
8	$C_6H_{12}O_4$	148.16	4	3	0.39	0
9	$C_5H_8O_5$	148.11	5	3	0.18	0
10	$C_6H_{10}O_5$	162.14	5	3	0.34	0
11	$C_9H_{16}O_8$	252.22	8	5	0.37	0
12	$C_5H_8O_4$	132.11	4	2	0.45	0
13	$C_9H_8O_2$	148.16	2	1	1.55	0
14	$C_{19}H_{18}O_2$	278.35	2	1	2.79	0
15	$C_8H_8O_4$	168.15	4	2	1.40	0
16	$C_{14}H_{18}O_9$	330.29	9	5	1.88	0
17	$C_{25}H_{24}O_{15}$	564.45	15	7	1.77	3
18	$C_{19}H_{26}O_{13}$	462.40	13	7	1.35	2
19	$C_{22}H_{12}O_5$	356.33	5	1	2.52	0
20	$C_7H_{14}O_4$	162.18	4	2	0.94	0
21	$C_{23}H_{14}O_4$	354.35	4	1	2.41	0
22	$C_{15}H_{18}O_9$	342.30	9	6	0.23	1
23	$C_{10}H_{12}O_7$	244.20	7	5	0.63	0
24	$C_{13}H_{24}O_9$	324.32	9	5	1.95	0
25	$C_7H_{12}O_5$	176.17	5	3	0.24	0
26	$C_{13}H_{12}O_7$	280.23	7	3	1.54	0
27	$C_{13}H_{18}O_6$	270.28	6	4	1.60	0
28	$C_{15}H_{20}O_9$	344.31	9	5	2.05	0
29	$C_{21}H_{32}O_{10}$	444.47	10	6	1.89	1
30	$C_6H_{10}O_3$	130.14	3	1	1.06	0
31	$C_{15}H_{16}O_9$	340.28	9	5	1.04	0

32	$C_{16}H_{18}O_9$	354.31	9	6	0.96	1
33	$C_7H_{12}O_6$	192.17	6	5	-0.12	0
34	$C_{23}H_{24}O_4$	364.43	4	2	3.70	0
35	$C_7H_{12}O_4$	160.17	4	2	0.94	0
36	$C_{17}H_{20}O_9$	368.34	9	4	2.54	0
37	$C_{18}H_{30}O_9$	390.43	9	5	2.35	0
38	$C_9H_8O_4$	180.16	4	3	0.97	0
39	$C_9H_8O_6$	212.16	6	3	0.24	0
40	$C_9H_{16}O_5$	204.22	5	2	1.55	0
41	$C_{15}H_{14}O_7$	306.27	7	6	0.98	1
42	$C_6H_{12}O_3$	132.16	3	2	1.17	0
43	$C_6H_6O_6$	174.11	6	3	-0.13	0
44	$C_{20}H_{32}O_{10}$	432.46	10	6	1.57	1
45	$C_{16}H_{24}O_{10}$	376.36	10	6	1.26	1
46	$C_{27}H_{30}O_{15}$	594.52	15	9	1.80	3
47	$C_{15}H_{22}O_5$	282.33	5	0	2.75	0
48	$C_{10}H_{16}O_8$	264.23	8	4	0.97	0
49	$C_{10}H_{14}O_4$	198.22	4	1	2.32	0
50	$C_{12}H_{20}O_4$	228.28	4	2	2.04	0
51	$C_{11}H_{18}O_2$	182.26	2	0	3.05	0
52	$C_{14}H_{26}O_5$	274.35	5	3	2.34	0
53	$C_{15}H_{22}O_5$	282.33	5	3	2.09	0
54	$C_{12}H_{18}O_4$	226.27	4	2	1.46	0
55	$C_{13}H_{18}O_5$	254.28	5	0	3.07	0
56	$C_9H_8O_3$	164.16	3	2	0.95	0
57	$C_{13}H_{18}O_5$	254.28	5	3	1.82	0
58	$C_9H_{10}O_3$	166.17	3	1	1.77	0
59	$C_{26}H_{28}O_{14}$	564.49	14	8	2.11	3
60	$C_{21}H_{20}O_{11}$	448.38	11	7	1.27	2
61	$C_{10}H_{18}O_5$	218.25	5	3	0.96	0
62	$C_{12}H_{18}O_5$	242.27	5	2	1.81	0
63	$C_{21}H_{32}O_9$	428.47	9	5	1.97	0
64	$C_{15}H_{18}O_4$	262.30	4	1	2.03	0
65	$C_{10}H_{10}O_4$	194.18	4	2	1.62	0
66	$C_{34}H_{26}O_9$	578.56	9	6	3.45	2
67	$C_{14}H_{24}O_5$	272.34	5	1	2.71	0
68	$C_{16}H_{26}O_8$	346.37	8	4	2.06	0
69	$C_{12}H_{22}O_4$	230.30	4	2	1.83	0
70	$C_{27}H_{30}O_{14}$	578.52	14	8	1.89	3
71	$C_{28}H_{28}O_{18}$	652.51	18	9	0.94	3
72	$C_{21}H_{38}O_7$	402.52	7	4	2.83	0
73	$C_{13}H_{12}O_6$	264.23	6	3	1.70	0
74	$C_{10}H_{18}O_5$	218.25	5	3	1.32	0
75	$C_{29}H_{30}O_{19}$	682.54	19	9	1.95	3

76	$C_9H_6O_4$	178.14	4	2	1.25	0
77	$C_{26}H_{24}O_4$	400.47	4	0	4.45	1
78	$C_9H_{14}O_2$	154.21	2	0	1.63	0
79	$C_{27}H_{26}O_{15}$	590.49	15	5	1.94	2
80	$C_{15}H_{22}O_4$	266.33	4	2	2.38	0
81	$C_{15}H_{20}O_5$	280.32	5	2	1.76	0
82	$C_{13}H_{14}O_6$	266.25	6	3	2.33	0
83	$C_{28}H_{30}O_{17}$	638.53	17	11	1.81	3
84	$C_{21}H_{38}O_7$	402.52	7	4	2.83	0
85	$C_{27}H_{26}O_{16}$	606.49	16	9	2.59	3
86	$C_{26}H_{28}O_{13}$	548.49	13	8	0.66	3
87	$C_{12}H_{22}O_6$	262.30	6	4	1.32	0
88	$C_{15}H_{22}O_4$	266.33	4	2	2.35	0
89	$C_{10}H_{14}O$	150.22	1	0	2.27	0
90	$C_{27}H_{28}O_{16}$	608.50	16	9	1.66	3
91	$C_9H_{16}O_4$	188.22	4	2	1.44	0
92	$C_{27}H_{28}O_{16}$	608.50	16	9	1.66	3
93	$C_{10}H_{16}O_3$	184.23	3	1	2.03	0
94	$C_{28}H_{32}O_{14}$	592.55	14	8	0.80	3
95	$C_{14}H_{24}O_4$	256.34	4	1	3.26	0
96	$C_9H_{18}O_3$	174.24	3	2	1.83	0
97	$C_{27}H_{28}O_{14}$	576.50	14	8	1.95	3
98	$C_{22}H_{20}O_{12}$	476.39	12	6	2.02	2
99	$C_{23}H_{22}O_{13}$	506.41	13	7	1.61	3
100	$C_{15}H_{22}O_4$	266.33	4	2	2.46	0
101	$C_{16}H_{22}O_9$	358.34	9	5	1.24	0
102	$C_{18}H_{32}O_6$	344.44	6	5	2.95	0
103	$C_{12}H_{20}O_5$	244.28	5	2	1.91	0
104	$C_9H_{16}O_2$	156.22	2	1	2.15	0
105	$C_{14}H_{26}O_4$	258.35	4	2	2.49	0
106	$C_{18}H_{24}O_4$	304.38	4	2	3.45	0
107	$C_{21}H_{20}O_{10}$	432.38	10	6	2.11	1
108	$C_{13}H_{12}O_7$	280.23	7	3	0.62	0
109	$C_{28}H_{30}O_{16}$	622.53	16	8	1.81	3
110	$C_{15}H_{16}O_4$	260.29	4	2	2.73	0
111	$C_{20}H_{26}O_7$	378.42	7	3	1.97	0
112	$C_{15}H_{20}O_4$	264.32	4	2	1.97	0
113	$C_{15}H_{22}O_4$	266.33	4	3	2.59	0
114	$C_{14}H_{22}O_4$	254.32	4	3	2.19	0
115	$C_{23}H_{22}O_{11}$	474.41	11	5	2.31	1
116	$C_{14}H_{24}O_4$	256.34	4	2	2.66	0
117	$C_{11}H_{16}O_2$	180.24	2	2	2.04	0
118	$C_{17}H_{22}O_2$	258.36	2	0	4.10	0
119	$C_{13}H_{12}O_9$	312.23	9	5	0.55	0

120	$C_{28}H_{30}O_{16}$	622.50	4	3	2.59	1
121	$C_{17}H_{28}O_{7}$	344.40	7	2	2.59	0
122	$C_{28}H_{30}O_{14}$	590.53	14	7	1.76	3
123	$C_{15}H_{22}O_{4}$	266.33	4	2	2.19	0
124	$C_{15}H_{24}O_{4}$	268.35	4	3	2.87	0
125	$C_{14}H_{22}O_{4}$	254.32	4	1	2.59	0
126	$C_{10}H_{16}O_{3}$	184.23	3	2	1.65	0
127	$C_{10}H_{18}O_{4}$	202.25	4	2	1.77	0
128	$C_{13}H_{12}O_{6}$	264.23	6	3	1.70	1

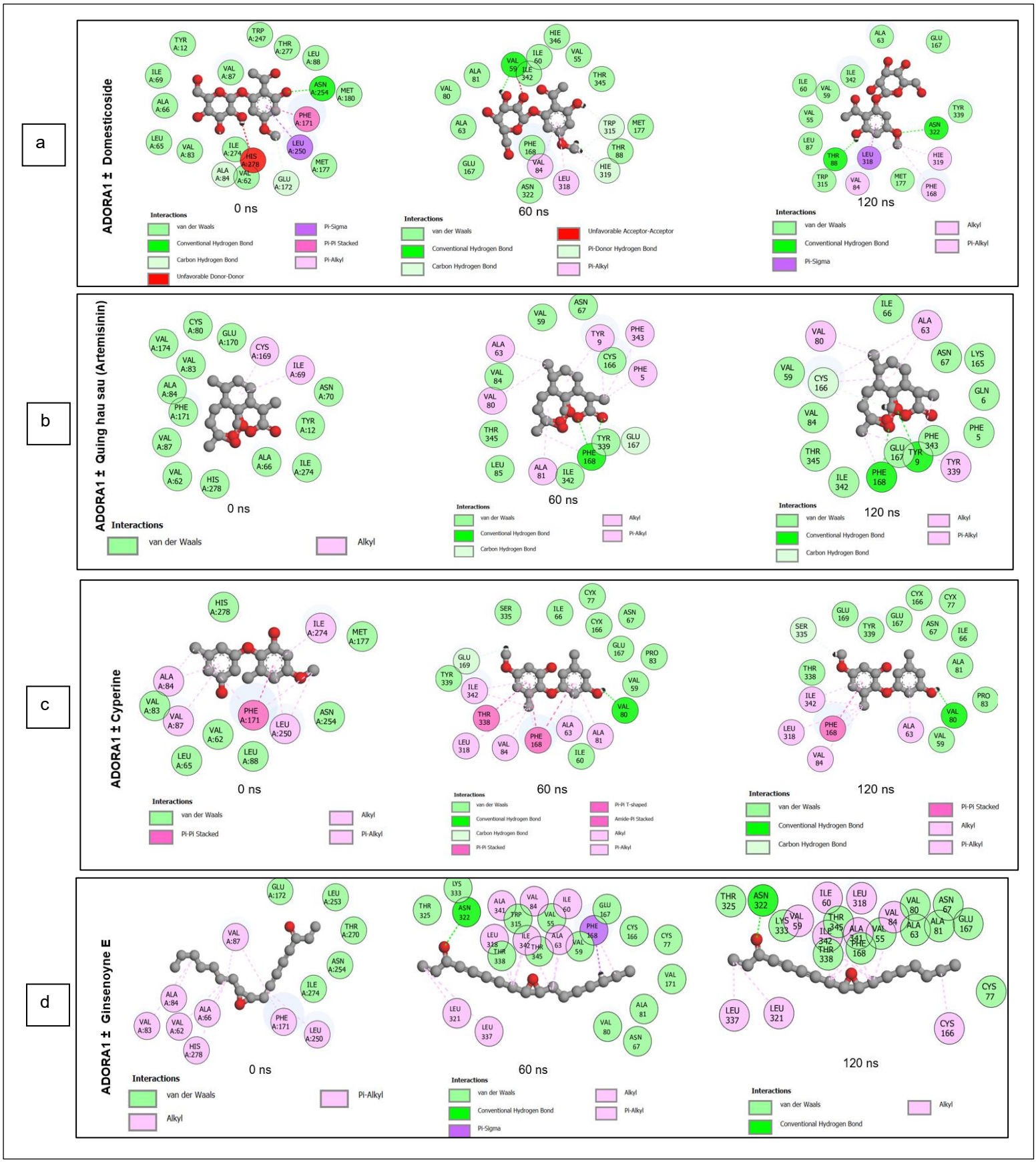

Figure S3: 2-D interaction plots of target gene *ADORA1* with bioactive constituents present in CS: a) domesticoside, b) quing hau sau, c) cyperine and d) ginsenoyne E over a 120-ns simulation

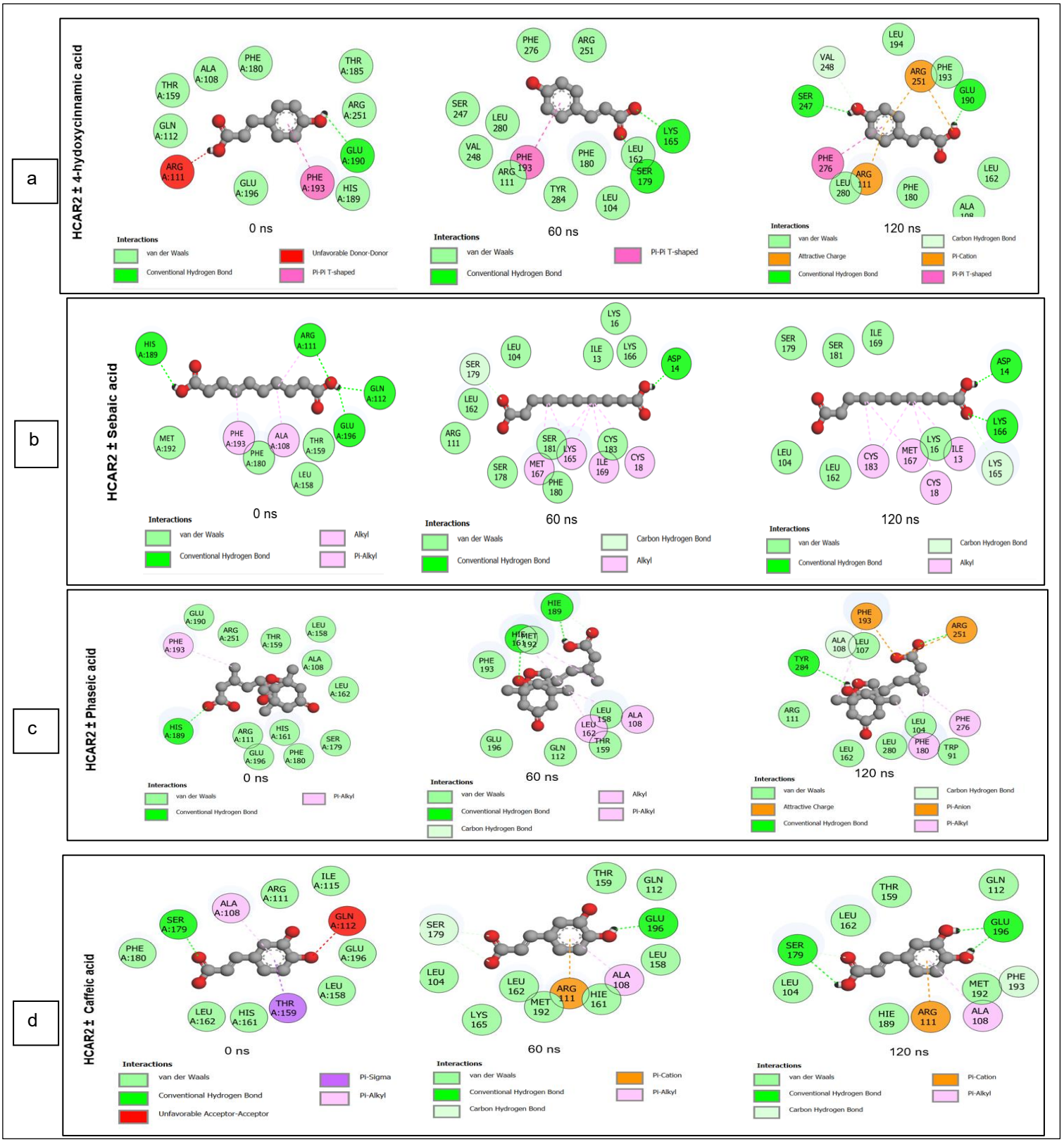

Figure S4: 2-D interaction plots of target gene *HCAR2* with bioactive constituents present in CS: a) 4-hydroxycinnamic acid, b) sebacic acid, c) phaseic acid and d) caffeic acid over a 120-ns simulation

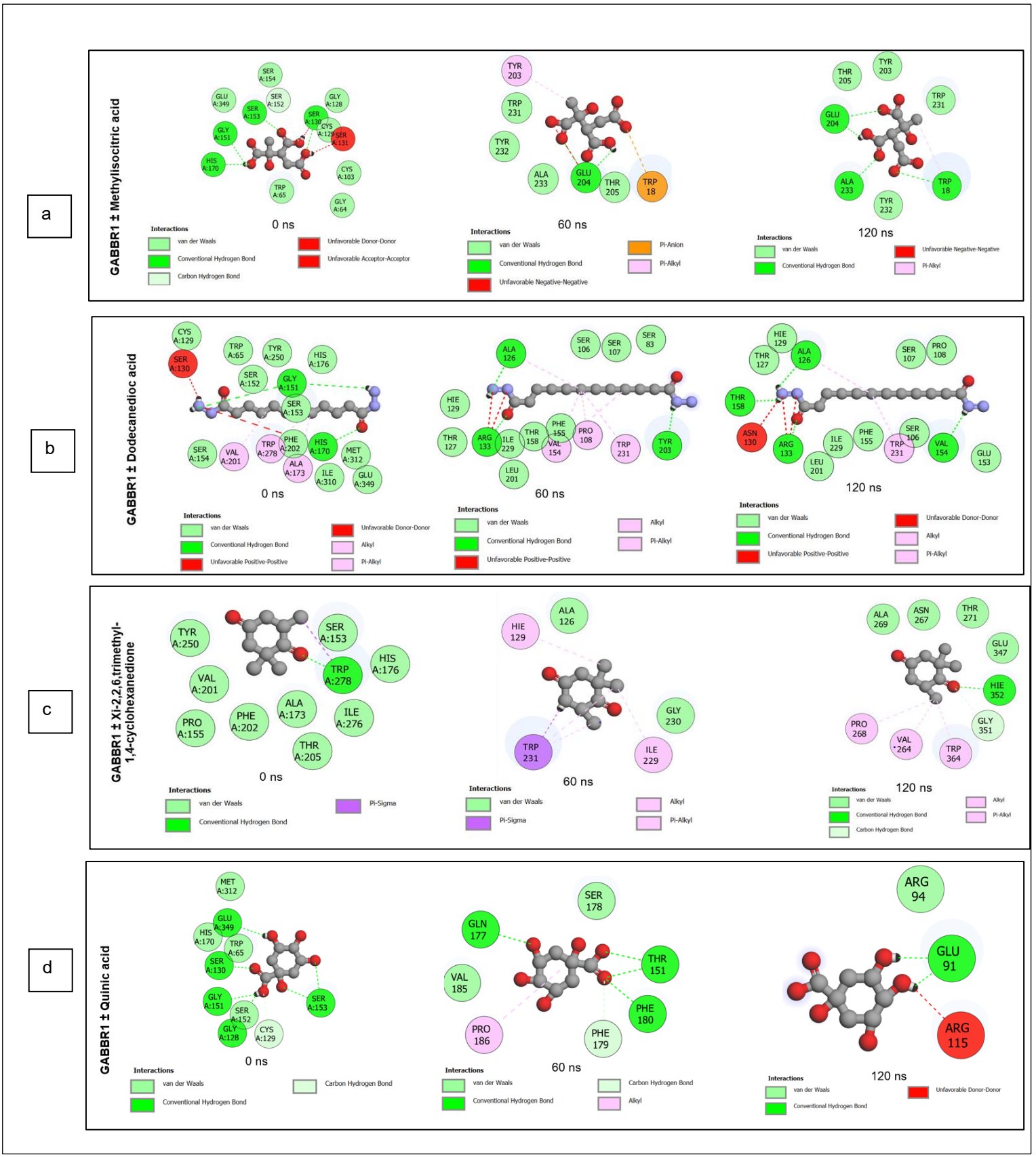

Figure S5: 2-D interaction plots of target gene *GABBR1* with bioactive constituents present in CS: a) methylisocitric acid, b) dodecanedioc acid, c) xi-2,2,6,trimethyl-1,4-cyclohexanedione and d) quinic acid, over a 120-ns simulation.

Chapter five

Unveiling the mechanism of action of corn silk in type 2 diabetes mellitus intervention through down regulation of *ADORA1* and *GABBR1* in HepG2 cells

This chapter was submitted in this format for publication in the *Journal of Functional Foods* (Impact Factor: 3.8)

Unveiling the mechanism of action of corn silk in type 2 diabetes mellitus intervention through down regulation of *ADORA1* and *GABBR1* in HepG2 cells

Ayesha Akoonjee, Terisha Ghazi, Anil Amichung Chuturgoon and Saheed Sabiu*

Department of Biotechnology and Food Science, Faculty of Applied Sciences, Durban University of Technology, Durban 4000, South Africa

Discipline of Medical Biochemistry and Chemical Pathology, School of Laboratory Medicine and Medical Science, College of Health Sciences, Howard College Campus, University of KwaZulu-Natal, Durban, South Africa

*Correspondence: sabius@dut.ac.za

Abstract

This study aims to validate the antidiabetic potential of different extracts (aqueous, hydro-ethanolic and ethanolic) of premature and mature CS in HepG2 cells. This was achieved through an initial 3-(4,5-dimethylthiazol-2-yl)-2,5-diphenyltetrazolium bromide cell viability and glucose consumption assays to establish their optimal doses, and subsequently by real-time polymerase chain reaction (RT-qPCR) to understand their modulatory effect on the expression of adenosine receptor A1 (*ADORA1*) and gamma-aminobutyric acid type B subunit 1 (*GABBR1*) as obtained from the network pharmacology study. At 75 – 100 µg/mL, the investigated extracts promoted viability of HepG2 cells, with ethanolic extract of the mature CS (75 µg/mL) being the most prominent compared with the reference standards-treated and the untreated cells. In the glucose uptake assay, the highest glucose consumption in both normal (7.38 mmol/L) and insulin-resistant (4.13 mmol/L) HepG2 cells observed with the aqueous extract of mature CS could be attributed to its profiled metabolites. A further probe into the modulatory effect of the CS extracts at their optimal doses on the expression of the profiled genes revealed that the aqueous extract of the premature CS (100 µg/mL) proficiently downregulated the expression of *ADORA1* and *GABBR1* in insulin-resistant HepG2 cells relative to the effects observed with the controls. These observations with the extract could be associated with its high abundance of gallicynoic acid B and tetradecanedioc acid identified as effective modulators of *ADORA1* and *GABBR1,* respectively. The findings of this study not only suggest the possible mechanism of antidiabetic action of CS in HepG2 cells through the downregulation of *ADORA1* and *GABBR1* resulting in increased glucose uptake, but will contribute towards the development of CS as an antidiabetic agent for the management of T2DM.

Keywords: *ADORA1*; Antidiabetic; Corn silk; *GABBR1*; Gene expression; Glucose uptake; HepG2 cells.

1. Introduction

Diabetes mellitus (DM) is a chronic metabolic disorder stemming from irregular glucose metabolism that poses substantial burdens on health care systems and economies worldwide (Pheiffer *et al*., 2018). As of 2021, approximately 537 million adults aged 20 to 79 were affected by DM worldwide, with projections indicating a rise to 783 million by 2045 if no effective intervention is provided (Yagasaki *et al*., 2022). Type 2 diabetes mellitus (T2DM), constituting roughly 90% of DM cases, represents the most prevalent form of DM (Lankatillake *et al*., 2019). If left untreated, T2DM can lead to many severe complications including renal disease, ocular damage, cardiovascular issues, myocardial infarctions, strokes, heightened fracture risks, neuropathy, dermatological problems, foot complications (foot ulcers, amputation), increased susceptibility to Alzheimer's disease, and auditory impairment (Yagasaki *et al*., 2022). A significant portion of T2DM patients rely on the use of synthetic medications, namely biguanides (metformin), sulfonylureas, thiazolidinediones, meglitinides, dipeptidyl peptidase-4 inhibitors, sodium-glucose co-transporter 2 inhibitors, glucagon-like peptide-1 receptor agonists and injectable insulin etc., to maintain glycaemic control and prevent possible secondary complications (Paddy *et al*., 2014; Padhi *et al*., 2020). While the effectiveness of these conventional medications as management options is undoubtable, they are associated with prolonged treatment durations, high expense, limited accessibility, variations in individual responses, and absence of target specificity (Padhi *et al*., 2020). Additionally, the extended use of these medications is correlated with the manifestation of adverse side effects in several individuals (Michaelidou *et al*., 2023). Therefore, the development of novel and promising antihyperglycemic agents that can be used as complementary alternatives or synergistically with conventional therapeutics is highly sought after (Abo *et al*., 2008; Xiao *et al*., 2018; Padhi *et al*., 2020).

Numerous cultures, including Chinese, Indian, European, Australian, Korean, Middle Eastern, American (North, South, and Central), and African, have utilized medicinal plants and their derived products to address and/or mitigate an array of health conditions (Van Wyk *et al*., 2018), including T2DM (Hasani-Ranjbar *et al*., 2008). Corn silk (CS), an abundant waste material discarded after corn cultivation has promising therapeutic

properties, including diuretic, antihyperlipidemic, antihypertensive, anti-obesity, anti-microbial, neuroprotective, anti-cancer, anti-depressant, antioxidant, anti-inflammatory, and antidiabetic (Hasanudin *et al*., 2012; Chen *et al*., 2013; Wang *et al*., 2016; Žilić *et al.,* 2016; Chaiittianana *et al*., 2017; Shalihah *et al*., 2020). While the promising antidiabetic potential of CS is well-documented (Chen *et al*., 2013; Zhang *et al*., 2015; Pan *et al*., 2017; Jia *et al*., 2020; Dong *et al*., 2022; Liang *et al*,. 2024), its mechanism of action has not been fully elucidated.

For instance, a previous *in silico* study that adopted integrated network pharmacology and MD simulation profiled significant modulation of adenosine receptor A1 (*ADORA1*), hydroxycarboxylic acid receptor 2 (*HCAR2*) and gamma-aminobutyric acid type B receptor subunit 1 (*GABBR1*) of the cyclic AMP (cAMP) pathway as the two most crucial key targets of interest implicated in antidiabetic potential of CS (Akoonjee *et al*., 2023). Despite that the study postulated a possible mechanism of action of CS in the management of T2DM, the experimental validation in an appropriate model was lacking. Experimental validation is crucial to ensure the safety and optimal therapeutic dose(s) of a therapeutic agent and can complement the results of *in silico* analysis to ascertain the mechanism of action of a drug candidate (Venkateswaran *et al*., 2020). Mammalian cells such as HepG2 cells have been previously used *in vitro* to establish the antidiabetic potential of therapeutics (Liu *et al*., 2017; Alaaeldin *et al*., 2021; Bourebaba *et al*., 2021; Yarahmadi *et al*., 2021; Zhou *et al*., 2021) and the findings from such studies have been adjudged reliable and reproducible (Huang *et al*., 2015; Liu *et al*., 2017). Consequent upon the foregoing and building on the already established modulatory role of CS metabolites on *ADORA1* and *GABBR1*, the present study investigated how CS extracts could influence glucose uptake and subsequent expression of *ADORA1* and *GABBR1* in insulin-resistant HepG2 cells.

2. Materials and methodology

2.1.Reagents and kits used

Human HepG2 cell line (ATCC Cat number: HB-8065) was kindly donated by Professor Chuturgoon of the Discipline of Medical Biochemistry and Chemical Pathology, University of KwaZulu-Natal, Durban, South Africa. Metformin, insulin (human), dimethyl sulfoxide (DMSO) and reagents such as 3-(4,5-dimethylthiazol-2-yl)-2,5-diphenyltetrazolium bromide (MTT) and Qiazol lysis reagent were purchased from Sigma-Aldrich (St Louis, Missouri, United States of America). All cell culture reagents [Dulbecco's medium eagle

media (DMEM; supplemented with 4500 mg/l glucose stable glutamine, sodium pyruvate and sodium bicarbonate), Dulbecco's phosphate buffered saline (DPBS, pH 7.4 with calcium and magnesium), penicillin-streptomycin, foetal bovine serum (FBS), 1% L-glutamine] were purchased from Lonza Biotechnology (Basel, Switzerland). Polymerase chain reaction (PCR) iScript cDNA synthesis kit and iScript One-Step RT-PCR kit with SYBR Green were products of Lasec (Cape Town, South Africa), while the PCR primers (for *ADORA1*, *GABBR1* and *GAPDH)* were purchased from Inqaba Biotech (Pretoria, South Africa). Except otherwise stated, all other reagents/kits used were of analytical grades.

2.2.Corn silk collection, processing and preparation of extracts

Fresh CS of the commonly consumed commercial hybrid ILHYB22 was collected at the Cedara College of Agriculture, KwaZulu-Natal, South Africa at the premature and mature stages. The CS samples obtained were further processed as earlier reported (Akoonjee *et al*., 2023). The CS stock solutions were prepared by dissolving its extracts in 100% DMSO to obtain a stock concentration of 100 000 µg/mL from which dilutions were made with HEPES buffer to obtain final concentrations of 5, 25, 50, 75 and 100 µg/mL, which served as the CS treatments used in this study, with the final concentration of DMSO ≤ 0.1% to prevent DMSO cytotoxicity to the HepG2 cells (Dludla *et al*., 2018).

2.3.Cell viability assay

To determine the effect of CS treatments on HepG2 cells (passage 3), the MTT assay protocol of Mosman (1983), which details the colorimetric measurement of the reduction of the yellow tetrazolium dye, was performed with slight modification (Dludla *et al*., 2018). HepG2 cells were cultured at 37°C with 5% CO_2 to 90% confluency in 96 well culture plates containing complete culture media (DMEM supplemented with 10% FBS and 1% penicillin-streptomycin). Briefly, following exposure of CS treatments for 24 h, HepG2 cells in 96 well plates were stained with 2 mg/mL MTT solution prepared in DPBS. Complete culture media was used as negative control whereas insulin (1 µM) (Mazibuko-Mbeje *et al*., 2021) and metformin (1 µM) (Dludla *et al*., 2020) were used as positive controls. Thereafter, DMSO and Sorenson's glycine buffer (0.1 M glycine and 0.1 M NaCl, adjusted to pH 10.5 with 0.1 mM NaOH) were added to solubilize the dye before absorbance was read at 570 nm using a microplate reader (ELx800, BioTek Instruments Incorporated, Winooski, Vermont, United States of America) and Gen 5 (BioTek

Instruments Incorporated, Winooski, Vermont, United States of America) software for data acquisition (Mosman, 1983; Dludla *et al*., 2018).

2.4. Establishment of experimental model of insulin resistance in HepG2 cells and corn silk treatment

Human HepG2 cells (1.5 x 10^6, passage 3) were cultured at 37°C with 5% CO_2 to 90% confluency in 25 cm^3 cell culture flasks containing complete culture media (DMEM supplemented with 10% FBS and 1% penicillin-streptomycin) (Ghazi *et al*., 2020). Upon 90% confluency, insulin resistance was induced in the HepG2 cells by exposing cells to 0.005 µM of insulin for 24 h (Alaaeldin *et al*., 2021). The cells were subsequently treated with optimal concentrations (75 or 100 µg/mL) of CS extracts as obtained from MTT assay for 24 h. Complete culture media was used as negative control whereas insulin (1 µM) (Mazibuko-Mbeje *et al*., 2021) and metformin (1 µM) (Dludla *et al*., 2020) were used as positive controls (Dludla *et al*., 2018).

2.5. Glucose consumption by normal and insulin-resistant HepG2 cells

The glucose concentration of the culture media containing HepG2 cells was measured through the conversion of glucose to gluconolactone using an Accu-Chek Active kit (including the Accu-Chek Glucometer and glucose test strips) (Roche Holding AG, Basel, Switzerland) as detailed by Nayak *et al*. (1997). HepG2 cells were cultured at 37°C with 5% CO_2 to 90% confluency in 96 well culture plates containing complete culture media (DMEM supplemented with 10% FBS and 1% penicillin-streptomycin) (Ghazi *et al*., 2020). Glucose concentration was measured in the culture media of HepG2 cells treated with optimal concentrations (75 or 100 µg/mL) of CS extracts prior to and following treatment with 0.005 µM of insulin to induce insulin resistance. Insulin and metformin were used as positive controls and complete culture media (untreated) was used as negative control (Choy *et al*., 2007; Eames *et al*., 2010). The amount of glucose consumption (mmol/L) was obtained by subtracting the glucose concentration of the normal and insulin-resistant HepG2 cells from the glucose concentration of a blank well (Huang *et al*., 2015).

2.6. RNA isolation, complementary DNA synthesis and real time quantitative polymerase reaction

2.6.1. RNA Isolation

Total RNA was extracted from CS extract-treated insulin-resistant HepG2 cells as described by Ghazi *et al*. (2019). Briefly, HepG2 cells were rinsed in 0.1 M DPBS and incubated for 5 min at room temperature in 500 µL Qiazol lysis reagent and 500 µL 0.1 M DPBS. Subsequently, cells were removed from cell culture flask using a cell scraper and transferred to sterile 1.5 mL microcentrifuge tubes. Cellular lysates were incubated for 24 h at −80°C. Thereafter, 100 µL chloroform was added and centrifuged (12,000 × *g*, 4°C, 15 min). The aqueous phase containing the RNA was transferred to a sterile 1.5 mL micro-centrifuge tube and 100% cold isopropanol (250 µL) was added to each sample prior to incubation for 24 h at −80°C. The samples were then centrifuged at 12,000 × *g*, 4°C for 20 min and the RNA pellets were washed in 75% cold ethanol (500 µL). Finally, samples were centrifuged (7,400 × *g*, 4°C, 15 min), RNA pellets were air dried for 30 min at room temperature, resuspended in 15 µL nuclease-free water and incubated for 3 min at room temperature. The RNA was quantified using the NanoDrop 2000 spectrophotometer (Thermo Fischer Scientific, Waltham, Massachusetts, United States of America) and standardized to 1,000 ng/µL. The A260/A280 absorbance ratio was used to assess RNA purity.

2.6.2. Complementary DNA synthesis

Complementary DNA (cDNA) synthesis was performed as previously described by Ghazi *et al*. (2019). The RNA isolated was used to prepare cDNA using the iScript cDNA synthesis kit (BioRad, Hercules, California, United States of America), as per the manufacturer's instructions. A master mix was prepared for each RNA isolate by adding 4 µLof 5x iScript reaction mix, 1 µL iScript reverse transcriptase and 15 µL nuclease-free water into a sterile 0.2 mL centrifuge tube. Thereafter, 1 µLof RNA template (1,000 ng/µL) was added before being subjected to a MiniAmp Thermal Cycler (Thermo Fischer Scientific, Waltham, Massachusetts, United States of America) and incubated at 25°C for 5 min, 42°C for 30 min and 95°C for 5 min. Once cDNA synthesis has been completed, 80 µL nuclease-free water was added and the cDNA samples were stored at -20°C until needed for quantitative polymerase chain reaction (qPCR).

2.6.3. Quantitative polymerase chain reaction

The expression of *ADORA1* and *GABBR1* was analysed using the iScript One-Step RT-PCR kit with SYBR Green (BioRad, Hercules, California, United States of America) as per the manufacturer's instructions. Glyceraldehyde 3-phosphate dehydrogenase (*GAPDH*) was used as an internal control gene (housekeeping gene) for normalizing mitochondrial

RNA (mRNA) expression. Per reaction, 9 µL of qPCR master mix [5 µL SYBR Green, 2 µL nuclease-free water, 1 µL sense primer (24 µM) and 1 µL anti-sense primer (25 µM)] was mixed with 1 µL cDNA (1000 ng/µL) into a 96 well PCR plate. Thereafter, the plate was sealed using an adhesive plate seal and centrifuged (1000 × *g*; 24°C for 1 min). All qPCR experiments were conducted using the CFX96 Real Time PCR System (BioRad, Hercules, California, United States of America) and analysed using the Bio-Rad CFX Manager™ Software version 3.1 (BioRad, Hercules, California, United States of America). The common "Double Delta threshold cycle (Ct)" method was used to determine relative changes in expression (Ghazi *et al*., 2019), as per the following equation:

% Relative quantification $=(2^{-\Delta\Delta Ct})*100$

Where:

i. $\Delta\Delta Ct = \Delta Ct_{(test)} - \Delta Ct_{(calibrator\ sample)}$

ii. $\Delta Ct_{(test)} = Ct_{(target\ gene\ in\ test)} - Ct_{(reference\ gene\ in\ test)}$

iii. $\Delta Ct_{(calibrator\ sample)} = Ct_{(target\ gene\ in\ calibrator)} - Ct_{(reference\ gene\ in\ calibrator)}$

2.7.Statistical analysis

GraphPad Prism version 5.0 (GraphPad Prism Software, Dotmatics, Boston, Massachusetts, United States of America) was used to perform all statistical analyses. Results are presented as relative abundance percentage ± standard deviation (n=3). Statistical significance was considered at $p < 0.05$.

3. Results

3.1.Effect of corn silk treatments on viability of HepG2 cells

The results from the MTT assay used to measure the metabolic activity, and thus viability, of the HepG2 cells upon treatment with CS extracts, metformin and insulin for 24 h relative to untreated are presented in Figure 1. The results demonstrated that HepG2 cell proliferation was enhanced by CS extracts from both the premature and mature stages, when administered at concentrations ranging from 75 to 100 µg/mL, in comparison to the untreated and positive controls (metformin and insulin) ($p<0.05$). The mature extracts of CS showed a higher percentage of cell viability in comparison to the premature CS ($p<0.05$). A dose-dependent effect was observed in the percentage of cell viability of

HepG2 cells upon treatment with the aqueous extracts of CS, with the highest percentage of viability occurring at a concentration of 100 µg/mL for the aqueous extract of premature (108.69%) and mature (124.93%) CS (Figure 1). Initially, both hydro-ethanolic and ethanolic extracts of CS at both developmental growth stages exhibited an increase in HepG2 cell viability between concentrations of 25 to 75 µg/mL but showed a decrease at the highest investigated concentration (100 µg/mL). The ethanolic mature extract of CS (145.28%) displayed the highest percentage cell viability in comparison to all the treatments including the controls (Figure 1).

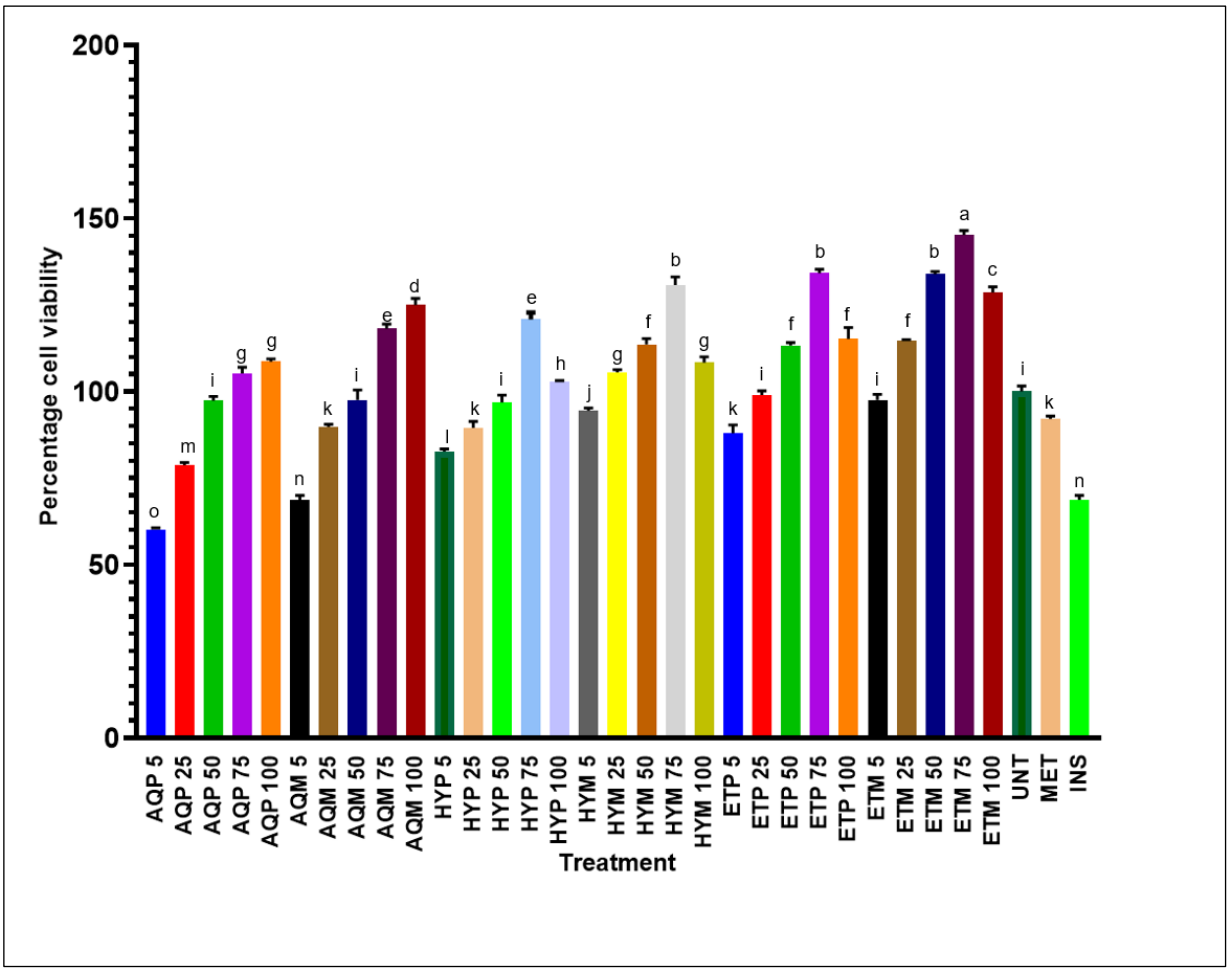

Figure 1: The effect of corn silk extracts (5 – 100 µg/mL) on cell viability based on mitochondrial activity in normal HEPG2 cells in comparison to culture media (untreated; negative control), insulin (1 µM) and metformin(1 µM) (positive controls). AQP; aqueous extract of premature CS, ETH MAT: ethanolic extract of mature CS, ETH PRE: ethanolic extract of premature CS, HYD MAT: hydro-ethanolic extract of mature CS, HYD PRE: hydro-ethanolic extract of premature CS,

UNT: untreated, MET: metformin, INS: insulin. Bars carrying different letters across each treatment are significantly different ($p < 0.05$)

3.2.Glucose consumption by normal and insulin-resistant HepG2 cells

The glucose concentration of the media consisting of normal and insulin-resistant HepG2 cells following treatment with CS extracts at two different developmental growth stages are presented in Supplementary Figure S1. For all treatments assessed, the insulin-resistant HepG2 cells had higher glucose concentrations in comparison to the normal HepG2 cells ($p<0.05$), confirming the formation of an insulin-resistant HepG2 model. Compared with the untreated cells, lower concentrations of glucose in both normal and insulin resistant cells was observed following treatment with CS extracts. In addition, all CS extracts at both developmental stages, except the hydro-ethanolic extract of mature CS (75 µg/mL), had lower concentrations of glucose, compared to insulin (1 µM) and metformin (1 µM), in both normal and insulin-resistant HepG2 cells. The lowest concentrations of glucose in both normal (16.50 mmol/l) and insulin-resistant (19.75 mmol/l) HepG2 cells were observed with the aqueous extract of premature CS. The amount of glucose consumed by normal and HepG2 cells following treatment with different CS extracts relative to a blank well containing only culture media (no HepG2 cells) are presented in Table 1 and Figure 2. Normal HepG2 cells exhibited higher glucose consumption in comparison to insulin-resistant HepG2 cells. In addition, treatment with all CS extracts, except for hydro-ethanol extract of the mature CS (6.11 mmol/L), resulted in a higher amount of glucose consumed compared to metformin, in both normal and insulin-resistant HepG2 cells. Aqueous extract of mature CS demonstrated the highest amount of glucose consumption in both normal (7.38 mmol/L) and insulin-resistant (4.13 mmol/L) HepG2 cells.

Table 1: The effect of different corn silk extracts on the consumption of glucose in normal and insulin-resistant HepG2 cells

Treatment	Glucose consumption in normal HepG2 cells (mmol/L)	Glucose consumption in insulin-resistant HepG2 cells (mmol/L)
Aqueous extract of premature CS (100 µg/mL)	7.06	3.81

Aqueous extract of mature CS (100 µg/mL)	7.38	4.13
Hydro-ethanolic extract of premature CS (75 µg/mL)	6.18	2.93
Hydro-ethanolic extract of mature CS (75 µg/mL)	6.11	2.86
Ethanolic extract of premature CS (75 µg/mL)	6.61	3.36
Ethanolic extract of mature CS (75 µg/mL)	6.66	3.41
Untreated	5.16	1.91
Metformin (1 µM)	6.16	2.91
Insulin (1 µM)	5.98	2.73

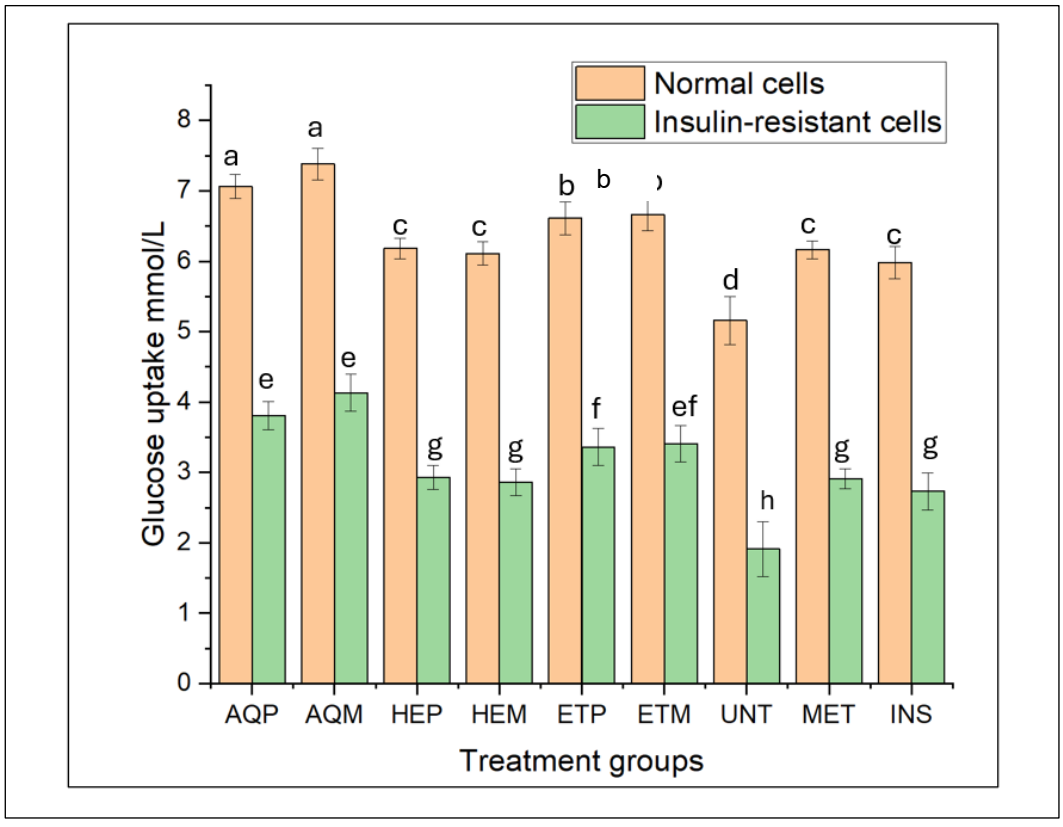

Figure 2: The effect of CS extracts on the uptake of glucose present in the culture media consisting of normal and insulin-resistant HepG2 cells in comparison to culture media (untreated; negative control), insulin and metformin (positive controls). AQP: aqueous extract of premature CS (100 µg/mL) , AQM: aqueous extract of mature CS (100 µg/mL), HEP: hydro-ethanolic

extract of premature CS (75 µg/mL), HEM: hydro-ethanolic extract of mature CS (75 µg/mL), ETP: ethanolic extract of premature CS (75 µg/mL), ETM: ethanolic extract of mature CS (75 µg/mL); UNT: untreated, MET: metformin (1 µM), INS: insulin (1 µM). Bars carrying different letters across each treatment are significantly different ($p < 0.05$)

3.3.Expression of *ADORA1* and *GABBR1* following treatment with CS extracts

The effect of CS extracts (100 µg/mL aqueous and 75 µg/mL hydro-ethanolic and ethanolic) on the expression of *ADORA1* and *GABBR1* in insulin-resistant HepG2 cells after 24 h, compared to untreated, metformin and insulin treatments are presented in Figure 3a and 3b, respectively. Exposure to aqueous (100 µg/mL), hydro-ethanolic and ethanolic (75 µg/mL) extracts of premature and mature CS significantly ($p>0.05$) reduced the expression of *ADORA1* and *GABBR1*, in contrast to the untreated insulin-resistant HepG2 cells. Although, metformin (1 µM) and insulin (1µM) treatment displayed lower expression of *ADORA1* and *GABBR1* in the cells compared to the untreated cells, gene expression was significantly higher compared to the investigated CS extracts. Aqueous extract of premature CS (100 µg/mL) enhanced the highest reduction in the expression of *ADORA1* (3.15%) and *GABBR1* (2.19%) relative to all other treatment groups. Metformin (1µM) had a greater reduction of *ADORA1* expression compared to insulin (Figure 3a), whereas insulin further reduced the expression of *GABBR1* in comparison to metformin (Figure 3b).

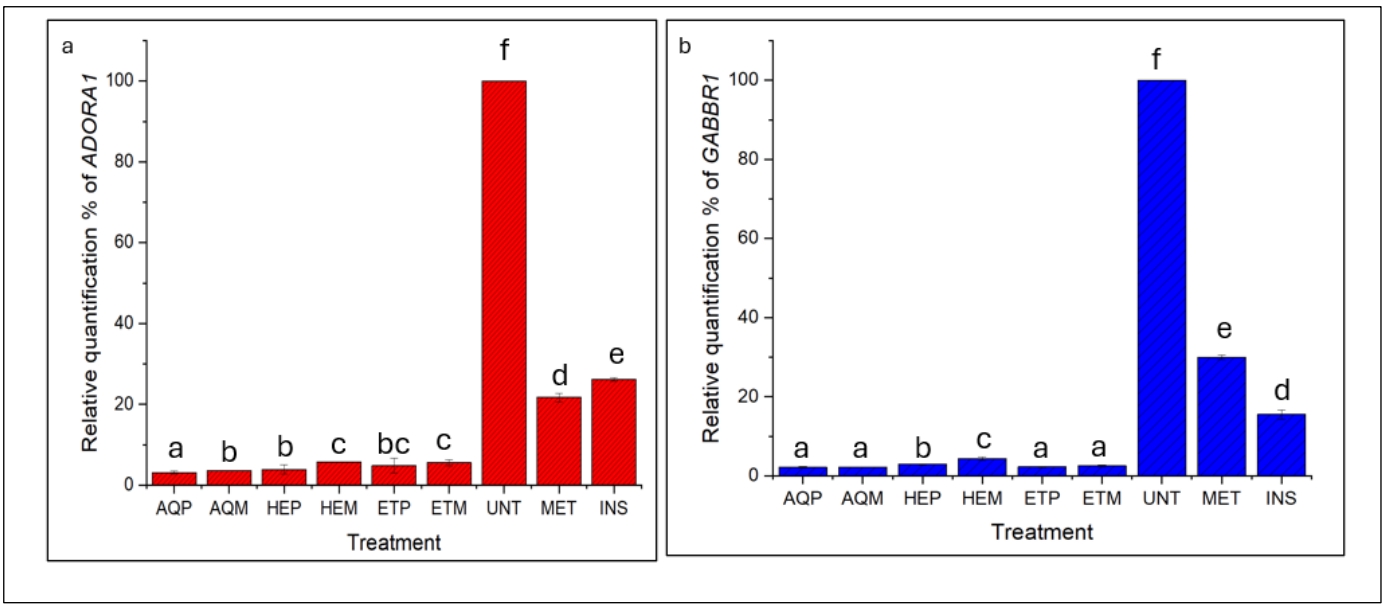

Figure 3: Effect of corn silk, metformin and insulin treatments on the expression of a) *ADORA1* and b) *GABBR1* in insulin-resistant HepG2 cells. AQP: aqueous extract of premature CS (100 µg/mL) , AQM: aqueous extract of mature CS (100 µg/mL), HEP: hydro-ethanolic extract of premature CS (75 µg/mL),

HEM: hydro-ethanolic extract of mature CS (75 µg/mL), ETP: ethanolic extract of premature CS (75 µg/mL), ETM: ethanolic extract of mature CS (75 µg/mL); UNT: untreated, MET: metformin (1 µM), INS: insulin (1 µM). Bars carrying different letters across each treatment are significantly different ($p < 0.05$)

4. Discussion

Natural products, particularly those originating from plants, have been invaluable sources of medicinal compounds over the course of human history (Salehi *et al*., 2019). Consequently, they emerge as an abundant source for identifying and developing potential lead drug candidates on a global scale (Sofowora *et al*., 2013; Salehi *et al*., 2019). Corn silk (CS) is a plentiful plant waste material with considerable therapeutic potential (Sabiu *et al*., 2016), yet its utilization remains largely untapped in South Africa (Sabiu *et al*., 2016; 2019). The present study serves to validate the anti-hyperglycaemic mechanism of action of CS extracts on glucose uptake and expression of *ADORA1* and *GABBR1* in insulin-resistant HepG2 cells.

Of the various types of viability assays that rely on a living cell's ability to convert a substrate to a chromogenic product, the MTT assay stands as one of the most versatile and commonly used techniques (Kumar *et al*., 2018). The MTT assay is based on the conversion of a water-soluble yellow dye MTT by living cells into an insoluble purple formazan crystal, thus determining the mitochondrial activity of the living cells (Cotner *et al*., 2023). Given that the total mitochondrial activity typically correlates with the number of viable cells among most cell populations, the MTT assay finds broad utility in accessing the *in vitro* cytotoxic effects of a drug candidate on cell lines or primary patient cells (Van Meerloo *et al*., 2011; Kumar *et al*., 2018). The MTT assay showed that CS extracts at 75 µg/mL (hydro-ethanolic and ethanolic) and 100 µg/mL (aqueous) induced the highest cell viability in HepG2 cells, with mature CS extracts outperforming premature ones, attributed to the secondary metabolites present in the mature samples of CS. The ethanolic mature extract of CS reported the highest percentage of HepG2 cell viability, due to the high abundance of plant compounds such as quing hau sau (artemisinin), 3-hydroxy-4-butanolide, 2-hydroxydecanedioic acid, esculetin, diaportinol, curvularol, carvone, quercetin 3-o-(6"-acetyl-glucoside), pandangolide 1a and (R)-7-butyl-6,8-dihydroxy-3-[(3E)-pent-3-en-1-yl]-3,4-dihydroisochromen-1-one as previously reported by Akoonjee *et al*. (2024). Although, there are currently no studies investigating the effect of CS on the viability of HepG2 cells by MTT assay, studies have investigated the cytotoxic effects of its extracts on other cell lines. For example, Al-Oqail *et al*. (2019) demonstrated the effect

of methanolic extract of CS on the percentage viability of human breast cancer (MCF-7) and normal human mesenchymal (hMSC-TERT4) cells. It was revealed that concentrations of up to 50 µg/mL and 100 µg/mL were non-toxic to the cells, respectively (Al-Oqail *et al*., 2019). Similarly, to assess the natural photoprotective properties of an ethanolic extract of CS, its cytotoxic potential against MRC-5 human fibroblast cells was evaluated by Azevedo *et al*. (2022). At the highest concentration of 1000 µg/mL of the CS extract, a cell viability of over 70 percent, indicating that it possessed a low cytotoxic profile (Azevedo *et al*., 2022). Sawangwong *et al*. (2024) revealed that 0.1 – 10 mg/mL of CS extracts did not affect the percentage viability of human dermal fibroblast cells. Wang *et al*. (2019) demonstrated that CS extracts at concentrations of 50 – 200 µg/mL did not exhibit any cytotoxic effects on mesangial cells. In agreement with the Al-Oqail *et al*. (2019), Wang *et al*. (2019) and Sawangwong *et al*. (2024), the CS extracts investigated in the present study at concentrations of 75 – 100 µg/mL did not have any cytotoxic effects on HepG2 cells. This observation is also consistent with the findings on the cytotoxic effects of plants such as *Allophylus cominia* and *Ficus carica* with no observable cytopathic effects at concentrations 1 – 100 µg/mL (Semaan *et al*., 2018) and 82.29 µg/mL(Zhang *et al*., 2019), respectively on HepG2 cells.

Mammalian cells consist of ubiquitous and facilitative glucose transport systems which are responsible for transporting glucose across cell surface membranes. Evaluating glucose uptake is important in the study of numerous diseases (Yamamoto *et al*., 2015), including T2DM (Anthony *et al*., 2019). The ability of a lead drug candidate to enhance glucose uptake by living cells is the true reflection of its anti-hyperglycaemic potentials, which can potentially contribute to the development of novel antidiabetic agents (Zhou *et al*., 2024). In agreement with Alaaeldin *et al*. (2021), the decrease in glucose consumption in the HepG2 cells exposed to 0.005 µM of insulin for 24 h compared to untreated HepG2 cells confirms the establishment of insulin-resistance model. Interestingly, treatment with most of the CS extracts in this study promoted the glucose uptake in normal and insulin-resistant cells compared to the observations with the metformin- and insulin-treated cells. While glucose uptake among the aqueous CS samples did not significantly differ from each other, both exhibited higher glucose uptake in normal and insulin-resistant HepG2 cells compared to other CS extracts, metformin, insulin, and untreated controls. The aqueous CS samples are rich in various metabolites, including ascorbic acid, mevalonic acid, CNP0447999, chlorogenic acid, quinic acid, caffeic acid, D-leucic acid, acetovanillone (apocynin),

tetradecanedioic acid, and gallicynoic acid B (more abundant in aqueous extracts of mature CS), as well as (7'R)-(+)-lyoniresinol 9'-glucoside, kaempferol 3-rhamnoside 7-galacturonide, (3R,4S,6S)-3,4,5-trihydroxy-6-[5-hydroxy-2-(4-hydroxyphenyl)-4-oxo-3-[(2S,3S,5R)-3,4,5-trihydroxy-6-methyloxan-2-yl]oxychromen-7-yl]oxyoxane-2-carboxylic acid, blennin D, and gallicynoic acid F (more abundant in aqueous extract of premature CS) (Akoonjee *et al*., unpublished). The presence of these metabolites in aqueous extracts of CS are likely to be responsible for the enhanced glucose uptake observed in HepG2 cells. Although the effect of CS on the uptake of glucose in HepG2 cells has not been previously performed, studies have reported enhanced glucose uptake in HepG2 cells following treatment with plant extracts including flowers from *Edgeworthia gardneri* (Wall.) Meisn, *Sambucus nigra* L. (*Adoxaceae*) and *Lauridia tetragona* as well as metabolites such as chrysin, carpachromene, kaempferol, xdesmethylagrimonolide, quercetin, luteolin (Bhattacharya *et al*., 2013; Huang *et al*., 2015; Ho *et al*., 2017; Oyedemi *et al*., 2019; *Zhang et al*., 2020; Alaaeldin *et al*., 2021; Zhou *et al*., 2021). Although research on the effect of CS on the uptake of glucose in mammalian cells is limited, Guo *et al*. (2019) reported that polysaccharides isolated from aqueous extract of CS enhanced the uptake of glucose in L6 skeletal muscle cells (Guo *et al*., 2019).

Based on the results from a previous network pharmacology study, *ADORA1* and *GABBR1* were identified as key therapeutic target genes from the cyclic adenosine monophosphate (cAMP) pathway that are modulated by the metabolites present in CS (Akoonjee *et al*., 2023). Adenosine A1 receptor (*ADORA1*) is a member of the G-protein coupled receptor that modulates the effects of adenosine and play a role in regulating cell metabolism and gene transcription (Lv *et al*., 2022). Adenosine A1 receptor (*ADORA1*) has been identified as an important drug target for numerous diseases (Nieto Gutierrez *et al*., 2018), including cancer (Nomiri *et al*., 2022), Parkinson's disease (Duyu *et al*., 2020), obesity and T2DM (Lv *et al*., 2022). Adenosine A1 receptor (*ADORA1*) inhibits the activation of adenylate cyclase (Wojcik *et al*., 2010; Lv *et al*., 2022), reducing cAMP levels (Nomiri *et al*., 2022), inhibiting the activity of protein kinase A, leading to decreased glycogen storage, altered glycogen synthesis, reduced gluconeogenesis, reduced mobilization of glucose and impaired insulin signalling (Shpakov *et al*., 2013; Yang *et al*., 2016). The abrogation of *ADORA1* signalling has been shown to enhance insulin release and improve insulin signalling, making *ADORA1* a promising therapeutic target for preventing the progression of T2DM (Yang *et al*., 2015). SDZ WAG-994 (N-cyclohexyl-2'-O-methyladenosine) was

one of the first potent and selective *ADORA1* gene agonists identified, capable of lowering serum glucose levels, blood pressure, and heart rate in hypertensive rats with hyperglycaemia (Ishikawa *et al*., 1998). Subsequently, other *ADORA1* agonists have been discovered with similar therapeutic effects for T2DM, including improving glucose tolerance, enhanced insulin sensitivity, insulin resistance, and glycogen synthesis (Wojcik *et al*, 2010)

The investigated CS extracts (100 µg/mL aqueous and 75 µg/mL hydroethanolic and ethanolic) from both developmental stages significantly decreased *ADORA1* expression in insulin-resistant HepG2 cells, outperforming the effects observed with metformin and insulin treatments. This reduction could be attributed to the presence of gallicynoic acid B, identified through computational analysis as a key modulator of *ADORA1* (Akoonjee *et al*., 2023). Among the different treatments, the aqueous samples proficiently downregulated *ADORA1* expression, and this effect might be attributable to the high abundance of gallicynoic acid B. Although no studies have specifically examined the modulation of *ADORA1* by CS treatment in HepG2 cells, Lv *et al*. (2022) showed that morusin, a metabolite found in Mulberry (Morus alba L.) leaves, repressed *ADORA1* gene expression in normal human liver L02 cells at concentrations of 2.5 and 5 µmol/L. This repression also impacted the glucose consumption of the cells. (Lv *et al*., 2022).

Gamma-aminobutyric acid type B receptor subunit 1 (*GABBR1*) along with gamma-aminobutyric acid type B receptor subunit 2 (*GABBR2*) form part of a heterodimeric guanine nucleotide-binding protein G protein-coupled receptor (GPCR), known as gamma-aminobutyric acid B [GABA(B)] (White *et al*., 1998). Within the heterodimer complex, *GABBR1* binds to agonists whilst GABBR2 mediates coupling to G-proteins (Nomura *et al*., 2008). Both *ADORA1* and *GABBR1* are involved in the regulation of adenylate cyclase (Hill, 1985; Nomiri *et al*., 2022), which could possibly contribute to CS's reported antidiabetic action (Sphakov *et al*., 2013). Rachdi *et al*. (2020) demonstrated that baclofen, a GABA(B) agonist modulates cAMP signalling in the human beta cell line ECN90, which subsequently decreased the expression of beta-specific genes, modulating beta cell differentiation and reduced insulin signalling (Rachdi *et al*., 2020). Corn silk treatment (100 µg/mL aqueous and 75 µg/mL hydroethanolic and ethanolic) from both developmental stages significantly inhibited *GABBR1* expression in insulin-resistant HepG2 cells, outperforming untreated cells, insulin, and metformin. This inhibition is attributed to the secondary metabolite tetradecanedioic acid, with the aqueous extracts showing the greatest

reduction, regardless of the developmental stage. The modulation of *GABBR1* by the aqueous extracts is likely due to the high abundance of tetradecanedioic acid, leading to enhanced glucose uptake in the cells (Akoonjee *et al*., 2023; Akoonjee *et al*., unpublished).

5. Conclusion

The antidiabetic mechanism of action of CS extracts was elucidated through their modulatory potential on *ADORA1* and *GABBR1* from the cAMP signalling pathway in insulin-resistant HepG2 cells. Aqueous (75 µg/mL) , hydro-ethanolic and ethanolic (100 µg/mL) extracts of CS had no cytotoxic effects on HepG2 cells and instead promoted the viability of the cells compared to untreated (culture media), metformin and insulin. Ethanolic mature extract of CS displayed higher viability of HepG2 cells compared to the other samples, potentially due to the high abundance of several plant compounds. The investigated CS extracts (75 - 100 µg/mL) from both developmental stages stimulated glucose uptake in both normal and insulin-resistant HepG2 cells. Aqueous extracts from mature CS, rich in compounds such as ascorbic acid, mevalonic acid, CNP0447999, chlorogenic acid, quinic acid, caffeic acid, D-leucic acid, apocynin, tetradecanedioic acid, and gallicynoic acid B, exhibited the highest glucose uptake compared to untreated cells, metformin, and insulin. Aqueous extract of premature CS (75 µg/mL) displayed the highest reduction in *ADORA1* and *GABBR1* expression in insulin-resistant HepG2 cells compared to observation with treatment with metformin and insulin, and could be attributed to the high concentrations of gallicynoic acid B and tetradecanedioc acid. It is proposed that the downregulation of *ADORA1* and *GABBR1* causes an increase in glucose consumption in insulin-resistant HepG2 cells, contributing to the antidiabetic properties of CS. This findings could support towards the development of CS as a therapeutic agent for the management of T2DM.

Author Contribution: A.A. was involved in the methodology, formal analysis, data curation, and preparation of original draft; T.G. was involved in the review and editing of the draft; A.C. was involved in the experimentation co supervision and S.S. conceptualized and administered the project, supervised, and provided funding. All authors have read and agreed to the published version of the manuscript.

Funding: The authors specially acknowledge the financial assistance of the Directorate of Research and Postgraduate Support, Durban University of Technology, the South African Medical Research Council (SAMRC) under a Self-Initiated Research Grant, the Technology

Innovative Agency as well as the National Research Foundation's (NRF) Competitive Programme for Rated Researchers Support (SRUG2204193723) to S. Sabiu. The views and opinions expressed in this paper are those of the authors and do not necessarily represent the official views of the funders.

Institutional Review Board Statement: Not Applicable

Informed Consent Statement: Not Applicable

Acknowledgments: The assistance of the Directorate of Research and Postgraduate Support, Durban University of Technology, for the Master's Scholarship Scheme to A. Akoonjee is duly and thankfully acknowledged. The Centre for High Performance Computing (CHPC), Cape Town, South Africa is equally acknowledged for granting access to the computing software and modules used in this study.

Conflicts of Interest: The authors declared no known competing financial interests or personal relationships that could have appeared to influence the work reported in this paper.

References:

Abo, K.A., Fred-Jaiyesimi, A.A. and Jaiyesimi, A.E.A. 2008. Ethnobotanical studies of medicinal plants used in the management of diabetes mellitus in South Western Nigeria. *Journal of Ethnopharmacology,* 115, 67.

Ahren, B. 2009. Islet G protein-coupled receptors as potential targets for treatment of type 2 diabetes. *Nature Reviews Drug Discovery,* 8, 369.

Akoonjee, A., Lanrewaju, A.A., Balogun, F.O., Makunga, N.P. and Sabiu, S. 2023. Waste to medicine: Evidence from computational studies on the modulatory role of corn silk on the therapeutic targets implicated in type 2 diabetes mellitus. *Biology*, 12, 1509.

Alaaeldin, R., Abdel-Rahman, I.A., Hassan, H.A., Youssef, N., Allam, A.E., Abdelwahab, S.F., Zhao, Q.L. and Fathy, M. 2021. Carpachromene ameliorates insulin resistance in HepG2 cells via modulating IR/IRS1/PI3k/Akt/GSK3/FoxO1 pathway. *Molecules*, 26, 7629.

Al-Oqail, M.M., Al-Sheddi, E.S., Farshori, N.N., Al-Massarani, S.M., Al-Turki, E.A., Ahmad, J., Al-Khedhairy, A.A. and Siddiqui, M.A. 2019. Corn silk (*Zea mays* L.) induced apoptosis in human breast cancer (MCF-7) cells via the ROS-mediated mitochondrial pathway. *Oxidative Medicine and Cellular Longevity*, 2019.

Antony, J., Debroy, S., Manisha, C., Thomas, P., Jeyarani, V. and Choephel, T. 2019. *In-vitro* cell line Models and Assay methods to study the Anti-diabetic Activity. Research *Journal of Pharmacy and Technology*, 12, 2200-2206.

Azevedo, A.S.D., Seibert, J.B., Amparo, T.R., Antunes, A.D.S., Sousa, L.R.D., Souza, G.H.B.D., Teixeira, L.F.M., Vieira, P.M.D.A., Santos, V.M.R.D., Nascimento, A.M.D. and Nascimento, A.M.D. 2022. Chemical constituents, antioxidant potential, antibacterial study and photoprotective activity of Brazilian corn silk extract. *Food Science and Technology*, 42, 98421.

Barber, R.D., Harmer, D.W., Coleman, R.A. and Clark, B.J. 2005. GAPDH as a housekeeping gene: analysis of GAPDH mRNA expression in a panel of 72 human tissues. *Physiological Genomics*, 21, 389.

Bhattacharya, S., Christensen, K.B., Olsen, L.C., Christensen, L.P., Grevsen, K., Færgeman, N.J., Kristiansen, K., Young, J.F. and Oksbjerg, N. 2013. Bioactive components from flowers of *Sambucus nigra* L. increase glucose uptake in primary porcine myotube cultures and reduce fat accumulation in Caenorhabditis elegans. *Journal of Agricultural and Food Chemistry*, 61, 11033.

Chaiittianan, R., Sutthanut, K. and Rattanathongkom, A. 2017. Purple corn silk: A potential anti-obesity agent with inhibition on adipogenesis and induction on lipolysis and apoptosis in adipocytes. *Journal of Ethnopharmacology*, 201, 9. .

Chen, S., Chen, H., Tian, J., Wang, Y., Xing, L. and Wang, J. 2013. Chemical modification, antioxidant and α-amylase inhibitory activities of corn silk polysaccharides. *Carbohydrate Polymers*, 98, 428.

Cheng, J.T., Chi, T.C. and Liu, I.M. 2000. Activation of adenosine A1 receptors by drugs to lower plasma glucose in streptozotocin-induced diabetic rats. *Autonomic Neuroscience*, 83, 127.

Cotner, M., Meng, S., Jost, T., Gardner, A., De Santiago, C. and Brock, A. 2023. Integration of quantitative methods and mathematical approaches for the modeling of cancer cell proliferation dynamics. *American Journal of Physiology-Cell Physiology*, 324, 247-262.

Dludla, P.V., Jack, B., Viraragavan, A., Pheiffer, C., Johnson, R., Louw, J. and Muller, C.J. 2018. A dose-dependent effect of dimethyl sulfoxide on lipid content, cell viability and oxidative stress in 3T3-L1 adipocytes. *Toxicology Reports*, 5, 1014-1020.

Dludla, P.V., Muller, C.J., Louw, J., Mazibuko-Mbeje, S.E., Tiano, L., Silvestri, S., Orlando, P., Marcheggiani, F., Cirilli, I., Chellan, N. and Ghoor, S. 2020. The combination effect of aspalathin and phenylpyruvic acid-2-o-β-d-glucoside from rooibos against hyperglycemia-induced cardiac damage: An in vitro study. *Nutrients*, 12, 1151.

Dong, W., Zhao, Y., Hao, Y., Sun, G., Huo, J. and Wang, W. 2022. Integrated molecular biology and metabolomics approach to understand the mechanism underlying reduction of insulin resistance by corn silk decoction. *Journal of Ethnopharmacology*, 284, 114756.

Duyu, T., Khanal, P., Khatib, N.A. and Patil, B.M. 2020. *Mimosa pudica* modulates neuroactive ligand-receptor interaction in Parkinson's disease. *Indian Journal of Pharmaceutical Education and Research*, 54, 732.

Erdemli, M.E., Doğan, Z., Çiğremiş, Y., Akgöz, M., Altinöz, E., Gecer, M. and Türköz, Y. 2015. Amelioration of subchronic acrylamide toxicity in large intestine of rats byorganic dried apricot intake. *Turkish Journal of Biology,* 39, 872-878.

Geng, Y., Bush, M., Mosyak, L., Wang, F. and Fan, Q.R. 2013. Structural mechanism of ligand activation in human GABAB receptor. *Nature*, 504, 254.

Guo, J., Liu, T., Han, L. and Liu, Y. 2009. The effects of corn silk on glycaemic metabolism. *Nutrition and Metabolism*, 6, 1.

Guo, H., Guan, H., Yang, W., Liu, H., Hou, H., Chen, X., Liu, Z., Zang, C., Liu, Y. and Liu, J. 2017. Pro-apoptotic and anti-proliferative effects of corn silk extract on human colon cancer cell lines. *Oncology Letters*, 13, 973.

Guo, Q., Chen, Z., Santhanam, R.K., Xu, L., Gao, X., Ma, Q., Xue, Z. and Chen, H. 2019. Hypoglycemic effects of polysaccharides from corn silk (*Maydis stigma*) and their beneficial roles via regulating the PI3K/Akt signaling pathway in L6 skeletal muscle myotubes. *International Journal of Biological Macromolecules*, 121, 981.

Hasanudin, K., Hashim, P. and Mustafa, S. 2012. Corn silk (*Stigma maydis*) in healthcare: a phytochemical and pharmacological review. *Molecules*, 17, 9697.

Hamza, A.H., Al-Bishri, W.M., Damiati, L.A. and Ahmed, H.H. 2017. Mesenchymal stem cells: a future experimental exploration for recession of diabetic nephropathy. *Renal Failure*, 39, 67.

Hasani-Ranjbar, S., Larijani, B. and Abdollahi, M. 2008. A systematic review of Iranian medicinal plants useful in diabetes mellitus. *Archives of Medical Science*, 4, 285.

Hasanudin, K., Hashim, P. and Mustafa, S. 2012. Corn silk (*Stigma maydis*) in healthcare: a phytochemical and pharmacological review. *Molecules*, 17, 9697.

Hill, D.R. 1985. GABAB receptor modulation of adenylate cyclase activity in rat brain slices. *British Journal of Pharmacology*, 84, 249.

Ho, G.T.T., Kase, E.T., Wangensteen, H. and Barsett, H. 2017. Effect of phenolic compounds from elderflowers on glucose-and fatty acid uptake in human myotubes and HepG2-cells. *Molecules,* 22, 90.

Hong, Y., Zheng, N., He, X., Zhong, J., Ma, J., Zhao, A., Zheng, X., Gu, Y., Yao, J., Li, Y. and Yuan, L. 2019. Inhibition of ADORA1 attenuates hepatic steatosis by gut microbiota-derived acetic acid from *Astragalus* polysaccharides. *BioRxiv*, 639195.

Huang, Q., Chen, L., Teng, H., Song, H., Wu, X. and Xu, M. 2015. Phenolic compounds ameliorate the glucose uptake in HepG2 cells' insulin resistance via activating AMPK: anti-diabetic effect of phenolic compounds in HepG2 cells. *Journal of Functional Foods*, 19, 487.

Huang, Q., Chen, L., Teng, H., Song, H., Wu, X. and Xu, M. 2015. Phenolic compounds ameliorate the glucose uptake in HepG2 cells' insulin resistance via activating AMPK: anti-diabetic effect of phenolic compounds in HepG2 cells. *Journal of Functional Foods*, 19, 487.

Ishikawa, J., Mitani, H., Bandoh, T., Kimura, M., Totsuka, T. and Hayashi, S. 1998. Hypoglycemic and hypotensive effects of 6-cyclohexyl-2′-O-methyl-adenosine, an adenosine A1 receptor agonist, in spontaneously hypertensive rat complicated with hyperglycemia. *Diabetes Research and Clinical Practice*, 39, 3.

Jia, Y., Xue, Z., Wang, Y., Lu, Y., Li, R., Li, N., Wang, Q., Zhang, M. and Chen, H. 2021. Chemical structure and inhibition on α-glucosidase of polysaccharides from corn silk by fractional precipitation. *Carbohydrate Polymers*, 252, 117185.

Kerimi, A., Jailani, F. and Williamson, G. 2015. Modulation of cellular glucose metabolism in human HepG2 cells by combinations of structurally related flavonoids. *Molecular Nutrition and Food Research*, 59, 894-906.

Kifle, Z.D., Yesuf, J.S., Atnafie, S.A. 2020. Evaluation of *in vitro* and *in vivo* anti-diabetic, anti-hyperlipidemic and anti-oxidant activity of flower crude extract and solvent fractions of *Hagenia abyssinica* (rosaceae). *Journal of Experimental Pharmacology*, 151-167.

Kumar, P., Nagarajan, A. and Uchil, P.D. 2018. Analysis of cell viability by the MTT assay. *Cold Spring Harbor Protocols*, 2018, 6.

Lankatillake, C., Huynh, T. and Dias, D.A. 2019. Understanding glycaemic control and current approaches for screening antidiabetic natural products from evidence-based medicinal plants. *Plant Methods*, 15, 1.

Liang, H., Zhang, R., Zhou, L., Wu, X., Chen, J., Li, X., Chen, J., Shan, L. and Wang, H. 2024. Corn stigma ameliorates hyperglycemia in zebrafish and GK rats of type 2 diabetes. *Journal of Ethnopharmacology*, 325, 117746.

Lv, Q., Lin, J., Wu, X., Pu, H., Guan, Y., Xiao, P., He, C. and Jiang, B. 2022. Novel active compounds and the anti-diabetic mechanism of mulberry leaves. *Frontiers in Pharmacology*, 13, 986931.

Mazibuko-Mbeje, S.E., Mthembu, S.X., Tshiitamune, A., Muvhulawa, N., Mthiyane, F.T., Ziqubu, K., Muller, C.J. and Dludla, P.V. 2021. Orientin improves substrate utilization and the expression of major genes involved in insulin signalling and energy regulation in cultured insulin-resistant liver cells. *Molecules*, 26, 6154.

Michaelidou, M., Pappachan, J.M. and Jeeyavudeen, M.S. 2023. Management of diabesity: current concepts. *World Journal of Diabetes*, 14, 396.

Nayak, R.C. and Herman, I.M. 1997. Measurement of glucose consumption by hybridoma cells growing in hollow fiber cartridge bioreactors: use of blood glucose self-monitoring devices. *Journal of Immunological Methods*, 205, 109.

Nieto Gutierrez, A., and McDonald, P.H. 2018. GPCRs: Emerging anti-cancer drug targets. *Cellular Signaling.* 41, 65.

Nomiri, S., Karami, H., Baradaran, B., Javadrashid, D., Derakhshani, A., Nourbakhsh, N.S., Shadbad, M.A., Solimando, A.G., Tabrizi, N.J., Brunetti, O. and Nasseri, S. 2022. Exploiting

systems biology to investigate the gene modules and drugs in ovarian cancer: A hypothesis based on the weighted gene co-expression network analysis. *Biomedicine and Pharmacotherapy,* 146, 112537.

Nomura, R., Suzuki, Y., Kakizuka, A. and Jingami, H. 2008. Direct detection of the interaction between recombinant soluble extracellular regions in the heterodimeric metabotropic γ-aminobutyric acid receptor. *Journal of Biological Chemistry*, 283, 4665.

Paddy, V., Van Tonder, JJ. and Steenkamp, V. 2014. The antidiabetic activity of a polyherbal tea mixture and its constituents *in vitro*. *17th World Congress of Basic and Clinical Pharmacology*. 13.

Padhi, S., Nayak, A.K. and Behera, A. 2020. Type II diabetes mellitus: a review on recent drug based therapeutics. *Biomedicine and Pharmacotherapy*, 131, 110708.

Pan, Y., Wang, C., Chen, Z., Li, W., Yuan, G. and Chen, H. 2017. Physicochemical properties and antidiabetic effects of a polysaccharide from corn silk in high-fat diet and streptozotocin-induced diabetic mice. *Carbohydrate Polymers*, 164, 370. .

Pasquini, S., Contri, C., Merighi, S., Gessi, S., Borea, P.A., Varani, K. and Vincenzi, F. 2022. Adenosine receptors in neuropsychiatric disorders: fine regulators of neurotransmission and potential therapeutic targets. *International Journal of Molecular Sciences*, 23, 1219.

Pheiffer, C., Pillay-van Wyk, V., Joubert, J.D., Levitt, N., Nglazi, M.D. and Bradshaw, D. 2018. The prevalence of type 2 diabetes in South Africa: A systematic review protocol. *BMJ Open,* 8, 021029.

Rachdi, L., Maugein, A., Pechberty, S., Armanet, M., Hamroune, J., Ravassard, P., Marullo, S., Albagli, O. and Scharfmann, R. 2020. Regulated expression and function of the GABAB receptor in human pancreatic beta cell line and islets. *Scientific Reports*, 10, 13469.

Sabiu, S., O'Neill, FH. and Ashafa, AOT. 2016. Kinetics of α-amylase and α-glucosidase inhibitory potential of *Zea mays* Linnaeus (Poaceae), *Stigma maydis* aqueous extract: An *in vitro* assessment. *Journal of Ethnopharmacology*. 183, 1.

Sabiu, S., Madende, M., Ajao, A.A.N., Ogundeji, O.A., Lekena, N. and Alayande, K.A. 2019. The scope of phytotherapy in southern African antidiabetic healthcare. *Transactions of the Royal Society of South Africa,* 74, 1.

Salehi, B., Ata, A., V. Anil Kumar, N., Sharopov, F., Ramírez-Alarcón, K., Ruiz-Ortega, A., Abdulmajid Ayatollahi, S., Valere Tsouh Fokou, P., Kobarfard, F., Amiruddin Zakaria, Z. and Iriti, M. 2019. Antidiabetic potential of medicinal plants and their active components. *Biomolecules*, 9, 551.

Sawangwong, W., Kiattisin, K., Somwongin, S., Wongrattanakamon, P., Chaiyana, W., Poomanee, W. and Sainakham, M. 2024. The assessment of composition, biological properties, safety and molecular docking of corn silk (*Zea mays* L.) extracts from the valorization of agricultural waste products in Thailand. *Industrial Crops and Products*, 212, 118352.

Semaan, D.G., Igoli, J.O., Young, L., Gray, A.I., Rowan, E.G. and Marrero, E. 2018. *In vitro* anti-diabetic effect of flavonoids and pheophytins from *Allophylus cominia* Sw. on the glucose uptake assays by HepG2, L6, 3T3-L1 and fat accumulation in 3T3-L1 adipocytes. *Journal of Ethnopharmacology*, 216, 8.

Singh, J., Inbaraj, B.S., Kaur, S., Rasane, P. and Nanda, V. 2022a. Phytochemical analysis and characterization of corn silk (*Zea mays*, G5417). *Agronomy*, 12, 777.

Singh, J., Rasane, P., Nanda, V. and Kaur, S. 2022b. Bioactive compounds of corn silk and their role in management of glycaemic response. *Journal of Food Science and Technology*, 1.

Sofowora, A., Ogunbodede, E. and Onayade, A. 2013. The role and place of medicinal plants in the strategies for disease prevention. *African Journal of Traditional, Complementary and Alternative Medicines*, 10, 210.

Shpakov, A.O. and Derkach, K.V. 2013. The functional state of hormone-sensitive adenylyl cyclase signaling system in diabetes mellitus. *Journal of Signal Transduction*, 2013.

Takanaga, Hitomi, Bhavna Chaudhuri, and Wolf B. Frommer. 2008. GLUT1 and GLUT9 as major contributors to glucose influx in HepG2 cells identified by a high sensitivity intramolecular FRET glucose sensor. *Biochimica et Biophysica Acta (BBA)-Biomembranes* 1778, 1091-1099.

Van Meerloo, J., Kaspers, G.J. and Cloos, J. 2011. Cell sensitivity assays: the MTT assay. *Cancer Cell Culture: Methods and Protocols*, 237.

Van Wyk, B.E. and Wink, M., 2018. Medicinal plants of the world. Cabi.

Venkateswaran, M., Jayabal, S., Hemaiswarya, S., Murugesan, S., Enkateswara, S., Doble, M.. Periyasamy, S. 2021. Polyphenol-rich Indian ginger cultivars ameliorate GLUT4 activity in C2C12 cells, inhibit diabetes-related enzymes and LPS-induced inflammation: an *in vitro* study. *Journal of Food Biochemistry*, 45, 13600.

Wang, K.J. and Zhao, J.L. 2019. Corn silk (*Zea mays* L.), a source of natural antioxidants with α-amylase, α-glucosidase, advanced glycation and diabetic nephropathy inhibitory activities. *Biomedicine and Pharmacotherapy*, 110, 510.

White, J.H., Wise, A., Main, M.J., Green, A., Fraser, N.J., Disney, G.H., Barnes, A.A., Emson, P., Foord, S.M. and Marshall, F.H. 1998. Heterodimerization is required for the formation of a functional GABAB receptor. *Nature*, 396, 679.

Wojcik, M., Zieleniak, A. and A Wozniak, L. 2010. New insight into A1 adenosine receptors in diabetes treatment. *Current Pharmaceutical Design*, 16, 4237.

Xiao, E. and Luo, L. 2018. Alternative therapies for diabetes: a comparison of western and traditional Chinese medicine (TCM) approaches. *Current Diabetes Reviews*, 14, 487.

Xie, L.J., Xie, X.Z., Zhou, Y.W., Liang, C., Jiang, Y.Y. and Chen, Z. 2016. Effect of heat stress on the expression of GABA receptor mRNA in the HPG axis of Wenchang chickens. *Brazilian Journal of Poultry Science*, 18, 277.

Yagasaki, K. and Muller, C.J. 2022. The effect of phytochemicals and food bioactive compounds on diabetes. *International Journal of Molecular Sciences*, 23, 7765.

Yamamoto, N., Ueda-Wakagi, M., Sato, T., Kawasaki, K., Sawada, K., Kawabata, K., Akagawa, M. and Ashida, H. 2015. Measurement of glucose uptake in cultured cells. *Current Protocols in Pharmacology*, 71, 12.

Yang, T., Gao, X., Sandberg, M., Zollbrecht, C., Zhang, X.M., Hezel, M., Liu, M., Peleli, M., Lai, E.Y., Harris, R.A. and Persson, A.E.G. 2015. Abrogation of adenosine A 1 receptor signalling improves metabolic regulation in mice by modulating oxidative stress and inflammatory responses. *Diabetologia*, 58, 1610.

Yang, H. and Yang, L. 2016. Targeting cAMP/PKA pathway for glycemic control and type 2 diabetes therapy. *Journal of Molecular Endocrinology*, 57, 93-108.

Yasuda, N., Inoue, T., Horizoe, T., Nagata, K., Minami, H., Kawata, T., Hoshino, Y., Harada, H., Yoshikawa, S., Asano, O. and Nagaoka, J. 2003. Functional characterization of the

adenosine receptor contributing to glycogenolysis and gluconeogenesis in rat hepatocytes. *European Journal of Pharmacology*, 459, 159.

Zhang, Y., Wu, L., Ma, Z., Cheng, J. and Liu, J. 2015. Anti-diabetic, anti-oxidant and anti-hyperlipidemic activities of flavonoids from corn silk on STZ-induced diabetic mice. *Molecules*, 21, 7.

Zhang, Y., Chen, J., Zeng, Y., Huang, D. and Xu, Q. 2019. Involvement of AMPK activation in the inhibition of hepatic gluconeogenesis by *Ficus carica* leaf extract in diabetic mice and HepG2 cells. *Biomedicine and Pharmacotherapy*, 109, 188.

Zhang, Y., Yan, L.S., Ding, Y., Cheng, B.C.Y., Luo, G., Kong, J., Liu, T.H. and Zhang, S.F. 2020. *Edgeworthia gardneri* (Wall.) Meisn. water extract ameliorates palmitate induced insulin resistance by regulating IRS1/GSK3β/FoxO1 signaling pathway in human HepG2 hepatocytes. *Frontiers in Pharmacology*, 10, 1666.

Zhang, J., Hou, Y., Du, X.L., Chen, D., Sui, G., Qi, Y., Licinio, J., Wong, M.L. and Yang, Y. 2021. ADORA1-driven brain-sympathetic neuro-adipose connections control body weight and adipose lipid metabolism. *Molecular Psychiatry*, 26, 2805.

Zhou, Y.J., Xu, N., Zhang, X.C., Zhu, Y.Y., Liu, S.W. and Chang, Y.N. 2021. Chrysin improves glucose and lipid metabolism disorders by regulating the AMPK/PI3K/AKT signaling pathway in insulin-resistant HepG2 cells and HFD/STZ-induced C57BL/6J mice. *Journal of Agricultural and Food Chemistry*, 69, 5618.

Zhou, J.N., Li, M.Y. and Zhang, T.T. 2024. Synergistic effects of three traditional herbs green tea, mulberry leaf and corn silk on glucose uptake level of L6 myoblasts and the hypoglycemic mechanism. *Traditional Medicine Research*, 9, 37.

Žilić, S., Janković, M., Basić, Z., Vančetović, J. and Maksimović, V. 2016. Antioxidant activity, phenolic profile, chlorophyll and mineral matter content of corn silk (*Zea mays* L): comparison with medicinal herbs. *Journal of Cereal Science*, 69, 363.

Supplementary materials

Table S1: Temperatures used for qualitative polymerase chain reaction

Stage	Number of cycles	Temperature	Time (minutes: seconds)
Hold	1	50 °C	02:00
		95 °C	10:00
Polymerase chain reaction	40	95 °C	00:15
		60 °C	01:00
		95 °C	00:15
Melt curve	1	95 °C	00:15
		60 °C	01:00
		95 °C	00:01
Hold stage	Infinite	4 °C	Infinite

Table S2: Cell viability based on mitochondrial activity of HepG2 cells treated with different corn silk extracts, untreated, insulin and metformin

Treatment	Cell viability % Run 1	Cell viability % Run 2	Cell viability % Run 3	Cell viability % average	Standard deviation
AQP 5 µg/mL	59.84	60.63	60.24	60.24	0.39
AQP 25 µg/mL	79.53	77.95	78.74	78.74	0.79
AQP 50 µg/mL	97.64	96.06	98.43	97.38	1.20
AQP 75 µg/mL	107.24	104.02	104.41	105.22	1.76
AQP 100 µg/mL	107.95	108.66	109.45	108.69	0.75
AQM 5 µg/mL	67.72	68.50	70.08	68.77	1.20
AQM 25 µg/mL	88.98	90.55	89.76	89.76	0.79
AQM 50 µg/mL	95.28	96.85	100.79	97.64	2.84
AQM 75 µg/mL	116.54	118.90	118.90	118.11	1.36
AQM 100 µg/mL	125.20	126.77	122.83	124.93	1.98
HYP 5 µg/mL	81.89	82.68	83.46	82.68	0.79
HYP 25 µg/mL	90.55	87.40	90.55	89.50	1.82

HYP 50 µg/mL	99.21	95.28	96.06	96.85	2.08
HYP 75 µg/mL	122.83	120.87	118.90	120.87	1.97
HYP 100 µg/mL	103.15	102.76	102.36	102.76	0.39
HYM 5 µg/mL	94.49	95.28	93.70	94.49	0.79
HYM 25 µg/mL	106.30	104.72	105.51	105.51	0.79
HYM 50 µg/mL	114.17	111.81	114.96	113.65	1.64
HYM 75 µg/mL	128.35	130.71	133.07	130.71	2.36
HYM 100 µg/mL	110.24	107.87	107.09	108.40	1.64
ETP 5 µg/mL	85.83	87.40	90.55	87.93	2.41
ETP 25 µg/mL	97.64	100.00	99.21	98.95	1.20
ETP 50 µg/mL	114.17	112.60	113.39	113.39	0.79
ETP 75 µg/mL	133.07	135.43	133.86	134.12	1.20
ETP 100 µg/mL	112.60	118.90	114.17	115.22	3.28
ETM 5 µg/mL	96.06	99.21	97.64	97.64	1.57
ETM 25 µg/mL	114.17	114.57	114.96	114.57	0.39
ETM 50 µg/mL	133.07	133.86	134.65	133.86	0.79
ETM 75 µg/mL	144.09	146.46	145.28	145.28	1.18
ETM 100 µg/mL	129.92	126.77	129.13	128.61	1.64
UNT	101.57	98.43	100.00	100.00	1.57
MET (1 µM)	92.13	91.34	92.91	92.13	0.79
INS (1 µM)	70.08	67.72	68.50	68.77	1.20

%: percentage AQP: aqueous extract of premature CS, AQM: aqueous extract of mature CS, HYP: hydro-ethanolic extract of premature CS, HYM: hydro-ethanolic extract of mature CS, ETP: ethanolic extract of premature CS, ETM: ethanolic extract of mature CS, UNT: untreated, MET: metformin, INS: insulin.

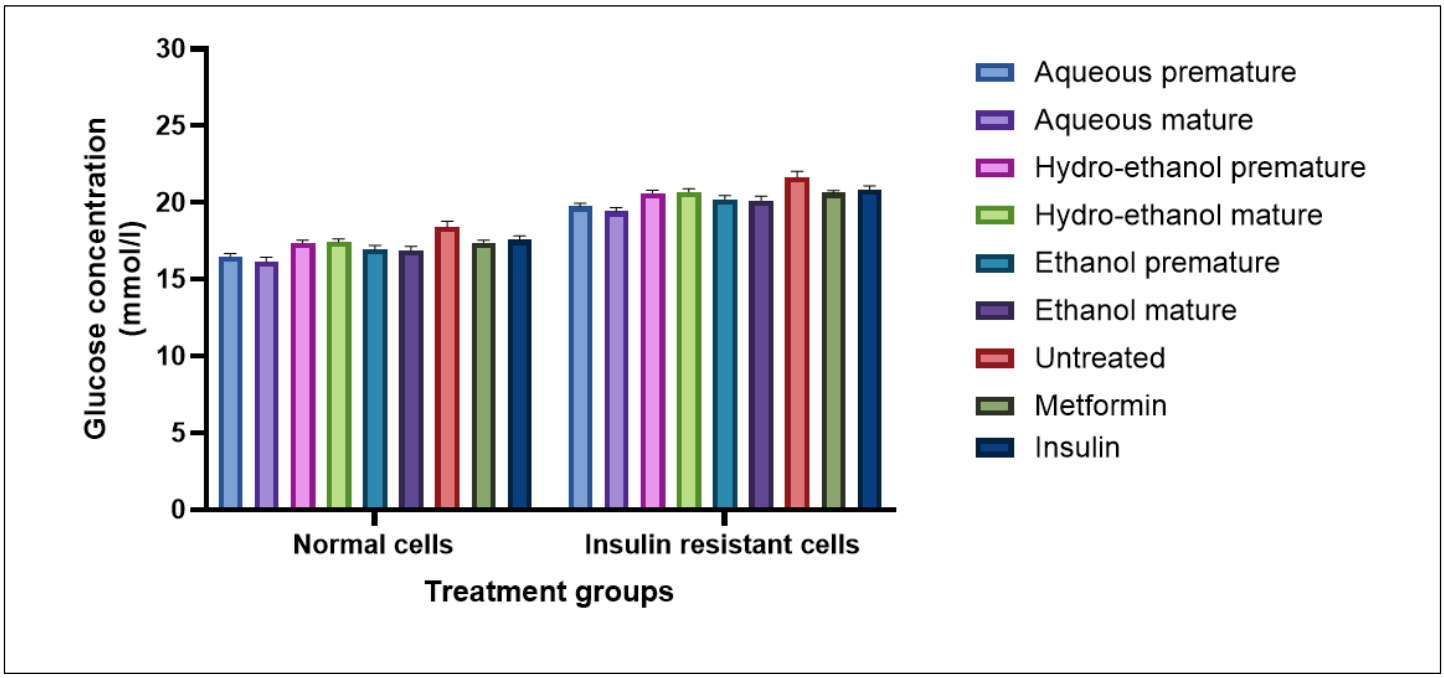

Figure S1: The effect of CS extracts on the concentration of glucose present in the culture media consisting of normal and insulin-resistant HepG2 cells in comparison to culture media (untreated; negative control), insulin and metformin (positive controls). Aqueous extract of premature CS (100 µg/mL), aqueous extract of mature CS (100 µg/mL), hydro-ethanolic extract of premature CS (75 µg/mL), hydroethanolic extract of mature CS (75 µg/mL), ethanolic extract of premature CS (75 µg/mL), ethanolic extract of mature CS (75 µg/mL), metformin (1 µM) and insulin (1 µM)

Table S3: Concentration of glucose following treatment with different extracts of corn silk, untreated, insulin and metformin

Type of HepG2 cell	Treatment	Glucose concentration 1	Glucose concentration 2	Glucose concentration 3	Glucose concentration 4	Average	Standard deviation
Normal	AQP 100 µg/mL	16.60	16.20	16.60	16.60	16.50	0.17
	AQM 100 µg/mL	15.90	16.00	16.40	16.40	16.18	0.23
	HEP 75 µg/mL	17.20	17.30	17.40	17.60	17.38	0.15
	HEM 75 µg/mL	17.40	17.60	17.20	17.60	17.45	0.17
	ETP 75 µg/mL	16.90	17.10	17.20	16.60	16.95	0.23

	ETM 75 µg/mL	16.80	17.00	17.20	16.60	16.90	0.22
	UNT	18.30	18.80	18.60	17.90	18.40	0.34
	MET 1 µM	17.30	17.40	17.30	17.60	17.40	0.12
	INS 1 µM	17.70	17.80	17.60	17.20	17.58	0.23
Insulin-resistant HepG2 cells	AQP 100 µg/mL	19.85	19.45	19.85	19.85	19.85	0.20
	AQM 100 µg/mL	19.15	19.25	19.65	19.65	19.65	0.26
	HEP 75 µg/mL	20.45	20.55	20.65	20.85	20.85	0.17
	HEM 75 µg/mL	20.65	20.85	20.45	20.85	20.85	0.19
	ETP 75 µg/mL	20.15	20.35	20.45	19.85	19.85	0.26
	ETM 75 µg/mL	20.05	20.25	20.45	19.85	19.85	0.26
	UNT	21.55	22.05	21.85	21.15	21.15	0.39
	MET 1 µM	20.55	20.65	20.55	20.85	20.85	0.14
	INS 1 µM	20.95	21.05	20.85	20.45	0.26	20.95

Aqueous premature: aqueous extract of premature CS (100 µg/mL), aqueous mature: aqueous extract of mature CS (100 µg/mL), hydro-ethanolic premature: hydro-ethanolic extract of premature CS (75 µg/mL), hydro-ethanolic mature: hydro-ethanolic extract of mature CS (75 µg/mL), ethanol premature: ethanolic extract of premature CS (75 µg/mL), ethanol mature: ethanolic extract of mature CS (75 µg/mL), UNT: untreated, MET: metformin, INS: insulin.

Table S4: Cycle threshold (cT) values obtained for polymerase chain reaction of *ADORA1* and *GABBR1*

Gene	Treatment	cT mean run 1	cT mean run 2	Δ Δ cT run 1	Δ Δ cT run 2	RA 1	RA 2	RA %	RA %
ADORA1	AQP 100 µg/mL	35.13	37.26	4.86	5.13	0.03	0.03	2.05	2.86
	AQM 100 µg/mL	38.86	37.40	5.03	4.41	0.03	0.05	3.07	4.70
	HEP 75 µg/mL	28.69	28.53	4.79	4.79	0.04	0.04	3.63	3.61
	HEM 75 µg/mL	29.17	29.17	4.10	4.11	0.06	0.06	5.80	5.79
	ETP 75 µg/mL	34.47	36.58	4.81	4.02	0.04	0.06	3.56	6.15
	ETM 75 µg/mL	35.51	30.60	4.32	4.02	0.05	0.06	5.01	6.12
	MET 1 µM	23.75	36.11	2.26	2.15	0.21	0.22	20.94	22.46
	INS 1 µM	24.11	21.67	1.95	1.92	0.26	0.26	25.83	26.46
	UNT	22.13	36.58	0.00	0.00	1	1	100	100.00
GABBR1	AQP 100 µg/mL	35.57	36.44	5.61	5.42	0.02	0.02	2.05	2.33
	AQM 100 µg/mL	38.58	37.01	5.06	5.12	0.03	0.02	3.00	2.87
	HEP 75 µg/mL	27.99	28.10	5.39	5.50	0.02	0.02	2.39	2.30
	HEM 75 µg/mL	29.19	28.99	4.16	4.42	0.41	0.47	4.09	4.68
	ETP 75 µg/mL	34.80	36.99	5.45	5.55	0.02	0.02	2.28	2.14
	ETM 75 µg/mL	36.31	29.05	5.42	5.20	0.02	0.27	2.33	2.75
	MET 1 µM	22.95	35.85	1.75	1.72	0.29	0.30	29.56	30.40
	INS 1 µM	24.47	20.56	2.61	2.77	0.16	0.15	16.37	14.66
	UNT	21.83	36.99	0.00	0.00	1.00	1.00	100	100.00

cT: cycle threshold, RA: relative abundance, RA %: percentage relative abundance

Chapter six

Chapter six

1. General discussion

Diabetes mellitus (DM) is one of the oldest known human diseases in history (Olokoba *et al*., 2012). Among the types of DM, type 2 diabetes mellitus (T2DM) is the most prevalent, constituting roughly 90% of global cases (Galicia-Garcia *et al*., 2020). It is characterized by elevated blood glucose levels due to relative insulin deficiency resulting from abnormal insulin production and/or resistance to insulin (Caturano *et al*., 2023). If not properly managed or left untreated, T2DM can result in severe secondary complications which affect diverse organs of the body (Bhatti *et al*., 2022). These secondary complications encompass cardiovascular diseases (congestive heart failure, arterial hypertension, ischemic heart disease, heart failure), diabetic neuropathy, nephropathy, diabetic retinopathy (e.g., blurred vision, floaters and blindness), diabetic ketoacidosis, diabetes-induced coma, liver cirrhosis, increased susceptibility to infections (not limited to urinary tract infections, skin infections and frequent yeast infections), slow wound healing, sexual dysfunction and mental health-associated problems such as depression and heightened anxiety (Lankatillake *et al*., 2019; Farmaki *et al*., 2020). Therefore, to minimize the risk of secondary complications as well as prevent premature mortality, effective management of the disease is crucial (Lankatillake *et al*., 2019; Sabiu *et al*., 2019). Apart from maintaining a healthy diet, engaging in regular physical activity, and effectively managing weight loss (Paddy *et al*., 2014), the administration of synthetic medications stands as the prevailing and efficacious approach for managing T2DM (Michaelidou *et al*., 2023). However, implementing and maintaining lifestyle modifications for prolonged periods of time is challenging for a majority of patients due to the accessibility of caloric dense foods and sedentary diets (Ahmad *et al*., 2022). Additionally, synthetic medications used in T2DM therapy are expensive, not readily available and are often accompanied by signficant adverse effects (Lankatillake *et al*., 2019). Consequently, there is a strong pursuit for novel therapeutic agents with promising antidiabetic potentials that can be used as complementary adjuncts or alternatives to synthetic medications for the management of T2DM and its associated complications.

The use of natural products within traditional systems of medicine continues to be esteemed as a preferred healthcare approach in numerous communities with more than 60% of the world's population, particularly around 80% in developing nations, relying on medicinal plants for their healthcare needs (Chaachouay *et al*., 2023). Several factors such as affordability, accessibility,

and safety considerations have contributed to the use of medicinal plants for the treatment of many human diseases (Mushtaq *et al*., 2018), including T2DM (Mohammed *et al*., 2022). The practice of developing medicines from natural sources is not a recent phenomenon (Mintah *et al*., 2019), with many commercially available pharmaceutical products having plant-based origins (Shakya *et al.,* 2016; Mintah *et al*., 2019). For example, opium, aspirin, digitalis, quinine and metformin are a handful of synthetic drugs that have been discovered through ethnopharmacological investigations (Balunas *et al*., 2005; Sarkar *et al*., 2015). Modern medicine currently compromises of active compounds which have been isolated from plants, with around 80% of these ingredients showing a favorable correlation between modern therapeutic applications and their traditional uses (Sarkar *et al*., 2015). Given that a majority of herbal remedies often diverge from strictly adhering to scientific evidence, continuous and comprehensive research on medicinal plants becomes imperative for advancing the development of new medicines and/or treatment methods (Mintah *et al*., 2019). Africa serves as a promising source for novel therapeutic agents due to its rich biodiversity and expansive repository of medicinal plants that have provided therapeutic potential against a range of diseases (Mohammed *et al*., 2022). Several indigenous African flora play a fundamental role in African traditional systems of medicine and are used for the treatment of T2DM and its associated complications (Odeyemi *et al*., 2018).

Corn silk (CS) exemplifies a natural product with extensive therapeutic potentials, including diuretic, antihyperlipidemic, antihypertensive, anti-obesity, anti-microbial, neuroprotective, anti-cancer, anti-depressant, antioxidant, anti-inflammatory, and antidiabetic (Kaur *et al*., 2023). It is an abundant waste material of corn cultivation (Hasanudin *et al*., 2012), and has been used as traditional medicine to address several diseases (Chen *et al*., 2013b), including cystitis, jaundice, kidney disorders, oedema, gout, rheumatism, arthritis, prostate disorders, heart ailments, malaria, obesity, bladder and urinary infections, psychological conditions, cancer, microbial infections and hyperglycemia (Grases *et al*., 1993; Hasanudin *et al*., 2012; Wang *et al*., 2012; Chen *et al*., 2013b; Sabiu *et al*., 2016; Wang *et al*., 2019). While the antidiabetic properties of CS has been well-documented (Guo *et al*., 2019; Zhao *et al*., 2012; Chen *et al*., 2013b; Pan *et al*., 2017; Chaudhary *et al*., 2022), there is limited evidence on its exact mechanism of action of CS, particularly its relationship with the key therapeutic targets implicated in the pathogenesis of T2DM. Using metabolomics and advanced computational approaches, the study lent scientific credence to possible mechanisms of antidiabetic action of

CS. The results of the computational assessment of CS metabolites on key therapeutic genes implicated in T2DM were thereafter validated *in vitro* in HepG2 cells.

Ultra-performance liquid chromatography-mass spectrometry (UPLC-MS) analysis of four samples of CS (raw and three extracts: aqueous, hydro-ethanolic, and ethanolic) at two growth stages (premature and mature) identified 128 secondary metabolites (Supplementary Table S1, Chapter 3). All samples contained these metabolites, but their quantities varied significantly ($p > 0.05$). Apart from the raw samples, the mature CS samples had a higher overall abundance of metabolites than premature ones (Figure 3, Supplementary Table S2, Chapter 3). The maturity of a plant plays a significant role in the qualitative and quantitative extraction of plant compound (Tsao *et al*., 2006; Adegbaju *et al*., 2020). This observation is in agreement with Adegbaju *et al*. (2020) , in which aqueous extracts of mature *Celosia argentea L* produced significantly higher yield of secondary metabolites compared to the premature one (Adegbaju *et al*., 2020). Additionally, among the different solvents employed for extraction of CS secondary metabolites, the hydro-ethanolic extract from mature CS had the highest relative abundance of a majority of metabolites (Supplementary Table S2, Chapter 3). This observation is attributed to the polarity of the solvent, in which hydro-ethanol is moderately polar, allowing for the extraction of more polar and less polar compounds more efficiently (Bitwell *et al*., 2023). Once the library of the metabolites were generated, it was possible to elucidate their relationship with targets implicated in the pathogenesis of T2DM.

Discovering and developing novel therapeutic agents that target specific enzymes involved in glucose metabolism and insulin signalling is a crucial strategy for advancing antidiabetic treatments (Kanwal *et al*., 2022). By modulating the activity of these key enzymes, researchers aim to improve glucose control, enhance insulin sensitivity, and address the metabolic imbalances characteristic of diabetes. (Kanwal *et al*., 2022; Balogun *et al*., 2023). These approaches aim to improve blood glucose control, enhance insulin sensitivity, and reduce the risk of long-term complications in individuals with T2DM (Oboh *et al*., 2014; Sharma *et al*., 2021; Thakur *et al*., 2021). In this study, the inhibition of six enzymes implicated in the pathogenesis of T2DM and its associated secondary complications by CS metabolites was investigated using computer-aided drug design approaches, such as molecular docking and molecular dynamics (MD) simulation. Alpha-amylase (AA) and alpha-glucosidase (AG) are key enzymes in carbohydrate metabolism, accelerating the breakdown of carbohydrates into simple sugars, which can cause rapid increases in blood glucose levels (Nair *et al*., 2013). Dipeptidyl peptidase-4 (DPP-4) deactivates glucagon-like peptide-1, an incretin hormone that

promotes insulin release and inhibits glucagon secretion—both critical for maintaining blood glucose balance (Duez *et al*., 2012; Gilbert *et al*., 2020). Protein tyrosine phosphatase 1B (PTP1B) impairs insulin signalling by dephosphorylating insulin receptors and downstream signalling molecules, reducing insulin sensitivity in muscles, liver, and adipose tissue, which leads to decreased glucose uptake and elevated blood glucose levels (Thareja *et al*., 2012). Aldose reductase (AR) and sorbitol dehydrogenase (SDH) are central to the polyol pathway, which converts glucose to sorbitol and sorbitol to fructose, respectively (Omotosho *et al*., 2014; Sabiu *et al*., 2017). The accumulation of sorbitol and fructose can cause osmotic and oxidative stress, contributing to diabetic complications, particularly in insulin-independent tissues such as the eyes, kidneys, and nerves (Tang *et al*., 2012; Omotosho *et al*., 2014).

Molecular docking, a structure-based drug design method (Pagadala *et al*., 2017), facilitated the evaluation of how CS metabolites bind to the active sites of the six investigated enzymes, providing valuable insights on the interactions between the CS metabolite-enzyme complexes (Pagadala *et al*., 2017; Pantsar *et al*., 2018). The most negative docking scores of CS metabolites aesculin, austricin, (6e)-1-(4-hydroxyphenyl)-7-phenylhepta-4,6-dien-3-one, (-)-11-hydroxy-9,10-dihydrojasmonic acid 11-beta-D-glucoside, phaseic acid and erythronolide B against AA, AG, AR, DPP-4, PTP1B and SDH, respectively, in comparison to the respective standards (Table 1, Chapter 3), indicating their better binding affinities, interaction, superiority and their greater suitability or fitness as bioactive compounds (Agarwal *et al*., 2016; Lanrewaju *et al*., 2023a). Molecular docking analysis has been used to explore how CS metabolites interact with T2DM-related targets (Sawangwong *et al*., 2024), particularly enzymes such as α-glucosidase, protein tyrosine phosphatase 1-B, dipeptidyl peptidase-4, and α-amylase. Studies by Alvarado *et al*. (2019) and Chaudhary *et al*. (2022) demonstrated that CS metabolites have good binding affinity with these therapeutic targets, suggesting their potential as effective modulators.

Subsequently, MD simulation, a computational approach which allows the analysis on the behavior of molecules over time (Shode *et al*., 2022), was employed to appraise molecular conformational changes that resulted from the binding of the CS metabolite to the target enzymes (Chapter 3). The study employs the Molecular Mechanics/GB Surface Area (MM/GBSA) technique to compute binding free energies (ΔG_{bind}) with lower ΔG_{bind} values correlating with heightened binding affinity between a ligand and a specific target protein (Hata *et al*., 2021). The high negative ΔG_{bind} values for R)-7-butyl-6,8-dihydroxy-3-[(3e)-pent-3-en-1-yl]-3,4-dihydroisochromen-1-one, 1-O-vanilloyl-beta-D-glucose, (-)-11-hydroxy-9,10-

dihydrojasmonic acid 11-beta-D-glucoside, p-coumaroyl malic acid, 2-hydroxydecanedioic acid, and (-)-11-hydroxy-9,10-dihydrojasmonic acid 11-beta-D-glucoside indicate a robust binding affinity to AA, AG, AR, DPP-4, PTP1B, and SDH, respectively (Table 2, Chapter 3). Most CS metabolites displayed reduced ΔG_{bind} values when bound to the investigated enzymes compared to the reference standards, highlighting the greater potential of CS metabolites for modulating the investigated enzymes respectively (Table 2, Chapter 3). Assessment of post-MD simulation components, including root mean square deviation (RMSD), root mean square fluctuation (RMSF), radius of gyration (ROG), solvent accessible surface area (SASA) and number of intramolecular hydrogen bonds (H-bonds), revealed that the CS metabolites formed more thermodynamically stable complexes with the enzyme targets compared to the apo-eznyme and the respective standards (Table 3, Chapter 3). Additionally, ligand-receptor interaction plots denoted a higher number of interactions between the CS metabolites and target enzymes, compared to the reference standard investigated (Figures 11 – 17, Chapter 3), highlighting the stability between the CS metabolites-enzyme complexes. Several studies have used MD simulation to investigate the mechanism of antidiabetic action of natural plants such as *Aegle marmelos*, *Helianthus annuus* (sunflower) seed, *Momordica charantia*, *Englerophytum magalismontanum, Azadirachta indica, Aspalathus linearis* and *Trigonella foenum-graecum* (fenugreek) (Rampogu *et al*., 2018; Arif *et al*., 2021; Akoonjee *et al*., 2022; Olaokun *et al*., 2022; Sharma *et al*., 2022; Abdullah *et al*., 2023; Rampadarath *et al*., 2023) as well as plant compounds such as chlorogenic acid, luteolin and dihydropyrimidinone derivatives (Singh *et al*., 2021; Ilyas *et al*., 2022; Kahksha *et al*., 2023). Therefore, the inhibition of the six investigated target enzymes by metabolites present in CS is denoted as a potential mechanism of action conferring CS with its antidiabetic properties. The antidiabetic mechanism of action of CS is through the modulation of AA, AG, AR, DPP-4, PTP1B, and SDH by CS metabolites R)-7-butyl-6,8-dihydroxy-3-[(3e)-pent-3-en-1-yl]-3,4-dihydroisochromen-1-one, 1-O-vanilloyl-beta-D-glucose, (-)-11-hydroxy-9,10-dihydrojasmonic acid 11-beta-D-glucoside, p-coumaroyl malic acid, 2-hydroxydecanedioic acid, and (-)-11-hydroxy-9,10-dihydrojasmonic acid 11-beta-D-glucoside respectively, demonstrating their potential to prevent carbohydrate and glucagon-like peptide 1 breakdown, enhance insulin signaling and reduce sorbitol and fructose accumulation in cells. These actions contribute to CS's antidiabetic effects by targeting enzymes involved in T2DM pathogenesis and its complications.

Density functional theory (DFT), a computational quantum mechanical modelling technique (Assadi *et al*., 2013) was employed to access the molecular characteristics of the CS metabolites (Table 9, Figure 17, Chapter 3). Energy gap (ΔE) calculations derived from the highest occupied molecular orbital (HOMO) and the lowest unoccupied molecular orbital (LUMO) are crucial for understanding the mechanism of action of lead compounds, as they provide insights into the compounds' reactivity, kinetic stability, and chemical characteristics (Karabacak *et al*., 2012; Rampadarath *et al*., 2023). A wide energy gap suggests firmness, low chemical reactivity, and hardness, while a small energy gap indicates softness and high chemical reactivity (Esha *et al*., 2024). The chemical hardness evaluates the chemical stability of a molecule and plays a crucial role in investigations pertaining to drug design elucidations, with soft molecules distinguished by elevated level of polarizability compared to hard molecules, primarily because of their reduced energy demand for excitation (Larenwaju *et al*., 2023). The lowest energy gaps, higher chemical softness and lower chemical hardness observed by some of the top-ranked CS compounds did not correlate with their ΔG_{bind}, and this could be due to the observed relative residue fluctuations and increased surface area of the enzyme targets upon ligand binding. This result is consistent with Rampadarath *et al*. (2023) in which the higher negative binding energy of Formoxanthone B complexed with MMP1 did not correlate with the lower energy gap. Remarkably, all the top-ranked CS metabolites had electrophilicity index above 1.5 eV, suggesting they are strong electrophiles with a significant electrophile presence around the molecules. The high electrophilicty of the CS metabolites highlights their ability to form covalent bonds with a target protein, leading to enhanced interaction between the protein and metabolite (McQuade *et al*., 2016). Additionally, it provides insights into the reactivity and specificity of the ligand, resulting in reactive ligands with enhanced specificity towards a target protein (McCammon *et al*., 2007; Rees, 2017).

In addition to enzymes, notable links have been established between signaling pathways and the pathogenesis of T2DM (Ahmad *et al*., 2022). A number of signaling pathways substantially control the advancement of pathological alterations occurring in T2DM such as insulin-resistance, β-cell dysfunction and other additional pathogenic disturbances (Cao *et al*., 2020). Signaling pathways regulate key processes, including chronic inflammation, incretin dysregulation, hyperglycemia, lipolysis, central appetite dysregulation, irregular gastric emptying, gut dysbiosis and deposition of islet amyloid polypeptide, all of which are involved in the pathophysiology of T2DM (Ahmad *et al*., 2022). A thorough comprehension of signaling pathways is crucial for in-depth understanding on the pathological mechanisms underlying

T2DM, as well as for advancing the development of novel targeted drugs and interventions to address T2DM and its associated complications (Perreault *et al*., 2021).

Network pharmacology analysis was used to investigate how CS metabolites interact with signalling pathways and genes related to T2DM. This approach, which combines systems biology, bioinformatics, high-throughput histology, pharmacology, and information networks, is cost-effective and efficient (Zhou *et al*., 2020). It allows the discovery of potential drug candidates by regulating multiple signalling pathways, improving drug efficacy, reducing side effects, enhancing clinical trial success rates, and lowering drug discovery costs (Zhang *et al*., 2013; Chandan *et al*., 2017; Zhou *et al*., 2020). Through network pharmacology analysis, the mechanism of action of CS against many diseases, including obesity, Alzheimer's and gout, has been elucidated (Oh *et al*., 2021; Zhang *et al*., 2022; Tao *et al*., 2023). In the present study, network pharmacology was employed to elucidate the molecular mechanism of antidiabetic action of CS through investigating the effect the plant material has on different signalling pathways and the genes involved in these pathways (Chapter 4). Kyoto encyclopaedia of genes and genomes (KEGG) pathway enrichment analysis revealed Cyclic adenosine 3,5-monophosphate (cAMP) pathway as the hub signalling pathway (Figure 5, Table 1, Chapter 4). The cAMP signalling pathway has been implicated in the maintenance of glucose homeostasis through several avenues, including insulin and glucagon secretion, glucose uptake, glycogen synthesis and breakdown, gluconeogenesis, maintenance of β-cell differentiation, and neural control of glucose homeostasis (Chen *et al*., 2013a: Deb *et al*., 2017). Within this pathway, a higher number of CS metabolites modulated the activity of adenosine A1 receptor (*ADORA1)*, hydroxycarboxylic acid receptor 2 (*HCAR2)* and gamma-aminobutyric acid type B receptor subunit 1 (*GABBR1)* (Figure 8, Chapter 4), suggesting their potential as therapeutic target genes for the management of T2DM.

The activation of adenosine A1 receptor (*ADORA1*), a G-protein-coupled receptor (Wojcik *et al*., 2010; Lv *et al*., 2022) inhibits the activity of adenylate cyclase, resulting in a reduction in cAMP levels (Nomiri *et al*., 2022), which are pleiotropic messengers that mediate the effects of various hormones involved in the regulation of metabolism (Almahariq *et al*., 2014). Reduced cAMP levels result in the downregulation of protein kinase A activity, which leads to decreased glycogen breakdown and altered glycogen synthesis, impaired cellular response to hormones (reduced mobilization of glucose, impaired insulin signalling and insulin resistance) as well as diminished transcriptional activation of key metabolic genes (Shpakov *et al*., 2013; Almahariq *et al*., 2014; Yang *et al*., 2016). Therefore, inhibition of *ADORA1* promotes

adenylate cyclase activity resulting in higher cAMP levels leading to elevated activation of protein kinase A, stimulating gluconeogenesis and glycogenolysis, improving insulin sensitivity, increasing glucose uptake (Cheng *et al*., 2000; Yang *et al*., 2015). This highlights its importance as a therapeutic target for several diseases, including T2DM (Nieto Gutierrez *et al*., 2018; Nomiri *et al*., 2022; Duyu *et al*., 2020).

Hydroxycarboxylic acid receptor 2 (*HCAR2*), a G-protein-coupled receptor primarily expressed in the brain (Moutinho *et al*., 2022), is responsible for mediating the antilipolytic actions of niacin and the lowering of blood lipid levels (Newman *et al*., 2014). The expression of *HCAR2* in mammalian cells affects the regulation of inflammatory factors, inhibition of lipolysis, glucose homeostasis and the inhibition of insulin secretion (Wang *et al*., 2016). Therefore, *HCAR2* plays a crucial role in several diseases, including obesity, aging associated hepatic steatosis, colitis and T2DM (Jadeja *et al*., 2019; Tuteja, 2019, Shon *et al*., 2021; Zhang *et al*., 2023). Liu *et al*. (2014) demonstrated that individuals with T2DM had higher expression levels of *HCAR2* in their peripheral blood leukocytes compared to healthy individuals, indicating that *HCAR2* signalling may be involved in T2DM and the regulation of inflammatory cytokines (Liu *et al*., 2014). A human study found that treatment with 500-2000 mg/day of metformin, an antidiabetic agent used to manage T2DM, led to a decrease in *HCAR2* expression compared to a control group not receiving metformin (Xu et al., 2017), highlighting *HCAR2* as a promising target for the management of T2DM (Liu *et al*., 2014; Xu *et al*., 2017).

Gamma-aminobutyric acid B [*GABA(B)*] is heterodimeric guanine nucleotide-binding protein G protein-coupled receptor (GPCR) consists of gamma-aminobutyric acid type B receptor subunit 1 (*GABBR1*) and gamma-aminobutyric acid type B receptor subunit 2 (*GABBR2*) (White *et al*., 1998). Within *GABA(B)*, *GABBR1* binds to agonists whilst *GABBR2* mediates coupling to G-proteins (Nomura *et al*., 2008). In pancreatic β-cells, *GABA(B)* plays a role in the regulation of glucose homeostasis through the inhibition of insulin secretion (Bonaventura *et al*., 2008). Upon the binding of ligands to the GABA receptor, the occurrence of conformational changes arise which triggers signalling via the guanine nucleotide-binding proteins as well as modulates the cAMP pathway and down-stream effectors such as adenylate cyclase (Hill, 1985; Geng *et al*., 2013). As previously mentioned, the adenylate signalling system is implicated in the pathogenesis and aetiology of T2DM and its associated secondary complications (Sphakov *et al*., 2013). Additionally, G-protein-coupled receptors (GPCRs) in islet β-cells are recognized for their involvement in regulating islet function, making them potential therapeutic targets for the treatment of T2DM (Ahren, 2009). Rachdi *et al.* (2020)

demonstrated that baclofen, a GABA(B) agonist modulates cAMP signalling in the human beta cell line ECN90, which subsequently decreased the expression of beta-specific genes, modulating beta cell differentiation and insulin signalling (Rachdi *et al*., 2020).

Gene ontology analysis showed that CS metabolites are involved in several key biological processes, cellular components, and molecular functions, with drug response, exosomes, and ion binding being the most significant, respectively (Figure 7, Chapter 4). Since drug response, exosomes, and ion binding are linked to the pathogenesis of T2DM (Yon Rhee *et al*., 2008; Huang-Doran *et al*., 2017; Li *et al*., 2023), this suggests that the antidiabetic effects of CS metabolites may be due to their modulation of these pathways. Subsequently, molecular docking identified the top five CS metabolites which inhibit the target genes investigated, in which quing hau sau, phaseic acid and tetradecanedioc acid had the best pose at the active site of *ADORA1*, *HCAR2* and *GABBR1*, respectively. Most of the CS metabolites reported significantly higher negative docking scores against the target genes compared to the respective standards (metformin and resveratrol) (Table2, Chapter 4) This highlights the potential of the CS metabolites as inhibitors of *ADORA1*, *HCAR2* and *GABBR1* target genes. Thereafter, ΔG_{bind} calculations produced after a 120 ns MD simulation revealed that gallicynoic acid B (-48.74 kcal/mol), dodecanedioc acid (-34.53 kcal/mol) and tetradecanedioc acid (-36.80 kcal/mol) had the highest negative ΔG_{bind} against *ADORA1*, *HCAR2* and *GABBR1* respectively (Table 3, Chapter 4), attributing to superior binding between the CS metabolites and gene targets. Post-MD simulation component analysis, including RMSD, RMSF, ROG, SASA, and number of intramolecular hydrogen bonds (H-bonds) (Figure 9-13, Chapter 4), revealed the formation of more thermodynamically stable complexes in comparison to the apo-gene, metformin and resveratrol [an antidiabetic agent which modulates the cAMP pathway (Vallianou *et al*., 2013)]. In agreement with the thermodynamic energy and post-MD simulation components, the type and amount of ligand-receptor interactions between the CS metabolites and the respective target genes were explored, in which the CS metabolites formed a greater number of interactions with the respective target genes compared to metformin and resveratrol (Figure 14, Figure 15 and Figure 16; Supplementary Figures S3–S5, Chapter 4), highlighting the stability of the CS metabolite-gene complexes. These findings suggest the potential of the CS metabolites as inhibitors of the investigated target genes *ADORA1*, *HCAR2* and *GABBR1* from the cAMP pathway.

The molecular (structural and chemical reactivity) properties of the top-ranked CS metabolites identified through network pharmacology analysis was investigated through DFT analysis. The

lower energy gap and chemical softness observed in ginsenoyne E, caffeic acid, and quinic acid against *ADORA1*, *HCAR2*, and *GABBR1*, respectively, suggests their high reactivities relative to other CS metabolites' reactivity. However, the highest chemical hardness value exhibited by quing hau sau, dodecanedioc acid, and tetradecanedioc acid against *ADORA1*, *HCAR2*, and *GABBR1*, respectively, suggest their resistance to charge transfer and are the least reactive, as evidenced by their relatively high energy gap. The top-scoring compounds' high electronegativity as well as electrophilicity index suggests their readiness to accept electrons and act as electrophiles respectively.

Although computational techniques provide valuable insights in the discovery of novel drugs, experimental validation—such as *in vitro* and *in vivo* studies—is essential to ensure the reliability, accuracy, efficacy, and safety of potential drug candidates (Shalaby *et al*., 2014). *In vitro* techniques such as cell line studies, have demonstrated the hypoglycemic properties of various plants, including *Helichrysum petiolare*, *Laurus nobilis*, *Enicostema littorale* blume, *Sonchus oleraceus* Linn and certain plant metabolites (quercetin, agrimonolide, desmethylagrimonolide, luteolin, luteolin-7-O-glucoside, kaempferol, chlorogenic acid, caffeic acid and apigenin) (Huang *et al*., 2015; Mokashi *et al*., 2017; Chen *et al*., 2019; Aladejana *et al*., 2020; Chen *et al*., 2020; Bourebaba *et al*., 2021; Yarahmadi *et al*., 2021). Chen *et al.* (2019) employed the human carcinoma cell line to reveal that caffeic acid and chlorogenic acid from *Sonchus oleraceus* Linn extract attenuated insulin resistance and modulated the uptake of glucose in HepG2 cells (Chen *et al*., 2019). However, there are presently no studies investigating the antidiabetic potential of CS through the use of a cell line study, a gap this project aimed to fulfill through elucidating the molecular mechanism of different extracts (aqueous, hydro-ethanolic and ethanolic) made from CS at two different growth stages (premature and mature) on the uptake of glucose as well as the modulation of *ADORA1* and *GABBR1* in insulin-resistant HepG2 cells.

The 3-(4,5-dimethylthiazol-2-yl)-2,5-diphenyltetrazolium bromide (MTT) assay revealed that upon treatment with different CS extracts, concentrations of 100 µg/mL (aqueous) and 75 µg/mL (hydro-ethanolic and ethanolic), induced the highest percentage of cell viability in the HepG2 cells compared to untreated, metformin and insulin (Figure 1, Chapter 5). The mature CS displayed a percentage cell viability in comparison to the premature (Figure 1, Chapter 5), possibly due to the higher abundance of a several metabolites in the mature CS samples (Chapter 3, Supplementary figure S5-S6, Supplementary Table S2). Out of all the treatments examined, the ethanolic mature extract of CS (145.28%) demonstrated the highest percentage

HepG2 cell viability, suggesting the metabolites present in the ethanolic mature CS, such as quing hau sau (artemisinin), 3-hydroxy-4-butanolide, 2-hydroxydecanedioic acid, esculetin, diaportinol, curvularol, carvone, quercetin 3-o-(6"-acetyl-glucoside), pandangolide 1a and (R)-7-butyl-6,8-dihydroxy-3-[(3E)-pent-3-en-1-yl]-3,4-dihydroisochromen-1-one, induced the viability of HepG2 cells. Although there are no studies reporting the effect of CS on HepG2 cell viability using the MTT assay, various CS extracts have been tested for cytotoxicity on different cell lines, including human breast cancer (MCF-7) and normal human mesenchymal cells (hMSC-TERT4) (Al-Oqail *et al*., 2019), human dermal fibroblast cells (Sawangwong *et al*., 2024), and mesangial cells (Wang *et al*., 2019). While CS extracts haven't been tested on HepG2 cells, other natural products have. For instance, extracts of *Allophylus cominia* showed no cytotoxic effects on HepG2 cells at 1-100 µg/mL (Semaan *et al*., 2018), and the antidiabetic activity of *Ficus carica* leaves had a half-maximal inhibitory concentration of 82.29 µg/mLafter 24 hours on HepG2 cells (Zhang *et al*., 2019).

Glucose transport is an essential process in mammalian cells which provides cellular fuel across cell surface membranes, allowing for an efficient supply of glucose needed for efficient energy metabolism (Ojo *et al*., 2023). Consequently, an understanding on these systems and the uptake of glucose in mammalian cells is crucial in studying numerous diseases (Yamamoto *et al*., 2015), including T2DM (Anthony *et al*., 2019). The decrease in glucose consumption in the HepG2 cells exposed to 0.005 µM of insulin for 24 h compared to normal HepG2 cells confirmed the establishment of insulin-resistance model in this study (Figure 2, Chapter 5), concurring with the report of Alaaeldin *et al*. (2021). At concentrations of 75 µg/mL (hydro-ethanolic and ethanolic extracts of premature and mature CS) and 100 µg/mL (aqueous extracts of CS) induced the uptake of glucose in normal and insulin-resistant HepG2 cells, compared to untreated, metformin and insulin (Table 1, Chapter 5). This effect is likely due to the presence of secondary metabolites in the CS, which aided in the uptake of glucose by the HepG2 cells. While the uptake of glucose between the aqueous (100 µg/mL) samples of CS were not significantly different from one another, both demonstrated higher uptake of glucose in both normal and insulin-resistant HepG2 cells compared to the other investigated CS extracts, metformin, insulin and untreated. Aqueous CS is abundant in several metabolites including ascorbic acid, mevalonic acid, CNP0447999, chlorogenic acid, quinic acid, caffeic acid, D-leucic acid, acetovanillone (apocynin), tetradecanedioic acid and gallicynoic acid B (more abundant in aqueous extracts of mature CS) as well as (7'R)-(+)-lyoniresinol 9'-glucoside, kaempferol 3-rhamnoside 7-galacturonide, (3R,4S,6S)-3,4,5-trihydroxy-6-[5-hydroxy-2-(4-

hydroxyphenyl)-4-oxo-3-[(2S,3S,5R)-3,4,5-trihydroxy-6-methyloxan-2-yl]oxychromen-7-yl]oxyoxane-2-carboxylic acid, blennin D and gallicynoic acid F (more abundant in aqueous extract of premature CS) (Chapter 3, Supplemetary Figure S5-S6, Table S1-S2), which are likely to be responsible for the enhanced uptake of glucose in the HepG2 cells. Although the effect of CS on the uptake of glucose in HepG2 cells is not well-reported, studies have report the enhanced glucose uptake in HepG2 cells following treatment with plant extracts including flowers from *Edgeworthia gardneri* (Wall.) Meisn, *Sambucus nigra* L. (Adoxaceae) and *Lauridia tetragona* as well as plant compounds such as chrysin, carpachromene, kaempferol, xdesmethylagrimonolide, quercetin, luteolin (Bhattacharya *et al*., 2013; Huang *et al*., 2015; Ho *et al*., 2017; Oyedemi *et al*., 2019; Zhang *et al*., 2020; Alaaeldin *et al*., 2021; Zhou *et al*., 2021). Additionally, several studies have reported that CS treatment resulted in an increase of glucose uptake in several animal models (Guo *et al*., 2009; Pan *et al*., 2017). The effect of CS on the uptake of glucose in mammalian cell lines is limited, with Guo *et al*. (2019) and Zhou *et al*. (2024) demonstrating the enhanced effect of CS on the uptake of glucose in L6 skeletal muscle cells (Guo *et al*., 2019; Zhou *et al*., 2024).

It was determined that the CS metabolites formed more thermodynamically stable complexes with *ADORA1* and *GABBR1* compared to *HCAR2*, evident post-dynamic component parameters including lower RMSD, RMSF, ROG, SASA and a higher number of hydrogen bonds (Akoonjee *et al*., 2023). In addition, the CS metabolites gallicynoic acid B and tetreadecanedioc acid displayed higher negative ΔG_{bind} against *ADORA1* and *GABBR1*, in comparison to the lower ΔG_{bind} reported from the binding of dodecanedioc acid and *HCAR2* (Akoonjee *et al*., 2023). Therefore, further analysis focused on modulation of *ADORA1* and *GABBR1*expression by the CS extracts in insulin-resistant HepG2 cells using quantitative Polymerase Chain Reaction (qPCR), a technique which simultaneously amplifies and quantifies a targeted DNA molecule (Garibyan *et al*., 2013). At concentrations of 75 µg/mL (hydro-ethanolic, and ethanolic) and 100 µg/mL (aqueous) extracts of premature and mature CS significantly ($p<0.05$) inhibited the expression of *ADORA1* and *GABBR1* in insulin-resistant HepG2 cells, compared to untreated cells, insulin, and metformin (Figure 3, Chapter 5). This finding was attributed to the metabolites present in the different samples of CS. The mature samples of CS displayed a higher reduction in the expression of *ADORA1* and *GABBR1*, in comparison to the premature (Figure 3, Chapter 5), potentially due to the relative abundance of the CS metabolites being more highly abundant in mature compared to premature (Chapter 3, Supplemetary Figure S5-S6, Table S1-S2). Among the different samples, the aqueous CS

had the highest downregulation of *ADORA1* and *GABBR1* expression, the different growth stages performing comparably with one another. Aqueous extract of mature CS (100 µg/mL) showed the greatest reduction in *ADORA1* (3.15%) and *GABBR1* expression (2.19%) compared to all other treatment groups (Figure 3, Chapter 5). Metabolomic profiling revealed that the aqueous samples of CS were rich in gallicynoic acid B and tetradecanedioc acid (Supplementary Figure S5-S6, Table S2, Chapter 3), lead compounds that modulate *ADORA1* and *GABBR1* respectively (Akoonjee *et al*, 2023). While there are no studies available showing the modulation of *ADORA1* and *GABBR1* by CS treatment in mammalian cells (such as HepG2), there are studies reporting the modulation of *ADORA1* and *GABBR1* by metabolites morusin and baclofen, which effected glucose homeostasis and insulin signalling (Lv *et al*., 2022; Rachdi *et al*., 2020). It can be said that the antidiabetic activity of CS is through the modulation of *ADORA1* and *GABBR1*, enhancing the uptake of glucose in HepG2 cells.

2. Conclusions and recommendations

- Diabetes mellitus, a complex metabolic disease, currently impacts approximately 540 million individuals globally;
- Type 2 diabetes mellitus (T2DM) accounts for approximately 90% of DM cases and is characterized by defective insulin production and/or insulin resistance in the body
- The utilization of natural products within traditional systems of medicine remains highly valued as a preferred healthcare approach in many communities, with over 60% of the global population, particularly around 80% in developing nations such as countries in Africa, still dependent on medicinal plants;
- Factors such as affordability, accessibility, and safety contribute to the use of medicinal plants for treating many human diseases;
- Corn silk (CS), an abundant waste material of corn cultivation has been used as a traditional medicine for the treatment of several diseases, including T2DM;
- Although, CS has significant therapeutic properties, including antidiabetic, its use remains underutilized in South Africa, a country where corn is one of the top three cereal crops produced yearly;
- While the antidiabetic potential of CS is well-reported, there is a knowledge gap regarding its mechanism of action;
- This study identified and validated the antidiabetic mechanism of action of CS through metabolomic profiling, computational bioprospection and experimental validation
- The findings of this study revealed that:

- Corn silk (CS) has 128 metabolites revealed by ultra-performance liquid chromatography-mass spectrometry analysis
- The developmental stage at which the CS is harvested plays a role in the relative abundance and types of its metabolites, with the mature CS having higher abundance of most of the metabolites;
- The solvent of extraction also plays a role in the type and relative abundance of metabolites in CS, with the hydro-ethanolic extract of mature CS being the most metabolites'-rich;
- The high negative binding free energy (ΔG_{bind}) of CS metabolites R-7-butyl-6,8-dihydroxy-3-[(3E)-pent-3-en-1-yl]-3,4-dihydroisochromen-1-one, 1-O-vanilloyl-beta-D-glucose, (-)-11-hydroxy-9,10-dihydrojasmonic acid 11-beta-D-glucoside, p-coumaroyl malic acid, 2-hydroxydecanedioic acid and (-)-11-hydroxy-9,10-dihydrojasmonic acid 11-beta-D-glucoside against alpha-amylase, alpha-glucosidase, aldose reductase, dipeptidyl peptidase-4, protein tyrosine phosphatase-1B and sorbitol dehydrogenase respectively, reveals their potential as modulators of the investigated enzymes;
- Post-dynamic component analysis and the ligand-free interactions revealed the CS metabolites formed more thermodynamically stable final complexes with the enzymes, compared to the respective standards;
- Therefore CS modulates the activity of alpha-amylase, alpha-glucosidase, aldose reductase, dipeptidyl peptidase-4, protein tyrosine phosphatase B and sorbitol dehydrogenase, preventing the breakdown of carbohydrates and glucagon-like peptide-1, promotes insulin signalling and reduces the accumulation of sorbitol and fructose in cells, mitigating the pathogenesis of T2DM and its secondary complications,
- Network pharmacology analysis identified the cyclic adenosine monophosphate (cAMP) pathway as the hub signalling pathway, in which *ADORA1*, *HCAR2*, and *GABBR1* were identified as the top target genes modulated by the CS metabolites;
- The high negative ΔG_{bind} of gallicynoic acid B, dodecanedioc acid and tetradecanedioc acid against *ADORA1*, *HCAR2*, and *GABBR1* respectively, compared to standards metformin and resveratrol, highlights their superior potential as inhibitors of the investigated target genes;

- The post-MD component analysis and ligand-receptor interaction plots revealed the formation of more stable final complexes between the CS phytoconstituents and *ADORA1*, *HCAR2*, and *GABBR1*, compared to the respective standards, further indicating their potential as inhibitors of the investigated target genes;
- Concentrations of 75 µg/mL (hydro-ethanolic and ethanolic extracts of CS) and 100 µg/mL (aqueous extracts of CS) promoted the viability of HepG2 cells and did not show cytotoxic effects, attributed to the abundancy of metabolites present in the different extracts of CS;
- Aqueous extracts of CS were rich in ascorbic acid, mevalonic acid, CNP0447999, chlorogenic acid, quinic acid, caffeic acid, D-leucic acid, acetovanillone (apocynin), tetradecanedioic acid, gallicynoic acid B, (7'R)-(+)-lyoniresinol 9'-glucoside, kaempferol 3-rhamnoside 7-galacturonide, (3R,4S,6S)-3,4,5-trihydroxy-6-[5-hydroxy-2-(4-hydroxyphenyl)-4-oxo-3-[(2S,3S,5R)-3,4,5-trihydroxy-6-methyloxan-2-yl]oxychromen-7-yl]oxyoxane-2-carboxylic acid, blennin D and gallicynoic acid F, which potentially promoted the uptake of glucose in normal and insulin-resistant HepG2 cells;
- Aqueous (100 µg/mL), hydro-ethanolic and ethanolic (75 µg/mL) extracts of CS at both growth stages inhibited the expression of *ADORA1* and *GABBR1* in insulin-resistant HepG2 cells compared to untreated, insulin and metformin. Aqueous samples reported the highest downregulation of *ADORA1* and *GABBR1* expression, which is attributed to the high abundance of metabolites gallicynoic acid B and tetradecanedioc acid, compounds which were identified to modulate *ADORA1* and *GABBR1* in the network pharmacology and molecular dynamics simulation study;
- Aqueous extracts of mature CS contained 41.84% gallicynoic acid B and 44.02% tetradecanedioc acid, while the aqueous extracts of premature CS samples contained 40.34% and 44.09%, respectively;
- The high concentration of gallicynoic acid B and tetradecanedioc acid in CS modulated the expression of *ADORA1* and *GABBR*1, resulting in increased consumption of glucose as well as the storage of glucose in HepG2 cells;
- Research has suggested that *ADORA1* and *GABBR1* are involved in adenylate cyclase signalling, which is responsible for the production of cAMP. Therefore, inhibition of *ADORA1* and *GABBR1* promotes adenylate cyclase signalling, resulting in higher cAMP levels leading to elevated activation of protein kinase

A, stimulating gluconeogenesis and glycogenolysis, improving insulin sensitivity and increasing glucose uptake;
    - It is therefore postulated that the antidiabetic mechanism of action of CS is through the downregulation of *ADORA1* and *GABBR1*, promoting glucose metabolism and uptake;
- Although this study has provided evidence-based data on the possible mechanisms of antidiabetic action of CS, it remains an underutilized waste material with immense therapeutic properties in South Africa;
- It is recommended that the report of this study be disseminated to communities that rely on corn as a staple diet, including developing countries such as South Africa, with a view to fully harnessing its therapeutic potential especially in the management of T2DM;
- Further *in vitro* (enzymatic assays), *in vivo* and clinical trial scientific explorations, can be performed to investigate the level of inhibition CS metabolites R-7-butyl-6,8-dihydroxy-3-[(3E)-pent-3-en-1-yl]-3,4-dihydroisochromen-1-one, 1-O-vanilloyl-beta-D-glucose, (-)-11-hydroxy-9,10-dihydrojasmonic acid 11-beta-D-glucoside, p-coumaroyl malic acid, 2-hydroxydecanedioic acid and (-)-11-hydroxy-9,10-dihydrojasmonic acid 11-beta-D-glucoside) have on target enzymes alpha-amylase, alpha-glucosidase, aldose reductase, dipeptidyl peptidase-4, protein tyrosine phosphatase and sorbitol dehydrogenase, respectively.
- In addition, for the development of gallicynoic acid B and tetradecanedioc acid as novel antidiabetic therapeutic agents, further research is required. For example, a HepG2 cell line exploring the cytotoxic and antidiabetic effects of the individual compounds, rather than the plant extracts can be performed.

References

Abdullah, A., Biswas, P., Sahabuddin, M., Mubasharah, A., Khan, D.A., Hossain, A., Roy, T., Rafi, N.M.R., Dey, D., Hasan, M.N. and Bibi, S. 2023. Molecular Dynamics simulation and pharmacoinformatic integrated analysis of bioactive phytochemicals from *Azadirachta indica* (Neem) to treat diabetes mellitus. *Journal of Chemistry*, 2023, 1-19.

Ahmad, E., Lim, S., Lamptey, R., Webb, D.R. and Davies, M.J. 2022. Type 2 diabetes. *The Lancet*, 400, 1803-1820.

Ahren, B. 2009. Islet G protein-coupled receptors as potential targets for treatment of type 2 diabetes. *Nature Reviews Drug Discovery*, 8, 369-385.

Akoonjee, A., Rampadarath, A., Aruwa, C.E., Ajiboye, T.A., Ajao, A.A.N. and Sabiu, S. 2022. Network pharmacology-and molecular dynamics simulation-based bioprospection of *Aspalathus linearis* for type-2 diabetes care. *Metabolites*, 12, 1013.

Alaaeldin, R., Abdel-Rahman, I.A., Hassan, H.A., Youssef, N., Allam, A.E., Abdelwahab, S.F., Zhao, Q.L. and Fathy, M. 2021. Carpachromene ameliorates insulin resistance in HepG2 cells via modulating IR/IRS1/PI3k/Akt/GSK3/FoxO1 pathway. *Molecules*, 26, 7629.

Aladejana, A.E., Bradley, G. and Afolayan, A.J. 2020. *In vitro* evaluation of the anti-diabetic potential of *Helichrysum petiolare* Hilliard and BL Burtt using HepG2 (C3A) and L6 cell lines. *F1000Research*, 9, 1240.

Almahariq, M., Mei, F.C. and Cheng, X. 2014. Cyclic AMP sensor EPAC proteins and energy homeostasis. *Trends in Endocrinology and Metabolism*, 25, 60-71.

Al-Oqail, M.M., Al-Sheddi, E.S., Farshori, N.N., Al-Massarani, S.M., Al-Turki, E.A., Ahmad, J., Al-Khedhairy, A.A. and Siddiqui, M.A. 2019. Corn silk (*Zea mays* L.) induced apoptosis in human breast cancer (MCF-7) cells via the ROS-mediated mitochondrial pathway. *Oxidative Medicine and Cellular Longevity*, 2019.

Alvarado-Díaz, C.S., Gutiérrez-Méndez, N., Mendoza-López, M.L., Rodríguez-Rodríguez, M.Z., Quintero-Ramos, A., Landeros-Martínez, L.L., Rodríguez-Valdez, L.M., Rodríguez-Figueroa, J.C., Pérez-Vega, S., Salmeron-Ochoa, I. and Leal-Ramos, M.Y. 2019. Inhibitory effect of saccharides and phenolic compounds from maize silks on intestinal α-glucosidases. *Journal of Food Biochemistry*, 43, 12896.

Arif, R., Ahmad, S., Mustafa, G., Mahrosh, H.S., Ali, M., Tahir ul Qamar, M. and Dar, H.R. 2021. Molecular docking and simulation studies of antidiabetic agents devised from hypoglycemic polypeptide-P of *Momordica charantia*. *BioMed Research International*, 2021, 5561129.

Assadi, M.H. and Hanaor, D.A. 2013. Theoretical study on copper's energetics and magnetism in TiO2 polymorphs. *Journal of Applied Physics*, 113, 233913

Balunas, M.J. and Kinghorn, A.D. 2005. Drug discovery from medicinal plants. *Life Sciences*, 78, 431-441.

Bhatti, J.S., Sehrawat, A., Mishra, J., Sidhu, I.S., Navik, U., Khullar, N., Kumar, S., Bhatti, G.K. and Reddy, P.H. 2022. Oxidative stress in the pathophysiology of type 2 diabetes and related complications: Current therapeutics strategies and future perspectives. *Free Radical Biology and Medicine*, 184, 114-134.

Bitwell, C., Indra, S.S., Luke, C. and Kakoma, M.K. 2023. A review of modern and conventional extraction techniques and their applications for extracting phytochemicals from plants. *Scientific African*, 19, 01585.

Bonaventura, M.M., Catalano, P.N., Chamson-Reig, A., Arany, E., Hill, D., Bettler, B., Saravia, F., Libertun, C. and Lux-Lantos, V.A. 2008. GABAB receptors and glucose homeostasis: evaluation in GABAB receptor knockout mice. *American Journal of Physiology-Endocrinology and Metabolism*, 294, 157-167.

Bourebaba, N., Kornicka-Garbowska, K., Marycz, K., Bourebaba, L. and Kowalczuk, A. 2021. *Laurus nobilis* ethanolic extract attenuates hyperglycemia and hyperinsulinemia-induced insulin resistance in HepG2 cell line through the reduction of oxidative stress and improvement of mitochondrial biogenesis–Possible implication in pharmacotherapy. *Mitochondrion*, 59, 190-213.

Chaachouay, N. and Zidane, L. 2024. Plant-derived natural products: a source for drug discovery and development. *Drugs and Drug Candidates*, 3, 184-207.

Chaudhary, R.K., Karoli, S.S., Dwivedi, P.S., Bhandari, R. 2022. Anti-diabetic potential of corn silk (*Stigma maydis*): an *in-silico* approach. *Journal of Diabetes and Metabolic Disorders*, 21, 445-454.

Chen, P.C., Kryukova, Y.N. and Shyng, S.L. 2013a. Leptin Regulates KATP Channel Trafficking in Pancreatic β-Cells by a Signaling Mechanism Involving AMP-activated Protein Kinase (AMPK) and cAMP-dependent Protein Kinase (PKA). *Journal of Biological Chemistry*, 288, 34098-34109.

Chen, S., Chen, H., Tian, J., Wang, Y., Xing, L. and Wang, J. 2013. Chemical modification, antioxidant and α-amylase inhibitory activities of corn silk polysaccharides. *Carbohydrate Polymers*, 98, 428-437.

Chen, L., Teng, H. and Cao, H. 2019. Chlorogenic acid and caffeic acid from *Sonchus oleraceus* Linn synergistically attenuate insulin resistance and modulate glucose uptake in HepG2 cells. *Food and Chemical Toxicology*, 127, 182-187.

Chen, L., Lin, X., Fan, X., Qian, Y., Lv, Q. and Teng, H. 2020. *Sonchus oleraceus* Linn extract enhanced glucose homeostasis through the AMPK/Akt/GSK-3β signaling pathway in diabetic liver and HepG2 cell culture. *Food and Chemical Toxicology*, 136, 111072.

Cheng, J.T., Chi, T.C. and Liu, I.M. 2000. Activation of adenosine A1 receptors by drugs to lower plasma glucose in streptozotocin-induced diabetic rats. *Autonomic Neuroscience*, 83, 127-133.

Cao, R., Tian, H., Zhang, Y., Liu, G., Xu, H., Rao, G., Tian, Y. and Fu, X. 2023. Signaling pathways and intervention for therapy of type 2 diabetes mellitus. *MedComm*, 4, 283.

Caturano, A., D'Angelo, M., Mormone, A., Russo, V., Mollica, M.P., Salvatore, T., Galiero, R., Rinaldi, L., Vetrano, E., Marfella, R. and Monda, M. 2023. Oxidative stress in type 2 diabetes: impacts from pathogenesis to lifestyle modifications. *Current Issues in Molecular Biology*, 45, 6651-6666.

Deb, D.K., Bao, R. and Li, Y.C. 2017. Critical role of the cAMP-PKA pathway in hyperglycemia-induced epigenetic activation of fibrogenic program in the kidney. *The FASEB Journal*, 31, 2065.

Duyu, T., Khanal, P., Khatib, N.A. and Patil, B.M. 2020. *Mimosa pudica* modulates neuroactive ligand-receptor interaction in Parkinson's disease. *Indian Journal of Pharmaceutical Education and Research*, 54, 732-739.

Farmaki, P., Damaskos, C., Garmpis, N., Garmpi, A., Savvanis, S. and Diamantis, E. 2020. Complications of the type 2 diabetes mellitus. *Current Cardiology Reviews*, 16, 249-251.

Galicia-Garcia, U., Benito-Vicente, A., Jebari, S., Larrea-Sebal, A., Siddiqi, H., Uribe, K.B., Ostolaza, H. and Martín, C. 2020. Pathophysiology of type 2 diabetes mellitus. *International Journal of Molecular Sciences*, 21, 6275.

Garibyan, L. and Avashia, N. 2013. Research techniques made simple: polymerase chain reaction (PCR). *The Journal of investigative Dermatology*, 133, 6.

Geng, Y., Bush, M., Mosyak, L., Wang, F. and Fan, Q.R. 2013. Structural mechanism of ligand activation in human GABAB receptor. *Nature*, 504, 254-259.

Ghazi, T., Nagiah, S., Naidoo, P. and Chuturgoon, A.A. 2019. Fusaric acid-induced promoter methylation of DNA methyltransferases triggers DNA hypomethylation in human hepatocellular carcinoma (HepG2) cells. *Epigenetics*, 14, 804-817.

Ghazi, T., Nagiah, S., Dhani, S. and Chuturgoon, A.A. 2020. Fusaric acid-induced epigenetic modulation of hepatic H3K9me3 triggers apoptosis *in vitro* and *in vivo*. *Epigenomics*, 12, 955-972.

Grases, F., March, J.G., Ramis, M. and Costa-Bauzá, A. 1993. The influence of *Zea mays* on urinary risk factors for kidney stones in rats. *Phytotherapy research*, 7, 146-149.

Guo, J., Liu, T., Han, L. and Liu, Y. 2009. The effects of corn silk on glycaemic metabolism. Nutrition and Metabolism, 6, 1-6.

Huang-Doran, I., Zhang, C.Y. and Vidal-Puig, A. 2017. Extracellular vesicles: novel mediators of cell communication in metabolic disease. *Trends in Endocrinology and Metabolism*, 28, 3-18.

Hasanudin, K., Hashim, P. and Mustafa, S. 2012. Corn silk (Stigma maydis) in healthcare: a phytochemical and pharmacological review. *Molecules*, 17, 9697.

Hill, D.R. 1985. GABAB receptor modulation of adenylate cyclase activity in rat brain slices. *British Journal of Pharmacology*, 84, 249.

Huang, Q., Chen, L., Teng, H., Song, H., Wu, X. and Xu, M. 2015. Phenolic compounds ameliorate the glucose uptake in HepG2 cells' insulin resistance via activating AMPK: anti-diabetic effect of phenolic compounds in HepG2 cells. *Journal of Functional Foods*, 19, 487-494.

Ilyas, U., Nazir, B., Altaf, R., Muhammad, S.A., Zafar, H., Paiva-Santos, A.C., Abbas, M. and Duan, Y. 2022. Investigation of anti-diabetic potential and molecular simulation studies of dihydropyrimidinone derivatives. *Frontiers in Endocrinology*, 13, 1022623.

Jadeja, R.N., Jones, M.A., Fromal, O., Powell, F.L., Khurana, S., Singh, N. and Martin, P.M. 2019. Loss of GPR109A/HCAR2 induces aging-associated hepatic steatosis. *Aging (Albany NY)*, 1, 386.

Kahksha, Alam, O., Al-Keridis, L.A., Khan, J., Naaz, S., Alam, A., Ashraf, S.A., Alshammari, N., Adnan, M. and Beg, M.A. 2023. Evaluation of antidiabetic effect of

luteolin in STZ induced diabetic rats: molecular docking, molecular dynamics, *in vitro* and *in vivo* studies. *Journal of Functional Biomaterials*, 14, 126.

Kanwal, A., Kanwar, N., Bharati, S., Srivastava, P., Singh, S.P. and Amar, S. 2022. Exploring new drug targets for type 2 diabetes: success, challenges and opportunities. *Biomedicines*, 10, 331.

Kaur, P., Singh, J., Kaur, M., Rasane, P., Kaur, S., Kaur, J., Nanda, V., Mehta, C.M. and Sowdhanya, D. 2023. Corn silk as an agricultural waste: a comprehensive review on its nutritional composition and bioactive potential. *Waste and Biomass Valorisation*, 14, 1413-1432.

Landeros-Martínez, L.L., Campos-Almazán, M.I., Sánchez-Bojorge, N.A., Flores, R., Palomares-Báez, J.P. and Rodríguez-Valdez, L.M. 2023. Theoretical studies for the discovery of potential sucrase-isomaltase inhibitors from maize silk phytochemicals: an approach to treatment of type 2 diabetes. *Molecules*, 28, 6778.

Lankatillake, C., Huynh, T. and Dias, D.A. 2019. Understanding glycaemic control and current approaches for screening antidiabetic natural products from evidence-based medicinal plants. *Plant Methods*, 15, 1.

Lanrewaju, A.A., Enitan-Folami, A.M., Nyaga, M.M., Sabiu, S. and Swalaha, F.M. 2023. Metabolites profiling and cheminformatics bioprospection of selected medicinal plants against the main protease and RNA-dependent RNA polymerase of SARS-CoV-2. *Journal of Biomolecular Structure and Dynamics*, 2023, 1-21.

Li, C., Yang, W., Meng, Y., Feng, L., Sun, L., Li, Z., Liu, X. and Li, M. 2023. Exploring the therapeutic mechanism of Banxia Xiexin Decoction in mild cognitive impairment and diabetes mellitus: a network pharmacology approach. *Metabolic Brain Disease*, 38, 2315-2325.

Liu, F., Fu, Y., Wei, C., Chen, Y., Ma, S. and Xu, W. 2014. The expression of GPR109A, NF-kB and IL-1β in peripheral blood leukocytes from patients with type 2 diabetes. *Annals of Clinical and Laboratory Science*, 44, 443-448.

Lv, Q., Lin, J., Wu, X., Pu, H., Guan, Y., Xiao, P., He, C. and Jiang, B. 2022. Novel active compounds and the anti-diabetic mechanism of mulberry leaves. *Frontiers in Pharmacology*, 13, 986931.

Paddy, V., Van Tonder, JJ. and Steenkamp, V. 2014. The antidiabetic activity of a polyherbal tea mixture and its constituents *in vitro*. *17th World Congress of Basic and Clinical Pharmacology*. 115, 151.

Pan, L., Li, Z., Wang, Y., Zhang, B., Liu, G. and Liu, J. 2020. Network pharmacology and metabolomics study on the intervention of traditional Chinese medicine Huanglian Decoction in rats with type 2 diabetes mellitus. *Journal of Ethnopharmacology*, 258, 112842.

Perreault, L., Skyler, J.S. and Rosenstock, J. 2021. Novel therapies with precision mechanisms for type 2 diabetes mellitus. *Nature Reviews Endocrinology*, 17, 364-377.

McCammon, J.A. and Hwang, H.J.A. 2007. Reactivity and selectivity of electrophilic ligands: Implications for drug design. *Biochemical Society Transactions*, 35, 257-262.

McQuade, K.L. and Lynch, D.M., 2016. Covalent bond formation in drug design: Insights into electrophilic ligands. *Journal of Medicinal Chemistry*, 59, 9898-9909.

Michaelidou, M., Pappachan, J.M. and Jeeyavudeen, M.S. 2023. Management of diabesity: current concepts. *World Journal of Diabetes*, 14, 396-411.

Mintah, S.O., Asafo-Agyei, T., Archer, M.A., Junior, P.A.A., Boamah, D., Kumadoh, D., Appiah, A., Ocloo, A., Boakye, Y.D. and Agyare, C. 2019. Medicinal plants for treatment of prevalent diseases. *Pharmacognosy-Medicinal Plants*, 177, 1-19.

Mohammed, A. and Tajuddeen, N. 2022. Antidiabetic compounds from medicinal plants traditionally used for the treatment of diabetes in Africa: A review update (2015–2020). *South African Journal of Botany*, 146, 585-602.

Mokashi, P., Khanna, A., Pandita, N. 2017. Flavonoids from *Enicostema littorale* blume enhances glucose uptake of cells in insulin resistant human liver cancer (HepG2) cell line via IRS-1/PI3K/Akt pathway. *Biomedicine and Pharmacotherapy*, 90, 268-277.

Moutinho, M., Puntambekar, S.S., Tsai, A.P., Coronel, I., Lin, P.B., Casali, B.T., Martinez, P., Oblak, A.L., Lasagna-Reeves, C.A., Lamb, B.T. and Landreth, G.E. 2022. The niacin receptor HCAR2 modulates microglial response and limits disease progression in a mouse model of Alzheimer's disease. *Science Translational Medicine*, 14, 7634.

Mushtaq, S., Abbasi, B.H., Uzair, B. and Abbasi, R. 2018. Natural products as reservoirs of novel therapeutic agents. *EXCLI Journal*, 17, 420.

Newman, J.C. and Verdin, E. 2014. β-hydroxybutyrate: much more than a metabolite. *Diabetes Research and Clinical Practice*, 106, 173-181.

Nieto Gutierrez, A., and McDonald, P.H. 2018. GPCRs: Emerging anti-cancer drug targets. *Cellular Signal*. 41, 65-74.

Nomiri, S., Karami, H., Baradaran, B., Javadrashid, D., Derakhshani, A., Nourbakhsh, N.S., Shadbad, M.A., Solimando, A.G., Tabrizi, N.J., Brunetti, O. and Nasseri, S. 2022. Exploiting systems biology to investigate the gene modules and drugs in ovarian cancer: A hypothesis based on the weighted gene co-expression network analysis. *Biomedicine and Pharmacotherapy*, 146, 112537.

Nomura, R., Suzuki, Y., Kakizuka, A. and Jingami, H. 2008. Direct detection of the interaction between recombinant soluble extracellular regions in the heterodimeric metabotropic γ-aminobutyric acid receptor. *Journal of Biological Chemistry*, 283, 4665-4673.

Olaokun, O.O., Manonga, S.A., Zubair, M.S., Maulana, S. and Mkolo, N.M. 2022. Molecular docking and molecular dynamics studies of antidiabetic phenolic compound isolated from leaf extract of *Englerophytum magalismontanum* (Sond.) TD Penn. *Molecules*, 27, 3175.

Olokoba, A.B., Obateru, O.A. and Olokoba, L.B. 2012. Type 2 diabetes mellitus: A review of current trends. *Oman Medical Journal*, 27, 269.

Rachdi, L., Maugein, A., Pechberty, S., Armanet, M., Hamroune, J., Ravassard, P., Marullo, S., Albagli, O. and Scharfmann, R. 2020. Regulated expression and function of the GABAB receptor in human pancreatic beta cell line and islets. *Scientific Reports*, 10, 13469.

Rampadarath, A., Balogun, F.O. and Sabiu, S. 2023. Insights into the mechanism of action of *Helianthus annuus* (sunflower) seed essential oil in the management of type-2 diabetes mellitus using network pharmacology and molecular docking approaches. *Endocrines*, 4, 327-349.

Rampogu, S., Parameswaran, S., Lemuel, M. and Lee, K. 2018. Exploring the therapeutic ability of fenugreek against type 2 diabetes and breast cancer employing molecular docking and molecular dynamics simulations. *Evidence-based Complementary and Alternative Medicine : eCAM*. 2018.

Rees, S.C. 2017. Designing safe and effective therapeutic agents: The role of electrophilic ligands. *Drug Discovery Today*, 22, 22-29.

Sabiu, S., O'Neill, FH. and Ashafa, AOT. 2016. Kinetics of α-amylase and α-glucosidase inhibitory potential of *Zea mays* Linnaeus (Poaceae), *Stigma maydis* aqueous extract: An *in vitro* assessment. *Journal of Ethnopharmacology*. 183, 1-18.

Sarkar, S., Zaidi, S., Chaturvedi, A.K., Srivastava, R., Dwivedi, P.K. and Shukla, R. 2015. Search for a herbal medicine: anti-asthmatic activity of methanolic extract of *Curcuma longa*. *Journal of Pharmacognosy and Phytochemistry*, 3, 59-72.

Sawangwong, W., Kiattisin, K., Somwongin, S., Wongrattanakamon, P., Chaiyana, W., Poomanee, W. and Sainakham, M. 2024. The assessment of composition, biological properties, safety and molecular docking of corn silk (*Zea mays* L.) extracts from the valorization of agricultural waste products in Thailand. *Industrial Crops and Products*, 212, 118352.

Semaan, D.G., Igoli, J.O., Young, L., Gray, A.I., Rowan, E.G. and Marrero, E. 2018. *In vitro* anti-diabetic effect of flavonoids and pheophytins from *Allophylus cominia* Sw. on the glucose uptake assays by HepG2, L6, 3T3-L1 and fat accumulation in 3T3-L1 adipocytes. *Journal of Ethnopharmacology*, 216, 8-17.

Shakya, A.K. 2016. Medicinal plants: Future source of new drugs. *International Journal of Herbal Medicine*, 4, 59-64.

Shalaby, N.M., Abd-Alla, H.I., Aly, H.F., Albalawy, M.A., Shaker, K.H. and Bouajila, J. 2014. Preliminary *in vitro* and *in vivo* evaluation of antidiabetic activity of *Ducrosia anethifolia* Boiss. and its linear furanocoumarins. *BioMed Research International*, 2014.

Sharma, P., Joshi, T., Mathpal, S., Chandra, S. and Tamta, S. 2022. *In silico* identification of antidiabetic target for phytochemicals of *A. marmelos* and mechanistic insights by molecular dynamics simulations. *Journal of Biomolecular Structure and Dynamics*, 40, 10543-10560.

Shon, J. and Park, Y.J. 2021. Effects of dietary butyrate on diet-induced obesity and lipid metabolism. *Current Developments in Nutrition*, 5, 525.

Shpakov, A.O. and Derkach, K.V. 2013. The functional state of hormone-sensitive adenylyl cyclase signaling system in diabetes mellitus. *Journal of Signal Transduction*, 2013,

retrieved from https://www.hindawi.com/journals/jst/2013/594213/, accessed on 01/04/2024.

Shrestha, P.M. and Dhillion, S.S. 2003. Medicinal plant diversity and use in the highlands of Dolakha district, Nepal. *Journal of Ethnopharmacology*, 86, 81-96.

Singh, A. and Raghuvanshi, R.S. 2021. Development and evaluation of value-added fiber rich laddoo supplemented with processed corn silk. *International Journal of Research and Analytical Reviews*, 8, 909-922.

Singh, J., Rasane, P., Nanda, V. and Kaur, S. 2023. Bioactive compounds of corn silk and their role in management of glycaemic response. *Journal of Food Science and Technology*, 60, 1695-1710.

Tsao, R., Khanizadeh, S. and Dale, A. 2006. Designer fruits and vegetables with enriched phytochemicals for human health. *Canadian Journal of Plant Science*, 86, 773-786.

Tuteja, S. 2019. Activation of HCAR2 by niacin: benefits beyond lipid lowering. *Pharmacogenomics*, 20, 1143-1150.

Wang, N., Guo, D.Y., Tian, X., Lin, H.P., Li, Y.P., Chen, S.J., Fu, Y.C., Xu, W.C. and Wei, C.J. 2016. Niacin receptor GPR109A inhibits insulin secretion and is down-regulated in type 2 diabetic islet beta-cells. *General and Comparative Endocrinology*, 237, 98-108.

Wang, K.J. and Zhao, J.L. 2019. Corn silk (*Zea mays* L.), a source of natural antioxidants with α-amylase, α-glucosidase, advanced glycation and diabetic nephropathy inhibitory activities. *Biomedicine and Pharmacotherapy*, 110, 510-517.

White, J.H., Wise, A., Main, M.J., Green, A., Fraser, N.J., Disney, G.H., Barnes, A.A., Emson, P., Foord, S.M. and Marshall, F.H. 1998. Heterodimerization is required for the formation of a functional GABAB receptor. *Nature*, 396, 679-682.

Wojcik, M., Zieleniak, A. and A Wozniak, L. 2010. New insight into A1 adenosine receptors in diabetes treatment. *Current Pharmaceutical Design*, 16, 4237-4242.

Xu, X., Lin, S., Chen, Y., Li, X., Ma, S., Fu, Y., Wei, C., Wang, C. and Xu, W. 2017. The effect of metformin on the expression of GPR109A, NF-κB and IL-1β in peripheral blood leukocytes from patients with type 2 diabetes mellitus. *Annals of Clinical and Laboratory Science*, 47, 556-562.

Yang, T., Gao, X., Sandberg, M., Zollbrecht, C., Zhang, X.M., Hezel, M., Liu, M., Peleli, M., Lai, E.Y., Harris, R.A. and Persson, A.E.G. 2015. Abrogation of adenosine A 1 receptor signalling improves metabolic regulation in mice by modulating oxidative stress and inflammatory responses. *Diabetologia*, 58, 1610-1620.

Yang, H. and Yang, L. 2016. Targeting cAMP/PKA pathway for glycemic control and type 2 diabetes therapy. *Journal of Molecular Endocrinology*, 57, 93-108.

Yarahmadi, A., Sarabi, M.M., Sayahi, A. and Zal, F. 2021. Protective effects of quercetin against hyperglycemia-induced oxidative stress in hepatic HepG2 cell line. Avicenna *Journal of Phytomedicine*, 11, 269-280.

Yip, L., Taylor, C., Whiting, C.C. and Fathman, C.G. 2013. Diminished adenosine A1 receptor expression in pancreatic α-cells may contribute to the pathology of type 1 diabetes. *Diabetes*, 62, 4208-4219.

Yon Rhee, S., Wood, V., Dolinski, K. and Draghici, S. 2008. Use and misuse of the gene ontology annotations. *Nature Reviews Genetics*, 9, 509-515.

Zhang, Y., Chen, J., Zeng, Y., Huang, D. and Xu, Q. 2019. Involvement of AMPK activation in the inhibition of hepatic gluconeogenesis by *Ficus carica* leaf extract in diabetic mice and HepG2 cells. *Biomedicine and Pharmacotherapy*, 109, 188-194.

Zhang, Y., Li, Z., Liu, X., Chen, X., Zhang, S., Chen, Y., Chen, J., Chen, J., Wu, F. and Chen, G.Q. 2023. 3-Hydroxybutyrate ameliorates insulin resistance by inhibiting PPARγ Ser273 phosphorylation in type 2 diabetic mice. *Signal Transduction and Targeted Therapy*, 8, 190.

Zhao, W., Yin, Y., Yu, Z., Liu, J. and Chen, F. 2012. Comparison of anti-diabetic effects of polysaccharides from corn silk on normal and hyperglycemia rats. *International Journal of Biological Macromolecules*, 50, 1133-1137.